ANNUAL REPORTS ON
NMR SPECTROSCOPY

Edited by

G. A. WEBB

Department of Chemistry, University of Surrey, Guildford, Surrey, England

VOLUME 22



ACADEMIC PRESS

Harcourt Brace Jovanovich, Publishers

London • San Diego • New York
Berkeley • Boston • Sydney • Tokyo • Toronto

ACADEMIC PRESS LIMITED
24–28 Oval Road,
LONDON NW1 7DX

U.S. Edition Published by

ACADEMIC PRESS INC.
San Diego, CA 92101

This book is printed on acid free paper ♾

Copyright © 1990 ACADEMIC PRESS LIMITED

All Rights Reserved

No part of this book may be reproduced or transmitted in any form or by any means, electronic or mechanical, including photocopying, recording, or any information storage and retrieval system without permission in writing from the publisher

British Library Cataloguing in Publication Data
Annual reports on NMR Spectroscopy, Vol. 22
1. Nuclear magnetic resonance spectroscopy
—periodicals
QD96.N8.
ISBN 0-12-505322-3
ISSN 0066-4103

Typeset by Mathematical Composition Setters Ltd, Salisbury, England
Printed in Great Britain by St Edmundsbury Press Limited
Bury St Edmunds, Suffolk

List of Contributors

I. Ando, *Department of Polymer Chemistry, Tokyo Institute of Technology, Ookayama, Meguro-ku, Tokyo, Japan.*

A.A.S. Bright, *Schering Agrochemicals Limited, Chesterford Park Research Station, Saffron Walden, Essex CB10 1XL, UK.*

David J. Craik, *School of Pharmaceutical Chemistry, Victorian College of Pharmacy Limited, 381 Royal Parade, Parkville, Victoria 3052, Australia.*

Torbjörn Drakenberg, *Division of Physical Chemistry 2, Chemical Center, University of Lund, POB 124, S-221 00 Lund, Sweden.*

Kerry A. Higgins, *School of Pharmaceutical Chemistry, Victorian College of Pharmacy Limited, 381 Royal Parade, Parkville, Victoria 3052, Australia.*

Klaus Horchler, *Laboratorium für Anorganische Chemie der Universität Bayreuth, Postfach 101251, D-8580 Bayreuth, Federal Republic of Germany.*

Charlotta Johansson, *Division of Physical Chemistry 2, Chemical Center, University of Lund, POB 124, S-221 00 Lund, Sweden.*

Jozef Kowalewski, *Division of Physical Chemistry, Arrhenius Laboratory, University of Stockholm, S-106 91 Stockholm, Sweden.*

H. Kurosu, *Department of Polymer Chemistry, Tokyo Institute of Technology, Ookayama, Meguro-ku, Tokyo, Japan.*

R.G. Ratcliffe, *Department of Plant Sciences, University of Oxford, Agricultural Science Building, Parks Road, Oxford OX1 3PF, UK.*

G.A. Webb, *Department of Chemistry, University of Surrey, Guildford, Surrey GU2 5XH, UK.*

Bernd Wrackmeyer, *Laboratorium für Anorganische Chemie der Universität Bayreuth, Postfach 101251, D-8580 Bayreuth, Federal Republic of Germany.*

T. Yamanobe, *Department of Polymer Chemistry, Tokyo Institute of Technology, Ookayama, Meguro-ku, Tokyo, Japan.*

Preface

As with previous volumes of this series, the present one encompasses aspects of NMR relating to a wide diversity of scientific interests.

The areas covered include metal-ion NMR studies on ion binding, some recent aspects of NMR studies relevant to small-molecule–large-molecule interactions, applications of NMR to investigations of agrochemicals and pesticides, some studies of NMR shielding and the electronic structures of macromolecules, lead NMR, and a consideration of the general aspects and inorganic applications of nuclear spin relaxation in diamagnetic fluids.

It is a pleasure for me to thank all of the contributors for their diligence and kind cooperation, without which this volume would not have been produced.

University of Surrey
Guildford

G.A. WEBB

Metal-Ion NMR studies of Ion Binding

CHARLOTTA JOHANSSON and TORBJÖRN DRAKENBERG

Division of Physical Chemistry 2, Chemical Center, University of Lund, P.O.B. 124, S-221 00 Lund, Sweden

1. Introduction 1
2. Small ligands 2
2.1. Alkali metals 2
2.2. Alkaline-earth metals 7
2.3. Transition metals 8
2.4. Group IIA and IIIA metals 21
3. Metal-ion binding to macromolecules 26
3.1. Alkali metals 26
3.2. Alkaline-earth metals 30
3.3. Transition metals 35
3.4. Thallium 47
4. Ion binding to aggregates and cells 47
4.1. Gramicidin channels 47
4.2. Whole-cell studies 49
References 50

1. INTRODUCTION

In this review we have chosen to cover only studies where NMR has been used as a tool to investigate the interaction between an ion and another ion or a molecule or an aggregate. We have excluded most studies of, for example, stable complexes where the interest has been exclusively in NMR parameters. This area has been covered by several recent reviews.[1-8] The borderline between what we should and should not include is of course not very straight, and our own interests have naturally affected our choice.

We wavered somewhat regarding which NMR nuclei should be incorporated, and have decided to limit ourselves to metals. Furthermore, we shall discuss only work dealing with ion binding, therefore excluding almost all studies of metallo-organic compounds. It may at first seem an overwhelming task to include all metal nuclei in one review; however, the

ANNUAL REPORTS ON NMR SPECTROSCOPY
VOLUME 22 ISBN 0-12-505322-3

Copyright © 1989 Academic Press Limited
All rights of reproduction in any form reserved

limits outlined above result in a drastic reduction in the amount of literature that need be taken into consideration.

Obviously the vast majority of NMR studies of ion binding have dealt with alkali and alkaline-earth ions, and moreover most of these studies have been on biologically or biochemically interesting systems, with only a minor proportion dealing with "pure" inorganic chemistry. Throughout this review, when we discuss "free" ions we in fact mean solvated ions.

We have tried to cover the literature from 1980 up to 1988, but have no claims to completeness. In addition, a few older studies are included, especially in connection with more recent work.

We have organized this review in a what we feel to be the most logical way, starting with interactions among small molecules, moving on to more and more complex systems, and ending with studies of whole living cells.

2. SMALL LIGANDS

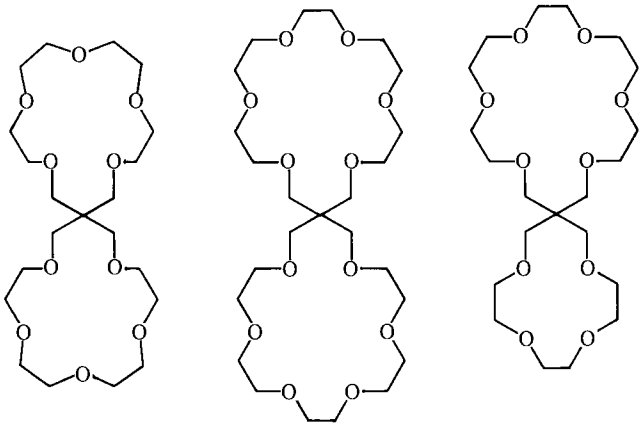
2.1. Alkali metals

Fraenkel *et al.*[9] used ^{6}Li and ^{13}C NMR to study the Li^+ exchange between various aggregates of propyllithium. The data show that the exchange results from the collision of two aggregates. Olsher *et al.*[10] used ^{7}Li and ^{1}H NMR to investigate the binding of Li^+ ions to polydentate amino ethers, and van Lier *et al.*[11] and Kolodziejski and Maciel[12] studied some kinds of ion binding with ^{7}Li NMR. There have been some reports on ion-pair formation using ^{23}Na NMR; this subject is on the borderline of the area covered by this review, and therefore we shall simply give references here, with no further discussion of the results.[13-19]

During the last few years there have been a number of NMR studies of metal-ion binding to crown ethers and cryptands using various NMR nuclei: ^{6}Li,[20,21] ^{7}Li,[22-26] ^{23}Na,[20,22,26-46] ^{39}K,[26,47-52] ^{87}Rb[22,53] and ^{133}Cs.[22,26,54-57] Popov and coworkers[24-26] also used ^{7}Li NMR to study Li^+ binding to crown ethers and cryptands in molten salts. In agreement with previous data[28] for non-aqueous solutions, they found that the stability of the complexes is in the order 15-crown-5 > 12-crown-4 > 18-crown-6 and that the Li^+ ion is in all cases in rapid exchange. For some Li–cryptand complexes they found the order of stability to be C221 > C222 > C222B; however, the exchange rate for the Li^+ ion is significantly higher for the C222 complex than for the others, showing that the entrance of the Li^+ ion is more hindered in the case of the C222B ligand. Lin and Popov[27] used ^{23}Na NMR to study the binding of Na^+ ions to various crown ethers and cryptands in different solvents. The stability of the complexes was found to

vary in the order Na^+18-crown-6 > Na^+15-crown-5 > Na^+D15-crown-5. Only in the case of 18-crown-6 was the cation exchange sufficiently slow to allow observation of separate lines for free and bound $^{23}Na^+$ ions.

In a series of articles ^{23}Na NMR has been utilized quite extensively for a thorough study of Na^+-ion binding to crown ethers.[29,35,36,40,41] Bouquant *et al.*[29] studied spiro-bis-crown ethers and a substituted 16-crown-5 crown ether. They found that 16-crown-5 and "O_6–O_4" formed a 1 : 1 complex



and a sandwich complex, whereas both "O_5–O_5" and "O_6–O_6" formed complexes with one sodium ion in each crown ether ring. In both of the latter cases there is a strong negative cooperativity between the sites in the two identical rings. For all ligands the sandwich complex has a slower ^{23}Na relaxation rate owing to higher symmetry. The authors also tried to analyse the temperature dependence of the linewidth in order to extract rate constants for the ion exchange. This proved to be successful only for the substituted 16-crown-5 crown ether—all of the others appeared to be too complicated for analysis. Detellier and coworkers have studied the aggregation of sodium tetraphenylborate–dibenzo-24-crown-8 complexes dissolved in nitromethane.[35] The dependence of the ^{23}Na shift on the ratio [crown]/[sodium] shows that a strong 1 : 1 complex is formed. They also found interesting shapes of the dependences of T_1^{-1} and T_2^{-1} on the ratio [crown]/[sodium], as shown in Fig. 1. The field dependence of T_2^{-1} shows that the maximum at a ratio of *ca.* 0.7 is due to an intermediate exchange between free and bound sodium ions, and the maximum in T_1^{-1} shows that more than one complex is formed. The data have been analysed assuming the formation of aggregates of the type ($Na_{i+1}crown_i$), with the agreement

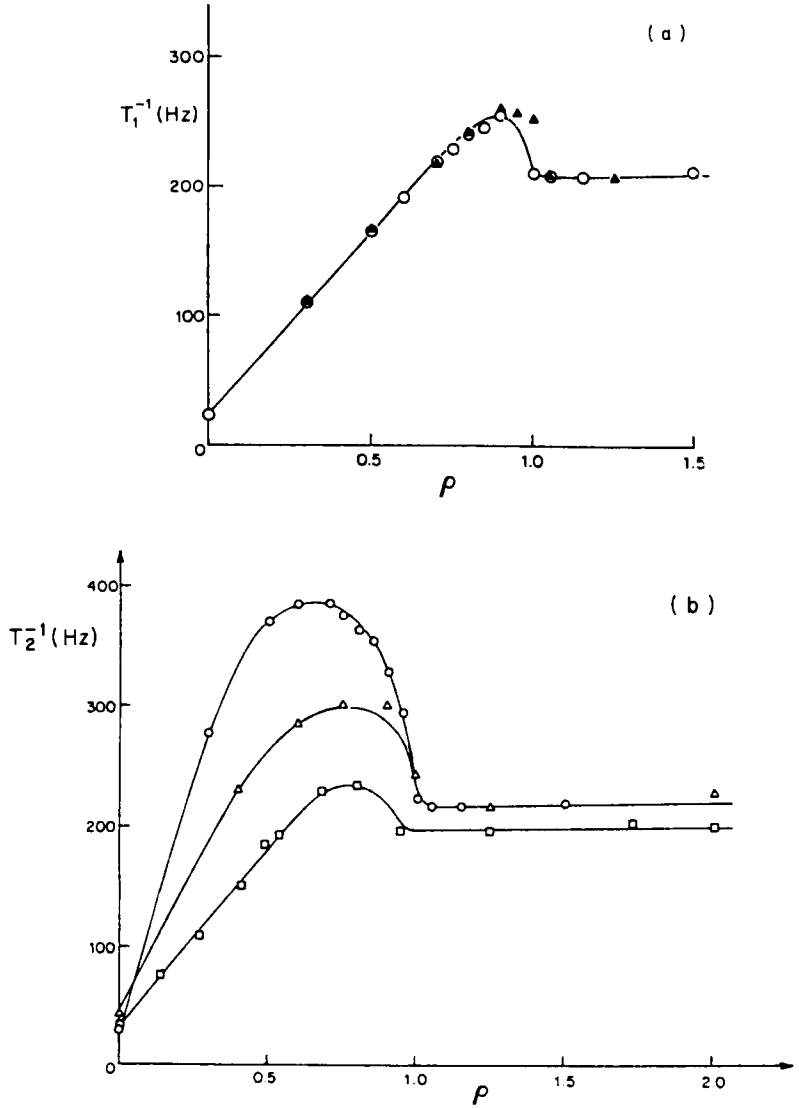


Fig. 1. ^{23}Na relaxation rates as functions of the ratio [crown]/[Na^+]. (a) T_1 relaxation at 79.35 MHz (○) and 52.92 MHz (△). (b) T_2 relaxation at 79.35 MHz (○), 52.92 MHz (△) and 21.04 MHz (□). From Ref. 35, with permission.

shown in Fig. 1. In another paper[36] they analysed the exchange in more detail and tested two models for the exchange:

(a) a unimolecular exchange (decomplexation)

$$\text{crownNa} \rightarrow \text{crown} + \text{Na}$$

(b) a bimolecular cation interchange

$$\text{crownNa} + \text{Na}^* \rightarrow \text{crownNa}^* + \text{Na}$$

For mechanism (a) the exchange should be concentration-independent, whereas for (b) the exchange rate should be linearly dependent on $[Na^+]$. Figures 2 and 3 show clearly that the exchange depends on the Na^+ concentration, and at concentrations above 10^{-3} M there is an almost-linear dependence in agreement with mechanism (b). At lower concentrations mechanism (a) appears to contribute to the exchange as well. The kinetic parameters for both mechanisms have been deduced. As for the DB18-crown-6–Na^+ complex, it has also been shown for the 18-crown-6–Na^+ complex that the metal-ion exchange can take place through either a unimolecular or bimolecular route.[35] In acetone solution the exchange follows the unimolecular route almost exclusively. For four different solvents the free energy of activation for the unimolecular exchange was

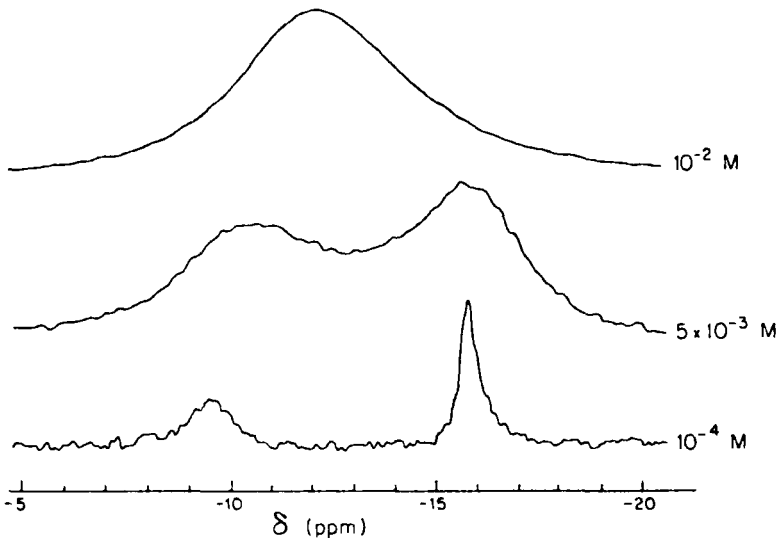


Fig. 2. ^{23}Na NMR spectra at 79.35 MHz of sodium tetraphenylborate solution in nitromethane in the presence of DB24-crown-8 at different sodium concentrations. [DB24-crown-8]/$[Na^+]$ = 0.5. From Ref. 36, with permission.

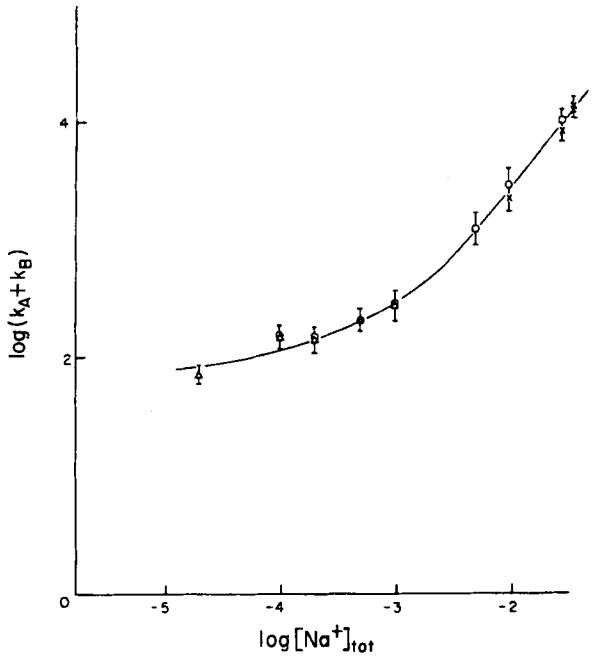


Fig. 3. Sodium exchange rate as a function of log $[Na^+]_{tot}$. From Ref. 36, with permission.

found to be similar, whereas the enthalpies and entropies of activation vary dramatically between the solvents.

Desroches *et al.*[44] studied the binding of metal ions to substituted crown ethers using, among other methods, ^{23}Na NMR, and Galiano-Roth and Collum[22] studied the effect of cryptate formation on the reactivity of metallated *N,N*-dimethylhydrazones.

Schmidt and Popov[48] studied the binding of K^+ ions to 18-crown-6 in various non-aqueous solvents. The chemical shift of ^{39}K bound to 18-crown-6 does not vary more than 5 ppm between the various solvents, whereas the shift difference for "free" K^+ is 22 ppm. This is an indication of the formation of inclusion complexes. From bandshape analysis of the ^{39}K NMR signals, they find that the enthalpy and entropy of activation vary dramatically with solvent and that there is only a small effect on the free energy of activation. For a 1,3-dioxalane solution the exchange was studied at two different K^+ concentrations. The exchange rate was found to be independent of $[K^+]$ at constant crown ether concentration, in agreement with the bimolecular mechanism (b) above.

Detellier and coworkers[50,51] found that dibenzo-30-crown-10 forms

complexes with either one or two potassium ions. In the 1 : 1 complex the K^+ ion is, according to ^{39}K chemical shifts, completely surrounded by the crown ether, whereas in the 2 : 1 complex there is some solvent and counterion interaction with the metal ion. Kauffmann *et al.*[54] used ^{133}Cs NMR to study the binding of caesium ions to various cryptands, and found that, for example, for the system C222–caesium octanoate in tetrahydrofuran, with some water, there is an equilibrium between inclusion and exclusion complexes.

Laszlo and coworkers[58] continued their ^{23}Na NMR studies on the self-assembly of 5′-guanosine monophosphate, finding that at high concentration there is a disorder–order transition with a highly cooperative nature. The phase-separation model could be used to reproduce the results satisfactorily with $\Delta H^\circ = -17$ kcal mol^{-1} and $\Delta S^\circ = -51$ cal mol^{-1} K^{-1}. Neurohr *et al.*[49] studied the binding of potassium ions to some ionophores with ^{39}K NMR, and Amat *et al.*[59,60] used ^{23}Na NMR in a study of the exchange between free sodium ions and sodium ions bound to monensin dissolved in methanol or methanol–water mixtures. The concentration dependence of the exchange rate shows that the dominant mechanism for the exchange is the dissociation of the Na–monensin complex.

During the years covered by this review there has been some work in developing new shift reagents for cations, especially for ^{23}Na and ^{39}K.[61–72] The Guptas[62–64] showed that complexes between Dy^{3+} and tripolyphosphate are effective shift reagents for $^{23}Na^+$ ions, and, by adding the shift reagent to the extracellular space of a skeletal muscle they could obtain well-separated ^{23}Na NMR signals for intra- and extra-cellular sodium ions. Springer and coworkers[65–68] tested several different paramagnetic lanthanide-complex anions and found, like the Guptas, that the tripolyphosphate complex is most effective; however, the effect is strongly pH-dependent. The triethylenetetraminehexaacetate ($TTHA^{6-}$) complex is not as effective a shift reagent as the tripolyphosphate complex, but has the advantage of being pH-independent in the interval 5–12. More recently, Sherry *et al.*[71,72] showed that a new chelate tetraazacyclododecane-*N*,*N*′,*N*″,*N*‴-tetramethylenephosphonate is a most effective shift reagent for cations.

2.2. Alkaline-earth metals

Jaber and Thomas-David[73] used ^9Be and ^{13}C NMR to study the binding of Be^{2+} to malonate. They were able to confirm the formation of three complexes, as suggested on the basis of Raman-spectroscopic data.[74]

Bouhoutsos-Brown *et al.*[75] studied the binding of Mg^{2+} and Ca^{2+} ions to

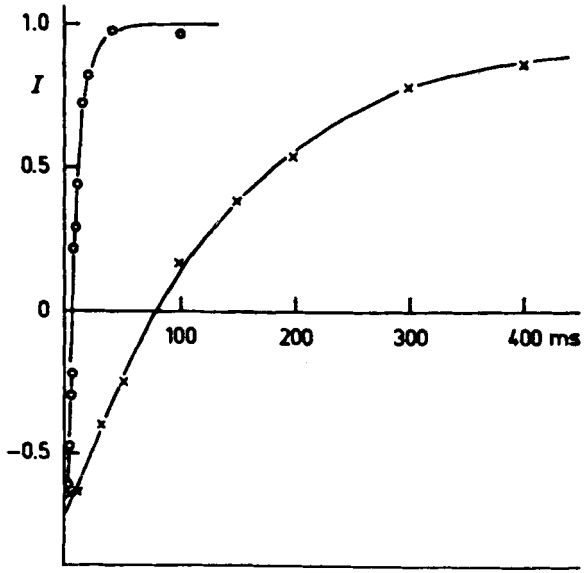


Fig. 4. ^{43}Ca signal intensity as a function of the delay time in inversion-recovery experiments: ×, CaEDTA; ○, CaEGTA. From Ref. 77, with permission.

EDTA at various pHs and temperatures using ^{25}Mg and ^{43}Ca NMR. They were in both cases able to observe resonances from both free solvated ions and ions bound to EDTA. Also, Farmer and Popov[76] observed resonances from free and EDTA-bound ^{43}Ca ions. Drakenberg[77] performed a more comprehensive ^{43}Ca NMR study of Ca^{2+} binding to a few ligands. Figure 4 shows the results from ^{43}Ca T_1 measurements for the complexes CaEDTA and CaEGTA. These two seemingly similar complexes have widely different T_1 values, which can only be explained in terms of quadrupole coupling constants of 0.5 MHz for CaEDTA and 2.1 MHz for CaEGTA. It is therefore obvious that the symmetries of the complexes are very different. The same has been observed for the corresponding Cd^{2+} complexes, *cf.* Section 2.3.

2.3. Transition metals

For most transition metals very little work has been published on what can be considered as ion binding. There are some studies with ^{45}Sc and ^{139}La that will be discussed below. For Group IVB elements there is nothing, and for ^{51}V we list a series of articles even though it is questionable whether they

should be classified as ion-binding studies. From Groups 6B to 8B only ^{195}Pt has been used to any great extent in metal-ion-binding studies; ^{103}Rh has also been used, but less frequently. The elements in Group 2B, especially ^{113}Cd, have been employed in NMR studies of metal-ion binding in a number of investigations.

There have recently appeared a few review articles dealing with some of the transition metals from a pure NMR point of view. Rehder[5] covered the first-row nuclei (Sc to Zn), Minelli *et al.*[6] discussed Group 6B nuclei (Cr, Mo and W), and Drakenberg[7] presented the transition metals that have quadrupole moments. Furthermore, Summers[8] has recently given a review on Cd NMR.

Rehder and Speh[78] studied the binding of the Sc^{3+} ion to alanine and some oligopeptides. They found that the Sc^{3+} exchange is intermediate to slow on the NMR timescale. At temperatures below 343 K a broad resonance assigned to the Sc–alanine complex can be observed (Fig. 5), and for temperatures below 313 K a third resonance assigned to $[Sc(H_2O)_5OH]^{2+}$ is also seen. ^{89}Y has, as far as we know, not been used for ion-binding studies, and the same seems to be the case for ^{175}Lu. ^{139}La NMR has been reviewed[7] and has since been used to study organometallic complexes.[79,80] Geraldes and Sherry[81–83] studied complexes between La^{3+} ions and various polyaminocarboxylates. They found that there is a correlation between the ^{139}La chemical shift and the number of nitrogen and oxygen ligands following

$$\delta = 50N + 30O,$$

where N and O are the number of neutral nitrogen and negative oxygen ligands respectively. Geraldes and Sherry also reported the width of the ^{139}La resonances for the various complexes, and discussed the variation in terms of differences in the correlation time as well as in the symmetry at the metal ion. It is thus concluded that the $La(TTHA)^{3-}$ and $La(DTPA)^{2-}$ complexes are more symmetric than $La(EDTA)^{-}$, which is much more symmetric than $La(HEDTA)^{-}$.

Very little has been published on titanium and zirconium NMR, and in fact none of these reports can be classified as ion-binding studies.[84–89]

Tracy and coworkers[90–92] studied the binding of various ligands to the vanadate ion using ^{51}V NMR. In the first work they found that both $EtOVO_3H^-$ and $(EtO)_2VO_2^-$ are formed with stability constants of 10 and 2.5 respectively. From the coalescence of the two resonances from $EtOVO_3H^-$ and $H_2VO_4^-$ they determined the rate constant for the formation of $EtOVO_3H^-$ to be 10 s^{-1} at 328 K. Using ethylene glycol instead of ethanol as a ligand results in the formation of a cyclic ester in addition to the acyclic mono- and di-esters. From the concentration dependence of the

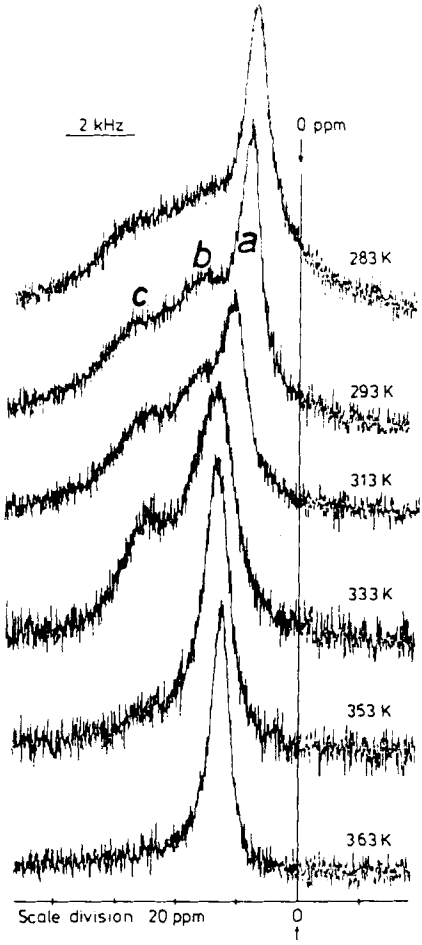


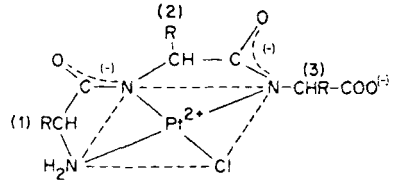
Fig. 5. 87.5 MHz ^{45}Sc NMR spectra of a $Sc(NO_3)_3$ alanine solution in water at pH 4 and a ratio [alanine]/[Sc^{3+}] of 6 at various temperatures as indicated. From Ref. 78, with permission.

intensities of the various ^{51}V signals, the authors concluded that the only cyclic ester present in measurable amounts is the dimer, with a chemical shift of -522 ppm as compared with -560 ppm for $H_2VO_4^-$ at pH 7.5. Tracy and Gresser[94] also showed, using ^{51}V NMR, that phenol and tyrosine form esters with vanadate, and they discussed the possibility that this may be responsible for the observation that vanadate has an effect *in vivo* on systems that are regulated by reversible phosphorylation of tyrosine residues. Tracy *et al.* have continued to study the binding of vanadium

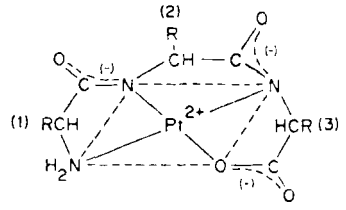
oxyanions to various ligands like phosphate and arsenate[95] and to acids[96] and the dependence of the ester formation on the pK_a of the alcohol or phenol.[97] This series of papers is in our opinion a very good example of how useful NMR can be in studies of complex formation. It is unfortunate, however, that the authors persist in trying to find linear relationships to prove various assumptions instead of fitting the raw data directly to one model or the other. The use of linearized relations is a remnant from the time when there were no microcomputers in the laboratory, and should in our opinion be avoided nowadays.

^{103}Rh NMR has been used to study the binding of Cl^- ions[98] to $Rh(H_2O)_6^{3+}$, forming a series of complexes, $RhCl_n(H_2O)_{6-n}^{3-n}$. Similarly, Mann and Spencer[99,100] studied the formation of $RhCl_nBr_{6-n}^{3-}$ complexes in solutions with mixtures of concentrated HCl and HBr. In the latter case they observed the "inverse halogen effect" and also found that the replacement of a water ligand by a Cl^- results in a low-frequency shift of 230 to 420 ppm. This is contrary to what is found for the more widely studied $^{113}Cd^{2+}$, but similar to ^{195}Pt.[100]

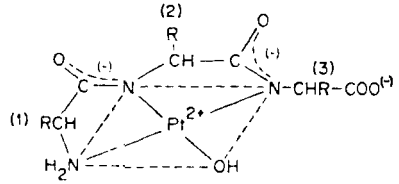
Appleton *et al.*[101] used a multinuclear approach to study the formation of complexes between $Pt(NH_3)_2(H_2O)_2^{2+}$ ion and various ligands. By the combined use of ^{195}Pt, ^{15}N and ^{1}H, ^{13}C or ^{15}N NMR, they were able to deduce the structure of several of the formed complexes. For several ligands under suitable concentration and pH conditions they detected the formation of hydroxo-bridged complexes. In an accompanying article Appleton *et al.*[102] studied complexation between $Pt(H_2O)_4^{2+}$ and a series of ligands bound via oxygen. They also studied the effect of Cl^-, and found a strongly negative chemical shift from replacement of a H_2O by Cl^-, in agreement with earlier observations.[103] Appleton *et al.*[104] also studied the complexes formed between glycine and either $Pt(H_2O)_4^{2+}$ or $Pt(NH_3)_2(H_2O)_2^{2+}$. Using ^{15}N-glycine, they could show that glycine is complexed to platinum solely through its oxygen in $Pt(H_2O)_3Gly$ and $Pt(H_2O)_2Gly_2$. For $Pt(NH_3)_2(H_2O)_2^{2+}$ it was found that under certain conditions the chelate complex $Pt(NH_3)_2Gly$ was formed. Appleton *et al.*[105–110] have continued their ^{195}Pt NMR studies of complexes of the type $Pt(NH_3)_2 \cdot X \cdot Y$. They have thus found, using ^{195}Pt and ^{15}N NMR, that β-alanine and γ-amino-butyric acid, when mixed with $Pt(NH_3)_2(H_2O)_2$, form an oxygen complex, and in contrast with glycine, there is no formation of a chelate even after several weeks. However, on increasing the pH of the β-alanine complex to 5.5 and heating to 80°C for 30 min a new ^{195}Pt resonance appears that can be assigned to a chelate where both amino and carboxyl groups in β-alanine are coordinated to platinum. In the pH range 9–11 only glycine reacts with $Pt(NH_3)_2(OH)_2$ to form a mixture of *cis*-$Pt(NH_3)_2(OH)$(Gly–N), $Pt(NH_3)_2$(Gly–N,O)$^+$ and *cis*-$Pt(NH_3)_2$(Gly–N)$_2$. Appleton *et al.*[111] also



I $Pt^{II}(H_2G_3)Cl^{2-}$ for R=H



II $Pt^{II}(H_2G_3)^-$ for R=H

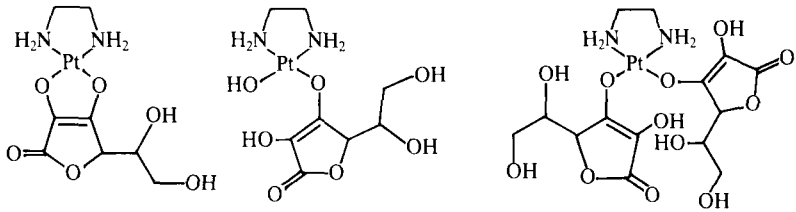


III $Pt^{II}(H_2G_3)OH^{2-}$ for R=H

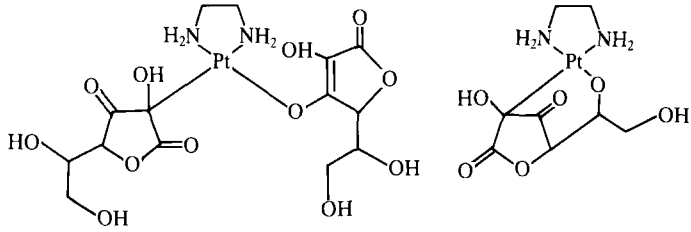
Fig. 6. Suggested structures of the Pt–triglycine complex.

studied the complexes between $Pt(NH_3)_2(H_2O)_2^{2+}$ and methionine or *S*-methylcysteine. They found that when the reaction takes place at pH 5 a chelate is formed in which S and N are bound to platinum. When the complexes are formed below pH 0.5 S, O chelates are observed. Kirvan and Margerum[112] studied the binding of $PtCl_4^{2-}$ to triglycine. They suggested that three different complexes are formed, all with three Pt—N bonds with both amide nitrogens deprotonated as shown in Fig. 6.

Hollis and coworkers[113–116] studied platinum complexes with vitamin C, which have antitumour properties. They found that $Pt(RNH_2)_2(H_2O)_2^{2+}$ forms a multitude of complexes with vitamin C. The kinetically preferred products are oxygen linked with vitamin C, complexes I–III, whereas the thermodynamically stable complexes are those where vitamin C is bound



I II III



IV V

via carbon 2, IV and V. The ^{195}Pt spectra in Fig. 7 have been used to reach this conclusion, and Fig. 8 shows the time dependence in the concentration of the various C-linked complexes. A pH titration of the chelate complex shows that the complex has a pK_a of 2, as can be seen from Fig. 9. This is shown to be due to the protonation of the ligating oxygen O5. The protonated complex is more water-soluble than the unprotonated one; however, it is not stable at pH < 2.

Marzilli and coworkers[117,118] studied the interaction between the anticancer drug displatin and nucleosides or nucleotides. They found, in agreement with Dijt *et al.*,[119] that an earlier interpretation[120] of the ^{195}Pt NMR spectra from the adduct between GMP and *cis*-$Pt(NH_3)_2Cl_2$ was in error. Also, Sarrazin *et al.*[121] studied *cis*-$Pt(NH_3)_2Cl_2$ and its interaction with adenosine phosphates. There are several other studies where ^{195}Pt has been used; however, these cannot be considered as ion-binding studies. All ^{195}Pt NMR studies up to 1985 have been covered in a review by Pregosin,[122] and here we shall just mention some of the more recent studies where ^{195}Pt NMR has been used to characterize complexes. Hassan *et al.*,[123] Hope *et al.*,[124] Al-Najjar *et al.*,[125] Green *et al.*,[126] Colton *et al.*[127] and Kraaijkamp *et al.*[128] used, among other techniques, ^{195}Pt NMR to study the binding of phosphorus-containing ligands to platinum(II). Kerrison and Sadler,[129] Brownlee *et al.*,[130] Galbraith *et al.*,[131] and Cramer *et al.*[132] studied complexes with sulphur ligands.

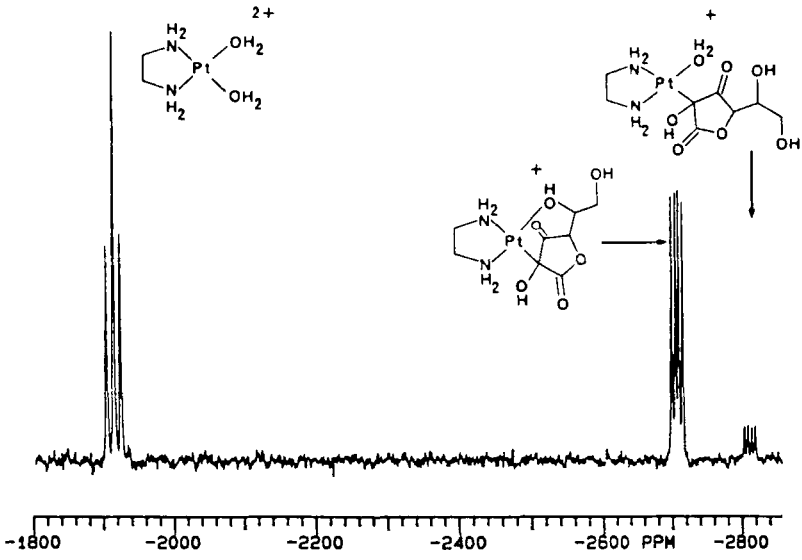


Fig. 7. ^{195}Pt spectrum of the reaction between [Pt(^{15}en)(C2, 05-Asc)] and HNO_3. From Ref. 115, with permission.

There are a few reports where ^{67}Zn has been used to study metal-ion binding. Carson and Dean[133] studied Zn^{2+} complexs with some thiolates and selenolates. They found that the ^{67}Zn chemical shift varies between 261 and 362 ppm for $Zn(SR)_4^{2-}$ complexes and the linewidth varies for the same complexes from 55 to 1200 Hz. They concluded that the main problem with ^{67}Zn NMR is the existence of broad lines, as expected. Li and Popov[134] showed that the ^{67}Zn shift and linewidth of Zn^{2+} ions varies with solvent, but they could not detect any resonances from Zn^{2+} ions bound to ligands like EDTA or crown ethers. Also, Köhnlein *et al.*[135] studied simple zinc salt solutions and reported concentration-dependent relaxation times. Shimizu *et al.*[136] used ^{67}Zn NMR to study the binding of Zn^{2+} to imidazoles, carboxylic acids and peptides. From the effect on the linewidth from the added ligand, boric acid apparently does not bind at all to Zn^{2+} ions, and acetate interacts only weakly, whereas lactate seem to bind more strongly, as judged from the broadening induced by addition of these ligands. Imidazole induces twice as much broadening as lactate, whereas the effect from 2-methylimidazole is much less. The strongest effect on the linewidth is reported for Boc-His-OMe. In a study of the temperature dependence, Kodaka *et al.*[137] showed that the Zn^{2+} exchange is fast, on the Zn NMR timescale, for the imidazole complex but slow when bound to thermolysin,

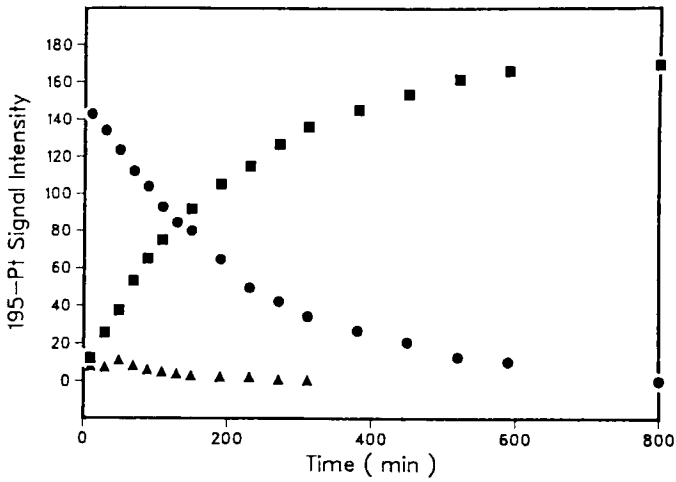


Fig. 8. Plot of ^{195}Pt signal intensities versus time for the reaction between [Pt(S, S-dach)(C2, O5-Asc)] and HNO_3: •, [Pt(S, S-dach)(C2,O5-Asc)]; ▲, [Pt(S, S-dach)(C2, HAsc)(H_2O)]$^+$; ■, [Pt(S, S-dach)$(H_2O)_2$]$^{2+}$. From Ref. 115, with permission.

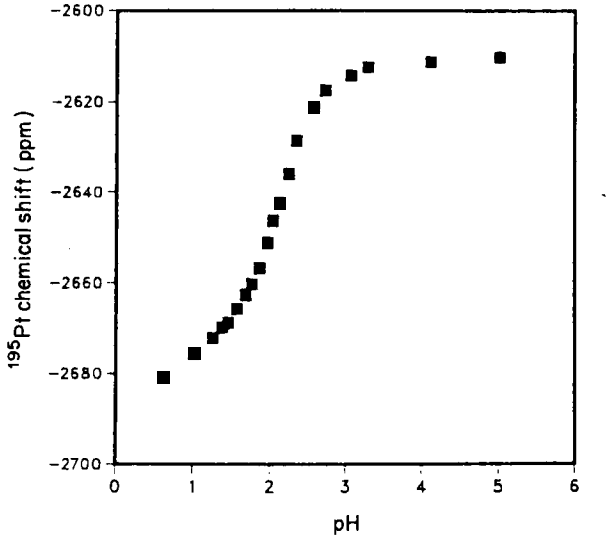


Fig. 9. ^{195}Pt chemical shift as a function of pH for [Pt(S, S-dach)(C2, O5-Asc)]. From Ref. 115, with permission.

thyrocalcitonin or DNA. Delville and Detellier[138] performed the most extensive ^{67}Zn NMR study reported to date. The binding of Zn^{2+} ions to penicillamine at various pHs has been studied by measuring both T_1 and T_2. They found, using literature values for the binding constants and assuming fast chemical exchange, that the width of ^{67}Zn resonance in the Zn–penicillamine complex is 6000 Hz, whether or not the ligand is monoprotonated, supporting the accepted solution-state structure where zinc is coordinated to the sulphydryl and amino groups and not to the carboxylate. We do not find it sufficiently proven that the metal-ion exchange is fast, since the exchange would affect T_1 and T_2 equally as long as the exchange rate is much less than the relaxation rate of complexed Zn^{2+} ions. A slow exchange could also explain why there is no observed change in the chemical shift of the ^{67}Zn resonance.

^{113}Cd is a very popular ion to use for NMR studies of ion binding, and Cd NMR has recently been reviewed by Summers.[8] It is quite obvious why this is so. ^{113}Cd is a spin-$\frac{1}{2}$ nucleus with a natural abundance of *ca.* 12%, resulting in a receptivity of 7.6 relative to ^{13}C, and the experimentalist is not plagued by the broad lines encountered for most metal nuclei owing to efficient quadrupole relaxation. Furthermore, Cd^{2+} ions can be used as probes in studies of ion binding to a multitude of proteins, since they can replace either Zn^{2+} or Ca^{2+}, as will be discussed in Section 3.3.

Pure cadmium halide complexes were studied quite early in the ^{113}Cd NMR history—first in a survey by Kostelnik and Bothner-By[139] and a few years later in more detail by Drakenberg *et al.*[140] and Ackerman *et al.*[141] In these studies only a single ^{113}Cd resonance was observed, and the chemical shift of the resonance was studied as a function of halide-ion concentration. From this concentration dependence, the ^{113}Cd shifts for the various complexes could be calculated assuming known binding constants. The uncertainty in the chemical shifts obtained in this way is clearly demonstrated from a comparison of the data reported in these two articles. In one extreme case, $CdBr_3^-$, there is a difference in the reported values of 200 ppm. In order to avoid this problem to some extent, Ackerman *et al.*[141] ran some solid-state NMR experiments on well-defined complexes; however, only a few are available and also in the solid state variations of up to 30 ppm were observed. A more satisfactory method has been developed by the Ackermans[142], using supercooled aqueous solutions. In this way they have been able to observe the ^{113}Cd chemical shifts directly for all four cadmium iodide complexes.

Summers *et al.*[143] observed that the halide-ion exchange is slow for the system Cd^{2+}–benzimidazole–halide in DMSO. They explained this unexpected finding by invoking the formation of a pocket that inhibits the interaction between the Cd^{2+} ion and solvent whenever the pocket is

occupied by Cl^-, Br^- or I^-. There are also two papers by Colton and Dakternieks[144,145] dealing with cadmium halide complexes. By recording the spectra at low temperature ($-80°C$) in dichloromethane solution, they were able to resolve the resonances from all mixed complexes, CdX_nY_{4-n} and $CdX_nY_mZ_{4-n-m}$. These authors have used the same technique to study the mixed tributylphosphine–halide complexes with cadmium.

There are a few published papers dealing with binding of Cd^{2+} ions to amino acids and peptides.[146-150] Considering the number of articles that have appeared in which cadmium-ion binding to proteins is discussed, it is somewhat surprising that so little attention has been paid to the building blocks of proteins—the amino acids. First, the Ackermans[146] and then Jakobsen and Ellis[147] showed that the various Cd(II)–Gly complexes could be studied under slow-exchange conditions in supercooled aqueous solutions. Jakobsen and Ellis showed convincingly, using ^{15}N-enriched glycine, that the glycine ligand is bound to the Cd^{2+} ion via its nitrogen (Fig. 10) and that complexes with up to three glycines bound to cadmium are formed with an incremental shift of about 100 ppm for each glycine ligand. Both studies were performed at pH 7. At this pH the predominant complexes will be chelates where both the carboxylate and amino group of the glycine ligand are utilized. In three later studies[148-150] it was assumed that at low pH there is a complex formed between the protonated amino acid and the Cd^{2+} ion where only the carboxylate group is involved, with a negative shift for the ^{113}Cd resonance. We have unpublished results showing that the shift for the complex with one $-COO^-$ group is *ca.* -30 ppm.

Jensen *et al.*[151] performed a multifield study of the Cd–EDTA complex and have found that one water molecule is coordinated to the cadmium ion in this complex, whereas Bryden and Reiley[152] have not found any bound water to the very similar Cd–CyDTA complex. Jensen *et al.* also reported the chemical shift and its pH dependence. The shift was found to be constant at 85 ppm in the pH interval 4.5–11, which is identical with a previously reported value.[153] Keller *et al.*[154] also studied Cd^{2+}-ion binding to EDTA and other ligands. They found that the symmetry of the Cd–EDTA and Cd–EGTA complexes differs, as seen from the difference in the chemical-shift anisotropy. The chemical-shift anisotropy relaxation mechanism appears to be much more effective for Cd–EGTA than for Cd–EDTA. This indicates that the Cd–EGTA complex is less symmetric than Cd–EDTA, in agreement with what has been shown for the corresponding Ca^{2+} complexes.[77] Baumann *et al.*[155] and Summers and Marzilli[156] studied Cd^{2+}-ion binding to amines. Ligands like ethylenediamine form stable complexes in DMSO, with slow exchange between "free" solvated and complexed ions (see Fig. 11). They also found a correlation between the ^{113}Cd chemical shift and the number and type of ligating N

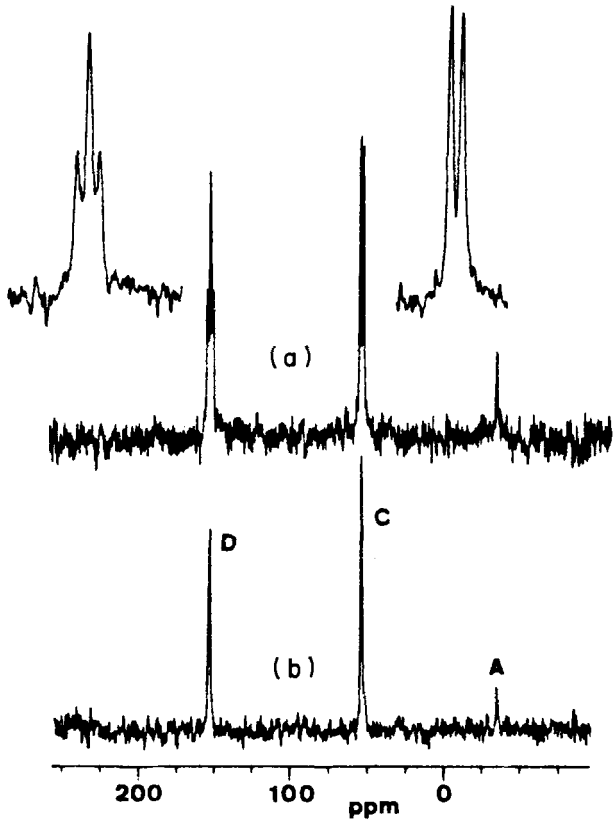


Fig. 10. Natural-abundance ^{113}Cd NMR spectra at $-40^{\circ}C$ of 0.1 M $Cd(ClO_4)_2$ and 0.25 M glycine: (a) with ^{15}N-glycine; (b) with normal ^{14}N-glycine. From Ref. 147, with permission.

donors:

$$\delta = 75A + 51B + 31C,$$

where A, B and C are the numbers of primary, secondary and tertiary amine donors respectively. More recently, the same group have extended their study to include other ligands, not only N donors, and also made the necessary corrections for the correlation to be valid in water solution instead of DMSO. This has allowed them to test their correlation on reported ^{113}Cd shifts for proteins. This has turned out to be surprisingly good. Munakata *et al.*[157] studied the $[Cd(en)_3]^{2+}$ complex using various solvents, concentrations and counterions, finding very small variations in the ^{113}Cd chemical shift. Also, complexes with 4-methylpyridine and imidazole have been studied. In these cases the exchange at room tempera-

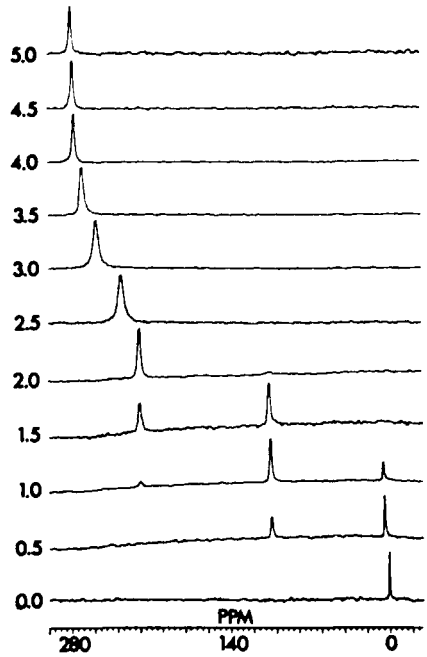


Fig. 11. ^{113}Cd NMR spectra of 1 M $Cd(NO_3)_2$ in DMSO with $N,N'-(CH_3)_2en(L)$ at [L]/[Cd] ratios as indicated. From Ref. 156, with permission.

ture is too fast to result in separate lines for the various species. Therefore the study was performed in ethanol solution at $-90^{\circ}C$, where sharp lines are obtained. (Fig. 12).

Rodesilar *et al.*[158] have recorded the ^{113}Cd NMR spectrum for the Cd^{2+}–tetraphenylporphyrin complex in $CDCl_3$ solution, and they found a concentration-dependent ^{113}Cd shift that varied from 419 to 454 ppm. Jakobsen *et al.*[159] performed a thorough NMR study of the same complex and reported a solution-state ^{113}Cd chemical shift for the pyridine adduct at 426.8 ppm. This value is in good agreement with the one obtained in the solid state, 432 ppm. The chemical shift of the Cd–tetraphenylporphyrin complex and its pyridine or dioxane adducts do not agree with the shift–ligand correlation suggested by Baumann *et al.*[155] This disagreement is not surprising, considering the difference in symmetry of the various complexes.

Since the pioneering ^{113}Cd NMR work on Cd^{2+} bound to sulphur ligands[153] there have appeared a few more recent works,[160–166] all reporting strong high-frequency shifts for ^{113}Cd bound to sulphur or to selenium[166]. There appears to be a general agreement that the cadmium

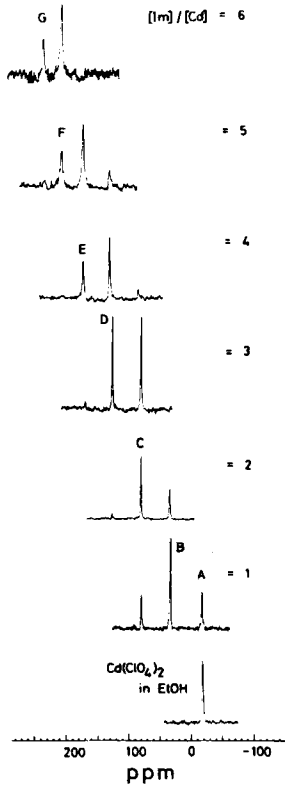


Fig. 12. ^{113}Cd NMR spectra of ethanol solutions at $-90°C$. Solutions contained 0.5 M $Cd(NO_3)_2$ and [imidazole]/[Cd] ratios as indicated. From Ref. 157, with permission.

chemical shift induced by various ligands increases in the order O < N < S, Se, and the most promising attempt to make a more detailed shift–ligand correlation is that of Baumann *et al.*,[115] which seems to apply to several Cd^{2+}–protein systems. However, there is still a long way to go before we can in general predict with any certainty the ^{113}Cd chemical shift for a new complex, small or large—as can for example be seen from the chemical shifts reported for two cryptates, where ^{113}Cd has a shift of 46 ppm when bound to four nitrogens and +78 ppm when bound to two nitrogens.[154]

There are also a few other ^{113}Cd NMR studies dealing with ion binding to ATP[167] and to phosphines.[168,169]

Bach *et al.*[170] and Bach and Vardhan[171] used ^{199}Hg NMR to determine binding constants for CH_3Hg^+ to various ligands, mainly in CH_2Cl_2 solution. They found, in agreement with previous studies[172] with

$Hg(ClO_4)_2$, that open-chain dithiaethers and tetrathiaethers form complexes that are at least two orders of magnitude stronger than those formed by 14- and 16-membered macrocyclic tetrathiaethers. Charland *et al.*[173] used ^{199}Hg NMR in combination with ^{1}H and ^{13}C NMR to study the disproportionation of methylmercury–adenine derivatives. They found that (CH_3Hg)–9-Me-adenine disproportionates into $(CH_3Hg)_2$–9-Me-adenosine and free 9-Me-adenosine. They also observed that the rotation around the C6–N6 bond was slow on the ^{199}Hg NMR timescale since they observed separate resonances for *syn* and *anti* $HgCH_3$ groups. Colton and Dakternieks[174–176] studied the formation of various halide and phosphine complexes with mercury, and Dean and Srivastava[177] studied some ditertiary phosphines.

2.4. Group IIA and IIIA metals

Hinton and coworkers[178–180] studied the ion-pair equilibria for $TlNO_3$ in ammonia and for TlOAc in DMSO and trifluoroethanol. By recording the ^{205}Tl chemical shift as a function of concentration, they determined the equilibrium constant for ion-pair formation, K_{ip}, and from the temperature dependence in K_{ip} they calculated ΔH and ΔS for the process. For TlOAc in either DMSO or trifluorethanol ion-pair formation is dominated by entropic effects, whereas the difference in K_{ip} between the two solvents is due to differences in ΔH_{ip}. Glaser and Henrikson[181–183] studied halide-ion binding to Tl^{3+} using ^{205}Tl NMR. At low total concentration (0.05 M) they found that the exchange

$$Tl^{3+} + X^- \rightarrow TlX^{2+}$$

is sufficiently slow to result in separate signals for Tl^{3+} and TlX^{2+} in the ^{205}Tl NMR spectrum for both Cl^- and Br^-. Also, the exchange

$$TlBr^{2+} + Br^+ \rightarrow TlBr_2^+$$

is slow on the ^{205}Tl NMR timescale. For higher total concentrations (1.0 and 2.6 M) all exchanges are fast, resulting in average ^{205}Tl resonances. The dependence of the ^{205}Tl chemical shift on the halide concentration at various Tl concentrations was used to calculate both binding constants and ^{205}Tl chemical shifts for the various complexes. Since there is not a monotonic variation in the chemical shift for the various complexes with increasing number of bound halide ions, the curves of chemical shift versus halide-ion concentration have maxima for Cl^- and minima for Br^- as shown in Fig. 13. Glaser *et al.*[183] also studied the Tl^+–Cl^- system. In this case all exchanges are fast and only a single resonance is observed; however,

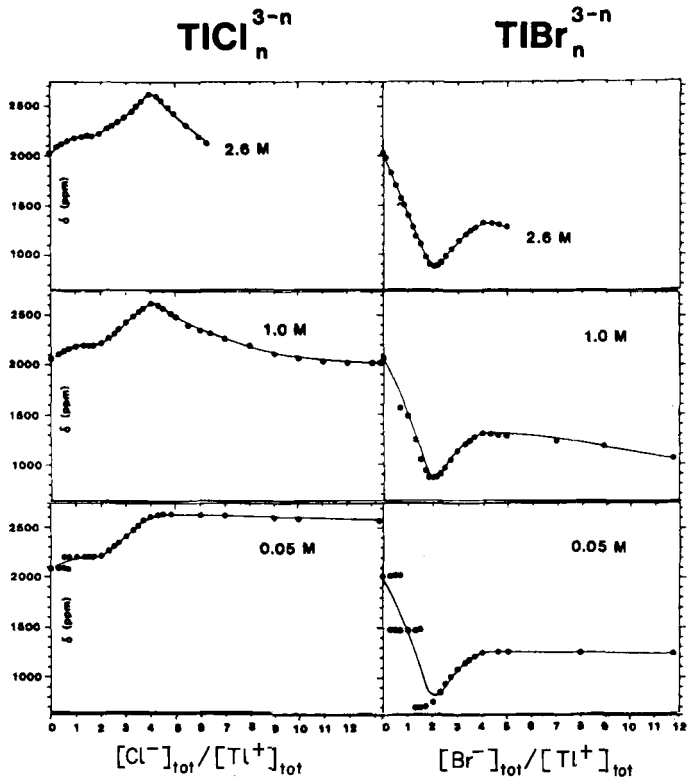


Fig. 13. ^{205}Tl chemical shifts from aqueous solutions of Tl(III) as functions of $[X^-]/[Tl^+]$ ratios for X = Cl or Br. From Ref. 181, with permission.

the chemical shift of this resonance varies by more than 400 ppm and both chemical shift and binding constants can be obtained with good accuracy.

Hinton and coworkers[184–190] studied the binding of Tl^+ ions to various ionophores. In a series of papers they studied the interaction between Tl^+ and gramicidin under various conditions, in trifluoroethanol and DMSO solution. They found that the gramicidin dimer in trifluoroethanol has two strong binding sites for Tl^+ and that the gramicidin monomer in DMSO has one strong binding site. The fact that the resonances for Tl^+ complexed to gramicidin in trifluoroethanol and DMSO appear at significantly higher frequencies than in dioxane suggests that the Tl^+ ion is still partially solvated in these solvents. The data from DMSO solution can be described very well assuming a single strong binding site as shown in Fig. 14. For trifluoroethanol, on the other hand, the assumption of two strong binding

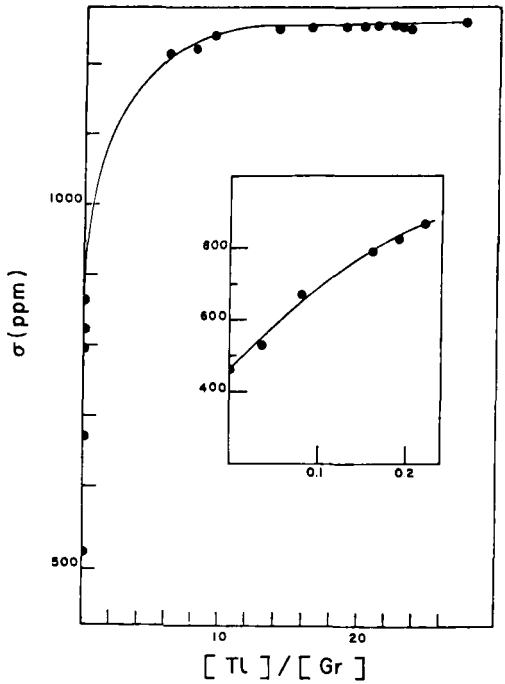
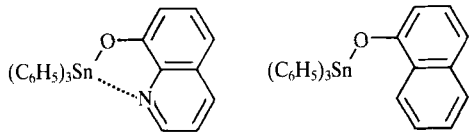


Fig. 14. ^{205}Tl chemical shift as a function of $[Tl^+]/[gramicidin]$ ratio in DMSO. From Ref. 188, with permission.

sites per dimer is not sufficient to explain the experimental data at high Tl^+ concentration, as can be seen in Fig. 15. A second set of weaker binding sites must be considered.

Tin and lead, especially the latter, are obvious candidates for ion-binding studies using metal-ion NMR—both having high-sensitivity spin-$\frac{1}{2}$ isotopes. Surprisingly little has, however, been reported. In fact, for ^{207}Pb there is to our knowledge only one publication dealing with lead-ion binding. Nakashima and Rabenstein[191] showed the potential use of ^{207}Pb NMR in studies of relatively weak complexes like with carboxylic acids. Harrison *et al.*[192] used ^{207}Pb NMR and X-ray diffraction to study the complex formed between Pb^{2+} and EDTA. Otera *et al.*[193] reported chemical shifts for ^{119}Sn and ^{207}Pb for seven-coordinated organometal chelates, and Dean[194,195] studied various phosphine complexes with either lead or tin. Lycka, Holecek and coworkers[196–200] have made quite extensive use of ^{119}Sn NMR in their studies of (mostly) organotin compounds. From measurements of the temperature dependence in the ^{119}Sn chemical shifts of compounds VI



VI VII

and VII in various solvents shown in Fig. 16, they estimated the thermodynamic parameters for formation of complexes between VI or VII and the solvent molecules in either pyridine or hexamethylphosphoramide (HMPA).[198] Holecek *et al.*[200] used the same technique to evaluate the thermodynamic parameters for the formation of complexes $R_3SnCl \cdot S$,

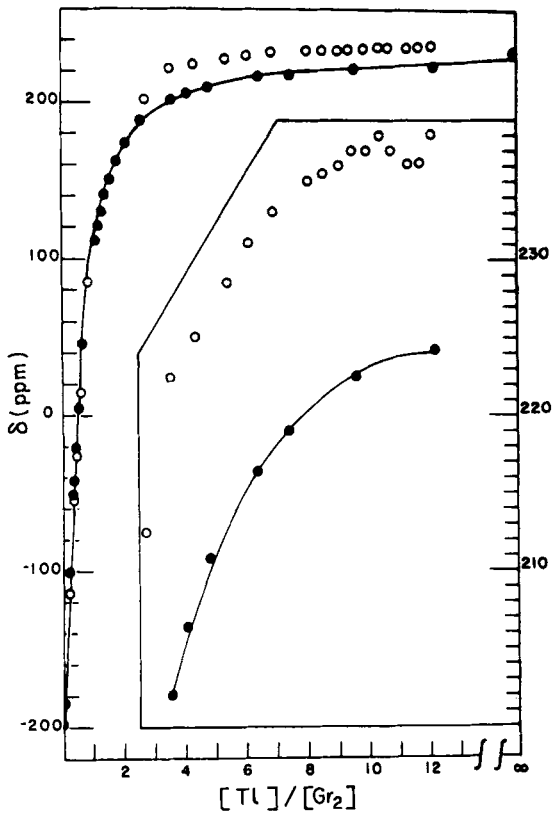


Fig. 15. ^{205}Tl chemical shift as a function of $[Tl^+]/[gramacidin]$ ratio in trifluoroethanol. From Ref. 187, with permission.

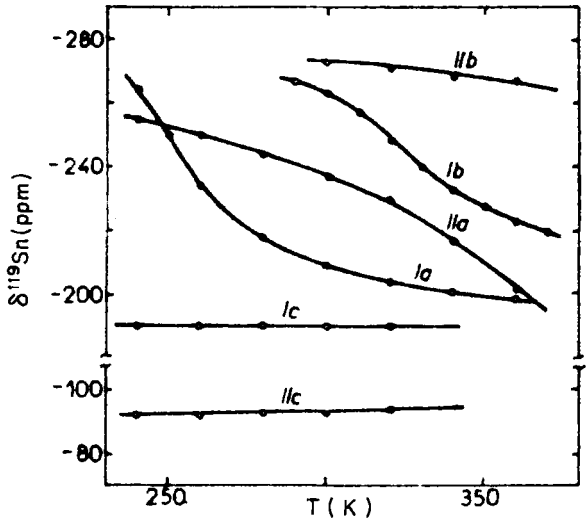


Fig. 16. Temperature dependence of ^{119}Sn chemical shifts for compounds VI (I) and VII (II) in pyridine (a), hexamethylphosphoramide (b) and deuteriochloroform (c). From Ref. 198, with permission.

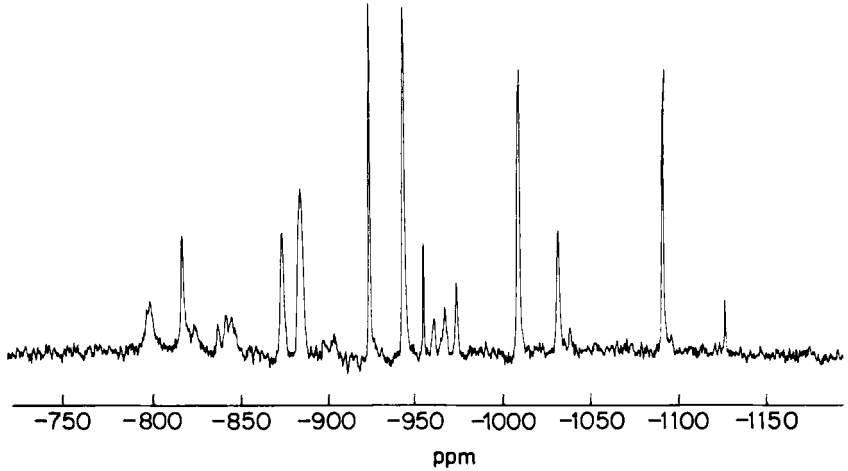


Fig. 17. 149 MHz ^{119}Sn NMR spectrum at $-30^{\circ}C$ of a methanolic solution containing $SnBr_4$ (1 M) and KSCN (3 M). From Ref. 201, with permission.

where S is pyridine, DMSO or HMPA. In all cases HMPA forms the strongest complexes and pyridine the weakest.

Blunden *et al.*[201] and Dillon and Marshall[202] used the pairwise interaction model to calculate the ^{119}Sn chemical shifts for various series of complexes. Blunden *et al.*[201] thus identified most of the 34 complexes in $SnBr_n(MeOH)_m(NCS)_{6-n-m}$, where $n = 0, \ldots, 4$ and $m = 0, \ldots, 2$. Figure 17 shows a ^{119}Sn spectrum containing *ca.* 20 different resonances recorded at $-30\,^{\circ}$C in methanol. Also, Saraswat and Mason[203], Chandler *et al.*[204] and Cardin and Roy[205] have used ^{119}Sn NMR to study various tin complexes.

3. METAL-ION BINDING TO MACROMOLECULES

Macromolecules have been studied using a limited number of NMR sensitive nuclei, owing to the size and complexity of the systems. However, of the available nuclei, both the alkali and the alkaline-earth metals, as well as ^{113}Cd have been used extensively. Other metal nuclei have also been employed, but to a much lesser extent.

3.1. Alkali metals

Of the alkali metals, ^{23}Na and ^{7}Li NMR are the nuclei mostly employed for NMR studies, but ^{39}K and ^{133}Cs are also used. The macromolecules studied are both biological, such as proteins and DNA, and various synthetic polymers.

^{23}Na NMR has been employed by many groups to study cationic interactions with DNA.[206-217] Most have used a two-state model, with "free" (F) and "bound" (B) sodium ions, in evaluating their results. The observed relaxation rate can then be written as

$$R = R_F + r(R_B - R_F)\frac{[P]}{[Na]_{tot}},$$

where r is the extent of association of Na^{2+} with DNA ($p_B = r[P]/[Na]$). The dependence of the ^{23}Na linewidth on the ratio $[P]/[Na]_{tot}$ is linear[206,207] at high ionic strength, thus $r(R_B - R_F)$ is constant. Bleam *et al.*[206] interpreted this as r being constant.

Bleam *et al.*[206] also titrated NaDNA with $MgCl_2$ to determine the upper bound of r° and R_B. To do this, they assumed R_B to be constant. Under this assumption r° can be calculated using the equation

$$R = R_F + r^{\circ}(R_B - R_F)\frac{[P]}{[Na]} - np_m(R_B - R_F)\frac{[P]}{[Na]}\frac{[Mg]}{[P]},$$

where

$$p_m = \frac{[Mg]_B}{[Mg]_{tot}}, \quad n = \frac{r^\circ[P] - [Na]_B}{[Mg]_B}, \quad r^\circ = \frac{[Na]_B}{[P]}.$$

When $[Mg] = 0$, r° can be calculated from extrapolation of the initial slope of the curve in a plot of $\delta\nu_{1/2}$ for ^{23}Na versus $[Mg]/[P]$ (Fig. 18). This resulted in $r^\circ = 0.34$, which is in good agreement with the Poisson–Boltzmann (PB) theory.

To get a better agreement with the PB theory, Nordenskiöld *et al.*[214] included a Mg^{2+} dependence in R_B and therefore set out to determine the NMR relaxation rates (T_1^{-1} and T_2^{-1}). They then deconvulated the non-Lorentzian line into two resonances and calculated the correlation time t_c to approximately 3 ns for natural B-DNA. An upper bound of 0.3 for r°/np_m is also obtained, which is approximately equal to the PB value. In this work Nordenskiöld *et al.* also studied some synthetic DNA whose conformations differed from that of the natural B-DNA, and found that t_c varies significantly, with no correlation with the GC content.

In all of the studies the interaction between Na^+ and DNA is shown to be electrostatic. However, when Delville *et al.*[209] titrated NaDNA with a series

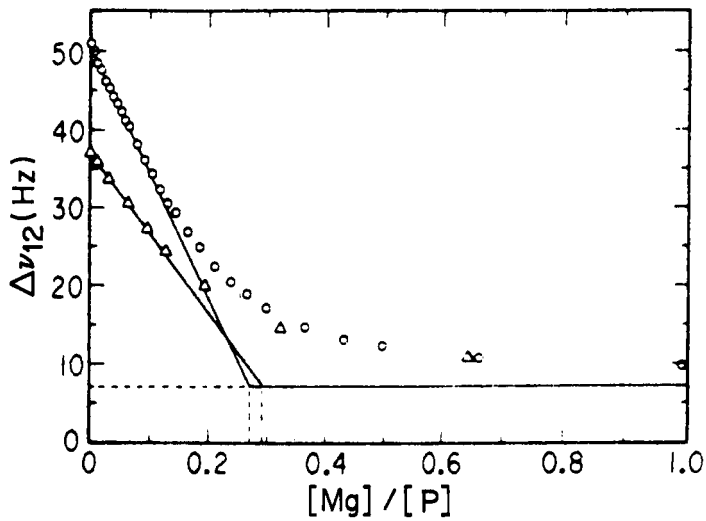


Fig. 18. ^{23}Na linewidths $\Delta\nu_{1/2}$ versus $[Mg]/[P]$ at constant $[Na]/[P]$: 0.013 M calf thymus DNA at 20.3°C with $[Na]/[P] = 1.5$ (○) or $[Na]/[P] = 2.2$ (△). Linear least-squares fit of data for which $[Mg]/[P] = 0.07$ are represented by straight lines. The broken horizontal line has an ordinate equal to the intercept at $[P]/[Na] = 0$ of a plot of $\Delta\nu_{1/2}$ versus $[P]/[Na]$ for a comparable titration of NaDNA with NaCl. From Ref. 206, with permission.

of quaternary ammonium salts Q^+Br^-, with increasing carbon-chain length of the cation, they found that the fraction of complexed sodium ions decreases with the size of Q^+. This indicates site binding between DNA and the surfactant counterion. Moreover, this interaction bears a strong resemblance to the result from operation of hydrophobic forces (Fig. 19).

In other studies DNA was titrated with different polyamines[210,218] and various monovalent,[207] divalent[210,211] or trivalent[210,212] cations, and even intercalating drugs,[208] mostly involving ^{23}Na NMR but also ^{39}K NMR[213] and ^{59}Co NMR.[212]

Other charged macromolecules that have been studied with ^{23}Na NMR are various polymers such as polystyrenesulphonic acid (PSA),[219,220] polyacrylic acid (PAA)[219] and polymethylacrylate.[221] Leyte and coworkers[219,220] found a biexponential behaviour of R_2, which could be a consequence of an increasing electrostatic persistence length and an increasing screen length upon lowering the polyion concentration. The variation of $R_{2,\text{fast}}$ with ionic strength, polymer concentration, charge and molecular weight was also analysed.

Florin[222] examined the relaxation rate for ^{23}Na, ^{7}Li and ^{133}Cs in aqueous solution on addition of polyethylene oxide (PEO). The relaxation curves fall in categories according to the kind of cation, but, irrespective of the anion, Cl^- or Br^-. At higher PEO concentrations the relaxation rate increases. PEO is known to affect the H_2O molecules in its immediate proximity, and ions that penetrate into this zone will be affected owing to disturbance of the surrounding water shells, leading to shorter relaxation rates than in pure water. Moreover, the increase in ether–oxygen contacts as the PEO concentration increases leads to strongly increased relaxation rates.

Other polymers that have been investigated are perfluorosulphonate ion-exchange resin,[223] polyuronates,[218] hyaluronate and chondroitin[224] and the sodium salts of polyacrylic acid and chondroitin-4-sulphate.[225] The results have in most cases been evaluated with either the Poisson–Boltzmann (PB) theory or the Manning counterion condensation theory (CC).

With the aim of proposing a molecular model for the action of pyruvate kinase (PK), Raushel and Villafranca[226] determined the distances between various monovalent cations such as $Li^+, Na^+, K^+, Rb^+, NH_4^+$ and Cs^+ bound to the monovalent and the divalent cation sites on PK with the aid of NMR. In the distance determination the Solomon–Blombergen equation

$$r = C\frac{3t_c T_{1m}}{1 + w_I^2 t_c^2}$$

was used, were T_{1m} is the paramagnetic contribution to T_1 for M^+ from the

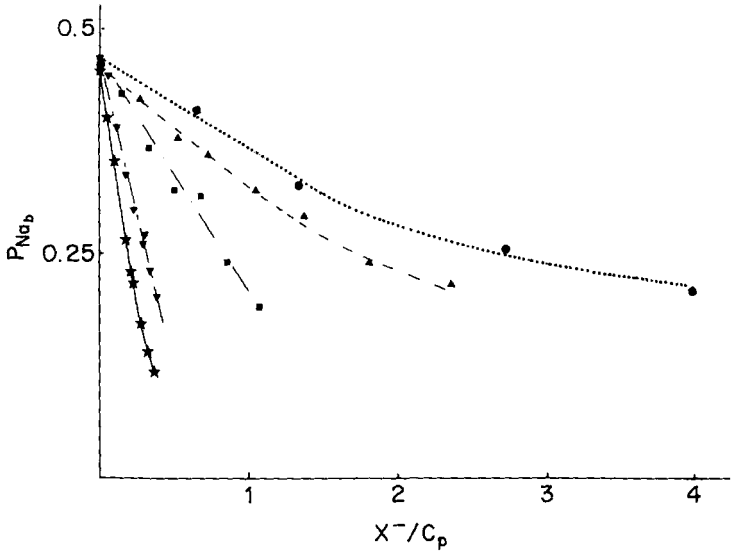


Fig. 19. Mole fraction of complexed sodium ions as a function of surfactant addition: •, NPr_4^+; ▲, NH_4^+; ■, NPe_4^+; ▼, NHe_4^+; ★, NMe_4Do^+. From Ref. 209, with permission.

Mn^{2+} ions bound to PK. To do this, t_c was determined by a method outlined by Raushel and Villafranca[226,227] using two NMR-sensitive isotopes for one ion. For example the T_1 values for $^6Li^+$ and $^7Li^+$ were obtained at the same field with ^6Li and ^7Li NMR respectively. The ratio of these values could be used to calculate a t_c value for the enzyme–Mn^{2+} complex according to the Solomon–Blombergen equation (Fig. 20). For PK the distance between Mn^{2+} and M^+ is reduced by 2–3 Å when the substrate phosphoenolpyruvate (PEP) is added. Moreover, the Mn^{2+}–M^+ distance in the PK–PEP complex is much closer for cations such as NH_4^+ and Tl^+, which are better activators for the protein, than for Li^+ and Cs^+.

The same method was applied by Raushel and Villafranca[228] and van Divender and Grisham[229] for distance determinations in PK and by Kasprzyk *et al.*[230] and Raushel *et al.*[231] for carbamoyl phosphate synthetase.

In contrast with the studies reported above, where the signals from free alkali-metal ions were observed, Rhyu *et al.*[232] studied $^7Li^+$ bound to the enzyme complex phosphoglucomutase–substrate. They followed the change in the chemical shift of the ^7Li NMR signal as the substrates varied during the enzymatic process.

Both ^{23}Na and ^{39}K NMR have been employed to study the interaction

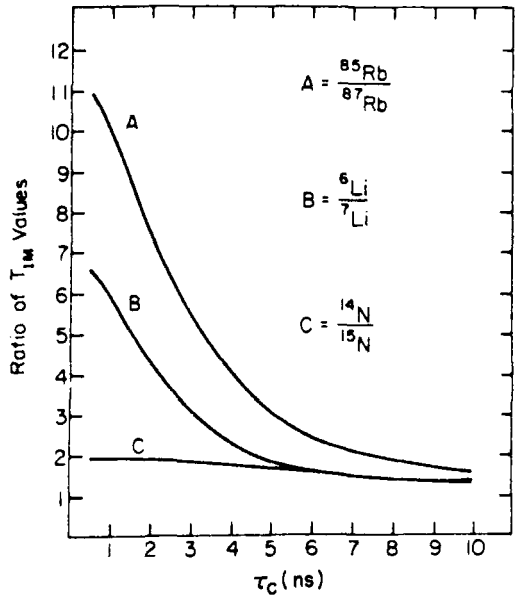


Fig. 20. Determination of the correlation time for the dipolar interaction of enzyme–Mn^{2+} from T_{1M} ratios for the isotopes of Li^+, NH_4^+ and Rb^+. From Ref. 226, with permission.

between Na^+ and K^+ ions and macromolecules such as calmodulin and its tryptic fragments,[233] troponin C and its tryptic fragments,[234] chondroitin sulphate–5% protein and dermatansulphate–5% protein,[235] the egg-yolk protein phosvitin,[236] carp ($pI = 4.25$) parvalbumin[237] and, as mentioned above, pyruvate kinase.[226]

3.2. Alkaline-earth metals

The only alkaline-earth metals studied with NMR are ^{25}Mg and ^{43}Ca. Both are quadrupole nuclei: ^{43}Ca has $I = \frac{7}{2}$ and ^{25}Mg has $I = \frac{5}{2}$. Moreover, the natural abundance of ^{43}Ca is very low. In spite of the low sensitivity of the nuclei, both have been used extensively to determine kinetic parameters in calcium and magnesium binding to macromolecules.

^{25}Mg and ^{43}Ca NMR studies are useful in the investigation of ion binding to proteins. The methods provide information on (i) association constants, (ii) competition of other cations for Mg^{2+} and Ca^{2+} binding sites, (iii) effects of other ligands on the protein, and (iv) dynamic parameters such as

the exchange rates and correlation times. Neurohr *et al.* in their review in Vol. 2 of ref. 1 give more information of ^{25}Mg and ^{43}Ca NMR.

The first ^{43}Ca NMR spectrum containing an NMR signal from a quadrupolar nucleus bound to a protein was claimed by Andersson *et al.*[238] Since then, ^{43}Ca NMR has been of great use in determining dynamic parameters for many calcium-binding proteins.

Various calcium-binding proteins have been investigated with ^{43}Ca and ^{25}Mg NMR.[238-254] The protein that has been subject to the most extensive studies is calmodulin (CaM)—both the intact protein and its two tryptic fragments TR_1C and TR_2C. To begin with, the correlation time τ_c and quadrupole coupling constant χ were determined from the ratio of T_1 and T_2;[239,240] a value of $\tau_c = 8.2$ ns was obtained. T_1 was determined in an inversion-recovery experiment and T_2 from the equation $T_2 = (\pi\delta\nu_{1/2})^{-1}$. Later, Drakenberg *et al.*[241] derived the equations necessary for a total bandshape analysis, starting from the modified Bloch equations for a general two-site exchange. In an iterative procedure the best fit between calculated and experimental bandshapes as a function of the temperature was obtained, and thereby χ, τ_c and k_{off} were determined. Using the model with two pairs of equal sites for CaM, the exchange rates for those pairs were determined as 10^3 s^{-1} and approximately 30 s^{-1} respectively, and a value of 1 MHz was obtained for χ. In a paper by Teleman *et al.*[242] the same dynamic parameters were determined for CaM and its tryptic fragments, both at low ionic strength and in 0.1 M $KClO_4$ or 0.1 M KCl. The fast exchanging sites were found to be located in the N-terminal half of the molecule, TR_1C. In the intact CaM the observed k_{off} for the fast process is slowed down by a factor of two in the presence of 0.1 M $KClO_4$, but 0.1 M KCl has no effect on the k_{off} observed in TR_1C. Tsai *et al.*[243] used ^{25}Mg NMR to study the Mg^{2+}-ion binding to CaM and its kinetics. The result was that sites I and II in CaM, which bind Ca^{2+} weakly, bind Mg^{2+} more strongly than sites III and IV do. From the total bandshape analysis, k_{off} is seen to be virtually identical for all four sites, whereas the association constant K_a is a factor of 10 higher at sites I and II. The authors also speculate that the role of Mg^{2+} in sites I and II is to maintain CaM in a conformation ready to interact with the target enzyme.

Since the chemical-shift range in ^{43}Ca NMR is very small, the signals often overlap, as, for example, in the case of the signals from free Ca^{2+} and protein-bound Ca^{2+} in CaM. Vogel *et al.*[244] and Vogel and Braunlin[249] used shift reagents (SR) such as $Dy(PPP)_2^{7-}$ to separate the signals. When the SR is added, only the resonance from the $^{43}Ca^{2+}$ ion that is free or rapidly exchanging experiences a shift. This method is used to show that when the CaM antagonist TFP is added to a CaM–Ca^{2+} solution the exchange rate between Ca^{2+} bound to the protein and free Ca^{2+} decreases;

the decrease in linewidth of the resonance from free Ca^{2+} is not due to the release of Ca^{2+} from the protein, as proposed by Shimizu *et al.*[245] Shimizu and Hatano[247] have recently attempted to study CaM with ^{43}Ca NMR. However, they give the CaM concentration to three decimal places, and, starting from this value, add what they seem to believe is exactly four equivalents of Ca^{2+}. In our opinion, it is impossible to determine the CaM concentration this accurately. The CaM concentration determined from published or standard extinction coefficients almost always give too-high values. If the CaM concentration is incorrectly determined then the interpretation of the ^{43}Ca NMR spectra will be in error (Fig. 21). In the spectrum shown in Fig. 21(c) the narrow signal is said to be from Ca^{2+} bound to the weak Ca^{2+}-binding sites I and II, whereas we believe that the signal is actually due to an excess of Ca^{2+} ions that are free in solution.

Other macromolecules or proteins that have been studied by ^{43}Ca NMR are troponin C,[238-241,248,253,254] parvalbumin,[239,240,253] calbindin D_{9k},[251] protein A,[255] bone γ-carboxyglutamic acid protein,[256] hemocyanin,[257] the polypentapeptide of elastin,[258] prophospholipase A_2,[241,252,259] pancreatic phospholipase A_2,[259] Ca(II)–DNA,[260] proteoglycans, heparin and ficoll,[261] bovine serine proteases and their zymogens,[262] human factor XIII[263] and prothrombin fragment 1.[264]

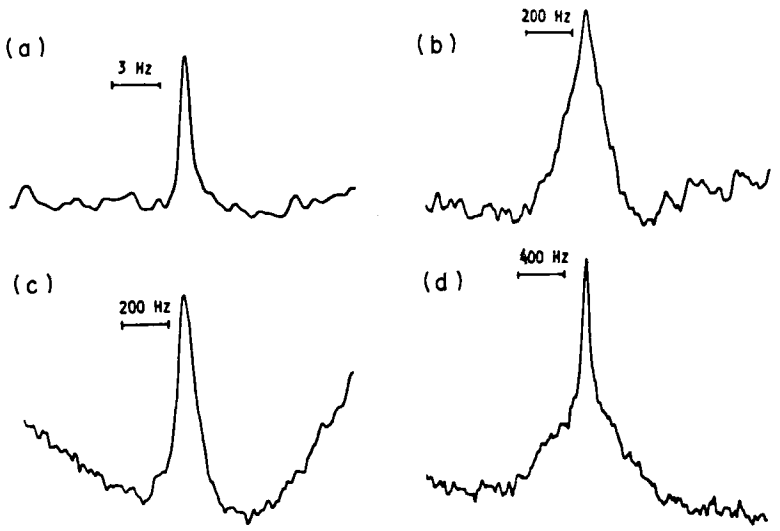


Fig. 21. ^{43}Ca NMR spectra of (a) $^{43}Ca^{2+}$ (2.9 mM), (b) $^{43}Ca^{2+}$ (2.9 mM)–calmodulin(0.725 mM), (c) $^{43}Ca^{2+}$ (2.9 mM)–calmodulin(0.725 mM)–melittin(1.0 mM) in 0.15 M HEPES–K^+ buffer (pH 7.2). From Ref. 24, with permission.

^{25}Mg NMR studies have been reported for Mg^{2+}–ATP, ADP–creatine kinase complexes,[265] acetate kinase[266] and DNA.[267,268]

Of the protein studies listed above, it is worth mentioning that the linewidth determined for $^{43}Ca^{2+}$ bound to saliva protein A (100 Hz)[255] is much narrower than any, up to that date, reported for Ca^{2+}-binding proteins. Braunlin *et al.*[255] suggested that this is due to a short correlation time and thus a high degree of flexibility of the binding site.

Phospholipase A_2 (PLA_2) and its zymogen prophospholipase A_2 ($PPLA_2$) have been studied by various workers at our laboratory.[241,252,253,259] Drakenberg *et al.*[259] found that the quadrupole coupling constant χ for PLA_2 ($\chi = 1.4$ MHz) is almost twice as large as χ for $PPLA_2$ ($\chi = 0.8$ MHz). Moreover, χ for PLA_2 is significantly larger than that reported for EF-hand proteins such as CaM, indicating a less-symmetric site. However, χ for $PPLA_2$ is smaller than χ for the EF-hand in CaM, thus the calcium-binding site in $PPLA_2$ is somewhat more symmetric.

The ion binding of proteoglycans from cartilage and some of the charged disaccharides of which proteoglycans consist, for example heparin and chondroitin sulphate, were studied by Lerner and Torchia.[261] They used ^{23}Na, ^{39}K, ^{25}Mg and ^{43}Ca NMR to see if there was any difference between the monovalent and divalent cations. It was found that sodium ions do not interact strongly with the macromolecules in solution, but that proteoglycan aggregates bind Mg^{2+} and Ca^{2+} in solution—however, not very strongly. From these results the authors concluded that the ionic dependence of the mechanical properties of cartilage is due to electrostatic shielding, rather than specific binding.

The binding of divalent cations to DNA has been subject to NMR studies by Braulin *et al.*[260] and Murk Rose *et al.*[267,268] Both ^{43}Ca NMR[260] and ^{25}Mg NMR[267,268] were used. ^{25}Mg NMR studies where Mg^{2+} was added to a DNA–phosphate solution and competition titrations with other cations such as Ca^{2+} and Na^{+} led Murk Rose *et al.*[267,268] to suggest two reasons for the ^{25}Mg NMR resonance being non-Lorentzian. The first reason was incomplete averaging of the first-order nuclear electric quadrupole interaction in the vicinity of the DNA molecule; however, the calculated spectrum for this did not properly match the experimental spectrum (Fig. 22). The second suggestion was that the signal consisted of two resonances—one broad and one narrow. The competition titrations with, for example, Ca^{2+} suggested that this is the correct interpretation of the spectrum. Braulin *et al.*[260] used ^{43}Ca NMR and also found evidence for Ca^{2+}, both territorially and site-bound to DNA. However, the interaction appears weaker than in the case of magnesium, since Mg^{2+} effectively displaces Ca^{2+}. This is monitored by a decrease in ^{43}Ca NMR linewidth towards the value of free Ca^{2+} upon addition of Mg^{2+}. The best fit of the Ca^{2+}-concentration

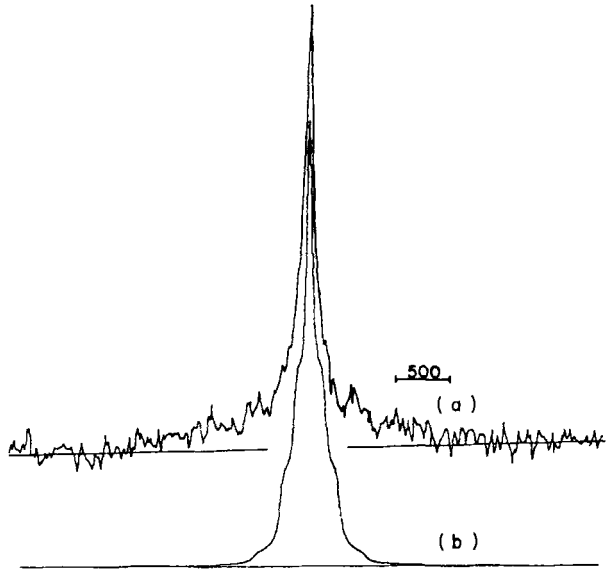


Fig. 22. (a) ^{25}Mg NMR spectrum recorded at 3.45 MHz and 295 K for an unsonicated calf thymus DNA solution containing 8.3 mM DNA phosphate and 114 mM $MgCl_2$. (b) ^{25}Mg NMR powder pattern calculated assuming a 60 Hz linewidth for an individual Lorentzian component and 1.6 kHz quadrupole coupling constant. From Ref. 268. Copyright 1982 John Wiley & Sons, Inc.

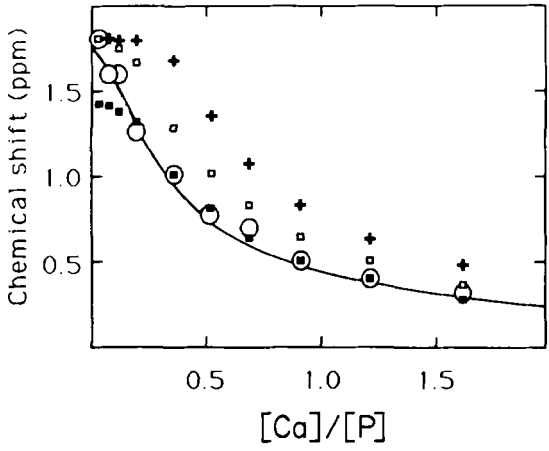


Fig. 23. Experimental determinations and theoretical predictions for the change in the $^{43}Ca^{2+}$ chemical shift for a titration of DNA with calcium salt: ○, experimental data; +, CC-model prediction for $\delta_B = 1.8$ ppm; □, PB prediction for $\delta_B = 1.9$ ppm; ■, PB prediction for $\delta_B = 1.5$ ppm. The solid line is the best fit of the data (all points included) to the site-exclusion binding model. The parameters obtained for $\delta_B = 2.1$ ppm are $K_{obs} = 900\,l\,mol^{-1}$ and $n = 3.5$. From Ref. 260. Copyright 1987 John Wiley & Sons, Inc.

dependences of the linewidth at half-height and of the chemical shift was obtained for $K_{obs} = 2.7 \times 10^3$ M^{-1} and $n = 2.9$ (from $\delta\nu_{1/2}$ versus [Ca^{2+}]) or $K_{obs} = 2.5 \times 10^3$ M^{-1} and $n = 2.6$ ($\delta_B = 1.5$ ppm) (Fig. 23).

Shimizu and Hatano[265,266] investigated how the addition of ATP, ADP and kinases (acetate and creatine) to a Mg^{2+} solution affect the ^{25}Mg NMR linewidth from free Mg^{2+}. In all cases they found a broadening of the ^{25}Mg signal, this broadening being greatest for the ternary complexes of $^{25}Mg^{2+}$–ATP–enzyme.

3.3. Transition metals

^{51}V NMR spectroscopy is a well-established method for the investigation of diamagnetic vanadium compounds, but the use of ^{51}V NMR to study larger systems of biological relevance have been very sporadic. The few studies of ^{51}V NMR of proteins are by Borak *et al.*,[269] Butler *et al.*[270] and Vilter and Rehder.[271]

Borak *et al.*[269] used uridine vanadate as a transition-state analogue for ribonuclease A, and Butler *et al.*[270] studied the binding of ^{51}V to the iron-transport protein human transferrin.

The first work where a vanadium-binding protein—*Ascophyllum nodosum* peroxidase (A.n.I.)—was studied by ^{51}V NMR was performed by Vilter and Rehder;[271] in their paper the authors also reported on the chemical shift and linewidth for albumin-bound vanadate. The ^{51}V NMR resonance for A.n.I. originally showed a chemical shift of -1070 ppm and shifted to *ca.* -1250 ppm when treated with additional vanadate. The lines are around 6 kHz broad (Fig. 24).

The only iron isotope active in NMR, ^{57}Fe, is not a very sensitive nucleus: $I = \frac{1}{2}$, 2.2% natural abundance, $\nu_L = 11.7$ MHz at 8.45 T and relaxation times are usually very long. This is the reason why the first observation of a ^{57}Fe NMR spectrum of a protein was reported as late as 1985. Independently, both Lee *et al.*[272] and Baltzar *et al.*[273] presented ^{57}Fe NMR spectra of iron bound to carbonylmyoglobin (MbCO). The chemical shift obtained at 23°C was 8227 ppm[272] downfield from $Fe(CO)_5$ and the linewidth was approximately 55 Hz.[272] Through an inversion-recovery experiment, Lee *et al.* determined T_1 as 17 ± 3 ms, while Baltzar *et al.* estimated it as 30 ms. The main relaxation mechanism is chemical-shift anisotropy; thus larger proteins would require lower fields, in order to avoid the signal becoming too broad.

La Mar *et al.*[274] also determined the MbCO chemical shift obtained through a double-resonance experiment. The linewidth of the doublet from ^{13}CO, monitored by ^{13}C NMR, has a minimum when the doublet collapses on the centre line, i.e. on resonance for ^{57}Fe NMR.

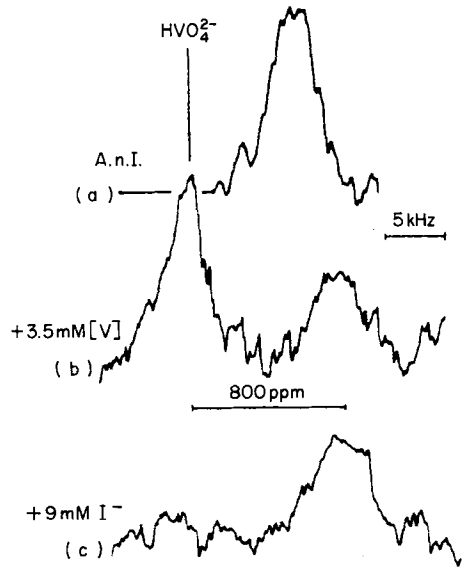


Fig. 24. ^{51}V NMR specta of peroxidase from *Ascophyllum nodosum*, reactivated with vanadate in tris-buffer, showing enzyme-bound vanadate: (a) total concentration 1.46 mM; (b) addition of 3.4-fold excess of vanadate to $[V]_{tot} = 5.0$ mM (c) A.n.I. in imidazole buffer with [KI] = 9.0 mM. From Ref. 271, with permission.

Furthermore, Baltzar and Landergren[275] studied the equilibrium

$$Fe(PPIX)(CO) + B \rightarrow Fe(PPIX)(CO)(B); \qquad PPIX = \text{protoporphyrin-IX}$$

for several different bases B, and found a linearly decreasing relationship in the ^{57}Fe NMR chemical shift versus log K.

Raj *et al.*[276] used ^{59}Co NMR to monitor the interaction of bovine serum albumin with hexacyanocobaltate(III) ion at different pH values. The ^{59}Co linewidth increases with decreasing pH. This is due to a sum of effects probably involving a distribution of binding sites.

Another nucleus that has been used extensively in NMR studies but very rarely for binding to macromolecules is ^{95}Mo ($I = \frac{5}{2}$). Bristow *et al.*,[277] however, employed ^{95}Mo NMR to observe the binding of $[MoO_4]^{2-}$ and $[MoS_4]^{2-}$ to the widely studied protein bovine serum albumin.

^{67}Zn NMR has, in analogy with ^{43}Ca and ^{25}Mg NMR, been employed to determine dynamic parameters for $^{67}Zn^{2+}$ ion binding—however, only rarely.

Because of the excellent spectroscopic properties of ^{113}Cd, $^{113}Cd^{2+}$ has been used as a metal probe for many metalloproteins. The ^{113}Cd NMR shift spans a wide range from 750 ppm to -200 ppm, and the nature of the

coordinating ligands and coordination number to $^{113}Cd^{2+}$ are strongly reflected in the chemical shift.

The largest chemical shift reported up to now for ^{113}Cd is for Cd^{2+} bound to the non-catalytic Zn^{2+} site of horse liver alcohol dehydrogenase ($\delta = 751$ ppm).[278,279] Here Cd^{2+} is coordinated to four cysteine residues. At the other extreme is the chemical shift of $^{113}Cd^{2+}$ bound to horseradish peroxidase ($\delta = -193$ ppm),[280] where Cd^{2+} is coordinated only to oxygen ligands at the high-affinity Ca^{2+} site.

The ^{113}Cd NMR spectra of bovine insulin has been obtained by Sudmeier *et al.*[281] and displays two signals: at 165 ppm and at -36 ppm. The resonance at 165 ppm is $^{113}Cd^{2+}$ bound to the Zn^{2+} site on insulin, where Cd^{2+} is coordinated to three imidazole nitrogens and three water molecules, and the resonance at -36 ppm is due to a Cd^{2+} ion bound to a Cd^{2+} site with only oxygen ligands. Shimizu and Hatano[282] have recorded ^{67}Zn NMR spectra in the presence of insulin. They calculated T_1, T_2, τ_c and χ (quadrupole coupling constant) to be 126 μs, 79.9 μs, 5.1 ns and 1.86 MHz respectively. From the values of τ_c and χ, they suggested that the reorientation of ^{67}Zn in the Zn^{2+}–insulin complex is fairly fast and that the environment around Zn^{2+} in insulin at acidic pH is not very symmetric. Shimizu and Hatano[266,283] have also attempted to study thermolysin using ^{67}Zn NMR.

A protein that has been extensively studied by ^{113}Cd NMR is metallothionein (MT).[284–295] In these studies metallothionein from different species have been investigated, and Armitage and coworkers have in various articles[284–287] shown that Cd-MTs from mammalians are very similar to each other, but the native metal composition in MT differs even after injection of enriched $^{113}Cd^{2+}$. However, the ^{113}Cd NMR spectra from invertebrate crab Cd_7–MT differ significantly from mammalian MT spectra. Otvos and Armitage[288] proposed a structure for the metal-binding sites in mammalian MT, which also has been verified in later work by Armitage and coworkers.[284–286,289,290] There are two distinct clusters of metal ions, one four-metal cluster and one three-metal cluster, where each Cd^{2+} in both clusters is coordinated by four cysteine residues (Fig. 25).

In mammalian MT there is a total of 20 cysteines, 11 of which participate in the Cd^{2+} coordination in the four-metal cluster, which has been shown to lie in the C-terminal fragment (residues 30–61) of MT.[290] The N-terminal fragment contains the other 9 cysteine residues, which are responsible for Cd^{2+} coordination in the three-metal cluster. Invertebrate crab MT has been shown to contain two three-metal clusters instead.[285]

The ^{113}Cd NMR spectra of native Cd,Zn–MT consists of much more than the seven resonances normally expected. This has been explained by (i) heterogeneity in the amino-acid sequence and (ii) unequal distribution of

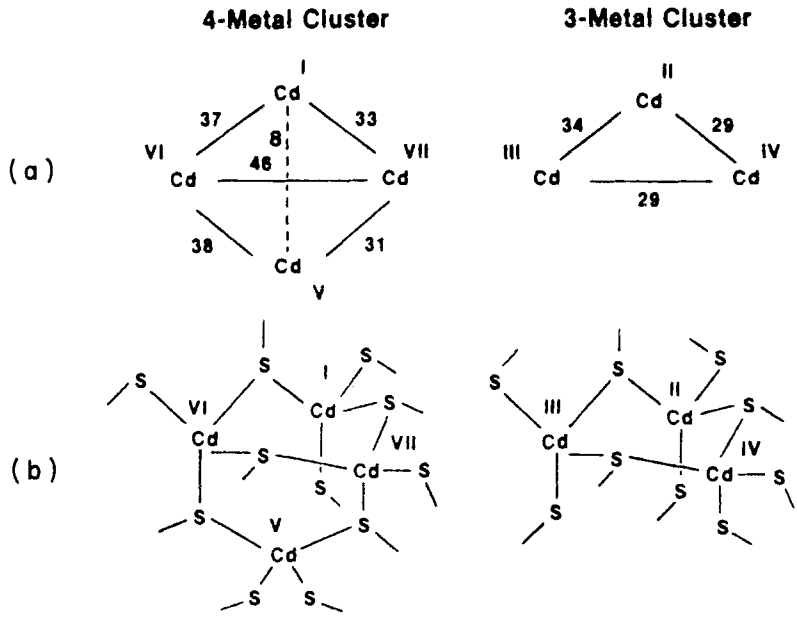


Fig. 25. (a) Schematic representations of the metal clusters in Cd_7–MT-2 showing the ^{113}Cd–^{113}Cd two-bond (solid lines) and four-bond (dashed line) scalar-coupling interactions between metals. The roman numeral beside each Cd refers to the corresponding resonance in Fig. 26, and the numbers on each line are the observed ^{113}Cd–^{113}Cd coupling constants. (b) Postulated structures for the metal–thiolate clusters based on ^{113}Cd NMR analyses. From Ref. 289, with permission.

Zn^{2+} among the sites. In addition to this, Otvos *et al.*[289] showed that MT undergoes oligomerization during preparation if there is an excess of metal ions. After they had prepared the monomeric MT, a simple ^{113}Cd NMR spectrum with seven resonances resulted, with chemical shifts for the resonances between 762 and 625 ppm (Fig. 26).

Furthermore, Nettesheim *et al.*[291] showed that Cd,Zn–MT generated *in vitro* by Cd^{2+} substitution of Zn_7–MT was not the same as the native Cd,Zn–MT produced *in vivo*, even though the Cd^{2+} to Zn^{2+} ratio was the same (2 : 1). However, the Cd,Zn–MT produced by adding Zn_7–MT to a solution of $^{113}Cd_7$–MT with a Cd^{2+} to Zn^{2+} ratio of 2 : 1 gave the same ^{113}Cd NMR spectrum as the Cd,Zn–MT generated *in vivo*. This metal-ion exchange is suggested to have both thermodynamic and kinetic driving forces.

Finally, Live *et al.*[296] used ^1H-detected heteronuclear multiquantum coherence (HMQC) for Cd^{2+} with multiple long-range couplings to protons. This enabled them to easily identify all the ^{113}Cd-coupled cysteine

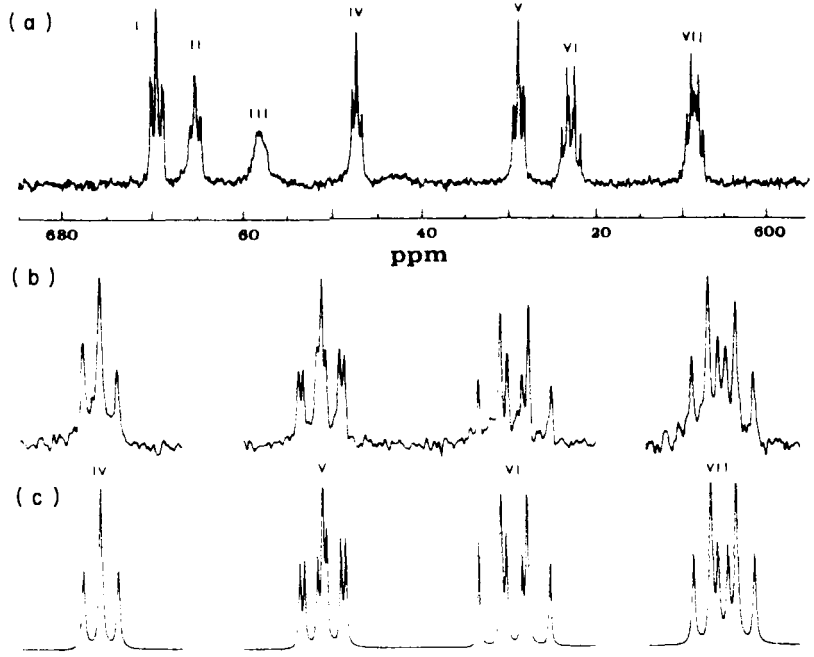


Fig. 26. (a) ^{113}Cd NMR spectrum at 44°C of 7 mM monomeric $^{113}Cd_7$–MT-2. (b) Expanded plots of resonances IV–VII from (a) after multiplication of the free-induction decay by a Gaussian function. (c) Spectral simulations of the multiplet structures of the resonances IV–VII using the spin-coupling constants and coupling connectivities shown in Fig. 25(a). From Ref. 289, with permission.

β-protons in each of the multiple Cd–Cys_4 sites in crab MT and then from homonuclear 2D ^1H NMR assign these cysteine protons.

Another protein that has been thoroughly studied not only by ^1H NMR but also by ^{113}Cd NMR and ^{31}P NMR is alkaline phosphatase (AP). AP has three metal-binding sites A, B and C in each of its two identical domains. Otvos and Armitage[297] and Gettins and Coleman[298,299] showed that addition of up to two equivalents of $^{113}Cd^{2+}$ to AP without P_i present showed one signal whose intensity decreases upon further addition of Cd^{2+} and completely disappears when six equivalents of Cd^{2+} have been added. The ^{113}Cd NMR signal at 169 ppm is from Cd^{2+} bound to the A site. When P_i is added to Cd_2-AP the resonance is shifted upfield and split into two resonances located at 144 ppm and 52 ppm. The resonance that is shifted to the lower frequency is from $^{113}Cd^{2+}$ in site B; that is, Cd^{2+} has migrated from site A to site B when AP is phosphorylated. From mixed metal hybrids of AP[300] it is suggested that the A-site metal has the greatest

influence on the activity of AP linked by the pK_a value, and that there is considerable subunit–subunit interaction in AP. Finally, Gettins and Coleman[301] studied the binding of arsenate to AP by ^{113}Cd NMR.

Different isozymes of carbonic anhydrase have been studied by ^{113}Cd NMR, where Cd^{2+} has substituted Zn^{2+} in the active site.[302] The chemical exchange rates differ for human erythrocyte carbonic anhydrase isozyme B and C—approximately $10^3\ s^{-1}$ for B and $10^5\ s^{-1}$ for C. This chemical exchange process is speculated to be a conformational flux accompanying solvent exchange in the coordination sphere of Cd^{2+}, and from this a mechanism of carbonic anhydrase is proposed. Furthermore, these authors and Evelhoch *et al.*[303] have found that various anionic inhibitors bind directly to the metal ion, for example, the two ^{15}N-labelled sulphonamides that Evelhoch *et al.* used were found to bind via the sulphonamide nitrogen.

The number of binding sites on yeast inorganic pyrophosphatase (PPase) have been determined as four high-affinity Cd^{2+} sites and two P_i sites per subunit by Welsh and Cooperman.[304] They suggested from ^{113}Cd NMR and equilibrium dialysis measurements in the presence of P_i that there are two classes of Cd^{2+} sites with two roughly equivalent sites in each class. The binding constant for Cd^{2+} is increased when P_i is added. Competition experiments with Mg^{2+} have also been performed.[304,305] The first two equivalents of Mg^{2+} added to PPase–$Cd_4(P_i)_3$ is predicted to bind to sites on PPase different from the Cd sites, but at higher Mg^{2+} concentrations there are direct competetive results. From the results of Welsh and Cooperman an updated model for the active-site structure of PPase is suggested (Fig. 27).

The locked conformation of concanavalin A (conA), as investigated with ^{113}Cd NMR by Palmer *et al.*,[306] gives rise to three signals at 68, 46 and −125 ppm, whereas the unlocked conformation only shows one signal,

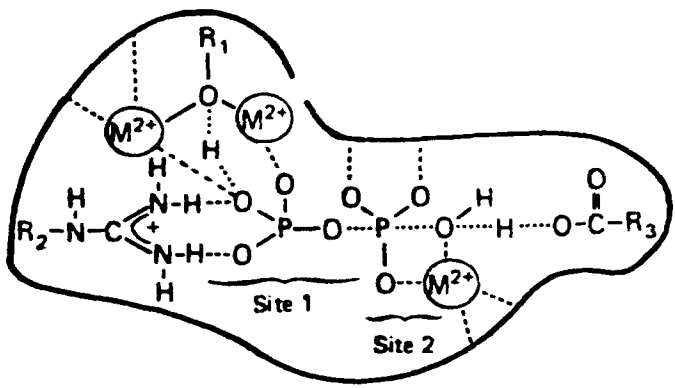


Fig. 27. Proposed model for the active-site structure of PPase. From Ref. 304, with permission.

indicating fast exchange between the metal-binding sites and free Cd^{2+}. The signals are due respectively to free Cd^{2+} or Cd^{2+} weakly associated with the protein, Cd^{2+} bound to the S1 site where normally Mn^{2+} binds and Cd^{2+} bound to the S2 site where normally Ca^{2+} binds. Addition of saccharides to conA show that S2, but not S1 is affected upon binding. Ellis *et al.*[307] also studied conA with ^{113}Cd NMR. They focused on the differences in Cd^{2+} binding to S1 and S2 and in the field dependence of the ^{113}Cd T_1.

In addition to this, Bhattacharyya *et al.*[308] studied lentil (LcH) and pea (PSA) lectins and made a comparison with conA. The ^{113}Cd NMR data for all three $(^{113}Cd^{2+})_2$-proteins were very similar, indicating close homology of their metal-ion binding sites, which is confirmed through amino-acid sequence data that show conservation of the amino acids in LcH and PSA, which constitutes the S1 and S2 sites in conA. $^{113}Cd^{2+}$–LcH has two resonances at 44.6 and -129.4 ppm, while the corresponding signals for $^{113}Cd^{2+}$–PSA are 46.6 and -130.4 ppm. A difference from conA is that PSA and LcH bind $^{113}Cd^{2+}$ tightly.

The ^{113}Cd NMR chemical shift for $^{113}Cd^{2+}$ bound to other proteins and the type of coordinating ligands for these proteins are reported in Table 1.

A somewhat unusual application of ^{113}Cd NMR was employed by Linse *et al.*[309] in an attempt to study the binding of $^{113}Cd^{2+}$ to polystyrene-sulphonate. However, the large span of chemical shifts for ^{113}Cd, which is of great use in protein studies, is a problem here, where $^{113}Cd^{2+}$ mostly is electrostatically bound.

The calcium-binding proteins calmodulin, troponin C, parvalbumin and calbindin D_{9k} have all been studied using ^{113}Cd NMR, where $^{113}Cd^{2+}$ has replaced Ca^{2+} in the binding sites. All four proteins belong to the same superfamily of proteins, and most of the Ca^{2+}-binding sites in all the proteins are what is called an EF-hand. The Cd^{2+} ions are octahedrally coordinated by oxygens, resulting in strongly negative chemical shifts.

Calmodulin (CaM), which has four Ca^{2+} binding sites, all EF-hands, has been extensively studied by the Forsén and Drakenberg group.[310–317] The ^{113}Cd NMR spectra at room temperature and neutral pH show two signals at -88 ppm and -114 ppm,[310,311] which were assigned by Andersson *et al.*[312] and Forsén *et al.*[311] to Cd^{2+} bound to sites IV and III respectively. The signals are assigned using the tryptic and thrombic fragments of CaM. These are the two cooperative high-affinity sites on CaM; the low-affinity sites I and II did not result in any ^{113}Cd NMR signals unless a drug that binds to CaM was added. The effect on the ^{113}Cd NMR spectra from the interaction of various drugs, such as D600 (a methoxy derivative of verapanil), trifluoroperazine, mastoparan and TNS, with CaM has also been studied[312–315] (Fig. 28). Intact CaM was used by Andersson *et al.*,[310] whereas tryptic fragments were used by Thulin *et al.*[314] and Andersson *et al.*[312]

Table 1.

Protein	Chemical shift (relative $Cd(ClO_4)_2$)	Coordinating ligands
Horseradish peroxidase[280]	−193	High-affinity Ca-site, only oxygen ligands
Horse liver alcohol dehydrogenase[278,279]	751	4 Cys, non-catalytic Zn site
	483	2 Cys, 1 His and presumably H_2O or OH^-, catalytic Zn site
	442	Catalytic site: NADH or NAD^+ bound
Bovine superoxide dismutase (BSD)[330]	310	Cd_2–BSD irregular tetrahedron
	320	Cd_2Cu_2BSD 3 His N, 1 carboxy O from Asp
Osteocalcin (BGP)[331]	20 (broad)	BGP + 2Cd
	0 (broad)	BGP + 2Cd + P_i: ^{111}Cd NMR
Bovine insulin[281]	165	3 imidazole N + $3H_2O$, Zn site
	−36	6 glutamyl carboxylate, Ca site
Phospholipase C (PhoC)[332,333]	85	Cd–PhoC structural site
	115	ZnCd–PhoC, catalytic site; mixture of N and O ligands
Blue copper protein:[334,335]		
Plastocyanin (PC)	432	2 His N, 1 Cys S, 1 Met S
Azurine(1)	372	As PC + 1 peptide carbonyl
Azurine(2)	379	As PC + 1 peptide carbonyl
Stellacyanin	380	2 His, 1 Cys thiolate, 1 Cys + 1 peptide carb.
Carboxypeptidase A (CPA)[336]	120 (<280 K)	2 His N, 2 O from Glu72, 1 H_2O
	127–137	Inhibitors added, coordinated as above
	335–350	Thioglycolic acid or DL-thiolactic acid added, coordination as above but binding through thiol group
a-Lactalbumin (alac)[337]	−80	Cd : Alac 1 : 1, only oxygen ligands
	−85	Cd : Alac 2 : 1

Phosmoglucomutase (PGM)[338]	22	PGM–Cd, mostly oxygen ligands
	75	PGM–Cd–Glu–P, one oxygen exchanged for nitrogen (His?)
Bovine serine proteases:[262]		
b-Trypsin	−54.5	
Trypsinogen	−55.8	Octahedral symmetry
Chymotrypsin	0 (broad)	Only oxygen ligands
Chymotrypsinogen	−10 (broad)	
Bovine serum albumin[339]	150	2 or 3 His, N and O ligands
	28	Probably oxygen ligands, less than octahedral geometry
Metallothionein (MT)[291]	671.3(site I)	
	630.9(V)	Four-metal cluster
	625.0(VI)	Only S-Cys ligands
	611.3(VII)	
	668.8(II)	
	659.0(III)	Three-metal cluster
	649.2(IV)	Only S-Cys ligands
Mammalian erythrocyte carbonic anhydrase (CA):[302]		
Bovine CA isozyme B	218	
Bovine CA isozyme A	157	
Human CA isozyme B	238	Cl^- added, alkaline pH
Alkaline phosphatase (AP)[297,298]	169	$(AP)Cd_2$, site A
	144	$(AP)(Cd_2)P_i$, site A
	52	$(AP)(Cd_2)P_i$, site B
Yeast inorganic pyrophosphatase (PPase)[304]	12.2	$(PPase)(Cd_4)(P_i)_2$
	−14.2	Coordinated to oxygens
	−16.5	
	−28.4	

(Continued)

Table 1. (*Continued*)

Protein	Chemical shift (relative $Cd(ClO_4)_2$)	Coordinating ligands
Concavalin A (ConA)[306]	68	Free Cd^{2+}
	46	Cd^{2+} in site S1
	−125	Cd^{2+} in site S2
Lentil lectin (LcH)[308]	44.6	
	−129.4	
Pea lectin (PSA)[308]	46.6	
	−130.4	
Calmodulin (CaM)[310,311]	−88	Site IV octahedrally coordinated
	−114	Site III by 6 oxygens
Calbindin D_{9k}[251]	−105(site II)	Calbindin (Cd^{2+})
	−110(II)	Calbindin $(Cd^{2+})_2$ octahedrally coordinated
	−155(I)	Calbindin $(Cd^{2+})_2$ by 6 oxygens
Parvalbumin (PA)[324,325]	−93	CD-site octahedral coordinated by oxygens
Carp PA, $pI = 4.47$	−97	EF-site
Skeletal muscle troponin C[328]	−101.5(site I)	
	−108.5(II)	Coordination number 8,
	−106.8(IV)	Coordinated by oxygens
	−112.8(III)	
Cardiac muscle troponin C[326]	−107	Coordinated by oxygens
	−114	

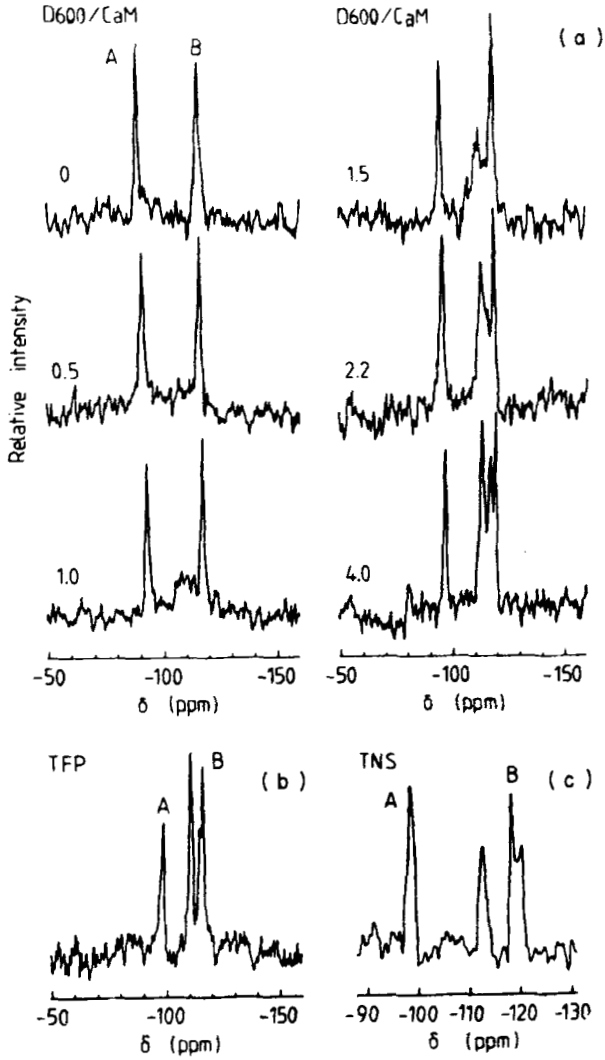


Fig. 28. The ^{113}Cd NMR spectra of CaM with the addition of different drugs: (a) 2.5 ml 1.2 mM CaM–Cd_4, pH 7.6 as a function of added 55 mM D600 dissolved in ethanol; (b) 1.4 mM CaM–Cd_4 and 2.8 mM TFP, pH 7.0; (c) 1.1 mM CaM–Cd_4 and 6.6 mM TNS, pH 7.5. The spectra in (a) and (b) were obtained at 56.55 MHz, while the spectrum in (c) was obtained at 80.24 MHz. From Ref. 313, with permission.

Calbindin D_{9k} has two calcium-binding sites, one EF-hand (site II) and the other a somewhat disordered "pseudo" EF-hand (site I). The EF-hand site binds Cd^{2+} somewhat more strongly than the other site; this resulted in NMR spectra with only one signal at -105 ppm when less than one equivalent of Cd^{2+} was added. Upon further addition of Cd^{2+}, the signal shifted to -110 ppm and a second broad signal at -155 ppm appeared.[318] The change in chemical shift for Cd^{2+} bound to site II, upon Cd^{2+} binding to site I, shows that there is an interaction between the two sites. Further work has been carried out on mutants of calbindin D_{9k} prepared by site-directed mutagenesis and produced in *Escherichia coli*.[251,319-323]

For example, Linse *et al.*[251] prepared four mutant proteins, where they tried to turn the pseudo-EF Ca^{2+}-binding site into an EF-hand. The mutant proteins were studied using ^{113}Cd NMR, since it was thought that an additional EF-hand should give a resonance around -80 to -120 ppm. However, this was not observed.

All parvalbumins have two strong Ca^{2+} binding sites, and some have an additional weak site. The ^{113}Cd NMR spectra display two resonances between -80 and -100 ppm. The assignment of the high-field signal to the EF-site and the low-field signal to the CD-site was made by competition experiments with various lanthanide ions by Drakenberg *et al.*[324] Svard and Drakenberg[237] studied the effect of the paramagnetic Mn^{2+} on the ^{113}Cd NMR spectra. A further ^{113}Cd NMR study of parvalbumin was made by Cavé *et al.*[325]

Both skeletal troponin C (STnC) and cardiac troponin C (cTnC) have been investigated by ^{113}Cd NMR. STnC has four Ca^{2+}-binding sites (two high-affinity sites and two low-affinity sites), whereas cTnC has only three Ca^{2+} binding sites, two of which are high-affinity sites. The ^{113}Cd NMR spectra for cTnC was recorded by Teleman *et al.*,[326] there are two signals at -107 and -114 ppm at both room temperature and at 4°C. The authors suggest that there is cooperative binding of Ca^{2+} or Cd^{2+} to the two strong Ca^{2+} sites. Both Ellis *et al.*[327,328] and Drakenberg *et al.*[329] studied STnC; however, Drakenberg *et al.* used the tryptic fragments of the protein instead of the intact protein. Ellis *et al.*[328] found four signals in the ^{113}Cd NMR spectra recorded at 4°C, at -101.5 and -108.5 ppm and -106.8 and -112.8 ppm. They confirmed the assignments made by Drakenberg *et al.*[329] that the two signals at -101.5 and -108.5 ppm arise from the *Ca^{2+}-regulatory sites, I and II respectively*, and that the two signals at *-106.8 and -112.8 ppm come from Cd^{2+} bound to the structural* Ca^{2+}–Mg^{2+} sites, IV and III respectively. The coordination number for Ca^{2+} (Cd^{2+}) in each site is proposed to be eight, and in STnC as in cTnC cooperative Cd^{2+} binding is indicated for the two high-affinity structural Cd^{2+} sites. In the review article by Sudmeier and Green[340] ^{113}Cd NMR shifts for some of these proteins are reported.

3.4. Thallium

^{205}Tl has been used as an NMR probe for the investigation of the proteins transferrin,[341-343] S-adenosylmethionine synthetase[343] and protein C, activated protein C (APC), a proteolytic derivative of protein C (GDPC) and the corresponding activated derivative (GDAPC).[344,345]

Bertini and coworkers[341-343] studied $^{205}Tl^{3+}$ binding to the two sites of transferrin. The chemical-shift range in ^{205}Tl NMR is very large and depends strongly on the ligands that coordinate to the Tl^+ ion. The Bertini group therefore concluded from the small shift difference between $^{205}Tl^{3+}$ in the two sites (20 ppm), that the sites were very similar. They also found evidence for the presence of two tyrosines and two histidines among the ligands to the metal.

Hill et al.[345] and Hill and Castellino[346] investigated $^{205}Tl^+$ binding to protein C and various derivatives of the protein. From titrations of the proteins with Tl^+, monitored with ^{205}Tl NMR, the K_d values were calculated. Hill *et al.*[345] found that these values are very similar for Tl^+–protein C and Tl^+–GDPC. Furthermore, Hill and Castellino[346] estimated the distances between the monovalent- and divalent-cation sites in GDPC and GDAPC to 6.7 ± 0.2 Å and 8.3 ± 0.2 Å respectively. To do this, they used paramagnetic Mn^{2+} and employed Salomon–Bloembergen theory.

4. ION BINDING TO AGGREGATES AND CELLS

4.1. Gramicidin channels

As discussed in Section 2.4, Hinton and coworkers studied the binding of Tl^+ ions to gramicidin in various solvents.[184-190] They also studied model systems in attempts to gain more information regarding the interaction between the thallous ion and gramicidin channels.[347-350] When gramicidin was incorporated into lysolecithin micelles Hinton *et al.*[347] found that there is only one Tl^+-binding site available in the gramicidin dimer, with a binding constant of 900 M^{-1}. Under these advantageous circumstances, it was unusually easy to determine the number of binding sites simply by comparing the theoretical curves for the concentration dependence, assuming one or two Tl^+-ion binding sites. The same authors have also performed a study of the temperature dependence in the binding constant to determine the enthalpy and entropy of binding. In a study using pure gramicidin A, B or C in lysophosphatidylcholine micelles they found that only half of the analytical gramicidin concentration was available for Tl^+ binding. The

binding constants were found to be 580, 1950 and 390 M^{-1} for gramicidin A, B and C, respectively. Using ^{205}Tl NMR in competition experiments they also determined the binding constants for the alkali metal ions to gramicidin dimers. In the most recent study they investigated the binding of Tl^+ ions to gramicidin A in dimyristoylphosphatidylcholine vesicles. In this case they observed that there are two Tl^+-ion binding sites on the gramicidin dimer, $K_1 = 500$ and $K_2 = 10$ M^{-1}. The two sites have chemical shifts for the bound Tl^+ ions in different directions with respect to the "free" solvated Tl^+ ion. This made it quite clear that a second site had to be included to explain the concentration dependence as shown in Fig. 29.

In another series of papers Urry *et al.*[352-358] used alkali-metal ions directly to study the interaction between them and the gramicidin channels. Using the effect on either chemical shift or relaxation rate from the binding to the gramicidin channels, they were able to obtain the binding constants for all five alkali-metal ions. The value of the strong binding site for ^{87}Rb is only a lower limit (30 M^{-1}) owing to the high concentration of Rb^+ ions that had to be used in order to get sufficient signal-to-noise ratios. The correlation times for the bound ions were also obtained, and, assuming that it is due to exchange of ions, the channel current could be calculated. It is interesting to note here that during the T_1 measurements close to the null

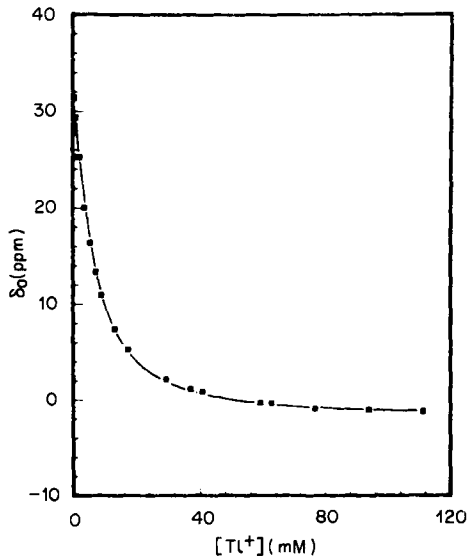


Fig. 29. Concentration dependence of ^{205}Tl chemical shift in the presence of gramicidin A and dimyristoylphosphatidylcholine vesicles. From Ref. 351, with permission.

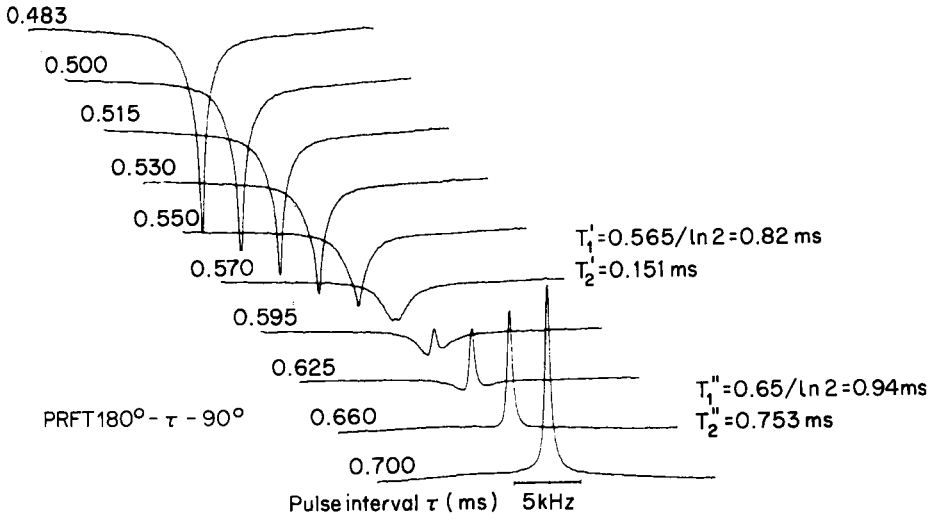


Figure 30. Partially relaxed inversion-recovery spectra close to the null point for 2.0 M RbCl in the presence of 3.16 M gramicidin channels. From Ref. 358, with permission.

point, two signals with slightly different chemical shifts and widely different linewidth are observed. Furthermore, the narrow line has the faster apparent relaxation rate (see Fig. 30). This shows that the T_1 relaxation measured in the usual way is not a true relaxation time.

Riddell and coworkers[359,360] studied the ionophore-mediated transport of alkali-metal ions. They used either monensin or nigericin as ion carriers and found, by recording the width of the ^{23}Na or ^{39}K resonances, that the K^+–nigericin complex is 4–5 times stronger than the Na^+–nigericin complex; however, Na^+ transport is 3.5 times faster than K^+ transport.

Elgavish and Elgavish[361] used ^{23}Na NMR to study Na^+-ion transport across brush-border membrane. In a system with brush-border membrane vesicles they found that Na^+-ion transport is fast on the NMR timescale since they observed one narrow ^{23}Na resonance, even in the presence of the shift reagent $Dy(EDTA)_2^{5-}$ in the extra vesicular space.

4.2. Whole-cell studies

Melamud *et al.*,[362] Ogino *et al.*[363] and Brophy *et al.*[364] all used ^{23}Na and/or ^{39}K NMR to obtain the amount of Na^+ or K^+ inside cells. To differentiate between inside and outside resonances, shift reagents were used.

Petegrew *et al.*[365,366] used ^{23}Na NMR to study the state of Na^+ in various cells. They thus demonstrated that the sodium-ion concentration in human erthrocytes as determined by NMR agrees well with that determined by flame photometry. They also found that a fraction of the intracellular sodium ions had a relatively long correlation time. They studied the state of Na^+ ions in intact bovine lens and in vitreous humour as well. From T_1 and T_2 measurements, they deduced that in the bovine lens there is a Na^+–protein interaction with a lifetime of about 3×10^{-9} s. This is similar to the interaction reported by Delville *et al.* for the proteins calmodulin[233] and troponin C.[234]

Ong and Cheung[367] studied human red-cell ghosts from hypertensive and normotensive subjects. From relaxation-time measurements on ^{23}Na as a function of total Na^+ concentration, they found that the ghosts from normotensives have a higher binding constant (500–1000 M^{-1}) than the ghosts from hypertensives (100 M^{-1}). Höfeler *et al.*[368] studied the efflux of sodium from sodium-loaded yeast cells, and Jans *et al.*[369] found that only 64% of the intracellular sodium from renal epithelial cells is NMR-visible.

REFERENCES

1. *NMR of Newly Accessible Nuclei* (ed. P. Laszlo). Academic Press, London, 1983.
2. *The Multinuclear Approach to NMR Spectroscopy* (ed. J.B. Lambert and F.G. Riddell). Reidel, Boston, 1983.
3. *Multinuclear NMR* (ed. J. Mason). Plenum, New York, 1987.
4. S. Forsen and B. Lindman, in *Annual Reports on NMR Spectroscopy*, Vol. 11B (ed. G.A. Webb), p. 183. Academic Press, London, 1983.
5. D. Rehder, *Magn. Reson. Rev.*, 1984, **9**, 125.
6. M. Minelli, J.H. Enemark, R.T.C. Brownlee, M.J. O'Connor and A.G. Wedd, *Coord. Chem. Rev.*, 1985, **68**, 169.
7. T. Drakenberg, in *Annual Reports on NMR Spectroscopy*, Vol. 17 (ed. G.A. Webb), p. 231. Academic Press, London, 1986.
8. M.F. Summers, *Coord. Chem. Rev.*, 1988, **86**, 43.
9. G. Fraenkel, M. Hendrichs, J.M. Hewitt, B. Miing Su and M.J. Geckle, *J. Am. Chem. Soc.*, 1980, **102**, 3341.
10. U. Olsher, G.A. Algavish and J. Jagur-Grodzinski, *J. Am. Chem. Soc.*, 1980, **102**, 10.
11. J.J.C. van Lier, L.J.M. van de Ven, J.W. de Haan and H.M. Buck, *J. Phys. Chem.*, 1983, **87**, 3501.
12. W. Kolodziejski and G.E. Maciel, *J. Phys. Chem.*, 1983, **87**, 4694.
13. A. Delville, C. Detellier, A. Gerstmans and P. Laszlo, *J. Am. Chem. Soc.*, 1980, **102**, 6559.
14. A. Delville, C. Detellier, A. Gerstmans and P. Laszlo, *J. Magn. Reson.*, 1981, **42**, 14.
15. W. Kolodziejski, P. Laszlo and A. Stockis, *Mol. Phys.*, 1982, **45**, 939.
16. J.H. Medley, E.S. Mooberry and M.C. Day, *Can. J. Chem.*, 1983, **61**, 558.
17. J.L. Gray and G.E. Maciel, *J. Phys. Chem.*, 1983, **87**, 5290.
18. J.L. Gray and G.E. Maciel, *J. Phys. Chem.*, 1983, **87**, 5418.
19. W. Kolodziejski, *J. Mol. Struct.*, 1987, **159**, 335.

20. A.S. Galiano-Roth and D.B. Collum, *J. Am. Chem. Soc.*, 1988, **110**, 3446.
21. N. Kallman and D.B. Collum, *J. Am. Chem. Soc.*, 1987, **109**, 7466.
22. B. Parbhoo and O.B. Nagy, *J. Chem. Soc. Faraday Trans. 1*, 1986, **82**, 1789.
23. F. Taulelle and A.I. Popov, *Polyhedron*, 1983, **2**, 889.
24. R.R. Rhinebarger, J.W. Rovang and A.I. Popov, *Inorg. Chem.*, 1984, **23**, 2558.
25. R.R. Rhinebarger and A.I. Popov, *Polyhedron*, 1988, **7**, 1341.
26. E. Schmidt, A. Housahis and A.I. Popov, *Inorg. Chim. Acta*, 1981, **52**, 91.
27. D. Lin and A.I. Popov, *J. Am. Chem. Soc.*, 1981, **103**, 3773.
28. A.J. Smetana and A.I. Popov, *J. Solution Chem.*, 1980, **9**, 183.
29. J. Bouquant, A. Delville, J. Grandjean and P. Laszlo, *J. Am. Chem. Soc.*, 1982, **104**, 686.
30. A. Ricard, F. Lafuma and C. Quivoran, *Polymer*, 1982, **23**, 907.
31. A. Kaifer, H.D. Durst, L.E. Echegoyen, D.M. Dishong, R.A. Schultz and G.W. Gokel, *J. Org. Chem.*, 1982, **47**, 3195.
32. M. Brisnaire, C. Detellier and D. Nadon, *Can. J. Chem.*, 182, **60**, 3071.
33. W. Offermann and E. Weber, *Chem. Ber.*, 1984, **117**, 234.
34. S.F. Lincoln, I.M. Brereton and T.M. Spotswood, *J. Chem. Soc. Faraday Trans. 1*, 1985, **81**, 1623.
35. H.D. Stöver, A. Delville and C. Detellier, *J. Am. Chem. Soc.*, 1985, **107**, 4167.
36. A. Delville, H.D. Stöver and C. Detellier, *J. Am. Chem. Soc.*, 1985, **107**, 4172.
37. B.O. Strasser, K. Hallenga and A.I. Popov, *J. Am. Chem. Soc.*, 1985, **107**, 789.
38. B.O. Strasser and A.I. Popov, *J. Am. Chem. Soc.*, 1985, **107**, 7921.
39. S.F. Lincoln, I. M. Brereton and T.M. Spotswood, *J. Am. Chem. Soc.*, 1986, **108**, 8134.
40. K.M. Briere and C. Detellier, *J. Phys. Chem.*, 1987, **91**, 6097.
41. A. Detellier, H.D.H. Stöver and C. Detellier, *J. Am. Chem. Soc.*, 1987, **109**, 7293.
42. S.F. Lincoln, A. White and A.M. Hounslow, *J. Chem. Soc. Faraday Trans. 1*, 1987, **83**, 2459.
43. H.P. Graves and C. Detellier, *J. Am. Chem. Soc.*, 1988, **110**, 6019.
44. J. Desroches, H. Dugas, M. Bouchard, T.M. Fyles and G.D. Robertson, *Can. J. Chem.*, 1987, **65**, 1513.
45. K.M. Aalamo and J. Krane, *Acta Chem. Scand.*, 1982, **A36**, 219.
46. H.D.H. Stöver, L.J. Maurice, A. Delville and C. Detellier, *Polyhedron*,, 1985, **4**, 1091.
47. E. Schmidt and A.I. Popov, *Spectrosc. Lett.*, 1981, **14**, 787.
48. E. Schmidt and A.I. Popov, *J. Am. Chem. Soc.*, 1983, **105**, 1873.
49. K.J. Neurohr, T. Drakenberg, S. Forsén and H. Lilja, *J. Magn. Reson.*, 1983, **51**, 460.
50. C. Detellier and M. Robillard, *Can. J. Chem.*, 1987, **65**, 1684.
51. H.D.H. Stöver, M. Robillard and C. Detellier, *Polyhedron*, 1987, **6**, 577.
52. J.-S. Shih and A.I. Popov, *Inorg. Chem.*, 1980, **19**, 1689.
53. S. Khazaeli, J.L. Dye and A.I. Popov, *Spectrochim. Acta*, 1983, **39A**, 19.
54. E. Kauffmann, J.L. Dye, J.-M. Lehn and A.I. Popov, *J. Am. Chem. Soc.*, 1980, **102**, 2274.
55. S. Khazaeli, A.I. Popov and J.L. Dye, *J. Phys. Chem.*, 1986, **86**, 5018.
56. A. Ricard and F. Lafuma, *Polymer*, 1986, **27**, 133.
57. G. Rounaghi, and A.I. Popov, *Polyhedron*, 1986, **5**, 1935.
58. M. Borzo, C. Detellier, P. Laszlo and A. Paris, *J. Am. Chem. Soc.*, 1980, **102**, 1124.
59. E. Amat, B.G. Cox, J. Rzeszotarska and H. Schneider, *J. Am. Chem. Soc.*, 1988, **110**, 3368.
60. E. Amat, B.G. Cox and H. Schneider, *J. Magn. Reson.*, 1987, **71**, 259.
61. C.C. Bryden, C.N. Reilley and J.F. Desreux, *Anal. Chem.*, 1981, **53**, 1418.
62. R.K. Gupta and P. Gupta, *J. Magn. Reson.*, 1982, **47**, 344.
63. R.K. Gupta, P. Gupta and W. Negendank, in *Ions, Cell Proliferation and Cancer* (ed. A.L. Boynton *et al.*), p. 1. Academic Press, New York, 1982.

64. R.K. Gupta, P. Gupta and R.D. Moore, *Annu. Rev. Biophys. Bioengng.*, 1984, **13**, 221.
65. M.M. Pike and C.S. Springer, *J. Magn. Reson.*, 1982, **46**, 348.
66. M.M. Pike, S.R. Simon, J.A. Balshi and C.S. Springer, *Proc. Natl Acad. Sci. USA*, 1982, **79**, 810.
67. M.M. Pike, D.M. Yarmush, J.A. Balshi, R.E. Lenkinski and C.S. Springer, *Inorg. Chem.*, 1983, **22**, 2388.
68. S.C. Chu, M.M. Pike, E.T. Fossel, T.W. Smith, J.A. Balshi and C.S. Springer, *J. Magn. Reson.*, 1984, **56**, 33.
69. M.H. Hayer and F.G. Riddell, *Inorg. Chim. Acta*, 1984, **92**, L37.
70. S.M. Anson, R.B. Homer and P.S. Belton, *Inorg. Chim. Acta*, 1987, **138**, 241.
71. A.D. Sherry, C.F.G.C. Geraldes and W.P. Cacheris, *Inorg. Chim. Acta*, 1987, **139**, 137.
72. A.D. Sherry, C.R. Malloy, M.H. Jeffrey, W.P. Cacheris and C.F.G.C. Geraldes, *J. Magn. Reson.* 1988, **76**, 528.
73. M. Jaber and G. Thomas-David, *Bull. Soc. Chim. Fr.*, 1985, 644.
74. M. Jaber and G. Thomas-David, *Bull. Soc. Chim. Fr.*, 1986, 59.
75. E. Bouhoutsos-Brown, D. Murk Rose and R.G. Bryant, *J. Nucl. Inorg. Chem.*, 1981, **43**, 2247.
76. R.M. Farmer and A.I. Popov, *Inorg. Nucl. Chem. Lett.*, 1981, **17**, 51.
77. T. Drakenberg, *Acta Chem. Scand.*, 1982, **A36**, 79.
78. D. Rehder and H. Speh, *Inorg. Chim. Acta*, 1987, **135**, 73.
79. S.H. Eggers and R.D. Fischer, *J. Organomet. Chem.*, 1986, **315**, C61.
80. S.H. Eggers, M. Adam, E.T.K. Haupt and R.D. Fischer, *Inorg. Chim. Acta*, 1987, **139**, 315.
81. C.F.G.C. Geraldes, M.C. Alpoim, M.P.M. Maques, A.D. Sherry and M. Singh, *Inorg. Chem.*, 1985, **24**, 3876.
82. C.F.G.C. Geraldes and A.D. Sherry, *J. Magn. Reson.*, 1986, **66**, 274.
83. A.D. Sherry, M. Singh and C.F.G.C. Geraldes, *J. Magn. Reson.*, 1985, **66**, 511.
84. J.A. Peters and A.P.G. Kieboom, *Recl. Trav. Chim. Pays-Bas*, 1983, **102**, 381.
85. P.G. Gassman, W. H. Campbell and D.G. Macomber, *Oragonometallics*, 1985, **3**, 385.
86. A. Dormond, M. Fauconet, J.C. Leblanc and C. Moise, *Polyhedron*, 1984, **3**, 897.
87. M.J. Glinchey and D.G. Bickley, *Polyhedron*, 1985, **4**, 1147.
88. W.C. Finch, E.V. Anslyn and R.H. Grubbs, *J. Am. Chem. Soc.*, 1988, **110**, 2406.
89. R. Benn and A. Rufinska, *J. Organomet. Chem.*, 1989, **273**, C51.
90. M.J. Gresser and A.S. Tracey, *J. Am. Chem. Soc.*, 1985, **107**, 4215.
91. M.J. Gresser and A.S. Tracey, *J. Am. Chem. Soc.*, 1986, **108**, 1935.
92. A.S. Tracey and M.J. Gresser, *Proc. Natl Acad. Sci. USA*, 1986, **83**, 609.
93. M.J. Gresser, A.S. Tracey and K.M. Parkinson, *J. Am Chem. Soc.*, 1986, **108**, 6229.
94. A.S. Tracey, M.J. Gresser and K.M. Parkinson, *Inorg. Chem.*, 1987, **26**, 629.
95. A.S. Tracey, B. Galeffi and S. Mahjour, *Can. J. Chem.*, 1988, **66**, 2294.
96. B. Galeffi and A.S. Tracey, *Can. J. Chem.*, 1988, **66**, 2565.
97. A.S. Tracey and M.J. Gresser, *Can. J. Chem.*, 1988, **66**, 2570.
98. C. Carr, J. Glaser and M. Sandstrom, *Inorg. Chim. Acta*, 1987, **131**, 153.
99. B.E. Mann and C.M. Spencer, *Inorg. Chim. Acta*, 1982, **65**, L57.
100. B.E. Mann and C.M. Spencer, *Inorg. Chim. Acta*, 1983, **76**, L65.
101. T.G. Appleton, R.D. Berry, C.A. Davis, J.R. Hall and H.A. Kimlin, *Inorg. Chem.*, 1984, **23**, 3514.
102. T.G. Appleton, J.R. Hall, S.F. Ralph and C.S.M. Thompson, *Inorg. Chem.*, 1984, **23**, 3521.
103. Ö. Gröning, T. Drakenberg and L.I. Elding, *Inorg. Chem.*, 1982, **21**, 1820.
104. T.G. Appleton, J.R. Hall and S.F. Ralph, *Inorg. Chem.*, 1985, **24**, 673.
105. T.G. Appleton, J.R. Hall and S.F. Ralph, *Inorg. Chem.*, 1985, **24**, 4685.
106. T.G. Appleton, J.R. Hall and I.J. McMahon, *Inorg. Chem.*, 1986, **25**, 720.

107. T.G. Appleton, J.R. Hall and I.J. McMahon, *Inorg. Chem.*, 1986, **25**, 726.
108. T.G. Appleton, J.R. Hall and S.F. Ralph, *Aust. J. Chem.*, 1986, **39**, 1347.
109. T.G. Appleton, J.R. Hall and M.A. Williams, *Aust. J. Chem.*, 1987, **40**, 1565.
110. T.G. Appleton and J.R. Hall, *J. Chem. Soc. Chem. Commun.*, 1983, 911.
111. T.G. Appleton, J.W. Connor and J.R. Hall, *Inorg. Chem.*, 1988, **27**, 130.
112. G.E. Kirvan and D.W. Margerum, *Inorg. Chem.*, 1985, **24**, 3017.
113. L.S. Hollis, A.R. Amundsen and E.W. Stern, *J. Am. Chem. Soc.*, 1985, **107**, 274.
114. L.S. Hollis, E.W. Stern, A.R. Amundsen, A.V. Miller and S.L. Doran, *J. Am. Chem. Soc.*, 1987, **109**, 3596.
115. L.S. Hollis and E.W. Stern, *Inorg. Chem.*, 1988, **27**, 2826.
116. W.I. Sundquist, K.J. Ahmed, L.S. Hollis and S.J. Lippard, *Inorg. Chem.*, 1987, **26**, 1524.
117. S.K. Miller and L.G. Marzilli, *Inorg. Chem.*, 1985, **24**, 2421.
118. M.D. Reily and L.G. Marzilli, *J. Am. Chem. Soc.*, 1986, **108**, 6785.
119. F.J. Dijt, G.W. Canters, J.H.J. den Hartog, A.T.M. Marcelis and J. Reedijk, *J. Am. Chem. Soc.*, 1984, **106**, 3644.
120. G.M. Clore and A.M. Gronenborn, *J. Am. Chem. Soc.*, 1982, **104**, 1369.
121. M. Sarrazin, V. Peyrot and C. Briand, *Inorg. Chim. Acta*, 1986, **124**, 87.
122. P.S. Pregosin, in *Annual Reports on NMR Spectroscopy*, Vol. 17 (ed. G.A. Webb), p. 285. Academic Press, London, 1986.
123. F.S.M. Hassan, D.M. McEwan, P.G. Pringle and B.L. Shaw, *J. Chem. Soc. Dalton Trans.*, 1985, 1501.
124. E.G. Hope, W. Levason and N.A. Powell, *Inorg. Chim. Acta*, 1986, **115**, 187.
125. I.M. Al-Najjar, *Inorg. Chim. Acta*, 1987, **128**, 93.
126. L.M. Green, Young-ae Park and D.W. Meek, *Inorg. Chem.*, 1988, **27**, 1658.
127. R. Colton, J. Ebner and B.F. Hoskins, *Inorg. Chem.*, 1988, **27**, 1993.
128. J.G. Kraaijkamp, D.M. Grove, G. van Koten and A. Schmidpeter, *Inorg. Chem.*, 1988, **27**, 2612.
129. S.J.S. Kerrison and P.J. Sadler, *Inorg. Chim. Acta*, 1985, **104**, 197.
130. R.T.C. Brownlee, W.D. McFadyen, M.J. O'Connor, T.J. Rook, I.A.G. Roos and L.P.G. Wakelin, *Magn. Reson. Chem.*, 1987, **25**, 492.
131. J.A. Galbraith, K.A. Menzel, E.M.A. Ratilla and N.M. Kostik, *Inorg. Chem.*, 1987, **26**, 2073.
132. R.E. Cramer, R.E. Kirkup and M.J.J. Carrie, *Inorg. Chem.*, 1988, **27**, 123.
133. C.K. Carson and P.A.W. Dean, *Inorg. Chim. Acta*, 1982, **66**, 157.
134. Zhi-fen Li and A.I. Popov, *J. Solution Chem.*, 1982, **11**, 17.
135. D. Köhnlein, O. Lutz and D. Ruppert, *J. Magn. Resonance*, 1984, **57**, 486.
136. T. Shimizu, M. Kodaka and M. Hatano, *Biochem. Biophys. Res. Commun.*, 1982, **106**, 988.
137. M. Kodaka, T. Shimizu and M. Hatano, *Inorg. Chim. Acta*, 1983, **76**, 155.
138. A. Delville and C. Detellier, *Can. J. Chem.*, 1986, **64**, 1845.
139. R.J. Kostelnik and A.A. Bothner-By, *J. Magn. Reson.*, 1974, **14**, 141.
140. T. Drakenberg, N.O. Björk and R. Portanova, *J. Phys. Chem.*, 1978, **82**, 2423.
141. J.J.H. Ackerman, T.V. Orr, V.J. Bartuska and G.E. Maciel, *J. Am. Chem. Soc.*, 1979, **101**, 341.
142. M.J.B. Ackerman and J.J.H. Ackerman, *J. Am. Chem. Soc.*, 1985, **107**, 6413.
143. M.F. Summers, J. van Rijn, J. Reedijk and L.G. Marzilli, *J. Am. Chem. Soc.*, 1986, **108**, 4254.
144. R. Colton and D. Dakternieks, *Aust. J. Chem.*, 1980, **33**, 1677.
145. R. Colton and D. Dakternieks, *Aust. J. Chem.*, 1980, **33**, 2405.
146. M.J.B. Ackerman and J.J.H. Ackerman, *J. Phys. Chem.*, 1980, **84**, 3151.
147. H.J. Jakobsen and P.D. Ellis, *J. Phys. Chem.*, 1981, **85**, 3367.

148. S.M. Wang and R.K. Gilpin, *Anal. Chem.*, 1983, **55**, 493.
149. S.M. Wang and R.K. Gilpin, *Talanta*, 1985, **32**, 329.
150. G. Battistuzzi Gavioli, M. Borzari, G.C. Pellaconi, L. Menabue, M. Sola and A. Bonamartini Corradi, *Inorg. Chem.*, 1988, **27**, 1587.
151. C.F. Jensen, S. Deshmukh, H.J. Jakobsen, R.R. Inners and P.D. Ellis, *J. Am. Chem. Soc.*, 1981, **103**, 3659.
152. C.C. Bryden and C.N. Reiley, *J. Am. Chem. Soc.*, 1982, **104**, 2697.
153. R.A. Haeberkorn, L. Que, W.O. Gillum, R.H. Holm, C.S. Liu and R.C. Lord, *Inorg. Chem.*, 1976, **15**, 2408.
154. A.D. Keller, T. Drakenberg, R.W. Briggs, and I.M. Armitage, *Inorg. Chem.*, 1985, **24**, 1170.
155. G.C. Baumann, M.F. Summers, J.P. Hutchinson, J. Zubieta and L.G. Marzilli, *Inorg. Chem.*, 1984, **23**, 3104.
156. M.F. Summers and L.G. Marzilli, *Inorg. Chem.*, 1984, **23**, 523.
157. M. Munakata, S. Kitigawa and F. Yagi, *Inorg. Chem.*, 1986, **25**, 964.
158. P.F. Rodesilar, E.H. Griffith, P.D. Ellis and E.L. Amma, *J. Chem. Soc. Chem. Commun.*, 1980, 492.
159. H.J. Jakobsen, P.D. Ellis, R.R. Innes and C.F. Jensen, *J. Am. Chem. Soc.*, 1982, **104**, 7442.
160. G.K. Carson, P.A.W. Dean and M.J. Stillman, *Inorg. Chim. Acta*, 1981, **56**, 59.
161. G.K. Garson and P.A.W. Dean, *Inorg. Chim. Acta*, 1982, **66**, 37.
162. R.A. Bulman, J.K. Nicholson, D.P. Higham and P.J. Sadler, *J. Am. Chem. Soc.*, 1984, **106**, 1118.
163. P.A.W. Dean and J.J. Vittal, *Inorg. Chem.*, 1985, **24**, 3722.
164. I.G. Dance and J.K. Saunders, *Inorg. Chim. Acta*, 1985, **96**, L71.
165. P.A.W. Dean and J.J. Vittal, *Inorg. Chem.*, 1986, **25**, 514.
166. P.A.W. Dean, J.J. Vittal and N.C. Payne, *Inorg. Chem.*, 1987, **26**, 1983.
167. S. Biagini, M. Casu, A. Lai, R. Caminiti and G. Crisponi, *Chem. Phys.*, 1985, **93**, 461.
168. D. Dakternieks, *Aust. J. Chem.*, 1982, **35**, 469.
169. D. Dakternieks and C.L. Rolls, *Inorg. Chim. Acta*, 1985, **105**, 213.
170. R.D. Bach, S.J. Rajan, H.B. Vardhan, T.J. Lang and N.G. Albrecht, *J. Am. Chem. Soc.*, 1981, **103**, 7727.
171. R.D. Bach and H.B. Varhan, *J. Org. Chem.*, 1986, **51**, 1609.
172. T.E. Jones, L.S.W.L. Sokol, D.B. Rorabacher and M.D. Glick, *J. Chem. Soc. Chem. Commun.*, 1979, 140.
173. J.-P. Charland, Minh Tan Phan Viet, M. St.-Jaques and A.L. Beauchamp, *J. Am. Chem. Soc.*, 1985, **107**, 8202.
174. R. Colton and D. Dakternieks, *Aust. J. Chem.*, 1980, **23**, 955.
175. R. Colton and D. Dakternieks, *Aust. J. Chem.*, 1980, **23**, 1463.
176. R. Colton and D. Dakternieks, *Aust. J. Chem.*, 1981, **24**, 323.
177. P.A.W. Dean and R.S. Srivastava, *Can. J. Chem.*, 1985, **63**, 2829.
178. J.F. Hinton, *Magn. Reson. Chem.*, 1987, **25**, 659.
179. J.F. Hinton and K.R. Metz, *J. Sol. Chem.*, 1980, **9**, 197.
180. G.L. Turner, J.F. Hinton and F.S. Millett, *J. Sol. Chem.*, 1982, **11**, 379.
181. J. Glaser and U. Henriksson, *J. Am. Chem. Soc.*, 1981, **103**, 6642.
182. U. Henriksson and J. Glaser, *Acta Chem. Scand*, 1985, **A39**, 331.
183. J. Glaser, U. Henriksson and T. Klason, *Acta Chem. Scand*, 1986, **A40**, 344.
184. R.W. Briggs, F.E. Etzkorn and J.F. Hinton, *J. Magn. Reson.*, 1980, **37**, 523.
185. J.F. Hinton and G.L. Turner, *J. Magn. Reson.*, 1984, **59**, 262.
186. J.F. Hinton, G.L. Turner and F.S. Millett, *J. Magn. Reson.*, 1981, **45**, 42.

187. G.L. Turner, J.F. Hinton and F.S. Millett, *Biochemistry*, 1982, **21**, 646.
188. G.L. Turner, J.F. Hinton and F.S. Millett, *J. Magn. Reson.*, 1983, **51**, 205.
189. J.F. Hinton, G.L. Turner, G. Young and K.R. Metz, *Pure Appl. Chem.*, 1982, **54**, 2359.
190. J.F. Hinton, G. Young and F.S. Millett, *Biochim. Biophys. Acta*, 1983, **727**, 217.
191. T.T. Nakashima and D.L. Rabenstein, *J. Magn. Reson.*, 1983, **51**, 223.
192. P.G. Harrison, M.A. Healy and A.T. Steel, *Inorg. Chim. Acta*, 1982, **67**, L15.
193. J. Otera, A. Kusaba, T. Hinoishi and Y. Kawasaki, *J. Oraganomet. Chem.*, 1982, **228**, 223.
194. P.A.W. Dean, *Can. J. Chem.*, 1982, **60**, 2921.
195. P.A.W. Dean, *Can. J. Chem.*, 1983, **61**, 1795.
196. A. Lycka, M. Nadvornik, K. Handlir and J. Holecek, *Coll. Czech. Chem. Commun.*, 1984, **49**, 2903.
197. J. Holecek, K. Handlir, A. Lycka, T.K. Chattopadhyay, B. Majee and A.K. Kumar, *Coll. Czech. Chem. Commun.*, 1986, **51**, 1100.
198. J. Holecek, A. Lycka and R. Wagener, *Coll. Czech. Chem. Commun.*, 1986, **51**, 2116.
199. A. Lycka and J. Holecek, *Inorg. Chim. Acta*, 1986, **122**, 15.
200. J. Holecek, K. Handlir, V. Cerny, M. Nadvornik and A. Lycka, *Polyhedron*, 1987, **7**, 1037.
201. S.J. Blunden, P.A. Cusack and D.G. Gillies, *Magn. Reson. Chem.*, 1986, **24**, 921.
202. K.B. Dillon and A. Marshall, *J. Chem. Soc. Dalton Trans.*, 1987, 315.
203. B.S. Saraswat and J. Mason, *Polyhedron*, 1986, **9**, 1449.
204. C.D. Chandler, G.D. Fallon, A.J. Koplick and B.O. West, *Aust. J. Chem.*, 1987, **40**, 1427.
205. C.J. Cardin and A. Roy, *Inorg. Chim. Acta*, 1986, **125**, 63.
206. M.L. Bleam, C.F. Anderson and M.T. Record, *Biochemistry*, 1983, **22**, 5418.
207. M.L. Bleam, C.F. Anderson and M.T. Record, *Proc. Natl Acad. Sci. USA*, 1980, **77**, 3085.
208. Y.H. Mariam and W.D. Wilson, *J. Am. Chem. Soc.*, 1983, **105**, 627.
209. A. Delville, P. Laszlo and R. Schyns, *Biophys. Chem.*, 1986, **24**, 121.
210. W.H. Braunlin, C.F. Anderson and M.T. Record, *Biopolymers*, 1986, **25**, 205.
211. M. Casu, A. Lai, C. Meloni and G. Saba, *Chem. Phys. Lett.*, 1987, **137**, 533.
212. W.H. Braunlin, C.F. Andersson and M.T. Record, *Biochemistry*, 1987, **26**, 7724.
213. W.H. Braunlin and L. Nordenskiold, *Eur. J. Biochem*, 1984, **142**, 133.
214. L. Nordenskiold, D.K. Chang, C.F. Anderson and M.T. Record, *Biochemistry*, 1984, **23**, 4309.
215. H. Sterk, H. Schrunner and A. Sax, *J. Mol. Liq.*, 1985, **30**, 171.
216. D.R. Burton, S. Forsén and P. Reimarsson, *Nucleic Acids Res.*, 1981, **9**, 1219.
217. L. van Dijk, M.L.H. Gruwell, W. Jesse, J. de Bleijser and J.C. Leyte, *Biopolymers*, 1987, **26**, 261.
218. H. Grasdalen and B.J. Kvam, *Macromolecules*, 1986, **19**, 1913.
219. M. Levij, J. de Bleijser and J.C. Leyte, *Chem. Phys. Lett.*, 1981, **83**, 183.
220. M. Levij, J. de Bleijser and J.C. Leyte, *Chem. Phys. Lett.*, 1982, **87**, 34.
221. C.W.R. Mulder, J. de Bleijser and J.C. Leyte, *Chem. Phys. Lett.*, 1980, **69**, 354.
222. E. Florin, *Macromolecules*, 1985, **18**, 360.
223. R.A. Komoroski, *Polym. Prepr. Am. Chem. Soc. Div. Polym. Chem.*, 1980, **19**, 341.
224. L. Piculell, B. Lindman and R. Einarsson, *Biopolymers*, 1984, **23**, 1683.
225. G. Gunnarsson and H. Gustavsson, *J. Chem. Soc. Faraday Trans. 1*, 1982, **78**, 2901.
226. F.M. Raushel and J.J. Villafranca, *Biochemistry*, 1980, **19**, 5481.
227. J.J. Villafranca and F.M. Raushel, *Ann. Rev. Biophys. Bioeng.*, 1980, **9**, 363.
228. F.M. Raushel and J.J. Villafranca, *J. Am. Chem. Soc.*, 1980, **102**, 6618.
229. J.M. van Divender and C.M. Grisham, *J. Biol. Chem.*, 1985, **25**, 14060.
230. P.G. Kasrzyk, E. Whalen-Pederson, P.M. Andersson and J.J. Villafranca, *Bioorg. Chem.*, 1985, **13**, 98.
231. F.M. Raushel, P.M. Anderson and J.J. Villafranca, *Biochemistry*, 1983, **22**, 1872.

232. G.I. Rhyu, W.J. Ray and J.L. Markley, *Biochemistry*, 1985, **24**, 2536.
233. A. Delville, J. Grandjean, P. Laszlo, C. Gerday, H. Brezeska and W. Drabikowski, *Eur. J. Biochem.*, 1980, **109**, 515.
234. A. Delville, J. Grandjean, P. Laszlo, G. Gerday, Z. Grabarek and W. Drabikavski, *Eur. J. Biochem.*, 1980, **105**, 289.
235. H. Gustavsson, G. Siegel, B. Lindman and L.-A. Fransson, *Biochim. Biophys. Acta*, 1981, **677**, 23.
236. W.H. Braunlin, H.J. Vogel and S. Forsén, *Eur. J. Biochem.*, 1984, **142**, 139.
237. M. Svard and T. Drakenberg, *Acta. Chem. Scand.*, 1986, **B46**, 689.
238. T. Andersson, T. Drakenberg, S. Forsén and E. Thulin, *FEBS Lett.*, 1981, **125**, 39.
239. S. Forsén, T. Andersson, T. Drakenberg, E. Thulin and M. Svard, *Fed. Proc.*, 1982, **41**, 2981.
240. T. Andersson, T. Drakenberg, S. Forsén, E. Thulin and M. Sward, *J. Am. Chem. Soc.*, 1982, **104**, 576.
241. T. Drakenberg, S. Forsén and H. Lilja, *J. Magn. Reson.* 1983, **53**, 412.
242. A. Teleman, T. Drakenberg and S. Forsén, *Biochim. Biophys. Acta*, 1986, **873**, 204.
243. M.-D. Tsai, T. Drakenberg, E. Thulin and S. Forsén, *Biochemistry*, 1987, **26**, 3635.
244. H.J. Vogel, T. Andersson, W.H. Braunlin, T. Drakenberg, and S. Forsén, *Biochem. Biophys. Res. Commun.*, 1984, **122**, 1350.
245. T. Shimizu, M. Hatano, S. Nagao and Y. Nozawa, *Biochem. Biophys. Res. Commun.*, 1982, **106**, 1112.
246. T. Shimizu and M. Hatano, *Inorg. Chem.*, 1985, **24**, 2003.
247. T. Shimizu and M. Hatano, *Inorg. Chim. Acta*, 1988, **152**, 257.
248. S. Forsén, T. Andersson, T. Drakenberg, H. Lilja and E. Thulin, *Period. Biol. (Jugoslav.)*, 1983, **85**, 31.
249. H.J. Vogel and W.H. Braunlin, *J. Magn. Reson.*, 1985, **62**, 42.
250. S. Forsén, T. Drakenberg and H. Wennerstrom, *Q. Rev. Biophys.*, 1987, **19**, 83.
251. S. Linse, P. Brodin, T. Drakenberg, E. Thulin, P. Sellers, K. Elmden, T. Grundstrom and S. Forsén, *Biochemistry*, 1987, **26**, 6723.
252. T. Andersson, T. Drakenberg, S. Forsén, T. Wieloch and M. Lindstrom, *FEBS Lett.*, 1981, **123**, 115.
253. S. Forsén, T. Andersson, T. Drakenberg, E. Thulin and T. Wieloch, in *Advances in Solution Chemistry* (ed. I. Dertini, L. Lunazzi and A. Dei), p. 192. Plenum, 1981.
254. T. Andersson, T. Drakenberg, S. Forsén, E. Thulin and M. Svard, *J. Am. Chem. Soc.*, 1982, **104**, 576.
255. W.H. Braunlin, H.J. Vogel, T. Drakenberg and A. Bennick, *Biochemistry*, 1986, **25**, 584.
256. M. Svard, T. Drakenberg, T. Andersson and P. Fernlund, *Eur. J. Biochem.*, 1986, **158**, 373.
257. T. Andersson, E. Chiancone and S. Forsén, *Eur. J. Biochem.*, 1982, **125**, 103.
258. D.W. Urry, T.L. Trapane and C.M. Venkatachalam, *Calcif. Tissue*, 1982, **34**, S41.
259. T. Drakenberg, T. Andersson, S. Forsén and T. Wieloch, *Biochemistry*, 1984, **23**, 2387.
230. W.H. Braunlin, T. Drakenberg, and L. Nordenskiold, *Biopolymers*, 1987, **26**, 1047.
261. L. Lerner and D. Torchia, *J. Biol. Chem.*, 1986, **261**, 12706.
262. E. Chiancone, T. Drakenberg, O. Teleman and S. Forsén, *J. Mol. Biol.*, 1985, **185**, 201.
263. M.M. Sarasua, K.A. Koehler, C. Skrzynia and J.M. McDonagh, *J. Biol. Chem.*, 1982, **257**, 14102.
264. E. Bouhoutsos-Brown, C.H. Pletcher, G.L. Nelestuen and R.G. Bryant, *J. Inorg. Biochem.*, 1984, **21**, 337.
265. T. Shimizu and M. Hatano, *Biochem. Biophys. Res. Commun.*, 1982, **104**, 720.
266. T. Shimizu and M. Hatano, *Inorg. Chim. Acta*, 1983, **80**, L37.
267. D. Murk Rose, M.L. Bleam, M.T. Record and R.G. Bryant, *Proc. Natl Acad. Sci. USA*, 1980, **77**, 6289.

268. D. Murk Rose, C.F. Polnaszek and R.G. Bryant, *Biopolymers*, 1982, **21**, 653.
269. B. Borak, C. Chen, W. Egan, M. Miller, A. Wlodawer and J.S. Cohen, *Biochemistry*, 1985, **24**, 2058.
270. A. Butler, M.J. Danzitz and H. Eckert, *J. Am. Chem. Soc.*, 1987, **109**, 1864.
271. H. Viltar and D. Rehder, *Inorg. Chim. Acta*, 1987, **136**, L7.
272. H.C. Lee, J.K. Gard, T.L. Brown and E. Oldfield, *J. Am. Chem. Soc.*, 1985, **107**, 4087.
273. L. Baltzar, E.D. Becker, R.G. Tschudiu and O.A. Gansow, *J. Chem. Soc. Chem. Commun.*, 1985, 1040.
274. G.N. La Mar, C.M. Dellinger and S.S. Sankar, *Biochem. Biophys. Res. Commun.*, 1985, **128**, 628.
275. L. Baltzar and M. Landergren, *J. Chem. Soc. Chem. Commun.*, 1987, 32.
276. T. Raj, C.R. Bennet and R.G. Bryant, *Anal. Biochem.*, 1980, **106**, 373.
277. S. Bristow, C.D. Garner, S.K. Hagyard, G.A. Morris, J.R. Nicholson and C.F. Mills, *J. Chem. Soc. Chem. Commun.*, 1985, 4709.
278. B.R. Bobsein and R.J. Myers, *J. Am. Chem. Soc.*, 1980, **102**, 2454.
279. B.R. Bobsein and R.J. Myers, *J. Biol. Chem.*, 1981, **256**, 5313.
280. I. Morishima, M. Kurono and Y. Shiro, *J. Biol. Chem.*, 1986, **261**, 9391.
281. J.L. Sudmeier, S.J. Bell, M.C. Storm and M.F. Dunn, *Science*, 1981, **202**, 560.
282. T. Shimizu and M. Hatano, *Inorg. Chim. Acta*, 1983, **76**, L17.
283. M. Kodaka, T. Shimizu and M. Hatano, *Inorg. Chim. Acta*, 1983, **78**, L55.
284. R.W. Briggs and I.M. Armitage, *J. Biol. Chem.*, 1982, **257**, 1259.
285. J.D. Otvos, R.W. Olafson and I.M. Armitage, *J. Biol. Chem.*, 1982, **257**, 2427.
286. Y. Boulanger, C.M. Goodman, C.P. Forte, S.W. Fesik and I.M. Armitage, *Proc. Natl Acad. Sci. USA*, 1983, **80**, 1501.
287. I.M. Armitage, J.D. Otvos, R.W. Briggs and Y. Boulanger, *Fed. Proc.*, 1982, **41**, 2974.
288. J.D. Otvos and I.M. Armitage, *Proc. Natl Acad. Sci. USA*, 1980, **77**, 7094.
289. J.D. Otvos, H.R. Engeseth and S. Wehrli, *Biochemistry*, 1985, **24**, 6735.
290. Y. Boulanger, I.M. Armitage, K.-A. Miklossy and D.R. Winge, *J. Biol. Chem.*, 1982, **257**, 13717.
291. D.G. Nettesheim, H.R. Engeseth and J.D. Otvos, *Biochemistry*, 1985, **24**, 6744.
292. J.K. Nicholson, P.J. Sadler, K. Cain, D.E. Holt, M. Webb and G.E. Hawkes, *Biochem. J.*, 1983, **22**, 1046.
293. D.M. Templeton, P.A.W. Dean and M.G. Cherian, *Biochem. J.*, 1986, **234**, 685.
294. P.A.W. Dean, A.Y.C. Law, J.A. Szymanska and M.J. Stillman, *Inorg. Chim. Acta*, 1983, **78**, 275.
295. M. Vasak, G.E. Hawkes, J.K. Nicholson and P.J. Sadler, *Biochemistry*, 1985, **24**, 740.
296. D. Live, I.M. Armitage, D.C. Dalgarno and D. Cowburn, *J. Am. Chem. Soc.*, 1985, **107**, 1775.
297. J.D. Otvos and I.M. Armitage, *Biochemistry*, 1980, **19**, 4031.
298. P. Gettins and J.E. Coleman, *Fed. Proc.*, 1982, **41**, 2966.
299. P. Gettins and J.E. Coleman, *J. Biol. Chem.*, 1983, **258**, 396.
300. P. Gettins and J.E. Coleman, *J. Biol. Chem.*, 1984, **259**, 4987.
301. P. Gettins and J.E. Coleman, *J. Biol. Chem.*, 1984, **259**, 4991.
302. A.J.M. Schoot Uiterkamp, I.M. Armitage and J.E. Coleman, *J. Biol. Chem.*, 1980, **255**, 3911.
303. J.L. Evelhoch, D.F. Bocian and J.L. Sudmeier, *Biochemistry*, 1981, **20**, 4951.
304. K.M. Welsh and B.S. Cooperman, *Biochemistry*, 1984, **23**, 4947.
305. K.M. Welsh, I.M. Armitage and B.S. Cooperman, *Biochemistry*, 1983, **22**, 1046.
306. A.R. Palmer, D.B. Bailey, W.D. Benhke, A.D. Cardin, P.P. Yang and P.D. Ellis, *Biochemistry*, 1980, **19**, 5063.
307. P.D. Ellis, P.P. Yang and A.R. Palmer, *J. Magn. Reson.*, 1983, **52**, 254.

308. L. Battacharyya, P.S. Marchetti, P.D. Ellis and C.F. Brewer, *J. Biol. Chem.*, 1987, **262**, 5616.
309. P. Linse, H. Gustavsson, B. Lindman and T. Drakenberg, *J. Magn. Reson.*, 1981, **45**, 133.
310. T. Andersson, T. Drakenberg, S. Forsén and E. Thulin, *Eur. J. Biochem.*, 1982, **126**, 501.
311. S. Forsén, E. Thulin, T. Drakenberg, J. Krebs and K. Seamon, *FEBS Lett.*, 1980, **117**, 189.
312. A. Andersson, S. Forsén, E. Thulin and H. Vogel, *Biochemistry*, 1983, **22**, 2309.
313. A. Andersson, T. Drakenberg, S. Forsén and E. Thulin, *Eur. J. Biochem.*, 1983, **134**, 459.
314. E. Thulin, A. Andersson, T. Drakenberg, S. Forsén and H.J. Vogel, *Biochemistry*, 1984, **23**, 1862.
315. S. Linse, T. Drakenberg and S. Forsén, *FEBS Lett.*, 1986, **199**, 28.
316. J. Krebs, E. Carafoli, E. Thulin and S. Forsén, *Ann. NY Acad. Sci.*, 1980, **356**, 397.
317. S. Forsén, T. Andersson, T. Drakenberg, O. Teleman, E. Thulin and H.J. Vogel, in *Calcium Binding Proteins 1983* (ed. B. deBernard *et al.*). Elsevier/North-Holland, Amsterdam, 1983.
318. H.J. Vogel, T. Drakenberg, S. Forsén, J.D. O'Neil and T. Hofmann, *Biochemistry*, 1985, **24**, 3870.
319. S. Forsén, S. Linse, P. Brodin, T. Drakenberg, E. Thulin, P. Sellers, C. Johansson, B. Wendt and T. Grundstrom, in *Alfred Benson Symposium 26*, p. 249. Munksgaard, Copenhagen, 1988.
320. S. Forsén, T. Drakenberg, E. Thulin, P. Brodin, S. Linse, P. Sellers and K. Elmdén, in *Calcium Binding Proteins in Health and Disease* (ed. A.W. Norman *et al.*). Academic Press, New York, 1986.
321. S. Forsén, T. Drakenberg, S. Linse, P. Brodin, P. Sellers, C. Johansson, E. Thulin and T. Grundstrom, in *Metal Ions in Biology*, Vol. 25 (ed. H. Siegel), p. 255. Marcel Dekker, New York, 1989.
322. S. Linse, P. Brodin, C. Johansson, E. Thulin, T. Grundstrom and S. Forsén, *Nature*, 1988, **335**, 651.
323. S. Forsén, M. Akke, P. Brodin, P. Bayley, T. Drakenberg, T. Grundstrom, C. Johansson, S. Linse, S. Martin and E. Thulin, in *Calcium Binding Proteins in Health and Disease* (ed. A. W. Norman *et al.*). Academic Press, New York, 1989.
324. T. Drakenberg, M. Svard, A. Cavé and J. Parello, *Biochem. J.*, 1985, **227**, 711.
325. A. Cavé, A. Saint-Yves, J. Parcello, M. Sward, E. Thulin and B. Lindman, *Mol. Cell Biochem.*, 1982, **44**, 161.
326. O. Teleman, T. Drakenberg, S. Forsén and E. Thulin, *Eur. J. Biochem.*, 1983, **134**, 453.
327. P.D. Ellis, P. Strang and J.D. Potter, *J. Biol. Chem.*, 1984, **259**, 10348.
328. P.D. Ellis, P.S. Marchetti, P. Strang and J.D. Potter, *J. Biol. Chem.*, 1988, **263**, 10284.
329. T. Drakenberg, S. Forsén, E. Thulin and H.J. Vogel, *J. Biol. Chem.*, 1987, **262**, 672.
330. D.B. Bailey, P.D. Ellis and J.A. Fee, *Biochemistry*, 1980, **19**, 591.
331. R.V. Prigodich, T. O'Connor and J.E. Coleman, *Biochemistry*, 1985, **24**, 6291.
332. K. Aalamo, J. Krane, C. Little and C.S. Storm, *Biochem. Soc. Trans.*, 1982, **10**, 367.
333. K. Aalamo, L. Hansen, E. Hough, K. Jynge, J. Krane, C. Lithe and C.B. Storm, *Biochemistry*, 1984, **8**, 27.
334. H.R. Engeseth, D.R. McMillin and J.D. Otvos, *J. Biol. Chem.*, 1984, **259**, 4822.
335. D. Live, C.L. Kojiro, D. Cowburn and J.L. Markley, *J. Am. Chem. Soc.*, 1985, **107**, 3043.
336. P. Gettins, *J. Biol. Chem.*, 1986, **261**, 15513.
337. L.J. Berliner, P.D. Ellis and K. Murakami, *Biochemistry*, 1983, **22**, 5061.
338. G.I. Rhyu, W.J. Ray and J.L. Markley, *Biochemistry*, 1985, **24**, 2536.
339. E.O. Martins and T. Drakenberg, *Inorg. Chem. Acta*, 1982, **67**, 71.
340. J.L. Sudmeier and D.B. Green, in *The Coordination Chemistry of Metalloenzymes* (ed. I. Bertini and R.S. Drago), p. 35. Reidel, New York, 1983.
341. I. Bertini, E. Borgi, C. Luchinat and A. Scozzafava, *J. Mol. Struct.*, 1984, **113**, 191.

342. I. Bertini, C. Luchinat and L. Messori, *J. Am. Chem. Soc.*, 1983, **105**, 1347.
343. I. Bertini, L. Messori, G.C. Pellacani and M. Sola, *Inorg. Chem.*, 1988, **27**, 761.
344. G.D. Markham, *J. Biol. Chem.*, 1986, **261**, 1507.
345. K.A.W. Hill, S.A. Steiner and F.J. Castellino, *J. Biol. Chem.*, 1987, **262**, 7098.
346. K.A.W. Hill and F.J. Castellino, *J. Biol. Chem.*, 1987, **262**, 7105.
347. J.F. Hinton, G. Young and F.S. Millett, *Biochemistry*, 1982, **21**, 651.
348. J.F. Hinton, G. Young and F.S. Millett, *Biochim. Biophys. Acta*, 1983, **727**, 217.
349. J.F. Hinton, R.E. Koeppe, D. Shungu, W.L. Whaley, J.A. Paczkowski and F.S. Millett, *Biophys. J.*, 1986, **49**, 571.
350. J.F. Hinton, W.L. Whaley, D. Shungu, R.E. Koeppe and F.S. Millett, *Biophys. J.*, 1986, **50**, 539.
351. D.C. Shungu, J.F. Hinton, R.E. Koeppe and F.S. Millett, *Biochemistry*, 1986, **25**, 6103.
352. D.W. Urry, C.M. Venkatachalam, A. Spisni, P. Lauger and M.A. Khaled, *Proc. Natl Acad. Sci. USA*, 1980, **77**, 2028.
353. D.W. Urry, C.M. Venkatachalam, S. Spisni, R.J. Bradley, T.L. Trapane and K.U. Prasad, *J. Membr. Biol.*, 1980, **55**, 29.
354. D.W. Urry, T.L. Trapane, C.M. Venkatachalam and K.U. Prasad, *J. Phys. Chem.*, 1983, **87**, 2918.
355. D.W. Urry, T.L. Trapane, C.M. Venkatachalam and K.U. Prasad, *Can. J. Chem.*, 1985, **63**, 1976.
356. D.W. Urry, T.L. Trapane, R.A. Brown, C.M. Venkatachalam and K.U. Prasad, *J. Magn. Reson.*, 1985, **65**, 43.
357. D.W. Urry, T.L. Trapane and C.M. Venkatachalam, *J. Membr. Biol.*, 1986, **89**, 107.
358. D.W. Urry, T.L. Trapane, C.M. Venkatachalam and K.U. Prasad, *J. Am. Chem. Soc.*, 1986, **108**, 1448.
359. F.G. Riddell, S. Arumugan, P.J. Brophy, B.C. Cox, M.C.H. Payne and T.E. Southon, *J. Am. Chem. Soc.*, 1988, **110**, 734.
360. F.G. Riddell and M.K. Hayer, *Biochim. Biophys. Acta*, 1985, **817**, 313.
361. G.A. Elgavish and A. Elgavish, *Biochem. Biophys. Res. Commun.*, 1985, **128**, 746.
362. R. Melamud, M. Risk and H. Gilboa, *Biochim, Biophys. Acta*, 1981, **678**, 311.
363. T. Ogino, J.A. den Hollander and R.G. Shulman, *Proc. Natl Acad. Sci. USA*, 1983, **80**, 5185.
364. P.J. Brophy, M.K. Hayer and F.G. Riddell, *Biochem. J.*, 1983, **210**, 916.
365. J.W. Petegrew, D.E. Woessner, N.J. Minshew and T. Glonek, *J. Magn. Reson.*, 1984, **57**, 185.
366. J.W. Petegrew, T. Glonek, N.J. Minshew and D.E. Woessner, *J. Magn. Reson.*, 1985, **63**, 439.
367. R.L. Ong and H.C. Cheung, *Biophys. Chem.*, 1986, **23**, 237.
368. H. Höfeler, D. Jensen, M.M. Pike, J.L. Dalayre, V.P. Cirillo, C.S. Springer, E.T. Fossel and J.A. Balshi, *Biochemistry*, 1987, **26**, 4953.
369. A.W.H. Jans, R. Willems, E.R. Kellenbach and R.K.H. Kinne, *Magn. Reson. Med.*, 1988, **7**, 292.

NMR Studies of Ligand–Macromolecule Interactions

DAVID J. CRAIK and KERRY A. HIGGINS

School of Pharmaceutical Chemistry, Victorian College of Pharmacy Limited, Victoria 3052, Australia

1. Introduction 61
2. Methods 62
2.1. Chemical-shift measurements 62
2.2. Relaxation-time measurements and linewidth changes . . 68
2.3. Magnetization-transfer experiments 72
2.4. Nuclear-Overhauser-effect measurements 76
2.5. Dynamic lineshape analysis 88
2.6. Paramagnetic probes 90
2.7. Other methods 95
3. Nuclear probes 97
3.1. ^{1}H NMR 97
3.2. ^{2}H NMR 98
3.3. ^{3}H NMR 99
3.4. ^{13}C NMR 99
3.5. ^{15}N NMR 100
3.6. ^{19}F NMR 102
3.7. ^{31}P NMR 102
3.8. Other nuclei 103
4. Applications 103
4.1. Protein (enzyme)–ligand interactions 114
4.2. Nucleic acids, membranes 132
5. Summary and conclusions 133
Acknowledgements 133
References 133

1. INTRODUCTION

The interaction between small molecules and large molecules is an essential facet of a wide range of biological processes. The "small" molecules may include neurotransmitters, hormones, endogenous effector ligands, drugs, enzyme substrates, coenzymes and inhibitors, while the large molecules may

ANNUAL REPORTS ON NMR SPECTROSCOPY
VOLUME 22 ISBN 0-12-505322-3

Copyright © 1989 Academic Press Limited
All rights of reproduction in any form reserved

be nucleic acids or proteins, including enzymes, transport proteins, or membrane-bound or nuclear "receptors". A detailed knowledge of the way in which the small molecules interact with their target macromolecules is an essential starting point for a complete understanding of how biological effects mediated by the macromolecule are achieved.

NMR spectroscopy has, of course, been widely applied in the separate study of small and large molecules. Studies in the former category include the key areas of structure determination and conformational analysis of organic species, while in the field of large molecules NMR is becoming an increasingly important tool in the three-dimensional (3D) structure determination of medium-sized proteins. Rather than examining these separate areas, this review will concentrate on NMR studies that involve the *interaction* between small and large molecules. The NMR methods and nuclei commonly used in such studies are described first, followed by applications in a range of chemical and biological problems.

2. METHODS

NMR is perhaps unique amongst the various forms of spectroscopy in that it has such a large number of spectral parameters that may be measured and used in solving chemical or biological problems. The primary parameters and methods that are useful in the study of small-molecule–large-molecule interactions are noted below.

2.1. Chemical-shift measurements

When a ligand binds to a macromolecule there will generally be a change in the immediate chemical environment of many of the nuclei on the ligand (and on the macromolecule), and thus there will potentially be a number of chemical-shift changes. Whether these measured shift changes will be of use in defining the interaction depends on a number of factors, including the size of the change and the nature of the binding kinetics.

Binding kinetics play a particularly important role in determining spectral appearance. The two extreme cases that may be encountered in studies of ligand binding are fast and slow exchange. As has been carefully pointed out by a number of authors,[1-4] these terms should always be quantified in terms of the parameter being measured: in this case, fast and slow exchange on the *chemical-shift* timescale. For a ligand exchanging between two states, free and bound, which have chemical shifts δ_A and δ_B

respectively, the appropriate conditions are

$$\text{slow exchange} \qquad k \ll |\delta_A - \delta_B|, \tag{1}$$

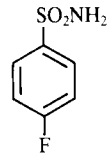
$$\text{fast exchange} \qquad k \gg |\delta_A - \delta_B|, \tag{2}$$

where k is the limiting rate constant for the exchange process for the macromolecule–ligand interaction. In the slow-exchange case separate signals for the free and bound ligand (and macromolecule) are potentially observable, while for fast exchange a single "averaged" resonance will be seen, with a shift given by

$$\delta^{obs} = P_A\,\delta_A + P_B\,\delta_B, \tag{3}$$

where δ_A and δ_B are the chemical shifts of the free and bound states respectively, and P_A and P_B are their relative mole fractions. The fast-exchange case generally applies to weakly binding ligands ($K_a \approx 10^3\ M^{-1}$), and chemical shifts of the free and bound forms may be extracted from plots of observed chemical-shift versus ligand/macromolecule ratio by fitting the data to the appropriate equilibrium expressions.[5] The derived bound shift may then be used to deduce information about the bound environment. The above plot is also a convenient method of determining the binding constant for the macromolecule–ligand interaction, although the need for caution in ensuring that the system is in "fast" rather than "intermediate" exchange has been stressed.[5]

The slow-exchange condition generally applies for tight-binding ligands ($K_a \geqslant 10^6\ M^{-1}$), and in this case determination of the bound shift is, in principle, more direct. However, whether both free- and bound-ligand signals are observed depends on a number of factors, including the relative mole ratios of free and bound species, the linewidth of the bound-ligand resonance, and the degree of overlap from other resonances. The latter factor may be reduced in ^{19}F NMR studies or in studies involving ^{13}C or ^{15}N labelling so that protein resonances do not interfere with observed ligand resonances, and in these cases bound-ligand signals are often readily detected, as seen in a number of examples in following sections. Figure 1 shows, for example, ^{19}F spectra of mixtures of the enzyme carbonic anhydrase and the inhibitor 4-fluorobenzenesulphonamide (**1**) at mole



1

ratios indicated on the traces. The broadened peak for the bound complex ($\delta \approx -6$ ppm) is in slow exchange with free inhibitors ($\delta = 0$ ppm). Note how the slow-exchange condition readily allows the stoichiometry of the complex to be determined, in this case 2 : 1.

Direct detection of signals from bound-ligand resonances is often much

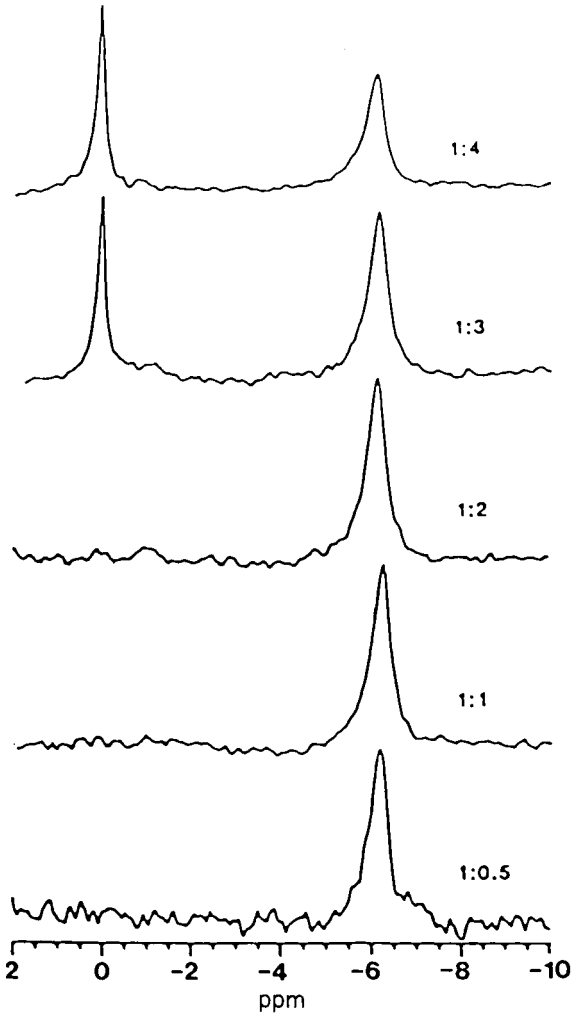


Fig. 1. ^{19}F NMR spectra at 282 MHz of the 4-fluorobenzenesulphonamide–carbonic-anhydrase-I system at various ratios of enzyme to inhibitor, as indicated on the traces. The peak at -6 ppm is due to bound inhibitor. The enzyme concentration was 1 mM at pH 7.2 in D_2O at 25°C. (Reprinted with permission from Ref. 6. © 1989 American Chemical Society.)

more difficult in ^{1}H NMR studies. The saturation-transfer technique (Section 2.3) is an extremely powerful way of overcoming this difficulty, and in many cases allows bound-ligand chemical shifts to be determined, even if the resonances are not directly detected in the spectrum, by transferring saturation from bound-ligand to more readily detected free-ligand signals. A number of early studies of ^{1}H NMR chemical-shift changes on coenzyme binding to dihydrofolate reductase made use of this technique (see e.g. Ref. 7).

While many of the above comments have related to ligand signals, in principle, changes in shifts on the macromolecule can also yield very significant information about the interaction. At the outset, however, it should be pointed out that perhaps the greatest difficulty in the interpretation of such chemical-shift changes is that it is often impossible to separate the direct effects due to ligand binding from those due to secondary conformation changes. For example, if the methyl protons of a threonine group on an enzyme shift upfield by 0.5 ppm following the binding of an aromatic inhibitor, this does not necessarily mean that the ligand-binding site is anywhere near the threonine residue, as a secondary conformational change in the enzyme may well account for the shift change.

In ^{1}H NMR experiments practical difficulties in making use of signals from the macromolecule include the problem of assignment and peak overlap. Two-dimensional NMR methods assist in both these areas and are increasingly being used in the study of macromolecular interactions. Figure 2 shows, for example, the use of 2D COSY spectra to detect chemical shift changes in aromatic resonances from the kringle 4 protein on binding of the ligands lysine and ε-aminocaproic acid (εACA).[8]

One area where chemical shifts from macromolecule resonances are widely used to monitor ligand interactions relates to pH profiles of ionizable groups on proteins. NMR is one of the few techniques that allows pK_a values of particular residues to be obtained, and changes in pK_a on ligand binding often yield significant information about the interaction. Histidine residues are widely studied by this technique because the C2–H proton is often well-resolved from other peaks,[2] and its chemical shift changes significantly with pH. Early studies showed, for example, increases of 1.2–1.8 pH units in the pK_a values of the active-site histidine of ribonuclease on the binding of mononucleotides, due to interactions between the histidine and phosphate groups.[2,9] The resolution of histidines is such that changes in pK_a can be determined even for the binding of very large ligands, for example for heparin to antithrombin III,[10,11] or in studies of protein–protein interactions (see e.g. Ref. 12).

The use of chemical shifts to determine pK_a and charge states also, of course, applies to ligand signals. Indeed, this is probably one of the most

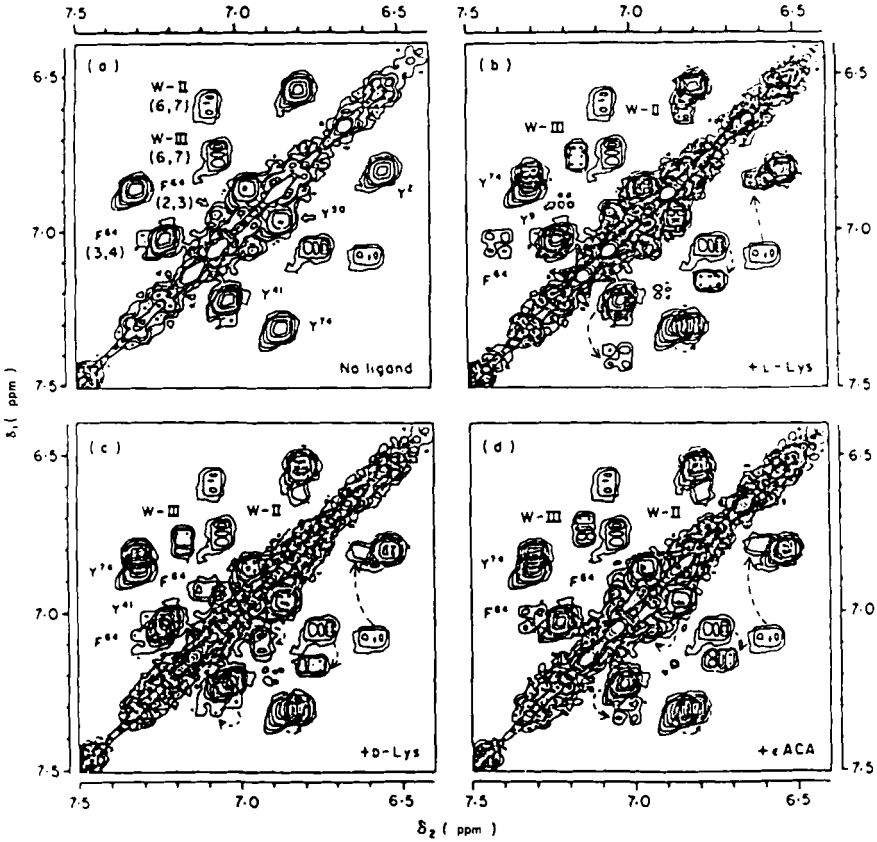


Fig. 2. Contour plots of the COSY spectra of kringle 4 at 300 MHz: aromatic region. (a) Kringle 4 with no added ligand. Off-diagonal cross-peaks are labelled according to their resonance assignments.[8] The numbers in parentheses identify cross-peaks according to the matrix convention whereby the first digit labels the row proton and the second indicates the column proton. Thus, for example, connectivity 6, 7 for W-II (Trp^{62}) in the upper-left triangle of spectrum (a) indicates that the indole H6 signal appears at a higher field position relative to the *J*-coupled vicinal H7. (b)–(d) Spectra of kringle 4 in the presence of excess ligand (heavy trace) superimposed on the spectrum (a) of kringle 4 with no ligand (light trace): (b) + L-Lys; (c) + D-Lys; (d) εACA. Shifts induced on the aromatic protons H7 of TrpII (Trp^{62}), H7 of TrpIII (Trp^{72}), H4 of Phe^{64} and H3,5 of Tyr^{74} due to ligand additions are indicated by broken-line arrows. Kringle 4 concentration, 1 mM, pH* 7.2, 310 K. (Reprinted with permission from Ref. 8. © 1989 Academic Press Limited.)

widely used applications of chemical shifts in the study of macromolecule–ligand interactions. A recent example is shown in Fig. 3, which is concerned with determination of the ionization state of methotrexate bound to a mutant dihydrofolate reductase, denoted dhfr-W21L.[13] Using ^{13}C-labelled methotrexate, it was found that the shift of C2 for methotrexate in the bound state (*ca.* 90.9 ppm), in either the presence or absence of coenzyme, corresponded more closely to the shift of N1-protonated methotrexate (89.2 ppm) than to that of the unprotonated species (95.1 ppm). From this it was concluded that methotrexate is protonated when bound to the mutant enzyme, as had earlier been concluded for the wild-type enzyme.[14]

Other recent illustrative examples include the use of ^{13}C NMR to determine the charge state of isocitrate bound to isocitrate dehydrogenase[15] and ^{15}N NMR to determine the ionization state of the inhibitor 4-fluorobenzenesulphonamide (**1**) bound to carbonic anhydrase.[6]

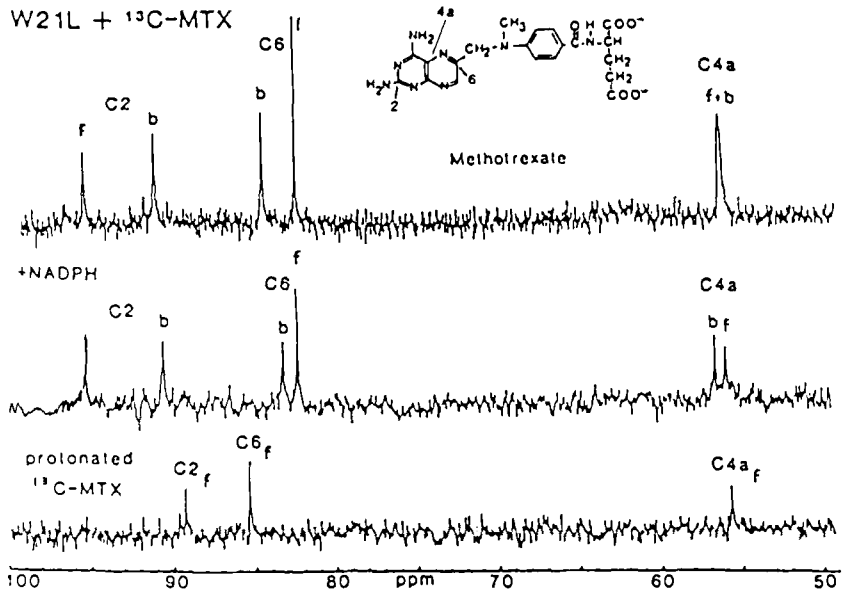


Fig. 3. Top: 125 MHz ^{13}C NMR spectra at 298 K of a sample containing [2,4a,6-^{13}C]methotrexate and dhfr-W21L in a ratio of 2 : 1 at pH 6.5* (bound and free methotrexate carbon resonances are indicated by "b" and "f"). Middle: same sample as in the top spectrum but with two equivalents of NADPH added. Bottom: [2,4a,6-^{13}C]methotrexate at pH* 2 in the absence of enzyme. (Reprinted with permission from Ref. 13. © 1989 American Chemical Society.)

2.2. Relaxation-time measurements and linewidth changes

The spin–lattice relaxation time T_1 and the spin–spin relaxation time T_2 are very dependent on both overall and internal molecular mobility, and hence provide a sensitive probe of binding. Measured relaxation times are potentially composed of contributions from several mechanisms such as dipole–dipole, chemical-shift anisotropy, spin rotation and quadrupolar interactions. In many cases the dipole–dipole interaction dominates and the dependence of relaxation parameters on motion is given by the following equations for relaxation of spin I by spin S:[16]

$$\frac{1}{T_1} = \frac{2}{15} \frac{\gamma_I^2 \gamma_S^2 S(S+1)\hbar^2}{r_{IS}^6} [J(\omega_I - \omega_S) + 3J(\omega_I) + 6J(\omega_I + \omega_S)], \quad (4)$$

$$\frac{1}{T_2} = \frac{1}{15} \frac{\gamma_I^2 \gamma_S^2 S(S+1)\hbar^2}{r_{IS}^6} \times [J(\omega_I - \omega_S) + 3J(\omega_I) + 6J(\omega_I + \omega_S) + 4J(0) + 6J(\omega_S)]. \quad (5)$$

Here the physical constants have their usual meanings and the $J(\omega)$ terms are spectral densities, which depend on the nature (e.g. isotropic/anisotropic) of the motion. For simple isotropic motion

$$J(\omega) = \frac{\tau_c}{1 + \omega^2 \tau_c^2} \quad (6)$$

where ω is the Larmor frequency and τ_c is the correlation time for molecular tumbling. Related expressions for a range of more complex motions, including internal flexing motions, have been derived. Measurement of T_1 and T_2 for macromolecular signals thus allows significant information on intramolecular dynamics to be obtained.[16] Changes in the relaxation parameters on ligand binding give some insight into the dynamic aspects of the macromolecule–ligand interaction, and thus provide information complementary to the static aspects of such interactions, which derive from X-ray crystallographic studies of macromolecule–ligand complexes. A recent example of such an approach made use of ^{13}C T_1 and T_2 values from three α-carbons of staphylococcal nuclease to detect a stiffening of the enzyme on binding of an inhibitor.[17] ^{19}F NMR relaxation measurements are also used to probe mobility at binding sites.[18]

Since the correlation time for overall tumbling of macromolecules (or ligands bound to macromolecules) is often significantly greater (10^{-9}–10^{-7} s) than for free ligands ($< 10^{-10}$ s), (4) and (5) show that the relaxation properties of a ligand are markedly affected by binding. Of particular importance are effects on T_2, since these have a direct bearing on

linewidth via

$$\mathrm{LW} = 1/\pi T_2 \tag{7}$$

As was the case for chemical shifts, the exchange kinetics of macromolecule–ligand interactions has a marked influence on relaxation properties and linewidths of observed peaks. "Slow" and "fast" exchange on the relaxation timescale are defined in terms of the size of the rate constant relative to the difference in relaxation rates in the free and bound states. Slow exchange is defined, for example, by

$$k \ll \left| \frac{1}{T_{1,2}^{\mathrm{A}}} - \frac{1}{T_{1,2}^{\mathrm{B}}} \right|, \tag{8}$$

with the opposite inequality applying for fast exchange. In the limit of very slow exchange peaks for bound and free states exhibit relaxation properties characteristic of the individual states, whereas in the limit of very fast exchange the observed relaxation rates are weighted averages:

$$\frac{1}{T_{1,2}^{\mathrm{obs}}} = \frac{P_{\mathrm{A}}}{T_{1,2}^{\mathrm{A}}} + \frac{P_{\mathrm{B}}}{T_{1,2}^{\mathrm{B}}}. \tag{9}$$

General expressions for intermediate conditions have been derived,[1,19] and simplified versions of those appropriate to macromolecule–ligand binding studies have been widely applied.[1,2]

In general, the simplified expressions have been derived for observation of the more easily detected ligand signals under conditions where the free-ligand signal is in excess: $P_{\mathrm{B}} < P_{\mathrm{A}} = 1 - P_{\mathrm{B}} \approx 1$.

For moderately slow exchange the following applies:

$$\frac{1}{T_2^{\mathrm{obs}}} = \frac{1}{T_2^{\mathrm{A}}} + \frac{P_{\mathrm{B}}}{P_{\mathrm{A}}} k_{\mathrm{off}}. \tag{10}$$

Note that it is often useful to discuss trends in T_2 in terms of "excess linewidth", given by

$$\Delta W_{\mathrm{ex}} = \frac{1}{\pi} \left(\frac{1}{T_2^{\mathrm{obs}}} - \frac{1}{T_2^{\mathrm{A}}} \right). \tag{11}$$

Measurement of peak broadening in this regime as a function of macromolecule/ligand ratio allows k_{off} to be determined. Measurement of linewidths of the ^{31}P resonance of the 2′-phosphate of $NADP^+$ in the presence of dihydrofolate reductase provides an example of this approach.[4,20]

For moderately fast exchange where free and bound peaks have no

chemical-shift difference the appropriate equation is†

$$\frac{1}{T_{1,2}^{obs}} = \frac{P_A}{T_{1,2}^{A}} + \frac{P_B}{T_{1,2}^{B} + 1/k_{off}} \tag{12}$$

On the other hand, if two states have a chemical-shift difference, the commonly applied equation[5,21] for T_2 is

$$\frac{1}{T_2^{obs}} = \frac{P_A}{T_2^{A}} + \frac{P_B}{T_2^{B}} + \frac{P_B(1 - P_B)^2 4\pi^2(\delta_A - \delta_B)^2}{k_{off}}. \tag{13}$$

The last term in (13) is often referred to as the "exchange contribution to linewidth". If this term dominates then a plot of excess linewidth versus $P_B(1 - P_B)^2 4\pi^2(\delta_A - \delta_B)^2$ will be linear, while if the second term dominates or (12) applies then the plot against P_B will be linear. An example of the latter may be seen for the binding of $NADP^+$ to isocitrate dehydrogenase,[22] and of the former for the binding of the ligand 4-(aminomethyl)bicyclo[2.2.2]octane-1-carboxylic acid, AMBOC, to the kringle 4 protein.[23] The plot for this case is shown in Fig. 4, from which the k_{off} value of $3.8 \times 10^3\ s^{-1}$ was derived for the interaction. In this study the procedure noted in Section 2.1 for determining the equilibrium constant K_a from the dependence of chemical shift on linewidth was also applied to yield $K_a = 48\ mM^{-1}$.[23] These two constants together allowed the on-rate to be determined from

$$K_a = k_{on}/k_{off}. \tag{14}$$

For AMBOC binding to kringle 4 protein this was found to be $1.8 \times 10^8\ M^{-1}\ s^{-1}$.

For intermediate exchange, lineshapes are complicated and the full generalized expression[1] must be applied. Note that because of the different conditions for fast/slow exchange for chemical shift, T_1 and T_2, and because, for macromolecules, $1/T_1$ is often much less than $1/T_2$, it is possible for the fast-exchange condition to apply to T_1, while chemical shifts and T_2 may be in slow exchange. Conversely, if δ and T_2 are in fast exchange, T_1 will always be in fast exchange.

The applications above relate to the direct use of relaxation parameters to obtain information about molecular dynamics or binding kinetics/thermo-

†Note that this equation is slightly modified from those appearing elsewhere,[1,19] where determinations were carried out for the assumption $P_A \approx 1$. Equations (12) and (13) reduce to the expected "weighted-average" expressions when exchange is very fast, i.e. $1/k_{off} \ll T_{1,2}^{B}$. Note also that the apparent anomaly of (13) as given above not reducing to (12) when $\delta_A - \delta_B = 0$ is resolved when it is seen that the denominator of the second term in equation (13) should, strictly, include the additional $1/k_{off}$ term. This is usually omitted, however, owing to the assumptions made in the derivation of (13) from the more generalized expressions.

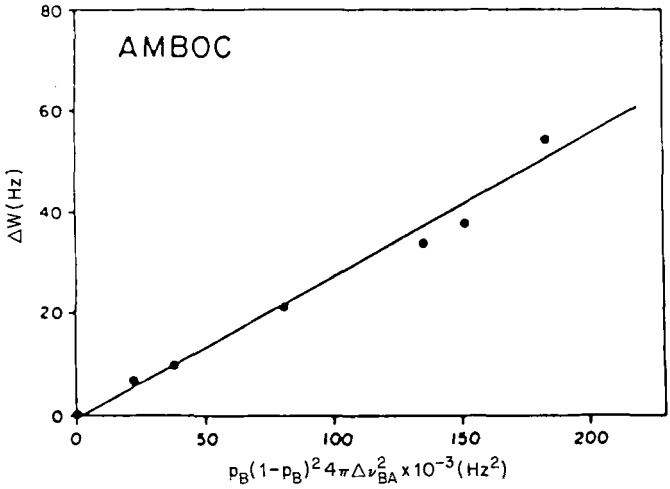
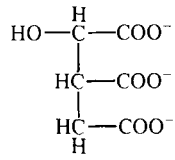


Fig. 4. Ligand titration of kringle 4 with AMBOC.[23] Excess linewidth ΔW was fitted to (13). (Reprinted with permission from Ref. 23. © 1989 American Chemical Society.)

dynamics. It is also important to consider the effects of relaxation parameters on spectral appearance, as this can have a marked influence on the ability to measure other spectral parameters such as chemical shifts.

Equations (5) and (7), for example, have an important bearing on the choice of site for ^{13}C labelling in studies of protein–ligand interactions. The $1/r^6$ distance dependence strongly indicates the desirability of avoiding protonated carbon sites if narrow lines are to be obtained for bound resonances. For example, substitution of a typical correlation time of 10^{-8} s into (2) for a C—H site on a bound ligand leads to a predicted linewidth of more than 50 Hz. By contrast, note that for the quaternary labelled sites in Fig. 3 the linewidths of the bound ligand are not significantly greater than for the free ligand. Likewise, in a study of isocitrate (**2**) binding to isocitrate



2

dehydrogenase[15] linewidths for the carboxyl ^{13}C-labelled site for bound substrate were of the order of 10 Hz, whereas those for the protonated ^{13}C-α site were too broad to be visible.

2.3. Magnetization-transfer experiments

Although the principles of magnetization transfer were developed in the early 1960s,[24] it has not been until recently that the technique has been widely used in biological applications. Over the last five to ten years, however, there has been a dramatic increase in the application of magnetization-transfer experiments to studies of ligand–molecule binding. The wide applicability of the technique in such studies arises because the basis of magnetization transfer involves chemical exchange, which is, of course, an integral part of any macromolecule–ligand interaction. Magnetization transfer also continues to find wide application in a range of more-chemical studies,[25,26] as well as making a major impact on studies of biochemical reactions in intact tissue samples.[27,28] Before examining some of the key applications with respect to ligand binding to macromolecules, a brief description of the theory of magnetization transfer follows.

The exchange of a ligand between free and bound states results in the transfer of nuclear magnetization between the two states. A simple illustration of the consequences of such exchange can be made by considering the two-site exchange between species A and B below.

$$\mathrm{A} \underset{k_2}{\overset{k_1}{\rightleftharpoons}} \mathrm{B}$$

The z magnetization of spin A may be described by the modified Bloch equations:

$$\frac{\mathrm{d}M_\mathrm{A}}{\mathrm{d}t} = \frac{M_\mathrm{A}^\circ - M_\mathrm{A}}{T_{1\mathrm{A}}} - k_1 M_\mathrm{A} + k_2 M_\mathrm{B}, \tag{15}$$

where M_A° is the equilibrium magnetization of A, M_A and M_B are the magnetizations of A and B at time t, k_1 and k_2 are the forward and reverse rate constants respectively, and $T_{1\mathrm{A}}$ is the spin–lattice relaxation time of A (in the absence of exchange). An analogous expression may be written for the magnetization of spin B. Equation (15) shows that the effect of exchange is to couple the time-dependent behaviour of the two spins, and while the coupled differential equations may be solved, this is cumbersome in practice and experiments studying the exchange phenomenon often make use of simplifying conditions.

2.3.1. Saturation transfer

The most commonly applied approach to simplifying the exchange problem is to selectively saturate one of the spins while observing the other. Thus if a selective radio-frequency (RF) field is placed on spin B to saturate it then

$M_B = 0$ and (15) becomes

$$\frac{dM_A}{dt} = \frac{M_A^\circ - M_A}{T_{1A}} - k_1 M_A. \tag{16}$$

If the saturating field is applied for long enough, the magnetization of spin A will reach a steady state (i.e. $dM_A/dt = 0$) and

$$\frac{M_A^\infty}{M_A^\circ} = \frac{1}{1 + k_1 T_{1A}}, \tag{17}$$

where M_A^∞ is the steady-state magnetization. It can be seen that the decrease in intensity of resonance A depends on a balance between the chemical exchange process, which tends to decrease the intensity, and spin–lattice relaxation, which tends to return it to its equilibrium value. The rates that can be studied by saturation transfer are limited on the one hand by the requirement that the signals must be in slow exchange on the chemical-shift timescale, i.e. the upper limit to k_1 is approximately $2\pi\ \delta\nu$ ($\delta\nu$ is the chemical-shift difference between irradiated and observed signals), and on the other by the smallest intensity change that can be measured.[25] In the most favourable case of long T_1 (say 5 s) and the ability to measure an intensity change of 0.5% by difference spectroscopy, a lower limit for k of $10^{-3}\ s^{-1}$ can be measured, although the typical range of k values covered is approximately 10^{-2}–$10^3\ s^{-1}$.

From (17) it can be seen that a determination of k_1 requires measurement of T_{1A}. If this cannot be independently measured then k_1 can still be obtained by following the time dependence of the decrease in M_A as B is saturated for variable lengths of time:[24]

$$M_A = \frac{M_A^\circ}{1 + k_1 T_{1A}} \left[1 + k_1 T_{1A} \exp\left(t \frac{1 + k_1 T_{1A}}{T_{1A}}\right)\right]. \tag{18}$$

A combination of the time constant for the above decay, $(1 + k_1 T_{1A})/\ T_{1A}$, and the value of $1/(1 + k_1 T_{1A})$ (derived from M_A^∞/M_A°) allows both k_1 and T_{1A} to be determined.

2.3.2. Inversion transfer

In this approach a selective 180° pulse is applied to one of the spins (B), and the magnetization of the other (A) is followed. As in saturation transfer, the chemical exchange causes inverted spins to exchange with uninverted spins, and results in intensity changes for both. An improved analytical procedure for the determination of unitary rate constants from inversion transfer experiments and its application to *cis–trans* isomerism of a peptide substrate have recently been described.[29]

2.3.3. Two-dimensional chemical exchange

Magnetization transfer can also be detected in 2D spectra and, in particular, in experiments that utilize the NOESY pulse sequence. The effects of exchange show up as cross-peaks between the species that are in exchange. A major advantage of the 2D technique is that all exchange processes are monitored simultaneously, without the need for selective irradiation or inversion of particular resonances. While peak quantitation has traditionally been more difficult in 2D than in 1D spectra, it is becoming less of a problem with advances in computer hardware and software for data processing. The time dependence of cross-peak intensity can be determined by performing the 2D experiment using various mixing times or by using the accordion technique.[30] Boyd *et al.*[31] have discussed the relative advantages/disadvantages of 1D and 2D techniques.

2.3.4. Application to ligand binding

While the above discussion of magnetization transfer for the simple equilibrium $A \rightleftharpoons B$ provides a convenient system to introduce the basic theory, a more appropriate description of the process occurring on macromolecule–ligand binding is given by the equilibrium

$$A + B \underset{k_{off}}{\overset{k_{on}}{\rightleftharpoons}} AB$$

where A represents the ligand, B the macromolecule and AB the bound complex. It might at first appear that saturation-transfer experiments would not be suitable for this case because k_{on} for such interactions is usually outside the range 10^{-2}–$10^{3}\ s^{-1}$ noted in Section 2.3.1. However, in this case the rate constant in (17) must be replaced with the apparent rate constant for the second-order binding process,[32,33] i.e. $k_{on}[B]$.

A consideration of typical magnitudes of kinetic constants and concentrations used in studies of macromolecule–ligand binding, shows, then, that magnetization transfer is applicable in such systems. Thus when a perturbation such as saturation by a selective RF field or inversion by a selective 180° pulse is applied to a resonance from a bound ligand, exchange of the ligand to the free state will result in a measurable intensity change in the free-ligand signal. For example, in a solution of a ligand and macromolecule prepared with typical initial concentrations of 5 mM and 1 mM respectively, if the association constant is $10^{6}\ M^{-1}$ then at equilibrium the unbound-macromolecule concentration [B] will be *ca.* 0.2 μM. For a diffusion controlled on-rate k_{on} of $10^{8}\ M^{-1}s^{-1}$ this yields an apparent rate constant for binding $k_1 = k_{on}[B]$ of $20\ s^{-1}$, which would result in a measurable change of intensity according to (17).

From the foregoing discussion it can be seen that magnetization-transfer methods provide a powerful means of determining kinetic information on ligand binding. Off-rates are usually of particular interest, and may be determined from (19):[7]

$$k_{\text{off}} = \frac{P_{\text{F}}}{P_{\text{B}}} k_1, \tag{19}$$

where k_1 is determined from (17) or (18), and P_{F} and P_{B} are the fractions of ligand in the free and bound states respectively. This approach was very successfully applied in early studies of the dihydrofolate reductase system,[7] where kinetic constants for ligand binding obtained from saturation transfer were consistent with those from line-broadening experiments.[20]

A perhaps more important aspect of saturation transfer is that it can be used to locate bound-ligand resonances that might otherwise not be visible. As noted earlier, for high-affinity interactions peaks due to free and bound ligand forms will often be in slow exchange on the chemical-shift timescale, so that two sets of ligand signals (free and bound) are present. It is frequently the case, however, that peaks from bound ligands are too broad, present in small relative mole fractions, or too overlapped with other resonances to be directly detected. By systematically stepping the saturating RF field over a frequency range of interest, it is often possible to detect the position of a bound ligand resonance by monitoring intensity changes in free ligand signals subject to saturation transfer. The bound chemical shift may then yield information about the bound environment.

Dihydrofolate reductase is perhaps the most extensively examined system in which saturation transfer has been used to determine chemical shifts of bound ligands. For reviews of early studies see Refs. 2, 4 and 34. Initial studies utilized mainly the 1D approach of systematically irradiating part of the spectrum where bound-ligand signals were expected while monitoring free-ligand resonances. In principle, if multiple bound conformations are present and they have different chemical shifts, they will be detected by this technique. This applies, for example, to the DHFR–folate–$NADP^+$ complex.[35] More recently, the 2D approach has been applied to the DHFR system.[4,36] This has the advantage of greater efficiency, since all exchange processes are detected in a single experiment. Further details are given in Section 4.1.3.

The saturation-transfer technique is not restricted to examining free- and bound-ligand signals, and can in principle also be applied to signals from a macromolecule in free and bound states. However, these applications tend to be rather specialized, being of use only in cases where unique circumstances exist that allow macromolecular signals to be readily detected. Such a case occurs for macromolecules that contain a paramagnetic metal centre

and consequently have a number of signals with very large well-resolved chemical shifts. An example of such a system, in which saturation transfer has recently been used to confirm assignments for resonances in the complexed macromolecule using previously assigned resonances in the unbound macromolecule, is horseradish peroxidase (HRP). On interaction with cyanide, the high-spin ferric HRP is converted to low-spin HRPCN, as follows:

$$HRP + CN^- \rightleftharpoons HRPCN$$

A combination of extensive isotope labelling and NOE experiments had led to the assignment of all the heme resonances of HRP.[37] The numbering scheme for this moiety is shown in Fig. 5, and the low-field hyperfine shifted portion of the 360 MHz ^1H NMR spectrum of a mixture of HRP and HRPCN is shown in trace A of Fig. 6. The broad peaks in the region 30–80 ppm all arise from HRP and had previously been assigned. Difference spectra obtained on saturation of the indicated HRP signals in traces B–F in Fig. 6 show saturation transfer to the corresponding peaks in HRPCN, which are sharper and occur in the region 10–30 ppm.

2.4. Nuclear-Overhauser-effect measurements

Nuclear-Overhauser-enhancement (NOE) measurements can be used to determine the proximity in space of two nuclei, or to help define molecular

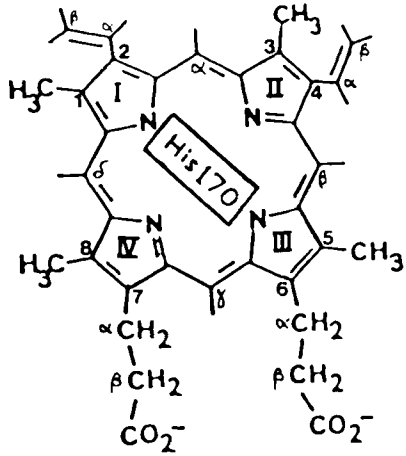


Fig. 5. Structure and numbering system for hemin in HRPCN with superimposed proximal histidine. (Reprinted with permission from Ref. 37. © 1989 American Chemical Society.)

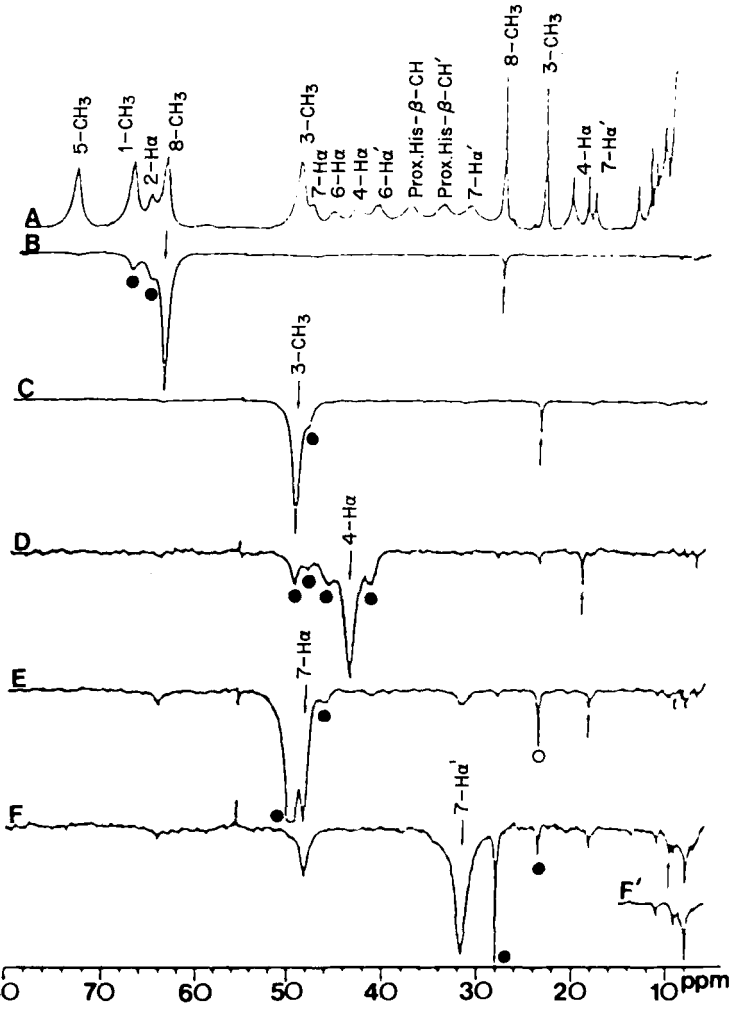


Fig. 6. The hyperfine shifted portions of the 360 MHz ^{1}H NMR spectrum of (A), a mixture of HRP/HRPCN in the ratio 65 : 35 in 100% D_2O at 55°C, pH 7.0.[37] B–F are saturation transfer difference spectra generated by subtracting the reference spectrum with the decoupler off resonance from a similar spectrum of the same sample in which the desired frequency was saturated. In each of the difference spectra B–F a downward arrow indicates the peak being saturated and an upward arrow saturation transfer. A filled circle denotes off-resonance power spillage, while an open circle denotes saturation transfer from off-resonance saturation. The difference spectra B–F show the saturation of 8-CH_3, 3-CH_3, 4-H_α, 7-H_α and 7-H_α' resonances of HRP respectively and the saturation transfer to their counterparts in HRPCN. The inset F′ shows the portion of the difference spectrum obtained using the sample without CN^-; note the disappearance of the resonance at 9.74 ppm. The other peaks in the inset are due to NOEs within the pure HRP complex. (From Ref. 37.)

mobility. While both features are useful in studies of macromolecule–ligand interactions, the distance information available from $^1H-^1H$ NOEs is of paramount importance. The use of NOEs for determining relative distances between protons in small molecules in solution has been widely demonstrated[38] and can be applied to determine conformations, provided that appropriate caution in the interpretation of the data is used.[2] An even greater potential exists for the determination of three-dimensional structures of proteins. This has arisen from the combination of interproton distances obtained from 2D NOESY experiments and distance–geometry algorithms to convert this distance into three-dimensional structures.[39–41]

In the current context, however, we are concerned not with separate studies of small molecules (ligands) and macromolecules but rather with their interaction. The NMR methods currently being developed for 3D structure determination of proteins offer outstanding promise of also yielding information on complete geometries of macromolecule–ligand complexes. However, most applications of NOE to date have been concerned with either establishing the proximity of certain residues on the macromolecule to those of the ligand (i.e. locating the binding site), or with determining the conformations of bound ligands. Both pieces of information are central to defining the nature of the macromolecule–ligand interaction, and both derive from the primary role of the NOE in indicating the proximity in space of pairs of nuclei.

2.4.1. Measurement, size and sign of NOEs

Proton–proton NOEs reflect the relative contribution of cross-relaxation between two protons to the total spin–lattice relaxation rate of the observed proton. If only the dipolar mechanism contributes to the relaxation of observed spin i and molecular tumbling is isotropic then the latter term is given by[42,43]

$$\rho_i = \sum_j \frac{\gamma^4 \hbar^2}{10 r_{ij}^6} \left(\tau_c + \frac{3\tau_c}{1+\omega^2\tau_c^2} + \frac{6\tau_c}{1+4\omega^2\tau_c^2} \right), \tag{20}$$

while the cross-relaxation rate between the ith and jth nuclei is given by

$$\sigma_{ij} = \frac{\gamma^4 \hbar^2}{10 r_{ij}^6} \left(\frac{6\tau_c}{1+4\omega^2\tau_c^2} - \tau_c \right). \tag{21}$$

From these equations it is apparent that in the extreme narrowing limit ($\omega\tau_c \ll 1$) proton–proton NOEs ($= \sigma/\rho$) are positive with a maximum value of $+0.5$, while when $\omega\tau_c \gg 1$ NOEs are negative with a maximum value of -1.0. The former case applies typically for free ligand molecules with $\tau_c < 10^{-10}$ s, while the latter applies to macromolecules or bound ligands,

which are characterized by longer correlation times ($\tau_c > 10^{-9}$ s). Contributions to dipolar relaxation of a given proton from other than the irradiated spin, or contributions from other relaxation mechanisms, reduce the size of the observed NOEs within these limits.

NOEs may be measured from either 1D spectra (from the intensity change in one resonance when another is irradiated) or from 2D spectra (from the intensity of cross-peaks in NOESY experiments). These measurements may be done either under steady-state conditions or by measuring the build-up rate of peak intensity in either 1D or 2D experiments where variable irradiation or mixing times respectively are used. The time-dependent experiments have the advantage that complications from spin diffusion, which tend to reduce the specificity of steady-state NOEs in slowly tumbling systems, are somewhat minimized.

As with homonuclear NOEs, the general expression for NOEs between an observed heteronucleus, I, and a different irradiated nucleus (usually the proton), S, also depends on the correlation time for molecular tumbling:[16]

$$\mathrm{NOE} = 1 + \frac{\gamma_S}{\gamma_I} \frac{6J(\omega_I + \omega_S) - J(\omega_I - \omega_S)}{J(\omega_I - \omega_S) + 3J(\omega_I) + 6J(\omega_I + \omega_S)}. \tag{22}$$

The most commonly utilized heteronuclear NOEs in studies of macromolecule–ligand binding are between protons and either ^{13}C, ^{15}N or ^{19}F. Substitution of the spectral density for isotropic molecular tumbling, (6), into (22) thus shows that the ranges of enhancement factors (= NOE − 1) for these nuclei are respectively $1.98 \rightarrow 0$, $-4.93 \rightarrow 0$ and $0.5 \rightarrow -1.0$, going from correlation times typical of free ligands ($\omega\tau \ll 1$) to those characteristic of macromolecule and bound-ligand signals ($\omega\tau \gg 1$). The need for appropriate caution in the use of ^{15}N and ^{19}F nuclei in particular can be seen, since signal nulling may occur for certain motion regimes.

Heteronuclear NOEs may be used alone, or in conjunction with relaxation-time measurements, to yield dynamic information in macromolecule–ligand complexes, and are also useful in establishing proximity of the heteronuclei to each other in the complexes (see e.g. Section 2.4.2). Such NOEs are usually measured in 1D experiments involving observation of the heteronucleus in the presence of broadband proton irradiation, but may also be observed in 2D experiments.[18,44]

2.4.2. Macromolecule–ligand NOEs

The observation of NOEs between protein or nucleic acid resonances and those of a ligand provides a powerful means of locating the binding site. Early examples of such effects were reported by Balaram *et al.*[45] and James.[46] More recent illustrations of this technique can be seen in studies of

ligands binding to kringle proteins[8,47] and dihydrofolate reductase.[13] Figure 7 shows, for example, control and NOE difference spectra for the binding of the ligand 4-benzylaminesulphonic acid (BASA) to kringle 1. Significant NOEs are detected in ligand resonances following irradiation of

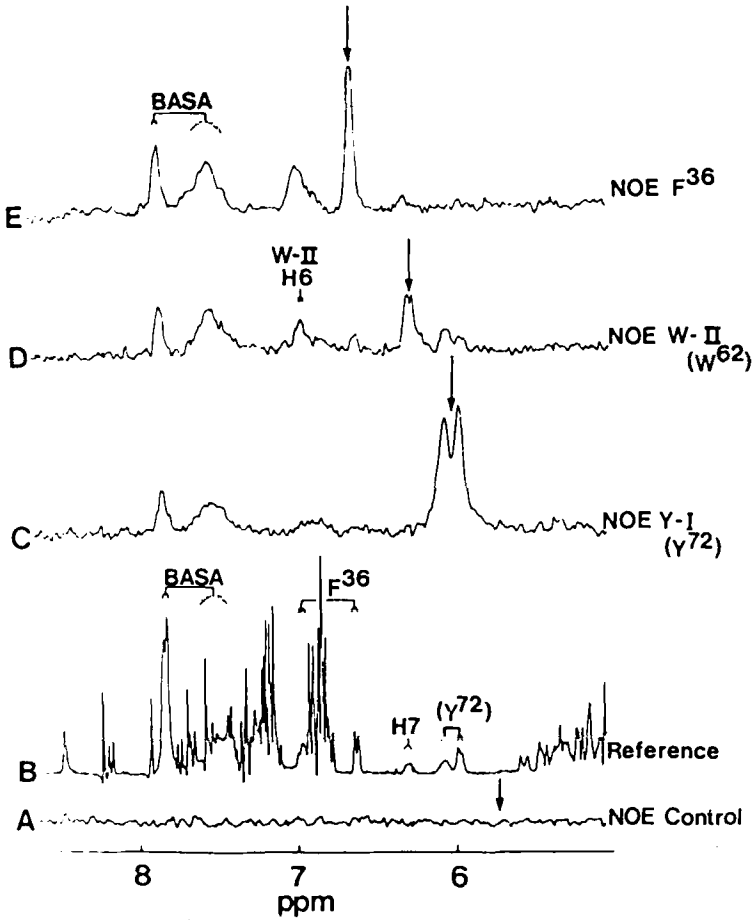


Fig. 7. Kringle-1–BASA protein–ligand NOE experiments at 300 MHz. (B) Kringle 1 aromatic reference spectrum. (C), (D) and (E) NOE difference spectra obtained by irradiating the Tyr^{72} H2,6 + H3,5, the Trp^{62} H7 and the Phe^{36} H2,6 transitions, respectively. Irradiation time 500 ms, using sufficient power to fully saturate the signals in about 20 ms; 2.5 s cycling time. (A) Control experiment in which irradiation was applied at a blank position, indicated by the arrow, about 50 Hz high-field-shifted relative to the closest Tyr^{72} doublet. Kringle concentration, 5×10^{-4} M, pH* 6.7, 50°C. [Kringle 1]/[ligand] ≈ 0.2. The labelling of residues as W-II, Y-I etc. reflected initial uncertainties in assignments, which have now been resolved. (Reprinted with permission from Ref. 47. © 1989 American Chemical Society.)

Tyr^{72}, Trp^{62} and Phe^{36} resonances, indicating their proximity to the binding site. Further discussion of kringle–ligand binding is given in Section 4.1.2. The power of the two-dimensional approach is seen in Fig. 8 for the binding of folate to the dihydrofolate–$NADP^+$ complex.[13] Under the pH conditions shown, the complex exists in one of three interconverting conformations, denoted conformation I. NOEs between the 7-proton of folate and three methyl protons indicates proximity of this part of the ligand to one or both methyl groups of Leu^{19} and Leu^{27} of DHFR.[13] Further discussion on the dihydrofolate reductase system is given in Section 4.1.3.

Even if definite assignments in the macromolecule have not been made, the chemical-shift region from which NOEs are observed often allows qualitative information about the nature of residues involved at the binding site to be deduced. For example, in the case of a substrate analogue binding to the large fragment of DNA polymerase I,[48] intermolecular NOEs indicated the proximity of hydrophobic amino acids with chemical shifts in the range 0.6–1.8 ppm, and an aromatic amino acid, possibly Tyr, to the

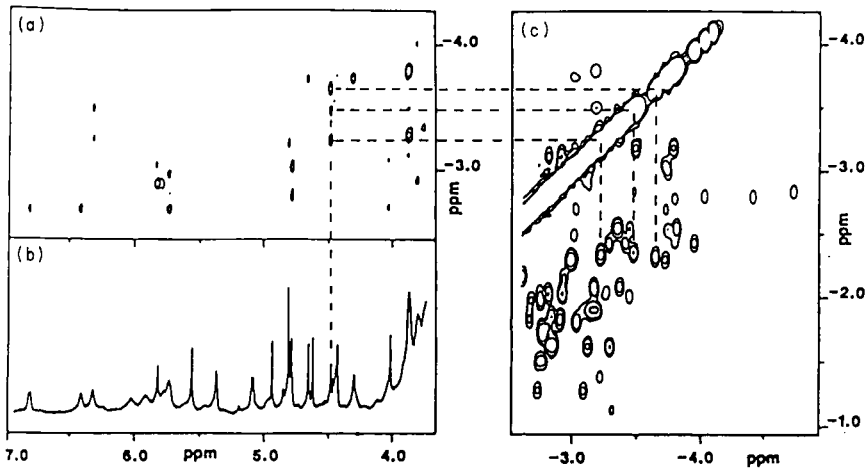
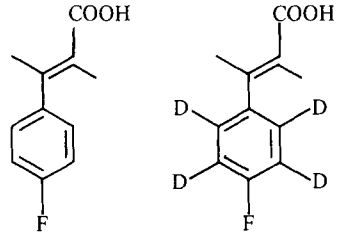


Fig. 8. Nuclear Overhauser effects involving the folate pteridine 7-proton and methyl groups of the protein in conformation I of the dihydrofolate-reductase–folate–$NADP^+$ complex (pH* 5). Spectrum (b) is the low-field part of the aromatic region of the one-dimensional ^1H spectrum of the complex, with the resonance of the 7-proton of bound folate indicated. Part (a) shows the region of the two-dimensional NOESY spectrum of the complex containing cross-peaks between low-field aromatic protons and methyl protons. Part (c) shows the high-field part of the two-dimensional ^1H COSY spectrum of the complex. The dashed lines connect the resonance of the folate 7-proton in (b) with its three NOESY cross-peaks in (a) and the corresponding COSY cross-peaks in (c). Chemical shifts are relative to dioxan. (Reprinted with permission from Ref. 36. © 1989 American Chemical Society.)

ligand at the binding site. Similar qualitative conclusions about the nature of amino acid residues near the binding site have been made on the basis of intermolecular NOEs in a number of other systems, including pepsin[49] and adenylate kinase.[50]

NOE experiments involving heteronuclei are also extremely useful in studies of macromolecule–ligand interactions. An example that shows the potential of heteronuclear protein–ligand NOEs for the location of binding sites was reported by Cairi and Gerig.[44] $^{19}F-\{^{1}H\}$ 2D NOESY experiments on the deuterated analogue (**3b**) of 4-fluorocinnamate (**3a**) were used to



3a **3b**

determine the shifts of protons on chymotrypsin which were in close proximity to the bound ligand. In this case, deuteration was carried out to decrease relaxation contributions to the fluorine nucleus from the ring protons of the ligand. A similar approach has been used to determine the nature of residues close to the fluorine atom of a 4-fluorophenylsulphonyl probe attached to the active site of chymotrypsin.[18]

Note that in most studies of ligand–macromolecule NOEs the observed NOEs are detected on free-ligand signals. This transfer of information between bound and free states is also used to great advantage in studies of intramolecular NOEs within ligands bound to macromolecules, as described in the next section.

2.4.3. Transferred NOE measurements

A major difficulty in the application of direct NOE measurements to determine conformation of ligands when bound to macromolecules is that the bound-ligand signals may be very broad and obscured by overlap with resonances from the macromolecule. These difficulties are overcome in the transferred nuclear Overhauser technique (TRNOE), which has now become a very powerful method for determining conformations of bound ligands.

The technique makes use of chemical exchange between the free and

bound ligand to transfer information concerning cross-relaxation between two bound nuclei from the bound to the free state. In the TRNOE experiment negative NOEs on the easily detectable free or averaged ligand resonances (depending on whether exchange is slow or fast on the chemical-shift timescale, Fig. 9) are measured following irradiation of other ligand resonances (free, bound or averaged) in order to obtain conformational information on the bound ligand. The phenomenon was first noted by Albrand *et al.*[51] in a study of the binding of trimethoprim and $NADP^+$ to dihydrofolate reductase. The theory of the technique was subsequently developed in more detail by Clore and Gronenborn[52] for an exchanging system with two spins in the bound state and two corresponding spins in the free state. It was shown that the change in intensity of one ligand proton resonance, I (average or free), when a second ligand proton resonance, S, is irradiated, $N_I(S)$, can be related to the cross-relaxation rate between the proton pair in the bound state, σ_{IS}^{BB}:

$$N_I(S) \propto \sigma_{IS}^{BB}, \tag{23}$$

provided that certain kinetic conditions are met, in particular that exchange between free and bound states is fast on the cross-relaxation timescale.

The ratio of distances between the protons S and T and a third proton I can then be determined using

$$\frac{r_{IS}^{BB}}{r_{IT}^{BB}} = \left(\frac{\sigma_{IT}^{BB}}{\sigma_{IS}^{BB}}\right)^{1/6} = \left[\frac{N_I(T)}{N_I(S)}\right]^{1/6}, \tag{24}$$

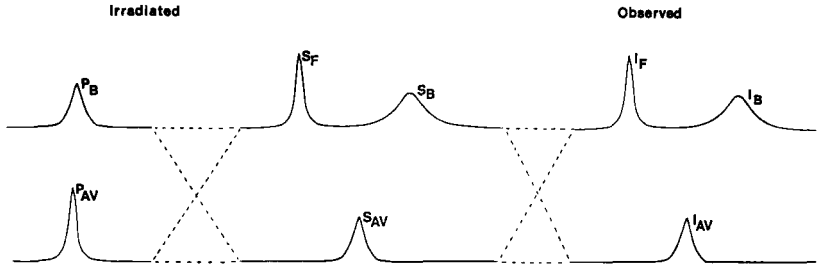
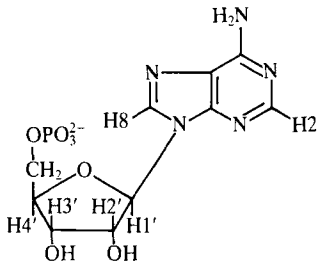


Fig. 9. Schematic illustration of the fact that TRNOE experiments may be carried out by observation of a free or averaged (I_F or I_{AV} respectively) ligand resonance following irradiation of either a free, bound or averaged resonance (S_F, S_B or S_{AV}) from another ligand proton, depending on exchange conditions on the chemical-shift timescale. Irradiation of S_B does not require that it be observed in the spectrum, since it may be located using a saturation-transfer experiment. Because the chemical-shift difference between the free and bound resonances for the two protons I and S may be different, it is possible either for both to be in fast exchange, both to be ion slow exchange, or one to be in fast and the other in slow exchange, in any individual system. TRNOE experiments are also possible in which bound or averaged macromolecule resonances P are irradiated while I_F or I_{AV} is observed.

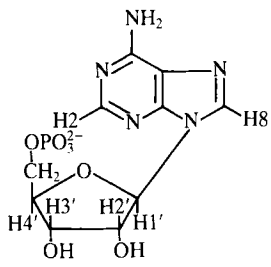
where r_{IS}^{BB} and r_{IT}^{BB} are respectively the distances between spins I and S and between I and T in the bound state. These distances can then be used to derive a conformation for the bound ligand.

A major advantage of the technique is that experiments can be performed with a large excess of ligand ($\leqslant 20$ fold), thus reducing the amounts of macromolecule required in cases where availability of the biological material is limited (as is usually the case!). Another important feature of the TRNOE method is that it can be applied to the binding of ligands to large proteins, as has been illustrated by examples[52] of 5′-AMP [4a,b] binding to horse-liver alcohol dehydrogenase, ADH (MW $\approx$ 80 000), yeast alcohol dehydrogenase (MW $\approx$ 150 000), and bovine-liver glutamate dehydrogenase (MW $\approx$ 300 000).

An important question often posed in such studies of nucleotide binding to enzymes is whether the bound conformation is *anti* (**4a**) or *syn* (**4b**).



4a



4b

Figure 10 shows TRNOE spectra of AMP binding to yeast ADH. At an approximately seven-fold excess of free to bound AMP a large negative TRNOE of about 50% is seen on the observed H8 resonance of the adenine ring following irradiation of the averaged H2′ resonance of the sugar ring. This, and the fact that no effect on H2 is observed on irradiation of H2′, provides strong evidence that AMP exists in the *anti* conformation when bound, as had earlier been inferred from X-ray studies. The specificity of the effect was demonstrated by recording an "action spectrum" where the intensity of H8 was monitored while the irradiation frequency was systematically stepped through the region of the spectrum containing other ligand resonances. In this experiment a constant short irradiation time was used to generate pre-steady-state TRNOEs. In the action spectrum shown in Fig. 11 the large negative TRNOE for H8 from H2′ and smaller effects from H3′ and H5′, as well as the absence of effects from H1′, are all consistent with the *anti* conformation being significantly populated in the

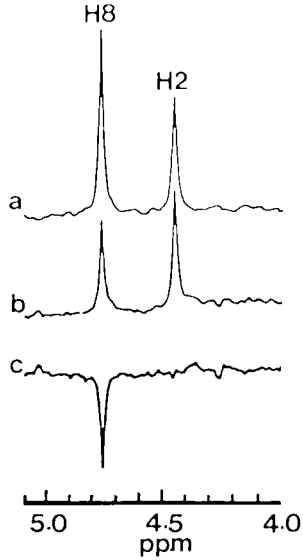


Fig. 10. Aromatic region of the 270 MHz ^{1}H NMR spectrum of 3.33 mM 5′-AMP in the presence of yeast ADH (corresponding to 0.4 mM in 5′-AMP binding sites): (a) control irradiation at 0.46 ppm; (b) irradiation of the observed H2′ sugar resonances at 1.06 ppm; (c) difference spectrum. Sample temperature 20°C. (Under these conditions, the positions of the observed resonances of 5′-AMP are at the positions of the corresponding resonances of free 5′-AMP.) Chemical shifts are expressed relative to dioxane. (Reprinted with permission from Ref. 52. © 1989 Academic Press.)

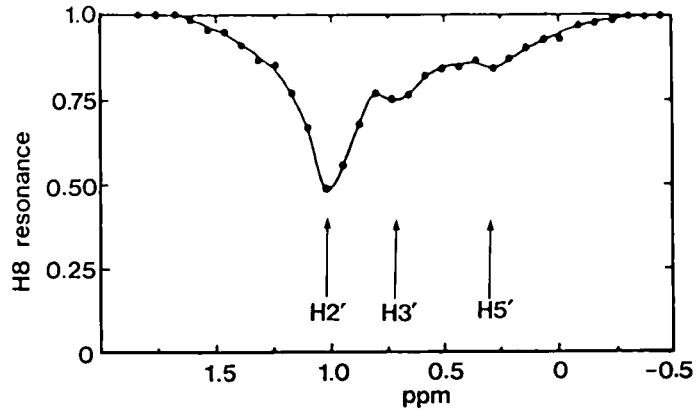


Fig. 11. Normalized intensity of the observed H8 resonance of the adenine ring of 5′-AMP (3.33 mM in the presence of 0.1 mM yeast ADH) as a function of irradiation frequency. The positions of observed H2′, H3′ and H5′ resonances are indicated. Chemical shifts are relative to dioxane. (Reprinted with permission from Ref. 52. © 1989 Academic Press.)

bound state. The absence of any effect on H2 following irradiation of any other proton confirms this.

In multispin systems with long correlation times spin diffusion may potentially reduce the specificity of NOE effects. To further improve the selectivity of the TRNOE method, the theory of time-dependent TRNOEs was subsequently developed.[53] In this approach cross-relaxation rates are derived from initial build-up rates of magnetization, $dM/dt|_{t=0}$ in experiments involving incremented irradiation periods.

Direct cross-relaxation effects may be distinguished from secondary effects by plotting NOEs as functions of irradiation time. This is illustrated in Fig. 12 for the binding of AMP to adenylate kinase.[50] Note the significant lag time associated with secondary effects at H2 compared with direct effects at H8 and H1′ when H2′ is irradiated.

Expressions for initial NOE build-up rates for primary effects[53] are given in Table 1, where it can be seen that the cross-relaxation rate between a proton pair in a ligand in the bound state, σ_{IS}^{BB}, or a macromolecule proton-bound ligand proton pair, σ_{IS}^{BX}, can be obtained directly from the initial slope. On the other hand, if the irradiated peak is an averaged or free ligand proton then the build-up rate is given by

$$\left.\frac{dM}{dt}\right|_{t=0} = (1 - a)\sigma_{IS}^{BB} + a\sigma_{IS}^{FF}, \tag{25}$$

and the desired cross-relaxation rate σ_{IS}^{BB} can still be obtained by either determining σ_{IS}^{FF} for the free ligand in a separate experiment or by measuring initial build-up rates at two ligand : macromolecule ratios to solve (25) for

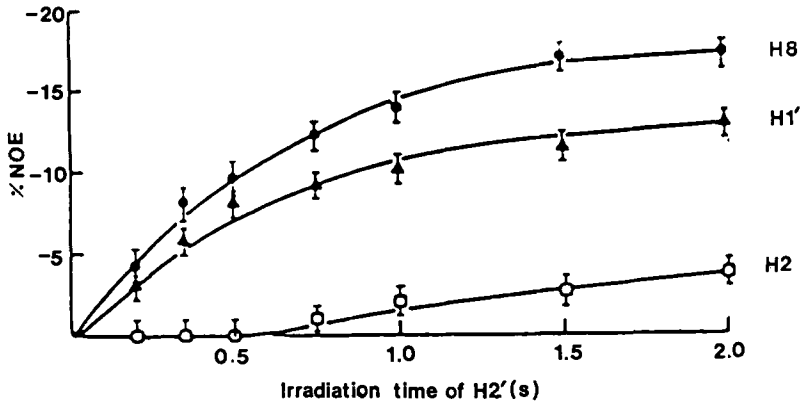


Fig. 12. NOE build-up curves for H8, H1′ and H2 following irradiation of the averaged resonance of H2′ of AMP bound to adenylate kinase. (Reprinted with permission from Ref. 50. © 1989 American Chemical Society.)

Table 1. NOE build-up rates in time-dependent TRNOE experiments[a].

Irradiated peak	$\left.\frac{dM_x}{dt}\right\|_{t=0}^{b,c}$
S_{AV}	$(1-a)\sigma_{IS}^{BB} + a\sigma_{IS}^{FF}$
S_B	$a\sigma_{IS}^{BB}$
S_F	$(1-a)\sigma_{IS}^{BB} + a\sigma_{IS}^{FF}$
P_{AV} or P_B	$(1-a)\sigma_{IT}^{BX}$

[a]Derived for the fast-exchange condition with respect to the cross-relaxation timescale.[53]
[b]Observed peak X is either I_{AV} or I_F; see text.
[c]Cross-relaxation rates σ are defined in the text; a is the fraction of free ligand.

both σ_{IS}^{FF} and σ_{IS}^{BB}. In many cases, however, even the above procedures are not necessary, since σ_{IS}^{FF} is usually very much smaller than σ_{IS}^{BB} and may often be neglected.

Once the cross-relaxation rates between one nucleus and two or more other nuclei have been obtained, (24) can be used to derive distance ratios. Absolute distances can be obtained if one of the proton–proton pairs involves a fixed distance, which can be used to calibrate other relative distances. Alternatively, if the correlation time τ_c is known or can be calculated independently then (21) may be used to determine individual internuclear distances (see e.g. Ref. 50).

The TRNOE method can be extended to two-dimensional experiments, which offer the significant advantage of simultaneously yielding information on cross-relaxation between all pairs of nuclei in the system without the need for separate irradiation. The standard NOESY pulse sequence is utilized for such experiments. An assessment of errors and a comparison of 1D and 2D approaches to TRNOE experiments has been reported,[54] as has a detailed discussion of the important features of the two-dimensional approach.[55]

Examples of applications of the TRNOE method include its use to determine the conformations of ligands bound to dihydrofolate reductase,[56] nucleotides to enzymes,[22,48,50,57–66] nucleotides to tRNA species,[67,68] peptides to enzymes,[69,70] peptides to phospholipid bilayers,[71–74] and other ligands to blood proteins.[55,75,76]

2.4.4. Isotope-edited NOE spectra

For cases where kinetic conditions or other factors make it inappropriate to

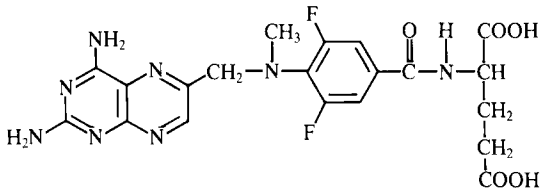
use the TRNOE technique to determine the bound conformation of ligands, it would be useful to have alternative means of measuring NOEs on bound ligands. As has been pointed out, the greatest difficulty with this approach is the complexity of and overlap in spectra of large complexes. Recently, however, several experimental approaches have been proposed to simplify complicated 2D NOE spectra.[49,77–80] These methods are based on the selective observation of protons attached to isotopically labelled nuclei. Examples of applications include the binding of inhibitors to pepsin,[49] described in Section 4.1.6, and atrial natriuretic factor (7–23) binding to micelles.[80]

2.5. Dynamic lineshape analysis

The importance of mutual flexibility of both ligand and target macromolecule in many interactions is increasingly being recognized. Indeed, there are now a number of documented examples of ligand–macromolecule complexes in which the ligand is able to convert reversibly, at the binding site, between stable conformations. For systems in which this occurs it is in principle possible to carry out the same sort of dynamic lineshape analysis (to obtain interconversion barriers and rates) that has been commonly applied in organic systems for many years.[81,82]

For the simple case of a two-site exchange a single resonance is observed when the system is in fast exchange, but as the temperature is lowered and interconversion rates decrease, coalescence and, finally, slow exchange (in which separate peaks for the two environments are present) occur. A theoretical lineshape analysis allows rates to be determined as a function of temperature, hence making it possible to derive thermodynamic parameters via the Eyring or Arrhenius equations.[82] A limitation on such an approach in biological systems is, of course, the temperature range over which the macromolecule–ligand complex is stable.

An example of this approach can be seen in the binding of 3′5′-difluoromethotrexate (**5**) to dihydrofolate reductase (DHFR).[83] Figure 13



5

shows ^{19}F spectra of the difluoromethotrexate–DHFR complex at temperatures between 273 and 308 K. At the highest temperature a single resonance is observed for both fluorine nuclei 1.04 ppm downfield from the resonance of free difluoromethotrexate. At temperatures below approximately 283 K two resonances of equal intensity are observed, indicating that the 3′ and 5′ nuclei experience different environments under these conditions. Because of the asymmetric nature of the binding site, any fixed orientation of the benzoyl ring should result in magnetic non-equivalence of the 3′ and 5′-^{19}F

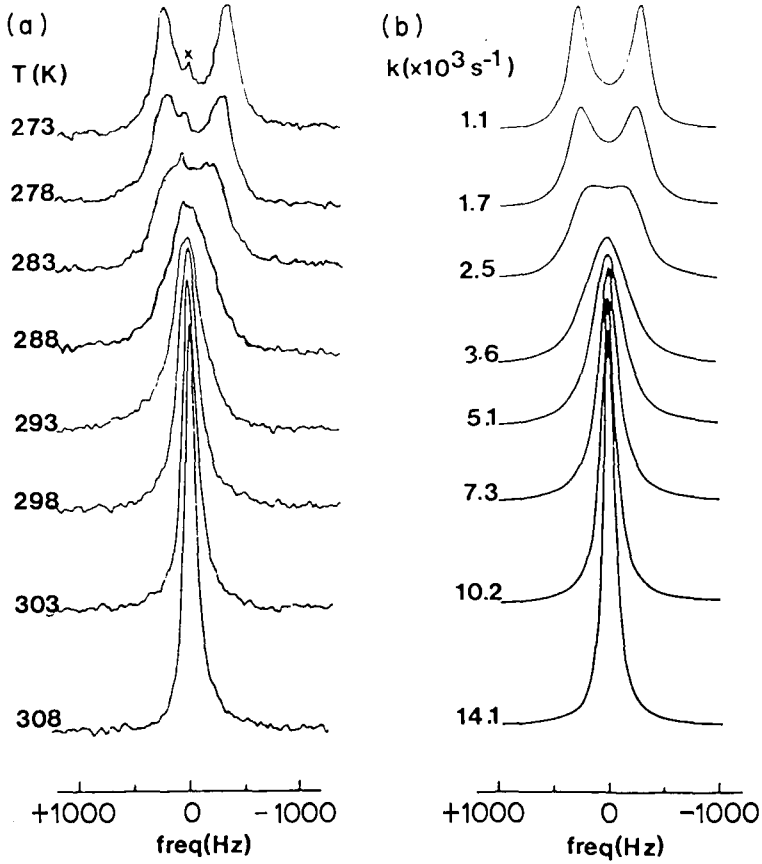
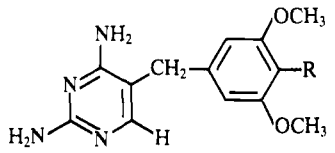


Fig. 13. Observed (a) and calculated (b) 188.3 MHz ^{19}F NMR spectra of 3′,5′-difluoromethotrexate bound to *L. casei* dihydrofolate reductase. The sample contained slightly less than one molar equivalent of difluoromethotrexate, so that all the ligand is bound to the enzyme. The small sharp resonance marked × represents a small amount (< 5%) of the impurity *N*-(3′,5′-difluoro-4-methylaminobenzoyl)-L-glutamate. (Reprinted with permission from Ref. 83.)

nuclei. The simplest process resulting in exchange of the 3′ and 5′ environments is motion about the symmetry axis of the benzoyl ring, i.e. simultaneous rotation about the N(10)—C(4′) and C(1′)—CO bonds. Fitting the experimental lineshape data to such a two-site model led to a calculated barrier of approximately 54 kJ mol^{-1}.[83] At 298 K this corresponds to a ring-flipping rate of 7.3×10^3 s^{-1}. Further ^{19}F experiments were carried out on enzyme–difluoromethotrexate–NADPH ternary complexes. The spectra were similar to those seen for the binary complex, and the rate of ring flipping for the ternary complexes was found to be 2.6–2.8 times that observed for the binary complex. It was suggested that this was because coenzyme binding has led to some changes in the protein conformation in the vicinity of the benzoyl-ring binding site. An attempt has been made to explain the change in terms of the differences observed for the crystal structure of the binary and ternary complexes.[83]

This study has been followed up more recently with similar dynamic NMR investigations involving ^{13}C-labelled trimethoprim derivatives.[84,85] ^{13}C-methoxy-labelled brodimoprim (**6**), for example, showed two equal-intensity ^{13}C signals at 274 K, which coalesced to a single peak at 287 K. The rate of ring flipping for this process was estimated to be 140 s^{-1} at 298 K compared with 250 s^{-1} for trimethoprim itself (**7**).



6 R = Br
7 R = OCH_3

2.6. Paramagnetic probes

Many proteins and enzymes require one or more metal centres for their function. In systems that incorporate paramagnetic metals these sites form a reference point from which distances to other parts of the protein or to binding ligands may be determined by relaxation or chemical-shift studies. For proteins or enzymes that incorporate diamagnetic metals it is often possible to substitute a paramagnetic nucleus and retain function. The replacement of Mg^{2+} by Mn^{2+} is a commonly used example, as illustrated in a recent study on tubulin.[86] In many instances the ligand itself may provide the paramagnetic metal ion, in which case distances to various

macromolecule resonances can be determined and used to locate the binding site. For systems not involving metal ions, stable organic free radicals, often containing a nitroxide moiety, can be used as spin-label probes. If the spin label is covalently attached to the ligand to be studied the distances from the bound probe to various nuclei of the macromolecule can be used to locate the binding site for the natural ligand if the probe does not cause a significant change in binding mode.

The theory and application of paramagnetic probes has been covered extensively by Dwek.[1] In the presence of a paramagnetic centre both chemical shifts and relaxation times of nearby nuclei may change significantly. The two major mechanisms by which unpaired electrons can interact with nuclear spins (and bring about these changes) are the Fermi *contact* interaction and the *dipolar* interaction. The former operates mainly through direct transfer of electron density from the metal to the observed nucleus, while the latter is a through-space effect that provides the basis for obtaining geometrical information from shifts and relaxation enhancements by paramagnetic centres. The separation of dipolar from contact contributions is an important aspect of interpretation of these experiments.[1,2,87]

2.6.1. Chemical-shift perturbations

On association with a paramagnetic ion, a given nucleus experiences shifts due to (i) electrostatic changes associated with complex formation, (ii) the Fermi contact interaction and (iii) a pseudocontact or dipolar interaction. The first of these can be estimated by binding of a suitable diamagnetic analogue of the paramagnetic ion, the second term is small and is usually ignored, and the third, and largest, term is the key parameter for deriving distance information. When various simplifying conditions are met, the term can be represented by the equation

$$\delta_p = D(3\cos^2\theta - 1)/r^3, \tag{26}$$

where D is a constant, θ is the angle between the metal–nucleus vector and the principal magnetic axis of the complex, and r is the corresponding distance. It is usual not to evaluate D directly but rather to obtain *relative* distances from the metal to several nuclei via equations like

$$\frac{\delta_{P1}}{\delta_{P2}} = \frac{(3\cos^2\theta_1 - 1)r_2^3}{(3\cos^2\theta_2 - 1)r_1^3}, \tag{27}$$

where the subscripts refer to separate ligand nuclei 1 and 2.[1,2]

When ligand binding to a metal-containing macromolecule is slow on the chemical-shift timescale, separate signals for free and complexed species may be detected. Saturation-transfer techniques may be used to assist

assignment of resonances in the complex if those in the free ligand have already been established.[87] When exchange is fast on the chemical-shift timescale, fitting of the observed (averaged) shift to the appropriate equilibrium equations allows limiting shifts to be derived.[87]

2.6.2. *Relaxation-rate perturbations*

The Solomon[42] and Bloembergen[88] equations describe the contribution of a paramagnetic centre to relaxation rates of nearby nuclei:

$$\frac{1}{T_{1M}} = \frac{2}{15}\frac{\gamma_I^2 g^2 S(S+1)\beta^2}{r^6}\left(\frac{3\tau_c}{1+\omega_I^2\tau_c^2}+\frac{7\tau_c}{1+\omega_S^2\tau_c^2}\right) + \tfrac{2}{3}S(S+1)\frac{A^2}{\hbar}\frac{\tau_c}{1+\omega_S^2\tau_e^2}, \tag{28}$$

$$\frac{1}{T_{2M}} = \frac{1}{15}\frac{\gamma_I^2 g^2 S(S+1)\beta^2}{r^6}\left(4\tau_c+\frac{3\tau_c}{1+\omega_I^2\tau_c^2}+\frac{13\tau_c}{1+\omega_S^2\tau_c^2}\right) + \tfrac{1}{3}S(S+1)+\frac{A^2}{\hbar}\left(\frac{\tau_e}{1+\omega_S^2\tau_e^2}\right). \tag{29}$$

Here T_{1M} and T_{2M} are respectively the longitudinal and transverse relaxation times of a nucleus in the bound complex; subscripts I and S refer to nuclear and electron spins respectively; γ is the gyromagnetic ratio, ω the Larmor frequency, g the Landé g factor, β the Bohr magneton, $A/\hbar$ the electron–nuclear hyperfine coupling constant, and r the distance between the nucleus and the paramagnetic centre. The correlation times are defined as

$$\frac{1}{\tau_c} = \frac{1}{\tau_s}+\frac{1}{\tau_m}+\frac{1}{\tau_r}, \tag{30}$$

$$\frac{1}{\tau_e} = \frac{1}{\tau_s}+\frac{1}{\tau_m}, \tag{31}$$

where τ_s is the electron-spin relaxation time, τ_m the lifetime of a nucleus in the bound state and τ_r the rotational correlation time.

The first term in each of (28) and (29) originates from dipolar interactions and the second from Fermi contact interactions. The latter are usually neglected and the former used to obtain geometrical information. The necessity of deriving correlation times can often be avoided by deriving relative distances via

$$\frac{(1T_{1,2M})_i}{(1/T_{1,2M})_j} = \frac{r_j^6}{r_i^6}, \tag{32}$$

where i and j are different nuclei. It is stressed that the assumptions implicit in deriving the above equations must be considered to see whether they are valid or not in individual cases.[1,2]

In the slow-exchange limit values of T_{1M} and T_{2M} can be measured directly from spectra. In the fast-exchange limit the following equations are used:[19,89]

$$\frac{1}{P_M q}\frac{1}{T_{1P}} = \frac{1}{P_M q}\left(\frac{1}{T_1^{obs}} - \frac{1}{T_1^{dia}}\right) = \frac{1}{P_M q T_1^{os}} + \frac{1}{T_{1M} + \tau_m}, \tag{33}$$

$$\frac{1}{P_M q}\frac{1}{T_{2P}} = \frac{1}{P_M q}\left(\frac{1}{T_2^{obs}} - \frac{1}{T_2^{dia}}\right)$$

$$= \frac{1}{P_M q T_2^{os}} + \frac{1}{\tau_m}\left(\frac{T_{2M}^{-1}(T_{2M}^{-1} + \tau_M^{-1}) + \Delta\omega_M^2}{(T_{2M}^{-1} + \tau_m^{-1})^2 + \Delta\omega_M^2}\right), \tag{34}$$

where P_M is the mole fraction of bound ligand, q is the coordination number and $\Delta\omega_M$ is the chemical-shift difference between bound and free species. T_{iP} $(i = 1, 2)$ represents the relaxation contribution from the paramagnetic ion, T_i^{obs} and T_i^{dia} $(i = 1, 2)$ are the observed relaxation time and that due to the diamagnetic control, and T_i^{os} $(i = 1, 2)$ are relaxation times due to outer-sphere relaxation (i.e. due to interactions with paramagnetic ions not bound to the ligand). It is assumed that $P_M q \ll 1$ in this derivation. When outer-sphere relaxation is neglected, and for $1/T_{2M} \gg \Delta\omega_M$, (23) and (34) reduce to

$$\frac{1}{T_{iP}} = \frac{P_M q}{T_{iM} + \tau_m} \quad (i = 1, 2). \tag{35}$$

Provided that $\tau_m < T_{2M}$, a plot of T_{iP} versus P_M allows T_{iM} to be determined. If $\tau_M \gg T_{iM}$ then relaxation is said to be "exchange-limited", and no geometrical information can be obtained.[87] This condition can occur fairly frequently, and the need for careful testing for partial or full exchange limitation (via frequency dependence of relaxation) has recently been emphasized.[90]

As noted above, many applications of the theory relate to the case of a ligand binding to a macromolecule already containing a paramagnetic centre. Relative distances from the paramagnetic centre to various ligand nuclei help to locate the binding site. Examples of the quantitative application of this theory are given in Section 4.1.7 for the binding of substrates to adenylate kinase. The alternative experiment involving paramagnetic ligands, where relaxation properties of the macromolecule are monitored, is also widely applied. It should also be noted that, even in a qualitative sense, the selective broadening of protein resonances on binding

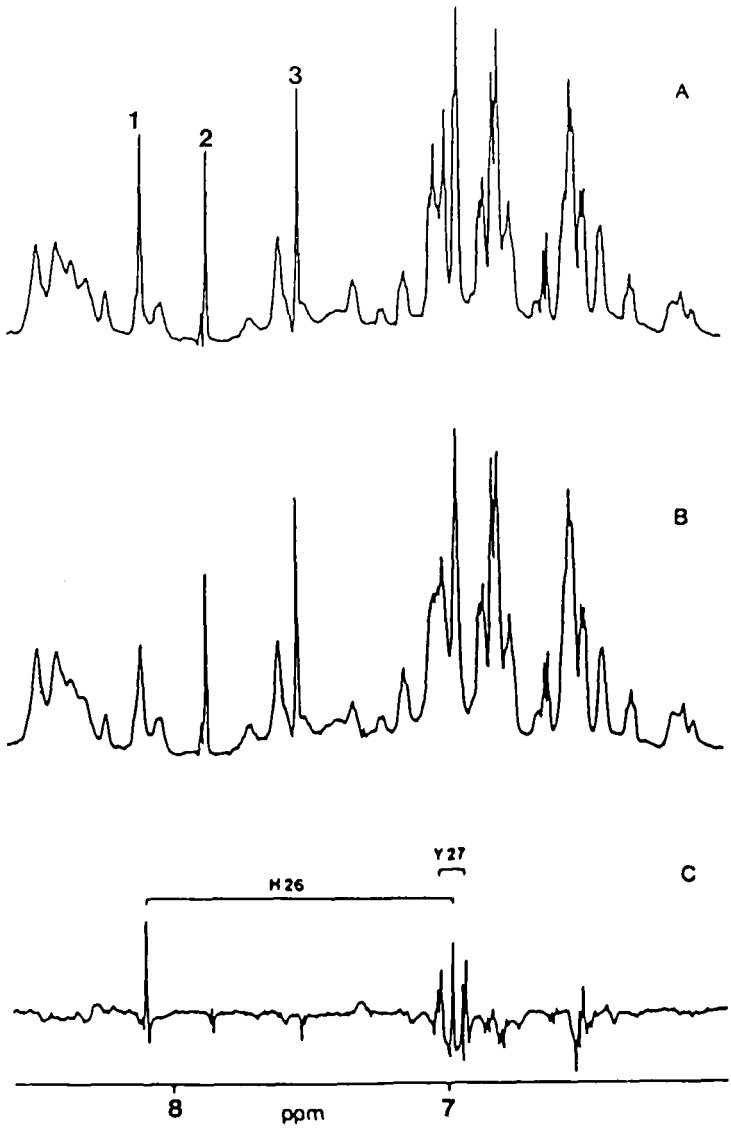


Fig. 14. Aromatic region of the 500 MHz ^{1}H NMR spectrum of oxidized cytochrome b_5: (A) native cytochrome b_5 at 24°C (pH 6.9). The C2—H proton resonances of the three surface histidines are labelled 1—3. (B) Cytochrome b_5 with Cu(II)NTA (0.11 M). (C) Difference spectrum A – B. The resonances of His^{26} and Tyr^{27} that are broadened by Cu(II)NTA are indicated in the difference spectra. These resonances were assigned by 2D double-quantum spectroscopy and NOESY spectra. (Reprinted with permission from Ref. 91. © 1989 Academic Press.)

of a metal containing ligand is an extremely useful method of determining the *site* of interaction of these ligands. Figure 14 shows how such broadening was used in a qualitative fashion to determine the Cu(II)NTA (NTA = nitrilotriacetic acid) bonds near His^{26} and Tyr^{27} residues of cytochrome b_5.[91] Two-dimensional difference spectroscopy also provides a convenient means of mapping binding sites of spin labelled ligands on macromolecules.[92]

Other studies that make use of paramagnetic centres to probe ligand binding involve observation of relaxation properties of water molecules. A paramagnetic site in water produces an increase in nuclear-spin relaxation rates of the water protons when a rapid coordination exchange of the water molecules occurs at the active site. This paramagnetic effect is reduced when the site is occupied by ligands other than water. Thus, by measuring the reduction of paramagnetic effects on the water protons in the presence of ligands that may bind to the paramagnetic site, it is possible to derive information about the coordination site. A recent illustrative example is a study of the copper site of dopamine β-mono-oxygenase by Obata *et al.*[93] Similarly, the effects on water relaxation of spin labels or paramagnetic metal ions bound to macromolecules can give valuable structural and thermodynamic information. On binding to a macromolecule, the relaxation rate of the water protons may be enhanced because of the hindrance of free rotation of the spin label and nearby water molecules, which increases the correlation time for dipolar interactions between the unpaired electron and water protons. An example is the interaction of a nitroxide spin labelled steroid substrate analogue with Δ^5-3-ketosteroid isomerase.[94]

2.7. Other methods

A range of other NMR techniques has been used in studies of macromolecule–ligand interactions. Many of these can be regarded as technological advances that make it easier to apply some of the methods discussed above. For example, polarization-transfer and spectral-editing techniques improve sensitivity and reduce spectral complexity, thus allowing chemical-shift information to be more readily observed. The development of 2D NMR has also made a major contribution in this area. Thus, while in the past studies of ligand binding for proteins of 10 kDa and above have tended to focus mainly on ligand signals, the recent expansion in the range of 2D techniques available has meant that macromolecular signals are increasingly being utilized. Current technology is such that significant numbers of assignments can now be made in systems approaching 20 kDa, including, for example, dihydrofolate reductase[95] and myoglobin.[96] The

Table 2. Properties and applications of NMR nuclei for small-molecule–large-molecule interactions.

Nucleus	Advantages	Disadvantages	Major applications
^{1}H	High sensitivity	Overlapped spectra in large macromolecules	Protein structure in solution
	Large amount of information accumulated on shifts, couplings, etc.	Complex nuclear relaxation in multispin systems	Geometries of ligand complexes with nucleic acids
			Conformations of bound ligands
^{2}H	Simple relaxation behaviour	Requires specific enrichment	Isotopic diluent for ^{1}H studies
	Isosteric with ^{1}H		Studies of membrane order
^{13}C	Widely dispersed chemical shifts	Low sensitivity and natural abundance	Probe of environment and dynamics of bound state
	Present in backbone of ligands and macromolecules	Requires specific enrichment for some applications	Dynamics of macromolecules and changes in flexibility on ligand binding
^{15}N	Large chemical-shift range	Very low sensitivity and natural abundance	Hydrogen bonding Protonation state of ligands
	Very sensitive to intra- and intermolecular interactions	Usually requires specific enrichment	
		Negative NOEs	
	Narrow spectral lines		
^{19}F	High sensitivity	Usually requires artificial incorporation into macromolecule or ligand	Determination of changes in ligand environment on binding
	No background signals	Negative NOEs for macromolecules	
	Very large chemical-shift range		
^{31}P	High sensitivity	Limited applicability to proteins	Studies of changes in nucleic acid conformation on ligand binding
	Sensitive probe of bond-angle changes		

ability to monitor changes in environments (chemical shifts) of a large number of protein sites following ligand binding should greatly assist in defining the interaction. Measurements of variation in exchange rates of macromolecule NH-protons may also be correlated with changes in hydrogen bonding on ligand binding.

Many of the following applications involve isotope labelling. In future it is likely that there will be an increasing use of NMR studies involving site-directed changes (either specific isotope labelling or substitution of amino acids) in proteins. This development will become possible because of major advances in molecular-biology techniques.

3. NUCLEAR PROBES

One of the major advantages of NMR over other methods for the study of structure, dynamics and molecular interactions is the site-specific nature of the information derived. It is an extremely valuable feature of NMR that many different nuclei can be detected separately, and that different nuclei have substantially differing types of information to deliver. Some of the methods described in Section 2 are applicable to certain nuclei but not to others, so that in any study of small-molecule–large-molecule interactions it is often possible to benefit from the varying advantages of different nuclear probes and thus obtain complementary information. Such an approach is illustrated in the applications described in Section 4, but it is useful first to briefly describe the pertinent properties of the nuclei most commonly used in studies of small-molecule–large-molecule interactions in biological systems. A summary of the major features of this discussion is given in Table 2. A more extensive survey of the application of these and other nuclei to a wider range of chemical studies may be found in several books on multinuclear NMR.[97–99]

3.1. ^{1}H NMR

The proton has traditionally been the nucleus most widely studied by chemists and biologists, and in large part this is due to its very high sensitivity to detection (exceeded only by tritium)[97] and general suitability for all the methods described in Section 2. As a result of the widespread study of this nucleus, a large body of knowledge on chemical shifts, coupling constants and other key parameters has been accumulated. This information, derived mainly from studies of organic molecules, is thus now

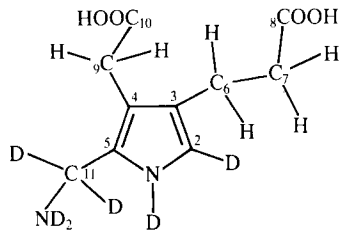
available for use in extrapolations to macromolecules and to macromolecule–ligand interactions.

The principal disadvantage of the ^{1}H nucleus for studies of small-molecule–large-molecule interactions is its small chemical-shift range, and the resulting potential for severely overlapped spectra of macromolecules. Despite this, it still remains the most widely utilized nucleus in ligand-binding studies.

3.2. ^{2}H NMR

Deuterium NMR finds extensive application in a number of specialist areas, although its general applicability is somewhat limited by the need for isotopic substitution in many cases. Areas of major application include studies of membrane ordering and mobility and liquid crystals. More often than not, the utility of deuterium arises not in direct studies of the nucleus itself, but in ^{1}H NMR studies where isotopic dilution by ^{2}H is used either to simplify spectra, to aid in assignments, or to delineate and study kinetics of exchangeable protons. An example of a system mentioned already in which deuterium substitution has been used to make assignments is HRP.[100,101]

Deuterium substitution is also of particular value in making ^{13}C detection easier in large proteins. Consideration of the relative gyromagnetic ratios and spin numbers for ^{1}H and ^{2}H in (5) suggests that replacement of each hydrogen by deuterium should lead to an approximate 16-fold reduction in the efficiency of dipolar relaxation; this in turn leads to much sharper and hence more intense spectral lines. The usual problem of multiplet splitting (and attendant signal-to-noise reduction) in ^{2}H spectra of small molecules is ameliorated in large proteins because rapid ^{2}H relaxation in the slowly tumbling species effectively decouples ^{13}C from ^{2}H. An illustration of the order-of-magnitude improvement of ^{13}C spectra of deuterated sites on ligands bound to macromolecules, brought about by the deuterium substitution, can be seen in a study of the binding of C-2 deuterated derivatives of porphobilinogen, PBG (**8**), to PBG synthase.[102] Based on a



8

correlation time of 245 ns at the bound site of the 280 kDa protein and a C—D bond length of 1.05 Å, the C-2 linewidth of PBG was calculated to be 21 Hz. (This compares with the experimental linewidth of *ca.* 55 Hz, presumed to be larger owing to contributions from chemical-shift-anisotropy relaxation.) In contrast, the calculated linewidth for the C-2 site in the protonated derivative is 420 Hz, which would make this resonance essentially unobservable.

3.3. ^{3}H NMR

Tritium is not commonly used in NMR studies of ligand binding, but is mentioned here because it has considerable potential as a probe nucleus. The widespread use of tritium as a radiotracer in binding studies means that there is available a body of expertise in the incorporation of this isotope into biological ligands. Combined with the very favourable NMR properties of ^{3}H, namely sensitivity 1.2 times that of the proton and high NMR frequency,[103] it may be a useful nucleus in cases where a proton study is appropriate but background signals interfere with resonances of interest. Such an application has recently been demonstrated by Evans *et al.*[104] for the binding of porphobilinogen to porphobilinogen-deaminase.

3.4. ^{13}C NMR

The large chemical-shift range of ^{13}C and the ubiquitous presence of carbon nuclei in the backbones of both small and macromolecular systems render it an extremely important probe nucleus for ligand–macromolecule binding. These major advantages are, in part, offset by the relatively low sensitivity to detection of ^{13}C NMR, but this is often overcome by specific ^{13}C labelling.

The sensitivity of ^{13}C chemical shifts to the charge state of molecules has made it an extremely useful probe of the ionization state of bound ligands. This applies not only when the probe ^{13}C nucleus is part of an ionizable carboxyl group, as was noted earlier for a study of the ionization of isocitrate bound to isocitrate dehydrogenase, but also when the ^{13}C probe site is adjacent to an N-protonation site, as in the methotrexate example illustrated in Fig. 3.

^{13}C NMR also finds widespread application in studies of enzyme–substrate interactions, where the large chemical-shift range of the nucleus make it a sensitive probe of hybridization changes occurring in the substrate

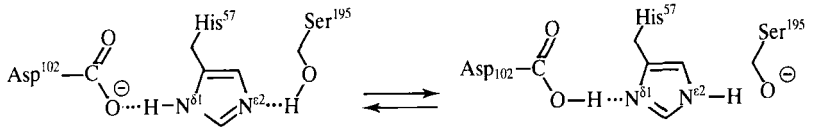
during enzyme-catalysed reactions.[105] Like those above, these studies normally utilize ^{13}C-labelled ligands.

Where sufficient protein or enzyme is available, ^{13}C NMR studies at natural abundance can be valuable in measuring overall and internal flexibility of proteins (from relaxation-time measurements at multiple backbone and sidechain sites) and in determining how this changes in the presence of binding ligands.[17] Selective ^{13}C labelling at key amino acid residues is also frequently applied.[16]

3.5. ^{15}N NMR

^{15}N suffers from very poor sensitivity owing to its low natural abundance (0.37%) and low gyromagnetic ratio ($\gamma_N \approx \frac{1}{10}\gamma_H$). However by ^{15}N enrichment, and with the use of polarization-transfer techniques[106,107] and inverse detection methods,[108,109] the sensitivity problem can be significantly reduced. ^{15}N NMR, then, has some attractive features for studies of proteins. These include the quite large chemical-shift range (*ca.* 150 ppm for protein resonances), sensitivity of amide nitrogen resonances to environmental changes,[109] and the substantially narrower lines than for protons or ^{13}C nuclei owing to the low gyromagnetic ratio of ^{15}N. These features mean that ^{15}N NMR spectra have intrinsically higher resolution than proton or ^{13}C spectra of proteins. Indeed, almost total resolution of all nitrogen sites for proteins of a few kilodaltons can be achieved in two-dimensional heteronuclear correlated spectra.[110]

The great sensitivity of ^{15}N shifts to hydrogen-bonding interactions makes specifically ^{15}N-labelled residues an attractive probe of such interactions as illustrated, for example, in a study of H-bonding in the "catalytic triad" or "charge relay" system **(9a)** ↔ **(9b)** at the active site of serine proteases.[111]



9a **9b**

Incorporation of histidine, labelled at both ring nitrogens, into α-lytic protease and measurement of ^{15}N shifts suggested that a strong hydrogen bond links the active-site histidine and serine residues in the resting enzyme

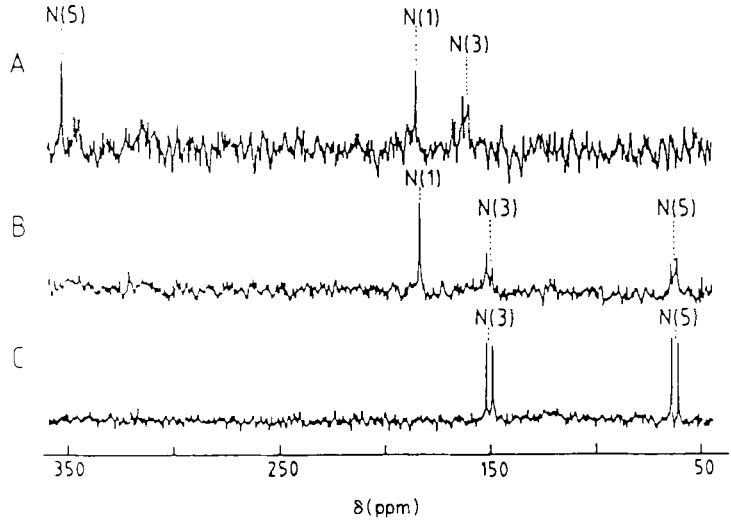
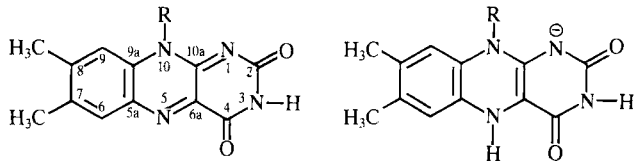


Fig. 15. ^{15}N NMR spectra of *Clostridium MP* apoflavodoxin reconstituted with [1,3,5-^{15}N]FMN in the oxidized state (A) (55 800 acquisitions) and in the reduced state (B and C). Spectrum B (119 800 acquisitions) was taken under proton-coupled conditions, and spectrum C (54 300 acquisitions) was obtained by applying the DEPT pulse sequence. (Reprinted with permission from Ref. 112. © 1989 American Chemical Society.)

in solution,[111] a conclusion that is at odds with X-ray diffraction data in the solid state.

^{15}N-Labelled ligands are also commonly used to probe electronic effects. Figure 15 shows the sensitivity of ^{15}N shifts to the oxidation state of riboflavin 5′-phosphate, FMN (**10**), bound to *Clostridium MP* flavodoxin.[112]



10a FMN (oxidized)

10b FMN (reduced)

Flavodoxins are a group of small (14–23 kDa) flavoproteins, and in the above study changes in ^{15}N (and ^{13}C) shifts in flavin–flavodoxin complexes from different species were used to make deductions about hydrogen

bonding and the electronic structure of the coenzyme. Note in Fig. 15 the significant increase in sensitivity for protonated nitrogens obtained by applying the DEPT pulse sequence. Caution must be exercised in measuring conventional ^{1}H-decoupled ^{15}N spectra of protein systems because of potential signal nulling from partial negative NOEs. In the above case NOEs for the N(3) site of bound FMN are -0.4, compared with -4.6 for free FMN (the latter value is close to the theoretical maximum[112]).

3.6. ^{19}F NMR

Its high sensitivity to detection and a lack of background interference from the macromolecule make ^{19}F NMR particularly useful for studying ligand–macromolecule interactions.[113,114] The ^{19}F nucleus is also very sensitive to environmental changes, making ^{19}F chemical shifts a valuable probe. ^{19}F occurs naturally in some drug molecules or enzyme inhibitors, but even if it is not normally present in the ligand being studied, its small size means that it can be incorporated into natural ligands or coenzymes without major loss of activity. Extensive use has been made, for example, of fluorinated derivatives of pyridoxal-5′-phosphate to probe the role of pyridoxal phosphate in glycogen phosphorylase.[115–117]

3.7. ^{31}P NMR

Like ^{19}F, the ^{31}P nucleus has the dual advantages of high sensitivity and relative lack of interference from unwanted background signals. The lack of ^{31}P nuclei in proteins or enzymes (except in phosphorylated systems) precludes the use of this nuclear probe in such systems. Applications thus tend to be confined to phosphorylated ligands (e.g. nucleotides or analogues) that bind to enzymes. In addition to the usual application of chemical-shift changes to probe environmental changes, the use of saturation-transfer methods to determine kinetics of binding of coenzymes and the rates of reactions involving phosphorylated substrates promises to be an increasingly important area of application. In an example of the latter approach, time-dependent ^{31}P saturation transfer has recently been used to determine rate constants for phosphate transfer on glucose-1-phosphate in the reaction catalysed by phosphoglucomutase.[118] The other major area of application of the ^{31}P nucleus is in studies involving ligand bonding to polynucleotides. Here the ^{31}P signals from the macromolecule are used as a probe for ligand binding.

3.8. Other nuclei

The nuclei discussed above are those most frequently encountered in ligand-binding studies, although many other nuclei are also widely applied. Metal ions are particularly valuable, both as direct probes of binding environments owing to their generally large chemical-shift range, and as perturbing probes in paramagnetic relaxation or chemical-shift studies (Section 2.6).

4. APPLICATIONS

A detailed description and analysis of macromolecule–ligand interaction studies carried out prior to 1981 is contained in the book by Jardetzky and Roberts,[2] which devotes two complete chapters to protein–ligand interactions as well as containing major sections on enzyme–substrate, protein–nucleic-acid and protein–membrane interactions. Some of the systems covered there include ribonuclease, stapylococcal nuclease, lysozyme, dihydrofolate reductase, antibody combining sites, alkaline phosphatase, gene 5 protein, various kinases, dehydrogenases and serine proteases, aspartate transcarbamylase, glycogen phosphorylase, concanavalin A, aspartate aminotransferase and glutamine synthetase. More recent reviews on the subject of macromolecule–ligand interactions include those by Blumenstein,[3] Roberts[4] and Feeney.[34] The following selected applications focus on studies since 1986.

Before examining specific applications in detail, it is instructive to give an overview of the general types of problems studied over recent years, and to attempt to illustrate the most widely used techniques. This has been done by listing (in Table 3) 80 examples of ligand–macromolecule interactions involving NMR, taken from a single journal (*Biochemistry*) for the period 1986–1988 inclusive. While we have not attempted to give a complete list of all studies carried out, nor a quantitative statistical compilation of methods, the table does allow some useful trends to be conveniently summarized. For example, features that may be discerned are the dominanance of ^{1}H and ^{31}P NMR in studies of nucleic acids, the widespread use of ^{13}C labelling in enzyme–substrate studies, the ubiquitous use of chemical-shift information in all types of macromolecule–ligand interactions, the importance of paramagnetic-relaxation studies in enzyme systems, and the high relative frequency with which ^{19}F studies appear, despite the fact that it is not widely found in "natural ligands". This points to its favourable properties as a probe nucleus.

Table 3. Nuclei and techniques used in studies of ligand–macromolecule interactions.

Study	Nucleus studied							Techniques[a]					Reference (all from the journal *Biochemistry*)
	^{1}H	^{13}C	^{15}N	^{19}F	^{31}P	^{2}H	Other	Chemical shift	Relaxation measurements	Magnetization transfer	NOE	Paramagnetic probes	
Enzyme–ligand													
Enzyme–substrate													
Porphobilinogen binding to porphobilinogen-deaminase	*	*					^{3}H	*		*			1986, **25**, 905
Prolidase-catalysed hydrolysis of L-alanyl-L-proline	*							*					1986, **25**, 1054
Tryptophan-synthase-catalysed isomerization of fluorinated tryptophan derivatives				*				*					1986, **25**, 4240
Large fragment of DNA polymerase I binding oligoriboadenylates and oligoribouridylates	*							*			*		1986, **25**, 5131
Interaction of α-chymotrypsin with 4-nitrophenyl-(phenylselenyl)-acetate							^{77}Se	*					1986, **25**, 5625
α-Lytic protease in complexes with phenylmethanesulphonyl fluoride and diisopropyl fluorophosphate	*		*					*					1986, **25**, 7751

Human carbonic anhydrase I catalysis of CO_2/HCO_3 exchange		*				*	*	*	*	*	1987, **26**, 183
Interaction of 6FPLP–glycogen phosphorylase–AMP with glucose-1-phosphate			*			*			*		1987, **26**, 360
Phosphoribosyl transferase binding of phosphoribosyl-1-pyrophosphate	*			*		*				*	1987, **26**, 1051
Adenylate kinase binding of AMP	*			*		*	*		*	*	1987, **26**, 1645
Isocitrate dehydrogenase binding of isocitrate and α-ketoglutarate		*				*					1987, **26**, 3461
Porphobilinogen synthase binding of amino levulinate		*				*					1987, **26**, 4258
Dopamine β-monooxygenase coordination of azide and cyanide	*					*	*			*	1987, **26**, 4962
ATP binding to adenylate kinase				*		*	*				1987, **26**, 6411
Isoleucyl tRNA synthase binding of L-isoleucine and L-valine	*					*			*		1987, **26**, 6531
Adenosine deaminase binding of purine ribosides		*				*	*				1987, **26**, 8450
Porphobilinogen synthase binding of [5,5-^{2}H,5-^{13}C]-5-aminolevulinate		*			*	*					1988, **27**, 4475

(*Continued*)

Table 3. (*Continued*)

Study	Nucleus studied							Techniques[a]					Reference (all from the journal *Biochemistry*)
	^{1}H	^{13}C	^{15}N	^{19}F	^{31}P	^{2}H	Other	Chemical shift	Relaxation measurements	Magnetization transfer	NOE	Paramagnetic probes	
Adenylate kinase complexes with ATP, GTP, GDP and AMP					*			*	*			*	1988, **27**, 8669
Phosphoglucomutase binding of glucose-1,6-bisphosphate					*			*		*			1989, **28**, 548
Alternative modes of substrate binding to dihydrofolate reductase	*							*		*	*		1989, **28**, 2297
Enzyme–inhibitor													
Dihydrofolate reductase complex with trimethoprim in the presence and absence of coenzymes		*						*					1986, **25**, 1925
Δ^{5}-3-Ketosteroid isomerase binding of spiro[doxyl-2,3′-5′α-androstan]-17′-β-ol	*							*	*			*	1987, **26**, 3927
α-Chymotrypsin binding of a dipeptide trifluoromethyl ketone	*	*		*				*					1987, **26**, 7603

Methotrexate analogues binding to dihydrofolate reductase	*						•						1987, **26**, 8585
Carbonic anhydrase I and II binding of 4-fluorobenzene sulphonamide	*		*	*			*	*	*				1988, **27**, 4310
Sheep-kidney Na,K ATP-ase binding of $Co(NH_3)_4$ ATP	*				*		*	*				*	1988, **27**, 4840
Porphobilinogen deaminase interaction with 5-aminolevulinic acid		*					*						1988, **27**, 7984
Pepsin complex with a tripeptide inhibitor	*		*				*				*		1988, **27**, 8297
Co(II)-substituted carboxy peptidase A binding of L- and D-phenylalanine and carboxylate inhibitors	*						*	*					1988, **27**, 8318
Ligand complexes formed with mutant dihydrofolate reductase	*	*			*		*						1989, **28**, 1353
Enzyme–coenzyme													
Glycogen phosphorylase complexes with 6FPAL and 6FPLP				*			*	*					1986, **25**, 1932
Reaction between apohaemoglobin and heme	*						*						1986, **25**, 5288
Lactoperoxidase binding of heme	*						*						1986, **25**, 5844

(*Continued*)

Table 3. (*Continued*)

Study	Nucleus studied							Techniques[a]					Reference (all from the journal *Biochemistry*)
	^{1}H	^{13}C	^{15}N	^{19}F	^{31}P	^{2}H	Other	Chemical shift	Relaxation measurements	Magnetization transfer	NOE	Paramagnetic probes	
Bacterial luciferase interaction with riboflavin-5′-phosphate (FMN)		*						*					1986, **25**, 8062
Bacterial luciferase interaction with FMN		*	*		*			*					1986, **25**, 8067
Actin peptide 114–118 binding ATP	*							*			*		1987, **26**, 1471
Creatine kinase binding of MgATP	*							*			*		1987, **26**, 5338
Actin peptide 106–124 binding of ATP and tripolyphosphate	*							*			*		1987, **26**, 6023
NAD binding to glutamate dehydrogenase	*							*				*	1987, **26**, 8443
NAD^{+} and NADH binding to UDP-galactose-4-epimerase					*			*	*				1989, **28**, 2645
Protein–ligand													
Antisickling ligands binding to haemoglobin	*							*	*			*	1986, **25**, 808

Cytochrome cd_1 complexes with electron-donating proteins	*						*		*			1986, **25**, 1089
Interaction of tropomysin with troponin T	*						*					1986, **25**, 4548
Dimerization of neurophysin	*						*					1986, **25**, 6579
Flavodoxin binding of FMN		*	*		*		*				*	1986, **25**, 6789
Interaction of a single neurophysin tyrosine with di- and tri-peptides	*						*					1987, **26**, 995
Antithrombin III interaction with heparin fragments	*						*					1987, **26**, 1391
Bovine neurophysin I (des 1–8 derivative) binding peptides	*						*					1987, **26**, 1518
Kringle 1 binding of εACA and BASA	*						*			*	*	1987, **26**, 3827
Antithrombin III binding to heparin	*						*					1987, **26**, 4403
Complex formation between cytochrome c and flavodoxins	*				*		*		*			1987, **26**, 4403
Tubulin binding of GTP and GTP(γP)				*	*		*		*			1987, **26**, 6099
Neurophysin binding of oxytocin and 8-Arg-vasopressin			*				*			*		1987, **26**, 6415
Cytochrome b_5 binding of Cu(II) NTA	*						*					1987, **26**, 7102

(*Continued*)

Table 3. (*Continued*)

Study	Nucleus studied							Techniques[a]					Reference (all from the journal *Biochemistry*)
	^{1}H	^{13}C	^{15}N	^{19}F	^{31}P	^{2}H	Other	Chemical shift	Relaxation measurements	Magnetization transfer	NOE	Paramagnetic probes	
Aliphatic ligand binding to kringle 4	*							*	*	*			1989, **28**, 1368
DNA–small-molecule													
Tomamycin binding to DNA	*							*					1986, **25**, 3021
Interaction between distamycin A and a symmetrical DNA dodecamer	*							*			*		1986, **25**, 3296
Mytomycin C binding to DNA	*							*					1986, **25**, 4337
Complex formation between the oligonucleotide d(TATC) mgAcr and the complementary strand d(GATA)	*							*			*		1986, **25**, 5357
Complex formation between d-$(GCATTAATGC)_2$ and a minor groove binding drug	*							*			*		1986, **25**, 5902
Complex formation between chromomycin A_3 and $d(ATGCAT)_2$	*				*			*			*		1987, **26**, 1058

Interaction of copper(II) isonictoinohydrazide with DNA			*		*			1987, **26**, 3781
λcro repressor complex with O_R3 DNA	*	*			*	*	*	1987, **26**, 7262
Interaction of $Co(NH_3)_6^{3+}$ with helical B-DNA				^{59}Co ^{23}Na	*	*		1987, **26**, 7724
Actinomycin D binding to oligodeoxyribonucleotides	*		*		*			1988, **27**, 915
Complex formation between d(T*TCTGT)-M_5Acr and the complementary sequence d(GCACAGAA)	*				*		*	1988, **27**, 1265
Complexes of echinomycin with the complementary d(ACGT) and d(TCGA) duplexes	*				*		*	1988, **27**, 1744
Interaction of nogalomycin with the duplex $d(5'\text{-GCATGC})_2$	*				*		*	1988, **27**, 4340
Hexamethonium 2H interaction with NaDNA				^{14}N ^{23}Na	*	*		1988, **27**, 4367
Actinomycin C binding to self-complementary oligodeoxyribonucleotides	*		*		*			1988, **27**, 6021
Interaction between Ff gene 5 protein and $d(pA)_{40-60}$	*				*		*	1988, **27**, 6947
Complex between distomycin A-$d(CGCGAATTCGCG)_{21}$	*				*		*	1988, **27**, 8088

(*Continued*)

Table 3. (*Continued*)

Study	Nucleus studied							Techniques[a]					Reference (all from the journal *Biochemistry*)
	^{1}H	^{13}C	^{15}N	^{19}F	^{31}P	^{2}H	Other	Chemical shift	Relaxation measurements	Magnetization transfer	NOE	Paramagnetic probes	
Lipid–protein													
Rhodopsin reconstituted into phospholipid bilayers					*	*		*	*				1986, **25**, 4818
D-Lactate dehydrogenase bound to model membrane systems				*				*					1987, **26**, 549
Pf1 coat protein bound to a model membrane system	*		*					*			*		1987, **26**, 1373
Bee-venom melittin interaction with dimyristoylphosphatidylcholine bilayers					*	*		*	*				1987, **26**, 5803
Lipid–small-molecule													
λ-Tocopherol interaction with a phospholipid model membrane						*		*	*				1986, **25**, 319
Gramicidin A and S in multimellar vesicles of dipalmitoylphosphatylcholine					*	*		*	*				1986, **25**, 3796

Inhibitors, 1,2-cyclohexanedione and dipyridamole interaction at membrane channels				^{35}Cl	*	*	1986, **25**, 7895
Cytochrome C interaction with mixed dimyristoylphospatidylcholine serine bilayers			*		*	*	1986, **25**, 3804
Bile acid movement across model membrane systems	*				*		1987, **26**, 1801
Tripeptide perturbation of phosphocholine bilayers			*		*	*	1987, **26**, 6127
Gramicidin interaction with liposomes and isolated human erythrocyte membranes		*			*		1987, **26**, 6613
Ubiquinone-10 interaction with plasmid membranes of *E. coli* and inner membranes of beetroot mitochondria			*		*	*	1987, **26**, 7702
λ-Tocopherol interaction with model membrane systems			*		*	*	1988, **27**, 1432
Gramicidin A in phospholipid membranes			*		*	*	1988, **27**, 2357

[a]Only the techniques (except dynamic NMR studies) listed in Section 2 are included, although many of the studies involve other techniques such as 2D NMR or polarization transfer.

4.1. Protein (enzyme)–ligand interactions

In most instances the techniques used to study ligand binding are similar, irrespective of whether the macromolecule is classed as a protein or an enzyme. If the interaction being studied is between an enzyme and a substrate then the additional complication of reactions occurring during the course of the NMR measurement is present. Even in these cases, however, NMR can be applied, and ^{13}C NMR, in particular, has proved invaluable in helping to define enzyme mechanisms.[105]

4.1.1. Neurophysins

The binding of peptide hormones such as oxytocin to neurophysins is a much-studied example of protein–ligand binding. Neurophysins are small proteins ($M_r = 10\,000$) that interact non-covalently with the peptide hormones oxytocin and vasopressin within the neurosecretory granules of the hypothalamo–neurohypophyseal tract.[119]

Previous ^{13}C NMR studies involving labelled hormones and neurophysins have yielded significant information on the nature of the complex.[3] More recently, ^{15}N NMR[120] has been applied in this system. These studies have taken advantage of developments such as polarization transfer and indirect detection, in combination with specific ^{15}N-labelling, to improve the sensitivity of detection of the ^{15}N nucleus. Live *et al.*,[120] for example, synthesized a number of ^{15}N-labelled derivatives (each singly labelled at a different position) of oxytocin and 8-arginine vasopressin (AVP) and recorded INEPT ^{15}N spectra of complexes of these ligands with neurophysin. These showed the systems to be generally in slow exchange on the chemical shift timescale. Chemical shifts of free and bound resonances are indicated in Table 4.

A previous model of the binding of AVP to neurophysin is summarized in Fig. 16.[119,121] This model incorporates a degree of hydrogen bonding for elements of the hormone backbone with the protein. This concept is supported by the data in Table 4. The largest binding-induced shifts occur, for example, for the amide nitrogen of residue 3. The ^{15}N of Phe-3 shifts 3.2 ppm downfield on binding, the direction associated with H-bonding. An accompanying change in the associated proton shift (0.76 ppm) is also observed. Proton shifts of this magnitude are associated with formation of strong NH H-bonds. In a previous study a similar large change (4.2 ppm) in the α-C resonance of position 3 of oxytocin had been observed, but this was attributed to some change in the sidechain conformation.[122] Although conformational changes cannot be completely discounted, the authors

Table 4. Effects of binding and pH on apparent chemical shifts of hormone in hormone–neurophysin mixtures.

	Chemical shift (ppm)					
			Hormone–neurophysin mixtures			
	Unbound hormone[a]		Bound		Free	
	pH 6	pH 3	pH 6	pH 2.6–3	pH 6	pH 2.6–3
[[^{15}N]Asn^{5}]oxytocin	116.1	116.1	114.2	114.4	116.1	116.1
[[^{15}N]Tyr^{2}]oxytocin		123.5	125.0	124.7		123.5
[[^{15}N]Asn^{5}]AVP	115.9	115.9	115.1	[115.7][b]	115.9	[115.7][b]
[[^{15}N]Tyr^{2}]AVP		123.1	124.7	124.4		123.1
[[^{15}N]Phe^{3}]AVP	120.2	120.8	123.9	123.4	120.2	120.8
[[^{15}N]Cys^{6}]AVP		119.7	120.9			

[a]With the exception noted, the chemical shifts of the free hormones represent those separately determined in the absence of protein. The chemical shift of unbound [[^{15}N]Phe^{3}]AVP at pH 6 was determined from two-dimensional ^{1}H[^{15}N] spectra in the presence of protein. The proton shift of the unbound hormone (determined in the absence of protein) was used to compute the chemical shift of the ^{15}N with which it was associated in hormone–protein mixtures.

[b]Bound and free peaks could not be resolved. The chemical shift shown represents the average peak position. (Data are from Ref. 120.)

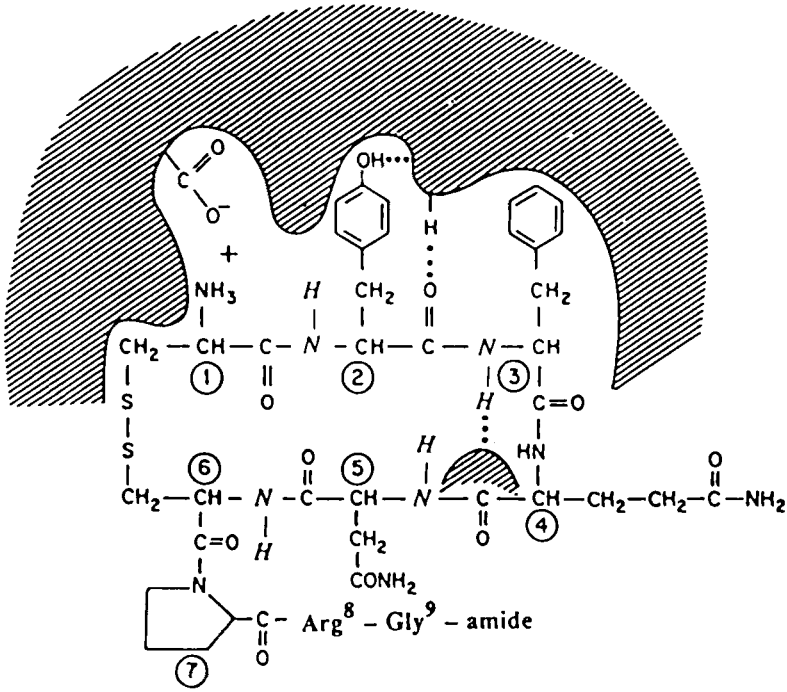


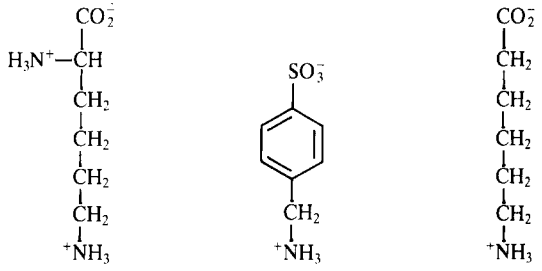
Fig. 16. Proposed bonding interactions between AVP and neurophysin. (Reprinted with permission from Ref. 120. © 1989 American Chemical Society.)

suggest that it seems unlikely that these would produce a shift of this magnitude.

Other recent investigations of neurophysins have probed the location of the peptide binding site using a combination of chemical modification and NMR studies,[123,124] and have provided insight into the self-association of neurophysin,[125] which is thermodynamically linked to peptide–hormone bonding.

4.1.2. Kringle proteins

Plasminogen contains five homologous modules of MW ≈ 10 000 each, known as kringles. The principal role of kringles appears to be the anchoring of the enzyme plasmin to its main target substrate, the fibrin matrix of blood clots. Kringle 1 and 4 domains have been shown to bind L-lysine (**11**) and a number of lysine analogues including BASA (**12**) and εACA (**13**). The lysine-binding ability is thought to be intimately related to the high affinity of plasminogen and plasmin for fibrin.



11 12 13

Ligand binding by kringles 1 and 4 has been the subject of many NMR studies. Some of the earlier work focused on quantitative analysis of 1D ^{1}H NMR experiments. For example, the binding of BASA to kringle 4, studied using ^{1}H NMR spectroscopy, showed that binding of BASA results in the perturbation of mainly aromatic rather than aliphatic resonances and produces a narrowing of many resonances, which suggests a change in flexibility of the protein.[126]

Subsequent studies showed that the Phe^{64}, Trp^{72} and, possibly, the Trp^{62} residues are at the lysine binding site, and that Tyr^{74} is probably in contact with Trp^{62}.[127,128] Consequently, it has been suggested that the aromatic residues provide a lipophilic contact site for the hydrophobic chain of the ligand, while the polar end groups are stabilized by interactions with ionic residues.

More recently, 2D ^{1}H NMR studies have been used to obtain a greater understanding of the interactions of ligands with the kringles.[8,23,47] Ramesh *et al.*[8] noted, for example, that in the aromatic region of COSY spectra of kringle 4 shift changes for Trp^{62} were fairly similar for the binding of L-Lys or D-Lys, while significantly different Phe^{64} shifts were induced by the two enantiomeric ligands (Fig. 2). It was suggested that the Phe residue was probably close to the enantiomeric C_α centre on the bound ligand, while the Trp^{62} residue at the bound site was nearer to the C_γ—C_δ—C_ε—N_ε segment of the aliphatic ligand chain. Later studies involving a range of lysine analogues as ligands provided support for this conclusion.[23] As was noted earlier, NOEs between ligand resonances and those of Trp^{62}, Phe^{64} and Trp^{72} also confirmed the proximity of these residues to the binding site.

Similar studies have been carried out for kringle 1.[47] In this case assignments of the aromatic region of the ^{1}H NMR spectrum of kringle 1 were again made with the assistance of COSY spectra. The effects of binding of BASA and εACA were then determined by comparing the aromatic regions of the 2D COSY spectrum of kringle 1 in the presence and absence of ligands. A combination of these experiments and protein–ligand

NOE measurements confirmed the involvement of Tyr^{62} and Tyr^{72} (which replaces Trp^{72} in kringle 4) at the binding site and, unlike the case for kringle 4, also suggested the proximity of Phe^{36}.

4.1.3. Dihydrofolate reductase

Dihydrofolate reductase is a key enzyme involved in the production of precursors for nucleocide synthesis, and is hence an important target in the design of cytotoxic and antibacterial agents. As such, the binding of substrate, coenzyme and inhibitors to the enzyme has been widely studied by NMR. Many of the studies done prior to 1986 have been summarized in reviews by Roberts[4] and Feeney.[34] Briefly, these studies utilized a variety of techniques including chemical-shift measurement, saturation transfer, transferred NOEs and dynamic lineshape analysis to obtain information about the conformation, ionization state, orientation, functional-group interactions, kinetics and mobility of ligands bound to dihydrofolate reductase. This system is also an ideal one with which to illustrate the advantages that can be gained from making use of several nuclear probes, including ^{1}H, ^{2}H, ^{13}C, ^{15}N, ^{19}F and ^{31}P.

In many of the early studies evidence was obtained for the existence of multiple conformations of enzyme–ligand complexes. This appears to be the case, for example, for the enzyme alone, for the enzyme–trimethoprim–$NADP^+$ complex and for enzyme–substrate–coenzyme complexes, but apparently not for complexes of methotrexate with the enzyme, in either the presence or absence of coenzyme (see Ref. 36 and references therein). Recent work has thus focused on further defining the nature of the various conformational states,[36] and on examining differences in the conformations and dynamics of ligand complexes formed with mutant enzymes containing key amino acid substitutions.[13]

For the dihydrofolate-reductase–folate–$NADP^+$ complex three conformations have been identified.[129] At low pH (<5.5) a single conformation, denoted I, was observed, while at high pH (>7.5) two other conformations, denoted IIa and IIb, were found to coexist in a ratio of 1 : 1.67. At intermediate pH all three forms were present. In recent work 2D exchange spectroscopy and 1D saturation-transfer experiments have been used to complete the assignment of aromatic and anomeric ^{1}H resonances of bound ligands. Figure 17 shows the aromatic region of a 2D exchange spectrum of a sample containing a two-fold molar excess of both $NADP^+$ and folate at pH 6.5. Under these conditions, most of the intense cross-peaks arise from chemical exchange of ligand molecules between free and bound states. (The exchange peaks can be distinguished from NOE cross-peaks because the former are present only when the sample contains

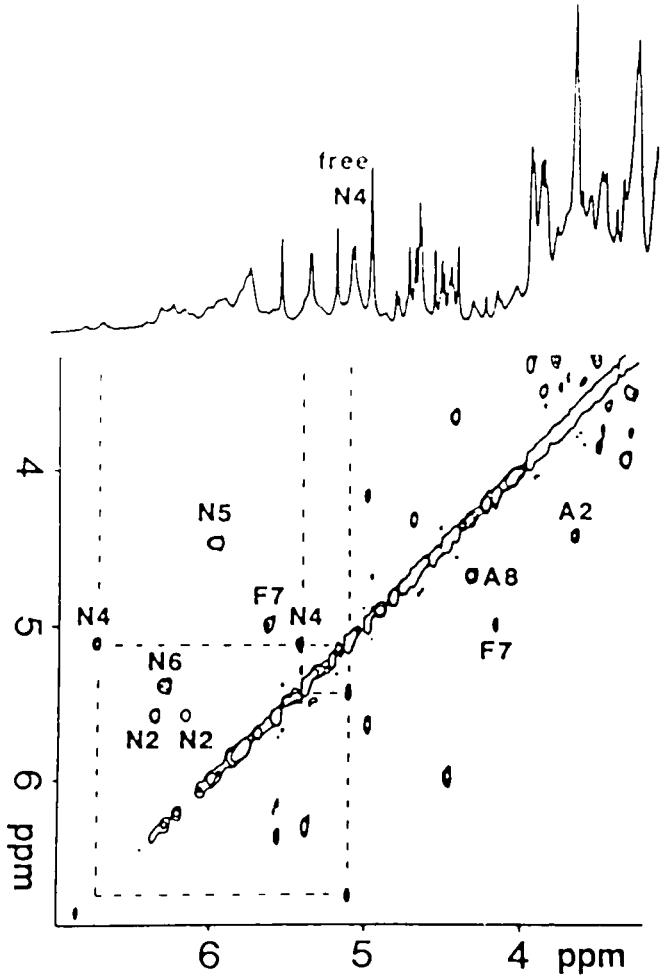


Fig. 17. Aromatic region of a two-dimensional ^{1}H NMR spectrum obtained from a sample containing dihydrofolate reductase and a two-fold molar excess of both $NADP^+$ and folate at pH* 6.5 using the NOESY pulse sequence with a mixing time of 100 ms. The corresponding region of the 1D spectrum is shown above. Under the conditions of this experiment, the cross-peaks shown arise from exchange of the ligands between the free state and conformations IIa and IIb of the complex. The ligand proton from which each cross-peak arises is indicated: N2–N6 denote the protons of the nicotinamide ring and A2–A8 the protons of the adenine ring of $NADP^+$, while F7 denotes the pteridine 7-proton of folate. (Reprinted with permission from Ref. 36. © 1989 American Chemical Society.)

Table 5. Chemical shifts of ligand nuclei in the three conformational states of the dihydrofolate-reductase–folate–$NADP^+$ complex and in the dihydrofolate-reductase–methotrexate (MTX)–$NADP^+$ complex.

	Chemical shift[a] (ppm)			
	Enzyme–folate–$NADP^+$			
Nucleus	I	IIa	IIb	Enzyme–MTX–$NADP^+$ [b]
Nicotinamide (^1H, ^{13}C)				
N2	6.32	6.30	6.12	6.34
N4	6.81	6.68	5.38	6.16
N5	5.74	5.92[c]	5.96[c]	5.34
N6	6.41	6.24	6.24	6.31
$^{13}CONH_2$	96.32	95.88	94.26	95.96[d]
Pyrrophosphate (^{31}P)	−14.4	−14.4	−14.4	−14.9
	−16.3	−16.3	−16.3	−16.5
Adenine (^1H, ^{31}P)				
A2	3.63	3.60	3.60	3.64
A8	4.30	4.26	4.26	4.31
2′PO_4	2.7	2.7	2.7	2.7
Pteridine (^1H, ^{15}N)				
H7	4.50	4.12	5.58	4.50
$^{15}N5$	2.5	9.9	10.7	
2′,6′H	2.25	1.84	1.84	
3′,5′H	3.37	3.26	3.26	

[a]Nicotinamide and adenine protons of the coenzyme are denoted N2–N6 and A2, A8 respectively. Data are from Ref. 36. ^1H and ^{13}C chemical shifts are given relative to dioxane, ^{15}N shifts relative to the resonance of free folate, pH* 6.3, and ^{31}P shifts relative to inorganic phosphate, pH* 8.0. Downfield shifts positive. ^{13}C and ^{31}P data are from Ref. 35. ^{15}N data are from Ref. 130. ^1H chemical shifts have been redetermined and are more precise than those obtained earlier from transfer of saturation experiments at 270 MHz.[35]

[b]Data from Refs. 7 and 20.

[c]Individual assignment to conformations IIa and IIb is uncertain.

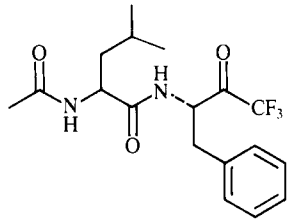
[d]Data (recalculated relative to dioxane) from Ref. 131.

significant populations of both free and bound ligand.) Note that in Fig. 17 the coexistence of conformations IIa and IIb is represented by the dotted line indicating exchange between the free ligand N4 proton and two bound states. From this and other experiments under conditions where conformation I was present, chemical shifts for the various conformations were derived, and are summarized in Table 5.

4.1.4. Chymotrypsin

Chymotrypsin and other serine proteases have also been widely studied by

NMR. For a summary of earlier studies see Ref. 2. A recent investigation[132] that illustrates the combined use of ^{1}H, ^{13}C and ^{19}F studies involved the slow binding inhibitor ($K_i = 1\ \mu M$) *N*-acetyl-L-leucyl-L-phenylalanyl trifluoromethyl ketone (**14**). On the basis of analogy with aldehydic peptides,



14

it has previously been proposed that peptidyl trifluoromethyl ketones react with the active-site serine to form a hemiketal. It is thought that the resemblance of this hemiketal to the tetrahedral adduct formed during the catalytic reaction is a major factor contributing to the tight binding. In the study by Liang and Abeles[132] a derivative of (**14**), ^{13}C-labelled at the ketone carbonyl, was synthesized, and from a comparison of ^{13}C shifts of the bound inhibitor with model hemiketals it was concluded that the trifluoroketone is present at the active site as an ionized hemiketal group. ^{19}F chemical shifts as a function of pH indicated that the pK_a of the hemiketal hydroxyl in the complex is approximately 4.9, 4.2 units lower than the pK_a of model hemiketals. This was suggested as evidence that serine proteases are able to stabilize the oxyanions of tetrahedral adducts. ^{1}H NMR shifts established the presence of an Asp–His H-bond and protonation of the imidazole group of His-57 in the tetrahedral adducts. A proposed structure of the adduct, based on the NMR studies, is shown in Fig. 18.

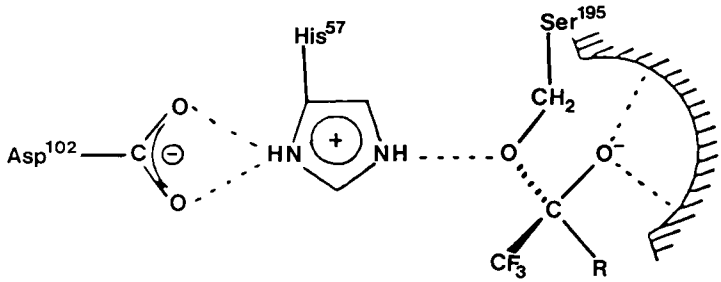
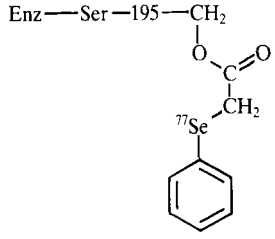


Fig. 18. Structure of the adduct formed between chymotrypsin and (**14**). R = $CH_3CONHCH[CH_2CH(CH_3)_2]CONHCH(CH_2Ph)$–. Striped area represents oxyanion hole. – – –, H bonds to Ser^{195} and Gly^{193} in the oxyanion hole. (Reprinted with permission from Ref. 132. © 1989 American Chemical Society.)

In other recent studies of the chymotrypsin system ^{19}F and ^{2}H relaxation measurements have been used to examine the mobility of a 4-fluorophenyl ring attached to the active site.[18] $^{19}F-^{1}H$ NOEs transferred from ligand to protein have been used to locate the binding site of 4-fluorocinnamate ligands,[44] and ^{77}Se NMR has been used to investigate a (phenylselenyl)acetyl-α-chymotrypsin reaction intermediate (**15**) in the α-chymotrypsin-catalysed hydrolysis of the substrate 4-nitrophenyl(phenylselenyl)acetate.[133]



15

4.1.5. Carbonic anhydrase

Carbonic anydrase is a zinc-containing metalloprotein found in two distinct forms, CAI and CAII, in human erythrocytes. CAII has extremely high activity in CO_2 hydration, limited only by availability of the substrate:

$$CO_2 + H_2O \rightleftharpoons HCO_3^- + H^+$$

CAI is more abundant than CAII in human erythrocytes; however, its activity is about a thousand-fold less than that of CAII. CAI is nearly completely inhibited by Cl^- at the concentration of the anion found in the erythrocyte, thus its biological function is not fully understood.

Aromatic and heterocyclic primary sulphonamides are particularly potent competitive inhibitors of carbonic anhydrase. NMR studies have demonstrated that sulphonamide inhibitors coordinate to the metal ion at the active site of carbonic anhydrase through the nitrogen atom of the SO_2NH_2 group, and that sulphonamide is an anion at the active site.[134-136] A more recent study by Dugad and Gerig[6] on the binding of the inhibitor 4-fluorobenzenesulphonamide, 4FBSA (**1**), provides an example of the application of many of the techniques described in Section 2, including ^{1}H, ^{19}F and ^{15}N shift measurements, linewidth and relaxation effects, NOE measurements and saturation-transfer studies.

The inhibitor in solution produces a single fluorine resonance, while addition of CAI or CAII results in a resonance appearing 6 ppm upfield of

the free 4FBSA signal. When 4FBSA is in excess, separate signals for the bound and free forms are observed as interaction with the inhibitor is slow on the NMR chemical-shift scale (Fig. 1). As was noted earlier, the stoichiometry of the interaction between 4FBSA and the anhydrases was determined by adding increasing amounts of the inhibitor to a known amount of enzyme (Fig. 1). ^{19}F experiments with both CAI and CAII showed that two molecules of inhibitor bind per molecule of enzyme. This was confirmed from ^{1}H NMR spectra of the anhydrases. These showed resonances down to -2.0 ppm, which were attributed to methyl groups close enough to aromatic rings in the tertiary structure to experience a ring current effect. Changes in these resonances were followed as the ratio of inhibitor to enzyme was increased. No further changes in the spectrum were observed once a 2 : 1 ratio was reached.

Saturation-transfer experiments were carried out to determine the exchange rates between inhibitor and anhydrases. For CAI these experiments were carried out in both directions, i.e. saturation of the free signal led to a 25% reduction in the bound signal, while saturation of the latter signal reduced the intensity of the free signal by 15%. Values derived for the forward and reverse rate constants, however, were not consistent with the observed concentration ratio of free to bound molecules. It was concluded that the simple equilibrium model used to obtain the rate-constant values was inadequate, and a more complex kinetic situation was indicated. However, in qualitative terms the value obtained for the dissociation rate constant of *ca.* 0.6 s^{-1} was not inconsistent with previous estimates,[137] and was used to predict the magnitude of exchange broadening to linewidths of the resonances.

Excess linewidth of the bound resonance was found to be strongly temperature-dependent, increasing by 130 Hz when the temperature was dropped from 25°C to 1°C. This observation could not be rationalized in terms of exchange broadening between free and bound species, but was consistent with an exchange process affecting only the bound inhibitor that becomes slower as temperature is lowered, leading to exchange broadening. This process presumably reflects rapid exchange between two sites in the bound complex. ^{15}N studies on enriched inhibitor provided further support for this in that a variable-temperature study showed a single ^{15}N resonance for the bound site at 25°C, but two closely spaced peaks at 2°C.[6]

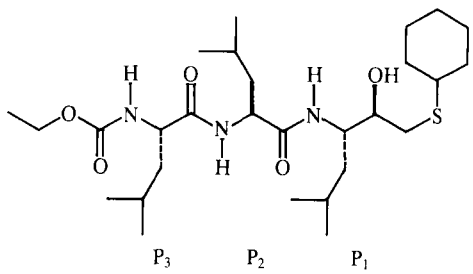
Spin–lattice relaxation and NOE experiments were also carried out on the inhibitor–enzyme complex. While T_1 for (**1**) in the absence of enzyme was 7.3 s, values for the "free" and bound peaks in Fig. 1 were 2.8 s and 0.42 s. The small value of the latter is consistent with that expected for a slow-tumbling macromolecule, while the value for the free state is reduced below that seen in the absence of enzyme (7.3 s), owing to exchange. This

exchange also results in a small negative $^{19}F-^{1}H$ NOE (-0.4), even for the free peak in Fig. 1. (No such NOE is detected in the absence of enzyme.)

Paramagnetic ^{13}C NMR relaxation studies have also recently been done on the kinetics and mechanism of HCO_3^-/CO_2 exchange catalysed by Mg(II)–carbonic-anhydrase I.[138] In this study measurements of paramagnetic relaxation rates $1/T_{1p}$ and $1/T_{2p}$ of the ^{13}C atom in HCO_3^- as a function of temperature, magnetic field strength, and substrate and apoenzyme concentration were fitted to (28) and (29) to obtain kinetic and geometric parameters associated with the reactions. The distance between the Mn^{2+} ion and the ^{13}C atom of HCO_3^- was determined to be 2.71 ± 0.03 Å, indicating that the bicarbonate is bound to the metal via two of its oxygen atoms in the central catalytic step. The interconversion rate for the reaction was deduced from inversion-transfer experiments in which signal intensities were monitored following selective inversion of HCO_3^- or CO_2 signals via a DANTE pulse sequence.[138]

4.1.6. Pepsin

A recent study of the binding of an inhibitor to the aspartic proteinase pepsin provides an example of the power of isotope-edited NOE spectroscopy.[49] The large size of the complex (*ca.* 35 kDa) meant that conventional NOE spectra would be severely overlapped; however, using an isotope-edited pulse sequence that detects only those protons attached to the ^{15}N-labelled sites, it was possible to considerably simplify spectra and determine bound conformations. In structure (**16**) of the inhibitor, the three peptide residues are P_1, P_2 and P_3.



16

Figure 19 shows isotope-edited NOE spectra in which the amide protons of the three residues are labelled on the diagonal, and cross-peaks to other protons are indicated. From these and other experiments involving ^{13}C labelling, as well as the observation of NOEs between bound inhibitors and the enzyme, it was possible to build a model of the binding-site conforma-

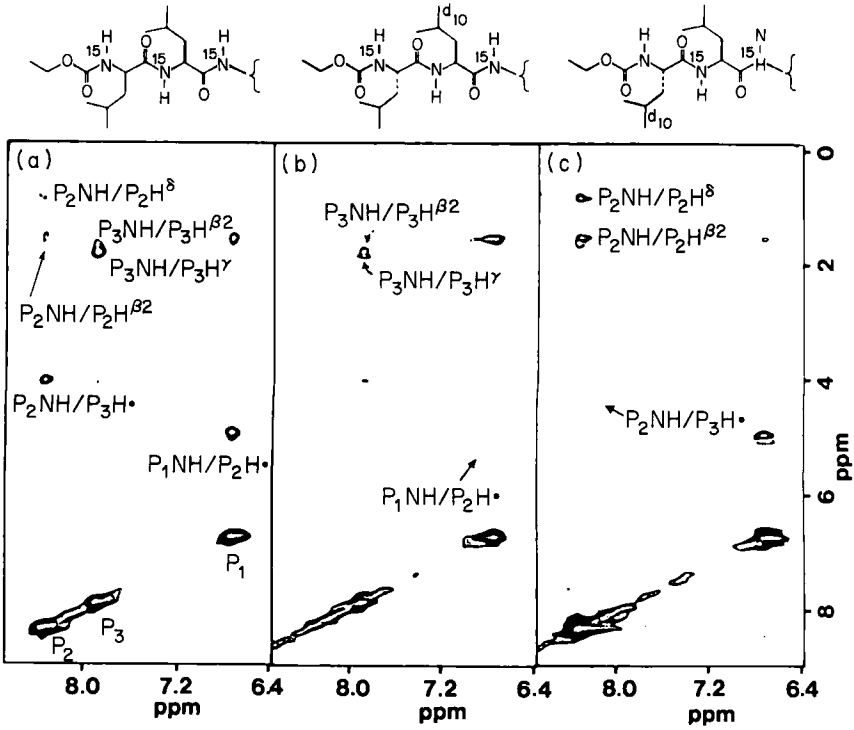


Fig. 19. ^{15}N isotope-edited 2D NOE spectra acquired with a mixing time of 50 ms of a pepsin/inhibitor (1/1) complex obtained using the labelled inhibitors shown at the top of the spectra. Nitrogen-labelled sites are marked "^{15}N". In (a) the diagonal peaks corresponding to the P_1–P_3 amide protons are labelled. In (b) and (c) the side chains marked d10 were fully deuterated and the arrows indicate the location in the spectra where cross-peaks are absent owing to deuterium labelling. The conformation of the bound inhibitor was derived from observed cross-peaks. (Reprinted with permission from Ref. 49. © 1989 American Chemical Society.)

tion, also based in part on X-ray data for the pepsin complex with a related inhibitor.[49]

4.1.7. Nucleotides binding to enzymes

This is one of the most widely studied types of macromolecule–ligand interactions. Because metal cofactors are often involved in enzymes that bind nucleotides, paramagnetic-relaxation methods are commonly utilized. The TRNOE technique is the other major method usually applied in such systems. The general principles involved in nucleoside binding to enzymes can be conveniently illustrated by examining studies on adenylate kinase.

This enzyme catalyses the reaction

$$\text{MgATP} + \text{AMP} \leftrightharpoons \text{MgADP} + \text{ADP}$$

Kinetic and NMR experiments have detected two distinct binding sites, one of which binds MgATP and MgADP, while the other is specific for uncomplexed AMP and ADP.[90] GTP and MgGTP are known to bind at the MgATP site, but the AMP site is highly specific for adenine nucleotides. Although the X-ray structure of the enzyme has been determined, there is continuing debate as to the location of the nucleoside binding sites.

Fry *et al.*[64] have previously used NMR to determine the conformation of enzyme-bound MgATP and to suggest a location for the MgATP binding site. In a more recent study the AMP site has been probed by examining the enzyme in the presence of Cr^{3+}AMPPCP (β,γ-methylenetriphosphate), a linear competitive inhibitor that binds at the MgATP site, and AMP. Distances from the metal to six protons and the phosphorus atom of AMP were determined using the paramagnetic T_1 probe method, while time-dependent TRNOEs were used to measure five interproton distances on enzyme-bound AMP. These two studies thus allowed the location and conformation of enzyme-bound AMP to be determined. Further information on the location of the site was provided from intermolecular NOEs to hydrophobic residues.[50]

In the paramagnetic-relaxation studies values of $1/T_{1P}$ and $1/T_{2P}$ ($= 1/\pi LW$) were measured as a function of $f =$ [bound Cr^{3+}AMPPCP]/[AMP]. After correction for outer-sphere relaxation, these were plotted against f to obtain the slopes shown in Table 6. Since the lower limit to the exchange rate of AMP, as derived from the maximum of $1/fT_2$, 6340 s^{-1}, is at least an order of magnitude greater than any of the $1/fT_{1P}$ values (Table 6), it was concluded that $1/T_{1P}$ was not exchange-limited.

Table 6. Paramagnetic relaxation rates for AMP bound to adenylate kinase.[a]

Atom	$1/fT_{1P}$ (s^{-1})[b]	$1/fT_{2P}$ (s^{-1})[b]	r (Å)[c]
P	474	6340	5.9 ± 0.3
H8	195	2160	8.9 ± 0.7
H2	228	1520	8.7 ± 0.6
H1′	106	1050	9.9 ± 0.7
H3′	299	—	8.3 ± 0.5
H4′	105	840	9.9 ± 0.7
H5′	374	2630	8.1 ± 0.5

[a]Data from Ref. 50.
[b]Obtained from slopes of plots of $1/T_{1,2P}$ (corrected for outer-sphere relaxation) versus f.
[c]Determined from (28); see text.

Thus, from (35) (with $f = P_{Mq}$), the values in Table 6 represent $1/T_{1M}$. These were substituted into (28) (with the last term neglected) to yield the distances (also shown in Table 6). The correlation time used in this expression was 3.5×10^{-10} s, derived from the frequency dependence of $1/T_{1P}$ of water protons due to enzyme-bound Cr^{3+}AMPPCP at 24.3, 250 and 260 MHz.[50]

Cross-relaxation rates between protons on bound AMP were determined from NOE build-up rates, as described in Section 2.4.3. Figure 12 shows a typical build-up curve, which immediately indicates the preference for an *anti* conformation, as deduced from the large NOE effects seen at H8 (and the negligible effect at H2) on irradiation of H2′. Further definition of the conformation was obtained from cross-relaxation rates and corresponding distances between other pairs of protons (Table 7). The results of the above studies, together with additional information from intermolecular NOEs, led to the proposed structure of the complex shown in Fig. 20.[50]

In other recent studies of the adenylate kinase system, Ray *et al.*[90] used the paramagnetic-relaxation method to determine distances between the metals Mn(II) or Co(II) and the phosphorous atoms of ATP, GTP, GDP and AMP nucleotides, and Shyy *et al.*[139] studies the stoichiometry of ligand binding from linewidth and coupling-constant measurements.

4.1.8. Porphobilinogen synthase and deaminase

While the traditional view has been that it may not be possible to observe substrates, intermediates or products bound to enzymes of greater than about 50 kDa molecular weight, recent studies[102,140] have demonstrated that quaternary carbons, or deuterated carbons, may be readily detected in

Table 7. Intramolecular NOEs and interproton distances within AMP bound to adenylate kinase.[a]

NOE	$-\sigma$ [b]	r (Å)[c]
H2′–H1′	0.21	2.70
H2′–H8	0.29	2.57
H3′–H8	0.31	2.53
H5′–H8	0.12	2.96
H4′–H1′	$\leqslant 0.07$	$\geqslant 3.24$
H1′–H8	$\leqslant 0.04$	$\geqslant 3.52$
H8–H1′	$\leqslant 0.04$	$\geqslant 3.57$

[a]Data obtained from Ref. 50.
[b]Obtained from time dependence of NOE (see text).
[c]Obtained from (21).

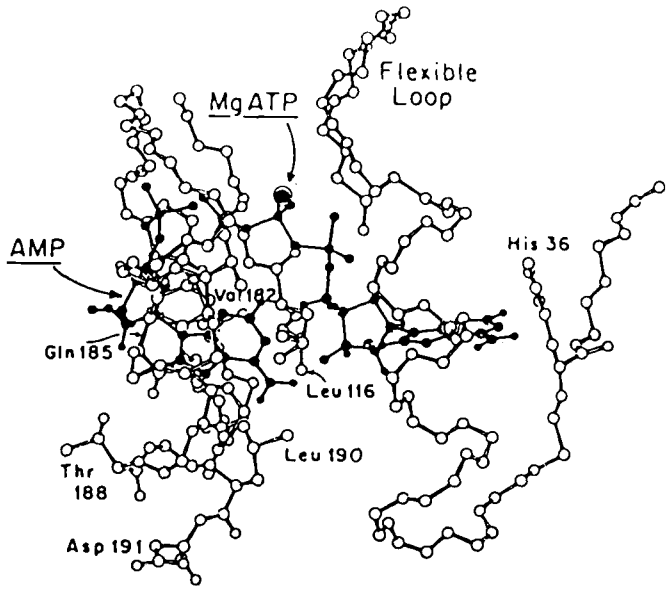
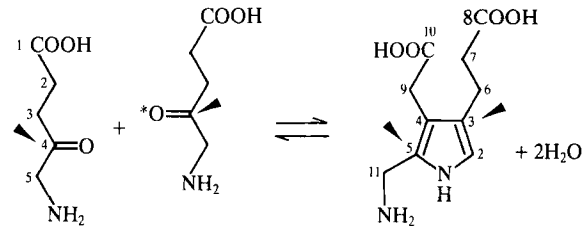


Fig. 20. Binding sites for AMP and MgATP on adenylate kinase as determined by NMR docking. The MgATP site was previously determined as described by Fry *et al.*[64] The AMP site was located on the basis of the conformation of bound AMP (Table 7), intersubstrate distances (Table 6) and intermolecular NOEs from protons of the enzyme to those of AMP. (Reprinted with permission from Ref. 50. © 1989 American Chemical Society.)

enzymes with molecular weights of several hundred kilodalton. Both types of site avoid the difficulty of significant line-broadening of protonated carbons due to dipolar interactions.[141,142] Figure 21 shows expanded regions of ^{13}C difference spectra of mixtures of the enzyme porphobilinogen synthase (PBG synthase), with the product [3,5-^{13}C]porphobilinogen derived from the labelled substrate [4-^{13}C]-5-aminolevulinate (ALA) (Scheme 1).

Porphobilinogen (PBG) synthase catalyses the above reaction, which is on the pathway for the biosynthesis of porphyrin, chlorophyll, vitamin B_{12} and a wide range of tetrapyrrole pigments. The reaction proceeds via a Schiff-base intermediate formed between one ALA and an active-site lysine. As seen in Fig. 21(c), [4-^{13}C]ALA (chemical shift 205.9 ppm) forms [3,5-^{13}C]PBG (chemical shift 121.0, C_5 and 123.0, C_3). In the equilibrium complex of [4-^{13}C]ALA and PBG two broadened peaks with chemical shifts of 121.5 and 127.2 are observed, possibly indicating the presence of a distorted form of PBG. When excess PBG is present exchange between free and bound species is slow on the NMR timescale, consistent with the



Scheme 1. Formation of [3,5-^{13}C]PBG from [4-^{13}C]ALA.

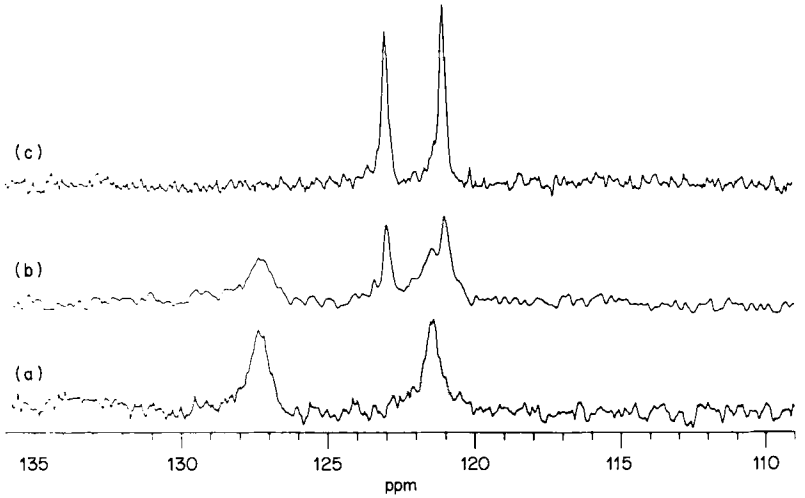


Fig. 21. Aromatic region of ^{13}C NMR spectra of PBG and PBG synthase complexes. (a) Difference spectrum of six ALA/octamer of holoenzyme, revealing the enzyme-bound PBG spectrum. (b) Difference spectrum of nine ALA/octamer of holoenzyme, showing both free and enzyme-bound PBG. (c) [3,5-^{13}C]PBG prepared from [4-^{13}C]ALA with catalytic amounts of PBG synthase. Spectra were processed with a 5 Hz line-broadening function. (Reprinted with permission from Ref. 140. © 1989 American Chemical Society.)

turnover rate of the enzyme.[140] Studies were also carried out with a methanethiosulphonate (MMTS) modified form of the enzyme that does not catalyse PBG formation, and in that case the predominant species observed in the complex was a Schiff-base adduct ($\delta = 166.5$ ppm). Activation of the MMTS-modified enzyme/Schiff-base complex with Cd^{2+} and 2-mercaptoethanol resulted in loss of the Schiff-base signal and the appearance of bound PBG signals.[140] This work has subsequently been extended via the use of double-labelled (^{2}H, ^{13}C) ALA analogues to allow methylene carbons that change hybridization during the reaction to be followed.[102]

^{13}C NMR and ^{3}H NMR have also recently been used to examine another enzyme on the porphyrin pathway, porphobilinogen-deaminase. In one study[104] ^{13}C NMR failed to detect signals from substrate bound to the 36 kDa enzyme, but the potential of ^{3}H NMR was demonstrated for studying systems in which there is a lack of an appropriate spectral "window" in the high-abundance background signal for ^{1}H NMR. Other

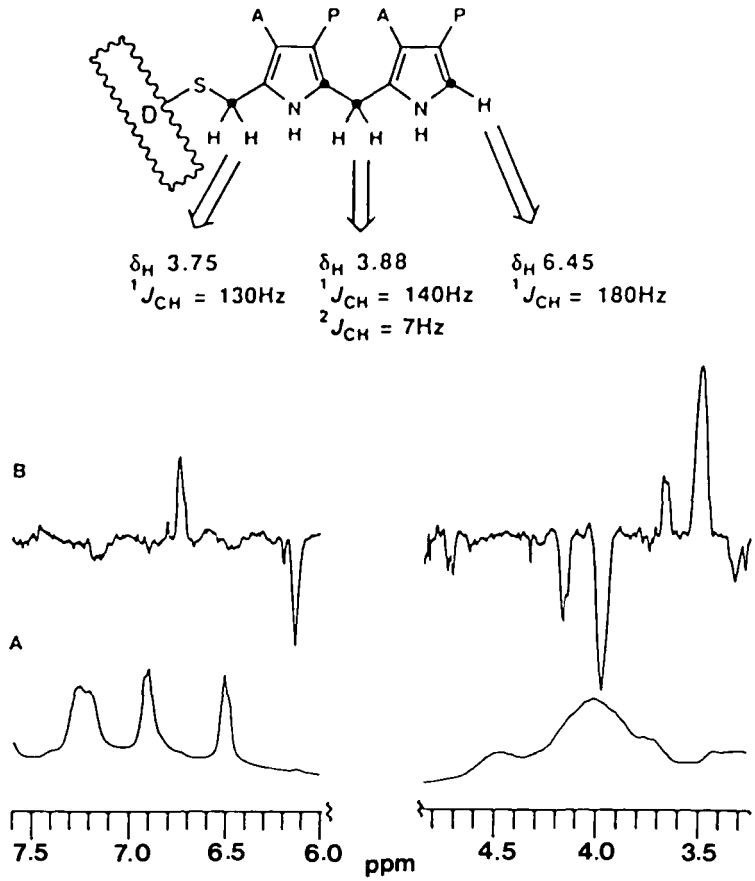
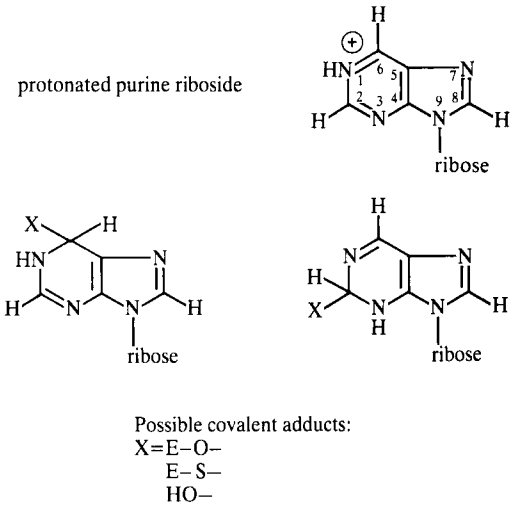


Fig. 22. 300 MHz ^{1}H NMR spectrum of PBG deaminase enriched from [5-^{13}C]ALA showing the relevant regions of (A) the normal proton spectrum and (B) the proton-detected zero and double-quantum coherence spectrum of the same region containing the three proton signals originating from the biosynthetically enriched dipyrromethane cofactor. The proton signals appear as antiphase multiplets. Conditions: 2.0 mM deaminase in 0.1 M phosphate buffer, pH 12.0, 20°C. Number of scans: (A) 384; (B) 6440. (Reprinted with permission from Ref. 143. © 1989 American Chemical Society.)



Scheme 2. Three possible structures of purine riboside–enzyme complex.

studies (see Ref. 143 and investigations described therein) have defined the active site of PBG deaminase to contain a dipyrromethane cofactor linked covalently to the enzyme via a cysteinyl sulphydryl group. In this case the power of heteronuclear multiple-quantum coherence experiments[144,145] for editing out the "bulk" proton signal and observing only protons attached to a specifically enriched ^{13}C nucleus was demonstrated. Figure 22 shows, for example, the simplification of the ^{1}H spectrum of PBG deaminase biosynthetically enriched with ^{13}C in its dipyrromethane cofactor. On the basis of chemical shifts of model dipyrromethanes attached to sulphur, the individual protons attached to ^{13}C sites were readily assigned, as indicated in the figure.[143]

4.1.9. Adenosine deaminase

This enzyme catalyses the hydrolysis of (deoxy)adenosine to deoxy(inosine). Purine riboside, which lacks a leaving group at C6, is an unreactive adenosine analogue and a potent reversible inhibitor of the enzyme. It is convenient to regard this compound as an example of a pseudo substrate which undergoes a reversible reaction at the binding site. Three possible structures have previously been proposed for purine riboside in the enzyme complex,[145] the first involving protonation at N-1, the second covalent adduct formation at C-2, and the third covalent adduct formation at C-6 (Scheme 2).

In a recent study by Kurz and Frieden[147] ^{13}C NMR spectroscopy was used to determine which of these structures is most likely, and consequently to gain some understanding of the mechanism of the enzyme. Purine riboside, ^{13}C-labelled at position C-2 or C-6, gave chemical shifts that differed from those in the free purine riboside by -3.7 and -73.1 ppm respectively when bound to the enzyme. In comparison with model compounds, it was suggested that differences in chemical shift are due to a change in the hybridization state of C-6 from sp^2 to sp^3, with formation of a new bond to oxygen or sulphur. Chemical-shift changes due to a change in the hybridization of C-2 or to protonation of the N-1 nitrogen were eliminated. These observations support a mechanism for the enzyme in which formation of a tetrahedral intermediate is the most difficult chemical step.

4.2. Nucleic acids, membranes

Interactions of ligands with nucleic acids and membranes are also of great biological importance. For example, the binding of many antitumour or antibiotic agents with nucleic acids results in significant perturbations to the conformation of the native nucleic acid. The perturbation is particularly severe in compounds that directly insert between the stacked base pairs of DNA, and it is this interaction that is primarily responsible for the pharmacological activity of these drugs. Several other modes of interaction of drugs with nucleic acids have now been established, including, for example, binding to the major and minor grooves of DNA.

Along with X-ray crystallography, NMR spectroscopy is now making a major contribution to detailed structure determination of complexes between drugs and oligonucleotides. Likewise, NMR is providing much insight into membrane surfaces and their interactions with drugs.[148] Limitations of space prevent a detailed examination here of applications in these areas, but some indication of the nuclei and methods used is available in Table 3. Generally, techniques similar to those applied in protein–ligand interactions are used to study ligand–nucleic-acid or ligand–membrane interactions, although there does tend to be a greater concentration on either ^{31}P or ^{1}H studies in nucleic acids and ^{2}H NMR in membranes.

Many of the techniques described in Section 2 can be extended beyond the realm of ligand–macromolecule studies, and can be used to investigate macromolecule–macromolecule interactions, including, for example, protein–protein, protein–DNA or protein–membrane interactions. The occurrence of spectral overlap and peak broadening, already a problem in studies of ligand–macromolecule interactions, is compounded in these

much larger systems, and so studies involving specific isotope labelling tend to be applied rather than ^{1}H NMR. For example, ^{19}F NMR of fluorotryptophan-labelled proteins has been used to study protein–lipid interactions,[149] and ^{15}N NMR has been used to study the interaction of a ^{15}N-labelled cro-repressor with O_R3 DNA.[150] Again, limitations of space prevent a detailed discussion of these types of applications, but some examples of protein–membrane and protein–DNA interactions are listed in Table 3.

5. SUMMARY AND CONCLUSIONS

It can be seen from the foregoing discussion that NMR can be used to provide answers to some very significant questions about ligand–macromolecule interactions. Information about the *location* of a binding site may be obtained from NOE measurements or paramagnetic probes, as can information about its *geometry*. The *ionization state* and general *electronic environment* of the ligand at the bound site can be probed with chemical-shift measurements, while the *bound-ligand conformation* can be obtained from TRNOE experiments. *Mobility* at the binding site can be examined via relaxation-time measurements and by dynamic NMR studies, and the *kinetics* of binding may be probed by linewidth studies or magnetization-transfer experiments. If multiple binding sites are present, it is often also possible to determine the *stoichiometry of binding* from various NMR titrations. For weak ligands, the *equilibrium constants* characterizing the interaction with the target macromolecule can be determined from chemical-shift changes as a function of ligand concentration.

While not every technique is applicable in all systems, and there are, of course, limitations on the amount of information that can be obtained in any one system, it is fair to say that there are very few aspects of ligand–macromolecule binding that cannot be addressed by NMR.

ACKNOWLEDGEMENTS

We thank Jackie King for her excellent typing of the manuscript, and Elaine Borg for the figures.

REFERENCES

1. R.A. Dwek, *Nuclear Magnetic Resonance in Biochemistry: Applications to Enzyme Systems.* Clarendon Press, Oxford, 1973.

2. O. Jardetzky and G.C.K. Roberts, *NMR in Molecular Biology*. Academic Press, London, 1981.
3. M. Blumenstein, in *The Peptides*, Vol. 7 (ed. V.J. Hruby), p. 356. Academic Press, New York, 1985.
4. G.C.K. Roberts, in *NMR in the Life Sciences* (ed. E.M. Bradbury and C. Nicolini), p. 73. Plenum, New York, 1985.
5. J. Feeney, J.G. Batchelor, J.P. Albrand and G.C.K. Roberts, *J. Magn. Reson.*, 1979, **33**, 519.
6. L.B. Dugad and J.T. Gerig, *Biochemistry*, 1988, **27**, 4310.
7. E.I. Hyde, B. Birdsall, G.C.K. Roberts, J. Feeney and A.S.V. Burgen, *Biochemistry*, 1980, **19**, 3738.
8. V. Ramesh, A.M. Petros, M. Llinás, A. Tulinsky and C.H. Park, *J. Mol. Biol.*, 1987, **198**, 481.
9. D.H. Meadows, G.C.K. Roberts and O. Jardetzky, *J. Mol. Biol.*, 1969, **45**, 491.
10. P. Gettins, *Biochemistry*, 1987, **26**, 1391.
11. P. Gettins and E.W. Wooten, *Biochemistry*, 1987, **26**, 4403.
12. J.R. Brisson, K. Golosinska, L.B. Smillie and B.D. Sykes, *Biochemistry*, 1986, **25**, 4548.
13. B. Birdsall, J. Andrews, G. Ostler, S.J.B. Tendler, J. Feeney, G.C.K. Roberts, R. W. Davies and H.T.A. Cheung, *Biochemistry*, 1989, **28**, 1353.
14. L. Cocco, J.P. Groff, C. Temple, J.A. Montgomery, R.E. London, N.A. Matwiyoff and R.L. Blakely, *Biochemistry*, 1981, **20**, 3972.
15. R.S. Ehrlich and R.F. Colman, *Biochemistry*, 1987, **26**, 3461.
16. R.E. London, in *Magnetic Resonance in Biology* (ed. J.S. Cohen), p. 1. Wiley, New York, 1980.
17. D.C. McCain, E.L. Ulrich and J.L. Markley, *J. Magn. Reson.*, 1988, **80**, 296.
18. M.E. Ando, J.T. Gerig and K.F.S. Luk, *Biochemistry*, 1986, **25**, 4772.
19. T.J. Swift and R.E. Connick, *J. Chem. Phys.*, 1962, **37**, 307.
20. E.I. Hyde, B. Birdsall, G.C.K. Roberts, J. Feeney and A.S.V. Burgen, *Biochemistry*, 1980, **19**, 3746.
21. J. Reuben and D. Fiat, *J. Chem. Phys.*, 1969, **51**, 4918.
22. R.S. Ehrlich and R.F. Colman, *Biochemistry*, 1985, **24**, 5378.
23. A.M. Petros, V. Ramesh and M. Llinás, *Biochemistry*, 1989 **28**, 1368.
24. S. Forsen and R. A. Hoffman, *J. Chem. Phys.*, 1963, **39**, 2892.
25. J.K.M. Sanders and J.D. Mersh, *Prog. NMR Spectrosc.*, 1982, **15**, 353.
26. J.K.M. Sanders and B.K. Hunter, *Modern NMR Spectroscopy*, Oxford University Press, Oxford, 1987.
27. A.P. Koretsky, S. Wang, M.P. Klein, T.L. James and M.W. Weiner, *Biochemistry*, 1986, **25**, 77.
28. P.G. Morris, in *Annual Reports in NMR Spectroscopy*, Vol. 20 (ed. G.A. Webb), p. 1. Academic Press, London, 1988.
29. G.F. King, C.R. Middlehurst and P.W. Kuchel, *Biochemistry*, 1986, **25**, 1054.
30. G. Bodenhausen and R.R. Ernst, *J. Am. Chem. Soc.*, 1982, **104**, 1304.
31. J. Boyd, K.M. Brindle, I.D. Campbell and G.K. Radda, *J. Magn. Reson.*, 1984, **60**, 149.
32. J.R. Alger and R.G. Shulman, *Q. Rev. Biophys.*, 1984, **17**, 83.
33. G.M. Clore, G.C.K. Roberts, A.M. Gronenborn, B. Birdsall and J. Feeney, *J. Magn. Reson.*, 1981, **45**, 151.
34. J. Feeney, *NMR in Living Systems* (ed. T. Axenrod and G. Ceccavelli), p. 347. Reidel, Amsterdam, 1986.
35. B. Birdsall, A. Gronenborn, E.I. Hyde, G.M. Clore, G.C.K. Roberts, J. Feeney and A.S.V. Burgen, *Biochemistry*, 1982, **21**, 5831.

36. B. Birdsall, J. Feeney, S.J.B. Tendler, S.J. Hammond and G.C.K. Roberts, *Biochemistry*, 1989, **27**, 2297.
37. V. Thanabal, J.S. de Ropp and G.N. La Mar, *J. Am. Chem. Soc.*, 1987, **109**, 265.
38. J.H. Noggle and R.E. Schirmer, *The Nuclear Overhauser Effect*. Academic Press, New York, 1971.
39. K. Wüthrich, *NMR in Biological Research: Peptides and Proteins*. North-Holland, Amsterdam, 1986.
40. K. Wüthrich, *Acc. Chem. Res.*, 1989, **22**, 36.
41. K. Wüthrich, *Science*, 1989, **243**, 45.
42. I. Solomon, *Phys. Rev.*, 1955, **99**, 559.
43. A. Kalk and H.J.C. Berendsen, *J. Magn. Reson.*, 1976, **24**, 343.
44. M. Cairi and J.T. Gerig, *J. Magn. Reson.*, 1985, **62**, 131.
45. P. Balaram, A.A. Bothner-By and E. Breslow, *J. Am. Chem. Soc.*, 1972, **94**, 4017.
46. T.L. James, *Biochemistry*, 1976, **15**, 4724.
47. A. Motta, R.A. Laursen, M. Llinás, A. Tulinsky and C.H. Park, *Biochemistry*, 1987, **26**, 3827.
48. L.J. Ferrin and A.S. Mildvan, *Biochemistry*, 1986, **25**, 5131.
49. S.W. Fesik, J.R. Luly, J.W. Erickson and C. Abad-Zapatero, *Biochemistry*, 1988, **27**, 8297.
50. D.C. Fry, S.A. Kruby and A.S. Mildvan, *Biochemistry*, 1987, **26**, 1645.
51. J.P. Albrand, B. Birdsall, J. Feeney, G.C.K. Roberts and A.S.V. Burgen, *Int. J. Macromolecules*, 1979, **1**, 37.
52. G.M. Clore and A.M. Gronenborn, *J. Magn. Reson.*, 1982, **48**, 402.
53. G.M. Clore and A.M. Gronenborn, *J. Magn. Reson.*, 1983, **53**, 423.
54. G.M. Clore and A.M. Gronenborn, *J. Magn. Reson.*, 1985, **61**, 158.
55. N.H. Andersen, H.L. Eaton and K.T. Nguyen, *Magn. Reson. Chem.*, 1987, **25**, 1025.
56. P.J. Cayley, J.P. Albrand, J. Feeney, G.C.K. Roberts, E.A. Piper and A.S.V. Burgen, *Biochemistry*, 1979, **18**, 3886.
57. A.M. Gronenborn and G.M. Clore, *Biochemistry*, 1982, **21**, 4040.
58. A.M. Gronenborn and G.M. Clore, *J. Mol. Biol.*, 1984, **172**, 559.
59. A.M. Gronenborn, G.M. Clore, L. Hobbs and J. Jeffrey, *Eur. J. Biochem.*, 1984, **145**, 365.
60. A. Banerjee, H.R. Levy, G.C. Levy and W.W.C. Chan, *Biochemistry*, 1985, **24**, 1593.
61. A. Banerjee, H.R. Levy, G.C. Levy, C. Li Muti, B.M. Goldstein and J.E. Bell, *Biochemistry*, 1987, **26**, 8443.
62. M. Machida, S. Yokoyama, H. Matsuzawa, T. Miyazawa and T. Ohta, *J. Biol. Chem.*, 1985, **260**, 16143.
63. L.J. Ferrin and A.S. Mildvan, *Biochemistry*, 1985, **24**, 6904.
64. D.C. Fry, S. A. Kruby and A.S. Mildvan, *Biochemistry*, 1985, **24**, 4680.
65. P.R. Rosevear, H.N. Bramson, C. O'Brien, E.T. Kaiser and A.S. Mildvan, *Biochemistry*, 1983, **22**, 3439.
66. P.R. Rosevear, V.M. Powers, D. Dowhan, A.S. Mildvan and G.L. Kenyon, *Biochemistry*, 1987, **26**, 5338.
67. A.M. Gronenborn, G.M. Clore, L.W. McLaughlin, E. Graeser, B. Lorber and R. Giege, *Eur. J. Biochem.*, 1984, **145**, 359.
68. G.M. Clore, A.M. Gronenborn and L.W. McLaughlin, *J. Mol. Biol.*, 1984, **174**, 163.
69. G.M. Clore, A.M. Gronenborn, G. Carlson and E.F. Meyer, *J. Mol. Biol.*, 1986, **190**, 259.
70. D. Kohda, G. Kawai, S. Yokoyama, M. Kawakarmi, S. Mizushima and T. Miyazawa, *Biochemistry*, 1987, **26**, 6531.
71. K. Wakamatsu, T. Higashijima, M. Fujini, T. Nakajima and T. Miyazawa, *FEBS Lett.*, 1983, **162**, 123.

72. K. Wakamatsu, A. Okada, M. Suzuki, T. Higashijima, Y. Masui, S. Sakakibara and T. Miyazawa, *Eur. J. Biochem.*, 1986, **154**, 607.
73. K. Wakamatsu, A. Okada, T. Higashijima and T. Miyazawa, *Biopolymers*, 1986, **25**, S193.
74. K. Wakamatsu, A. Okada, T. Miyazawa, Y. Masui, S. Sakakibara and T. Higashijima, *Eur. J. Biochem.*, 1987, **163**, 331.
75. I.M. Russu, A.K.L.C. Lin, C.-P. Yang and C. Ho, *Biochemistry*, 1986, **25**, 808.
76. P.R. Andrews, D.J. Craik and S.L.A. Munro, in *NMR Spectroscopy and Drug Development* (ed. J.W. Jaroszewski, K. Schaumburg and H. Kofod), p. 20. Munksgaard, Copenhagen, 1988.
77. G. Otting, H. Senn, G. Wagner and K. Wüthrich, *J. Magn. Reson.*, 1986, **70**, 500.
78. A. Bax and M.A. Weiss, *J. Magn. Reson.*, 1987, **71**, 571.
79. L.P. McIntosh, F.W. Dahlquist and A.G. Redfield, *J. Biol. Struct. Dyn.*, 1987, **5**, 21.
80. S.W. Fesik, R.T. Gampe and T.W. Rockway, *J. Magn. Reson.*, 1987, **74**, 366.
81. H. Gunther, *NMR Spectroscopy.* Wiley, New York, 1980.
82. J. Sandstrom, *Dynamic NMR Spectroscopy*. Academic Press, London, 1983.
83. G.M. Clore, A.M. Gronenborn, B. Birdsall, J. Feeney and G.C.K. Roberts, *Biochem. J.*, 1984, **217**, 659.
84. H.T.A. Cheung, M.S. Searle, J. Feeney, B. Birdsall, G.C.K. Roberts, I. Kompis and S.J. Hammond, *Biochemistry*, 1986, **25**, 1925.
85. M.S. Searle, M.J. Forster, B. Birdsall, G.C.K. Roberts, J. Feeney, I. Kompis and A.J. Geddes, *Proc. Natl Acad. Sci. USA*, 1988, **85**, 3787.
86. O. Monasterio, *Biochemistry*, 1987, **26**, 6099.
87. R.E. Lenkinski and J.D. Glickson, in *The Peptides*, Vol. 7 (ed. V.J. Hruby), p. 301. Academic Press, New York, 1985.
88. N. Bloembergen, *J. Chem. Phys.* 1957, **27**, 572.
89. Z. Luz and S. Meiboom, *J. Chem. Phys.*, 1964, **40**, 2686.
90. B.D. Ray, P. Rosch and B.D.N. Rao, *Biochemistry*, 1988, **27**, 8669.
91. L.S. Reid, H.B. Gray, C. Dalvit, P.E. Wright and P. Saltman, *Biochemistry*, 1987, **26**, 7102.
92. E.A.M. de Jong, C.A.A. Claesen, C.J.M. Daemen, B.J.M. Harmsen, R.N.H. Konings, G.I. Tesser and C.W. Hilbers, *J. Magn. Reson.*, 1988, **80**, 197.
93. A. Obata, H. Tanaka and H. Kawazura, *Biochemistry*, 1987, **26**, 4962.
94. A. Kuliopulos, E.M. Westbrook, P. Talalay and A.S. Mildvan, *Biochemistry*, 1987, **26**, 3927.
95. S.J. Hammond, B. Birdsall, M.S. Searle, G.C.K. Roberts and J. Feeney, *J. Mol. Biol.*, 1986, **188**, 81.
96. C. Dalvit and P.E. Wright, *J. Mol. Biol.*, **194**, 313.
97. R.K. Harris and B.E. Mann, *NMR and the Periodic Table.* Academic Press, London, 1978.
98. C. Brevard and P. Granger, *Handbook of High-Resolution Multinuclear NMR.* Wiley, New York, 1981.
99. P. Laszlo (ed.), *NMR of Newly Accessible Nuclei*, Vols. 1 and 2. Academic Press, London, 1983.
100. G.N. La Mar, J.S. de Ropp, K.M. Smith and K.C. Langry, *J. Biol. Chem.*, 1980, **225**, 6646.
101. J.S. de Ropp, G.N. La Mar, K.M. Smith and K.C. Langry, *J. Am. Chem. Soc.*, 1984, **106**, 4438.
102. E.K. Jaffe and G.D. Markham, *Biochemistry*, 1988, **27**, 4475.
103. A.L. Odell, in *NMR of Newly Accessible Nuclei*, Vol. 2 (ed. P. Laszlo), p. 27. Academic Press, New York, 1983.
104. J.N.S. Evans, G. Burton, P.E. Fagerness, N.E. Mackenzie and A.I. Scott, *Biochemistry*, 1986, **25**, 905.

105. N.E. Mackenzie, J.P.G. Molthouse and A.I. Scott, *Science*, 1984, **225**, 883.
106. G.A. Morris and R. Freeman, *J. Am. Chem. Soc.*, 1979, **102**, 428.
107. D.M. Doddrell, D.T. Pegg and M.R. Bendall, *J. Magn. Reson.*, 1982, **48**, 323.
108. A. Bax, R.H. Griffey and B.L. Hawkins, *J. Am. Chem. Soc.*, 1984, **106**, 7188.
109. O.H. Live, H.R. Wyssbord, A.J.M. Fischmann, W.C. Agosta and D. Cowburn, *J. Am. Chem. Soc.*, 1984, **106**, 1936.
110. R.A. Schiksnis, M.J. Bogusky, P. Tsang and S.J. Opella, *Biochemistry*, 1987, **26**, 1373.
111. W. W. Bachovchin, *Biochemistry*, 1986, **25**, 7751.
112. J. Vervoort, F. Muller, S.G. Mayhew, W.A.M. van der Berg, C.T.W. Moonen and A. Bacher, *Biochemistry*, 1986, **25**, 6789.
113. J.T. Gerig, in *Biological Magnetic Resonance*, Vol. 1 (ed. L.J. Berliner and J. Reuben), p. 139. Plenum Press, New York, 1978.
114. D.O. Shah and D.G. Gorenstein, *Biochemistry*, 1983, **22**, 6096.
115. Y-C. Chang and D. J. Graves, *J. Biol. Chem.*, 1985, **260**, 2709.
116. Y-C. Chang, R.D. Scott and D.J. Graves, *Biochemistry*, 1986, **25**, 1932.
117. Y-C. Chang, R.D. Scott and D.J. Graves, *Biochemistry*, 1987, **26**, 360.
118. C.B. Post, W.J. Ray and D.G. Gorenstein, *Biochemistry*, 1989, **28**, 548.
119. E. Breslow, in *Cell Biology of the Secretory Process* (ed. M. Kantin), p. 276. Karger, Basel, 1984.
120. D.H. Live, D. Cowburn and E. Breslow, *Biochemistry*, 1987, **26**, 6415.
121. B.A. Whittaker, N.M. Allewell, J. Carlson and E. Breslow, *Biochemistry*, 1985, **24**, 2782.
122. M. Blumenstein, V.J. Hruby, V. Viswanatha and D. Chaturvedi, *Biochemistry*, 1984, **23**, 2153.
123. V. Sardana, J.D. Carlson, E. Breslow and D. Peyton, *Biochemistry*, 1987, **26**, 995.
124. D. Peyton, V. Sardana and E. Breslow, *Biochemistry*, 1987, **26**, 1518.
125. D. Peyton, V. Sardana and E. Breslow, *Biochemistry*, 1986, **25**, 6579.
126. S.M. Hochschwender, R.A. Laursen, A. De Marco and M. Llinás, *Arch. Biochem. Biophys.*, 1983, **223**, 58.
127. M. Llinás, A. Motta, A. De Marco and R.A. Laursen, *J. Biol. Sci. Suppl.*, 1985, **8**, 121.
128. A. De Marco, R.A. Laursen and M. Llinás, *Arch. Biochem. Biophys.*, 1986, **244**, 727.
129. G. Birdsall, A.M. Gronenborn, G.M. Clore, G.C.K. Roberts, J. Feeney and A.S.V. Burgen, *Biochem. Biophys. Res. Commun.*, 1981, **101**, 1139.
130. B. Birdsall, J. De Graw, J. Feeney, S.J. Hammond, M.S. Searle, G.C.K. Roberts, W.T. Colwell and J. Crase, *FEBS Lett.*, 1987, **217**, 106.
131. J.L. Way, B. Birdsall, J. Feeney, G.C.K. Roberts and A.S.V. Burgen, *Biochemistry*, 1975, **14**, 3470.
132. T.-C. Liang and R.H. Abeles, *Biochemistry*, 1987, **26**, 7603.
133. G.P. Mullen, R.B. Dunlop and J.D. Odom, *Biochemistry*, 1986, **25**, 5625.
134. J.L. Evelhoch, D.F. Bocian and J.L. Sudmeier, *Biochemistry*, 1981, **20**, 4951.
135. G.M. Blackburn, B.E. Mann, B.F. Taylor and A.F. Worrall, *Eur. J. Biochem.*, 1985, **153**, 553.
136. K. Kanamori and J.D. Roberts, *Biochemistry*, 1983, **22**, 2658.
137. J.T. Gerig and J.M. Moses, *J. Chem. Soc. Chem. Commun.*, 1987, 482.
138. J.D. Led and E. Neesgaard, *Biochemistry*, 1987, **26**, 183.
139. Y.-J. Shyy, G. Tian and M.-D. Tsai, *Biochemistry*, 1987, **26**, 6411.
140. E.K. Jaffe and G.D. Markham, *Biochemistry*, 1987, **26**, 4258.
141. D.J. Wilbur, R.S. Norton, A.O. Clouse, R. Addleman and A. Allerhand, *J. Am. Chem. Soc.*, 1976, **98**, 8250.
142. A. Allerhand, *Methods Enzymol.*, 1979, **61**, 458.

143. A.I. Scott, C.A. Roessner, N.J. Stolowich, P. Karuso, H.J. Williams, S.K. Grant, M.D. Gonzalez and T. Hoshino, *Biochemistry*, 1988, **27**, 7984.
144. L. Muller, *J. Am. Chem. Soc.*, 1979, **101**, 4481.
145. J.A. Wilde, P.H. Bolton, N.J. Stolowich and J.A. Gerht, *J. Magn. Reson.* 1986, **68**, 168.
146. L.C. Kurz and C. Frieden, *Biochemistry*, 1983, **26**, 382.
147. L.C. Kurz and C. Frieden, *Biochemistry*, 1987, **26**, 8450.
148. M. Auger, I.C.P. Smith and H.C. Jarrell, in *NMR Spectroscopy and Drug Development* (ed J.W. Jaroszewski, K. Schaumburg and H. Kofod). p. 473. Munksgaard, Copenhagen, 1988.
149. G.S. Rule, E.A. Pratt, V. Simplaceanu and C. Ho, *Biochemistry*, 1987, **26**, 549.
150. P. Leighton and P. Lu, *Biochemistry*, 1987, **26**, 7262.

Applications of NMR in the Analysis of Agrochemicals and Pesticides

A.A.S. BRIGHT

Schering Agrochemicals Limited, Chesterford Park Research Station, Saffron Walden, Essex CB10 1XL, UK

R.G. RATCLIFFE

Department of Plant Sciences, University of Oxford, Agricultural Science Building, Parks Road, Oxford OX1 3PF, UK

1. Introduction 139
2. Structural information 140
   2.1. General considerations 140
   2.2. Detailed structural analysis 142
   2.3. Compounds of natural origin 167
3. Decomposition and metabolism 174
   3.1. Stability in model systems 174
   3.2. Metabolism of agrochemicals 177
   3.3. Metabolic effects and mode of action 188
4. Miscellaneous applications 192
   Appendix 195
   References 199

1. INTRODUCTION

Nuclear magnetic resonance (NMR) is an indispensible tool for the structural analysis of organic molecules, and NMR spectra are obtained routinely from virtually every compound that is screened as a potential agrochemical or pesticide. The emphasis is on the rapid characterization of the structural features of immediate interest, with publication of the data given a lower priority. Consequently, only a small fraction of the information finds its way into the literature, and in reviewing this material our intention is to highlight the many different NMR methods that may be required to achieve the necessary structural characterization.

ANNUAL REPORTS ON NMR SPECTROSCOPY
VOLUME 22 ISBN 0-12-505322-3

Copyright © 1989 Academic Press Limited
All rights of reproduction in any form reserved

The application of NMR to pesticides has been reviewed previously[1-3] and the present review concentrates on the more recent applications of NMR in the general area of agrochemical and pesticide research. While structural analysis (Section 2) is the most important theme, the opportunity has been taken to describe various NMR approaches to the decomposition and metabolic effects of agrochemicals (Section 3), and to draw attention to a number of proposals for using NMR to assay pesticides or their residues (Section 4). Compounds of natural origin (Section 2.3) are separated from their more numerous synthetic counterparts (Section 2.2), and the description of the structural analysis of the latter group of compounds has been subdivided to emphasize the role of NMR in stereochemical and conformational studies.

2. STRUCTURAL INFORMATION

2.1. General considerations

NMR has few rivals as a rapid means of identifying test material and likely impurities. Instrumental developments have increased the versatility of the technique and, with full computer control of the spectrometer, NMR users with only a few minutes instruction and virtually no experience can obtain good-quality spectra.[4] The walk-up user concept involves the selection of acquisition, processing and plotting options that are tailored to the needs of a particular laboratory and project. While this simplicity of operation is to be welcomed, the apparent ease with which spectra can be obtained presents special problems in sample handling and data management as the spectrometer output increases.

The sample-handling problem has been eased within the last few years by the availability of fully automated instrumentation that permits the automatic loading of the sample followed by acquisition, processing and plotting. Unattended operation over extended periods has been an established feature of NMR for many years, but the ability to change samples automatically after each acquisition is a valuable addition since it enables better use to be made of equipment and resources.

Analysis of novel compounds and unknowns is greatly assisted by comparisons with spectra of closely related analogues or established reference compounds. In this regard a sound database is invaluable and the large number of spectra provided by current instrumentation can provide this, although at a price in terms of computer storage. Extra experimental work is sometimes necessary to achieve a convincing match between test and

Table 1. Summary of one- and two-dimensional pulse NMR experiments and their areas of application.

Experiment	Applications	Refs.
1D METHODS		
^1H NMR		
Fully coupled	Measurement of chemical-shift and coupling-constant data	—
Spin-decoupled	Adjacent ^1H sequences	—
Presaturation	NOE (equilibrium and transient) for through-space relationships	13
	Exchange processes	14
	Solvent suppression	9, 15
^{13}C NMR		
^1H-decoupled	Measurement of chemical shift	—
Continuous-wave off-resonance	Multiplicity test	—
Single-frequency decoupled	Assignment of ^1H and ^{13}C resonances	—
INEPT	Peak selection using polarization transfer to increase sensitivity	16
DEPT		17
APT (*J*-modulated spin echo)	Attached proton test using NOE to increase sensitivity	18
Spectral editing	—	18
Gated decoupled	Coupling-constant data (with NOE)	—
Inverse gated decoupled	Measurement of peak intensity (without NOE)	—
2D METHODS		
^1H–^1H NMR		
2D *J*-resolved	Resolution of overlapped multiplets	19
COSY	Correlation of spins with a common *J*, ^1H sequences	20, 21, 22
Relayed-COSY	Extended COSY to give connectivity patterns	23, 24
NOESY	Through-space relationships and exchange processes	13, 25
^{13}C–^1H NMR		
Directly bonded		
^{13}C–^1H correlated	Assignment of resonances	
	using INEPT	26, 27
	using DEPT	28
	QWIKCORR	29
Long-range		
Fully coupled	Assignment of resonances and stereochemistry	30, 31 32, 33
Heteronuclear *J*-resolved 2D	Enhanced resolution of coupled resonances	34
COLOC	Shift correlation with ^1H–^1H decoupling, useful for quaternary carbons	35

reference spectra—for example, it may be necessary to vary the solvent, the solute concentration, the temperature or the observation frequency—but in general much data analysis is based on comparisons with previously assigned spectra.

Computer-searchable databases, based on chemical-shift and peak-intensity information, have the potential to rationalize the process of spectral comparison, and their use has been considered recently.[5-7] This approach is particularly suitable for ^{13}C NMR, since the carbon spectrum clearly defines the molecular skeleton in most cases, and the NIH/EPA Chemical Information System (CIS),[8] which includes spectra of standard reference pesticides, has been used to test an automated library search system for ^{13}C-NMR.[6]

^{1}H NMR spectra are more difficult to represent in coded form, and this is particularly unfortunate since the vast bulk of spectroscopic data is in the form of ^{1}H NMR spectra and, indeed, ^{1}H NMR is the only practicable NMR detection method for samples in limited supply. Spectral comparisons can be complicated by solvent effects, which may cause local chemical-shift changes, and by the effect of the field strength on the splitting patterns. These difficulties can all make for an unsuccessful computer search.[7]

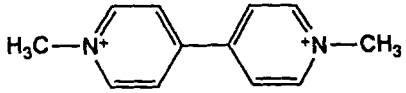
The chemist is primarily interested in the structural information that can be extracted from the spectrum, rather than in the spectrum itself, and in some cases a cursory analysis of the main spectral features may be sufficient to identify the compound of interest or to show that a starting material or impurity is still present. At the other extreme, it may be necessary to achieve a complete structural analysis of a newly isolated compound with no readily available analogues, and in this situation it is usually necessary to use several different NMR methods to solve the problem. Table 1 summarizes the most commonly used experiments, and further details of the pulse sequences can be found in several recent publications.[9-13]

The purpose of the following sections (2.2 and 2.3) is to illustrate the application of these methods in an agrochemical or pesticidal context, with examples ranging from the identification of simple compounds to the study of natural products.

2.2. Detailed structural analysis

2.2.1. Assignment of spectra

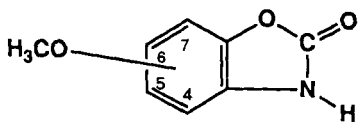
In general, assignment becomes more difficult as the level of molecular complexity increases, but even the analysis of structures with a small number of protons can be problematic. Paraquat (**1**), a powerful herbicide



1

with a wide range of uses, has been the subject of a reassignment. Earlier work[36] had considered that protons H-3 and H-5 should be at lower field than H-2 and H-6 owing to the presence of an aromatic ring at position 4. However, the effects of *N* substituents on the ring protons of a series of 1,1′-dialkyl-4,4′-bipyridinium salts[37] permitted a complete reversal of this assignment.

A common assignment problem concerns the position of substitution in ring systems, and this can be difficult to solve when there are relatively few protons in the structure. Proton-coupled carbon spectra can be useful here, and this approach has been used in a ^{13}C NMR analysis of 5-, 6- and 7-methoxybenzoxazolinones (**2**) (larval growth inhibitors for insect pests on



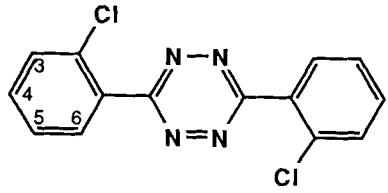
2

cereal). The isomers were identified by analysis of chemical shift and both direct and long-range carbon–proton coupling constants, obtained from gated decoupled spectra.[38] For the 6-isomer the methine carbons C-5 and C-7 were located as doublets of doublets, with directly bonded ($^1J_{CH}$) and long-range ($^3J_{CCCH}$) coupling. However, the remaining methine, C-4, showed no long-range effects. The quaternary carbons C-8 and C-9 were distinguished by the number of vicinal proton couplings, with C-9 displaying a greater multiplicity. For these quaternary carbons geminal couplings $^2J_{CCH}$ were sufficiently large to measure.

The assignment of spectra has been revolutionized by the development of two-dimensional (2D) methods for correlation of ^1H and ^{13}C resonances. These methods are used to establish molecular connectivity and enable the spectroscopist to deduce molecular structures of unknown compounds without reference to the spectra of related compounds. The routine application of this approach has become practicable over approximately the last five years and the main purpose of the following examples is to illustrate the usefulness of these 2D methods in analysis of the spectra of agrochemicals and pesticides.

The proton spectra of simple aromatic systems, obtained at even

moderately high field strength, can be difficult to interpret. In these circumstances extra spectral dispersion can be achieved through two-dimensional methods avoiding the need for even high field strength. This can be illustrated with a ^{1}H and ^{13}C NMR study of the acaricide clofentezine (**3**).[39]



3

This is a 1,2,4,5-tetrazine symmetrically substituted in the 3- and 6-positions.[40] As expected, the ^{1}H NMR spectrum is complex, even at an observation frequency of 300 MHz (Fig. 1a), but proton H-6 for each chlorophenyl ring can be identified at lowest field. In contrast, the ^{13}C NMR spectrum is a simple seven-line spectrum (Fig. 2). While single-frequency decoupling of H-6 identified carbon C-6, heteronuclear $^{13}C-^{1}H$ 2D chemical-shift correlation, using DEPT polarization transfer from ^{1}H to ^{13}C,[28] located all proton regions against their respective carbon resonances in a single experiment (Fig. 3). Molecular connectivity was finally established by proton spin-decoupling of H-6 (Fig. 1b). The greatest effect was centred at 7.54 ppm, and this region was assigned to H-5. A splitting of 2 Hz was removed in the region 7.55–7.60 ppm (H-4, *meta* to H-6), and a very narrowly space doublet coalesced into a singlet at 7.62 ppm (H-3). The assignment of all the methine carbons was then possible by a combination of both $^{13}C-^{1}H$ 2D correlation and proton spin-decoupling effects. Quaternary carbons were assigned on the basis of chemical shift.

Experimental spin–lattice relaxation times $T_{1,obs}$, obtained by the inversion–recovery method, showed most efficient relaxation for C-4 *para* to the tetrazine ring (see Table 2). This was consistent with a preferred rotation about the main axis of the molecule and, in combination with the spin-decoupling results, indirectly endorsed the assignment of H-6. Simulation permitted estimation of values of the chemical shifts and coupling constants (see Fig. 1(c) and Table 3) and confirmed the non-first-order nature of the spectrum; several minor transitions in the simulation matched small peaks in the measured spectrum.

1,3,4-Trisubstituted aromatic systems are relatively common in molecular structures of agrochemicals and pesticides, and identification of the characteristic ^{1}H NMR pattern is frequently required. For example,

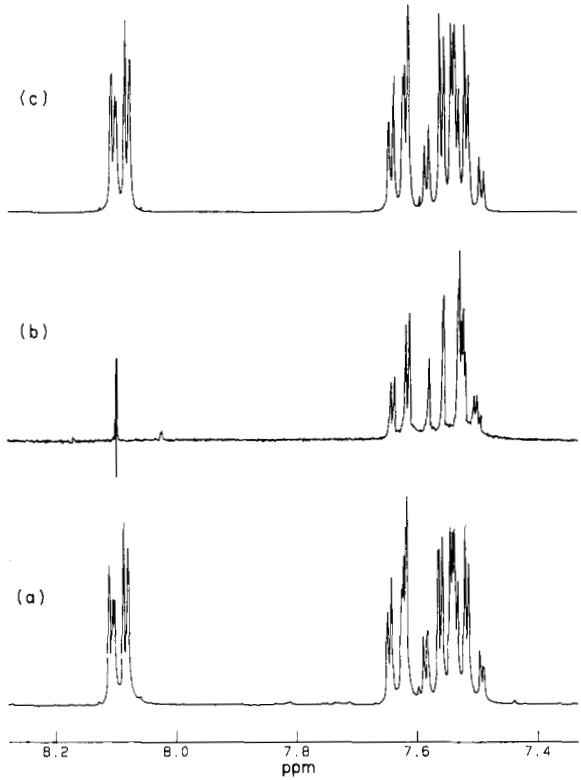
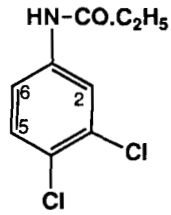


Fig. 1. ^{1}H NMR spectra of clofentezine (**3**) in $CDCl_3$: (a) coupled; (b) spin-decoupled with irradiation of H-6; (c) simulated.



4

propanil (**4**), representative of 3,4-dichloroaniline-derived herbicides, has been studied at an observation frequency of 500 MHz, to examine substituent effects on chemical shift.[41]

Several diphenyl ether herbicides present a more involved situation, with

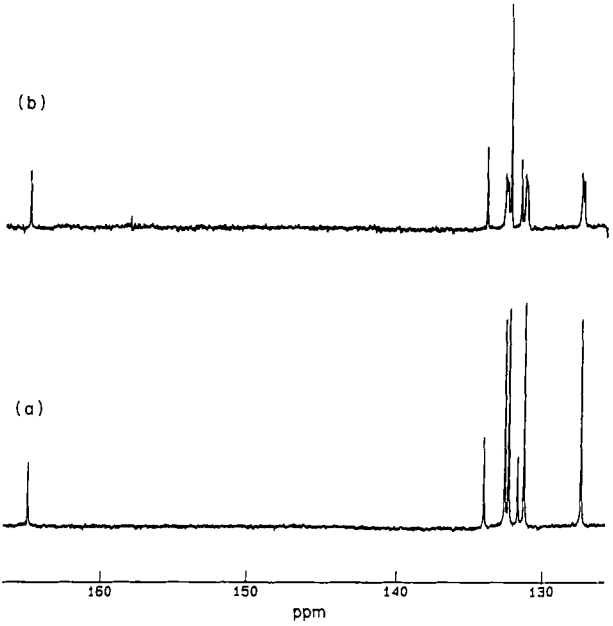


Fig. 2. ^{13}C NMR of clofentezine (**3**): (a) broadband decoupled; (b) single-frequency decoupled with irradiation of H-6.

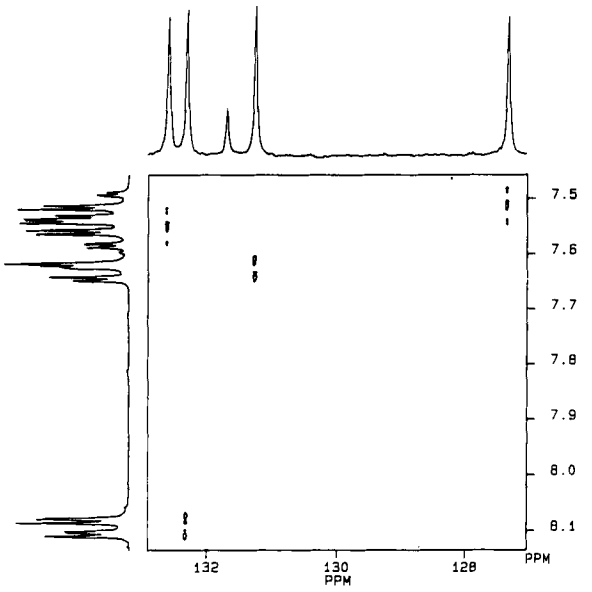


Fig. 3. 2D $^{13}C-^{1}H$ shift-correlated spectrum of (**3**).

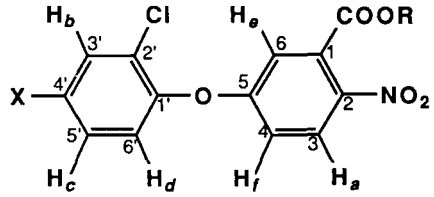
Table 2. ^{13}C–NMR data for clofentezine (**3**).

Carbon	Chemical shift (ppm)	$T_{1,obs}$ (s)
Chlorophenyl ring		
1	133.95	
2	131.62	
3	131.22	2.6
4	132.58	1.0
5	127.31	2.6
6	132.29	2.2
Tetrazine ring		
3, 6	164.94	

Table 3. Spectrum simulation parameters for clofentezine (**3**).

Chemical shift (ppm)		Indirect coupling (Hz)			
H-3	7.63	$J_{3,4}$	7.8	$J_{4,5}$	7.4
H-4	7.56	$J_{3,5}$	1.7	$J_{4,6}$	2.0
H-5	7.53	$J_{3,6}$	0.6	$J_{5,6}$	7.4
H-6	8.09				

two 1, 3, 4-trisubstituted fragments in the molecular structure. With a combination of one- and two-dimensional NMR techniques, complete assignment of the ^1H and ^{13}C NMR spectra is possible and has been demonstrated for acifluorfen (**5**), acifluorfen methyl (**6**) and bifenox (**7**).[42]



	X	R
5	$-CF_3$	Na
6	$-CF_3$	$-CH_3$
7	$-Cl$	$-CH_3$

Assignment of the ^1H NMR spectra for all three diphenylethers was possible using shift-correlated COSY experiments (see Fig. 4 for acifluorfen). The spin connections for acifluorfen are clearly and easily established between protons in the respective ring systems. While the assignment could have been achieved by one dimensional spin-decoupling,[43] the 2D method was preferred since it provided an easy method for correlating the protons in the respective ring systems. Indeed, the 2D method will always be preferable in more complicated spectra with overlapping resonances. Similarly, indirect assignment of the aromatic methine carbons by heteronuclear carbon–proton correlation was preferred to single frequency decoupling.[42]

The remaining aromatic quaternary carbons presented a more difficult problem, which was resolved by detection of long-range $^{13}C-^1H$ coupling.

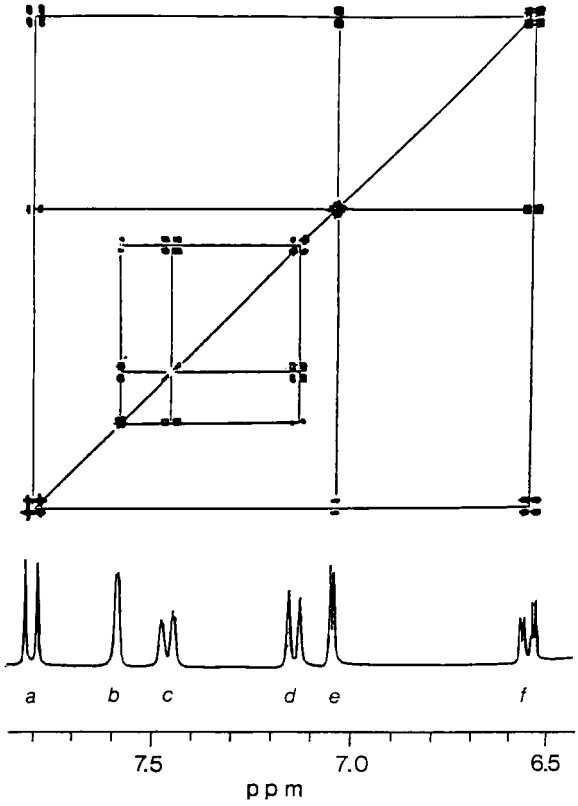


Fig. 4. Contour plot of the aromatic region of the proton *J*-correlated (COSY) spectrum of acifluorfen. (Adapted with permission from G.H. Lee, *J. Agric. Food Chem.* **33**, 499. Copyright (1985) American Chemical Society.)

Heteronuclear *J*-resolved 2D NMR, using selective 180° proton pulses, was employed. In this "spin-flip" experiment the broadband decoupled signals are modulated by the heteronuclear couplings and the long-range couplings measured in the second frequency domain. For acifluorfen methyl (**6**) two separate "spin-flip" correlations were performed, one on proton *a* and a second on proton *c*. Figure 5 illustrates the effect of long-range coupling

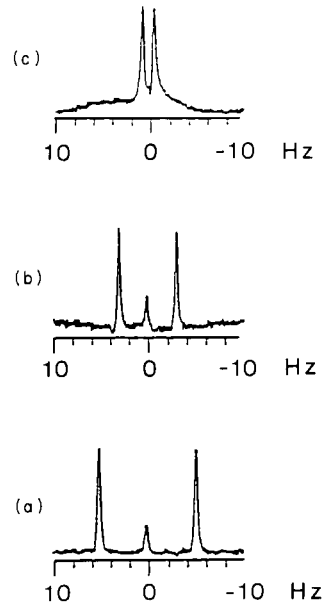
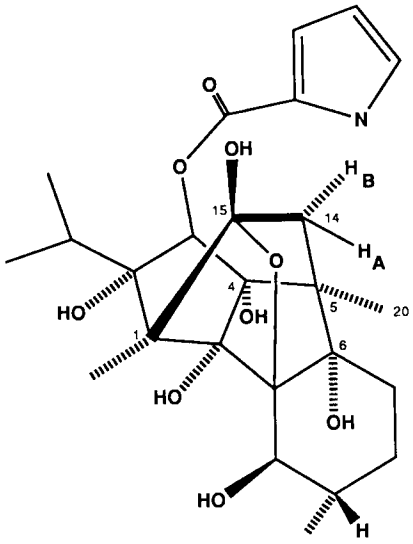


Fig. 5. Long-range coupling spectra of acifluorfen methyl when proton *a* was flipped in a hetereonuclear *J*-resolved 2D experiment. (a), (b) and (c) correspond to carbons C-5, C-1 and C-6 respectively. (Reprinted with permission from G.H. Lee, *Agric. Food Chem.* **33**, 499. Copyright (1985) American Chemical Society.)

Table 4. Long-range $^{13}C-^{1}H$ coupling in acifluorfen methyl (**6**).

Selected proton	Carbon resonance	*J* (Hz)
a	*meta* C-5	10.15
	meta C-1	5.95
	para C-6	1.18
c	*meta* C-1′	10.25
	para C-2′	1.78
	meta C-3′	7.08

detected on selection of proton *a*. From the magnitude of the heteronuclear couplings (see Table 4) the quaternary aromatic carbons in the *meta* position to the selected proton were assigned. Thus, by use of a combination of 1D and 2D NMR methods, nuclear connectivity was established and the molecular structure deduced without the need to compare the spectra of analogue compounds.



8

Ryanodine (**8**), an active constituent of the ground stem wood of the shrub *Ryania speciosa* and formerly marketed for some years as an insecticide, has been widely studied. However, assignment of the ^{1}H and ^{13}C NMR spectra has only been possible recently.[33] Fully coupled $^{13}C-^{1}H$ 2D correlation was necessary to identify and assign the large number of quaternary carbon atoms and to complete the analysis. The fully coupled correlated method detects all $^{13}C-^{1}H$ couplings, with none eliminated through refocusing pulses or broadband decoupling. Figure 6 illustrates, in schematic form, the partial correlation map for protons attached to C-14 and C-20 and the carbons C-14, C-1, C-4, C-5, C-6 and C-15. In the f1 dimension (*y* axis) both H-14A and H-14B are split into doublets by direct coupling $^{1}J_{ch}$. The ^{13}C resonance of C-14 is split into a methylene triplet in f2 (*x* axis), and the resulting correlation gives two rectangular contour-patterns. The methyl protons on C-20 correlate with the C-14 triplet to give three contours in f2, but spectral resolution is insufficient to detect splitting in f1 from long-range $^{2}J_{CCH}$ coupling. The quaternary carbons of interest

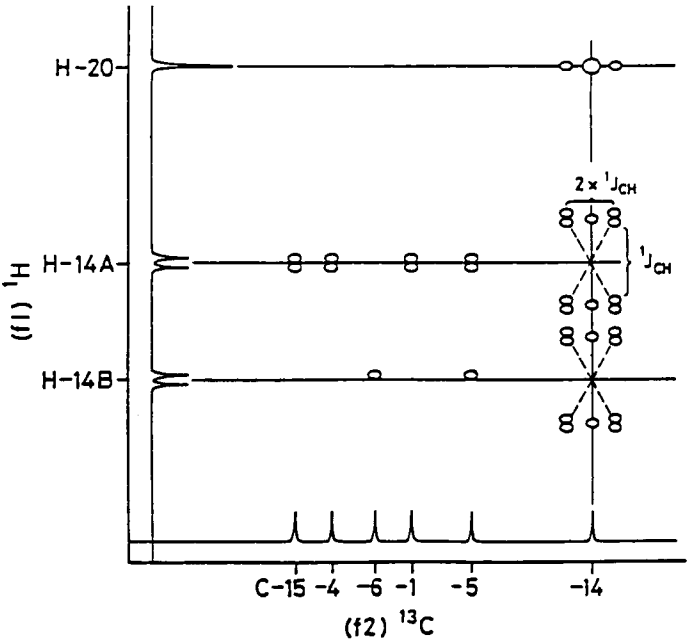
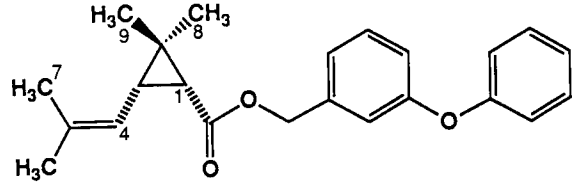


Fig. 6. A partial schematic of the fully coupled spectrum of ryanodine (**8**). (Reprinted with permission from A.L. Waterhouse, I. Holden and J.E. Casida, *J. Chem. Soc. Perkin Trans. 2*, 1011. Copyright (1985), The Royal Society of Chemistry.)

correlate with the protons on C-14 as singlets in the f2 dimension and can be readily distinguished.

Phenothrin, a non-systemic pyrethroid insecticide, effective by contact and as a stomach poison, is a public-health insecticide and is also used to protect stored grain. It is a mixture of (1*R*)-*cis* and (1*R*)-*trans* isomers. (1*R*)-*cis*-phenothrin (**9**) has been studied by NMR at a proton observation



9

frequency of 300 MHz and an unambiguous spectral assignment made.[44] Key elements in the analysis relied on connectivities established by directly-bonded and long-range $^{13}C-^{1}H$ correlation 2D NMR. The starting point

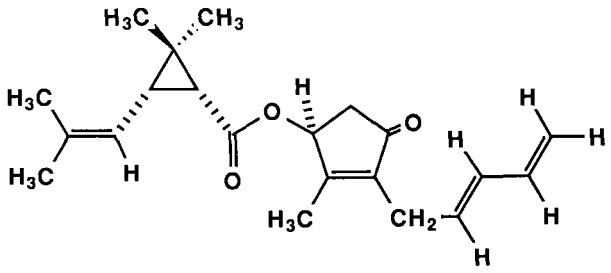
was assignment of the benzylic, vinylic and cyclopropyl protons using routine 1D NMR methods. The methyl and aromatic carbon resonances were assigned by comparison of directly bonded and long-range effects. In particular, the two geminal methyl carbons on the cyclopropyl ring were distinguished by detection of long-range coupling, effective for C-8 but not for C-9, through *trans* vicinal coupling to the cyclopropyl protons. In a similar manner, C-7 was assigned *trans* to the vinylic proton, H-4. Long-range correlations were obtained using a modification to an existing pulse sequence (COLOC) designed to remove $^{1}H-^{1}H$ coupling and so improve sensitivity compared with the fully coupled technique. The new sequence, COLOC-S (COLOC-selective), was found to be even more sensitive to long-range effects, and to have fewer artefacts. Directly bonded carbon–proton correlations were obtained via a pulse sequence known as QWIKCORR.

2.2.2. Stereochemistry

The complete characterization of molecular structures requires a description of the stereochemistry of unsaturated bonds and chiral centres. Assignment of the NMR spectrum does not lead immediately to a stereochemical analysis, since the main objective in assignment is the establishment of bonding patterns, and in this section we wish to illustrate the way in which stereochemical information is extracted from the NMR data.

Configuration at double bonds

Pyrethroids are effectively analogues of pyrethin I (**10**) but may contain



10

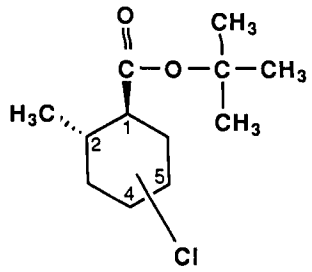
little, if any, of the functional groups present in the prototype. Isosteric replacements, with retention of the stereochemical features critical for activity, have given many active pyrethroids.[45] Both ^{1}H and ^{13}C NMR have been important in defining geometric configurations, for example, in series of oxime *O*-ethers[46,47] with pyrethroid-like activity, and in pyrethroids containing the alkoxyimino groups in the alcoholic side chain.[48] Characterization of *E* and *Z* derivatives was achieved by analogy with aliphatic[47] and aromatic[48] oximes, where *E* and *Z* forms are clearly distinguished by ^{13}C NMR. Here, the carbon in the aldoximes is at higher field for the *Z* isomers than for the *E* isomers. A combination of both optical rotation and ^{1}H and ^{13}C NMR permitted stereochemical assignment of several pyrethrins at high stereochemical purity.[49]

Pheromones are used in insect traps to assess the build-up of insect populations and so permit optimal timing for insecticide application. ^{13}C NMR has been used both to assign the structure of several insect sex pheromone components and structural analogues and to define the configuration of C=C double bonds present.[50] The chemical shift difference between carbons α to the C=C double bond in monoenic and dienic pheromones, and the equivalent carbon in the corresponding saturated compound was used to categorize configuration. Carbons in allylic position were shifted up-field for (*Z*)-double bonds and down-field for (*E*)-double bonds. Quantitative analysis of mixtures was performed by ^{13}C NMR in chloroform solution using the paramagnetic relaxation additive, chromium(III) acetylacetonate to shorten the spin–lattice relaxation times of all carbons and eliminate differential NOE. Mixtures of synthetic pheromone components, (*Z*)- and (*E*)-9-tetradecen-1-yl acetate and (*Z*)- and (*E*)-9,11-dodecadien-1-yl acetate were analysed to validate the method.

Configuration in ring systems

The configurations of some alkyl methylcyclohexaneacetates have been identified by ^{13}C NMR chemical shift in a study of attractant activity to the German cockroach (*Blatella germanica*).[51] Comparison was made with the corresponding dimethylcyclohexane compounds in order to assign *cis* and *trans* configuration.

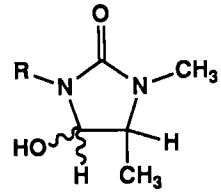
Enantiomers of the biologically active components of the insect attractant trimedlure, a synthetic lure used to attract male Mediterranean fruit flies, have been studied by ^{1}H and ^{13}C NMR.[52] Configurations of the most active components, t-butyl esters of *cis*-4- and *trans*-5-chloro-*trans*-2-



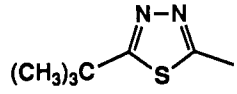
11

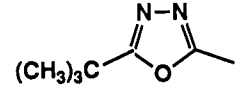
methylcyclohexanecarboxylic acids (**11**), were assigned on the basis of literature analogy, proton chemical shift and chromatographic separation order of some diastereomeric adducts of the acids.

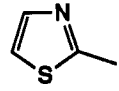
^{1}H NMR has been used to study the products of epimerization in some experimental urea-type herbicides[53] (**12**–**15**). For the isolated *cis* and *trans*

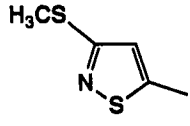


R

12 

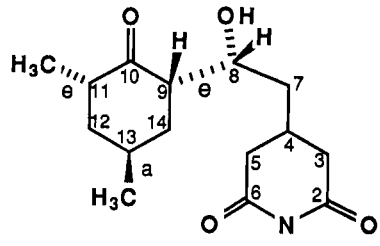
13 

14 

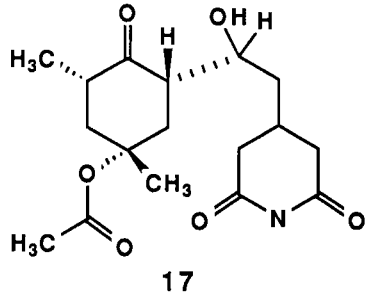
15 

isomers of (**15**) epimerization appeared to be dependent on the solvent; occuring in dimethyl sulphoxide but not in chloroform. This solvent effect implied mediation of an intermolecular hydrogen bond between the hydroxylic proton of the hydroxyimidazolidinone solute and dimethyl sulphoxide. With ready interconversion between *cis* and *trans* forms for (**12**), (**13**) and (**14**), an intramolecular hydrogen bond was thought likely between the hydroxylic proton and the α-nitrogen atom in each hetero-aromatic ring.

Cycloheximide (**16**), isolated from a cultured broth of *Streptomyces griseus*, is a by-product of streptomycin manufacture. It inhibits the growth, in culture, of many plant pathogenic fungi and is used to control powdery mildew on ornamentals, rusts and leaf spot on grasses. The antimicrobial activity of cycloheximide was reported in 1948,[54] but the structure and stereochemistry of this antibiotic was not available until 1965[55] (with confirmation by X-ray crystallography in 1977[56]). The stereochemistry of the cyclohexanone moiety was established by ^{1}H NMR using model ketones for comparison. The key to the analysis was that for reference cyclohexanone compounds axial methyl groups occurred at lower field than equatorial methyls, irrespective of substitution at the 2- or 4-position.



16



17

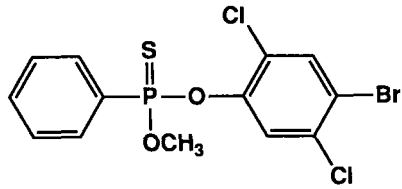
In contrast, a recent report describes a rapid elucidation of the molecular structure for 13-acetoxycycloheximide (**17**) by a combination of both 1D and 2D NMR techniques.[57] These included COSY and heteronuclear $^{13}C-^{1}H$ 2D correlation. The stereochemistry at C-9 and C-11 in the cyclohexanone ring was deduced from the magnitude of the coupling between H-9 and H-4 (axial) ($J = 13.2$ Hz), and between H-11 and H-12 (axial) ($J = 14.9$ Hz). This showed the methyl groups at both C-9 and C-11 to be equatorial, and established the stereochemistry at these positions. However, a complete mapping of the cyclohexanone proton connectivity, feasible for cycloheximide, was not possible here, as the acetoxy group effectively blocked correlation at the C-13 carbon.

In a synthesis study of cycloheximide isomers, the stereochemistry in the cyclohexanone ring was established by comparison of the methyl carbon chemical shifts with known natural isomers.[58] The stereochemistry of some demethylated analogues has also been assigned by carbon chemical shift,[59] and the biosynthesis of cycloheximide has been followed by ^{13}C NMR using ^{13}C-labelled materials.[60]

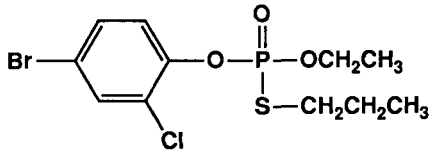
Valuable stereochemical information can be obtained from fully coupled $^{13}C-^{1}H$ 2D correlated spectra. The technique distinguishes between large and small vicinal couplings, which are themselves dependent on torsion angle. For example, in ryanodine (**8**) C-4 was found to correlate with H-14A but not with H-14B, implying a favourable torsion angle (close to 180°) between C-4 and H-14A (Fig. 6). Exactly the opposite was observed for C-6, where correlation with H-14B was found. Analysis of the fully coupled spectra therefore allowed an unequivocal assignment of H-14A and H-14B.[33]

Enantiomeric purity

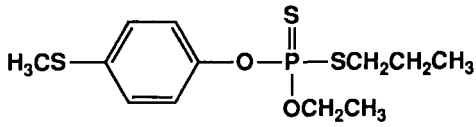
Optically active lanthanide shift reagents can be used to determine enantiomeric purity,[61] and this method has been used with several organophosphorus insecticides. Estimation of enantiomeric purity has been reported for leptophos (**18**),[62] profenofos (**19**)[63,64] and sulprofos (**20**),[64] after either



18



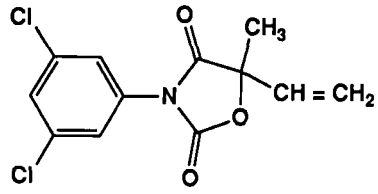
19



20

their chiral synthesis or isomer resolution. For leptophos and sulprofos, prior oxidation to the respective oxon and oxon sulphone was necessary because, while shift reagents associated effectively with compounds containing the phosphoryl moiety,[65,66] they do not interact with sulphur analogues, as sulphur is not a sufficiently strong Lewis base for complex formation.

The advantages offered by both chiral and achiral lanthanide shift reagents in studies at low field (60 MHz) have been investigated[67] with racemic vinclozolin (**21**), a selective contact fungicide. Optimal conditions for determination of optical purity showed that as little as 5% of the minor enantiomer was detectable.



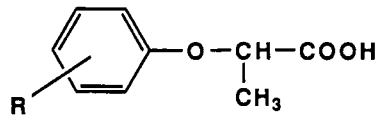
21

Paclobutrazol (**25**) (p. 159) is both a highly active plant growth regulator and a fungicide. Resolution to obtain the (2*S*, 3*S*) enantiomer has been monitored by ^{1}H NMR and the optical purity determined[68] using Eu(hfbc)$_3$. The (*S*, *S*) enantiomer was thought to be specific for plant growth regulator activity.

Formation of diastereomeric menthyl esters (using optically pure menthol), combined with ^{13}C NMR and lanthanide shift reagents, has been

useful in defining the optical purity of intermediates in pyrethroid synthesis.[69]

The microbial reduction and resolution of a series of 2-alkyl-2-aryloxyacetic acid herbicides (including dichlorprop (**22**), fenoprop (**23**) and mecoprop (**24**)) by the mould *Gloeosporium olivarum* has been



	R
22	2,4-di Cl
23	2,4,5-tri Cl
24	2-CH_3, 4-Cl

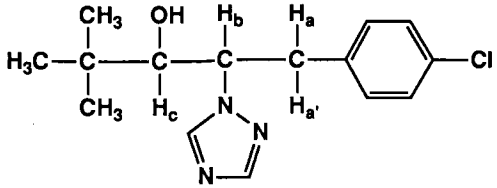
described.[70] Enantioselective reduction of the racemic substrate gave alcohols, classified by optical rotation, with the (*S*) configuration, and the enantiomeric purity of these alcohols was assessed by ^{1}H NMR using Mosher's method[71] with achiral lanthanide shift reagents. Esterification of the isolated alcohols with (*R*)-(+)-α-methoxy-α-trifluoromethylphenylacetyl chloride gave the corresponding acetates, and these were examined at 100 MHz in the presence of Eu(fod)$_3$. For one of the esters, corresponding to 2-methyl-2(-3-chlorophenoxy)ethanol, estimation of isomer ratio was achieved at 400 MHz without the need for a shift reagent.

Further applications of NMR are likely in this area, especially when the biological activity of an agrochemical is found to be due to a specific enantiomer. Here, development of microbial processes offer the possibility of replacing currently used racemates with specific isomers and would allow a significant reduction in the quantity of material applied in the environment.

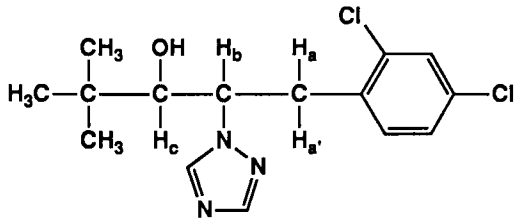
2.2.3. Conformational properties

The conformational properties of a flexible molecule are likely to be important in its mode of action, and NMR has been used in various ways to define conformations in solution. For example, an investigation aimed at understanding the significance of conformation in the mode of action of chiral fungicides involved the comparison of X-ray crystallographic and

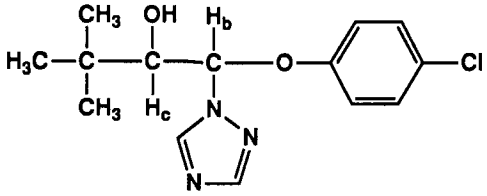
solution-phase ^{1}H NMR data.[72] In structural studies of some azolylmethanes, including paclobutrazol (**25**), diclobutrazol (**26**) and triadimenol (**27**),



25



26

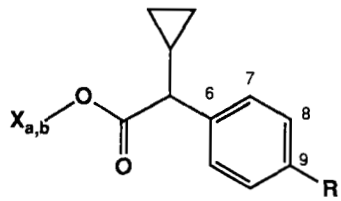


27

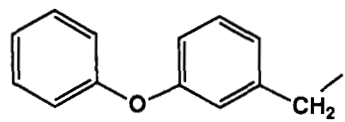
analysis of the coupling between the labelled protons (a, b, c and a′) using the Karplus equation[73] indicated the preferred conformations in solution. A mixed population of conformers was specified from an intermediate value of vicinal coupling between the extremes for *trans* (10–12 Hz) and *gauche* (1–3 Hz) conformations. The chemical shift of the t-butyl protons was also measured, as a greater value of chemical shift was expected for the t-butyl and triazole groups in *trans* rather than in *gauche* conformation.

With two chiral centres present, each molecule may exist as two enantiomeric pairs, (*RS*, *SR*) and (*RR*, *SS*) configurations. For the two most fungitoxic enantiomeric pairs, (*RR*, *SS*)-diclobutrazol and (*RS*, *SR*)-triadimenol, close correspondence was obtained between solution and crystal conformations. However, for the less active (*RS*, *SR*)-diclobutrazol and (*RR*, *SS*)-triadimenol the solution and crystal conformations differed. The possibility of different enantiomers having different modes of binding at the active site was considered.

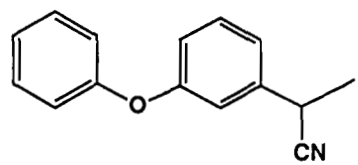
28



X_a



X_b

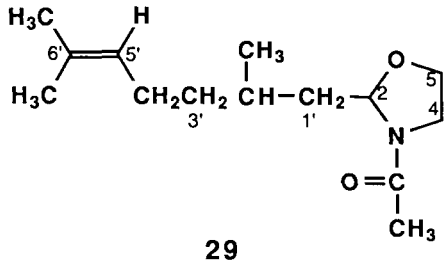


R **Cl, Br, CH_3, C_2H_5, F**

In pyrethroids (**28**), synthesized with α-cyano-3-phenoxybenzyl alcohol as the esterifying alcohol, small additional ^{13}C NMR shifts (relative to other esters) associated with the presence of the nitrile group have been interpreted in terms of restricted molecular motion.[69] Shifts were observed at C-6, C-7, C-8 and C-9 with the largest noted at C-6. From these induced shifts, the nitrile group was thought to align with the aryl group in a $\pi-\pi$ type electron–acceptor–donor interaction.

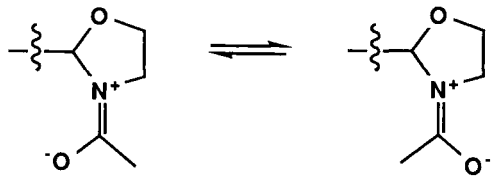
Conformational compositions of methyl- and propyl-methylcyclohexane acetates, at room temperature, were estimated from carbon chemical-shift data[51] in order to correlate conformation and attractant effect to *Blatella germanica*.

Diastereomers of the insect repellant 3-acetyl-2-(2′,6′-dimethyl-5′-heptenyl)oxazolidine (**29**), have been found to exist as *cis* and *trans*



29

rotational isomers in solution at ambient temperature.[74] ^{13}C NMR of (**29**) gave nine non-equivalent carbons in deuterochloroform solution with doubling of resonances for C-1′, C-3′, C-5′, C-6′, C-2, C-4, C-5 and the acetamide carbonyl and methyl carbons. The effect was attributed to restricted rotation about the amide bond with interconversion between species (**29a**) and (**29b**), and with (**29a**) giving rise to the major isomer. The



29a **29b**

chemical shift of the doubled signals differed by less than 1 ppm, except for C-1′ and C-4, where the shift difference was slightly greater. Coalescence was observed at 345 K in deuterobenzene solution.

Selective line broadening was observed in the 500 MHz ^1H-NMR spectrum of propanil (**4**)[41] (see Fig. 7). Protons *ortho* to the *N*-acetyl function were significantly broadened, and the effect was attributed to restricted rotation about the amide bond. The linewidths were close to the rapid-exchange limit, and lowering the temperature removed the residual broadening. Instead, at lower field strength the effect should be far less

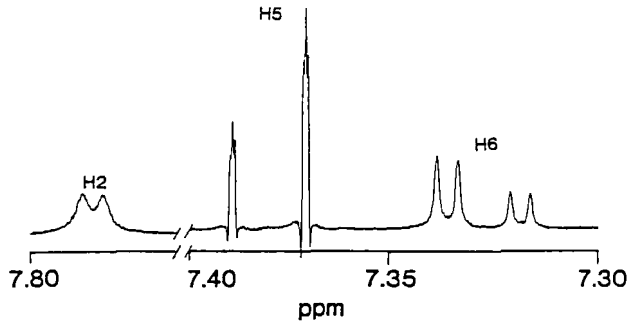
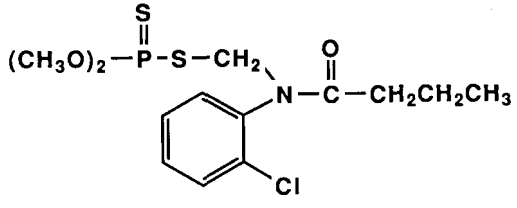


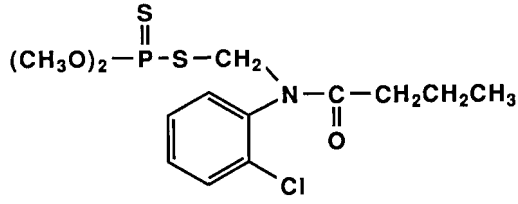
Fig. 7. The 500 MHz ^{1}H NMR spectrum of the aromatic protons of propanil (**4**) in methylene chloride at 301 K shows slight broadening of the two resonances *ortho* to the *N*-acetyl moiety (H-2, H-6). The free-induction decay was processed with Lorentzian to Gaussian filtering. (Reprinted from J.O. Ley, F.E. Evans and J.A. Hinson, *Biomed. Environ. Mass Spectrom.* **13**, 495. Copyright (1986) John Wiley & Sons, Ltd. Reprinted by permission of John Wiley & Sons, Ltd.)

noticeable. These effects demonstrate the need to consider molecular dynamics at an early stage in the design of experiments at high field.

Apparent non-equivalence of the phosphomethoxy and *N*-methylene protons observed in the ^{1}H NMR spectrum of fosmethilan (**30**), at ambient



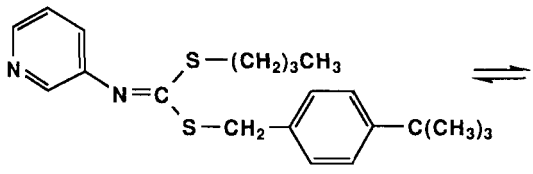
exo



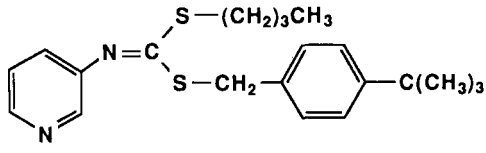
endo

30

temperature, has been interpreted as restricted rotation around the $N-C_{aryl}$ bond.[75] Here the unsymmetrically *ortho*-substituted *N*-aromatic ring gave rise to an asymmetric environment. Coalescence of the phosphomethoxy resonances, a pair of doublets of roughly equal intensity, occurred at 346 K. For hindered rotation about the amide bond, two rotameric forms, *exo* and *endo*, were possible. Moreover, the *exo* isomer with the chlorophenyl moiety *trans* to the carbonyl group would be preferred. However, there was no evidence for the presence of both isomers, even at low temperature, and consequently the *exo* form was thought to predominate.



anti

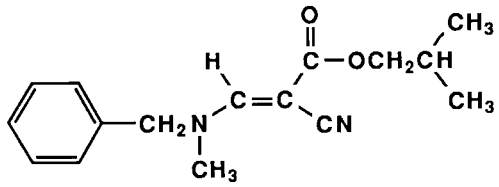


syn

31

In solution, at ambient temperature, buthiobate (**31**), a potent fungicide, displays considerable conformational freedom.[76] This contrasts with the crystal conformation where the 3-pyridyl and *S*-*p*-t-butylbenzyl groups were found in *syn* configuration about the C=N bond. At lower temperature (233 K), ^1H NMR in chlorobenzene solution showed the benzylic methylene protons as two peaks, with coalescence at 259 K on temperature increase. Isomer ratios were measured from spectra obtained below the coalescence points. Experiments with a series of *S*-alkyl analogues showed that for bulky groups the isomer ratio was reversed compared with groups with lower steric demand. Consequently, the major isomer of buthiobate was assigned the *anti* configuration.

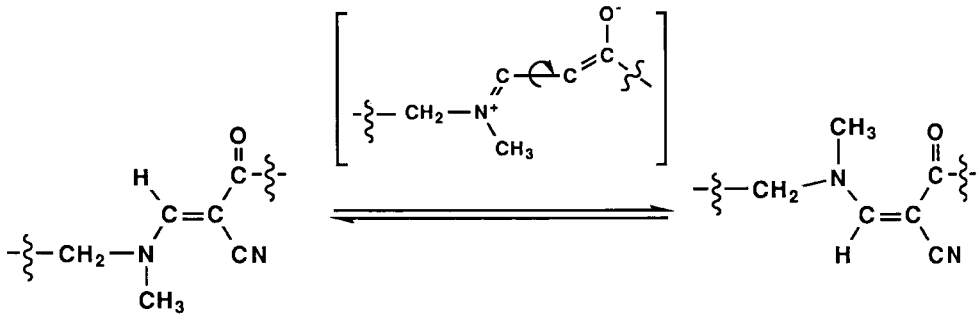
Variable-temperature studies can be extremely time-consuming, and saturation transfer[14,77,78] provides an alternative method for studying exchange processes. As an example of this approach, saturation transfer methods have been used to investigate hindered molecular rotation in the research fungicide isobutyl 3-(benzylmethylamino)-2-cyanoacrylate (**32**)[79].



32

The ^{1}H NMR spectrum of (**32**) (Fig. 8a) shows major and minor singlets for the =CH, N−CH_2 and N−CH_3 functions. On heating a solution in dimethyl sulphoxide, coalescence of the =CH singlets occurred at approximately 373 K and implied a two-site exchange process with a relatively high activation energy. However, in chloroform solution and at ambient temperature, irradiation of each minor signal (using a simple presaturation pulse sequence) gave a pronounced reduction in intensity for each corresponding major singlet (Fig. 9c). In addition, complementary reductions in signal intensity were seen for the minor singlets on selective saturation of the major signals. The saturation transfers obtained clearly identified an exchange process.

A quantitative analysis of the saturation transfers enabled the lifetimes of the rotamers of (**32**) to be determined in solution. The quotient of measured lifetimes τ_A/τ_B gave reasonable agreement with the quotient of rotamer concentrations R_A/R_B obtained from spectrum integration (Table 5), and indicated minimal interference from cross-relaxation phenomena. The relatively long lifetimes are consistent with a high activation energy and support a scheme for internal molecular rotation involving an apparent rotation about a C=C bond.



Scheme 1.

The correlations obtained in the spectrum of (**32**) by saturation transfer can be observed simultaneously in the 2D NOE correlated (NOESY) spectrum (Fig. 8b). For NOESY the presence of cross-peaks relates regions

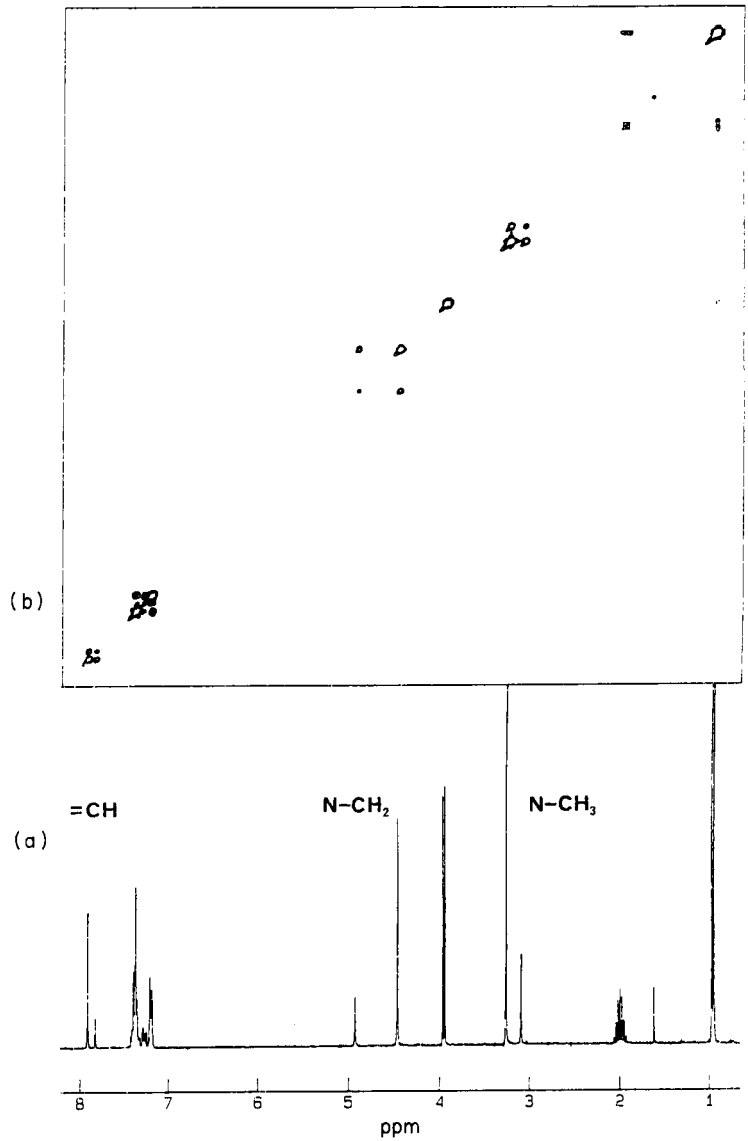


Fig. 8. (a) ^{1}H NMR and (b) NOESY spectra for (**32**) in $CDCl_3$ at 300 K.

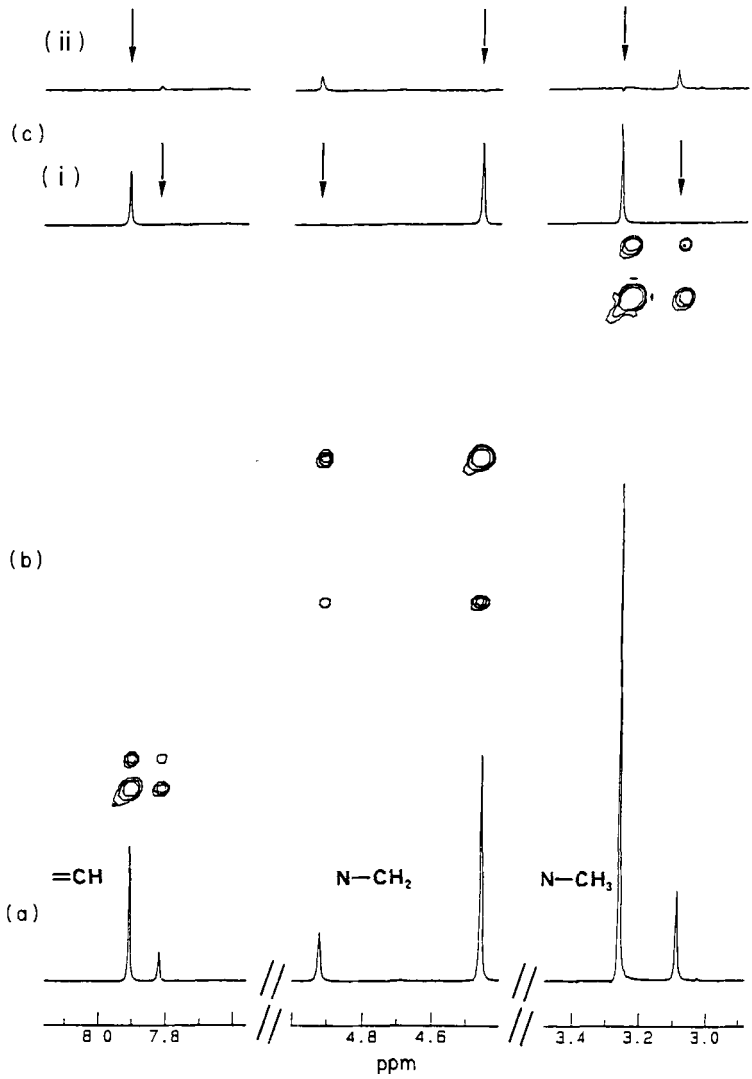


Fig. 9. Partial ^{1}H NMR spectra for the $=CH$, $N-CH_2$ and $N-CH_3$ moieties of (**32**): (a) 1D spectrum; (b) NOESY, showing regions related through rotamer exchange; and (c) saturation population transfer with irradiation of (i) minor singlets and (ii) major singlets.

Table 5. Rotamer lifetimes for (**32**).

	Lifetimes			Rotamer ratio
	τ_A (s)	τ_B (s)	τ_A/τ_B	R_A/R_B
=CH	1.4	0.4	3.5	4.0
N−CH_2	1.0	0.3	3.3	3.6
N−CH_3	1.2	0.3	4.0	3.9

of the spectrum coupled by NOE or by chemical exchange. In Fig. 9(b) the cross-peaks indicate regions of the spectrum related via rotamer exchange. A small dipolar coupling is also apparent between the major peaks of the =CH and N−CH_2 functions in Fig. 8(b).

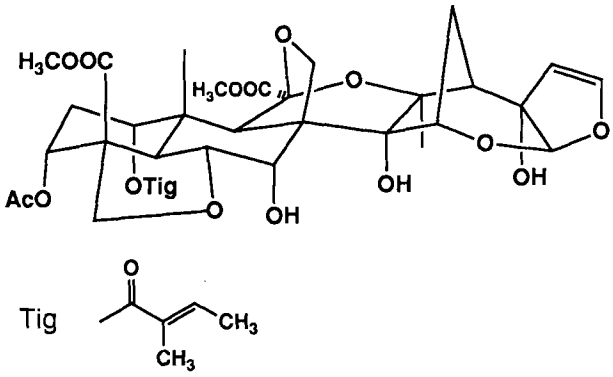
2.3. Compounds of natural origin

There is a growing interest in natural mechanisms as the basis for crop protection. This is largely due to an increasing difficulty in the discovery of novel synthetic compounds with suitable properties and more demanding regulations in relation to environmental protection. Indeed, the possibility that higher plants could afford valuable chemicals for future agrochemical or pesticidal use has been considered and reviewed.[80]

Although the industrial significance of products obtained by tissue extraction may be limited, some recent examples are given where NMR has been used to study biologically interesting compounds obtained from higher plants. Examples of NMR for compounds isolated from cell suspensions and culture media are also given.

Probably the most promising use for biologically active substances obtained from higher plants is in insect control. The limonoid natural products extracted from the neem tree, *Azadirachta indica* A. Juss, and from the related china berry tree, *Melia azedarach* L., display important biological activity and have been the subject of a number of international conferences in recent time.[81]

The most active component, azadirachtin, is a potent insect antifeedant and growth-regulating agent. Considerable effort has been expended on the elucidation of its molecular structure with three research groups working independently. Reviews of results from each group have been collectively published recently (Nakanishi's group,[82] Kraus's group[83] and Ley's group[84]). A summary highlighting the problems encountered has been provided.[85] This also indicates where lessons may be learnt for future investigation of complex systems.

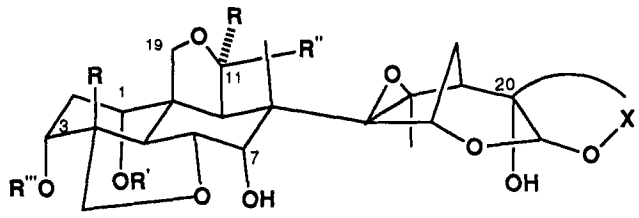


33

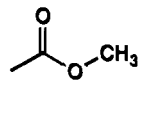
The structure for azadirachtin (**33**) proposed by Nakanishi[86] in 1975, was revised to (**34**) some ten years later by Kraus[87] and by Ley[88]. Problems in determination of the structure centred on the difficulty in establishing connectivity within the molecule by either ^{13}C or ^{1}H NMR, where spin–spin coupling through oxygen greatly reduced the size of the coupling constant. In addition, the full significance of temperature-dependent effects noted in the original work was not realized until later. These effects indicated possible internal molecular rotation about a single bond. Indeed, Nakanishi *et al.*[82] have used azadirachtin as a test case in structure assignment by NMR and redetermined its structure as if the material were an "unknown". The 7,11,20-trimethyl ether of azadirachtin was also studied in order to locate the hydroxyl functions in azadirachtin unambiguously. Both steady-state and kinetic NOE measurements were made for azadirachtin and for its trimethylether in order to define optimal conformations.

In the X-ray crystallographic work of Ley and coworkers[84] crystals of azadirachtin of sufficient quality could not be obtained. However, detigloyldihydroazadirachtin (**35**), prepared by degradation of azadirachtin, gave suitable crystals and revealed key structural fragments common to both compounds. Comparisons were also made by ^{1}H NMR.

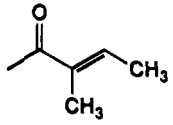
Subsequent to the reassignment of azadirachtin,[87] the structure of



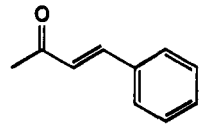
	R'	R''	R'''	X
34	Tig	OH	Ac	-CH=CH-
35	H	OH	Ac	$-(CH_2)_2-$
36	Tig	H	H	-CH=CH-
37	H	H	Tig	-CH=CH-
38	Tig	OH	Cin	-CH=CH-
39	Tig	OH	Ac	$-CH_2-CH(OCH_3)-$



R

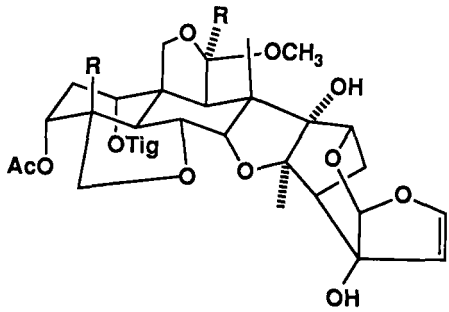


Tig

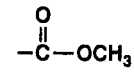


Cin

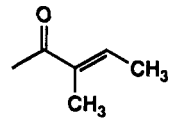
deacetylazadirachtinol[89] was reinvestigated.[84,90] Ley assigned the structure as 3-deacetyl-11-desoxyazadirachtin (**36**) and confirmed the position of the tigloyl group at C-1.[84] However, Kraus determined the tiglate group to be at the 3-position, and reassigned the structure as 3-deacetyl-3-tigloyl-11-desoxyazadirachtin (**37**).[90] Whereas Kraus observed a significant NOE from a C-19 methylene proton to H-1, no such effect was observed by Ley.



R



Tig



40

This discrepancy may be due, in part, to the origin and history of the samples under study—the melting points reported were significantly different.

Other structure determinations by NMR have been reported for 3-deacetyl-3-cinnamoylazadirachtin (**38**), 22,23-dihydro-23β-methoxy-azadirachtin (**39**) and 1-tigloyl-3-acetyl-11-methoxyazadirachtinin (**40**) obtained from *Azadirachta indica* extracts,[83] and for 1-cinnamoyl-melianolone (**41**) isolated from *Melia azedarach* L.[91]

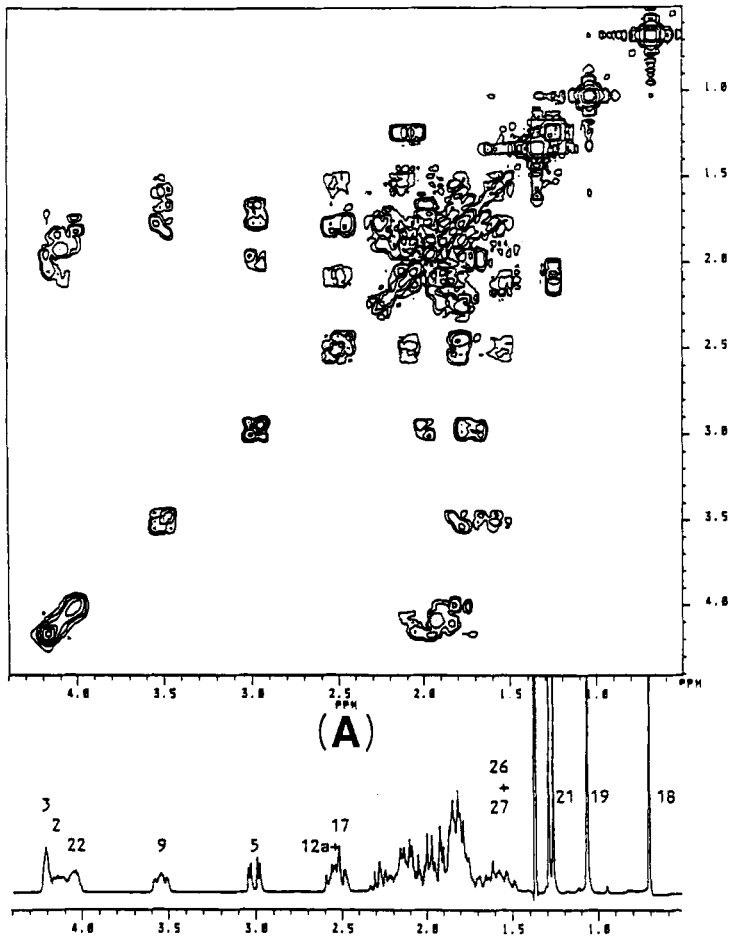
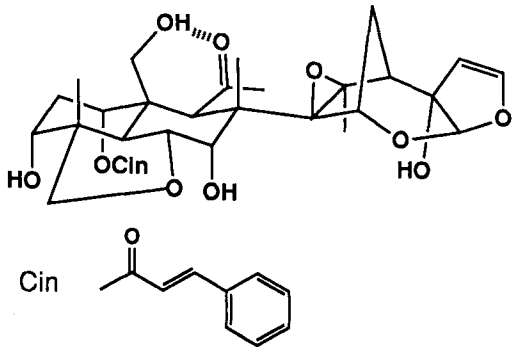
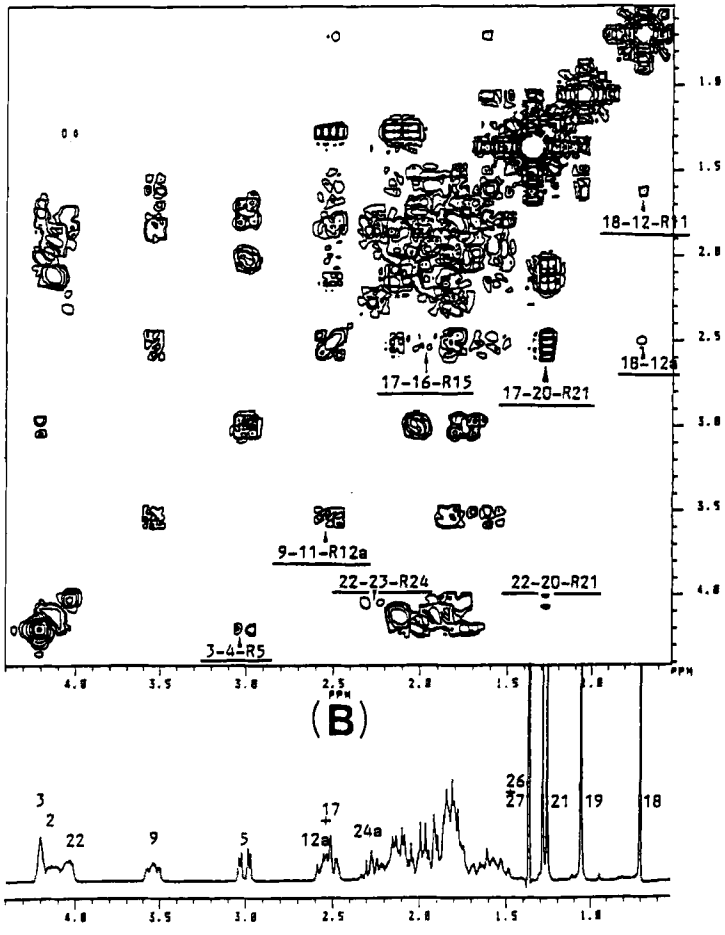


Fig. 10. (A) 2D COSY45 and (B) relayed COSY of ecdysone (**42**) in C_5D_5N. (Reprinted with permission from *J. Insect Physiol.* **34**, 701, J.P. Girault and R. Lafont, Copyright (1988), Pergamon Press PLC.)

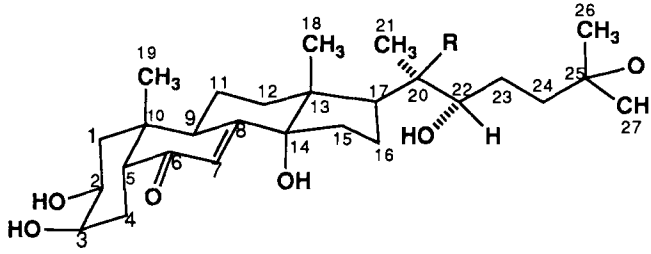

OH
O
O
O
O
HO
OCIn
O
OH
HO
Cin
O

41


18-12-R11
18-12a
17-16-R15
17-20-R21
9-11-R12a
22-23-R24
22-20-R21
3-4-R5
PPM
(B)
3
2
22
9
5
17
12a
24a
26
27
21
19
18

As in the case of pyrethrin manufacture, where supply of flower heads was critical, the dependence of azadirachtin production on the availability of neem seed would make for a poor commercial prospect. Indeed, the most likely development route for the azadirachtins would seem to be via discovery of simple synthetic analogues.[80,92]

A further example in the investigation of plant–insect relationships is the application of NMR in the structural studies of phytoecdysteroids. Ecdysteroids, a large group of steroid compounds, occur in both plants and insects. In insects they have hormonal functions controlling development. Consequently plant ecdysteroids acting as insect hormone mimics can afford protection against herbivores. Here ^{1}H NMR 2D correlation methods assume an increasing importance for spectral assignment purposes when sample quantity is severely limited and ^{13}C observation impracticable. To achieve the necessary molecular connectivity for assignment, networks of adjacent protons, recognized by COSY correlation, need to be augmented to include next-nearest neighbours. This is possible by optimizing COSY for small values of J (COSY long-range). However, where long-range couplings are too small, connectivity can be extended by relayed coherence transfer. In relayed COSY, new correlations, which appear in addition to the normal COSY cross-peaks, indicate relayed coherence or neighbouring non-coupled spins.



	R
42	H
43	OH

An illustration of relayed COSY is in assignment of the ^{1}H NMR spectrum of ecdysone (**42**).[93] The COSY45 and relayed COSY spectra are given in Figs 10(A) and 10(B) respectively. In particular, from the COSY45 spectrum the C-21 methyl protons (1.28 ppm) are seen to correlate with H-20 (2.12 ppm), and H-20 to couple with both H-17 (2.51 ppm) and H-22 (4.05 ppm). The normal COSY contours also occur in the relayed COSY

Table 6. NMR in structural studies of compounds obtained from plant extracts and cell cultures.

Compound	Structure[a]	Origin	Activity	NMR application	Refs
Azadirachtin and analogues	**(34)**	Neem tree	Insect antifeedant	See text	82, 83, 84, 87, 88, 90, 91
Phytoecdysteroids	**(43)**	Found in several plants and in insect larvae	Insect-hormone mimic	See text	93, 94
Trichilins (A, B, C and D)	—	Dried root bark of *Trichilia roka*	Insect antifeedant (vs American army worm)	^{1}H and ^{13}C spectra assigned by various techniques, including 2D *J*-resolved	98
Myricoside	—	Root of *Cleodendrum myricodes* (Verbendaceae)	Insect antifeedant (vs African army worm)	Linkages of various groups established in this phenolic glycoside by comparison of ^{13}C and ^{1}H chemical-shift data with the peracetylated compound	98
Phloretin 4′-*O*-β-D-glucopyranoside	**(A1)**	Fresh leaves of the apple *Malus pumila* var. *dulcissima* Mill (Rosaceae)	Insect antifeedant (vs greenbug aphid)	Preferred solution conformation described by $^{13}C-^{1}H$ coupling and $^{1}H-^{1}H$ NOE	99
Destruxins	—	Fungus culture *Metarrhizum anisopliae* (Metch.) Sorok	Insecticidal	Study of conformation in cyclodepsipeptides by ^{1}H NMR	100
Capsidiol Debneyol and analogues (phytoalexins)	**(A2)** **(A3)**	Plant tissue, and elicited from cellulase-treated cell suspension cultures of *Nicotiana tabacum*	Antifungal (raise resistance of the host plant to fungal attack)	Stereochemistry defined by ^{1}H and ^{13}C NMR	101–103
Phenanthrenes	**(A4)** **(A5)**	Peel of yams	Antifungal (preformed inhibitors for disease resistance)	Structure determined by comparison of ^{1}H chemical shifts with known compounds	104
Cycloheximide	**(16)**	By-product of streptomycin manufacture	Fungicidal	See text (Section 2.2.2)	55,58
Analogues of ovalifoliene	**(A6)**	Liverworts	Plant growth inhibition	Identification by ^{13}C NMR	105
Cytochalasin H and derivatives	**(A7)**	Culture extracts of *Phomopsis* sp.	Plant growth regulating activity in intact plants	^{1}H and ^{13}C NMR in a correlation of conformation and biological effect	106

[a] Structures prefixed with the letter **A** are given in the Appendix.

spectrum and, in addition, cross-peaks for C-21 methyl protons with H-17 and H-22 are present. Other correlations include relay between protons at C-22 and C-24, and between protons at C-17 and C-15. Consequently connectivity is indirectly established from C-24 through to C-15. Chemical shift assignments for ecdysone, achieved through the COSY correlation, were therefore confirmed and missing connections established through use of relayed coherence transfer.

Interestingly, the ^{1}H NMR assignment of 20-hydroxyecdysone (**43**) has been reported[94] in an investigation into resistance of *Heliothis* larva to dietary phytoecdysteroids found in several plants.[95–97]

Many other compounds obtained from natural sources, showing a variety of interesting biological activity have been studied by NMR. These are summarized in Table 6.

3. DECOMPOSITION AND METABOLISM

Exposure to the environment or metabolism by living systems has the potential to modify the structure of most plant protection agents. In principle, NMR should be an ideal technique for characterizing these structural changes, but in practice the limited quantities of material available for analysis result in NMR being used less frequently for following degradative and metabolic processes than for determining the structures of new compounds. However, the continuing improvements in NMR methodology are reducing some of the difficulties, and the investigation of the decomposition and metabolism of plant protection agents by NMR is likely to increase.

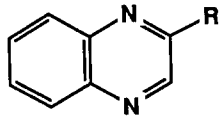
3.1. Stability in model systems

Evaluation of the chemical behaviour of agrochemical and pesticidal compounds is essential before the material can be released into the environment, and the results of such studies assist in the optimal design of the commercial product. Hydrolysis, oxidation and photochemical degradation are the processes of immediate interest and the conditions imposed on the material may be designed either to provide a good approximation to the natural environment or to cause the maximum chemical effect.

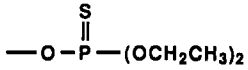
Environmental degradation often leads to complex mixtures of compounds that can only be obtained in very small quantities, and the isolation and detection of these products requires chromatographic techniques. Subsequently, the identity of each product is established by comparison

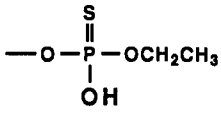
with the properties of synthetic samples of known structure. While NMR will almost certainly have been used to establish the structure of the synthetic material, an NMR analysis of the purified decomposition product is unlikely to be possible for many of the minor components of the original mixture.

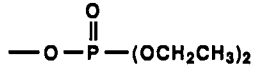
NMR is more useful in characterizing the structural changes that occur under conditions that favour a particular chemical transformation (Table 7). For example, ^{1}H NMR was used in combination with mass spectrometry and infrared spectroscopy to confirm possible structures for products formed during the catalytic hydrolysis[107] and photodegradation[108] of the insecticide quinalphos (**44**). Two products were identified after catalytic hydrolysis by homoionic clays: Cu-, Fe- and Al-montmorillonite gave 2-hydroxyquinoline while clays of the alkali and alkaline-earth metals caused dealkylation to (**45**). Photoirradiation with sunlight gave several products: (**45**) and (**46**) were formed on a glass plate, while (**45**), (**47**) and (**48**) were produced on soil surfaces.



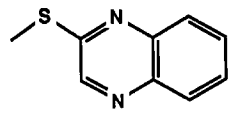
R

44 

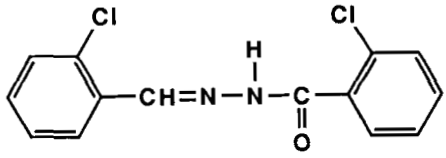
45 

46 

47 

48 

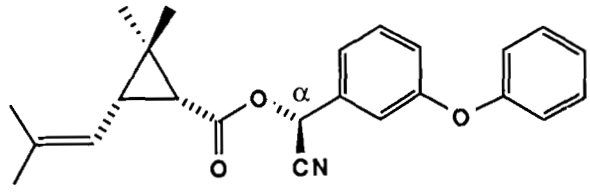
Although the spectrum of the starting material is usually fully characterized, the analysis of the changes caused by the degradation of the compound can sometimes produce interesting spectroscopic problems. Molecular decomposition does not necessarily lead to spectral simplification, and this is well illustrated by the degradation of the acaricide clofentezine (**3**). The principal degradation product (**49**) in soil arises from



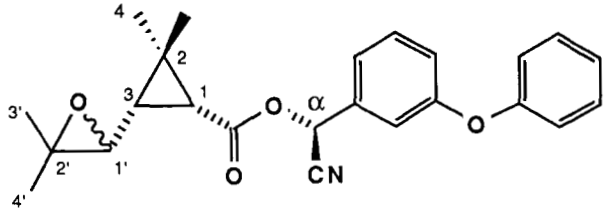
49

the hydrolytic cleavage of the tetrazine ring,[109] and the resulting isomeric mixture increases the number of ^{13}C resonances from 7 (Fig. 2a) to 28 (Fig. 11).

Several different pulse sequences may be necessary to obtain a complete understanding of the spectral changes caused by decomposition. For example, chemical oxidation of the pyrethroid insecticide (1*R*,*cis*,α*S*)-cyphenothrin (**50**) yields two diastereoisomers of (1*R*,*cis*,α*S*)-



50



51

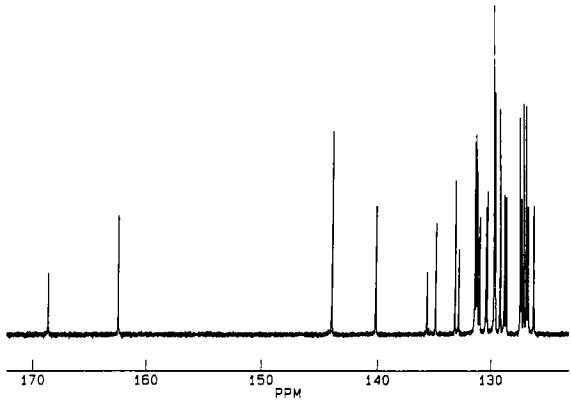


Fig. 11. ^{13}C-NMR spectrum of (**49**), the hydrolysis product of clofentezine (**3**) in $(CD_3)_2SO$.

epoxycyphenothrin (**51a,b**), and several NMR methods were needed to assign the structure and absolute configuration of these isomers.[110] Directly bonded and long-range heteronuclear $^{13}C-^{1}H$ correlation was used to obtain the ^{1}H and ^{13}C assignments, and the observation of *trans* vicinal coupling between C-3′ and H-1′ and between C-4 and H-1 gave an unambiguous assignment of the two methyl resonances (isomer **51a**) C-3′ 1.32 ppm, C-4 1.23 ppm; isomer (**51b**) C-3′ 1.34 ppm, C-4 1.20 ppm). The separation of the methyl groups differs in the two diastereoisomers. They are in close proximity in the (1′*R*) form and apart in the (1′*S*) form. In a ^{1}H NOESY experiment (Fig. 12) cross-correlation was only obtained between C-3′ and C-4 in the spectrum of (**51b**), indicating that this spectrum corresponded to the (1′*R*) isomer.

An interesting application has been considered for the ^{13}C NMR data obtained from some substitution methylthio s-triazine herbicides.[111] A correlation was established between the chemical shift of the carbon at the position of methylthio substitution in the triazine ring and the half-life for methanolysis. If methanolysis could be assumed to model environmental hydrolysis then the chemical shift of carbon atoms at reactive centres might indicate the likelihood of nucleophilic substitution in the environment.

3.2. Metabolism of agrochemicals

Attempts to use NMR to investigate the metabolism of agrochemicals can be frustrated by the insensitivity of the technique. Metabolites are often only available in small quantities, and the potential advantages of an NMR

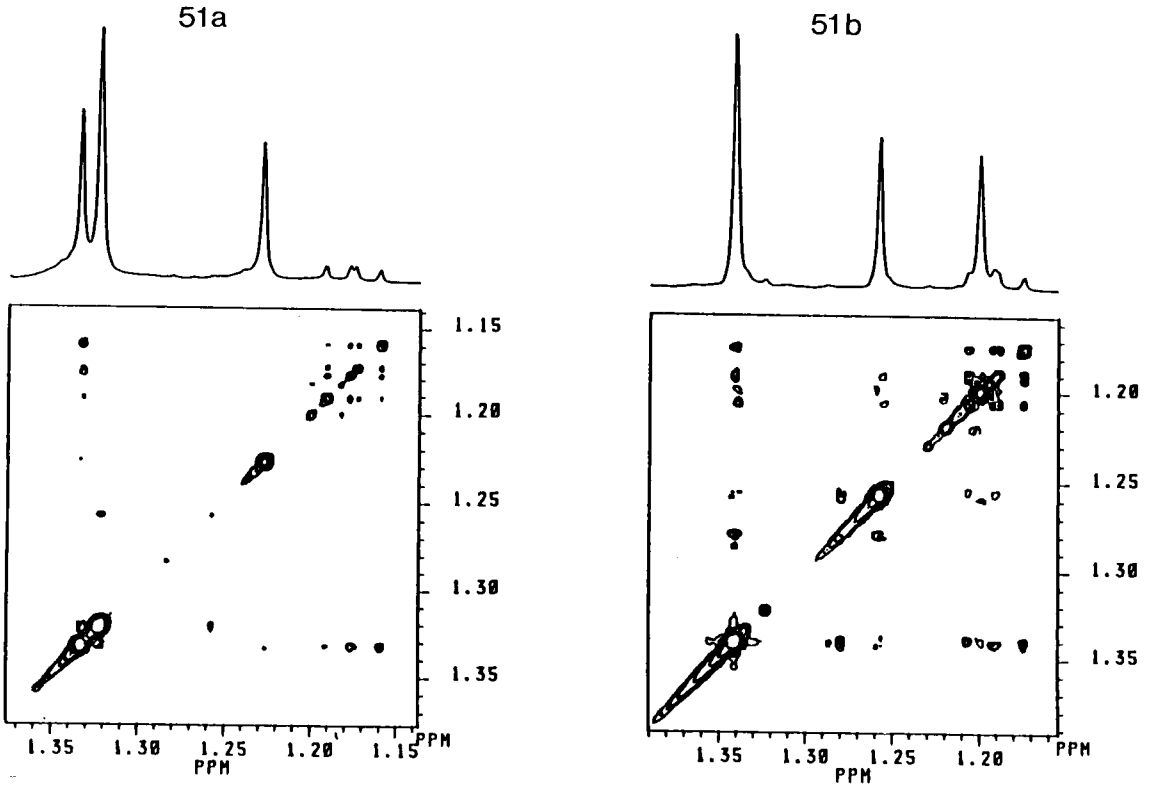


Fig. 12. NOESY spectra of diastereoisomers of (1*R*,*cis*,α*S*)-cyphenothrin (**51a,b**). (Reprinted with permission from V.V. Krishnamurthy, J.E. Casida and L.O. Ruzo, *J. Agric. Food Chem.* **35**, 504. Copyright (1987) American Chemical Society.)

Table 7. Structural changes characterized by NMR.

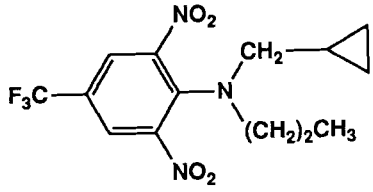
Process	Compound	Structure[a]	Activity[b]	Nucleus	NMR application	Refs
Epimerization	Rotenone	**(A8)**	I	^{13}C	Quantification of epimer ratios	139, 140
Hydrolysis	Clofentezine	**(3)**	I	^{13}C	Isomer formation during cleavage of the tetrazine ring	109
	Quinalphos	**(44)**	I	^{1}H	See text	107
	Chlozolinate	**(A9)**	F	^{1}H	Identification of decomposition products in wine	141
	Vinclozolin	**(21)**	F	^{1}H	Identification of decomposition products in wine	141
Oxidation	Cyphenothrin	**(50)**	I	$^{1}H/^{13}C$	Determination of the structure and absolute configuration of the two diastereoisomers of (1*R*,*cis*,α*S*)-epoxycyphenothrin **(51)** obtained by chemical oxidation of **(50)**	110
	Methfuroxam	**(A10)**	F	$^{1}H/^{13}C$	Observation of a 4,5-epoxyfuran intermediate (formed by peracid oxidation of **(A10)**); a model for microsomal oxidation of pyrethrins to ring-opened products	142, 143
	Propanil	**(4)**	H	^{1}H	Identification of *N*-oxidation decomposition products **(A11–A13)**	41
Photochemical changes	Allethrin and analogues	**(A14)**	I	$^{1}H/^{13}C$	Identification of photolysis products indicated that the propenyl group was not the major site for photodegradation in *S*-bioallethrin **(A15)**	144
	Fluazifop-butyl	**(A16)**	H	^{1}H	Identification of the isomerization that occurs during a photochemical rearrangement	145
	Isoproturon	**(A17)**	H	^{1}H	Authentication of reference compounds for identifying the products of photodecomposition	146
	Quinalphos	**(44)**	I	^{1}H	See text	108

[a] Structures prefixed with the letter **A** are given in the Appendix.
[b] I, insecticidal; H, herbicidal; F, fungicidal.

investigation may be outweighed by the impracticability or undesirability of scaling up the production of the metabolite. The small number of successful studies in this area fall into four categories: (a) analysis of body fluids; (b) analysis of tissue extracts; (c) solid-state analysis of freeze-dried tissues; (d) *in vivo* monitoring.

3.2.1. Analysis of body fluids

Abnormalities in metabolism and the presence of drug metabolites can be detected by high-resolution NMR studies of body fluids.[112] The need for high sensitivity favours the use of ^{1}H and ^{19}F NMR at the highest available field strengths, and under these conditions NMR provides a convenient analytical method that can complement other experimental approaches. The advantages of the method include the minimal preparation of the sample and the fact that the spectrum reports on all the metabolites in the solution. Although primarily developed in a clinical context, the same approach should be useful in metabolic studies of agrochemicals, and this view is confirmed by a number of recent publications.



52

^{19}F NMR has been used to identify metabolites of profluralin (**52**) in the urine of rats.[113] The chemical shift of the trifluoromethyl group was a useful indicator of the identity of the corresponding metabolites, and evidence was obtained for a number of metabolites that had not been recognized by other methods. A timecourse for the appearance of the metabolites in the urine was readily obtained by recording spectra from samples taken at different times after ingestion of the herbicide, and this information was used to suggest pathways for the degradation of profluralin.

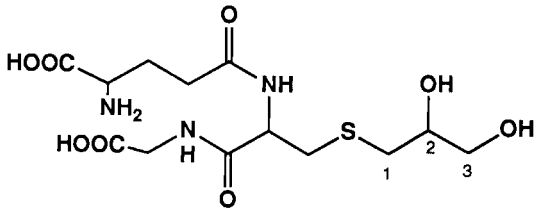
While the ^{19}F method has the advantage that each metabolite contributes a single resonance, the assignment of the resonance is not necessarily trivial since there is only one measurement—the chemical shift—constraining the identification. Four of the profluralin metabolites were isolated by chromatography and identified by ^{1}H NMR and mass spectrometry; but the majority of the assignments could only be based on a comparison between

the ^{19}F spectrum and the ^{19}F shifts of known compounds. The latter approach cannot distinguish between different compounds with the same chemical shift and it fails (as it did for some signals in the profluralin study) when no known compound corresponds to an observed resonance.

^{1}H and ^{13}C NMR have also been used to identify pesticide metabolites in body fluids, and here the assignment problem stems more from the complexity of the spectrum than from the difficulty of making unambiguous assignments. Direct comparison with the spectra of known compounds is more informative when the material is characterized by many different resonances, but it may still be necessary to simplify the spectrum by isolating a particular component from the metabolite mixture.

$CH_2BrCHBrCH_2Cl$

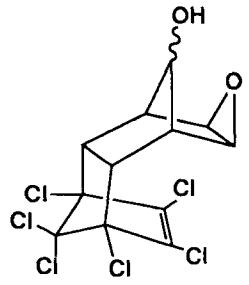
53



54

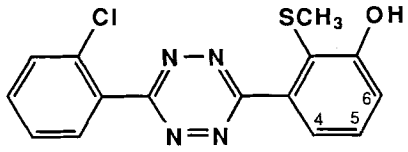
The identification of five small rodent metabolites of the nematicide DBCP (**53**) as glutathione (GSH) conjugates was achieved by a combination of ^{1}H and ^{13}C NMR using ^{13}C-enriched test material.[114] Directly bonded heteronuclear carbon–proton correlation was important in the spectral comparisons between the isolated material and the synthesized standards. A complete assignment of *S*-(2,3-dihydroxy-1-propyl)GSH (**54**) has been reported,[115] and the unambiguous assignment of the C-1 and C-3 resonances, on the basis of long-range carbon–proton correlations, was important in the analysis of the ^{13}C-labelled metabolites.

NMR data for synthetic standards relating to mammalian metabolites of the insecticides dieldrin and endrin have also been reported. Several major metabolites,[116] as well as a minor metabolite,[117] have been synthesized, and ^{1}H NMR was particularly useful in determining the configuration at C-12 for 12-hydroxyendrin (**55**). The hydroxy group in the *syn* isomer was



55

strongly hydrogen-bonded to the epoxy group and gave a doublet ($J \approx 12$ Hz) whereas the hydroxy group in the *anti* isomer gave a broad resonance.



56

As a final example, a small rodent metabolite (**56**) of clofentezine (**3**) has been studied by ^{1}H NMR at 300 MHz in methanol.[39] The aromatic region of the spectrum (Fig. 13) extends over just 1 ppm and is free of the major artefacts introduced by isolation and purification apparent in the aliphatic region of the spectrum. Regions I and II resembled the spectrum of clofentezine (Fig. 1a), but simulation of regions III and IV suggested the presence of a tri-substituted aromatic moiety (Fig. 13 and Table 8) and also indicated that the minor resonances in region III were not due to a minor component. Confirmation of the molecular structure was obtained by synthesizing the predicted compound and assigning regions III and IV using a COSY45 shift correlated spectrum.

3.2.2. Analysis of tissue extracts

The analysis of tissue extracts is marginally less attractive than the direct analysis of body fluids, because of the possibility of chemical changes during extraction, but the origin of the sample is of no consequence to the NMR analysis. A straightforward example is provided by a ^{13}C NMR study

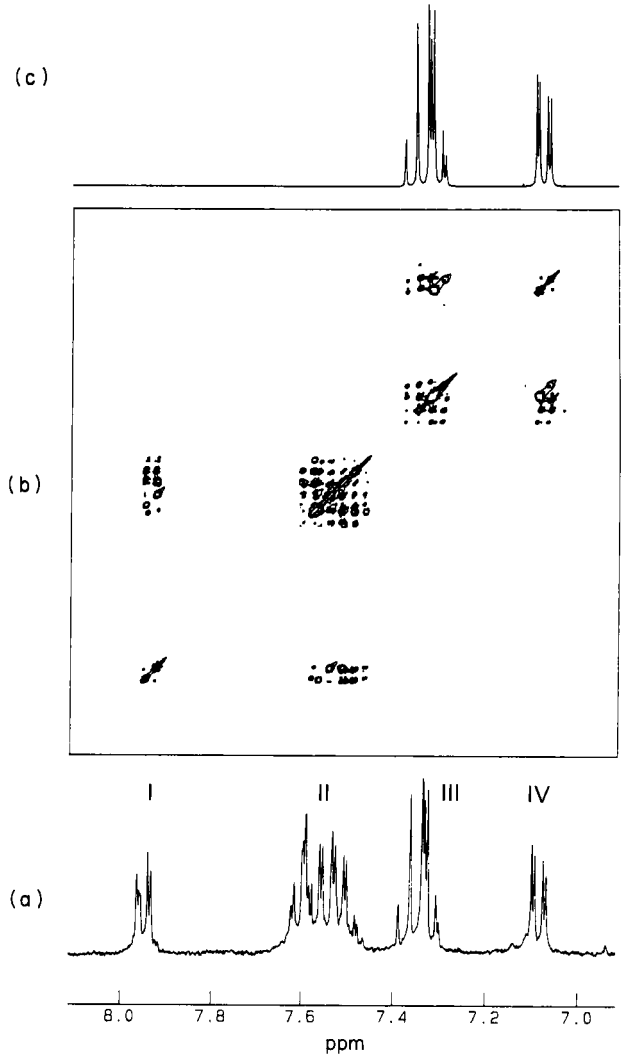
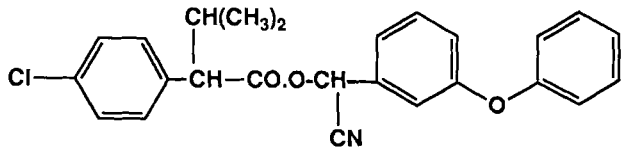


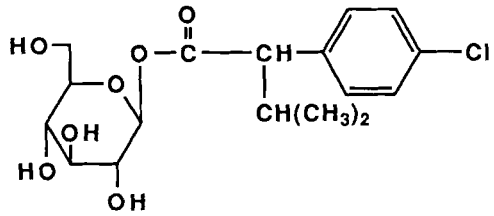
Figure 13. ^{1}H-NMR spectra of clofentezine metabolite (**56**) in CD_3OD: (a) coupled spectrum; (b) 2D COSY45; (c) spectrum simulation for the trisubstituted aromatic ring.

Table 8. Spectrum simulation parameters for clofentezine metabolite (**56**).

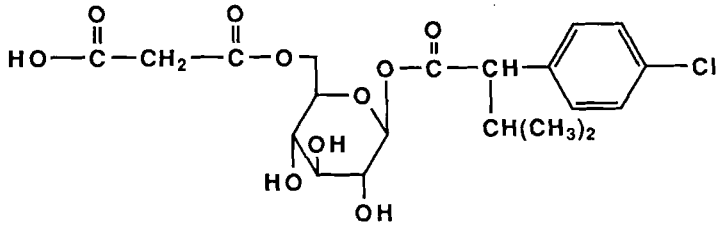
Chemical shift (ppm)		Indirect coupling (Hz)	
H-4	7.32	$J_{4,5}$	7.8
H-5	7.36	$J_{4,6}$	1.4
H-6	7.09	$J_{5,6}$	8.3



57

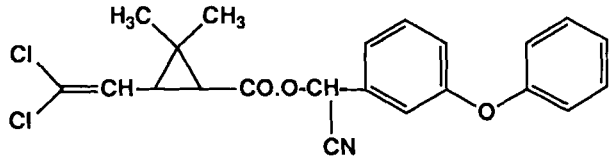


58

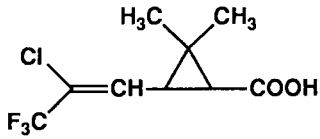


59

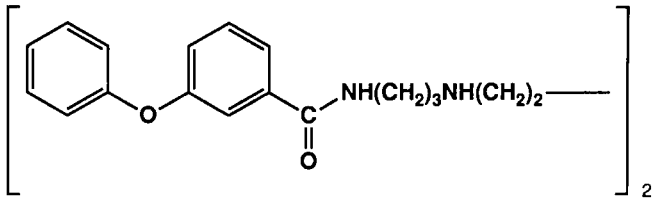
of the conjugation of the acid moiety of the insecticide fenvalerate (**57**) in plants.[118] Two metabolites were extracted from cabbage leaves and identified as (**58**) and (**59**). A more complicated example is provided by the conjugation of the pyrethroid cypermethrin (**60**) by earthworms.[119] Here the trifluoracetyl derivative of the principal metabolite, which had been prepared for chromatographic reasons, provided a convenient probe for a quantitative study by ^{19}F NMR. By using (**61**) as an internal standard for both ^{1}H and ^{19}F NMR it was possible to show that the unknown metabolite contained two 3-phenoxybenzoyl groups, and subsequently it was shown that the trifluoroacetyl derivative of N^{1},N^{12}-di-(3-phenoxybenzoyl)spermine (**62**) matched the unknown.



60



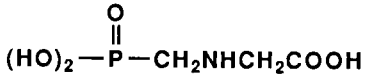
61



62

3.2.3. Solid-state analysis of freeze-dried tissues

High-resolution solid-state NMR spectra can be obtained by combining the resolution-enhancing techniques of magic-angle spinning and dipolar decoupling with the sensitivity-enhancing technique of cross-polarization.[120] Solid-state spectra can be obtained from freeze-dried tissues, and the potential of this technique for metabolic studies is well illustrated by a series of papers on the microbial metabolism of the herbicide glyphosate (**63**).[121–124]



63

Cell suspensions were incubated with ^{13}C- and/or ^{15}N-labelled glyphosate, and the distribution of the label was investigated by recording single and double cross-polarization spectra from the freeze-dried tissue. The single cross-polarization experiment, in which magnetization was transferred to either ^{13}C or ^{15}N, was used to identify the molecular form of the label, while the double cross-polarization experiment, in which magnetization was transferred between directly bonded ^{13}C and ^{15}N nuclei, was used to determine the fate of the two C—N bonds in the glyphosate molecule.

The NMR investigations focused on two pathways for glyphosate degradation: the aminomethylphosphonic acid (AMPA) pathway and the glycine pathway (Fig. 14). The double cross-polarization experiment was

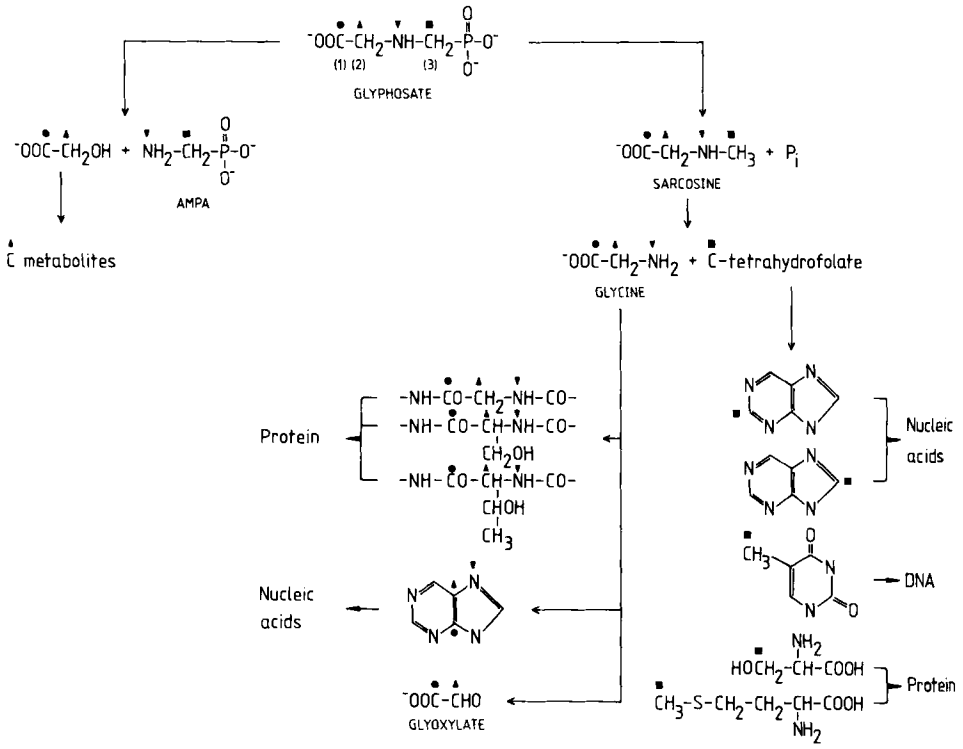


Fig. 14. Pathways for the bacterial degradation of glyphosate (**63**), showing the fate of the labelled carbon and nitrogen atoms.

able to distinguish between these pathways because the AMPA pathway breaks the nitrogen bond to carbon 2 and the glycine pathway breaks the nitrogen bond to carbon 3. In the soil *Pseudomonas* sp. PG2982,[121,122] glyphosate metabolism occurred via the glycine pathway, with the subsequent fate of the glycine depending on the nitrogen source supplied to the culture. For cells grown on ammonium, most of the glycine released from the glyphosate was incorporated intact into proteins and nucleic acids,[121,122] but for cells grown on glycine the glyphosate glycyl moiety was broken down completely.[121] The glycine pathway was also identified in the Gram-positive *Arthrobacter* sp. GLP-1,[123] whereas in *Pseudomonas* sp. strain LBr the dominant mechanism for glyphosate metabolism involved the AMPA pathway, with release of the bulk of the AMPA to the medium.[124]

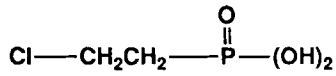
The main advantages of this approach to metabolism are the simple

sample preparation and the ease with which the labelling patterns can be interpreted. An equivalent radiolabelling experiment would be much more laborious because of the need for extraction, itself a potential source of uncertainty, followed by the difficult task of establishing the molecular location of the labels. In contrast to *in vivo* NMR (Sections 3.2.4 and 3.3), solid-state NMR signals are obtained from every component in the freeze-dried sample, and this is a particular advantage when the label accumulates in the macromolecular end products of biosynthesis without forming significant pools of low-molecular-weight precursors. The existence of the glycine pathway was deduced entirely from the labelling pattern of the nucleic acids and proteins, and, although potentially detectable, no labelled free glycine was observed. However, the lack of signals from intermediates in the pathway meant that it was not possible to decide from the NMR evidence whether the carbon–phosphorus bond in glyphosate was broken before or after the release of glycine, and the intermediate formation of sarcosine shown in Fig. 14 was established by the extraction of [3-^{14}C]sarcosine in pulse-labelling experiments with [3-^{14}C]glyphosate.[125]

3.2.4. In vivo *monitoring*

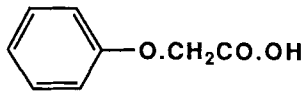
NMR is well established as a non-invasive method for studying the metabolism of living systems,[126,127] including plants.[128,129] In this approach tissues are maintained in a functional state within the detecting coil of a spectrometer and spectra are recorded from the freely mobile low-molecular-weight ions and molecules in the sample. ^{1}H, ^{14}N, ^{19}F, ^{23}Na, ^{31}P and ^{39}K in unlabelled systems and ^{13}C and ^{15}N in labelled systems are the most commonly detected isotopes of biological interest, and their usefulness *in vivo* depends on both the magnetic properties of the nucleus and the distribution of the isotope in the living system. The sensitivity of the detectable isotopes varies by several orders of magnitude, and this has an important influence on the application of the different nuclei. For example, in the case of the most popular *in vivo* nucleus, ^{31}P, the threshold for detection is a concentration of $\sim$1 mM averaged over the total volume within the detecting coil. This is sufficient for a number of important metabolites, such as glucose-6-phosphate, ATP, phosphocreatine and the ubiquitous orthophosphate, but insufficient to detect the submillimolar pools of many other important phosphorous compounds.

There are very few reports of *in vivo* NMR being used to monitor the metabolism of agrochemicals *in vivo*. In one study ^{31}P NMR was used to investigate the decomposition of the pre-harvest ripening agent ethephon (**64**) in olive leaves.[130] Spray applications of ethephon were only detectable

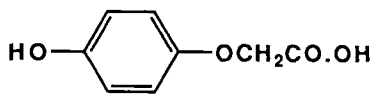


64

at concentrations >0.05 M, which is much greater than the level used for agricultural purposes, and it was necessary to use leaves from xylem-fed shoots to obtain useful *in vivo* spectra. Preliminary experiments indicated that NMR could be used to follow the absorption and hydrolysis of ethephon and to investigate the distribution of the compound between the cycloplasm and the vacuole. In a second study natural abundance ^{13}C NMR was used to investigate the metabolism of phenoxyacetic acid herbicides in carrot tissue.[131] Following vacuum infiltration with phenoxyacetic acid (**65**), spectra were recorded over a period of 18 h, and small changes in the spectrum were consistent with the formation of 4-hydroxyphenoxyacetic acid (**66**). Inadequate signal-to-noise ratio was a severe problem in this



65

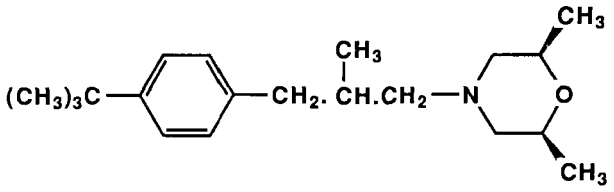


66

work and the use of ^{13}C-labelled phenoxyacetic acid or ^{1}H NMR detection of the herbicide were suggested as possible solutions to this problem.

3.3. Metabolic effects and mode of action

NMR has been used in various ways to characterize the metabolic effects of agrochemicals. In the simplest approach NMR may be used to characterize a metabolite that accumulates in a tissue exposed to the compound of interest. For example, a combination of ^{1}H NMR, IR, UV and mass spectroscopy was used to identify the accumulation of ergosta-8,14,24(28)-trien-3β-ol in *Penicillium italicum* treated with the fungicide fenpropimorph (**67**).[132] This indicated that ergosterol synthesis was blocked at



67

the step involving the reduction of the C-14(15) double bond, i.e. that fenpropimorph was an inhibitor of Δ^{14}-sterol reductase.

The interaction between an enzyme and its substrate or inhibitors can also be investigated by NMR, and a good illustration is provided by the ^{19}F NMR study of the mode of action of 3-octylthio-1,1,1-trifluoropropane-2-one, OTFP (**68**).[133] OTFP is a potent inhibitor of insect juvenile hormone esterase, and, prior to the NMR study, assays with OTFP derivatives had suggested that the inhibition was caused by the formation of a tetrahedral adduct between OTFP and a nucleophilic residue in the active site. The esterase was not available in sufficient quantity for an NMR study, and so, on the assumption that the active site would contain a serine residue, ^{19}F NMR was used to study the interaction between OTFP and the serine hydrolase enzyme acetylcholine esterase.

$CH_3(CH_2)_7SCH_2CO.CF_3$

68

$CH_3(CH_2)_7SCH_2C(OH)_2CF_3$

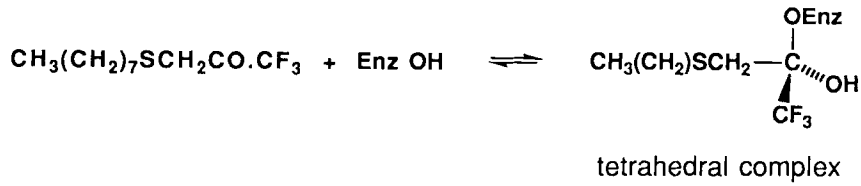
69

$CH_3(CH_2)_7SCH_2CH(OH)CF_3$

70

In chloroform solution the ^{19}F-NMR spectrum of OTFP consisted of a major peak at -0.49 ppm (relative to trifluoracetic acid) for the keto form, and a minor resonance at -10.15 ppm for the hydrate (**69**). However, in aqueous solution the hydrate form predominated. On inhibition of the enzyme by OTFP, the complex formed gave a grossly broadened peak (linewidth 66 Hz) centred at -9.26 ppm in the region for a tetrahedral or hydrated species. The broadening was consistent with formation of a protein-bound inhibitor with the rotational correlation time of the protein. To show that the effects observed were due to a specific interaction of

enzyme and inhibitor, experiments were performed with inactivated enzyme. The spectra obtained were consistent with the presence of unbound OTFP. Further, the alcohol (**70**) gave no induced fluorine shift in the presence of active enzyme. This implicated the keto form in the enzyme interaction. Thus NMR data showed that OTFP was a reversible inhibitor of the acetylcholine esterase and that it acted as a transition state analogue by forming a tetrahedral adduct in the active site as expected.

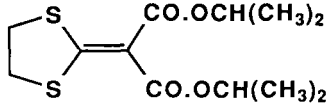


Scheme 2.

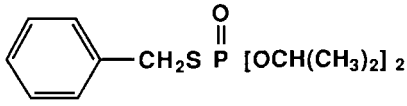
Another possibility in mode-of-action studies is to use NMR to investigate the effect of herbicides[134] and insecticides[135] on the properties of model membrane systems. ^{31}P NMR, in combination with X-ray diffraction data, indicated that phenylamide herbicides (e.g. propanil (**4**) and CIPC (**77**) (p. 193)) partitioned into the hydrocarbon region of phosphatidylcholine vesicles, causing disruption of the hydrocarbon-chain packing below the lipid phase-transition temperature.[134] ^{13}C-NMR T_1 measurements for the phosphatidylcholine resonances showed that the phenylamide alkyl-chain substituents were mainly responsible for the change in mobility of the hydrocarbon chains. Unfortunately, while this study provided interesting information on the interaction between the herbicides and the bilayer, it did not provide a physical basis for the differential metabolic effects of the phenylamide herbicides. In a similar ^{31}P NMR investigation of three organophosphorus insecticides, two compounds (chlorophos and OKh-30) were found to have no specific interaction with neutral or negatively charged liposomes while a third (GA-41) intercalated into the hydrocarbon region of the bilayer and made it permeable to a trivalent lanthanide ion above a critical concentration.[135]

Finally, *in vivo* NMR methods have also been used to observe the metabolic effects of agrochemicals.[136–138] For example, ^{13}C NMR was used to observe the effect of fungicides on the synthesis of choline from ^{13}C-labelled methionine in intact mycelia of *Pyricularia oryzae*.[136] Transmethylation caused the appearance of a signal from $\equiv\overset{\oplus}{N}-CH_3$ at the expense of the methionine methyl resonance, and analysis of extracts showed that choline, rather than phospatidylcholine, was the principal

contributor to the new resonance. Exposure to isoprothiolane (**71**) and the organophosphorus fungicide IBP (**72**) inhibited this process, showing that

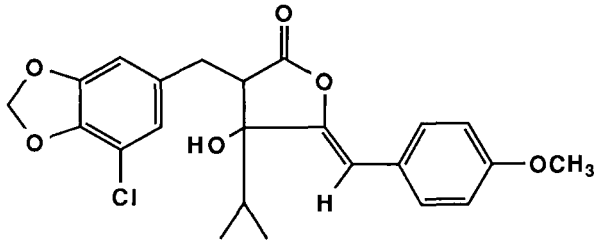


71



72

the fungicides interfered with the transmethylation step. Two ^{31}P *in vivo* NMR studies of agrochemicals have also been reported.[137,138] In the first study ^{31}P NMR was used to monitor the cytoplasmic pH in cells of the unicellular cyanobacterium *Synechococcus* sp. during treatment with the natural herbicide cyanobacterin (**73**).[173] The slow decline in the cytoplasmic

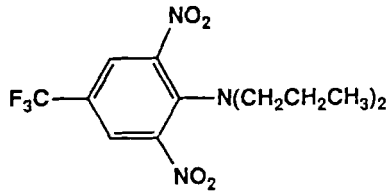


73

pH indicated that the compound affected the proton pumping mechanism in photosystem II. In the second study ^{31}P NMR was used to observe the effects of chlorophenols on the transmembrane pH gradient and nucleotide pools in a *Flavobacterium* sp. that degraded some, but not all, chlorinated phenols. Experiments with pentachlorophenol, which was degraded, and 2,4,5-trichlorophenol, which was not, suggested that the chlorophenols that were not degraded were resistant because they acted as proton dissipators.[138] These three *in vivo* NMR studies illustrated the potential of the method for obtaining metabolic information non-invasively, and with the rapid development of the *in vivo* technique in recent years further work of this kind can be anticipated.

4. MISCELLANEOUS APPLICATIONS

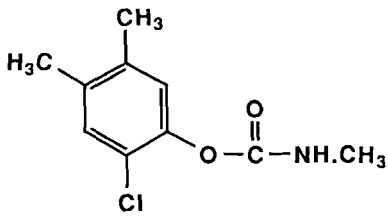
The possibility of using ^{19}F NMR in the determination of pesticide residues in food has been considered.[147] Rapid sample analysis with minimal sample clean-up were viewed as major advantages over other chromatographic techniques. Trifluralin (**74**), a pre-emergence herbicide, was easily mon-



74

itored down to a concentration of 0.1 ppm (at 75 MHz; ^{19}F). Spectra obtained from concentrated crop extracts showed the technique to be particularly attractive for relatively oil-free crops, but samples containing an appreciable amount of oil could not be concentrated to the same degree and data acquisition time became unacceptable. However, at higher field strength, with increased sensitivity, this problem should become less noticeable.

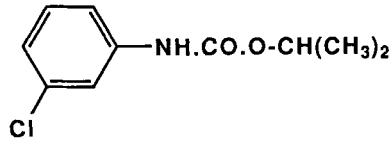
Detection of some organochlorine pesticides in water at low concentration has been achieved by application of nuclear double resonance (NDR) spectroscopy.[148] The technique involved monitoring the effects of cross-relaxation between proton and chlorine nuclei, and measurements were made for aqueous solutions of carbanolate (**75**), barban (**76**), CIPC (chlorpropham (**77**)), atrazine (**78**) and simazine (**79**), after extraction into



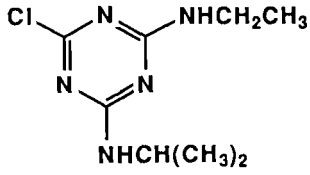
75



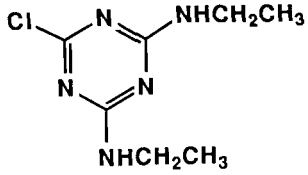
76



77



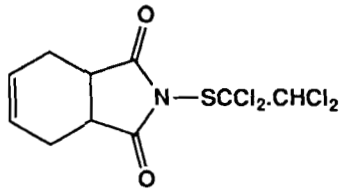
78



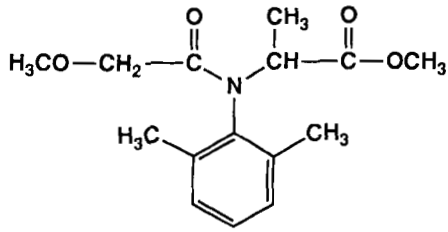
79

either chloroform or bromoform. The sensitivity of the technique was less than for electron-capture gas chromatography. However, as NDR measurements were made at $-20^{\circ}C$, heat-sensitive compounds, requiring derivatization for gas-chromatographic analysis, could be dealt with directly. Moreover, fats and oils in extracts did not cause interference.

^{1}H NMR in combination with mass spectrometry successfully identified captafol (**80**) as an impurity in specimens of a commercial formulation of metalaxyl (**81**).[149] Consequently, high genetic activity on diploid *Aspergillus nidulans* given by the metalaxyl specimens was shown to be due to the presence of captafol.

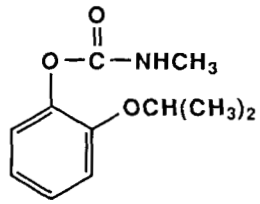


80



81

^{1}H NMR has proved a convenient technique for assay of the insecticide propoxur (**82**) in pesticide formulations.[150] The method uses methanol as an internal standard, and was devised as a rapid alternative to gas chromatographic methods where lengthy sample-derivatization is required to prevent thermal breakdown during analysis.



82

^{31}P NMR is a powerful technique for analysis of organophosphorus pesticides. High sensitivity, possible with modern instrumentation, and wide chemical-shift dispersion permit the identification of many minor components in the presence of a main active ingredient. Quantitative aspects, important for control of manufacturing processes, estimation of toxic contaminants and certification of analytical standards, have been discussed recently.[151,152] Due account must be taken of relaxation and NOE effects in order to validate the analytical methods.

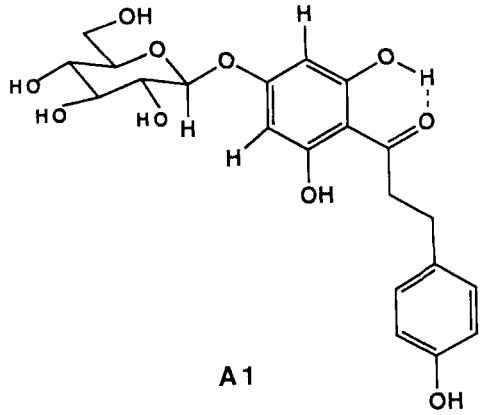
A ^{1}H NMR method for the screening of potential insecticides as inhibitors of cholinesterase has been described.[153] The principle of the

method is based on the determination of the initial rate of hydrolysis of acetylcholine by horse serum pseudocholinesterase. From measurements made with and without insecticide, a constant for inhibition was calculated.

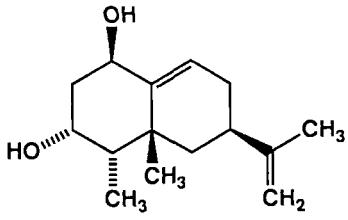
Both ^{13}C and ^{1}H NMR chemical shifts have been used in a quantitative structure–activity relationship (QSAR) study of benzotriazole derivatives active as plant growth regulators.[154] Chemical-shift data were obtained for the substituent carbon (and attached proton) connected to the nitrogen of both 1- and 2-substituted benzotriazole derivatives. Data from both isomer groups, including data for lipophilic character, could be successfully combined in a single correlation with biological activity, when carbon chemical shift was also included as a parameter. In previous work[155] dummy parameters had been required to take separate account of electronic and steric effects. This shows that an ensemble of molecular characteristics can be represented by a single parameter and demonstrates the value of NMR chemical shift as a parameter in QSAR investigations.

APPENDIX

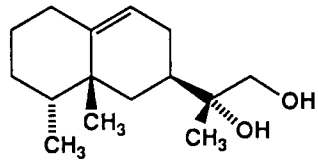
Molecular structures of compounds referred to in Tables 6 and 7



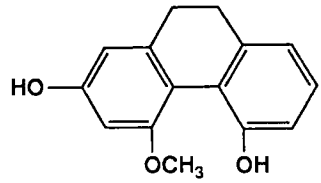
A1



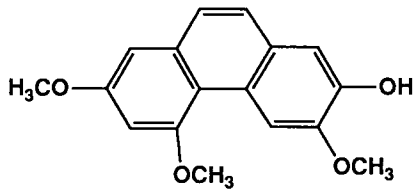
A2


OH
CH3
CH3
CH3
OH

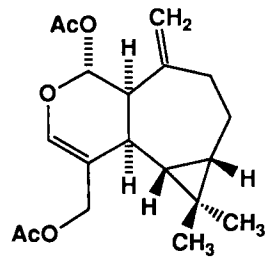
A3


HO
OCH3
OH

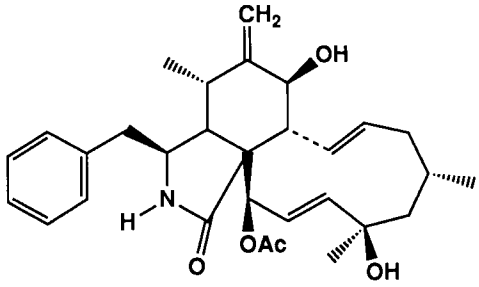
A4


H3CO
OH
OCH3
OCH3

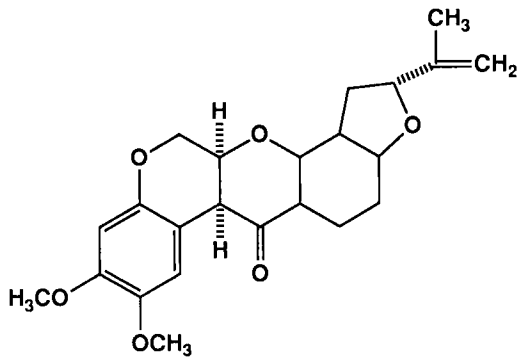
A5


AcO
CH2
H
O
H
H
H
CH3
CH3
AcO

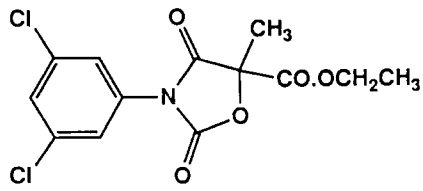
A6


CH2
OH
N
H
O
OAc
OH

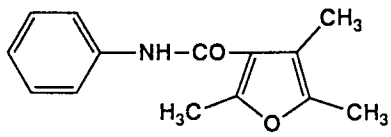
A7


CH3
CH2
H
O
O
O
H
H
O
H3CO
OCH3

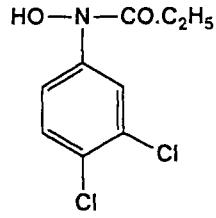
A8


Cl
O
CH3
CO.OCH2CH3
N
O
Cl
O

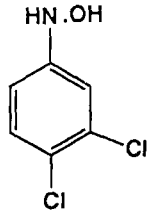
A9


CH3
NH–CO
H3C
O
CH3

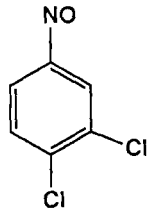
A10



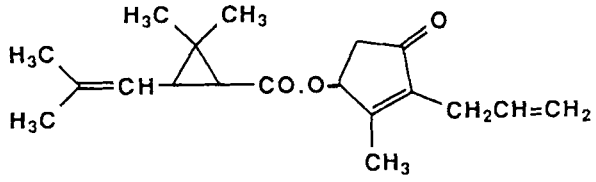
A11



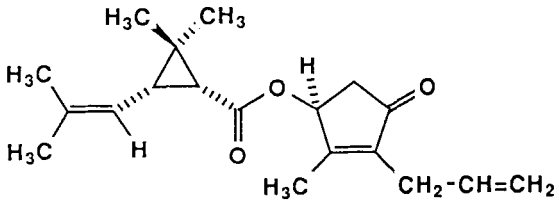
A12



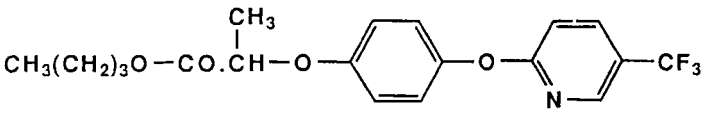
A13



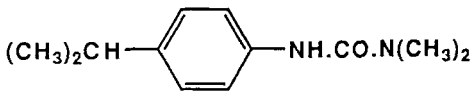
A14



A15



A16



A17

REFERENCES

1. R. Haque and D.R. Buhler, in *Annual Reports on NMR Spectroscopy*, Vol. 4 (ed. E.F. Mooney), p. 237. Academic Press, London, 1971.
2. N. Cyr, T. Cyr and R. Haque, *Anal. Methods Pestic. Plant Growth Regulator*, 1977, **9**, 51.
3. N.K. Wilson, in *Pesticide Analysis* (ed. K.G. Das), p. 263. Marcel Dekker, New York, 1981.
4. P.J. Moore, Private communication.
5. W. Bremser, *Angew. Chem. Int. Ed. Engl.*, 1988, **27**, 247.
6. R.W. Bally, D. van Krimpen, P. Cleij and H.A. van't Klooster, *Anal. Chim. Acta*, 1984, **157**, 227.
7. S.-i. Sasaki, T. Yamasaki, K. Tanaka and H. Abe, in *Computer Supported Spectroscopic Databases* (ed. J. Zupan), p. 133. Ellis Horwood, Chichester, 1986.
8. S.R. Heller, G.W.A. Milne and R.J. Feldmann, *Science*, 1973, **195**, 253.
9. C.J. Turner, *Prog. Nucl. Magn. Reson. Spectrosc.*, 1984, **16**, 311.
10. A.E. Derome, *Modern NMR Techniques for Chemical Research*. Pergamon Press, Oxford, 1987.
11. J.K.M. Sanders and B.K. Hunter, *Modern NMR Spectroscopy: A Guide for Chemists*. Oxford University Press, Oxford, 1987.
12. *Pulse Methods in 1D and 2D Liquid Phase NMR*. (ed. W.S. Brey). Academic Press, London, 1988.
13. D. Neuhaus and M.P. Williamson, *The Nuclear Overhauser Effect in Structural and Conformational Analysis*. VCH Publishers, New York, 1989.
14. I.D. Campbell, C.M. Dobson, R.G. Ratcliffe and R.J.P. Williams, *J. Magn. Reson.*, 1978, **29**, 397.

15. D.J. Rabenstein, S. Fan and T.T. Nakashima, *J. Magn. Reson.*, 1985, **64**, 541.
16. D.T. Pegg, D.M. Doddrell and M.R. Bendall, *J. Chem. Phys.*, 1982, **77**, 2745.
17. D.M. Doddrell, D.T. Pegg and M.R. Bendall, *J. Magn. Reson.*, 1982, **48**, 323.
18. O.W. Sørensen and H.J. Jakobsen, Polarization transfer and editing techniques, Chap. 3 in Ref. 12.
19. W.P. Aue, J. Karhan and R.R. Ernst, *J. Chem. Phys.*, 1976, **65**, 4226.
20. W.P. Aue, E. Bartholdi and R.R. Ernst, *J. Chem. Phys.*, 1976, **64**, 2229.
21. K. Nagayama, A. Kumar, K. Wüthrich and R.R. Ernst, *J. Magn. Reson.*, 1980, **40**, 321.
22. A. Bax and R. Freeman, *J. Magn. Reson.*, 1981, **44**, 542.
23. G. Eich, G. Bodenhausen and R.R. Ernst, *J. Am. Chem. Soc.*, 1982, **104**, 3731.
24. G. Wagner, *J. Magn. Reson.*, 1983, **55**, 151.
25. D.G. Davis and A. Bax, *J. Magn. Reson.*, 1985, **64**, 533.
26. A. Bax and G.A. Morris, *J. Magn. Reson.*, 1981, **42**, 501.
27. V. Rutar, *J. Magn. Reson.*, 1984, **58**, 306.
28. M.R. Bendall and D.T. Pegg, *J. Magn. Reson.*, 1983, **53**, 144.
29. W.F. Reynolds, D.W. Hughs, M. Perpick-Dumont and R.G. Enriquez, *J. Magn. Reson.*, 1985, **64**, 304.
30. G. Bodenhausen and R. Freeman, *J. Magn. Reson.*, 1977, **28**, 471.
31. G. Bodenhausen and R. Freeman, *J. Am. Chem. Soc.*, 1978, **100**, 320.
32. H. Bleich, S. Gould, P. Pitner and J. Wilde, *J. Magn. Reson.*, 1984, **56**, 515.
33. A.L. Waterhouse, I. Holden and J.E. Casida, *J. Chem. Soc. Perkin Trans. 2*, 1985, 1011.
34. A. Bax and R. Freeman, *J. Am. Chem. Soc.*, 1982, **104**, 1099.
35. H. Kessler, C. Griesinger, J. Zarbock and H.R. Loosli, *J. Magn. Reson.*, 1984, **57**, 331.
36. R. Haque, W.R. Coshow and L.F. Johnson, *J. Am. Chem. Soc.*, 1969, **91**, 3822.
37. J.H. Ross and R.I. Krieger, *J. Agric. Food Chem.*, 1980, **28**, 1026.
38. G.F. Nicollier, P.A. Hedin and F.M. Davis, *J. Agric. Food Chem.*, 1982, **30**, 1133.
39. A.A.S. Bright, NMR and agrochemicals. Poster presented at the 7th International Meeting on NMR, Cambridge, 1985; otherwise unpublished.
40. P.J. Brooker, J.H. Parsons, J. Reid and P.J. West, *Pestic. Sci.*, 1987, **18**, 179.
41. J.O. Ley, F.E. Evans and J.A. Hinson, *Biomed. Environ. Mass Spectrom.*, 1986, **13**, 495.
42. G.H. Lee, *J. Agric. Food Chem.*, 1985, **33**, 499.
43. W.M. Draper and J.E. Casida, *J. Agric. Food Chem.*, 1983, **31**, 1201.
44. V.V. Krishnamurthy and J.E. Casida, *Magn. Reson. Chem.*, 1987, **25**, 837.
45. M. Elliott and N.F. Janes, *Chem. Soc. Rev. (Lond.)*, 1978, **7**, 473.
46. M.J. Bull, J.H. Davies, R.J.G. Searle and A.C. Henry, *Pestic. Sci.*, 1980, **11**, 249.
47. G.E. Hawkes, K. Herwig and J.D. Roberts, *J. Org. Chem.*, 1974, **39**, 1017.
48. M. Elliot, A.W. Farnham, N.F. Janes and B.P.S. Khambay, *Pestic. Sci.*, 1988, **22**, 231.
49. T. Ando and J.E. Casida, *J. Agric. Food Chem.*, 1983, **31**, 151.
50. R. Rossi, A. Carpita, M. Quirici and C.A. Veracini, *Tetrahedron*, 1982, **38**, 639.
51. Y. Iida and R. Sugawara, *Agric. Biol. Chem.*, 1981, **45**, 1553.
52. P.E. Sonnet, T.P. McGovern and R.T. Cunningham, *J. Org. Chem.*, 1984, **49**, 4639.
53. T.L. Hough, I.R. Hough and R.W. Pannell, *J. Heterocyclic Chem.*, 1986, **23**, 1125.
54. A.J. Whiffen, *J. Bacteriol.*, 1948, **56**, 283.
55. F. Johnson, N.A. Starkovsky and W.D. Gurowitz, *J. Am. Chem. Soc.*, 1965, **87**, 3492.
56. J. Sayers, D. Schindler and M. Sundaralingam, *J. Am. Chem. Soc.*, 1977, **99**, 3848.
57. M. Iwata, H. Iwamatsu, S. Zushi, K. Tachibana and T. Watanabe, *Meiji Seika Kenkyu Nenpo*, 1985, **24**, 38.
58. S. Kudo, T. Oritani and K. Yamashita, *Agric. Biol. Chem.*, 1984, **48**, 2315.
59. H. Kondo, T. Oritani and K. Yamashita, *Agric. Biol. Chem.*, 1988, **52**, 129.
60. P.W. Jeffs and D. McWilliams, *J. Am. Chem. Soc.*, 1981, **103**, 6185.

61. G.R. Sullivan, in *Topics in Stereochemistry*, Vol. 10 (ed. E.L. Eliel and N.L. Allinger), p. 287. Wiley, New Jersey, 1978.
62. R. Allahyari, J.G. Hollingshaus, R.L. Lapp, E. Timm, R.A. Jacobson and T.R. Kukuto, *J. Agric. Food Chem.*, 1980, **28**, 594.
63. H. Leader and J.E. Casida, *J. Agric. Food Chem.*, 1982, **30**, 546.
64. A. Hirashima, H. Leader, I. Holden and J.E. Casida, *J. Agric. Food Chem.*, 1984, **32**, 1302.
65. T.M. Ward, I.L. Allcox and G.H. Wahl, *Tetrahedron Lett.*, 1971, 4421.
66. B.K. Eya and T.R. Fukuto, *J. Agric. Food Chem.*, 1985, **33**, 884.
67. A. Hatzis and R. Rothchild, *Appl. Spectrosc.*, 1986, **40**, 743.
68. B. Sugavanam, *Pestic. Sci.*, 1984, **15**, 296.
69. M. Elliott, A.W. Farnham, N.F. Janes, D.M. Johnson and D.A. Pulman, *Pestic. Sci.*, 1980, **11**, 513.
70. Y. Tsuda, K.-I. Kawai and S. Nakajima, *Chem. Pharm. Bull.*, 1985, **33**, 1955.
71. J. Dale and H.S. Mosher, *J. Am. Chem. Soc.*, 1973, **95**, 512.
72. N.H. Anderson, S.K. Branch, R.S.T. Loeffler, B.E. Mann, I.W. Newell and P.E. Walker, *Pestic. Sci.*, 1984, **15**, 310.
73. L.M. Jackson and S. Sternhell, *Applications of Nuclear Magnetic Resonance Spectroscopy in Organic Chemistry*, 2nd edn, pp. 292–298. Pergamon Press, Oxford, 1962.
74. W.G. Taylor and T.T. Nakashima, *Can. J. Chem.*, 1984, **62**, 96.
75. Z.H-Kovács, *Hung. J. Ind. Chem.*, 1987, **15**, 219.
76. S. Tanaka, T. Kato, S. Yamamoto, H. Yoshioka, Z. Taira and W.H. Watson, *Agric. Biol. Chem.*, 1978, **42**, 287.
77. S. Forsén and R.A. Hoffman, *J. Chem. Phys.*, 1963, **39**, 2892; *Ibid.*, 1964, **40**, 1189.
78. S. Forsén and R.A. Hoffman, *Prog. Nucl. Magn. Reson. Spectrosc.*, 1966, **1**, 173.
79. A.A.S. Bright, A study of molecular motion by saturation population transfer and 2D–NMR. Poster presented at the 8th International Meeting on NMR, Canterbury, 1987; otherwise unpublished.
80. J.S. McLaren, *Pestic. Sci.*, 1986, **17**, 559.
81. First International Neem Conference, Rottach-Egern, Germany, 1980; Second International Neem Conference, Giessen, Germany, 1983; Third International Neem Conference, Nairobi, Kenya, 1986.
82. C.J. Turner, M.S. Tempesta, R.B. Taylor, M.G. Zagorski, J.S. Termini, D.R. Schroeder, and K. Nakanishi, *Tetrahedron*, 1987, **43**, 2789.
83. W. Kraus, M. Bokel, A Bruhn, R. Cramer, I. Klaiber, A. Klenk, G. Nagl, H. Pöhnl, H. Sadlo and B. Vogler, *Tetrahedron*, 1987, **43**, 2817.
84. J.N. Bilton, H.B. Broughton, P.S. Jones, S.V. Ley, Z. Lidert, E.D. Morgan, H.S. Rzepa, R.N. Sheppard, A.M.Z. Slawin and D.J. Williams, *Tetrahedron*, 1987, **43**, 2805.
85. D.A.H. Taylor, *Tetrahedron*, 1987, **43**, 2779.
86. P.R. Zanno, I. Miura, K. Nakanishi and D.L. Elder, *J. Am. Chem. Soc.*, 1975, **97**, 1975.
87. W. Kraus, M. Bokel, A. Klenk and H. Pöhnl, *Tetrahedron Lett.*, 1985, **26**, 6435.
88. H.B. Broughton, S.V. Ley, A.M.Z. Slawin, D.J. Williams and E.D. Morgan, *J. Chem. Soc. Chem. Commun.*, 1986, 46.
89. K. Kubo, T. Matsumoto and J.N. Shoolery, *Tetrahedron Lett.*, 1984, **25**, 4729.
90. A. Klenk, M. Bokel and W. Kraus, *J. Chem. Soc. Chem. Commun.*, 1986, 523.
91. S.M. Lee, J.A. Klocke and M.F. Balandrin, *Tetrahedron Lett.*, 1987, **28**, 3543.
92. J.E. Casida, in *Natural Products for Innovative Pest Management* (ed. D.L. Whitehead and W.S. Bowers), p. 109. Pergamon Press, Oxford, 1983.
93. J.P. Girault and R. Lafont, *J. Insect Physiol.*, 1988, **34**, 701.
94. I. Kubo, A. Matsumoto and F.J. Hanke, *Agric. Biol. Chem.*, 1985, **49**, 243.

95. I. Kubo, T. Matsumoto and J.A. Klocke, *J. Chem. Ecol.*, 1984, **310**, 547.
96. I. Kubo, J.A. Klocke, I. Granjian, N. Ichikawa and T. Matsumoto, *J. Chromatogr.*, 1983, **257**, 157.
97. I. Kubo, A. Matsumoto and J.F. Ayafor, *Agric. Biol. Chem.*, 1984, **48**, 1683.
98. K. Nakanishi, *Chemistry of Natural Products: Proceedings of the Sino-American Symposium 1982*, p. 9. Science Press, Beijing, People's Republic of China.
99. I. Kubo and A. Matsumoto, *Chem. Pharm. Bull.*, 1985, **33**, 3817.
100. H. Naganawa, T. Takita, A. Suzuki, S. Tamura, S. Lee and N. Izumiya, *Agric. Biol. Chem.*, 1976, **40**, 2223.
101. G.I. Birnbaum, A. Stoessl, S.H. Grover and J.B. Stothers, *Can. J. Chem.*, 1974, **52**, 993.
102. D.G. Watson, D.S. Rycroft, I.M. Freer and C.J.W. Brooks, *Phytochemistry*, 1985, **24**, 2195.
103. I.M. Whitehead, D.F. Ewing, and D.R. Threlfall, *Phytochemistry*, 1988, **27**, 1365.
104. D.T. Coxon, S.K. Ogundana and C. Dennis, *Phytochemistry*, 1982, **21**, 1389.
105. A. Matsuo, K. Atsumi, K. Nadaya, M. Nakayama and S. Hayashi, *Phytochemistry*, 1981, **20**, 1065.
106. R.H. Cox, P. Morris, H.G. Cutler, R.E. Hurd and R.J. Cole, *J. Agric. Food Chem.*, 1983, **31**, 405.
107. A. Pusino, C. Gessa and H. Kozlowski, *Pestic. Sci.*, 1988, **24**, 1.
108. P. Dureja, S. Walia, and S.K. Mukerjee, *Pestic. Sci.*, 1988, **22**, 287.
109. D.J. Arnold, C.R. Leake and L. Somerville, *Proceedings of the British Crop Protection Conference on Pests and Diseases, Brighton 1986*, p. 851.
110. V.V. Krishnamurthy, J.E. Casida and L.O. Ruzo, *J. Agric. Food Chem.*, 1987, **35**, 504.
111. M.L. Tosato and D. Cesareo, *Anm. Ist. Super. Sanità*, 1984, **19**, 649.
112. J.D. Bell, J.C.C. Brown and P.J. Sadler, *Chem. Brit.*, 1988, **24**, 1021.
113. A.R. Jacobson and J.T. Gerig, *Chem. Res. Toxicol.*, 1988, **1**, 304.
114. D.R. Dohn, M.J. Graziano and J.E. Casida, *Biochem. Pharmacol.*, 1988, **37**, 3485.
115. V.V. Krishnamurthy, J.E. Casida and D.R. Dohn, *Magn. Reson. Chem.*, 1988, **26**, 542.
116. C.T. Bedford, A.E. Crane and R.K. Harrod, *Pestic, Sci.*, 1986, **17**, 659.
117. C.T. Bedford, A.E. Crane, E.H. Smith and N.R. Wellard, *Pestic. Sci.*, 1986, **17**, 33.
118. N. Mikami, N. Wakabayashi, H. Yamada and J. Mijamoto, *Pestic. Sci.*, 1985, **16**, 46.
119. E.A. Curl, P.J. Edwards, C. Elliott and J.P. Leakey, *Pestic. Sci.*, 1987, **20**, 207.
120. J. Klinowski and J.M. Thomas, *Endeavour*, 1986, **10**, 2.
121. G.S. Jacob, J. Schaefer, E.O. Stejskal and R.A. McKay, *J. Biol. Chem.*, 1985, **260**, 5899.
122. G.S. Jacob, J.R. Garbow, J. Schaefer and G.M. Kishore, *J. Biol. Chem.*, 1987, **262**, 1552.
123. R. Pipke, N. Amrhein, G.S. Jacob, J. Schaefer and G.M. Kishore, *Eur. J. Biochem.*, 1987, **165**, 267.
124. G.S. Jacob, J.R. Garbour, L.E. Hallas, N.M. Kimack, G.M. Kishore and J. Schaefer, *Appl. Environ. Microbiol.*, 1988, **54**, 2953.
125. D.L. Shinabarger and H.D. Braymer, *J. Bacteriol.*, 1986, **168**, 702.
126. D.G. Gadian, *Nuclear Magnetic Resonance and its Applications to Living Systems*. Clarendon Press, Oxford, 1982.
127. P.G. Morris, in *Annual Reports on NMR Spectroscopy*, Vol. 20 (ed. G.A. Webb), p. 1. Academic Press, London, 1988.
128. B.C. Loughman and R.G. Ratcliffe, *Adv. Plant Nutrition*, 1984, **1**, 241.
129. R.G. Ratcliffe, *Meth. Enzymol.*, 1987, **148**, 683.
130. G.A. Lang and G.C. Martin, *J. Am. Hort. Sci.*, 1986, **111**, 577.
131. B.C. Loughman, A.K. East, J.C. Maynard and T.E. Southon, in *Conjugated Plant Hormones: Structure, Metabolism and Function* (ed. K. Schreiber, H.R. Schutte and G. Sembnder), p. 376. VEB Kongress und Werbedruck, Oberlungwitz, East Germany, 1987.

132. A. Kerkenaar, J.M. van Rossum, G.G. Versluis and J.W. Marsman, *Pestic. Sci.*, 1984, **15**, 177.
133. R.J. Linderman, J. Leazer, R.M. Roe, K. Venkatesh, B.S. Selinsky and R.E. London, *Pestic. Biochem. Physiol.*, 1988, **31**, 187.
134. M.A. Stidham, J.N. Siedow, T.J. McIntosh, N.A. Porter and D.E. Moreland, *Biochim, Biophys. Acta*, 1985, **812**, 721.
135. I.I. Adrashitova, T.F. Aripov, F.G. Kamaev, B.A. Salakhutdinov and A.A. Abduvakhabov, *Khim. Prir. Soedin.*, 1988, 107.
136. M. Yoshida, S. Moriya and Y. Uesugi, *J. Pestic, Sci.*, 1984, **9**, 703.
137. W.J. Thoma and F.K. Gleason, *Biochemistry*, 1987, **26**, 2510.
138. J.G. Steiert, W.J. Thoma, K. Ugurbil and R.L. Crawford, *J. Bacteriol.*, 1988, **170**, 4954.
139. S.L. Abidi and M.S. Abidi, *J. Heterocyclic Chem.*, 1983, **20**, 1687.
140. R. Nunlist and J. Ralph, *J. Heterocyclic Chem.*, 1988, **25**, 351.
141. F.M. Pirisi, M. Meloni, P. Cabras, M.R. Bionducci and A. Serra, *Pestic. Sci.*, 1986, **17**, 109.
142. L.O. Ruzo, J.E. Casida and I. Holden, *J. Chem. Soc. Chem. Commun.*, 1985, 1642.
143. L.O. Ruzo, J.E. Casida, and I. Holden, *J. Agric. Food Chem.*, 1985, **33**, 622.
144. T. Ando, L.O. Ruzo, J.L. Engel and J.E. Casida, *J. Agric. Food Chem.*, 1983, **31**, 250.
145. A. Frigerio, A. Pusino and C. Gessa, *Pestic. Sci.*, 1987, **21**, 175.
146. G. Kulshrestha and S.K. Murkerjee, *Pestic. Sci.*, 1986, **17**, 489.
147. E.P. Mazzola, A.P. Borsetti, S.W. Page and D.W. Bristol *J. Agric. Food Chem.*, 1984, **32**, 1102.
148. R. Osredkar and P.K. Kadaba, *Bull. Environ. Contam. Toxicol.*, 1982, **28**, 513.
149. B.N. Ziogas and S.G. Georgopoulos, *Pestic. Sci.*, 1987, **20**, 193.
150. J.H. Lesser, S.I. Kreps and E. Friedman, *J. Assoc. Off. Anal. Chem.*, 1985, **68**, 565.
151. R.S. Wayne, G.W. Stockton and L.A. Wilson, Proceedings of International Congress on Pesticide Chemistry (ed. J. Miyamoto and P.C. Kearney)—*Pestic. Chem.*, 1983, **4**, 381.
152. R. Greenhalgh, B.A. Blackwell, C.M. Preston and W.J. Murray, *J. Agric. Food Chem.*, 1983, **31**, 710.
153. N. Rozani, D. Guillochon, C. Lange and J.J. Basselier, *Eur. J. Med. Chem. Chim. Ther.*, 1976, **11**, 310.
154. F. Sparatore, G. Caliendo, M.I. la Rotonda, E. Novellino, C. Silipo and A. Vittoria, *Quant. Struct.–Act. Relat.*, 1988, **7**, 178.
155. E. Sparatore, M.I. la Rotonde, G. Caliendo, E. Novellino, C. Silipo and A. Vittoria, *Il Farmaco Ed. Sci.*, 1988, **43**, 141.

NMR Nuclear Shielding and the Electronic Structures of Macromolecules

I. ANDO, T. YAMANOBE and H. KUROSU

Department of Polymer Chemistry, Tokyo Institute of Technology, Ookayama, Meguro-ku, Tokyo, Japan

G.A. WEBB

Department of Chemistry, University of Surrey, Guildford, Surrey, United Kingdom

1. Introduction 205
2. Theoretical aspects of nuclear shielding in macromolecules . . 206
3. Interpretations of nuclear shielding in terms of electronic structures . 210
   3.1. Nuclear shielding and intrachain interaction 210
   3.2. Nuclear shielding and configuration 212
   3.3. Nuclear shielding and interchain interaction 226
4. Conclusions 246
   References 246

1. INTRODUCTION

High-resolution NMR spectroscopy, combined with quantum chemistry, is able to provide detailed information on the electronic and stereochemical structures of macromolecules.[1] Accounts appear annually of NMR studies on synthetic macromolecules, natural macromolecules and high-resolution solid-state NMR data.[2] The large number of reviews and reports relating to high-resolution NMR studies on macromolecules is also detailed on an annual basis.[2] The main thrust of the present account is to attempt to relate the high-resolution nuclear magnetic shielding data of macromolecules to their electronic structures with the assistance of this approach. This *modus operandi* has been demonstrated previously[1] and requires no further explanation.

Quantum-chemical calculations produce values for all nine of the components of the nuclear shielding tensor. For molecules having preferred

ANNUAL REPORTS ON NMR SPECTROSCOPY
VOLUME 22 ISBN 0-12-505322-3

Copyright © 1989 Academic Press Limited
All rights of reproduction in any form reserved

orientations it is possible to experimentally determine all of these components individually. Clearly, a situation of this kind provides a more extensive opportunity to compare theory and experiment than do those cases where only the isotropic chemical shift and/or the shielding anisotropy are available.[3] However, the majority of NMR experiments on macromolecules only produce isotropic data[4]—thus the present account deals mainly with this situation and little mention is made of the individual components of the nuclear shielding tensor. In both the solid and solution states macromolecules may exist as mixtures of large numbers of conformers of comparable energies. Thus, in principle, the NMR spectra of macromolecules are rather complicated. The spectrum obtained may represent the superposition of the spectra of the various conformers, if molecular motion is slow on the NMR timescale. Low temperatures may help to achieve this situation. In contrast, rapid molecular motion can give rise to an NMR spectrum that is the weighted average of the spectra of the conformers present. Low-viscosity solvents and high temperatures are conducive to promoting this aim. In either of these extreme cases it is often possible to identify individual NMR signals and thus to obtain relevant shielding data from the spectra. Comparison of these with nuclear shieldings, produced by quantum-chemical calculations, permits some insight into the electronic structures of the macromolecules under investigation.

2. THEORETICAL ASPECTS OF NUCLEAR SHIELDING IN MACROMOLECULES

Details of the "atom in a molecule" approach to nuclear shielding calculations, and the various other approximations frequently encountered, have been covered in recent reviews of shielding calculations.[5-7] In general, calculations on small molecules using *ab initio* molecular orbital (MO) procedures can provide very satisfactory estimates of nuclear shielding. For larger monomeric species, semi-empirical molecular orbital calculations of various types are still the workhorse. In many cases very acceptable results are obtained. Progress in nuclear shielding calculations is reported annually.[2]

It has to be recognized that the results of molecular orbital calculations on monomeric species are not readily transferable to polymers on account of differences in electronic structure. Thus it becomes necessary to consider the basis of molecular orbital calculations on polymers. Since electrons are constrained to a finite region of space in small molecules, whereas this is not necessarily the case for polymers, some additional approximations are required. Periodic systems have the advantage of translational symmetry

when compared with aperiodic ones. It is possible to exploit this symmetry in order to reduce to reasonable proportions the formidable task of computing the electronic states of an extended system. From the point of view of calculating nuclear shielding, the tight-binding (TB) model of macromolecular electronic structure has been reasonably successful. One consequence of employing this model is that the electronic eigenfunctions, which are real for small finite molecules, now become complex. This point is illustrated by the presence of $i = (-1)^{1/2}$ in (1) below. In the present discussion the TB molecular orbital model is employed to describe the electronic structures of linear periodic polymers within the framework of a "linear combination of atomic orbitals" approximation for the electronic eigenfunctions.[8-11] By means of Bloch's theory,[12] the eigenfunction $\Psi_n(k)$ for an electron at position r, belonging to the nth crystal orbital is given by

$$\Psi_n(k) = N^{-1/2} \sum_{j=-(N-1)/2}^{(N-1)/2} \sum_{\nu=1}^{s} e^{ikjb} C_{\nu n}(k) \phi_\nu(r - jb), \tag{1}$$

where k is the eigenfunction number, ν is an orbital index for the jth cell, s is the total number of atomic orbitals in a given cell, N is the total number of cells considered and b is the unit vector of translational symmetry. In (1) $\phi_\nu(r - jb)$ represents the νth atomic orbital in the jth cell and $C_{\nu n}(k)$ its expansion coefficient in the linear combination of atomic orbitals. The limits of k, within a given Brillouin zone, are $-\frac{1}{2}\pi$ and $\frac{1}{2}\pi$. Using (1), the total electronic energy E of the polymer can be expressed as

$$E = \int_{-\pi/b}^{\pi/b} \sum_{n}^{\text{occ}} \langle \Psi_n(k) | H | \Psi_n(k) \rangle \, dk, \tag{2}$$

where $\Psi_n(k)$ is the Slater determinant composed of $\phi_n(k)$. H is the Hamiltonian, consisting of the kinetic energy, the potential energy of the electronic field of the polymer, and the electron repulsion energy. By solving (2), the expansion coefficients in (1) can be obtained. The advantage of (1) is that calculation of the electronic structure of an infinite polymer can be reduced to the calculation for a unit cell (monomer unit) interacting with all other unit cells, using the periodicity of the polymer. The formulation for the calculation of the electronic structure of the polymer has been considered within the CNDO/2 framework. The diagonal and off-diagonal elements of the Fock matrix, $F_{\mu\mu}(k)$ and $F_{\mu\mu'}(k)$, respectively, are expressed as follows:

$$F_{\mu\mu}(k) = -\tfrac{1}{2}(I_\mu + A_\mu) + \tfrac{1}{2}(1 - P_{\mu\mu})\gamma_{AA}^{00} + \sum_{B} \sum_{j=-M}^{M} (P_B - Z_B)\gamma_{AB}^{0j}$$

$$+ 2K_\pi \beta_A \sum_{j=1}^{M} S_{\mu\mu}^{0j} \cos kj - \sum_{j=1}^{M} \gamma_{AA}^{0j} P_{\mu\mu}^{-jR} \cos kj, \tag{3}$$

$$F_{\mu\mu'}(k) = \tfrac{1}{2} K_\pi(\beta_A + \beta_B) \sum_{j=-M}^{M} S_{\mu\mu'}^{0j} \, e^{ikj}$$
$$- \tfrac{1}{2} \sum_{j=-M}^{M} P_{\mu'\mu}^{-jR} \, \gamma_{AB}^{0j} \, e^{ikj}, \tag{4}$$

where I_μ and A_μ are the ionization potential energy and electron affinity respectively, γ_{AB} represents the Coulomb repulsion integral between the atomic orbital μ on atom A in the original cell and the atomic orbital μ' on atom B in the jth cell. This integral may be calculated using $1s$ or $2s$ orbitals even if the orbital concerned is a $2p$ orbital. $S_{\mu\mu'}(k)$ is the overlap integral between the μth atomic orbital in the original cell and the μ'th atomic orbital in the jth cell. $P_{\mu\mu'}$ is the bond order matrix, P_B the electron density on atom B and $P_{\mu'\mu}^{-jR}$ the bond order matrix between the μth atomic orbital in the original cell and the μ'th atomic orbital in the $\pm j$th cell, and Z_B is the core charge of atom B. K_π is a correction factor for the $\pi-\pi$ electron interaction,[12] here we take $K_\pi = 0.85$. β_A is the bonding parameter for atom A.

To calculate the shielding for the various nuclei in a given macromolecule, it is necessary to obtain values for the expansion coefficients $C_{\nu n}(k)$ in (1) and for the energies $E_n(k)$ of the crystal orbitals. These are obtainable by means of the variation procedure, as in more familiar molecular orbital calculations.[13-17] In principle, any level of molecular orbital approximation can be used to evaluate these terms. In practice, only semi-empirical methods have been used in nuclear shielding calculations to date. The semi-empirical values of $C_{\nu n}(k)$ and $E_n(k)$ can be incorporated in the sum-over-states perturbation expressions due to Pople[18,19] for the nuclear shielding tensor. Within this model, the total nuclear shielding σ is expressed as the sum of two opposing terms, σ^d and σ^p, which are the diamagnetic and paramagnetic terms respectively. For nucleus A the expressions obtained[13-15] as a function of k are

$$\sigma_A^d(k) = \frac{\mu_0 e^2}{6\pi m_e^2} \sum_{\nu}^{A} \sum_{\nu'}^{A} P_{\nu\nu'}(k) \langle \phi_\nu(r) \,|\, r^{-1} \,|\, \phi_{\nu'}(r) \rangle, \tag{5}$$

$$\sigma_{A,\alpha\beta}^p(k) = -\frac{\mu_0 \hbar^2 e^2}{4\pi m_e^2} \sum_{m}^{occ} \sum_{n}^{unocc} \sum_{j}^{A} \langle r^{-3} \rangle_{2p} ({}^1E_m^n - {}^1E_0)^{-1}$$
$$\times \sum_{j}^{B} \sum_{l}^{B} [X(j,m,n,\beta,\gamma) X(l,m,n,\gamma,\alpha)$$
$$- Y(j,m,n,\beta,\gamma) Y(l,n,m,\gamma,\alpha)$$
$$+ X(j,m,n,\gamma,\alpha) X(l,n,m,\beta,\gamma)$$
$$- Y(j,m,n,\gamma,\alpha) Y(l,n,m,\beta,\gamma)], \tag{6}$$

where e is the charge and m_e the mass of the electron, μ_0 is the permeability of free space and

$$P_{\nu\nu'}(k) = \sum_{m}^{\text{occ}} C^{*}_{\nu m}(k) C_{\nu' m}(k), \tag{7}$$

where m refers to the number of occupied crystal orbitals and n to those that are unoccupied, E_0 is the electronic energy of the ground state and E^n_m is the energy of the state created by promoting an electron from orbital m to orbital n. j and l are atomic orbitals on centres A and B respectively, and

$$X(j, m, n, \beta, \gamma) = C^{\mathrm{R}\beta}_{jm} C^{\mathrm{I}\gamma}_{jn} + C^{R\beta}_{jn} C^{\mathrm{I}\gamma}_{jm} - C^{\mathrm{R}\gamma}_{jn} C^{\mathrm{I}\beta}_{jm} - C^{\mathrm{R}\gamma}_{jm} C^{\mathrm{I}\beta}_{jn}, \tag{8}$$

$$Y(j, m, n, \beta, \gamma) = C^{\mathrm{R}\beta}_{jm} C^{\mathrm{R}\gamma}_{jn} + C^{R\gamma}_{jn} C^{\mathrm{R}\beta}_{jm} - C^{\mathrm{I}\beta}_{jn} C^{\mathrm{I}\gamma}_{jm} - C^{\mathrm{I}\gamma}_{jm} C^{\mathrm{I}\beta}_{jn}. \tag{9}$$

In (5) and (6) α, β and γ refer to the x, y and z components of the shielding tensor in cyclic order and R and I indicate the real and imaginary parts of the coefficients $C_{\mu n}(k)$. As shown by (5) and (6), the nuclear shielding is calculated as a function of the eigenfunction number k. In order to be able to compare the calculated and experimental values of the nuclear shielding, it is necessary to average the calculated data over k, within the first Brillouin zone, as given by

$$\sigma = \int_{-\pi/b}^{\pi/b} \sigma(k) D(k)\, \mathrm{d}k, \tag{10}$$

where $D(k)$ is the state density, namely the number of states per unit amount of energy. The nuclear shielding is a second-rank tensor. In principle, non-spinning NMR measurements in the solid state can yield values for the individual components of the shielding tensor $\boldsymbol{\sigma}$ as expressed by

$$\boldsymbol{\sigma} = \begin{pmatrix} \sigma_{xx} & 0 & 0 \\ 0 & \sigma_{yy} & 0 \\ 0 & 0 & \sigma_{zz} \end{pmatrix}, \tag{11}$$

where the σ_{ii} are the principal tensor components. Rapid isotropic motions in liquid or solution and solid-state CP/MAS (cross-polarization/magic-angle spinning) experiments ensure that the isotropic nuclear shielding σ_{iso} is given by one-third of the trace of $\boldsymbol{\sigma}$ as

$$\sigma_{\text{iso}} = \tfrac{1}{3}(\sigma_{xx} + \sigma_{yy} + \sigma_{zz}). \tag{12}$$

Equations (5), (6) and (10) have been used in studies of the ^{13}C nuclear shieldings of some polymers, as discussed in Section 3.

Before closing the present section, it is appropriate to note that one of the major difficulties encountered in the evaluation of the paramagnetic

component of the shielding tensor lies in the estimation of the excitation energy $E_m^n - E_0$.

Within the extended Hückel framework, this energy is taken to be the difference in energies between the occupied and unoccupied crystal orbitals.[13,14,17] When the CNDO/2 procedure is employed the excitation energy is more appropriately given by

$$^1E_m^n - {}^1E_0 = \varepsilon_n - \varepsilon_m - J_{nm} + 2K_{nm}, \tag{13}$$

where ε_n and ε_m refer to the energies of the unoccupied and occupied crystal orbitals respectively, and J_{nm} and K_{nm} are the Coulomb and exchange integrals respectively, where

$$J_{nm} = \frac{1}{N} \sum_j \sum_\nu \sum_\mu C_{\nu n}^* C_{\mu m}^* C_{\nu n} C_{\mu m} \gamma_{AB}^{0j}, \tag{14}$$

$$K_{nm} = \frac{1}{N} \sum_j \sum_\nu \sum_\mu C_{\nu n}^* C_{\mu m}^* C_{\mu n} C_{\nu m} \gamma_{AB}^{0j}. \tag{15}$$

In (14) and (15) γ_{AB}^{0j} represents the Coulomb repulsion integral between atomic orbital μ on atom A in the original cell and atomic orbital μ' on atom B in the jth cell.

A more recent development has been to use the semi-empirical INDO/S parametrization scheme.[20] This has previously been demonstrated to be advantageous in nuclear shielding calculations on smaller molecules.[5] When employed within the TB approximation, equations (13)–(15) are evaluated by means of INDO/S parameters in order to obtain an estimate of the excitation energies. The results so far reported for macromolecules are in better quantitative agreement with experiment than those from comparable CNDO/2-based calculations.

3. INTERPRETATIONS OF NUCLEAR SHIELDING IN TERMS OF ELECTRONIC STRUCTURES

3.1. Nuclear shielding and intrachain interaction

In the TB calculation, the calculated physical properties are obtained as functions of the eigenfunction number k. As the observed physical properties are not so dependent, the integration over k within the Brillouin zone as shown in (10) should be carried out in order to compare the calculated physical properties with the observed ones. In the numerical integration it is necessary to decide how finely to divide the range of k to obtain sufficiently accurate approximations to the true values of the desired quantities. As an

Table 1. Dependence of the total energy, electron density on carbon atom and ^{13}C NMR chemical shift of polyethylene in the *trans* zigzag form on the number of divisions for k.

No. of divisions for k	Total energy/a.u.	Electron density on carbon atom	^{13}C NMR chemical shift/ppm
10	−17.3794	3.9872	−40.2733
20	−17.3794	3.9872	−40.2781
40	−17.3794	3.9872	−40.2657
60	−17.3794	3.9872	−40.2611
80	−17.3794	3.9872	−40.2591
100	−17.3794	3.9872	−40.2580

example, we consider polyethylene; Table 1 shows the dependence of the calculated total energy and electron density on the number of carbon atoms, and the ^{13}C NMR chemical shifts of a polyethylene chain on the number of elements used in the total range of k. As shown in this table, the total energy and electron densities on the carbon atoms do not change with an increase in the number of divisions of k. On the other hand, the calculated ^{13}C NMR chemical shift changes slightly as the number of divisions increases. Since the magnitude of the change is small when compared with the experimental precision of the measurement of ^{13}C NMR chemical shifts in the solid state, 10 points seem to be sufficient to give the appropriate accuracy. Within the extended Hückel framework, 80 points as the number of divisions were necessary to obtain the appropriate accuracy.[13] In the CNDO/2 method, the convergence of the calculated physical properties is rapid.[15] Table 2 shows the dependence of the CNDO/2-calculated total energy, electron densities on the carbon atoms, and ^{13}C NMR chemical shifts of a polyethylene chain on the number M of interacting cells.[15] The original cell for which the calculation is carried out interacts with M neighbouring cells on both sides. As can be seen from Table 2, the total energy converges to a definite value

Table 2. Dependence of the total energy, electron density on carbon atoms and ^{13}C NMR chemical shift of polyethylene in the *trans* zigzag form on the number of interacting cells M.

M	Total energy/a.u.	Electron density of carbon atom	^{13}C NMR chemical shift/ppm
1	−17.3768	3.9870	−40.4742
2	−17.3794	3.9872	−40.3507
3	−17.3794	3.9872	−40.2813
4	−17.3794	3.9872	−40.2794
5	−17.3794	3.9872	−40.2781

when the number M of interacting cells exceeds 2. On the other hand, the electron densities on the carbon atoms and the ^{13}C NMR chemical shifts still vary slightly even when M is 5. In the extended Hückel method these quantities converge when M exceeds 3.[13] Because electron repulsion integrals are partially included in the CNDO/2 method, the long-range interactions still affect the electronic structure of a polymer chain. Taking into account the experimental precision, 5 interacting cells on either side of the original cell are sufficient to give the appropriate accuracy. In the following discussions the calculations are carried out with 20 points to cover the range of k and 5 interacting cells on either side of the cell of interest.

3.2. Nuclear shielding and configuration

^{13}C NMR chemical shifts reflect the magnetic environment of the atom considered, which depends on the configuration (structure) of the polymer concerned. In order to clarify the situation, the relationship between ^{13}C NMR chemical shifts and the electronic structure of polymers must be understood.

First, we consider polyethylene. The calculated ^{13}C NMR chemical shielding tensor obtained using the CNDO/2 method is compared with the observed one as shown in Fig. 1.[15] The calculated quantity is the nuclear shielding, σ, and so the negative sign means deshielding. On the other hand,

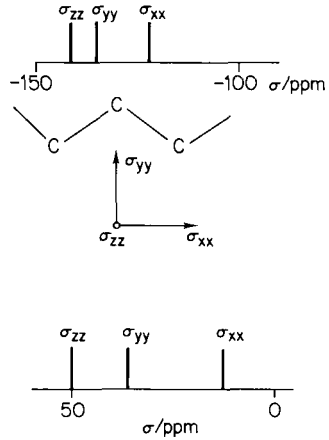


Fig. 1. The calculated principal values of the ^{13}C shielding tensors of polyethylene. The observed stick spectra and the directions of the principal axes are indicated at the bottom.

a negative sign of the observed chemical shift δ means an increase in shielding. The observed stick spectra and the direction of the principal axes of the tensor are shown in Fig. 1.[20,21] In the calculation the order of the principal values of the chemical shielding tensor is α_{xx}, σ_{yy} and σ_{zz} from low frequency, and the value of the breadth $\sigma_{xx} - \sigma_{zz}$ (corresponding to shielding anisotropy) is about 20 ppm.[15] The order of the principal values and the direction are in agreement with observation[22]. However, the calculated value of the breadth is somewhat small when compared with observation. Ando *et al.*[23] have examined the dependence of ^{13}C NMR chemical shifts on CNDO/2 parameters such as the bonding parameter and the correlation factor for $\pi-\pi$ interactions. The use of the parameters proposed reproduces the experimental values more reasonably.[23]

It is known from an X-ray diffraction study[24] that a polyoxymethylene chain in the crystalline region takes an all-*gauche* conformation with a 9/5 helix. However, in the non-crystalline region the structure is not exactly determined as yet because of the complicated conformation of the chain. Figure 2 shows the dependence of the calculated ^{13}C NMR isotropic shielding on the dihedral angle ψ.[25] The isotropic ^{13}C NMR shielding increases as ψ is increased from 50° to 90°, and the shielding decreases

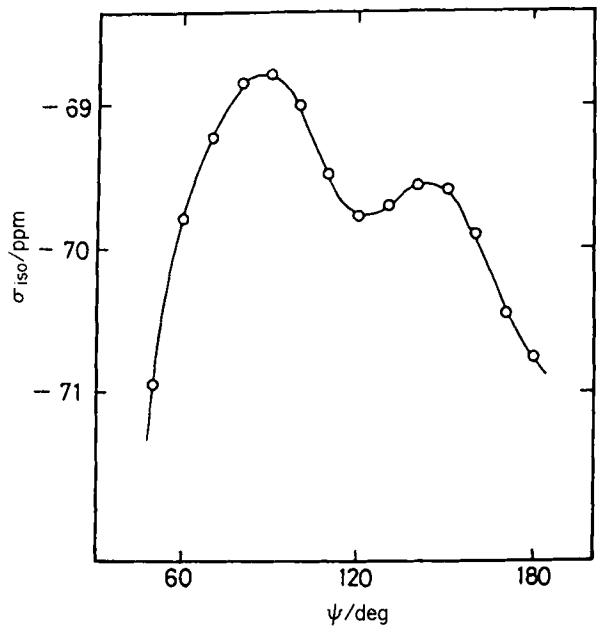


Fig. 2. The dependence of the calculated ^{13}C shielding of polyoxymethylene on the dihedral angle ψ.

through the minimum value as ψ is increased from 90° to 180°. The values of 60° and 180°, for ψ correspond to the all-*gauche* and the all-*trans* conformations respectively. The calculated isotropic ^{13}C NMR chemical-shielding values for all-*gauche* and all-*trans* conformations are listed in Table 3. As can be seen from this table, for the diamagnetic term the difference between the all-*gauche* and all-*trans* conformations is 0.1 ppm, and for the paramagnetic term the corresponding difference is 0.9 ppm. So, the contribution to the relative ^{13}C chemical shifts is due mainly to a change in the paramagnetic term. The diamagnetic term is determined by the ground state, whereas, as can be seen from (6), the paramagnetic term involves interactions between the ground and excited states. Thus it can be said that the observed chemical-shift difference between the crystalline and non-crystalline regions comes from a variable interaction due to a conformational change. Also, Fig. 2 and Table 3 show that the ^{13}C shielding for the all-*gauche* conformation is greater by 1.0 ppm than that for the all-*trans* conformation. Therefore it can be said that this calculated value explains well the experimental finding that the ^{13}C shielding for the crystalline region is greater by about 1 ppm than that for the non-crystalline region.

Next we consider anisotropy of the ^{13}C shielding tensor. Figure 3 shows the dependence of the calculated spectrum breadth $\Delta\sigma = \sigma_{yy} - \sigma_{zz}$ on ψ. It is found that the breadth increases as ψ is increased from 40° to 60° and decreases from 60° to 180° through the minimum value. The values of $\Delta\sigma$ for the all-*gauche* and all-*trans* conformations are listed together with the principal values of the shielding tensors in Table 3. As can be seen from Fig. 3 and Table 3, it is found that the value of $\Delta\sigma$ (37.7 ppm) for the all-*gauche* conformation is much larger than that (1.8 ppm) for the all-*trans* conformation. On the other hand, the experimental values of $\Delta\delta$ for the crystalline and non-crystalline regions are about 35 ppm and 7–10 ppm respectively.[25] Thus it can be said that the calculated and experimental values agree relatively well with each other. The fact that the calculated value of $\Delta\sigma$ for the all-*trans* conformation is rather small suggests that the electronic

Table 3. Calculated isotropic ^{13}C NMR chemical shieldings σ and components of the chemical-shielding tensors of polyoxymethylene[a] (in ppm).

	Isotropic			Tensor components			
Conformation	σ^d	σ^p	σ^t	σ_{11}	σ_{22}	σ_{33}	$\Delta\sigma^b$
All-*gauche*	55.7	−125.5	−69.8	−144.9	−124.3	−107.3	37.7
All-*trans*	55.6	−126.4	−70.8	−127.1	−126.8	−125.3	1.8

[a] The negative sign means deshielding.
[b] $\Delta\sigma = |\sigma_{11} - \sigma_{33}|$.

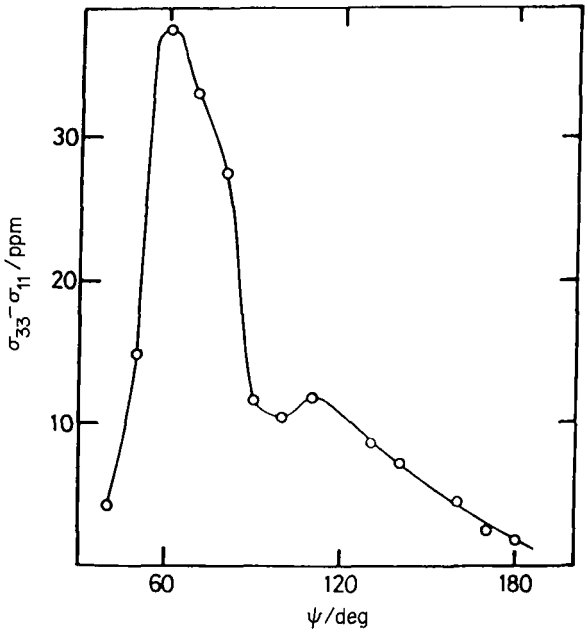


Fig. 3. The dependence of the calculated width of the powder pattern of polyoxymethylene on the dihedral angle ψ.

environment around the carbon nucleus considered here is relatively symmetric. Thus the small value of the observed $\Delta\delta$ may be due mainly to the high symmetry of the electronic environment in addition to the averaging of ^{13}C shielding anisotropy with molecular motion. Further, we are concerned with the behaviour of δ_{22}, the value of which is obtained from the apex of the tent-like powder pattern. In the experimental data, δ_{22} for the crystalline region appears at about 5 ppm to low frequency when compared with that for the non-crystalline region. However, as can be seen from Table 3, σ_{22} for the all-*gauche* conformation appears at lower frequency by about 2.5 ppm when compared with that for the all-*trans* conformation. Thus the calculation explains the observation reasonably despite the rough assumption of an all-*trans* conformation for the non-crystalline region.

Polyacetylene is the simplest conjugated polyene and has two isomers: *cis* and *trans*. These have been actively studied by both experimental and theoretical procedures. This is due to the discovery of a direct synthetic method for polyacetylene film[26] and a large increase in its electronic conductivity with doping.[27] The isotropic ^{13}C shielding and the full tensor have been employed in conformational studies. The observed values of the breadth of the spectra of *cis*- and *trans*-polyacetylenes are about 200 and

180 ppm respectively.[28,29] The observed values of δ_{zz}, δ_{xx} and δ_{yy} for *cis*-polyacetylenes are larger by about 1, 6 and 25 ppm respectively than those of the *trans* form. The large difference in δ_{yy} leads to the large difference observed in the isotropic ^{13}C chemical shift between *cis*- and *trans*-polyacetylenes. The observed differences between δ_{zz} and δ_{xx} for *cis*- and *trans*-polyacetylenes are 80 and 75 ppm respectively, and the observed differences between δ_{xx} and δ_{yy} for *cis*- and *trans*-polyacetylenes are 116 and 97 ppm respectively. The calculated ^{13}C shielding tensors and directions of principal axes are shown in Fig. 4,[15] where the observed results are also shown. The calculated values of the breadth $\sigma_{zz} - \sigma_{yy}$ for *cis*- and *trans*-polyacetylenes are 116.3 and 115.8 ppm respectively. Thus the calculations reproduce the experimental data on the ^{13}C shielding tensors satisfactorily. Comparing the calculated isotropic ^{13}C shieldings with the observed ones, we find that the calculated difference in shieldings between *cis*- and *trans*-polyacetylenes is much smaller than that observed. The observed difference in ^{13}C shielding between *cis*- and *trans*-polyacetylenes is about 10 ppm, whereas the calculated difference is about 0.4 ppm. It is reported[13] that the bond angles of *cis*- and *trans*-polyacetylenes are very important in discussing their ^{13}C chemical shifts.

From an X-ray diffraction study, the bond angle of *cis*-polyacetylene is reported to be 127° and that of *trans*-polyacetylene to be 123°.[30] The shielding calculation has been carried out by varying the bond angles of *cis*- and *trans*-polyacetylenes.[15] Figure 5 shows the dependence of the ^{13}C NMR

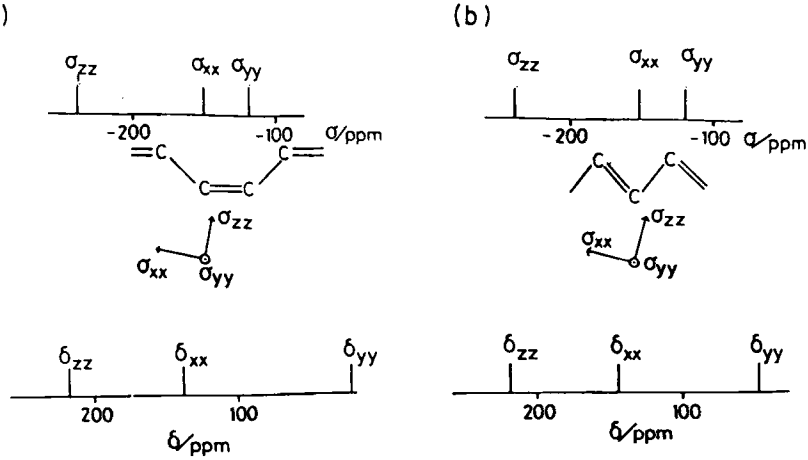


Fig. 4. The calculated principal values of the ^{13}C shielding tensors of *cis*-polyacetylene (a) and *trans*-polyacetylene (b). The observed stick spectra and the directions of the principal axes are indicated at the bottom.

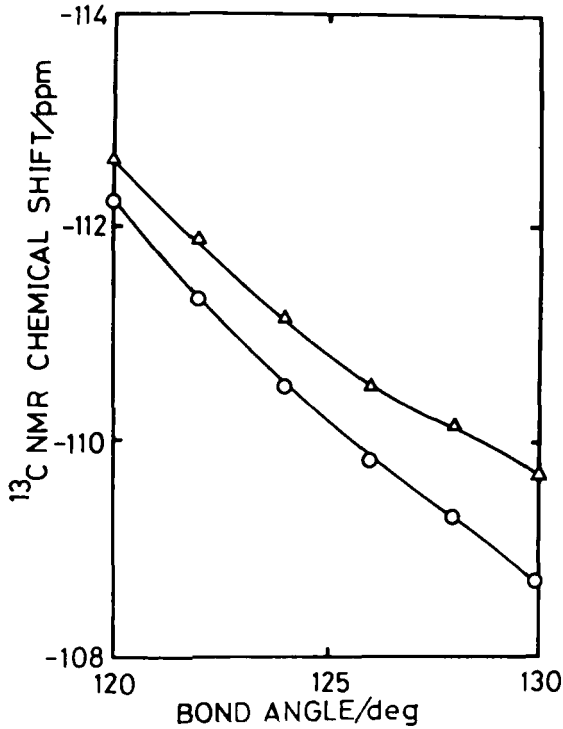


Fig. 5. The dependence of the calculated isotropic ^{13}C shieldings of *cis*-polyacetylene (△) and *trans*-polyacetylene (○) on bond angle C=C—C.

chemical shift on the bond angles for *cis*- and *trans*-polyacetylenes. As can be seen from this figure, the ^{13}C shieldings of both polyacetylenes increase, and their difference becomes larger, as the bond angle is increased. The ^{13}C shielding of *cis*-polyacetylene, with a bond angle of 127°, is − 109.6 ppm, while that of *trans*-polyacetylene, with a bond angle of 123°, is − 111.5 ppm. The difference is about 2 ppm, and it becomes larger when all of the bond angles are taken to be 120°. This explains the experimental data fairly well.

Figure 6 shows the dependence of the principal values of the ^{13}C shielding tensor on the bond angles in *cis*- and *trans*-polyacetylenes.[15] As can be seen from this figure, the predicted substantial change in ^{13}C shielding tensor (a change in the order of the principal values and the value of the signal breadth) is not detected even when the bond angle is varied. The most sensitive element of the ^{13}C shielding tensor, to bond-angle variation, is σ_{zz}. The variation quantities are about 5 and 8 ppm for *cis*- and *trans*-polyacetylenes respectively, and the direction of the principal value is almost

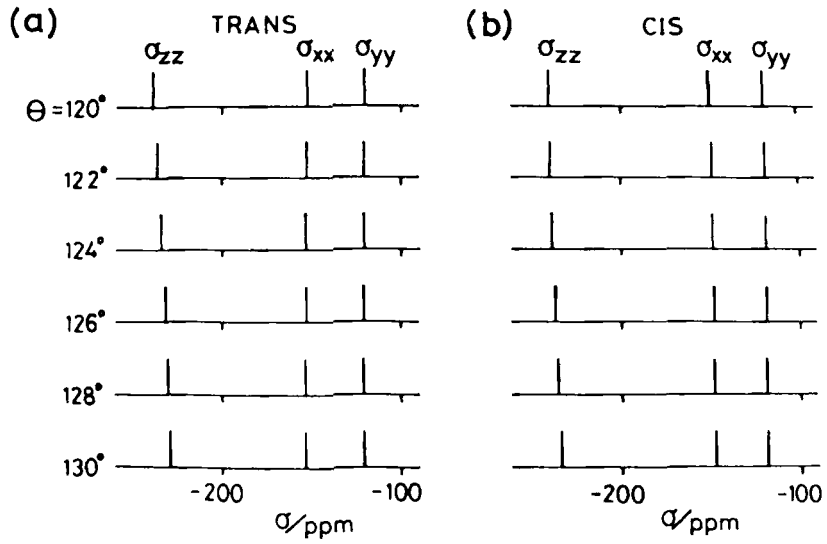


Fig. 6. The dependence of the calculated principal values of the ^{13}C shielding tensors of *cis*-polyacetylene (a) and *trans*-polyacetylene (b) on bond angle C=C−C.

perpendicular to the long axis. This can be understood since both *cis*- and *trans*-polyacetylenes have conjugation in the direction of the long axis and the electrons are most mobile along this direction (the ^{13}C shielding is mainly governed by the paramagnetic term, which arises from the distortion of electron distribution by the magnetic field). The directions of the principal axes have been determined only for *trans*-polyacetylene. The angle between the C−C single bond and the direction of the principal axis of the observed δ_{zz} is 40°, and the direction of δ_{yy} is perpendicular to the C−C=C plane. In the calculation the angle between the C−C single bond and the direction of the principal axis of σ_{zz} is 41°, and the direction of σ_{yy} is perpendicular to the C−C=C plane. The calculated directions of the principal axes are almost the same as the observed ones. From this result, it is found that the directions of the principal axes for *cis*-polyacetylene may be predicted by the calculation. The angle between the C−C single bond and the direction of σ_{zz} is about 37°, which is somewhat smaller than that of *trans*-polyacetylene. Table 4 shows the calculated principal values of the ^{13}C shielding tensors of *cis*- and *trans*-polyacetylenes (the bond angles for *cis* and *trans* are 123° and 127° respectively) and the corresponding observed data. The observed principal values of the shielding tensor decrease in going from *cis*- to *trans*-polyacetylene. The variations of δ_{xx} and

δ_{yy} are relatively large, but that of δ_{zz} is small. These trends are qualitatively reproduced by the calculations reported.

As can be seen from the above results, a more refined treatment is necessary to obtain satisfactorily quantitative agreement between experiment and calculation. Yamanobe *et al.*[20] have used the INDO/S method for the calculation of the ^{13}C shielding of polyacetylene. This is a modified INDO method,[31] providing more reliable excitation energies than the CNDO/2 and INDO methods. Table 5 shows the observed isotropic ^{13}C shieldings of *cis*- and *trans*-polyacetylenes together with the calculated ones within the frameworks of the CNDO/2 and INDO/S methods. As can be seen from this table, the differences in the isotropic ^{13}C shielding between *cis*- and *trans*-polyacetylenes, calculated by the CNDO/2 and INDO/S methods, are about 2.0 and 3.5 ppm respectively. The difference for the INDO/S method is about twice that obtained by the CNDO/2 method. However, the observed difference is about 10 ppm.[28,29] Both types of calculation somewhat underestimate the observed data in this case. It is found that the INDO/S calculation reproduces the observed data better than does the CNDO/2 calculation. The observed shielding increase for *cis*-polyacetylene is reproduced in both calculations, but the difference

Table 4. The observed and calculated ^{13}C isotropic chemical shifts and chemical-shielding tensors of *cis*- and *trans*-polyacetylenes (in ppm).

	Observed[a]				Calculated[b]			
	δ_{iso}	δ_{11}	δ_{22}	δ_{33}	σ_{iso}	σ_{zz}	σ_{xx}	σ_{yy}
cis	127.7	218 ± 2	138 ± 1	22 ± 2	−109.6	−235.2	−148.7	−118.9
trans	137.3	219 ± 2	144 ± 1	47 ± 2	−111.5	−236.0	−152.3	−120.2

[a] Ref. 28. From TMS.
[b] The negative sign means deshielding.

Table 5. The observed and calculated isotropic ^{13}C shieldings of *cis*- and *trans*-polyacetylenes (in ppm).

		Calculated[b]	
	Observed[a]	CNDO/2[31]	INDO/S
cis	127.7	−109.6	−129.2
trans	137.3	−111.5	−132.7

[a] Ref. 28. From TMS.
[b] The negative sign means deshielding.

between σ_{xx} and σ_{yy} is greatly underestimated in the CNDO/2 calculation. From both the isotropic ^{13}C shielding and its tensor components, it can be seen that the INDO/S method provides better results than the CNDO/2 method.

As shown in Fig. 7, the absolute values of σ_{zz} and σ_{xx} calculated by the INDO/S procedure are smaller by about 40 ppm than those obtained by the CNDO/2 calculation. The value of σ_{yy} calculated by the INDO/S method is larger by about 10 ppm than that obtained by the CNDO/2 calculation. Consequently, the separation between the values of σ_{xx} and σ_{yy} calculated by the INDO/S method is much larger than that obtained by the CNDO/2 approach. Further, it is shown that in going from the CNDO/2 to the INDO/S calculation the values of σ_{zz} and σ_{xx} are changed considerably. This may be because in going from the CNDO/2 to the INDO/S framework there is a change of the electronic structure that affects σ_{zz} and σ_{xx} more than σ_{yy}. The most remarkable difference between the INDO/S and CNDO/2 methods is the estimation of overlap integrals. In the INDO/S method the effective $\pi-\pi$ overlap would be screened differently than the $\sigma-\sigma$ overlap. The contribution from π electrons to ^{13}C shieldings calculated by the INDO/S procedure is very different from that calculated by the

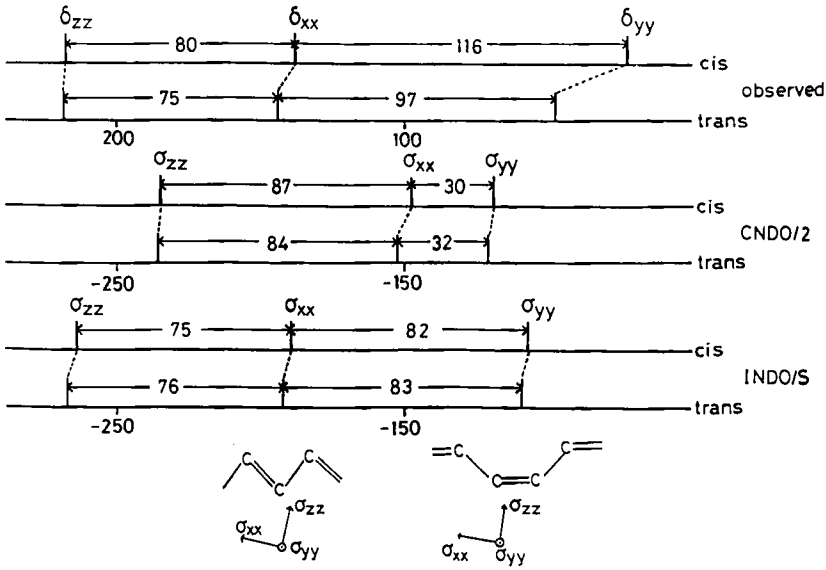


Fig. 7. The observed and calculated components of ^{13}C NMR shielding tensors of *cis*- and *trans*-polyacetylenes. The directions of the principal axes are indicated at the bottom (the angles between the C—H bond and the direction of σ_{zz} for *trans*- and *cis*-polyacetylenes are 16° and 17° respectively).

CNDO/2 method. From the above results, it is evident that the values of σ_{zz} and σ_{xx} are affected by the distribution of the π electrons. In order to discuss this in more detail, we note a change of the band structure in going from the CNDO/2 to the INDO/S method. Figure 8 shows the valence-band structures of *cis*- and *trans*-polyacetylenes calculated by the CNDO/2 and INDO/S methods. On comparing the band structures calculated by these two procedures, it can be seen that the energies of bands 1 and 2 decrease in going from the CNDO/2 to the INDO/S results. On the other hand, the energies of bands 3 to 5 increase—in particular, that of band 5, which has π symmetry. The band gaps (the energy differences between the highest

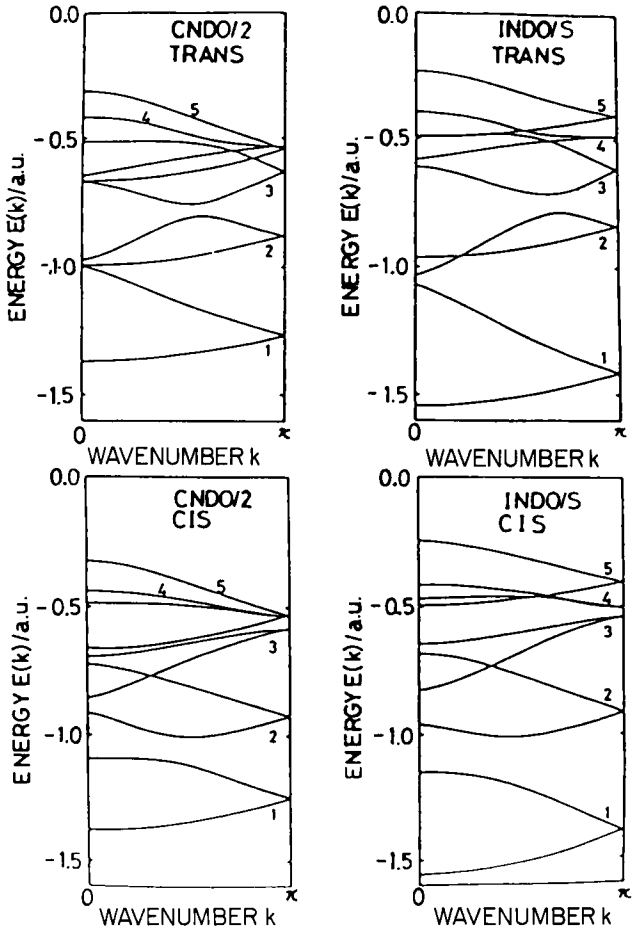


Fig. 8. The band structures of *cis*- and *trans*-polyacetylenes calculated within the framework of the CNDO/2 and INDO/S MO methods.

occupied and the lowest unoccupied bands) for *trans*-polyacetylene, calculated by the CNDO/2 and INDO/S methods, are about 8.0 and 4.2 eV respectively. The corresponding values for *cis*-polyacetylene are 8.4 and 4.3 eV respectively. The observed band gap, for *trans*-polyacetylene, determined from absorption spectra, is about 1.9 eV, and that for *cis*-polyacetylene is slightly larger than 1.9 eV.[23] The INDO/S method thus reproduces the observed band gap better than does the CNDO/2 procedure. From this, we may see why the INDO/S calculation of the ^{13}C shielding gives the better agreement with the experimental data.

Table 6 shows the sum of the contributions to the components of ^{13}C shielding tensor of the transitions from the valence band to all of the conduction bands. From this table, it can be seen that both σ_{xx} and σ_{zz} receive significant contributions from bands 3, 4 and 5 for both *cis*- and *trans*-polyacetylenes. However, the highest occupied band does not contribute to σ_{yy}. σ_{yy} has large contributions from bands 2, 3 and 4 (low-energy bands). Comparing the values of σ_{xx} for *trans*-polyacetylene calculated by the INDO/S and CNDO/2 methods, it can be seen that bands 3, 4 and 5 contribute to an increase in the absolute value of σ_{xx}. From (6), the paramagnetic contribution may be expressed as[5]

$$\sigma^{\mathrm{P}} \propto -\frac{1}{\Delta E_m^n} Q_{\mathrm{AB}}, \tag{16}$$

Table 6. The contribution of transitions from any specified valence band, to all conduction bands, to the components of the ^{13}C NMR shielding tensor of (a) *trans*-polyacetylene and (b) *cis*-polyacetylene calculated by the CNDO/2 and INDO/S methods (in ppm).

	CNDO/2[a]			INDO/S[a]		
Band no.	σ_{xx}	σ_{yy}	σ_{zz}	σ_{xx}	σ_{yy}	σ_{zz}
(a)						
1	−0.458	−6.043	−3.089	−0.737	−5.784	−2.597
2	−1.282	−25.028	−9.916	−1.051	−21.848	−11.774
3	−16.718	−38.512	−56.588	−23.418	−36.661	−63.858
4	−62.591	−50.551	−54.668	−82.085	−45.287	−69.542
5	−71.419	0.0	−113.511	−85.426	0.0	−120.986
(b)						
1	−0.211	−5.607	−2.371	−0.426	−5.222	−2.865
2	+0.250	−28.947	−4.808	+1.443	−25.548	−8.403
3	−30.209	−38.671	−35.960	−38.914	−37.417	−40.600
4	−48.314	−45.565	−78.062	−64.877	−39.126	−91.403
5	−70.462	0.0	−113.822	−85.577	0.0	−120.824

[a] The negative sign means deshielding.

where ΔE_m^n is the averaged excitation energy between the valance band m and the conduction band n, and Q_{AB} is a term containing bond orders and charge densities.[5] From this, the increase in the energies of bands 3, 4 and 5 is one of the factors leading to the deshielding of σ_{xx}, which implies a lower excitation energy. Of course, the Q_{AB} values for bands 3 and 4 might also contribute to deshielding. A similar trend appears in the calculation of σ_{xx} for *cis*-polyacetylene and σ_{zz} for *cis*- and *trans*-polyacetylenes. In order to reproduce the observed large difference in σ_{yy} between *cis*- and *trans*-polyacetylenes, using only an isolated chain, it may be necessary to use MOs that can properly describe bands 2, 3 and 4, which have σ symmetry.

There has also been some interest in polypeptides. It has been demonstrated that the ^{13}C chemical shifts of the C_α, C_β and carbonyl carbons are displaced by up to 7 ppm, depending on the particular conformations such as α-helix, β-sheet and ω-helix forms. Such conformation-dependent ^{13}C chemical shifts should be understood through changes of electronic structure varying with the dihedral angles (ϕ and ψ) of the skeletal bonds.

Table 7 shows the calculated and observed ^{13}C shieldings of a polyglycine chain with forms I and II.[17] The observed carbonyl ^{13}C signal for form I is shielded by about 4 ppm compared with that for form II. The calculated ^{13}C shielding for form I is larger by about 11 ppm than that of form II, which matches the experimental finding. There is no significant difference between the methylene ^{13}C chemical shifts for forms I and II within experimental error. At this stage, we cannot determine whether the methylene shielding for form I or for form II is the larger one. The calculated ^{13}C shielding for form I is smaller by about 3 ppm than that for form II, so the calculation predicts the existence of a shielding difference (about 3 ppm) between forms I and II. It appears that the calculated shieldings are somewhat exaggerated compared with the observed values. Nevertheless, the observed trend that the ^{13}C shielding difference for the methylene carbon is very small when compared with that for the carbonyl carbon is reproduced quantitatively by the calculation.

Table 7. The observed and calculated ^{13}C chemical shifts and chemical shieldings of an isolated polyglycine chain (in ppm).

	δ_{obs}[a]		σ_{calc}[b]	
	Form I	Form II	Form I	Form II
CH_2	43.5	43.5	−127.2	−124.4
C=O	168.4	172.3	−236.7	−248.1

[a] From TMS. The positive sign means deshielding.
[b] The negative sign means deshielding.

Next we consider the ^{13}C shielding of poly(L-alanine), which takes the α-helix form.[17] It is known that poly(L-alanine) has a right-handed α-helix (α_R-helix) form, but that the L-alanine residues are incorporated into the left-hand α-helix (α_L-helix) in a D-alanine sequence in the random copolymers consisting of L- and D-alanines. The observed Cα and carbonyl ^{13}C shieldings of L-alanine residues, incorporated into the α_L-helix form in the D-alanine sequence, are between those in the β-sheet and α_R-forms, and appear close to that in the sheet form, while the C_β shift of the α_L-helix is close to that of the α_R-helix.[32]

Table 8 shows the calculated and observed ^{13}C shieldings of poly(L-alanine).[17,33] As can be seen from this table, the calculated ^{13}C shieldings of the C_α, C_β and carbonyl carbons are respectively larger (6.7 ppm), smaller (−1.3 ppm) and larger (10.3 ppm) when the conformation changes from the α_R-helix to the α_L-helix form. Experimentally, the displacements of the signals are 3.3, 0.0 and 3.5 ppm for the C_α, C_β and carbonyl carbons respectively. This indicates that the calculation reproduces the experimental data reasonably well.

We now consider poly(β-benzyl L-aspartate), which takes various conformations. Poly(β-benzyl L-aspartate) normally takes the α_L-helix conformation in the solid state and in chloroform solution. However, the α_R helix is formed, either in monolayers at an air–water interface[32] or in films of low molecular weight polymers from chloroform solution by slow evaporation.[34] X-ray diffraction studies provide exact information about the main-chain conformation, but not always about side-chain conformations. ^{13}C shieldings of the carbonyl, C_α and C_β carbons for the α_R-helix and α_L-helix forms have been calculated as shown in Table 9, together with the corresponding experimental data.[35] It is obvious from the calculated data that the C_α, C_β and carbonyl signals of the α_R helix appear at higher frequency than do those of the α_L helix. The displacements of the signals on going from the α_L helix to the α_R helix conformation are 16.1, 11.9 and

Table 8. The observed and calculated ^{13}C chemical shifts and chemical shieldings of an isolated poly(L-alanine) chain (in ppm).

	δ_{obs}[a]			σ_{calc}[b]		
	α_R	α_L	β	α_R	α_L	β
$CH_3(C_\beta)$	14.9	14.9	19.9	−94.8	−96.1	−98.3
$CH(C_\alpha)$	52.4	49.1	48.2	−151.5	−144.8	−143.0
C=O	176.4	172.9	171.8	−278.1	−267.8	−245.8

[a] From TMS. The positive sign means deshielding.
[b] The negative sign means deshielding.

9.7 ppm for the C_α, C_β and carbonyl carbons respectively. In these calculated ^{13}C shieldings the difference in the value of σ^p depends largely on the conformational change from the α_L-helix to the α_R-helix form, but the value of σ^d does not. This means that the conformation-dependent ^{13}C shieldings are largely governed by the paramagnetic contribution. The carbonyl ^{13}C shielding provides useful information about the conformation around the skeletal bonds. Experimentally, the conformational change from the α_L-helix to the α_R-helix form leads to a decrease in shielding (3.8 ppm). This is in agreement with the calculated trend (9.7 ppm). This is comparable to the case of poly(L-alanine), despite the different sizes of the side groups involved. These data suggest that the ^{13}C-shielding differences of the main-chain carbonyl carbons in polypeptides arise mainly from changes of electronic structure varying with the dihedral angles of the skeletal bond rather than changes of electronic structure varying with the side group. For the main-chain C_α, the conformational change from the α_L-helix to the α_R-helix form leads to deshielding (2.5 ppm) experimentally. This is in agreement with the calculated trend (16.1 ppm). Similarly, a deshielding is found in the case of poly(L-alanine). Thus it is reasonable to ascribe the conformation-dependent ^{13}C shieldings of the main-chain carbons to changes of electronic structure accompanying changes of the dihedral angles of the skeletal bonds. For the side-chain C_β the conformational change from the α_L-helix to the α_R-helix form provides no significant experimental shielding change within experimental error.[35] However, a high-resolution ^{13}C NMR study of a copoly(Ala, Asp(OBzl))$_n$ in $CDCl_3$

Table 9. Calculated ^{13}C nuclear-shielding data and experimental ^{13}C chemical shift of poly(β-benzyl L-aspartate) in the solid state (in ppm).

	Experimental chemical shift δ^a		Calculated-nuclear shielding σ^b					
			α_R			α_L		
	α_R	α_L	σ^p	σ^d	σ	σ^p	σ^d	σ
C_α	53.4 (53.5)	50.9 (50.8)	−272.1	56.5	−125.6	−256.0	56.5	−199.5
C_β	33.8 (34.7)	33.8 (33.8)	−194.4	60.1	−134.3	−182.5	60.1	−122.4
CO(amide)	174.9 (174.2)	171.1 (171.6)	−342.2	49.2	−293.0	−332.6	49.3	−283.3

[a] From TMS Experimental error ±0.5 ppm. Data in parentheses are from solution NMR data of poly(Ala, Asp(OBzl)) where the molar ratio of Ala : Asp(OBzl) = 5 : 95. The positive sign means deshielding.

[b] The negative sign means deshielding.

solution shows that the C_β signal of the α_R-helix portion of the Asp(OBzl) residue is displaced to high frequency by 1.0 ppm compared with that of the α_L-helix. The calculated ^{13}C shielding for the α_R-helix form is larger by about 11.9 ppm than that for the α_L-helix form, so the calculation predicts the existence of a shielding difference between the α_R-helix and α_L-helix forms. Again these data are in agreement with the experimental findings.

The band gap between the highest filled and lowest unfilled bands of a poly(β-benzyl L-aspartate) chain may be considered on the basis of the experimental result for the ^{13}C shielding. This gap is closely related to properties such as electrical conductivity. Thus it is of interest to obtain information about it. The excitation energy is one of the important factors contained in the paramagnetic shielding term, and a small value of this term leads to an increase in nuclear shielding. Thus the observation of the ^{13}C shielding might provide information on the averaged excitation energy of a polymer chain, i.e. the band gap. On the basis of this, as well as for polyalanine,[17] the experimental results, which show the relatively small shieldings of the carbon atoms from the α_L helix to the α_R helix, might suggest a reduction in the band gap. The magnitudes of the calculated shieldings are somewhat exaggerated compared with the experimental values. The overestimation of the displacement of the calculated shielding may be due to the use of extended Hückel MO calculations for polar molecules, where there is a tendency to overestimate the electronic polarization, in contrast with the case of hydrocarbons. Improved data may be obtained when more rigorous wavelengths such as those found in CNDO, INDO or *ab initio* procedures are used. Nevertheless, it is emphasized that the extended Hückel MO calculation can predict the experimental trend of the conformation-dependent ^{13}C shieldings.

3.3. Nuclear shielding and interchain interaction

The crystal structure of a solid, which describes how the molecule condenses, is an important factor when discussing the properties of individual molecules. Solid-state NMR chemical shifts can give information on crystal structures.[16] Thus solid-state NMR combined with X-ray analysis provides a useful method for studying crystal structure. For this, we need to understand the origin of interchain interactions on the ^{13}C shieldings as demonstrated by quantum-chemical methods.

Experimentally, it can be seen that the ^{13}C shieldings of all of the n-paraffins and polyethylene in the orthorhombic form are almost constant (about 33 ppm) within experimental error, irrespective of the number of carbons.[16,36,37]

However, the ^{13}C shieldings of cyclic paraffins in the triclinic form are about 34 ppm.[16,38,39] In the cyclic paraffin $C_{160}H_{320}$, which takes the orthorhombic form, the ^{13}C shielding is about 33 ppm, which is very close to that for n-paraffins and polyethylene. This suggests that the difference of about 1 ppm may be due to a local change in intermolecular interactions resulting from the transition from the orthorhombic to the triclinic form. The solid-state ^{13}C shielding data may be used to differentiate the molecular packing. For the crystallographic form of the polyethylene and paraffins considered here, the result of X-ray diffraction suggests that the all-*trans* zigzag plane of any specified chain in the orthorhombic and triclinic forms is respectively perpendicular and parallel to that of the neighbouring chains. It has been reported[37] that the ^{13}C shielding of polyethylene with the monoclinic form is decreased by 1.4 ppm compared with that of polyethylene with the orthorhombic form, while the monoclinic form is very close to the triclinic form. Thus the solid-state ^{13}C shielding depends on the orientation of the C—C—C plane in *trans* zigzag chains.

Since in the solid the chains lie periodically in space, shielding calculations should be employed that take account of the three-dimensional structure, including interactions between chains. In the real calculation, however, it is not possible to handle chains having such three-dimensional structures because of limits on computer memory and available computation time. Therefore in this work two models using three chains for the triclinic and orthorhombic subcells are used to compute ^{13}C shieldings. Figure 9(A) is a model for polyethylene with the triclinic form, where the C—C—C planes in three chains are parallel to each other and R is the interchain distance. Figure 9(B) is a model for polyethylene with the orthorhombic form, where the neighbouring C—C—C planes in the three

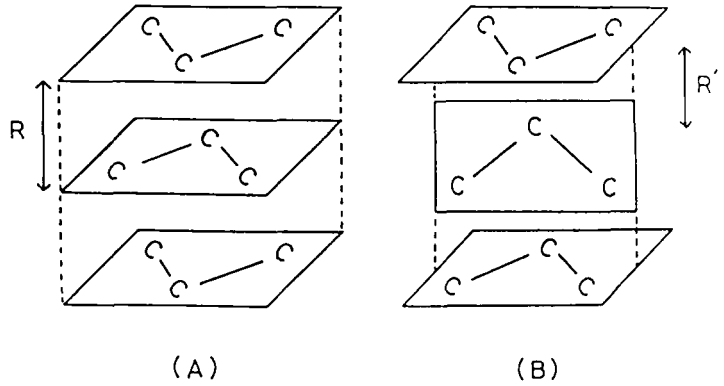


Fig. 9. The crystallographic models used for polyethylene in the ^{13}C shielding calculation: (A) triclinic form; (B) orthorhombic form.

chains are perpendicular to each other and R' is the distance between the neighbouring chain axes. Using these models, the calculations were carried out varying R or R' from 3 Å to 5 Å. The calculations reproduce the experimental data reasonably well. Figure 10(a) shows the dependences of the calculated ^{13}C shielding on R. For the orthorhombic form the ^{13}C NMR

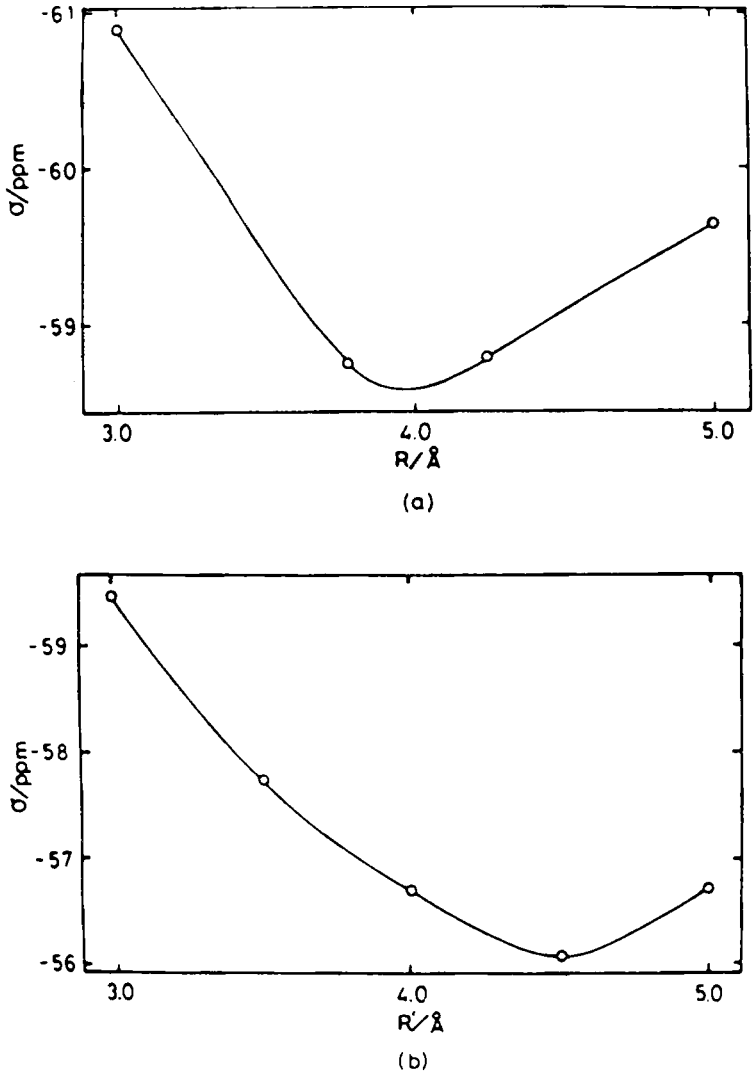


Fig. 10. The dependence of the calculated ^{13}C shielding of polyethylene on interchain distance (R or R'): (a) triclinic form; (b) orthorhombic form.

shielding (orth) increases as R' increases from 3 Å to 4.5 Å, and decreases as R' increases beyond 4.5 Å. For the triclinic form the overall tendency of the R dependence of the ^{13}C shielding (tri) is close to that for the orthorhombic form except for the value of R at which the decrease in shielding occurs, which is about 4.0 Å. In discussing the effect of the crystallographic form on the ^{13}C shielding, the appropriate values of R and R' should be chosen. In this work the values of R and R' are adopted on the basis of the lattice constant of cyclic $C_{34}H_{68}$ ($R = 4.08$ Å)[40] and polyethylene ($R' = 4.00$ Å).[41] Therefore, using these values of R and R', the ^{13}C shieldings calculated for the two models are $\sigma_{tri} = -58.6$ ppm and $\sigma_{orth} = -56.7$ ppm. The calculated difference between the tri and orth forms is 1.9 ppm, which is about twice as large as the experimental value (0.9 ppm). The ^{13}C shielding for the triclinic form is smaller than that for the orthorhombic form. This trend parallels the experimental one.

Next we consider polyoxymethylene. The calculation of the ^{13}C shielding, total energy and band gap by the TB-CNDO/2-SOS method, using a single chain, taking the 9/5 (or 29/16) and 2/1 helical conformations, has been carried out for trigonal and orthorhombic polyoxymethylene chains.[42] It is possible to use this single-polyoxymethylene-chain model to evaluate the conformational effect for a polyoxymethylene crystal form (trigonal or orthorhombic); however, it is not appropriate for calculation of the interchain interactions. Table 10 shows the calculated ^{13}C shielding, total energy and band gap for the single-chain model of trigonal and orthorhombic polyxoymethylene. Additionally, the averaged least-squares deviation $\alpha = [\frac{1}{5}\Sigma(\Delta\sigma_{obs} - \Delta\sigma_{calc})^2]^{1/2}$ is listed in this table, which is a measure of the deviations of the calculated values from the observed data for the ^{13}C shieldings. As can be seen from Table 10, the calculated ^{13}C shielding for

Table 10. The calculated ^{13}C NMR shielding and chemical-shielding tensor for trigonal and orthorhombic POMs using the single-polymer-chain model.

	σ_{iso}	σ_{11}	σ_{22}	σ_{33}	$\Delta\sigma$[b]	Band gap (eV)	Total energy (a.u.)
	(ppm)[a]						
Trigonal	−77.57	−149.9	−132.4	−117.8	32.1	16.532	−26.090
Orthorhombic	−74.81	−152.5	−127.3	−112.0	40.5	16.817	−26.004
Δ[c]	2.76	−2.6	5.1	5.8	8.4	0.285	0.086
α[d]			1.505				

[a] The negative sign means deshielding.
[b] $\Delta\sigma = |\sigma_{11} - \sigma_{33}|$.
[c] Orthorhombic–trigonal.
[d] Averaged least-squares deviation.

trigonal polyoxymethylene decreases by 2.76 ppm with respect to that for orthorhombic polyoxymethylene. The calculated value of $\Delta\sigma$ (32.1 ppm) for trigonal polyoxymethylene is smaller than that (40.5 ppm) for the orthorhombic form. The values of the total energy show that trigonal polyoxymethylene is energetically more stable than the orthorhombic form. The observed ^{13}C shielding for trigonal polyoxymethylene decreases by 2.4 ppm with respect to that for orthorhombic polyoxymethylene, and the observed values of $\Delta\sigma$ for trigonal and orthorhombic polyoxymethylene are about 35 ppm and 42 ppm respectively.[43] The calculation for this single chain explains the observed data reasonably well; in addition, the relative stability of the trigonal and orthorhombic polyoxymethylenes as predicted by the calculation agrees with the experimental result. However, the averaged least-squares deviation α obtained using this model is not so good when compared with that for the seven-polyoxymethylene-chain model mentioned below. This is thought to be due to the neglect of interchain interactions in the single-chain-model calculation.

The value of the band gap (16.817 eV) for orthorhombic polyoxymethylene is somewhat larger than that (16.532 eV) for trigonal polyoxymethylene. The magnitudes of these gaps indicate that these polymers are insulators. This explains well the experimental finding for trigonal polyoxymethylene (10^{14}–10^{16} Ω cm). These calculated results are compared with those calculated using the seven-chain model below.

The information about molecular packing (the relative interchain "sliding length" l and the relative rotation angle Ψ as defined in Figs 11 and 12) are needed when the seven-polyoxymethylene-chain model is used. Such information, for orthorhombic polyoxymethylene, is obtained from X-ray diffraction studies ($l = 0.5$ pitch and $\Psi = 90^\circ$), where any oxygen atom in a specified chain (e.g. chains number 1, 2 and 3 in Fig. 13) and carbon atoms in the other chains (chains number 4, ..., 7) are in the same plane, which is perpendicular to the helical axis. However, the corresponding information

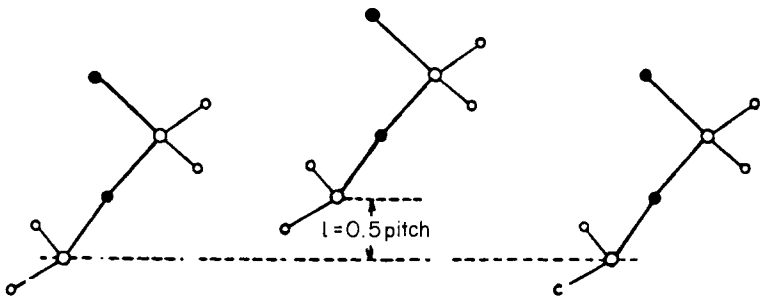


Fig. 11. The relative "sliding length" l defined for the model with seven polyoxymethylene chains.

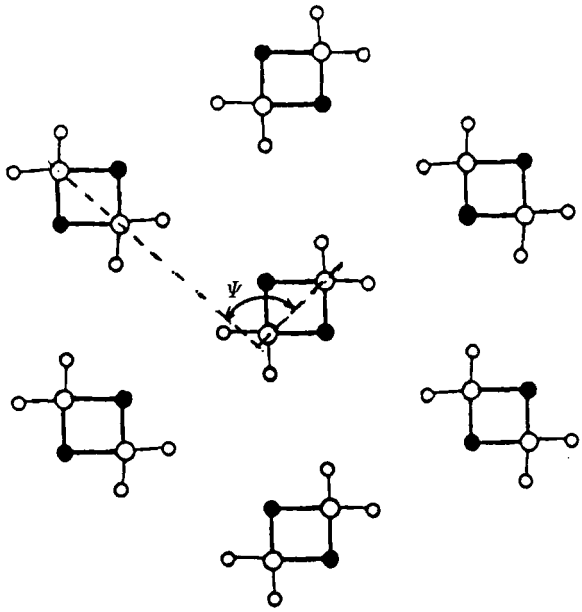


Fig. 12. The relative rotation angle Ψ defined for the model with seven polyoxymethylene chains.

for trigonal polyoxymethylene is unknown. We are concerned with the calculated total energy, ^{13}C shielding and its anisotropy for orthorhombic polyoxymethylene chains (Table 11). In the calculation the values of Ψ and l are 90° and 0.5 pitch, respectively. From the calculation, $\Delta\sigma = 34.29$ ppm was obtained. This is close to the observed value ($\Delta\delta = 42$ ppm). In the previous preliminary calculation on the orthorhombic system[43] the total energy and ^{13}C shielding calculated with respect to Ψ indicate that the most reasonable value for Ψ is 90°, which agrees with the value determined by X-ray diffraction. This gives an approximate indication of the reliability of the "optimum" Ψ value for the trigonal case. The relative interchain "sliding length" l and relative rotation angle Ψ for trigonal polyoxymethylene are unknown. Consequently, the TB calculations are carried out as functions of l and Ψ, and the acceptable values determined. For this purpose, TB calculations were performed for trigonal polyoxymethylene in the two cases $l = 0.5$ (case I) and $l = 0.0$ pitch (case II). In each case the value of Ψ is changed from 0° to 330°, in intervals of 30°. In Table 12 are listed the dependences of the calculated total energy, ^{13}C shielding and tensor components on Ψ for case I. For convenience, Fig. 14 shows the dependence of the calculated ^{13}C shielding on Ψ for the model with seven trigonal polyoxymethylene chains ($l = 0.5$ pitch). As can be seen from this

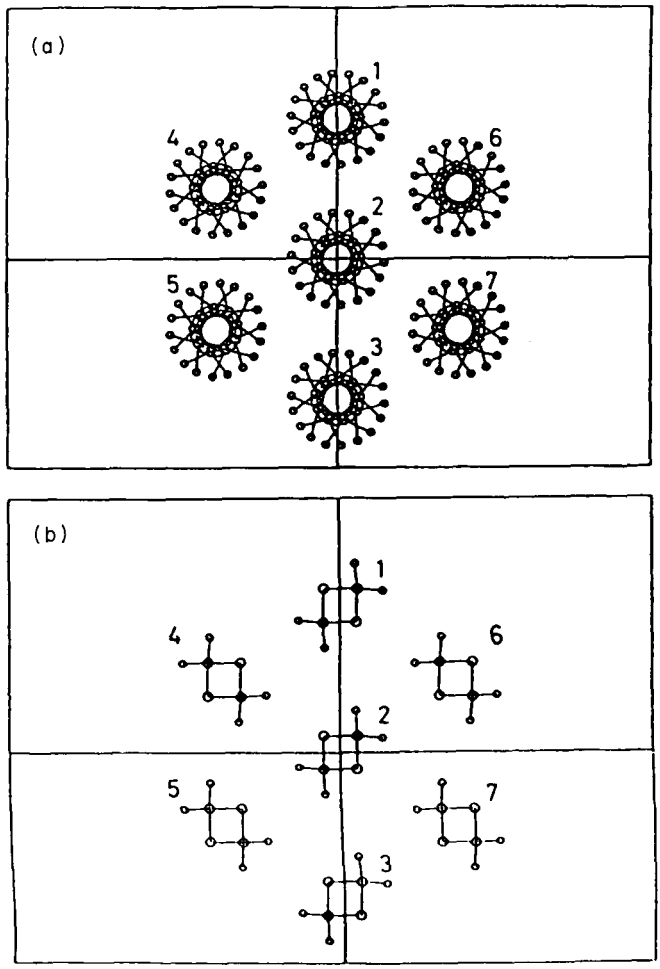


Fig. 13. The crystallographic models for polyoxymethylene used in the ^{13}C shielding calculations: (a) trigonal form; (b) orthorhombic form.

Table 11. The calculated ^{13}C NMR shielding, chemical-shielding tensor, band gap and total energy for the model with seven orthorhombic POM chains.[a]

σ_{iso}	σ_{11}	σ_{22}	σ_{33}	$\Delta\sigma$	Band gap/eV	Total energy/a.u.
		ppm				
−52.390	−126.333	−106.427	−92.042	34.291	16.0695	−182.0702

[a] The negative sign means deshielding.

Table 12. The calculated ^{13}C NMR shielding, chemical-shielding tensor, band gap, and total energy as functions of relative rotation angle for the model with seven trigonal POM chains for case I ($l = 0.5$ pitch).

	Rotation angle Ψ											
	0°	30°	60°	90°	120°	150°	180°	210°	240°	270°	300°	330°
σ_{iso}	−51.04	−53.14	−56.82	−57.67	−60.57	−55.13	−51.39	−52.58	−56.17	−54.15	−53.62	−54.55
σ_{11}	−120.56	−122.66	−123.76	−127.16	−120.14	−124.74	−120.91	−122.41	−126.18	−118.24	−123.43	−123.89
σ_{22} /ppm[a]	−107.30	−109.22	−113.03	−113.85	−116.41	−111.10	−107.56	−108.32	−111.77	−109.62	−110.02	−110.96
σ_{33}	−93.42	−95.42	−101.43	−99.76	−112.84	−97.25	−93.58	−95.05	−98.62	−102.63	−95.35	−96.61
$\Delta\sigma$	27.14	27.24	22.32	27.41	7.30	27.49	27.33	27.36	27.56	15.61	28.07	27.28
Band gap/eV	15.853	15.861	15.892	15.721	15.780	16.033	15.780	15.800	15.699	15.481	15.298	15.809
Total energy/a.u.	−182.689	−182.632	−182.558	−182.615	−182.674	−182.634	−182.621	−182.578	−182.571	−182.727	−182.720	−182.690

[a] The negative sign means deshielding.

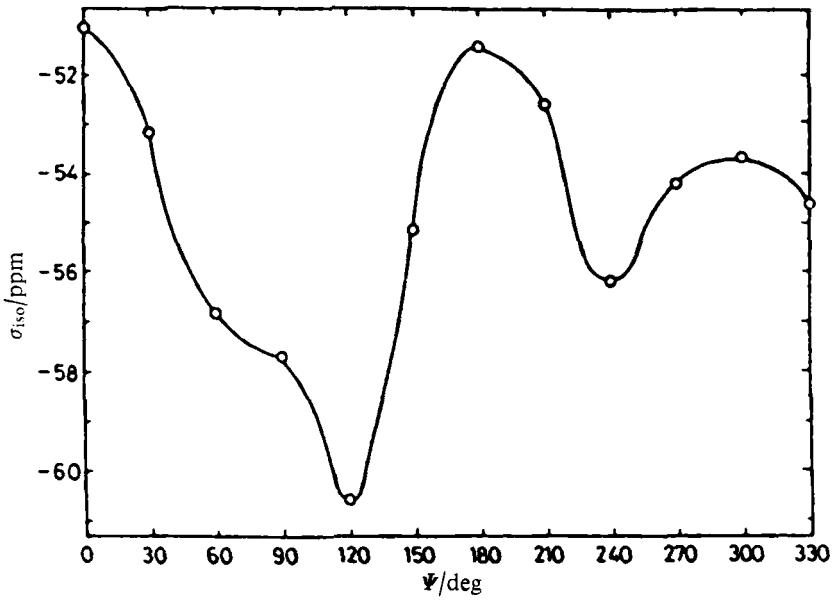


Fig. 14. The dependence of the calculated ^{13}C shielding on the relative rotation angle Ψ for the model with seven trigonal polyoxymethylene chains (case I: $l = 0.5$ pitch).

figure, the calculated ^{13}C shielding decreases as Ψ is increased from 0° to 120°; and as Ψ is increased from 120° to 330°, the shielding increases through the minimum value of Ψ. As described above, the observed ^{13}C shielding for trigonal polyoxymethylene decreases by 2.4 ppm with respect to that for orthorhombic polyoxymethylene. It is therefore expected that the ^{13}C shielding σ_{iso} for trigonal polyoxymethylene should be -54.8 ppm ($= -52.4 - 2.4$). As can be seen from Fig. 14, when values of 150°, 240° and 330° for Ψ are used, we have values close to -54.8 ppm (-55.13 ppm for $\Psi = 150°$, -56.17 ppm for $\Psi = 240°$ and -54.55 ppm for $\Psi = 330°$). This means that the value of Ψ for trigonal polyoxymethylene should be 150° and/or 240° and/or 330°. Table 13 shows the dependences of the calculated differences in the ^{13}C shielding tensors between the trigonal and orthorhombic polyoxymethylene chains on Ψ for case I. As can be seen from this table, the calculated order of the principal values for the ^{13}C tensor is in agreement with the observed one except for $\Psi = 0°$ and 180°. We are also concerned with the Ψ dependence of the calculated ^{13}C shielding tensor. As can be seen from Table 13, the values of the averaged least-squares deviation α at $\Psi = 150°$ and 240° are considerably smaller than those at other values of Ψ. However, the value of α at $\Psi = 330°$ is

Table 13. The calculated ^{13}C NMR shielding, chemical-shielding tensor, band gap, and total energy difference and averaged least-squares deviation as functions of the relative rotation angle for the model with seven trigonal POM chains for case I ($l = 0.5$ pitch).

	Rotation angle Ψ											
	0°	30°	60°	90°	120°	150°	180°	210°	240°	270°	300°	330°
$\Delta\sigma_{iso}$	−1.35	0.75	4.43	6.90	8.18	2.74	1.00	0.19	3.78	1.76	1.23	2.17
$\Delta\sigma_{11}$	−5.77	−3.68	−2.58	−1.68	−6.19	−1.60	−5.42	−3.93	−0.15	−8.10	−2.91	−2.44
$\Delta\sigma_{22}$ /ppm[a]	0.87	2.79	6.60	9.57	9.98	4.73	1.14	1.89	5.34	3.20	3.59	4.53
$\Delta\sigma_{33}$	1.38	3.37	9.39	12.94	20.80	5.20	1.54	3.01	6.58	10.59	3.31	4.57
$\Delta(\Delta\sigma)$	7.15	7.05	11.97	14.62	26.99	6.80	6.96	6.94	6.73	18.69	6.22	7.01
Band gap/eV	0.216	0.208	0.178	0.297	0.290	0.036	0.289	0.269	0.370	0.589	0.772	0.260
Total energy/a.u.	0.619	0.562	0.488	0.537	0.604	0.564	0.551	0.508	0.501	0.657	0.650	0.620
α[b]	4.214	2.484	3.096	5.431	11.811	1.137	3.974	2.853	0.892	6.574	2.201	1.564

[a] Δ : orthorhombic–trigonal.

[b] Averaged least-square deviation.

larger than these values at $\Psi = 150^\circ$ and 240°. From the above results for the shielding tensor, we can take the value of Ψ for trigonal polyoxymethylene as 150° and/or 240°. Further, judging from the total energies at $\Psi = 150^\circ$ and 240° (Table 12), it may be said that the arrangement for the trigonal polyoxymethylene chains at the former angle is slightly more stable than that at the latter angle. From these results, we may adopt $\Psi = 150^\circ$ as the arrangement for trigonal polyoxymethylene.

We now turn to case II ($l = 0.0$ pitch) in the seven-chain model. In this case, any oxygen atom in a specified chain (e.g. chains number 1, 2 and 3 in Fig. 13) and oxygen atoms in the other chains (chains number 4, ..., 7) are in the same plane, which is perpendicular to the helical axis. Figure 15 shows the relationship between the relative rotation angle Ψ and the ^{13}C shielding. At $\Psi = 120^\circ$ α takes the smallest value (1.655), but this value is larger than the value at $l = 0.5$ pitch and $\Psi = 150^\circ$. The calculation for the model with $l = 0.0$ pitch is not in good agreement with the observed data. However, in this calculation, only the relative stability for polyoxymethylene chains is explained reasonably well. This result shows that the ^{13}C shielding is more sensitive to a change in the structure compared with the total energy. From these results, it can be said that the model with $\Psi = 150^\circ$ and $l = 0.5$ pitch is in agreement with the crystal structure of trigonal polyoxymethylenes and can reproduce reasonably the observed data.

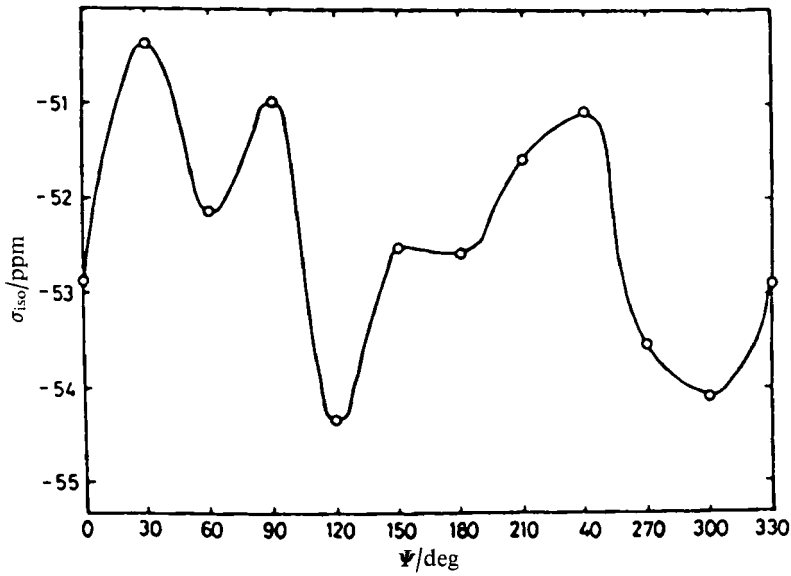


Fig. 15. The dependence of the calculated ^{13}C shielding on relative rotation angle Ψ for the model with seven trigonal polyoxymethylene chains (case II: $l = 0.0$ pitch).

Before discussing the results of the multichain-models calculation for polyacetylene (PA)[48], we compare the calculated ^{13}C NMR shielding of the single-chain model made using Teramae's geometrical parameters[44] with the observed shielding. As shown in Table 14, the calculated isotropic shielding (σ_{iso}) of *trans*-PA is smaller than that of *cis*-PA. This result agrees with that calculated previously using different geometrical parameters,[15] and qualitatively reproduces the experimental data. The difference in σ_{iso} between the *cis* and *trans* PA isomers is about 0.7 ppm, but this is very small when compared with the observed value (about 10 ppm). As for the thermal stability and the band gap, the trend of the calculated results qualitatively explains the observed phenomena that *trans*-PA is thermally more stable and has a higher conductivity than *cis*-PA. A specified polymer chain is locally surrounded by six neighbouring chains in the crystal, and these six chains can be separated into three groups. Each chain group consists of two chains, which are equivalent for the central chain. In the calculations for the seven-chain model the geometrical parameters used are given in Fig. 16. The calculated values depend on the chain arrangement. In addition, for the lattice parameters, various experimentally determined values are reported.[30,45,46] The ϕ values are ambiguous. Thus the values of b and ϕ in the calculation are varied. A small decrease from the original crystal-lattice values determined by X-ray methods leads to energetically stable results in the calculations for both PA isomers (Fig. 17). This comes from the fact that the CNDO/2 method slightly underestimates the interaction distances, as is already known.[47] However, the extreme decrease in the interchain distance leads to a large instability. Therefore, when comparing the *cis* and *trans* PA isomers, it might be appropriate to consider the arrangement with a somewhat shorter distance. With respect to the band gap, the smaller the b values are, the smaller the band gap values become. The decrease of the lattice parameters in the calculation corresponds to the PA system under high pressure, where a shrinkage of the interchain distance

Table 14. The calculated total energy, band gap and isotropic ^{13}C NMR shielding in the single-PA-chain model compared with the observed data.

	Total energy/a.u.	Band gap/a.u.	^{13}C NMR shielding/ppm	
			Calculated[a]	Observed[b]
cis	−28.4634	0.3275	−89.3	127.3
trans	−28.4644	0.3196	−90.0	137.3

[a] The negative sign means deshielding.
[b] From TMS. The positive sign means deshielding.

occurs. It is therefore suggested that the electronic conductivity of PA samples will increase with an increase in pressure. Comparing the isomers, the band-gap value of *trans*-PA is smaller than that of the *cis* form. This explains the experimental observation that *trans*-PA has a higher conductivity than *cis*-PA. The calculated values are very large for the arrangement given by the original lattice parameters. The arrangement with the small value of *b* is near to the form in the real crystal. It has been shown experimentally that the lattice parameters *a* and *b* for *cis*-PA are larger than those for *trans*-PA (Fig. 16); that is, the interchain distance of *cis*-PA is longer than that of *trans*-PA. This may be due to the different shapes of both of the PA chains. In the comb-like *cis*-PA chains some of the hydrogen and carbon atoms tend to be very close together, and so they become repulsive (in fact, the nearest-neighbour C–H distance between the

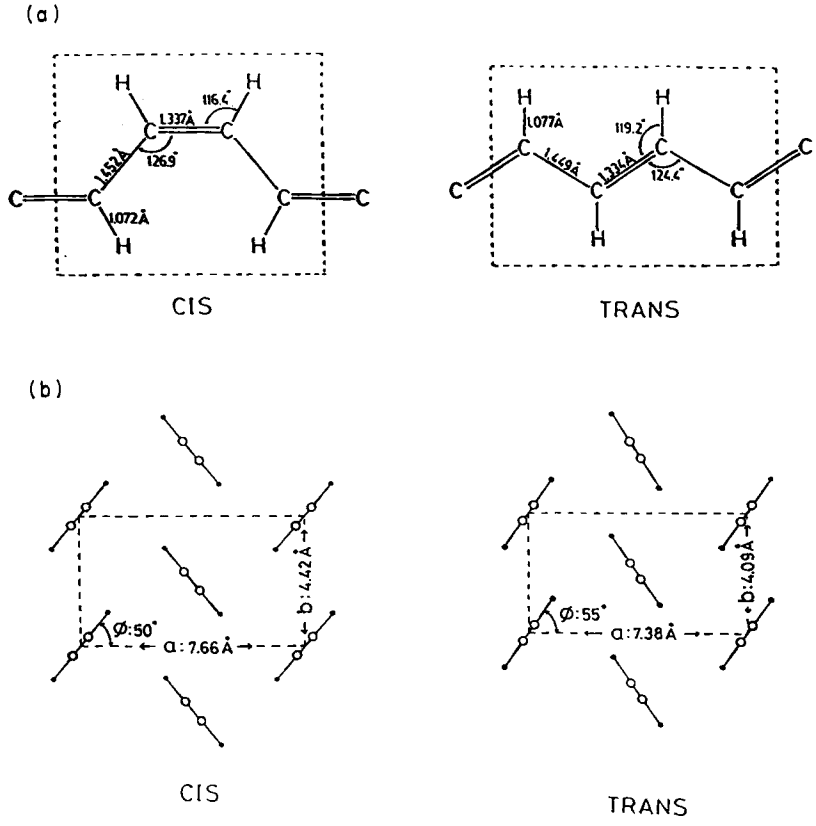


Fig. 16. Geometrical parameters of *cis*- and *trans*-polyacetylenes: (a) valence geometries; (b) lattice parameters.

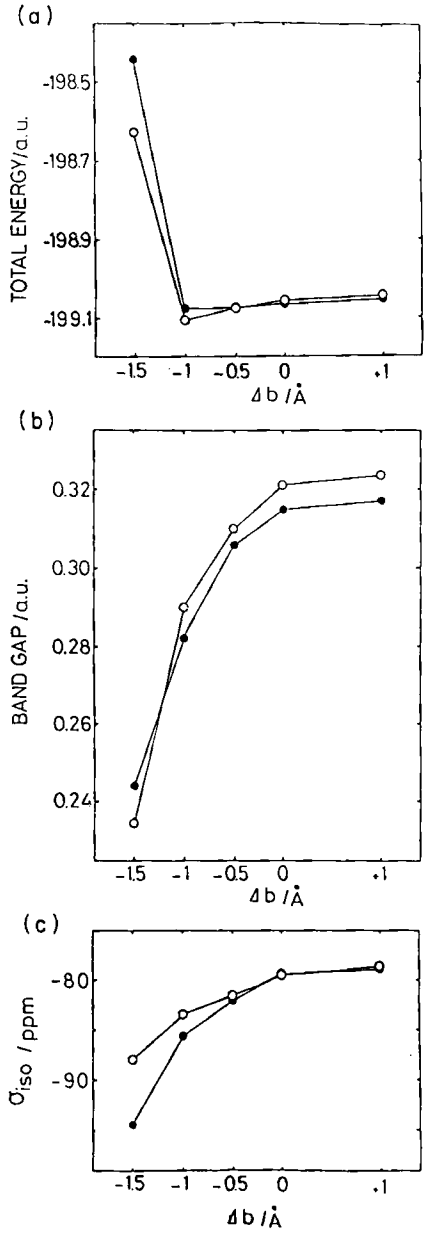


Fig. 17. The dependence on b of the calculated total energy (a), band gap (b) and isotropic ^{13}C shielding (c) of PA chains in the seven-chain model at $\Delta\phi = 0°$: ○, *cis*; ●, *trans*.

chains in *cis*-PA is shorter than that in *trans*-PA in the original geometries). Therefore the *cis*-PA crystal becomes more stable in the arrangement with the larger lattice parameters than does the *trans*-PA crystal, and these long interchain distances lead to the large band gap and so to a small conductivity for *cis*-PA.

In the arrangement with the original lattice parameters the calculated values of σ_{iso} do not reproduce the observed large difference between the two isomers. However, in the arrangement with short interchain distances the calculations agree well with the experiments. With regard to the shielding tensors, not only σ_{33} but also the components σ_{11} and σ_{22} decrease as the interchain distance is decreased (Fig. 18). The most variable component for a change of the interchain distance is σ_{22}, whose direction is along the direction of the molecular chain. The effect of the interchain interactions might appear strongly in this direction. At $\Delta b = -1$ Å, the difference in σ_{22} between the isomers quantitatively agrees with the experimental data. Figure 19 shows the dependence of the ^{13}C shieldings on the "setting angle" ϕ. It is supposed that at the small value of Δb the ϕ dependence is large. In fact, the conformational energy depends strongly on ϕ at $\Delta b = -1$ Å and it is indicated that the original value of ϕ is the appropriate value. However, with respect to the nuclear shielding, the ϕ dependence hardly appears, even at $\Delta b = -1$ Å. It is speculated that the central chain exists in the averaged field produced by the overlap of the interchain interactions among all of the chains. This is supported by the fact that the calculated shieldings of all of the surrounding chains become almost equal, and close to that of the central chain. From the above-mentioned results, it can be said that, although PA chains interact strongly with each other, the overlap of the interactions might produce an averaged field in the crystal.

Finally, we consider the interchain interaction of the ^{13}C shielding in polypeptides. Polyglycine has a hydrogen bond in both forms I and II. Form I has an antiparallel β-sheet structure, and each chain has a hydrogen bond with both sides of the chains in the sheet. Form II has a α_1-helix structure, and each chain is intermolecularly hydrogen-bonded to six surrounding chains. Therefore it is important to investigate the effects of hydrogen bonding on the ^{13}C shielding. A TB MO calculation of the ^{13}C shielding of polyglycine for forms I and II, considering the effect of the hydrogen bond, has been carried out.[17] The TB MO calculation of the ^{13}C shielding was performed as a function of the distance between the oxygen atom and the hydrogen atom bonded to the nitrogen atom, in order to evaluate the influence of the hydrogen bond on the shielding. The calculation for form II was carried out in a similar manner. Figure 20(a) shows the R dependence of the shielding of the carbonyl carbons for forms I and II. In

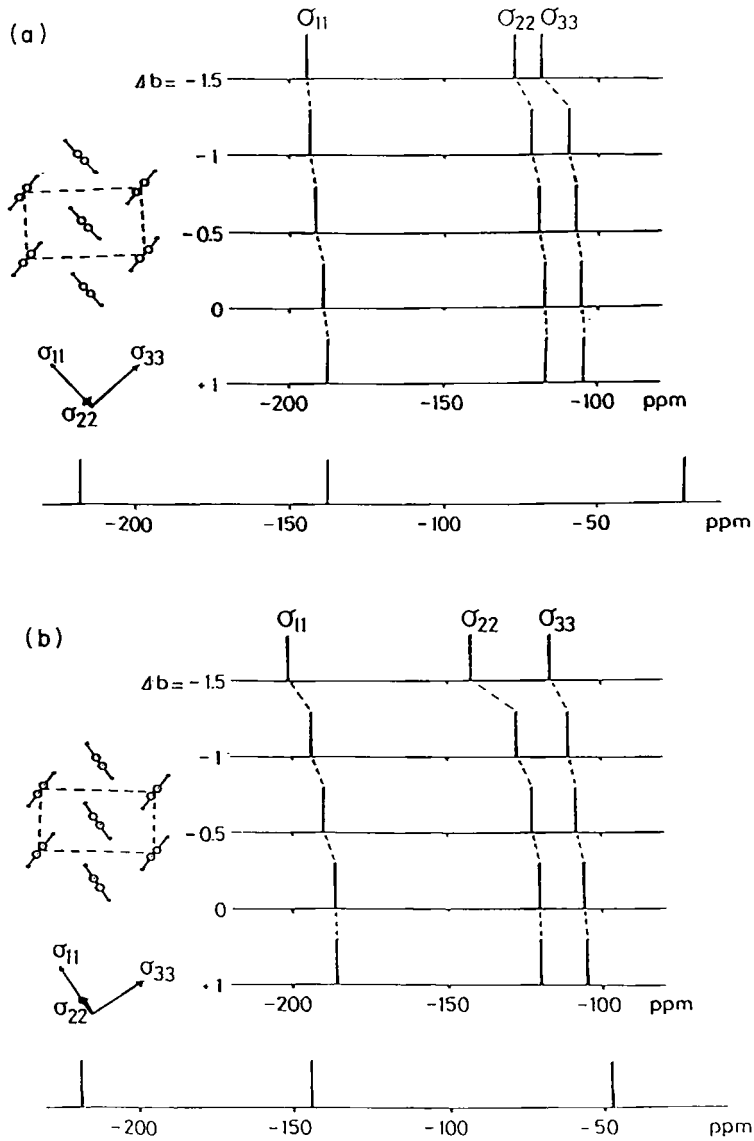


Fig. 18. The dependence on b of the calculated shielding tensors of the central PA chain in the seven-chain model at $\Delta\phi = 0^\circ$. The observed values are indicated at the bottom, and the left-hand-side arrows indicate the directions of the calculated principal axes. (a) *cis*; (b) *trans*.

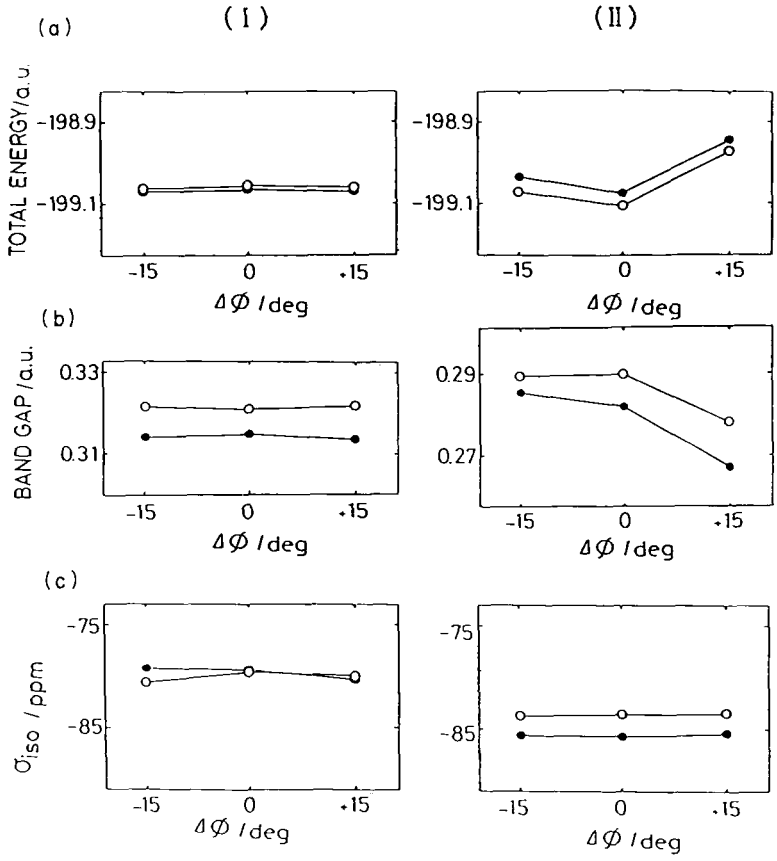


Fig. 19. The dependence on ϕ of the calculated total energy (a), band gap (b) and isotropic ^{13}C shielding (c) of PA chains in the seven-chain model PA at (I) $\Delta b = 0$ and (II), $\Delta b = -1$ Å: ○, *cis*; •, *trans*.

the case of form I the carbonyl shielding decreases as R increases from 2 Å to 3.2 Å, and increases as R increases beyond 3.2 Å. In the case of form II the carbonyl shielding decreases as R increases. Comparing this with the results for an isolated polymer chain, the carbonyl ^{13}C shieldings for both forms I and II generally appear to be small. This means that the carbonyl-shielding decrease is due to hydrogen bonding. At the minimum-energy position ($R = 2.5$ and 2.0 Å for forms I and II respectively), the carbonyl shieldings of forms I and II are -274.9 and -286.2 ppm respectively (Fig. 20a). Thus the carbonyl shielding for form I is larger than that for form II, which is again consistent with the experimental finding. Figure 20(b) shows the R dependence of the methylene ^{13}C shielding, which is much smaller

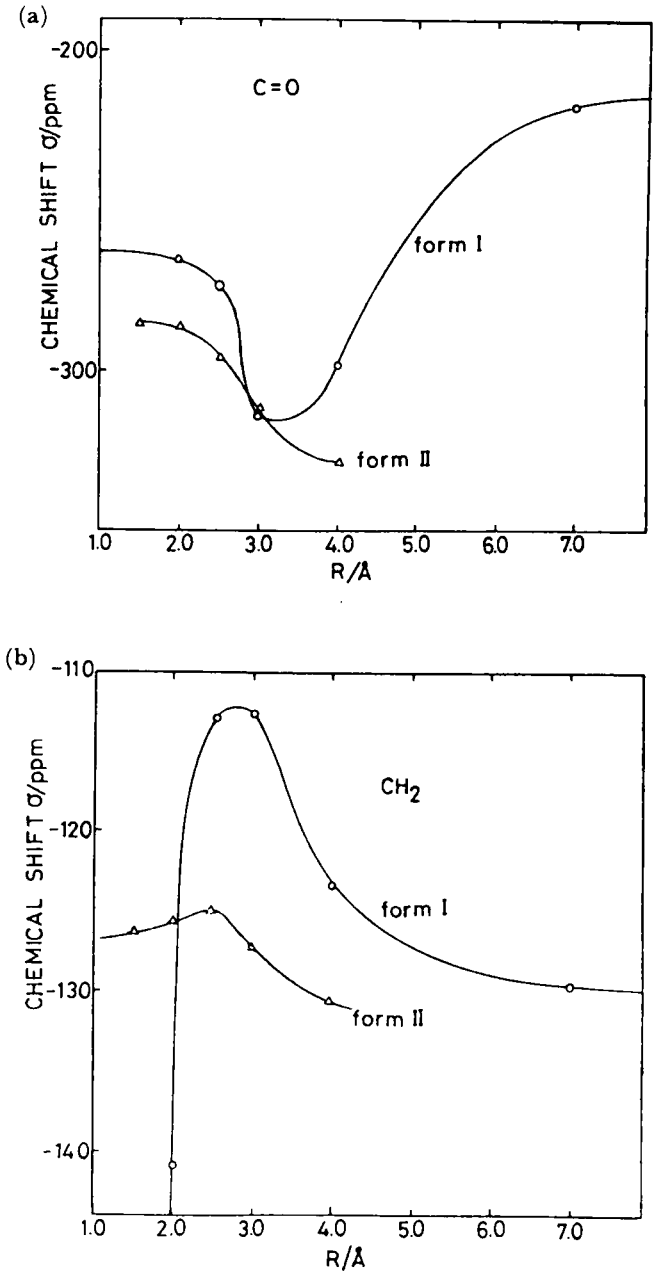


Fig. 20. The R dependence of the calculated ^{13}C shielding of the carbonyl carbon (a) and methylene carbon (b) in polyglycine: ○, form I; △, form II.

than that of the carbonyl carbon. In particular, the R dependence of the methylene shielding for form II is very small. This may be due to the fact that the carbonyl carbon is directly involved in the hydrogen bonding, but the methylene carbon is not. In the case of form I the methylene shielding increases as R increases from 2 Å to 2.8 Å and decreases as R increases beyond 2.8 Å. In the case of form II the ^{13}C shielding is similar to that of form I, but the magnitude of the change is much smaller in comparison with that for form I. At the minimum-energy position the ^{13}C shieldings of the methylene carbons for forms I and II are -112.9 and -126.0 ppm respectively. Therefore it appears that the difference in ^{13}C shielding of the methylene carbon between forms I and II is greatly overemphasized in the calculation since the experimental ^{13}C shielding of the methylene carbon for form I is almost the same as that in form II. The ^{13}C shielding of the methylene carbon for form I changes considerably in the vicinity of the energy-minimum position, especially in the range of R between 2.0 Å and 2.5 Å. This indicates that the electronic structure of form I changes considerably in this region. As shown in Fig. 20(b), the shielding of the methylene carbon for form I decreases as R decreases from its value at the energy minimum, and at about 2.3 Å it becomes almost equal to the shielding of the methylene carbon in form II. At this value of R the shielding of the carbonyl carbon for form I is larger than that for form II. This result coincides with observation. It is plausible that the R value obtained from energy minimization of the two chains might be slightly modified by taking into account many chains in the solid state. Thus, by considering the hydrogen bond, we can explain the behaviour of the ^{13}C shielding of forms I and II reasonably well.

In the above calculation (Section 3.2) for the α_R-helix and α_L-helix forms of poly(L-alanine) the O(=C) and H(–N) atoms making the hydrogen bond are included without difficulty. In the β-sheet form, where the hydrogen bonds are formed between chains, the ^{13}C shielding for the β-sheet form is calculated by taking into account the hydrogen bonds in a similar manner to that of polyglycine. Figures 21(a), (b) and (c) show the R dependences of the shieldings of the C_α, C_β and carbonyl carbons respectively. It can be seen that the shieldings of the C_α and C_β carbons increase as R increases from 2.0 Å to 3.6 Å and decrease as R increases beyond 3.6 Å. However, in the case of the carbonyl carbon the shielding decreases as R increases from 2 Å to 3.7 Å and then increases as R increases beyond 3.7 Å. The carbonyl-carbon shielding shows the largest R dependence. This result agrees with the result for polyglycine. The carbonyl carbon is bonded directly to the oxygen atom through a double bond, and a transfer of electrons from the carbon to the more electronegative oxygen probably occurs.

At the energy minimum ($R = 2.75$ Å) the shieldings of the C_α, C_β and

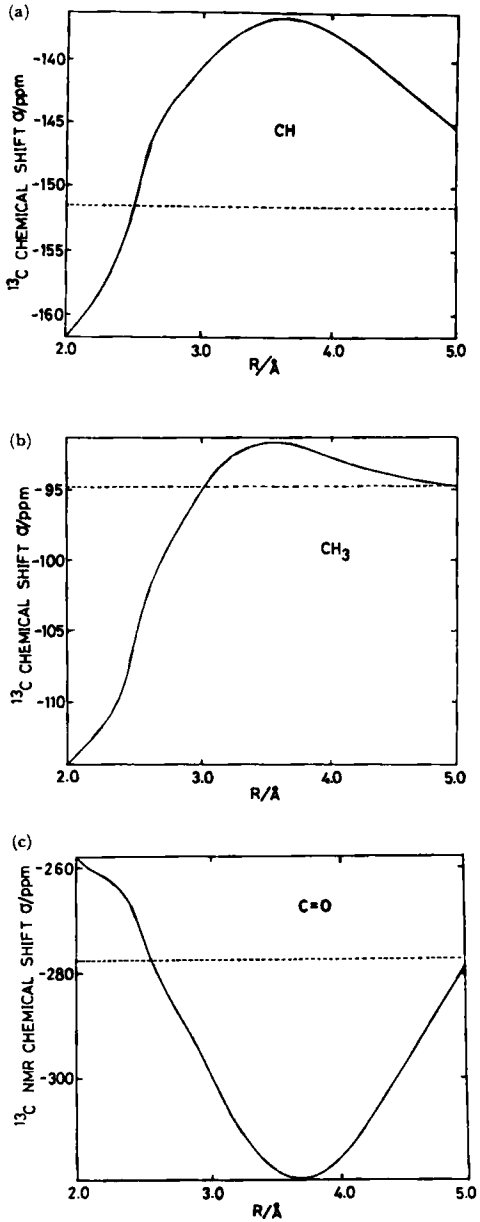


Fig. 21. The R dependence of the calculated ^{13}C shielding of poly(L-alanine) in the β-sheet. The solid line is for two hydrogen-bonded β-sheet chains. The dashed line indicates the ^{13}C shielding value for an isolated α-helix chain. (a) C_α; (b) C_β; (c) C=O.

carbonyl carbons are −144.5, −99.3 and −287.0 ppm respectively, as can be seen from Fig. 21. These values of the C_α, C_β and carbonyl carbon for the β-sheet form are respectively larger (7.0 ppm), smaller (−4.5 ppm) and smaller (−8.9 ppm) than the shielding values of the α_R-helix form (Table 8). Experimentally, however, the shieldings of the C_α, C_β and carbonyl carbon for the β-sheet form are respectively larger (4.2 ppm), smaller (−5.0 ppm) and larger (4.6 ppm) than those for the α_R-helix. Therefore it is shown that the calculated shielding for the carbonyl carbon at the minimum energy is not consistent with the experimental results, although the C_α and C_β shieldings are reproduced well. This is probably due to the fact that the carbonyl shielding is extremely sensitive to the hydrogen-bond distance R. Another possibility is that the R value determined by the energy minimum should be slightly modified when more than two chains are hydrogen-bonded in the real sheet form. It is therefore worthwhile to examine the R value that reproduces the experimental data instead of the R value at the energy minimum. For this, the ^{13}C shielding value for the α_R-form is indicated by the dashed line in Fig. 21. (The solid line indicates the ^{13}C shielding for the β-sheet form.) For the C_α, C_β and carbonyl carbons both the lines intersect at $R = 2.5$, 3.0 and 2.56 Å respectively. Accordingly, the approximate value of R at which the calculated results match the experimental result falls in the range of 2.5–2.56 Å. This range is still greater than the length of the hydrogen bond determined from X-ray diffraction. Such an argument, however, arises from the use of an inadequate wavefunction such as that employed in the extended Hückel MO approximation. It is likely that this sort of problem might easily be resolved when more accurate wavefunctions, such as those used in CNDO, INDO or non-empirical theories, are employed.

4. CONCLUSIONS

The present review shows that tight-binding MO calculations offer useful perspectives in interpreting the results of NMR nuclear shieldings in polymers, both in terms of the structure in the solid state and in understanding the effect of interchain interactions on nuclear shieldings. The latter are shown to operate through the electronic structures of the molecules considered. It is to be hoped that the examples chosen and the data presented serve to indicate some of the possible applications of the techniques described herein.

REFERENCES

1. I. Ando and T. Asakura, in *Annual Reports on NMR Spectroscopy*, Vol. 10A (ed. G.A. Webb), p. 81. Academic Press, London, 1980.

2. *Specialist Periodical Reports on NMR*, Vol. 18 (ed. G.A. Webb). Royal Society of Chemistry, London, 1989.
3. K.A.K. Ebraheem and G.A. Webb, *Prog. NMR Spectrosc.*, 1978, **11**, 149.
4. I. Ando and H. Saitô in *Annual Reports on NMR Spectroscopy*, Vol. 21 (ed. G.A. Webb), p. 209. Academic Press, London, 1989.
5. I. Ando and G.A. Webb, *Theory of NMR Parameters*. Academic Press, London, 1983.
6. H. Fukui, *Magn. Reson. Rev.*, 1987, **11**, 205.
7. D.B. Chesnut, in *Annual Reports on NMR Spectroscopy*, Vol. 21 (ed. G.A. Webb), p. 51. Academic Press, London, 1989.
8. *Electronic Structure of Polymers and Molecular Crystals* (ed. J.M. Andre and J. Ladik). Plenum Press, New York, 1974.
9. *Quantum Theory of Polymers* (ed. J.M. Andre, J. Delhalle and J. Ladik). Reidel, Dordrecht, 1978.
10. *Recent Advances in the Quantum Theory of Polymers* (ed. J.M. Andre, J.L. Bredas, J. Delhalle, J. Ladik, G. Leroy and C. Moser). Lecture Notes in Physics, Vol. 113. Springer-Verlag, Berlin, 1980.
11. *Quantum Chemistry of Polymers; Solid State Aspects* (ed. J. Ladik, J.M. Andre and M. See). Reidel, Dordrecht, 1984.
12. F. Bloch, *Z. Phys.*, 1928, **52**, 555.
13. T. Yamanobe, R. Chujo and I. Ando, *Mol. Phys.*, 1983, **50**, 123.
14. T. Yamanobe, I. Ando, H. Saitô, R. Tabeta, A. Shoji and T. Ozaki, *Chem. Phys.*, 1985, **99**, 259.
15. T. Yamanobe and I. Ando, *J. Chem. Phys.*, 1985, **83**, 3154.
16. T. Yamanobe, T. Sorita, T. Komoto, I. Ando and H. Sato, *J. Mol. Struct.*, 1985, **131**, 267.
17. T. Yamanobe, I. Ando, H. Saitô, R. Tabeta, A. Shoji and T. Ozaki, *Bull. Chem. Soc. Jpn*, 1985, **58**, 23.
18. J.A. Pople, *J. Chem. Phys.*, 1962, **37**, 53.
19. J.A. Pople, *J. Chem. Phys.*, 1962, **37**, 60.
20. T. Yamanobe, I. Ando and G.A. Webb, *J. Mol. Struct.*, 1987, **151**, 191.
21. D.L. VanderHart, *J. Chem. Phys.*, 1976, **64**, 830.
22. S.J. Opella and J.S. Waugh, *J. Chem. Phys.*, 1977, **66**, 4919.
23. M. Kondo, I. Ando, R. Chujo and A. Nishioka, *J. Magn. Reson.*, 1976, **24**, 315.
24. H. Tadokoro, M. Kobayashi, Y. Kawaguchi, A. Kobayashi and S. Murashashi, *J. Chem. Phys.*, 1963, **38**, 703.
25. H. Kurosu, T. Yamanobe, T. Komoto and I. Ando, *Chem. Phys.*, 1987, **116**, 391.
26. T. Ito, H. Shirakawa and S. Ikeda, *Polymer J.*, 1973, **4**, 460.
27. C.K. Chiang, C.R. Fincher, Y.W. Park, A.J. Heeger, H. Shirakawa, E.J. Louis, S.C. Gauand and A.G. MacDiarmid, *Phys. Rev. Lett.*, 1977, **39**, 1098.
28. T. Terao, S. Maeda, T. Yamabe, K. Akagi and H. Shirakawa, *Chem. Phys. Lett.*, 1987, **103**, 347.
29. M. Mehring, H. Weber, W. Miiller and G. Wegner, *Solid State Commun.*, 1987, **45**, 1079.
30. R.H. Baughman, S.L. Hsu, G.P. Pez and A.J. Signorelli, *J. Chem. Phys.*, 1978, **68**, 5405.
31. K. Krogh-Jesperson and M. Ratner, *J. Chem. Phys.*, 1966, **44**, 3289.
32. I. Ando, H. Saitô, R. Tabeta, A. Shoji and T. Ozaki, *Macromolecules*, 1984, **17**, 457.
33. H. Saitô, R. Tabeta, A. Shoji, T. Ozaki and I. Ando, 1983, **16**, 1050.
34. H. Kyotani and H. Kanetsuna, *J. Polym. Sci.*, 1972, **10**, 1932.
35. I. Ando, T. Ozaki and A. Shoji, *Chem. Lett.*, 1987, 1437.
36. D.L. VanderHart, *J. Magn. Reson.*, 1981, **44**, 117.
37. D.L. VanderHart and F. Khoury, *Polymer*, 1984, **25**, 1589.
38. I. Ando, T. Yamanobe, T. Sorita, T. Komoto, H. Sato, K. Deguchi and M. Imanari, *Macromolecules*, 1987, **17**, 1955.

39. I. Ando, T. Yamanobe, S. Akiyama, T. Komoto, H. Sato, T. Fujito, K. Deguchi and M. Imanari, *Solid State Commun.*, 1987, **62**, 785.
40. A. Newman and H. F. Kay, *J. Appl. Phys.*, 1967, **38**, 4105.
41. C.W. Bunn, *Trans. Faraday Soc.*, 1939, **35**, 482.
42. H. Kurosu, T. Yamanobe and I. Ando, *J. Chem. Phys.*, 1988, **89**, 5216.
43. H. Kurosu, T. Komoto and I. Ando, *J. Mol. Struct.*, 1988, **176**, 279.
44. H. Teramae, *J. Chem. Phys.*, 1986, **85**, 990.
45. G. Perego, G. Lugli, U. Pedretti and E. Cernia, *J. Phys., Paris, Colloq.*, 1983, **44 C3**, 93.
46. K. Shimamura, F.E. Karasz, J.A. Hirsch and J.C.W. Chien, *Makromol. Chem. Rapid Commun.*, 1981, **2**, 473.
47. K. Morokuma, *Chem. Phys. Lett.*, 1971, **19**, 129.
48. T. Ishii, H. Kurosu, T. Yamanobe and I. Ando, *J. Chem. Phys.*, 1988, **89**, 7315.

^{207}Pb-NMR Parameters

BERND WRACKMEYER and KLAUS HORCHLER

Laboratorium für Anorganische Chemie der Universität Bayreuth, Postfach 101251, D-8580 Bayreuth, Federal Republic of Germany

1. Introduction 249
2. Experimental 250
   2.1. Referencing 250
   2.2 Techniques for observing ^{207}Pb resonances 251
3. Nuclear spin relaxation 253
4. Chemical shifts δ^{207}Pb 255
   4.1. General 255
   4.2. Patterns of ^{207}Pb chemical shifts 256
5. Indirect nuclear spin–spin coupling constants $^{n}J(^{207}\mathrm{PbX})$ . . 261
   5.1. General 261
   5.2 Pattern of couplings $^{n}J(^{207}\mathrm{PbX})$ 262
6. ^{207}Pb NMR of solids 264
7. Conclusions 266
   Acknowledgements 266
   Tables 267
   References 301

1. INTRODUCTION

The chances of increasing industrial production and widespread application of organolead compounds are rather poor owing to the pressure of environmental problems. However, there is still considerable interest in lead chemistry. Inorganic lead compounds as stabilizers for polymers or as components in glasses, the toxicity of lead chemicals and basic research in organolead chemistry are important topics. We learn as an elementary fact that the chemistry of the heaviest main-group elements differs considerably from that of their lighter congeners, although the theoretical basis for this observation is rarely discussed in detail; in Group IV of the periodic table ^{207}Pb NMR may provide relevant information.

Comparison of the properties of analogous tin and lead compounds is attractive with regard to reactivity and reaction mechanisms as well as to

ANNUAL REPORTS ON NMR SPECTROSCOPY
VOLUME 22 ISBN 0-12-505322-3

Copyright © 1989 Academic Press Limited
All rights of reproduction in any form reserved

physical properties, including of course NMR parameters. In lead chemistry, as in other areas, NMR spectroscopy has become one of the prominent tools for studying lead compounds in solution, and there are already numerous indications that it may also be valuable for studying various classes of solid lead compounds. The advent of multinuclear equipment for PFT NMR spectrometers has been a great influence on the quality and thoroughness of NMR studies, and NMR measurements of nuclei other than ^{1}H or ^{13}C are becoming more popular.

NMR properties of the ^{207}Pb isotope

	Spin	Natural abundance	Magnetogyric ratio γ(rad $s^{-1}T^{-1}$)	$\Xi(^{207}Pb)$, Me_4Pb ($\Xi(^{1}H)$, Me_4Si = 100 MHz)	Receptivity $D^C(^{13}C = 1)$
^{207}Pb	$\frac{1}{2}$	22.6%	5.59×10^7	20 920 597 Hz	11.7

^{207}Pb NMR measurements are easy to perform—at least in liquids—and the results will be the main topic of this review. Section 6 deals briefly with some aspects of solid-state ^{207}Pb NMR without aiming at a complete review since this is a rapidly growing area at present. ^{207}Pb NMR has been reviewed several times;[105,131] however, no comprehensive review on ^{207}Pb NMR parameters (^{207}Pb chemical shifts $\delta^{207}Pb$, indirect nuclear spin–spin coupling constants $^{n}J(^{207}PbX)$ ($n = 1, 2, 3, \ldots$), ^{207}Pb-nuclear relaxation $T_1(^{207}Pb)$, $T_2(^{207}Pb)$) has appeared so far. The present review aims for a complete (literature covered until the end of 1988, and some selected references in 1989) data set of $\delta^{207}Pb$ values, together with references to other nuclei (except ^{1}H) that may have been measured for a particular compound. Listings of many representative $^{n}J(^{207}PbX)$ values are provided and some aspects of ^{207}Pb-nuclear relaxation are discussed.

2. EXPERIMENTAL

2.1. Referencing

One of the first ^{207}Pb NMR studies[104] dealt with solids and the $\delta^{207}Pb$ values were given in gauss relative to metallic lead, for which $\delta^{207}Pb = +11\,125 \pm 25$ relative to Me_4Pb can be calculated. Using modern PFT NMR spectrometers, it is most convenient to define fixed frequencies as a reference for all those nuclei for which an internal reference is not generally available. In the case of ^{207}Pb NMR this is the ^{207}Pb resonance frequency of Me_4Pb (80% in toluene), given as $\Xi(^{207}Pb) = 20\,920\,597$ Hz

(when the ^{1}H resonance of Me_4Si, $\Xi(^{1}H) = 100\,000\,000$ Hz[132]). Therefore the ^{207}Pb reference frequency for any other NMR spectrometer can be calculated once the exact ^{1}H resonance frequency of Me_4Si has been determined for that particular instrument. Further corrections may be required for different lock signals.

Sometimes the ^{207}Pb resonance of an aqueous solution (1 M) of $Pb(NO_3)_2$ is used as an external reference. These data are converted to the Me_4Pb scale by adding 2961 ppm.[33,102] As a consequence of differing procedures for referencing the δ^{207}Pb values for a particular compound, measured under comparable conditions, may vary over a range of several ppm.

2.2. Techniques for observing ^{207}Pb resonances

For most purposes the heteronuclear double-resonance techniques (INDOR) such as $^{1}H-\{^{207}Pb\}$[133] have been replaced by direct observation of ^{207}Pb NMR in the PFT mode (see Fig. 1), with or without ^{1}H-decoupling. Polarization-transfer techniques like INEPT[134] or DEPT[135] can be applied successfully (see Fig. 2) if the relaxation behaviour of the ^{207}Pb nuclei is taken into account (see below).

The large range of ^{207}Pb chemical shifts requires correct setting of the

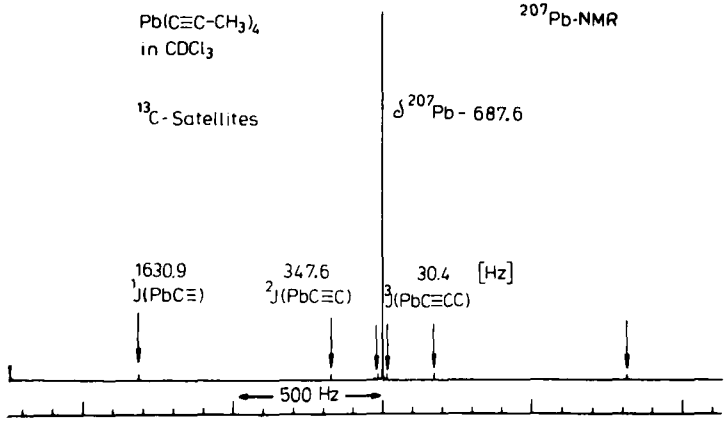


Fig. 1. 41.8 MHz $^{207}Pb-\{^{1}H\}$ NMR spectrum of tetra-1-propynyllead[22] in $CDCl_3$ (5%) in a 10 mm (o.d.) tube at 27°C. The spectrum was recorded within about 45 min by normal techniques in PFT mode using a pulse width of 8 μs (about 40°), a sweep width of 10 Hz and an acquisition time of 1.64 s. The observation of the ^{13}C satellites serves as evidence for the comparatively high sensitivity of the ^{207}Pb nucleus towards the NMR experiment.

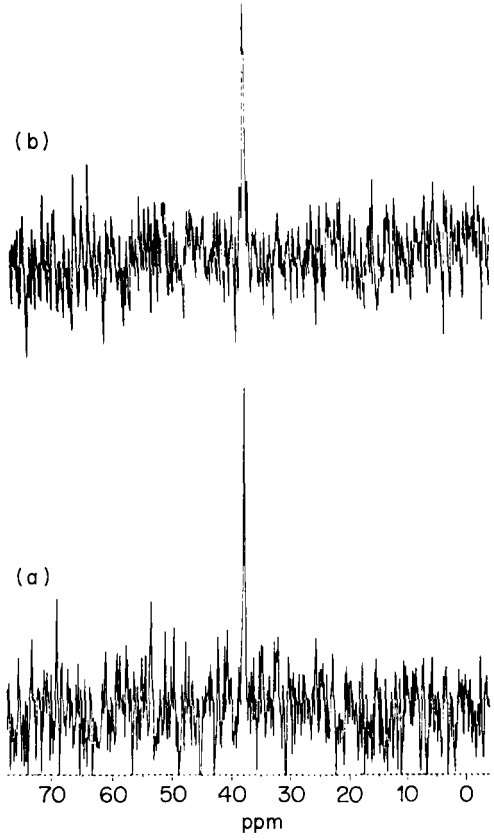


Fig. 2. 62.5 MHz ^{207}Pb NMR specta of a saturated $CDCl_3$ solution of triphenyllead chloride in a 5 mm (o.d.) tube at 27°C.[168] (a) Application of the refocused INEPT pulse sequence[134] with ^{1}H-decoupling (32 scans). (b) Normal observation mode with ^{1}H broadband decoupling (380 scans = the same time consumption as in (a)). The parameters for experiment (a) have not been optimized in order to simulate realistic conditions (spectral width 15 kHz, acquistion time 0.55 s, relaxation delay $D_1 = 6$ s, $D_2 = 0.25/J(\mathrm{PbH}) = 2.77$ ms, $D_3 = 0.0667/J = 0.74$ ms). The longitudinal relaxation time of the protons, $T_1(^1\mathrm{H})$ in Ph_3PbCl is rather long compared with $T_1(^{207}\mathrm{Pb})$, the correct $^3J(^{207}\mathrm{Pb}\,^1\mathrm{H})$ value is 108 Hz and the influence of $^nJ(^1\mathrm{H}\,^1\mathrm{H})$ on D_3 [170] has not been taken into account. The spectrum (b) shows that the normal ^{207}Pb–{^{1}H} measurement is almost equally efficient for samples with unknown NMR parameters. For most lead compounds the ^{207}Pb longitudinal relaxation time $T_1(^{207}\mathrm{Pb})$ is short if $B_0 \geqslant 4.7$ T owing to the contribution of chemical-shift anisotropy (CSA). Therefore a pulse width close to 90° (about 65° was used in (b)) can be applied. These experiments show that the polarization-transfer technique may be superior to normal techniques for ^{207}Pb NMR if the necessary information on the values of $^nJ(^{207}\mathrm{Pb}\,^1\mathrm{H})$ and $T_1(^1\mathrm{H})$ is already available. Otherwise, normal techniques are more readily applied, in particular when high field instruments are used. The linewidth of the ^{207}Pb resonance in (b) is slightly greater than in (a). This is a consequence of the greater temperature gradient in the sample for experiment (b) owing to the effect of normal high-power ^{1}H broadband decoupling.

spectral parameters (sweep width, pulse length), and frequently it is advisable to check whether the ^{207}Pb resonance is real or folded. Typical of heavy nuclei, the δ^{207}Pb values are markedly temperature-dependent, which accounts for some broadening of the ^{207}Pb resonances. Conditions as for ultrahigh-resolution NMR[136] are necessary to observe ^{207}Pb resonances that are close to the linewidth controlled by natural transverse relaxation processes (see below).

Furthermore, it is expected that two-dimensional (2D) NMR techniques will be useful,[137] although little work has been carried out so far in lead chemistry. Shift correlations (e.g. $\delta^{207}\mathrm{Pb}/\delta^{1}\mathrm{H}$) via appropriate 2D ^{207}Pb–{^{1}H} experiments may find some application to problems in organolead chemistry. ^{13}C–^{1}H chemical-shift correlation spectroscopy with proton homonuclear decoupling is useful for the assignment of the ^{207}Pb satellites in complex ^{1}H NMR spectra of organolead compounds and allows for the comparison of the sign of the coupling constants $J(^{207}\mathrm{Pb}^{13}\mathrm{C})$ with $J(^{207}\mathrm{Pb}^{1}\mathrm{H})$.[28] One can also consider reverse 2D ^{1}H-{^{207}Pb} experiments[138] for further improvement of the sensitivity (however, the theoretical factor $[\gamma(^{1}\mathrm{H})/\gamma(^{207}\mathrm{Pb})]^{3} = 104.5$ as compared with conventional detection cannot be achieved so far because of shortcomings inherent to the construction of the probes and because of ^{207}Pb relaxation processes).

3. NUCLEAR SPIN RELAXATION

For "normal" (motional narrowing limit $\omega_0^2\tau_0^2 \ll 1$, where ω_0 is the resonant angular frequency and τ_0 is the correlation time characterizing molecular motions) diamagnetic solutions, intramolecular interactions will be the dominant source of relaxation mechanisms. According to the following equation, there are four different mechanisms[139] contributing to the longitudinal relaxation time T_1:

$$(T_1)^{-1} = (T_1^{\mathrm{DD}})^{-1} + (T_1^{\mathrm{SR}})^{-1} + (T_1^{\mathrm{CSA}})^{-1} + (T_1^{\mathrm{SC}})^{-1}. \qquad (1)$$

The ^{1}H–^{207}Pb dipole–dipole interactions (T_1^{DD}) will be of minor importance owing to the $r_{\mathrm{Pb-H}}^{-6}$ dependence of this term (thus in most cases there is no benefit from the NOE = 2.38 for dominant ^{1}H–^{207}Pb dipolar relaxation). For most practical purposes scalar interactions contributing to T_1 (T_1^{SC}) are unimportant, leaving the spin–rotation interaction (T_1^{SR})[125,173] and the chemical-shift anistropy $\Delta\sigma$ (T_1^{CSA}) as the most important pathways for ^{207}Pb longitudinal relaxation. Spin–rotation interactions are more efficient for smaller molecules and at elevated temperatures, whereas at lower temperature, and particularly at higher magnetic field strengths (B_0^2

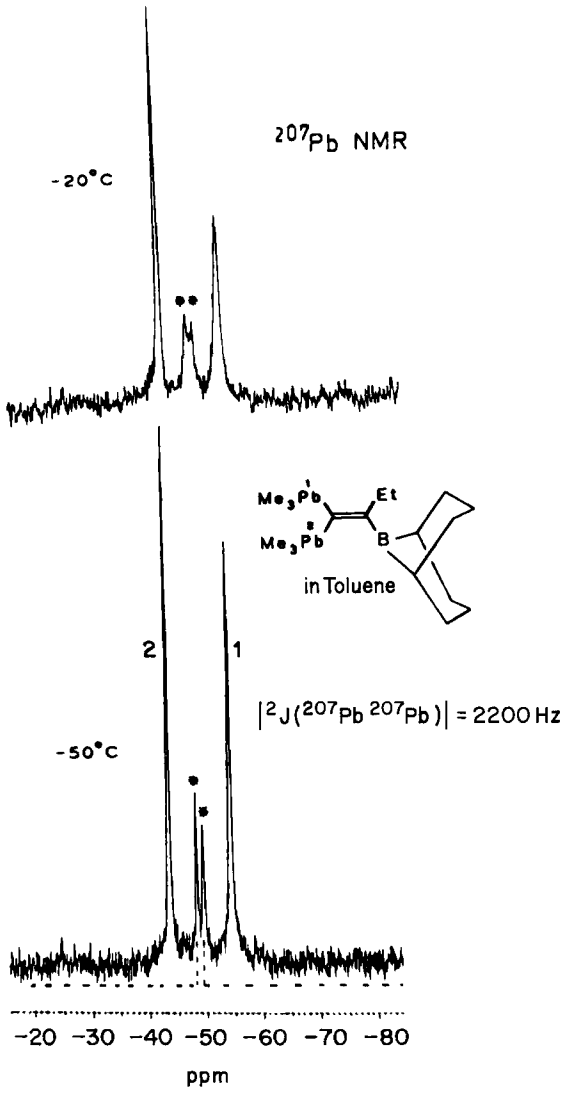


Fig. 3. 41.8 MHz ^{207}Pb–{^{1}H} NMR spectra of 1,1-bis(trimethylplumbyl)-2-(9-borabicyclo[3.3.1]non-9-yl)-1-butene (about 10% in C_7D_8).[168] The isotopomer containing two ^{207}Pb nuclei gives rise to an AB spin system, of which the intense inner lines are visible (*), $^2J(^{207}Pb\,^{207}Pb) = 2200$ Hz. At higher temperatures the ^{207}Pb resonance signals are significantly broadened owing to scalar relaxation of the second kind. Under these conditions, the quadrupolar relaxation rate of the ^{11}B nucleus is too slow for efficient averaging of the scalar coupling $^3J(^{207}Pb\,^{11}B)$; the differential broadening can be used for the assignment of the ^{207}Pb resonances, assuming that $^3J(^{207}Pb\,^{11}B)_{trans} > {}^3J(^{207}Pb\,^{11}B)_{cis}$.

dependence !), relaxation via the CSA mechanism becomes dominant compared with the contribution of spin–rotation. This is shown below for Me_3PbCl.

Longitudinal relaxation times $T_1(^{207}Pb)$ for Me_3PbCl (sat. in CH_2Cl_2/DMSO-d_6)[51]

Temperature (K)	T_1 (2.35T) (s)	Contribution of CSA (%)	T_1 (7.05T) (s)	Contribution of CSA (%)
260	1.60	66.2	0.25	94.6
298	1.36	17.8	0.56	66.0
320	1.14	11.4	0.64	48.9

Within the motional narrowing limit the following relations for the transverse relaxation time T_2 (which determines the natural linewidth $\Delta\nu_{1/2}$; for Lorentzian line shape $\Delta\nu_{1/2} = (\pi T_2)^{-1}$):

$$T_2^{DD} = T_1^{DD}, \quad T_2^{SR} = T_1^{SR}, \quad T_2^{CSA} = \tfrac{6}{7} T_1^{CSA}.$$

T_2^{SC} may be shortened by chemical exchange processes or by scalar relaxation of the second kind (i.e. by scalar interaction with quadrupolar nuclei). Since indirect nuclear spin–spin coupling between ^{207}Pb and other nuclei X can be quite large (see below), the proximity of the ^{207}Pb nucleus to quadrupolar nuclei may lead to rather broad ^{207}Pb resonances,[99] indicating that the quadrupolar relaxation rate is insufficient for complete averaging of the scalar coupling (see Fig. 3). Even in the absence of significant contributions from T_2^{SC}, the influence of CSA relaxation (typical of heavy nuclei[51,139]) may cause markedly broadened ^{207}Pb resonances and it may also hamper the observation of ^{207}Pb satellites in X-NMR spectra for the determination of $^nJ(^{207}PbX)$.

4. CHEMICAL SHIFTS δ^{207}Pb

4.1. General

At present, calculations of the nuclear screening constant $\sigma(A)$ of a heavy nucleus A by a rigorous theoretical treatment are not feasible. The complexity of the molecular terms $\sigma_d(A)$ (diamagnetic term) and (in particular) $\sigma_p(A)$ (paramagnetic term) in Ramsey's non-relativistic approach[140] is by no means reduced in the relativistic treatment[58,141] that is required for heavy nuclei A such as ^{207}Pb. It is possible to extract relativistic terms $\sigma_d(A)$ and $\sigma_p(A)$ that are analogous in their meaning as well as in their trends to

the corresponding non-relativistic terms. This applies to the usual influence of symmetry, charge density, bond order and to the presence of energetically low-lying excited states. The spin–orbit splitting of non-s shells increases the number of ground and excited states, giving rise to additional excitations.

Chemical-shift correlations for nuclei of the same group of the periodic table (e.g. $\delta^{119}Sn/\delta^{29}Si$,[34] $\delta^{119}Sn/\delta^{73}Ge$ [17]) are based on the expectation that the slope of the linear relationship corresponds closely to the ratio of the $\langle r_{np}^{-3}\rangle$ values (e.g. $\langle r_{5p}^{-3}\rangle_{Sn}/\langle r_{3p}^{-3}\rangle_{Si}$), where the terms $\langle r_{np}^{-3}\rangle$ have been calculated on the basis of non-relativistic wave functions.[164] In the case of the $\delta^{207}Pb/\delta^{119}Sn$ correlations for Pb(IV) and Sn(IV) compounds, e.g.

$$\delta^{207}Pb = 2.43\delta^{119}Sn + 34, \tag{2}$$

the slope (2.42 [34]–3.0,[86] depending on the selection of $\delta^{207}Pb$ and $\delta^{119}Sn$ values) is considerably greater than calculated for $\langle r_{6p}^{-3}\rangle_{Pb}/\langle r_{5p}^{-3}\rangle_{Sn}$ (≈ 1.4–1.9). This is reminiscent of similar observations for the linear correlations $\delta^{125}Te/\delta^{77}Se$ [142] and $\delta^{199}Hg/\delta^{111}Cd$.[143] The greater slope may be traced to relativistic contraction of the relevant orbitals of the heavy nuclei. Furthermore, in the case of the correlations $\delta^{207}Pb/\delta^{119}Sn$ it became apparent that many Pb(II) and Sn(II) compounds (lone electron pair on the lead or tin atom) do not fit into the relationship (2). Indeed, there is a second relationship with an even greater slope and a large intercept:[144]

$$\delta^{207}Pb = 3.30\delta^{119}Sn + 2336. \tag{3}$$

Interestingly, $\delta^{207}Pb$ and $\delta^{119}Sn$ values for stannocenes and plumbocenes are predicted approximately equally well by both relationships.[144] The greater slope and the magnitude of the intercept in (3) are related to the influence of the "inert" 6s electron pair at the lead atom and give an idea of the so-called HAHA-effect[4] (*h*eavy *a*tom shift of the *h*eavy *a*tom).

4.2. Patterns of ^{207}Pb chemical shifts

4.2.1. Coordination number

The increase in the lead coordination number (c.n.) from c.n. = 2 to higher c.n.s (e.g. formally to c.n. = 10 in plumbocenes, $(\eta^5\text{-}R_5C_5)_2Pb$) is accompanied by a large increase in ^{207}Pb-nuclear shielding. This can be predicted on grounds of the decreasing imbalance of charge distribution around the ^{207}Pb nucleus. In Fig. 4 a chart of ^{207}Pb values shows typical regions for the various c.n.s. The $\delta^{207}Pb$ values cover a range of about 16 000 ppm and it is interesting to note that $\delta^{207}Pb$ data for Pb(II) compounds

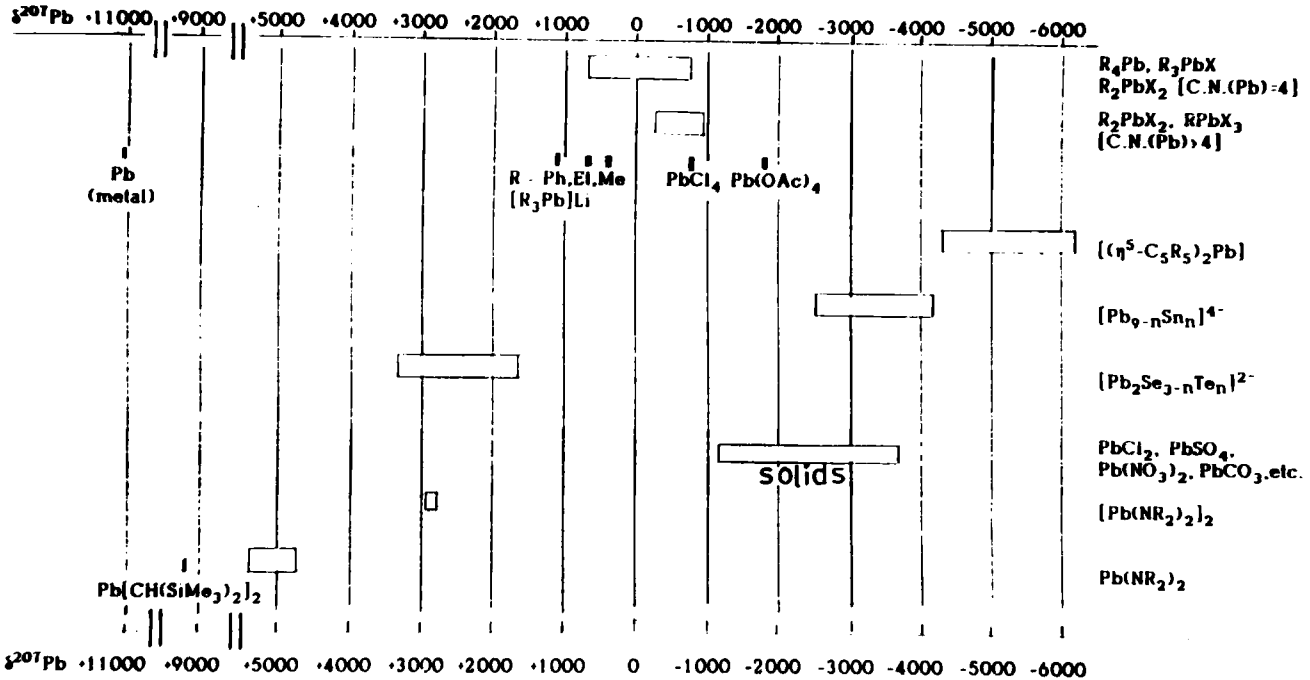


Fig. 4. Chart of ^{207}Pb chemical shifts $\delta^{207}Pb$.

are found at both extreme ends. Except for metallic lead itself (δ^{207}Pb + 11 125 ± 25 [104]), the most-deshielded ^{207}Pb nuclei are observed in the plumbylene [$(Me_3Si)_2CH]_2Pb$,[145] and the ^{207}Pb nuclei become most strongly shielded in plumbocenes such as $(\eta^5\text{-}Ph_5C_5)_2Pb$.[111]

In monomeric plumbylenes R_2Pb (R = alkyl, amino) the Pb $6p_z$ orbital is empty and there is only a small energy gap to the bonding σ-Pb−C states (magnetically active (B_0-induced) $\sigma \rightarrow \pi^*$ charge circulations !) in addition to the presence of the lone 6s-electron pair (magnetically active $n \rightarrow \pi^*$ charge circulations !). In contrast, the LUMO in the plumbocenes is expected to be of fairly high energy with respect to the HOMO, and B_0-induced paramagnetic charge circulations will be of minor importance.

The sensitivity of ^{207}Pb-nuclear shielding to small structural changes is reflected by a marked solvent dependence of δ^{207}Pb values.[33,55,68,70] This sensitivity can also be used for studying strongly and weakly associated species. If the association occurs by increase of the c.n. of the lead atom, a shift of the ^{207}Pb resonance to low frequency will be observed.[27,49] This is an important aspect for the comparison of δ^{207}Pb values from solutions and the solid state (see Section 6).

Other applications concern the determination of dissociation constants (e.g. for Me_3PbCl in H_2O or MeOH[68]) or equilibria involved in aqueous solutions of lead(II) acetate.[33] There are several examples of potential bioinorganic applications of ^{207}Pb NMR. The changes in the ^{207}Pb resonance frequency of an aqueous solution of $Pb(NO_3)_2$ on addition of EDTA (a molar ratio of $[EDTA]/[Pb^{2+}] = 0.16$ induces a high-frequency shift of the ^{207}Pb resonance by about 140 ppm) are remarkable,[44] and it turns out that δ^{207}Pb values for Pb^{2+} ions in aqueous solution are very sensitive to the presence of carboxylic acids or aminocarboxylic acids.[39] Two signals are observed (δ^{207}Pb ≈ −1400, ≈ −2600) in the ^{207}Pb NMR spectra of the product from the reaction between lead(II) acetate and adenosine 5′-triphosphate (ATP).[32]

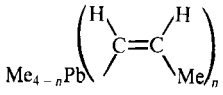
4.2.2. *Substituent effects, multiple substitution, interbond angles at the lead atom and isotope effects*

(a) Lead(IV) *compounds* (Tables 1–8). Organyl groups influence the ^{207}Pb-nuclear shielding in the usual way.

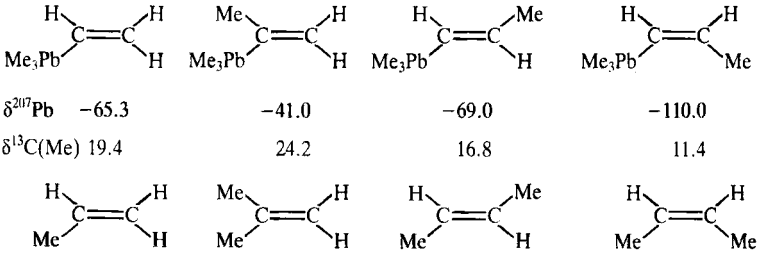
(i) Branching at the β-carbon atoms reduces the shielding whereas chain elongation increases the shielding (γ-carbon atoms are the main contributors):

	$Me_3Pb-CH_2-CH_3$	$Me_3Pb-CH(CH_3)_2$	$Me_3Pb-CH_2CH_2CH_2CH_3$
δ^{207}Pb:	+29.0	+62.0	+16.0

(ii) If the ^{207}Pb nucleus is adjacent to a C=C double bond (aryl or alkenyl group) or to a C≡C triple bond a substantial increase in ^{207}Pb-nuclear shielding is observed:

	$n=1$	2	3	4
$Me_{4-n}PbPh_n$	−38.5	−80.0	−118.9	−179.0
	−110.0	−220.0	−330.0	−440.0
$Me_{4-n}Pb(C\equiv C-Me)_n$	−139.8	−304.7	—	−685.8

(iii) In the series of alkenylplumbanes the influence of the substituents at the C=C double bond in geminal and vicinal (*trans*, *cis*) position with respect to the plumbyl group is strikingly analogous to the effects in ^{13}C NMR (δ^{13}C data from Ref. 165):

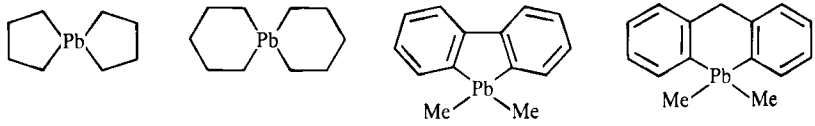


δ^{207}Pb	−65.3	−41.0	−69.0	−110.0
δ^{13}C(Me)	19.4	24.2	16.8	11.4

There is no complete δ^{207}Pb data set available for the series of compounds $R_{4-n}PbX_n$ (X = Cl, Br, I, OR, SR, SeR, NR_2, etc.; $n = 0, \ldots, 4$). In most cases the lead coordination number increases or sufficiently stable and soluble compounds cannot be prepared. Therefore most δ^{207}Pb values refer to $n = 1$ and only few examples have been reported for $n = 2$. These data indicate that substituent effects on the ^{207}Pb resonance frequencies are analogous to those observed for ^{119}Sn-nuclear shielding,[146] although the range of the δ^{207}Pb values is much larger by a factor of 2–3 (e.g. δ^{207}Pb data for compounds of the type $Me_3Pb-NR^1R^2$ are spread between δ^{207}Pb ≈ +350 .... +140, whereas the corresponding range of δ^{119}Sn values is ≈80 ppm[146,155]).

As one would expect, changes of the interbond angles at the lead atom induce large changes in the ^{207}Pb chemical shifts. There are numerous examples in the tables showing that in five-membered cyclic compounds the ^{207}Pb-nuclear shielding is much lower than in corresponding six-membered

rings or non-cyclic compounds. This behaviour is reminiscent of that of the δ^{119}Sn values of analogous tin compounds.[146,161]



δ^{207}Pb +416.3[86] −199.0[86] +0.3[107] −201.4[107]

(b) Lead(II) *compounds* (Tables 10–12). The peculiar electronic structure of monomeric lead(II) compounds[18] is evidenced by the extreme deshielding for the ^{207}Pb nuclei in the derivatives with a carbene-like plumbylene structure (see Section 4.2.1) and the extreme shielding for the plumbocenes. In the former compounds the substitution of two Pb—N bonds by two Pb—C bonds causes a decrease in ^{207}Pb nuclear shielding by >4000 ppm in contrast with fairly small changes found for comparable lead(IV) compounds (see Tables 7 and 8). In the dimeric diaminolead(II) derivatives the ^{207}Pb nuclear shielding increases by about 2000 ppm with respect to the monomers. This can be traced to the vanishing contribution from B_0-induced charge circulation between the σ-bonding framework and the formerly unoccupied Pb $6p_z$ orbital. However, the Pb 6s lone electron pair is still present and the δ^{207}Pb values of the dimers fit into the δ^{207}Pb/δ^{119}Sn relationship for comparable lead(II) and tin(II) compounds (see (3)).

Comparison of δ^{207}Pb values for monomer cyclic and non-cyclic diaminolead(II) compounds (Table 11) shows that the ^{207}Pb-nuclear shielding decreases from the four-membered rings to the five-membered rings and the lowest shielding is observed for the non-cyclic compounds. The latter influence is in contrast with the change of the δ^{207}Pb values for lead(IV) compounds. Therefore it is not advisable to look for a straightforward relationship between δ^{207}Pb data of lead(II) compounds and the interbond angles at the lead atom.

The ^{207}Pb-nuclear shielding of the Pb^{2+} cation depends markedly on the nature of the stabilizing ligand (see Table 10). Coordinative Pb–F–, Pb–O–, Pb–N interactions increase the shielding (F > O > N) in contrast with coordinative Pb–S, Pb–Se or Pb–P interactions (P > S ≈ Se).

(c) Isotope effects. A few organolead(IV) compounds have been studied with respect to the ^{12}C/^{13}C isotope effect on δ^{207}Pb.[22] As for the corresponding tin compounds, it appears that the magnitude and the sign of the isotope effect depend significantly upon the nature of the organyl group.[22]

5. INDIRECT NUCLEAR SPIN–SPIN COUPLINGS, $^{n}J(^{207}\mathrm{PbX})$

5.1. General

Assuming the dominance of the Fermi-contact term, the reduced indirect (electron mediated) spin–spin coupling

$$^{n}K(\mathrm{AB}) = 4\pi^2\ {}^{n}J(\mathrm{AB})(h\gamma_\mathrm{A}\gamma_\mathrm{B})^{-1} \tag{4}$$

can be expressed in the non-relativistic limit[149] as[151]

$$^{1}K(\mathrm{AB}) = -\ \tfrac{4}{9}\mu_0^2\beta^2\psi_\mathrm{A}(0)^2\psi_\mathrm{B}(0)^2\Pi_\mathrm{AB}, \tag{5}$$

where μ_0 and β have their usual meanings, $\psi_\mathrm{A}(0)^2$ is the valence-s electron density at the site of nucleus A and Π_AB is the mutual polarizability:

$$\Pi_\mathrm{AB} = 4 \sum_{i}^{\mathrm{occ}} \sum_{j}^{\mathrm{unocc}} \frac{C_{i\mathrm{A}}C_{j\mathrm{A}}C_{j\mathrm{B}}C_{i\mathrm{B}}}{E_j - E_i}. \tag{6}$$

It turns out that for the heavier elements relativistic effects become important and affect NMR parameters because of the spin–orbit splitting of the non-s shells and (most noticeable for spin–spin coupling) because of the contraction of s and p shells. A relativistic analogue of Ramsey's theory[149] has been developed[152] that combines all terms of coupling mechanisms in one relationship. However, the extraction of a "contact" part proved possible,[58] and for most examples studied it was shown that terms dealing with s densities give rise to dominant contributions to the one-bond couplings.[48,58]

In order to make practical use of these considerations, we compare the reduced coupling constants $^{1}K(^{207}\mathrm{PbX})$ with $^{1}K(^{119}\mathrm{SnX})$ (see Table 13). For large and positive or large and negative ^{1}K values we expect that their ratio differs significantly from that predicted on the basis of the ratio of the valence-s electron densities $\psi_\mathrm{Pb}(0)^2/\psi_\mathrm{Sn}(0)^2$ (≈ 1.5–1.7 [60]), calculated from non-relativistic wavefunctions. Using correction factors as suggested by Breit[153] leads to a ratio of about 3.0, and calculated relativistic s densities[58] for ^{207}Pb and ^{119}Sn nuclei give a ratio of about 3.4. Although these values are close to many experimental data for $K(^{207}\mathrm{PbX})/K(^{119}\mathrm{SnX})$, one should keep in mind that this use of relativistic s densities may just reflect the proportionality of the ^{1}K values for given elements in a qualitative way.

The spin–orbit splitting of the non-s shells may lead to additional contributions of either sign to $^{1}K(^{207}\mathrm{PbX})$. Comparison of $^{1}K(\mathrm{MX})$ data shows that for M = ^{207}Pb the sign of ^{1}K changes more readily than for M = ^{119}Sn. Owing to the existence of a data set for a large number of organotin and organolead compounds, correlations for $^{1}J(\mathrm{M}^{13}\mathrm{C})$ are available (see below)

in which M = ^{207}Pb, ^{119}Sn and the ^{13}C nucleus is part of a methyl group, an alkenyl or an alkynyl group.

5.2. Pattern of couplings $^{n}J(^{207}PbX)$

5.2.1. One-bond couplings $^{1}J(^{207}PbX)$

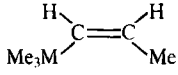
Many $^{1}J(^{207}PbX)$ values are available for X = ^{13}C (see Refs. 4, 5, 12, 22, 45, 46, 50, 53–56, 67, 70, 78, 81, 85, 90, 92, 93, 109, 112, 117, 162, among many!) and there are few data scattered in the literature for X = ^{1}H,[122,157] ^{11}B,[82,94] ^{15}N,[14,61,66,79,94,144,154] ^{77}Se,[94] ^{119}Sn,[94] ^{125}Te,[94] ^{183}W,[171] ^{195}Pt[42] and ^{207}Pb[119]. Representative $^{1}J(^{207}PbX)$ values together with the reduced coupling constants $^{1}K(^{207}PbX)$ (see (4)) and $^{1}J(^{119}SnX)$, $^{1}K(^{119}SnX)$ for corresponding or comparable tin compounds[146] are given in Table 13. There are analogous trends for changes in sign and magnitude for one-bond couplings involving the ^{207}Pb and ^{119}Sn nuclei, respectively. Many effects that are small in the case of ^{119}Sn become large and significant for ^{207}Pb. Examples can be found for X = ^{13}C in the series of alkynyl derivatives, where the magnitude of $^{1}K(^{119}Sn^{13}C{\equiv})$ is somewhat smaller than expected and $^{1}K(^{207}Pb^{13}C{\equiv})$ may even become <0.[55] For methyllead and methyltin compounds the $^{1}J(M^{13}C)$ values give a linear correlation[188]

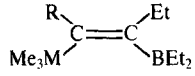
$$^{1}J(^{207}Pb^{13}C_{(Me)}) = -2.26\,^{1}J(^{119}Sn^{13}C_{(Me)}) - 556.6 \quad (r = 0.985), \quad (7)$$

which shows that the sign of $^{1}J(^{207}Pb^{13}C)$ in $[Me_3Pb]^-$ is negative. In the $[Ph_3Sn]^-$ anion the $|^{1}J(^{119}Sn^{13}C)|$ value is smaller than in Ph_4Sn, whereas in $[Ph_3Pb]^-$ the value of $|^{1}J(^{207}Pb^{13}C)|$ is much larger than in Ph_4Pb.[4] On the basis of the relationship[188]

$$^{1}J(^{207}Pb^{13}C_{(C=)}) = -1.79\,^{1}J(^{119}Sn^{13}C_{(C=)}) - 481.5 \quad (r = 0.985), \quad (8)$$

it is suggestive that both $^{1}K(^{119}Sn^{13}C)$ and $^{1}K(^{207}Pb^{13}C)$ are negative in $[Ph_3M]^-$ (M = Sn, Pb). This trend is already apparent from the change in the magnitude of $^{1}J(^{207}Pb^{13}C=)$ in alkenyllead compounds with additional electropositive substituents linked to the C=C double bond:[168]

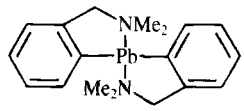




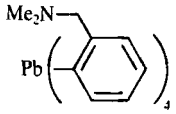
$^{1}J(M^{13}C=)$ (Hz)		R = H	Me	^{t}Bu	Ph	Me_3Si	Me_3Sn	Me_3Pb
M = ^{207}Pb	359.0[54]	434.1	534.6	571.2	436.0	230.7	164.7	120.0
M = ^{119}Sn	465.0[54]	498.0	536.0	545.0	486.1	347.1	344.9	346.3

The magnitude of $^{1}J(^{207}Pb^{13}C)$ in lead(II) compounds suggests that the

sign of this coupling constant is negative. In the case of bis[bis(trimethylsilyl)methyl]lead direct comparison of $^{1}J(^{207}Pb^{13}C)$ and $^{1}J(^{119}Sn^{13}C)$ (see Table 13) supports this argument. In bis[2-(dimethylaminomethyl)phenyl]-lead[50] it has been noted that $^{1}J(^{207}Pb^{13}C)$ is large. In the light of the new data, it is more likely that the influence of the lone electron pair causes sign inversion of $^{1}J(^{207}Pb^{13}C)$ with respect to the Pb(IV) compound rather than there being an increased s character of the Pb—C hybrid orbital.



$^{1}J(^{207}Pb^{13}C)$ (Hz) 1158.0



723.0

The reduced coupling constants $^{1}K(^{207}Pb^{15}N)$ appear to be large and negative in most cases studied, whereas $^{1}K(^{119}Sn^{15}N)$ in tin (IV)–nitrogen compounds can be small and of either sign (see Table 13). In the lead(II) amides large and presumably positive $^{1}J(^{207}Pb^{15}N)$ values ($^{1}K(^{207}Pb^{15}N) < 0$) have been observed.[14,144,154] As for other nuclei with a closed s shell, negative contributions to the Fermi contact term arise owing to the presence of the 6s lone electron pair. Chelate ligands such as 1,4,8,11-tetraazacyclotetradecane (= L)[77] or *trans*-1,2-diaminocyclohexane-*N,N,N'N'*-tetraacetate ion (= cydta^{4-}) have been used for the complexation of the Pb^{2+} ion.[66,77] The distorted structure is shown in the case of $[Pb(L)][NO_3]_2$ by two very different $^{1}J(^{207}Pb^{15}N)$ values:

	$[Pb(cydta)]^{2-}/H_2O$ (0.5 M)	$[Pb(L)][NO_3]_2$/DMSO (0.9 M)
$^{1}J(^{207}Pb^{15}N)$(Hz)	187.5	207.5, 19.8

Since the sign of these coupling constants is unknown, the assignment[66,77] of the small value (19.8 Hz) to coupling between ^{207}Pb and ^{15}N in axial position is rather tentative.

5.2.2. *Geminal couplings* $^{2}J(^{207}PbX)$

There is a wealth of data for $^{2}J(^{207}Pb^{1}H)$ (see Refs. 43, 109, 114, 119–121, 123, 190, among many!), which in most cases are readily obtained from ^{1}H NMR spectra. A number of Me_2Pb derivatives with c.n.(Pb) > 4 have been studied by ^{1}H NMR in various solvents, and $|^{2}J(^{207}Pb^{1}H)|$ values were found to increase with an increase in the donor strength of the solvent.[75,100] The correlation of $^{1}J(^{207}Pb^{13}C)$ and $^{2}J(^{207}Pb^{1}H)$ for MePb groups yields a crude linear relationship, reminiscent of the corresponding relationship for methyltin compounds:[159]

$$^{1}J(^{207}Pb^{13}C_{(Me)}) = -8.2\ ^{2}J(^{207}Pb^{1}H_{(Me)}) - 268.9 \quad (r = 0.988). \qquad (9)$$

A series of geminal coupling constants $^2J(^{207}PbX)$ across an olefinic carbon atom in alkenylplumbanes has been determined[5] (Table 15). There are some transition-metal complexes with plumbyl groups as ligands in *cis* or *trans* position relative to a phosphine ligand (Table 15). As for other geminal couplings across a transition metal, it is found that $|^2J(^{207}Pb\,^{31}P)_{trans}| \gg |^2J(^{207}Pb\,^{31}P)_{cis}|$.

5.2.3. *Vicinal coupling constants* $^3J(^{207}PbX)$

Few vicinal coupling constants $^3J(^{207}Pb\,^1H)$ have been measured for ethyllead[110,114,190] and vinyllead compounds[11,54,118,190] (see Table 14). The trends are fully in agreement with those observed for corresponding tin compounds, for which a much greater data set is available.[148] The data available for other $^3J(^{207}PbX)$ (in particular for X = ^{13}C) suggest that Karplus-type relationships between the magnitude of $^3J(^{207}PbX)$ and the respective dihedral angles will emerge, as has been shown in the case of $^3J(^{119}SnX)$.[146]

5.2.4. *Long-range coupling constants* $^nJ(^{207}PbX)$ ($n \geqslant 4$)

A systematic study of long-range coupling constants has not been carried out so far, although coupling through 4, 5 or 6 bonds between ^{207}Pb and ^1H or ^{13}C can be observed as for other nuclei provided a suitable coupling path is available (across the C=C=C system in allenes, across aromatic π systems or through bicyclic or tricyclic systems offering two or more equivalent coupling pathways).

6. ^{207}Pb NMR OF SOLIDS

Early studies on solids by ^{207}Pb NMR date back more than 30 years,[104,174] and $\delta^{207}Pb$ values of solids are included in the tables if it has proved possible to extract meaningful figures. Sometimes the referencing is not clear or no attention has been paid at all to referencing.[172] Glasses containing PbO have been studied frequently by ^{207}Pb NMR;[31,40,88,176] the ferroelectric phase transition of $PbHPO_4$ has been monitored by ^{207}Pb NMR;[15] the Knight shift and spin–lattice relaxation time for the ^{207}Pb nuclei in $BaPbO_3$ have been measured,[10] and conduction-band formation in lead layers intercalated in TaS_2 was investigated by determining the anisotropy of the NMR frequency K ($K_\perp$ and $K_\parallel$).[101] The large difference in the ^{207}Pb-nuclear shielding between $TlPbX_3$ and $CsPbX_3$ (X = Br, I), in particular for X = Br

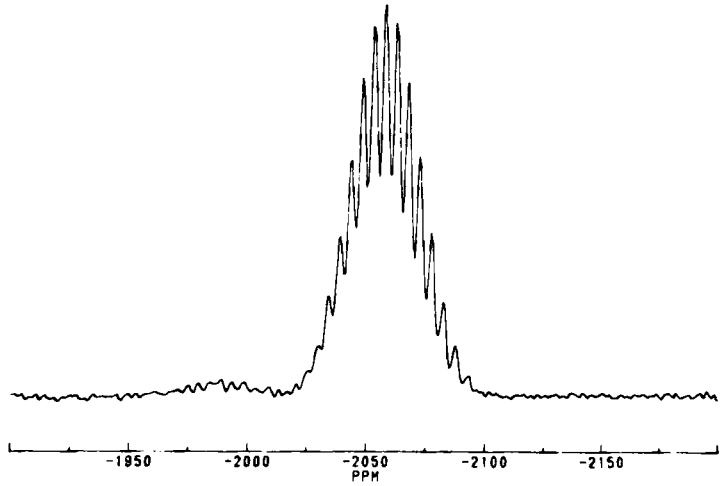


Fig. 5. 62.8 MHz $^{207}Pb-\{^1H\}$ MAS spectrum (spinning speed = 3982 Hz) of solid $[(NH_4)_2PbCl_6]$.[126] The splitting pattern results from scalar coupling $^1J(^{207}Pb\,^{35}Cl)$ (300 Hz; the presence of ^{37}Cl contributes mainly to the linewidth) and corresponds closely to the calculated intensities (15 of 19 lines are visible and the seven most-intense lines should have a 0.59 : 0.80 : 0.96 : 1 : 0.96 : 0.80 : 0.59 pattern). The spectrum shows that in this case $T_1(^{35}Cl)$ is sufficiently long in the solid state, in contrast with solutions.

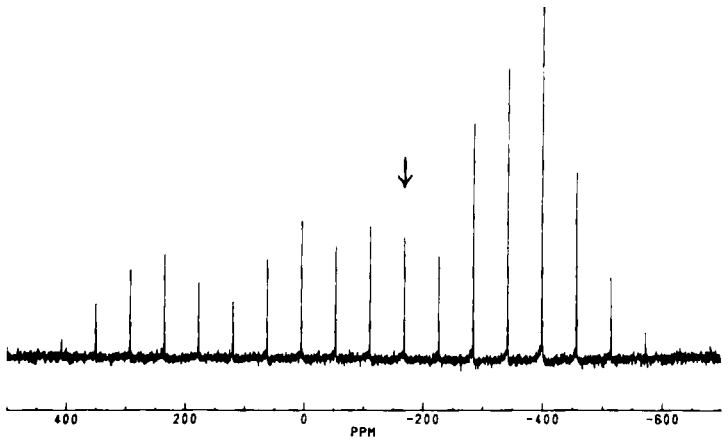


Fig. 6. 62.8 MHz ^{207}Pb CPMAS spectrum (spinning speed = 3625 Hz) of solid bis(trimethylplumbyl)ethyne $[Me_3Pb-C\equiv C-PbMe_3]$.[128] The isotropic $\delta^{207}Pb$ value is marked with an arrow. The $\delta^{207}Pb$ value is very similar to $\delta^{207}Pb$ in solution, showing that there is no change in the lead coordination number. Since there is only a single $\delta^{207}Pb$ value, all molecules are crystallographically equivalent. The envelope of the spinning sidebands corresponds closely to the characteristic powder pattern for axial symmetry, as expected. The great number of spinning sidebands results from the large anisotropy $\Delta\sigma(^{207}Pb) \approx 1100$ ppm, typical of heavy nuclei (compare with $\Delta\sigma(^{13}C) = 10$–$20$ ppm for tetracoordinate ^{13}C nuclei).

(deshielding by about 1400 ppm in $CsPbBr_3$ with respect to $TlPbBr_3$), indicates changes in the structure of the two perovskite-type crystals.[147] The isotropic $\delta^{207}Pb$ values of solid lead(II) halides have been determined and analysed theoretically by electronic structure calculations at the SCF–LCAO MO level.[196]

The advent of MAS (*m*agic-*a*ngle *s*pinning), if possible combined with CP (^1H-*c*ross *p*olarization, also for ^{19}F[89]), CP MAS,[166] has opened new dimensions for solid-state NMR of rare spins.[41,65,111,113,124,129,130] In addition to insoluble inorganic lead compounds (see Fig. 5 for the MAS ^{207}Pb NMR spectrum of $[(NH_4)_2PbCl_6]$), many solid organolead compounds that have been studied only in solution so far will be investigated by CP MAS ^{207}Pb NMR (see Fig. 6) in the near future.

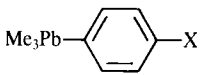
7. CONCLUSIONS

Multinuclear magnetic resonance is increasingly used for obtaining consistent information on the systems under consideration. For the preparative chemist dealing with lead compounds, ^{207}Pb NMR already is or soon will be a fascinating tool, revealing straightforward information—under realistic conditions—on the progress of complex reactions. At the same time, a larger set of ^{207}Pb NMR data aids our understanding of NMR parameters of the lighter magnetically active isotopes in Group IV of the periodic table, in particular for ^{119}Sn and ^{29}Si nuclei. Furthermore, ^{207}Pb NMR is of considerable interest from the theoretical point of view. ^{207}Pb NMR parameters serve as a crucial test of the validity of theoretical models aiming at the description of chemical and physical properties of the heavy elements. Finally, many "old" problems in the solid-state chemistry of lead can be tackled again, taking advantage of the improvements in modern NMR instrumentation.

ACKNOWLEDGEMENTS

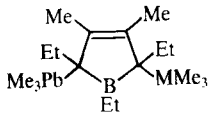
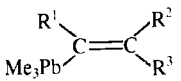
We thank the *Deutsche Forschungsgemeinschaft*, the *Fonds der Chemischen Industrie* and the *Stiftung Volkswagenwerk* for generous support of our experimental and spectroscopic work.

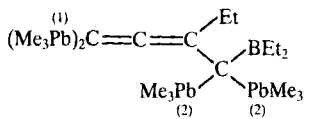
Table 1. Organotrimethyllead compounds.

Compound	δ^{207}Pb	Solvent	Notes	Refs.	Other nuclei	Refs.
Me_4Pb	0.0	Toluene, 80%	*a*	—	^{13}C	97, 78
	−2.4	Pyridine		97		
	+3.3	$CDCl_3$		22		
	+7.5	THF		168		
Me_3Pb-Et	+29.0	—		78	^{13}C	78, 110
$Me_3Pb-{}^iPr$	+62.0	$CDCl_3$		78	^{13}C	78, 110
Me_3Pb-Bu	+16	—		78		
 X						
H	+54.5	C_6D_{12}		6		
	+57.1	$CDCl_3$		6	^{13}C	6
Me	+60.4	C_6D_{12}		6		
	+63.1	$CDCl_3$		6	^{13}C	6
Ph	+62.4	C_6D_{12}		6		
	+65.6	$CDCl_3$		6	^{13}C	6
4-F−C_6H_4	+63.3	C_6D_{12}		6		
	+66.2	$CDCl_3$		6	^{13}C	6
F	+73.6	C_6D_{12}		6		
	+76.8	$CDCl_3$		6	^{13}C	6
$Me_3Pb-C(N_2)-CO_2Et$	+87.0	C_6D_6		69	^{13}C	84
$(Me_3Pb)_2CN_2$	+114.0	C_6D_6		69	^{13}C	84
$Me_3Pb-C(SnMe_3)_3$	+161.4	$CDCl_3$		21	^{13}C, ^{119}Sn	21
$(Me_3Pb)_2C(SnMe_3)_2$	+189.9	$CDCl_3$		21	^{13}C, ^{119}Sn	21
$(Me_3Pb)_3C-SnMe_3$	+221.5	$CDCl_3$		21	^{13}C, ^{119}Sn	21
$(Me_3Pb)_4C$	+256.5	$CDCl_3$		21	^{13}C	21
Me_3Pb-Ph	−38.5			105	^{13}C	90
$Me_3Pb-(4\text{-}F-C_6H_4)$	−38.5	—		97	^{19}F	97
$Me_3Pb-C_5H_5$	+127.0	C_6H_6	*b*	3		

(Continued)

Table 1. (*Continued*)

Compound			δ^{207}Pb	Solvent	Notes	Refs.	Other nuclei	Refs.
Me_3Pb—3-Furyl			−76.7	$CDCl_3$		38	^{13}C	38
$(\eta^5$-Me_3Pb—$C_5H_4)_2Fe$			+3.7	Acetone-d^6		12	^{13}C	12
		M						
		Sn	+180.8	C_7D_8	*b*	168	^{11}B, ^{13}C, ^{119}Sn	168
		Pb	+177.1	C_6D_6	*b*	168	^{11}B, ^{13}C	168
								
R^1	R^2	R^3						
H	H	H	−65.3	—		97	^{13}C	110
H	H	Me	−110.0	C_6D_6		54	^{13}C	54
H	Me	H	−69.0	C_6D_6		54	^{13}C	54
Me	H	H	−41	C_6D_6		54	^{13}C	54
Me_3Si	H	H	−21.2	$CDCl_3$		5	^{29}Si	5
Bu	H	Me_3Si	−82.7	$CDCl_3$	*c*	11	^{13}C, ^{29}Si	11
Ph	Me_3Si	H	−27.9	$CDCl_3$	*d*	11	^{13}C, ^{29}Si	11
Me_2NCH_2	H	Me_3Si	−86.2	$CDCl_3$	*e*	11	^{13}C, ^{29}Si	11
Me_3Ge	H	H	−24.8	$CDCl_3$		5		
Me_3Sn	H	H	−12.2	$CDCl_3$		5	^{119}Sn	5
Me_3Pb	H	H	+8.7	$CDCl_3$		5		
Et	Me	$SnMe_3$	−69.7	C_6D_6	*f*	150	^{13}C, ^{119}Sn	150
H	Et	BEt_2	−101.1	C_6D_6		168	^{11}B, ^{13}C	168
Me	Et	BEt_2	−65.6	C_6D_6		168	^{11}B, ^{13}C	45
Me	^{i}Pr	B^iPr_2	−76.5	C_6D_6		168	^{11}B, ^{13}C	168

^{t}Bu	Et	BEt_2	−100.0	C_7D_8	*g*	168	^{11}B, ^{13}C	168
Ph	Et	BEt_2	−65.3	C_6D_6		168	^{11}B, ^{13}C	168
Me	Ph	BPh_2	−41.3	CD_2Cl_2	*g*	168	^{13}C	168
Me	Et	BEt_2Me^-	−66.7	THF-d_8	*h*	168	^{11}B, ^{13}C	168
Me	Et	$BEt_2NH_2^-$	−146.5	THF-d_8	*n*	189	^{11}B, ^{13}C	189
Me_3Si	Et	BEt_2	−81.3	C_7D_8	*g*	168	^{13}C, ^{29}Si	168
Me_3Si	BEt_2	Et	−109.1	C_7D_8	*g*	168	^{13}C, ^{29}Si	168
Me_3Sn	Et	BEt_2	−73.9	C_7D_8	*g*	168	^{13}C, ^{119}Sn	168
Me_3Sn	BEt_2	Et	−86.7	C_7D_8	*g*	168	^{13}C, ^{119}Sn	168
Me_3Pb	Et	BEt_2	−43.4 −53.2(R^1)	C_7D_8	*g*	168	^{13}C	168
Li	H	H	−14.9	THF	*i*	16	^{13}C	16
			+31.3(1) +66.3(2)	C_7D_8	*j*	168	^{11}B, ^{13}C	168
$Me_3Pb-C\equiv C-H$			−130.3	Hexane, C_6D_6		168	^{13}C	168
$Me_3Pb-C\equiv C-Me$			−133.0	$CDCl_3$		55	^{13}C	55
			−139.8	C_6H_6		97		
			−140.9	Pyridine		97		
			−142.1	C_6D_6		55	^{13}C	55
$Me_3Pb-C\equiv C-{}^tBu$			−131.7	$CDCl_3$		55	^{13}C	55
			−140.6	C_6D_6		55	^{13}C	55
$Me_3Pb-C\equiv C-Ph$			−113.0	$CDCl_3$		168	^{13}C	168
			−123.0	C_6D_6		168	^{13}C	
$Me_3Pb-C\equiv C-C(Me)=CH_2$			−121.3	$CDCl_3$		55	^{13}C	55
			−130.4	C_6D_6		55	^{13}C	55
$Me_3Pb-C\equiv C-C\equiv C-PbMe_3$			−99.2	$CDCl_3$		168	^{13}C	168
			−108.6	C_6D_6		168	^{13}C	168
$Me_3Pb-C\equiv C-SiMe_3$			−130.0	$CDCl_3$	*k*	168	^{13}C, ^{29}Si	168
			−144.6	C_6D_6	*k*	168	^{13}C, ^{29}Si	168

(Continued)

Table 1. (*Continued*)

Compound	δ^{207}Pb	Solvent	Notes	Refs.	Other nuclei	Refs.
$Me_3Pb-C\equiv C-SnMe_3$	−140.1	$CDCl_3$	*l*	55	^{13}C, ^{119}Sn	55
	−153.1	C_6D_6	*l*	71	^{13}C, ^{119}Sn	22, 55, 71
$Me_3Pb-C\equiv C-PbMe_3$	−145.6	$CDCl_3$		55	^{13}C	55
	−158.8	C_6D_6		71	^{13}C	22, 55, 71
(solid)	−168.9	—		128	^{13}C	128
trans-$[Pt(PEt_3)_2(C\equiv C-PbMe_3)_2]$	−180.0	C_6D_{12}	*m*	167	^{13}C, ^{31}P, ^{195}Pt	167

Notes:

[a] Reference compound: 80% in toluene.

[b] Fluxional, metallotropic rearrangement.

[c] $^3J(^{207}Pb^{29}Si) = 71.2$ Hz.

[d] $^3J(^{207}Pb^{29}Si) = 138.9$ Hz.

[e] $^3J(^{207}Pb^{29}Si) = 65.6$ Hz.

[f] $^3J(^{207}Pb^{119}Sn) = 912.8$ Hz.

[g] At −40°C.

[h] $^3J(^{207}Pb^{11}B) = 54.8$ Hz.

[i] At −40°C; $^1J(^{207}Pb^{13}C=)$ 918.4 Hz; the sign of ^1J is presumably negative.

[j] $^5J(^{207}Pb^{207}Pb)$ 928.4, 881.5 Hz (two diastereomers).

[k] $^3J(^{207}Pb^{29}Si)$ (in C_6D_6) 5.8 Hz, (in $CDCl_3$) 3.1 Hz.

[l] $^3J(^{207}Pb^{119}Sn)$ (in C_6D_6) 23.5 Hz, (in $CDCl_3$) 32.0 Hz.

[m] $^3J(^{207}Pb^{195}PT)$ 325.0 Hz.

[n] At −74°C; lead coordination number = 5 because of intramolecular N–Pb coordination.

Table 2. Other tetraalkyllead compounds.

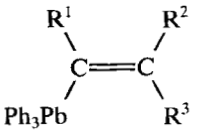
Compound	δ^{207}Pb	Solvent	Notes	Refs.	Other nuclei	Refs.
Et_4Pb	+71.0	—		3, 78	^{13}C	78, 96
	+71.9	$CDCl_3$		22		
Bu_4Pb	+40.0			78	^{13}C	78
	+65.0	C_6D_6	*a*	70		
	+68.0	$CDCl_3$	*a*	70		
	+66.9	HMPA	*a*	70		
$(^tBu-CH_2)_4Pb$	+47.0	CH_2Cl_2		86	^{13}C	110
$(CH_2)_4Pb(CH_2)_4$	+416.3	—		86	^{13}C	107
$(CH_2)_5Pb(CH_2)_5$	−199.0	CH_2Cl_2		86		
Et_3Pb-Me	+67.0	—		78	^{13}C	78, 96
Et_3Pb-Bu	+65.0	—		78		
	+65.5	C_6D_6		168	^{13}C	168
Bu_3Pb-Me	+36.0	—		78		
Bu_3Pb-Et	+57.0	—		78		
Me_2PbEt_2	+53.0	—		78	^{13}C	78
Me_2PbBu_2	+29.0	—		78		
$Me_2Pb(CH_2)_4$	+205.3	$CDCl_3$		107	^{13}C	107

Note:

[a] Bu_4Pb in C_6D_6 (50% v : v) has been selected as external reference compound; however, the δ^{207}Pb values appear to be incorrect by about 23–25 ppm (to high frequency).

Table 3. Organotriphenyllead compounds.

Compound	δ^{207}Pb	Solvent	Notes	Refs.	Other nuclei	Refs.
Ph_4Pb	−166	C_6H_6		3	^{13}C	28, 72, 76, 90
	−178	$CDCl_3$		73		
	−179	$CDCl_3$		78	^{13}C	78
	−182.7	$CDCl_3$		1		
	−155.4	0.1 M, $CDCl_3$	*a*	70		
	−155.8	0.1 M, HMPA	*a*	70		
Ph_3Pb-Me	−118.9	$CDCl_3$		73	^{13}C	62, 90
Ph_3Pb-Et	−114.5	CCl_4		102	^{13}C	62
	−116.2	$CDCl_3$		73		
Ph_3Pb-Pr	−123.6	$CDCl_3$		107	^{13}C	62
$Ph_3Pb-{}^{i}Pr$	−120.1	$CDCl_3$		73	^{13}C	62
Ph_3Pb-Bu	−122.0	$CDCl_3$		107	^{13}C	62
$Ph_3Pb-{}^{i}Bu$	−131.6	$CDCl_3$		107	^{13}C	62
$Ph_3Pb-{}^{t}Bu$	−111.5	$CDCl_3$		73	^{13}C	62
$Ph_3Pb-CH_2-{}^{t}Bu$	−141.8	$CDCl_3$		73	^{13}C	62
n						
$Ph_3Pb-CH(CH_2)_n$ 2	−107.7	$CDCl_3$		107	^{13}C	62
3	−127.7	$CDCl_3$		107	^{13}C	62
4	−107.8	$CDCl_3$		107	^{13}C	62
5	−149.2	$CDCl_3$		107	^{13}C	62
6	−119.2	$CDCl_3$		107	^{13}C	62
$Ph_3Pb-CH_2CH_2Ph$	−124.5	$CDCl_3$		107	^{13}C	107
$Ph_3Pb-CH_2-CH=CH_2$	−175.5	$CDCl_3$		107	^{13}C	107
$Ph_3Pb-CH_2-C(Me)=CH_2$	−167.8	$CDCl_3$		107	^{13}C	107
$Ph_3Pb-CH_2-CH=CH_2$	−121.3	$CDCl_3$		107	^{13}C	107
$Ph_3Pb-C_5H_5$	−101.0	C_6H_6	*b*	3		



R^1	R^2	R^3						
H	H	H	−199.7	$CDCl_3$		107	^{13}C	107
H	H	Me	−226.0	$CDCl_3$		107	^{13}C	107
H	Me	H	−199.4	$CDCl_3$		107	^{13}C	107
Me	H	H	−182.7	$CDCl_3$		107	^{13}C	107
H	Me	Me	−222.7	$CDCl_3$		107	^{13}C	107
Me	Et	BEt_2	−204.8	CD_2Cl_2	*c*	168	^{11}B, ^{13}C	168
Me	^{i}Pr	$B^{i}Pr_2$	−182.7	C_6D_6		168	^{11}B, ^{13}C	168
$Ph_3Pb-CH=C=CH_2$			−213	$CDCl_3$		107	^{13}C	107
$Ph_3Pb-C\equiv C-Me$			−266.5	$CDCl_3$		107	^{13}C	107
$Ph_3Pb-C\equiv C-Ph$			−259.7	$CDCl_3$		107	^{13}C	107
$Ph_3Pb-C\equiv C-PbPh_3$			−269.1	$CDCl_3$		107	^{13}C	107

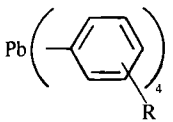
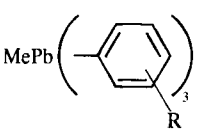
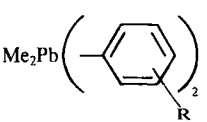
Notes:

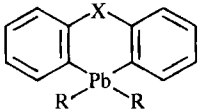
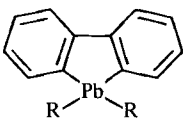
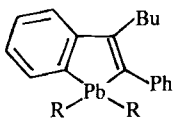
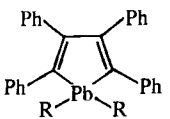
[a] Bu_4Pb in C_6D_6 (50% v:v) has been selected as external reference compound; however, the $\delta^{207}Pb$ values appear to be incorrect by about 23–25 ppm (to high frequency).

[b] Fluxional; metallotropic rearrangement.

[c] At −30°C.

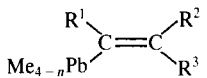
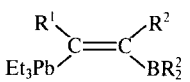
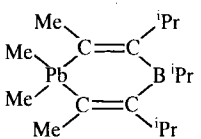
Table 4. Tetraaryllead and other aryllead compounds.

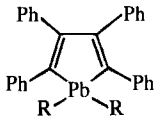
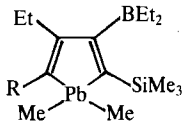
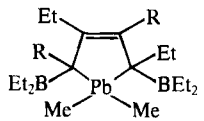
Compound	R	δ^{207}Pb	Solvent	Notes	Refs.	Other nuclei	Refs.
	2-Me	−161.6	$CDCl_3$		73	^{13}C	76, 80
	3-Me	−174.0	$CDCl_3$		78	^{13}C	76, 78, 80
		−175.3	$CDCl_3$		73		
	4-Me	−168.0	$CDCl_3$		78	^{13}C	78, 80, 90
		−166.6	$CDCl_3$		73		
	(solid)	−159.2	—				
	4-^{t}Bu	−181.8	$CDCl_3$		107		
	3-F	−171.1	$CDCl_3$		73		
	4-F	−153.5	CCl_4		97	^{19}F	97
		−156.2	$CDCl_3$		73		
	3-Cl	−169.1	$CDCl_3$		73	^{13}C	73
	4-Cl	−157.1	$CDCl_3$		73	^{13}C	73
	2-MeO	−195.6	$CDCl_3$		73	^{13}C	76, 80
	3-MeO	−166.0	CS_2		78	^{13}C	76, 80
		−166.5	$CDCl_3$		73		
	4-MeO	−153.0	$CHCl_3$		78	^{13}C	90
		−152	$CDCl_3$		73		
	4-MeS	−160.0	$CDCl_3$		78		
	2,4-$(MeO)_2$	−185.5	$CDCl_3$		73	^{13}C	76, 80
	2,5-$(MeO)_2$	−188.7	$CDCl_3$		73	^{13}C	76, 80
	4-Me	−113.4	$CDCl_3$		73	^{13}C	90
	4-F	−102.6	CCl_4		97	^{19}F	97
		−101.2	$CDCl_3$		73		
	4-Cl	−100.2	$CDCl_3$		73	^{13}C	90
	4-MeO	−103.9	$CDCl_3$		73	^{13}C	90
	H	−38.0	$CDCl_3$		107	^{13}C	90
		−80.0	?		105		
	4-F	−63.0	—		97	^{19}F	97

$(CH_2)_4PbPh_2$			+149.3	$CDCl_3$		107	^{13}C	107
$(C_5H_5)_2PbPh_2$			−30.0	C_6H_6		3		
$(Me-C\equiv C)_2PbPh_2$			−384.2	$CDCl_3$		168	^{13}C	168
			−382.7	C_6D_6		168	^{13}C	168
	X	R						
	CH_2	Me	−201.4	$CDCl_3$		107	^{13}C	107
	CH_2	Ph	−284.1	$CDCl_3$		107	^{13}C	107
	CH_2	1/2	−396.2	$CDCl_3$	*a*	107	^{13}C	107
	O	Ph	−333.4	$CDCl_3$		107	^{13}C	107
	NMe	Me	−238.0	$CDCl_3$		107	^{13}C	107
	NMe	Ph	−334.7	$CDCl_3$		107	^{13}C	107
	—	Me	+0.3	$CDCl_3$		107	^{13}C	107
	—	Ph	−95.4	$CDCl_3$		107	^{13}C	107
	—	4-Me−C_6H_4	−90.1	$CDCl_3$		107	^{13}C	107
	—	1/2	+10.7	$CDCl_3$	*a*	107	^{13}C	107
	—	4-Me−C_6H_4	−61.7	$CDCl_3$		107	^{13}C	107
	—	1/2	+92.2	$CDCl_3$		107	^{13}C	107
	—	4-Me−C_6H_4	−16.2	$CDCl_3$		107	^{13}C	107

Note:
[a] 1/2 denotes a spiro compound.

Table 5. Tetraalkenyllead and other alkenyllead compounds.

Compound				δ^{207}Pb	Solvent	Notes	Refs.	Other nuclei	Refs.
									
n	R^1	R^2	R^3						
2	H	H	Me	−220.0	C_6D_6		54		
2	H	Me	H	−137.0	C_6D_6		54		
2	Me	H	H	−86.0	C_6D_6		54		
2	Me	^{i}Pr	B^iPr_2	−121.8	C_6D_6		191	^{11}B, ^{13}C	191
3	H	H	Me	−330.0	C_6D_6		54		
3	Me	H	H	−121.0	C_6D_6		54		
4	H	H	H	−251.0	—		97	^{13}C	70
4	H	H	Me	−440.0	C_6D_6		54		
4	H	Me	H	−280.0	C_6D_6		54		
			R^1	R^2					
			Me	Et	−2.1	C_6D_6		168	^{11}B, ^{13}C	168
			Me	^{i}Pr	−15.6	C_6D_6		168	^{11}B, ^{13}C	168
			^{t}Bu	Et	−3.7	C_6D_6		168	^{13}C	168
					−195.0	C_6D_6		191	^{11}B, ^{13}C	191

	R						
	Me	+112.8	$CDCl_3$		107	^{13}C	107
	1/2	+190.2	$CDCl_3$	*a*	107	^{13}C	107
	R						
	Me	+319.0	C_6D_6		168	^{13}C, ^{29}Si	168
	Me_3Si	+543.2	CD_2Cl_2	*b*	168	^{13}C, ^{29}Si	168
$Me_2Pb(C_5H_5)_2$		+167.0	C_6H_6	*c*	3		
$Et_3Pb-C_5H_5$		+182	C_6H_6	*c*	3		
$Et_2Pb(C_5H_5)_3$		+200.0	C_6H_6	*c*	3		
	R						
	Me	+275.1	C_6D_6		168	^{11}B, ^{13}C	168
	Bu	+280.7	C_6D_6		168	^{11}B, ^{13}C	168

Notes:

[a] 1/2 denotes a spiro compound.

[b] At −34°C; $^2J(^{207}Pb^{29}Si_{2/5})$ 171.3, 168.8 Hz.

[c] Fluxional; metallotropic rearrangement.

Table 6. Tetraalkynyllead and other alkyl(alkynyl)lead compounds.

Compound	δ^{207}Pb	Solvent	Note	Refs.	Other nuclei	Refs.
$(Me-C\equiv C)_4Pb$	−685.5	C_6H_6		97		
	−698.9	Pyridine		97		
	−687.5	C_6D_6		55	^{13}C	55
	−687.0	$CDCl_3$		55	^{13}C	55
$Me_2Pb(C\equiv C-Me)_2$	−304.7	C_6H_6		97		
	−311.0	Pyridine		97		
	−306.4	C_6D_6		55	^{13}C	55
	−304.8	$CDCl_3$		55	^{13}C	55
(solid)	−301.4	—		128	^{13}C	128
$Me_2Pb(C\equiv C-Bu)_2$	−302.8	C_6D_6		168	^{13}C	168
	−296.0	$CDCl_3$		168	^{13}C	168
$Me_2Pb(C\equiv C-{}^tBu)_2$	−298.5	C_6D_6		168	^{13}C	168
	−288.9	$CDCl_3$		168	^{13}C	168
(solid)	−295.2	—		128	^{13}C	128
$Me_2Pb(C\equiv C-Ph)_2$	−282.8	C_6D_6		168	^{13}C	168
	−278.1	$CDCl_3$		168	^{13}C	168
$Me_2Pb(C\equiv C-SiMe_3)_2$	−322.5	C_6D_6	*a*	168	^{13}C, ^{29}Si	168
	−315.9	$CDCl_3$	*a*	168	^{13}C, ^{29}Si	168
(solid)	−315.0	—		128	^{13}C, ^{29}Si	128
$Et_3Pb-C\equiv C-H$	−38.5	C_6D_6		55	^{13}C	55
	−35.5	$CDCl_3$		55	^{13}C	55
$Et_3Pb-C\equiv C-Me$	−41.4	C_6D_6		55	^{13}C	55
	−35.7	$CDCl_3$		55	^{13}C	55
$Et_3Pb-C\equiv C-{}^tBu$	−34.9	C_6D_6		168	^{13}C	168
$Et_3Pb-C\equiv C-PbEt_3$	−48.2	C_6D_6		55	^{13}C	55
	−39.7	$CDCl_3$		55	^{13}C	55
$Et_2Pb(C\equiv C-Me)_2$	−230.0	C_6D_6		55	^{13}C	55
	−225.6	$CDCl_3$		55	^{13}C	55
(solid)	−205.0	—		128	^{13}C	128

Note:
[a] $^3J(^{207}Pb^{29}Si)$ (in C_6D_6) 7.8 Hz, (in $CDCl_3$) 6.7 Hz.

Table 7. Triorganolead–element compounds.

Compound	δ^{207}Pb	Solvent	Notes	Refs.	Other nuclei	Refs.
Me_3Pb-Cl	+390.0	$CHCl_3$		78	^{13}C	78, 110
	+374.8	$CDCl_3$		97		
	+432.0	CH_2Cl_2		86		
	+215.7	Pyridine		97	^{13}C	78
	+342.0	MeOH		78		
	+347.3	MeOH	*a*	68		
	+482.1	H_2O	*b*	68		
	+436.2	0.35 M, $CDCl_3$	*c*	70		
	+189.8	0.35 M, HMPA	*c*	70		
$Me_2EtPb-Cl$	+425.0	$CHCl_3$		78	^{13}C	78
$MeEt_2Pb-Cl$	+459.0	$CHCl_3$		78	^{13}C	78
Et_3Pb-Cl	+472.0	$CHCl_3$		78	^{13}C	78
	+425.0	C_6H_6		78	^{13}C	78
	+423.0	CCl_4		78	^{13}C	78
	+416.0	MeCN		78	^{13}C	78
	+403.0	Acetone		78	^{13}C	78
	+393.0	THF		78	^{13}C	78
	+325.0	DMF		78	^{13}C	78
	+310.0	DMSO		78	^{13}C	78
	+305.0	Pyridine		78	^{13}C	78
$^{i}Pr_3Pb-Cl$	+442.0	$CHCl_3$		78	^{13}C	78
$chex_3Pb-Cl$	+381.6	$CDCl_3$		128		
(solid)	+320.7	—		128		
Ph_3Pb-Cl	+33.0	$CDCl_3$		78	^{13}C	78
	+29.0	CH_2Cl_2(sat.)	*d*	23		
	+41.0	C_6H_6		3	^{13}C	109
	−67.0	THF		3		
	−186.0	DMSO		3	^{13}C	109

(Continued)

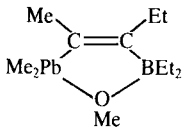
Table 7. (*Continued*)

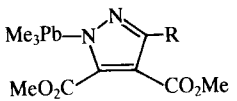
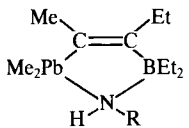
Compound	δ^{207}Pb	Solvent	Notes	Refs.	Other nuclei	Refs.
	−177.0	Pyridine		3		
	+59.8	0.5 M, $CHCl_3$	*c*	70		
	−182.2	0.5 M, HMPA	*c*	70		
	−73.0	CH_2Cl_2/DMEU	*e*	23		
	−53.0	CH_2Cl_2/DMPU	*e*	23		
(4-MeO−C_6H_4)$_3$Pb−Cl	+76.8	$CDCl_3$		73		
Me_3Pb−Br	+390.0	$CHCl_3$		78	^{13}C	78, 110
	+367.0	CH_2Cl_2		86		
	+382.0	$CDCl_3$		128	^{13}C	128
Et_3Pb−Br	+490.9	$CDCl_3$(sat.)		168	^{13}C	168
(^{t}Bu−CH_2)$_3$Pb−Br	+384.0	CH_2Cl_2		86	^{13}C	110
Ph_3Pb−Br	+0.6	$CDCl_3$		73		
	−3.0	$CHCl_3$		78	^{13}C	78
	−3.0	CH_2Cl_2		23		
	−63.0	THF		78	^{13}C	78
	−174.0	Pyridine		78	^{13}C	78
	+28.2	0.5 M, $CHCl_3$	*c*	70		
	−153.6	0.5 M, HMPA	*c*	70		
	−52.0	CH_2Cl_2/DMEU	*e*	23		
	−70.0	CH_2Cl_2/DMPU	*e*	23		
(4-MeO−C_6H_4)$_3$Pb−Br	+34.9	$CDCl_3$		73		
Me_3Pb−I	+171.0	$CHCl_3$		78	^{13}C	78, 110
	+203.6	CH_2Cl_2		86		
Et_3Pb−I	+303.0	CH_2Cl_2		86		
(^{t}Bu−CH_2)$_3$Pb−I	+336.0	CH_2Cl_2		86		
Ph_3Pb−I	−131.0	$CHCl_3$		78		
	−127.5	$CDCl_3$		73		
	−124.0	CH_2Cl_2		23		

	−125.0	CH_2Cl_2/DMEU	*e*	23		
	−130.0	CH_2Cl_2/DMPU	*e*	23		
(2,4,6-$Me_3-C_6H_2)_3Pb-I$	−356.8	$CDCl_3$		179		
(solid)	−350	—		179		
(4-$MeO-C_6H_4)_3Pb-I$	−152.8	$CDCl_3$		73		
$Me_3Pb-OMe$	+331.3	CH_2Cl_2		97		
$Me_3Pb-OAc$	+304.6	MeOH(sat.)		97		
	+264.8	MeOH/Pyridine		97		
	+428.0	H_2O		78	^{13}C	78
	+408.1	HOAc	*o*	102		
$[Me_3Pb(H_2O)_n]^+$	−730.0	H_2O	*f*	105		
$Et_3Pb-OAc$	+412.0	HOAc		102		
	+317.0	$CDCl_3$		78	^{13}C	78
	+372.7	0.5 M, $CDCl_3$	*c*	70		
	+169.8	0.5 M, HMPA	*c*	70		
$Pr_3Pb-OAc$	+370.0	$CHCl_3$		78	^{13}C	78
	+428.8	HOAc		102		
	+407.2	$CDCl_3$	*c*	70		
	+378.5	Aniline	*c*	70		
	+339.9	MeOH	*c*	70		
	+244.4	DMSO	*c*	70		
	+242.4	Pyridine	*c*	70		
	−168.9	HMPA	*c*	70		
$Bu_3Pb-OAc$	+383.0	$CHCl_3$		78	^{13}C	78
	+424.0	HOAc		102		
	+423.2	0.5 M, $CHCl_3$	*c*	70		
	+45.5	0.5 M, HMPA	*c*	70		
$^{i}Bu_3Pb-OAc$	+392.0	$CHCl_3$		78	^{13}C	78, 107
	+432.0	HOAc		102		
($^{t}Bu-CH_2)_3Pb-OH$	+288.0	CH_2Cl_2		86		

(Continued)

Table 7. (*Continued*)

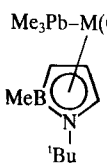
Compound	δ^{207}Pb	Solvent	Notes	Refs.	Other nuclei	Refs.
	+656.0	C_6D_6		168	^{11}B, ^{13}C	168
$Ph_3Pb-OAc$	−93.0	$CDCl_3$		78	^{13}C	78
	−89.4	$CDCl_3$		73		
	−299.1	0.5 M, HMPA	*c*	70		
$(4\text{-}MeO-C_6H_4)_3Pb-OAc$	−115.2	$CDCl_3$		73		
$Me_3Pb-SMe$	+214.0	—		86		
	+239.0	CH_2Cl_2		86		
$Me_3Pb-SEt$	+194.0	—		86		
	+215.0	CH_2Cl_2		86		
Me_3Pb-S^iPr	+177.5	—		86		
	+197.0	CH_2Cl_2		86		
Me_3Pb-S^tBu	+147.8	—		86		
	+161.4	CH_2Cl_2		86		
$Me_3Pb-SCH_2Ph$	+208.1	—		86		
	+217.4	CH_2Cl_2		86		
$Me_3Pb-SPh$	+243.0	—		86		
	+255.0	CH_2Cl_2		86		
$Et_3Pb-SMe$	+298.0	CH_2Cl_2		86		
$Et_3Pb-SEt$	+282.0	CH_2Cl_2		86		
Et_3Pb-S^tBu	+236.0	CH_2Cl_2		86		
$Et_3Pb-SCH_2Ph$	+282.0	CH_2Cl_2		86		
$Ph_3Pb-SMe$	+41.6	0.5 M, $CHCl_3$	*c*	70	^{13}C	70
	+3.4	0.5 M, HMPA	*c*	70	^{13}C	70
$(Ph_3Pb)_2S$	+3.1	$CDCl_3$	*g*	124	^{13}C	124

$Me_3Pb-SeMe$		+80.5	C_6H_6		94	^{77}Se	94
		+98.0	C_6H_6		86		
$Me_3Pb-SePh$		+133.0	CH_2Cl_2		86		
$Me_3Pb-NEt_2$		+242.0	C_6H_6		86	^{13}C, ^{15}N	168
$Me_3Pb-N(Me)Ph$		+226.5	C_6H_6		86	^{15}N	61, 94
$Me_3Pb-NC_4H_4$		+204.0	C_6D_6		24	^{13}C, ^{14}N	24
	R						
	Me_2As	+315.0	?		69	^{13}C	69
	Me_3Si	+350.0	?		69	^{13}C	69
$Me_3PbN(^tBu)SiMe_3$		+123.0	C_6D_6		169	^{13}C, ^{15}N, ^{29}Si	169
$Me_3Pb-N(SiMe_3)_2$		+170.0	?		69		
		+171.9	C_6D_6		169	^{13}C, ^{15}N, ^{29}Si	169
$Me_3Pb-N(^tBu)SnMe_3$		+144.0	C_6D_6		57	^{119}Sn	57
$Me_3Pb-N(SnMe_3)_2$		+242.0	C_6D_6		25	^{119}Sn	25, 57
$Me_3Pb-N(PbMe_3)SnMe_3$		+268.0	C_6D_6		61	^{119}Sn	57, 61
$Me_3Pb-N(^tBu)PbMe_3$		+173.0	C_6D_6		57		
$Me_3Pb-N(PbMe_3)_2$		+294.0	C_6D_6		57		
	R						
	H	+427.6	C_6D_6		189	^{11}B, ^{13}C, ^{15}N	189,168
		+367.4	THF-d_8		168	^{11}B, ^{13}C	168
	Me	+460.5	C_6D_6		168	^{11}B, ^{13}C, ^{15}N	168
$Me_3Pb-PPh_2$		+40.5	C_6H_6		86	^{31}P	61, 94
$Me_3Pb-SiMe_3$		−298.2	C_6D_6		187	^{13}C, ^{29}Si	187
$Ph_3Pb-GePh_3$		−271.5	$CHCl_3$		78	^{13}C	78
$Me_3Pb-SnMe_3$		−323.8	C_6H_6		94	^{119}Sn	94
$Me_3Pb-SnPh_3$		−263.1	C_6H_6		94	^{119}Sn	86, 94
$chex_3Pb-Snchex_3$		−92.4	$CDCl_3$	*h*	29	^{13}C, ^{119}Sn	29
$Ph_3Pb-SnPh_3$		−256.5	$CHCl_3$		78	^{13}C, ^{119}Sn	30
$Me_3Pb-PbMe_3$		−281.0	C_6H_6		94, 119	^{13}C	95, 110

(Continued)

Table 7. (*Continued*)

Compound	δ^{207}Pb	Solvent	Notes	Refs.	Other nuclei	Refs.
$(^tBu-CH_2)_3Pb-Pb(CH_2-^tBu)_3$	−237.0	CH_2Cl_2		86	^{13}C	110
$chex_3Pb-Pbchex_3$	+80.2	C_6D_6		26	^{13}C	29
(solid)	+140.6	—		127		
$Ph_3Pb-PbPh_3$	−79.8	$CDCl_3$		30	^{13}C	78
	−75.0	$CHCl_3$		78		
(solid)	−131.8, +14.5	—	*i*	127		
$Ph_3Pb-Pb(C_6H_4-4\text{-}OMe)_3$	−98.2(a)	$CDCl_3$	*j*	1		
(a) (b)	−63.3(b)					
$(2\text{-}Me-C_6H_4)_3Pb-Pb(C_6H_4-2\text{-}Me)_3$	−88.7	$CDCl_3$		26	^{13}C	26
$(4\text{-}Me-C_6H_4)_3Pb-Pb(C_6H_4-4\text{-}Me)_3$	−80.1	$CDCl_3$		26	^{13}C	26
	−77.6	$CDCl_3$		180		
(solid)	−95, −66	—	*i*			
$[Me_3Pb-BH_3]^-Li^+$	+166.0	THF	*k*	187	^{11}B, ^{13}C	187
$Me_3Pb-B[N(Me)CH_2]_2$	−362.0	C_6H_6		94	^{11}B	94
$[Me_3Pb]Li$	+512.0	THF	*k*	187	^{13}C	187
$[Et_3Pb]Li$	+744.6	THF	*k*	188	^{13}C	188
$[Ph_3Pb]Li$	+1062.6	THF	*l*	4	^{7}Li, ^{13}C	4
$[Ph_3Pb]K$	+1045.0	THF	*l*	4		
$Me_3Pb-M(CO)_3(C_5H_5)$ M						
Mo	+229.0	CH_2Cl_2/C_6D_6		171	^{95}Mo	171
W	−87.0	CH_2Cl_2/C_6D_6		171		



M					
Mo	+214.0	C_6D_6	63	^{11}B, ^{13}C	63
W	−106.0	C_6D_6	63	^{11}B, ^{13}C	63

$R_3Pb-M(CO)_3(C_5H_5)$	R	M						
	Et	Mo	+301.0	CH_2Cl_2/C_6D_6		171	^{95}Mo	171
	Et	W	+25.0	CH_2Cl_2/C_6D_6	*m*	171		
	Ph	Mo	+125.0	CH_2Cl_2/C_6D_6		171	^{95}Mo	171
	Ph	W	−217.0	CH_2Cl_2/C_6D_6	*n*	171		
cis-[$Ph_3Pb(Ph)Pt(PPh_3)_2$]			−100.0	CH_2Cl_2		42	^{31}P, ^{195}Pt	42, 100
trans-[$(Ph_3Pb)_2Pt(PPh_3)_2$]			+76.0	CH_2Cl_2		42	^{31}P, ^{195}Pt	42

Notes:

[a] 0.039 M; depends on concentration.

[b] 0.031 M; depends on concentration.

[c] Bu_4Pb in C_6D_6 (50% v:v) has been selected as external reference compound; however, the $\delta^{207}Pb$ values appear to be incorrect by about 23–25 ppm (to high frequency).

[d] Et_4Pb has been selected as reference compound; corrected for the Me_4Pb scale using $\delta^{207}Pb(Et_4Pb) = +71.0$.

[e] DMEU = dimethylethylene urea = 1,3-dimethyl-2-imidazolidinone; DMPU = dimethylpropylene urea = 1,3-dimethyl-3,4,5,6-tetrahydro-2(1*H*)-pyrimidinone.

[f] Concentration is not given.

[g] In the solid state: $\delta^{207}Pb = +30.3, +17.9$.

[h] $^1J(^{207}Pb\,^{119}Sn) = 2217$ Hz.

[i] Two different molecules per unit cell, in contrast with solid (2,4,6-$Me_3-C_6H_2)_6Pb_2$ ($\delta^{207}Pb = -141.3, -154.1$), where the non-equivalence of the ^{207}Pb nuclei is intramolecular in origin (no centre of symmetry).[127]

[j] A mixture of all $Ph_{6-n}(anisyl)_6Pb_2$ compounds ($n = 0, \ldots, 6$) has been studied.

[k] At −70°C.

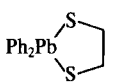
[l] Also in 2-methyl-THF, 1,2-dimethoxyethylene, DMPU[e].

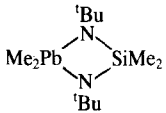
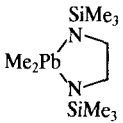
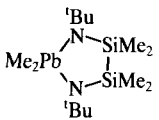
[m] $^1J(^{207}Pb\,^{183}W) = 115$ Hz.

[n] $^1J(^{207}Pb\,^{183}W) = 390$ Hz.

[o] See also Ref. 192, 193.

Table 8. Diorgano-, monoorganolead(IV)–element and lead(IV)–element compounds.

Compound	δ^{207}Pb	Solvent	Notes	Refs.	Other nuclei	Refs.
Me_2PbCl_2	−222.0	DMSO	*a*	78	^{13}C	78
Ph_2PbI_2	−391.8	$CDCl_3$		73		
$(4\text{-}MeO{-}C_6H_4)_2PbI_2$	−393.5	$CDCl_3$		73		
$Me_2Pb(OAc)_2$	−472.0	MeOH		78	^{13}C	78
	−538.0	Pyridine		78	^{13}C	78
$Me_2Pb(acac)_2$	−661.0	$CDCl_3$	*b*	49		
$Me_2Pb(pan)(acac)$	−799.0	$CDCl_3$	*b*	49		
$Me_2Pb(pan)(hfacac)$	−711.0	$CDCl_3$	*b*	49		
$Me_2Pb(pan)(oxin)$	−668.0	$CDCl_3$	*b*	49		
$Me_2Pb(pan)OAc$	−609.0	$CDCl_3$	*b*	49		
$Et_2Pb(OAc)_2$	−441.0	$CDCl_3$		78	^{13}C	78
$^{i}Pr_2Pb(OAc)_2$	−497.0	$CHCl_3$		78	^{13}C	78
	−662.0	Pyridine		78		
$Bu_2Pb(OAc)_2$	−448.0	$CDCl_3$		78	^{13}C	78
$Ph_2Pb(OAc)_2$	−688.0	$CHCl_3$		78		
	−859.0	Pyridine		78	^{13}C	78
	−611.6	$CDCl_3$		73		
	−692.1	0.5 M, $CHCl_3$	*c*	70		
	−911.3	0.5 M, HMPA	*c*	70		
$(2\text{-}MeO{-}C_6H_4)_2Pb(OAc)_2$	−561.5	$CDCl_3$		73		
$(3\text{-}MeO{-}C_6H_4)_2Pb(OAc)_2$	−591.0	$CDCl_3$		73		
$(4\text{-}MeO{-}C_6H_4)_2Pb(OAc)_2$	−490.1	$CDCl_3$		73		
 (solid)	+280.6	—		179		

	X						
$Ph_2Pb\text{-}SCH_2CH_2\text{-}X\text{-}CH_2CH_2S$	O	+90.1	$CDCl_3$		27	^{13}C	27
	S	+148.9	$CDCl_3$		27	^{13}C	27
		+209.1	C_6D_6		169	^{13}C, ^{15}N, ^{29}Si	169
		+296.1	C_6D_6	*d*	169	^{13}C, ^{15}N, ^{29}Si	169
		+159.3	C_6D_6	*e*	144	^{13}C, ^{15}N, ^{29}Si	144
	R M						
$R_2Pb[M(CO)_3(C_5H_5)]_2$	Ph Mo	+421.0	CH_2Cl_2/C_6D_6		171	^{95}Mo	171
	Et W	−128.0	CH_2Cl_2/C_6D_6	*f*	171		
	Ph W	−375.0	CH_2Cl_2/C_6D_6	*g*	171		
$Ph\text{-}Pb(OAc)_3$		−857.4	$CDCl_3$		73	^{13}C	76
$2\text{-}MeO-C_6H_4-Pb(OAc)_3$		−848.7	$CDCl_3$		73		
$4\text{-}MeO-C_6H_4-Pb(OAc)_3$		−795.5	$CDCl_3$		73		
$PbCl_4$		−767.7	—	*h*	99		

(Continued)

Table 8. (*Continued*)

Compound	δ^{207}Pb	Solvent	Notes	Refs.	Other nuclei	Refs.
$[NH_4]_2[PbCl_6]$ (solid)	−2058	—	*i*	126		
$Pb(OAc)_4$	−1869.0	$CDCl_3$		78		
$Pb(O_4C_2)_2$ (solid)	−1416	—	*j*	104		
PbO_2 (solid)	+4850	—	*k*	104		

Notes:

[a] c.n.(Pb) > 4.

[b] acac = acetylacetonato; pan = 1-(2-pyridylazo)-2-naphtolate; oxin = oxinate; hfacac = hexafluoroacetylacetonate.

[c] Bu_4Pb in C_6D_6 (50% v : v) has been selected as external reference compound; however, the δ^{207}Pb values appear to be incorrect by about 23–25 ppm (to high frequency).

[d] $^1J(^{207}Pb\,^{15}N) = 200.2$, $^2J(^{207}Pb\,^{29}Si) = 38.6$, $^1J(^{207}Pb\,^{13}C) = 342.8$, $^2J(^{207}Pb\,^{13}C) = 26.2$ Hz.

[e] $^1J(^{207}Pb\,^{15}N) = 172.7$, $^2J(^{207}Pb\,^{29}Si) = 62.3$ Hz.

[f] Proposed to be in mixture with $Et_3Pb{-}W(CO)_3(C_5H_5)$; $^1J(^{207}Pb\,^{183}W) = 135$ Hz.

[g] $^1J(^{207}Pb\,^{183}W) = 270$ Hz.

[h] Pure liquid under H_2SO_4.

[i] See Fig. 5.

[j] The δ^{207}Pb values are given in gauss; recalculation by assuming δ^{207}Pb $[Pb(NO_3)_2] = -2961$.

[k] The low shielding of the ^{207}Pb nucleus can be attributed to a Knight shift (PbO_2 is a conductor), and the broad resonance signal (in spite of the rutile structure) may be due to anisotropy and inhomogeneity of the Knight shift (impurities).[172]

Table 9. "Naked" cluster anions containing lead.

Compound	δ^{207}Pb	Solvent	Notes	Refs.	Other nuclei	Refs.
$[Pb_2Se_3]^{2-}$	+3290.0	en	*a*, *b*	2	^{77}Se	2
$[Pb_2Se_2Te]^{2-}$	+2894.0	en	*a*, *c*	2	^{77}Se, ^{125}Te	2
$[Pb_2SeTe_2]^{2-}$	+2375.0	en	*a*, *d*	2	^{77}Se, ^{125}Te	2
$[Pb_2Te_3]^{2-}$	+1727.0	en	*a*, *e*	2	^{125}Te	2
$[PbSn_8]^{4-}$ $4Na^+$	−2667.2	en	*a*, *f*	20	^{119}Sn	20
$[Pb_2Sn_7]^{4-}$ $4Na^+$	−2825.2	en	*a*, *f*	20	^{119}Sn	20
$[Pb_3Sn_6]^{4-}$ $4Na^+$	−3001.2	en	*a*, *f*	20	^{119}Sn	20
$[Pb_4Sn_5]^{4-}$ $4Na^+$	−3168.2	en	*a*, *f*	20	^{119}Sn	20
$[Pb_5Sn_4]^{4-}$ $4Na^+$	−3343.2	en	*a*, *f*	20	^{119}Sn	20
$[Pb_6Sn_3]^{4-}$ $4Na^+$	−3534.2	en	*a*, *f*	20	^{119}Sn	20
$[Pb_7Sn_2]^{4-}$ $4Na^+$	−3731.2	en	*a*, *f*	20	^{119}Sn	20
$[Pb_8Sn]^{4-}$ $4Na^+$	−3932.2	en	*a*, *f*	20	^{119}Sn	20
$[Pb_9]^{4-}$ $4Na^+$	−4150.2	en	*a*	20		
$[Pb_9]^{4-}$ $4Li^+$	−4185.2	en	*a*	20		
$[Pb_xPtL_y]^{q-}$ qK^+	−2988	en	*a*, *g*	35		

Notes:

[a] en = 1,2-diaminoethane.

[b] $J(^{207}Pb\,^{77}Se) = 149$ Hz.

[c] $J(^{207}Pb\,^{77}Se) = 188$ Hz; $J(^{207}Pb\,^{125}Te) = 915$ Hz.

[d] $J(^{207}Pb\,^{77}Se) = 227$ Hz; $J(^{207}Pb\,^{125}Te) = 994$ Hz.

[e] $J(^{207}Pb\,^{125}Te) = 1070$ Hz.

[f] Preliminary information is also given in Refs. 52, 79; $J(^{207}Pb\,^{119}Sn) = 555$, 562, 568, 572, 568, 562, 537, 488 Hz for 1, 2, 3, 4, 5, 6, 7 Pb atoms respectively: the δ^{207}Pb values as well as the $J(^{207}Pb\,^{119}Sn)$ values change slightly with the cation (Na^+, K^+, Rb^+, Cs^+); for the anions $[Sn_7PbTl]^{5-}$ and $[Sn_6Pb_2Tl]^{5-}$ coupling constants $J(^{207}Pb\,^{119}Sn) = 335$ Hz and 366 Hz (cation: Na^+) respectively are reported.[20]

[g] $J(^{207}Pb\,^{195}Pt) = 4122$ Hz; since no ^{31}P or ^{195}Pt NMR data are reported, the values for *q* and *y* and the nature of L remain uncertain.

Table 10. Anionic and cationic lead(II) compounds.

Compound	δ^{207}Pb	Solvent	Notes	Refs.	Other nuclei	Refs.
$Pb(AsF_6)_2$	−4066.0	SO_2(203 K)	*a*	47		
$PbCl_2$ (solid)	−1174	—	*b*	104		
$TlPbI_3$ (solid)	+371	—	*c*	147		
$Pb(ClO_4)_2$	−2839.0	1 M, H_2O	*d*	33		
$Pb(NO_3)_2$	−2961.2	1 M, H_2O	*d*	102		
$Pb(NO_3)_2$ (solid)	−3480	—	*b*	103, 104		
	−3562	—	*e*	64, 74		
$PbSO_4$ (solid)	−3575	—	*b*	104		
$PbCO_3$ (solid)	−2719	—		87		
$Pb(OAc)_2$	−1337.0	1 M, H_2O	*d*	102		
(solid)	−1416	—	*b*	104		
$Pb(OAc)_2 \cdot 3H_2O$ (solid)	−1906	—		181		
R						
$[Pb(O_2C-R)_2]_n$ C_5H_{12}	−2215		*f*	113		
C_7H_{16}	−2238					
C_9H_{20}	−2252					
$C_{11}H_{24}$	−2259					
$C_{13}H_{28}$	−2252					
$C_{15}H_{32}$	−2259					
$C_{17}H_{36}$	−2180					
$Pb(O_2CC_6F_5)_2$	−1044.0	0.1 M, THF	*d*	33		
$[Pb(MeNO_2)_2]^{2+}$	−3342.0	$MeNO_2$		37		
$[Pb(OPchex_3)_2]^{2+}$ $2AsF_6^-$	−1659.0	SO_2(203 K)	*a*	47	^{31}P	47
$[Pb(OPchex_3)_3]^{2+}$ $2AsF_6^-$	−1142.0	SO_2(203 K)	*a*	47	^{31}P	47
$PbCrO_4$ (solid)	−2360	—		87		
$PbMoO_4$ (solid)	−2078	—		87		
$PbWO_4$ (solid)	−2071	—		87		
$[Pb(SPh)_3]^-$	+2818.0	CD_3OD	*a*	36	^{13}C	36
$[Pb(SPchex_3)_3]^{2+}$ $2AsF_6^-$	+2457.0	SO_2(203 K)	*a*	47	^{31}P	47
$Pb[SP(S)(OEt)_2]_2$	−420.0	0.49 M, THF		33		
	−237.0	0.5 M, CH_2Cl_2		33		

$Pb[SP(S)(OBu)_2]_2$	−415.0	0.1 M, THF		33		
	−70.0	0.26 M, CH_2Cl_2		33		
$[Pb(SePh)_3]^-$	+3105.0	CD_3OD(213 K)		36	^{13}C, ^{77}Se	36
	+3188.0	CD_3OD(295 K)		36		
$[Pb(SPchex_3)_2(SePchex_3)]^{2+}2AsF_6^-$	+2719.0	SO_2(203 K)	*a*	47	^{31}P	47
$[Pb(SPchex_3)(SePchex_3)_2]^{2+}2AsF_6^-$	+2901.0	SO_2(203 K)	*a*	47	^{31}P	47
$[Pb(SePchex_3)_3]^{2+}$ $2AsF_6$	+3011.0	SO_2(203 K)	*a*	47	^{31}P	47
$[Pb(EDTA)]^{2+}$ $2NO_3^-$	−558.0	H_2O/D_2O (95 : 5)	*g*	39		
$[Pb(HEDTA)]^{2+}2NO_3^-$	−590.0	H_2O/D_2O	*g*	39		
$[Pb(NTA)]^-$	−813.0	H_2O/D_2O	*g*	39		
$[Pb(MIDA)]^{2-}$	−860.0	H_2O/D_2O	*g*	39		
$[Pb(Ph_2PCH_2CH_2PPh_2)]^{2+}$	+60.0	$MeNO_2$(260 K)		37	^{31}P	37
$[Pb(Ph_2PCH_2CH_2)_2PPh]^{2+}$	+56.0	$MeNO_2$		37	^{31}P	37
$[Pb(Ph_2PCH_2)_3CMe]^{2+}$	−190.0	$MeNO_2$		37	^{31}P	37
$[Pb(Ph_2PCH_2CH_2)_3P]^{2+}$	−269.0	$MeNO_2$		37	^{31}P	37
	−2.0	$MeNO_2$	*h*	37	^{31}P	

Notes:

[a] Referencing uncertain owing to contradictory use of the sign convention for δ values.

[b] $\delta^{207}Pb$ values were determined by the field-sweep method and are given in Gauss (calculated on the basis that $\delta^{207}Pb = -2961$ for an aqueous solution of $Pb(NO_3)_2$; the $\delta^{207}Pb$ values given in Ref. 105 are incorrect). See Ref. 192, 193 for $\delta^{207}Pb$ in aqueous solution.

[c] Single-crystal orthorombic $TlPbI_3$, calculated on the basis that $\delta^{207}Pb = -2854$ for an aqueous solution of $Pb(NO_3)_2$ at infinite dilution; $\delta^{207}Pb$ values for other perovskite-type structures ($TlPbBr_3$, $CsPbI_{3-n}Br_n$, with $n = 0,1,2,3$) and for $PbBr_2$, PbI_2 are given; however, owing to the extremely broad resonances, the $\delta^{207}Pb$ values are believed to differ considerably from the isotropic chemical shifts; qualitatively, the ^{207}Pb nuclei become deshielded by 600 ppm and 1390 ppm in $CsPbX_3$ (X = I and Br respectively) relative to $TlPbX_3$; similarly, the ^{207}Pb shielding in PbI_2 is reduced by about 900 ppm with respect to $PbBr_2$. See also Ref. 196.

[d] The dependence of $\delta^{207}Pb$ on the concentration has been studied. See also Ref. 192.

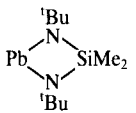
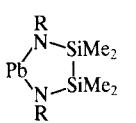
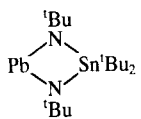
[e] Single-crystal; $\sigma_{\parallel} - \sigma_{\perp} = 53$ ppm; data in agreement with powder measurements.[87]

[f] All values are measured at 110°C without a solvent; CPMAS spectra (e.g. for $Pb(O_2C-C_{13}H_{28})_2$) have been determined ($\delta^{207}Pb$ −2138 and $\Delta\sigma = 424$ ppm; asymmetry $\eta = 0.1$; $\sigma_{11} = 1906$, $\sigma_{22} = 1945$ and $\sigma_{33} = 2562$ ppm). For $Pb(O_2C-C_9H_{20})_2$ see also Ref. 13.

[g] EDTA = ethylenediaminotetraacetic acid; HEDTA = *N*-hydroxyethylethylenediaminetriacetic acid; NTA = nitrilotriacetic acid; MIDA = methyliminodiacetic acid.

[h] $[Pb(Ph_2PCH_2CH_2)_2PCH_2CH_2P(H)Ph_2]^{3+}$.

Table 11. Monomeric diaminolead(II) compounds.

Compound		δ^{207}Pb	Solvent	Notes	Refs.	Other nuclei	Refs.
$Pb[N(^tBu)SiMe_3]_2$		+5271.0	C_6D_6	*a*	154	^{13}C, ^{15}N, ^{29}Si	154
$Pb[N(^tOct)SiMe_3]_2$		+5416.0	C_6D_6		154	^{13}C, ^{15}N, ^{29}Si	154
$Pb[N(SiMe_3)_2]_2$		+4916.0	C_6D_6		25	^{13}C, ^{15}N, ^{29}Si	14
		+4917.0	C_7D_8 (90°C)	*b*	14	^{13}C, ^{15}N, ^{29}Si	14
	R ^tBu ^tOct	+4900.0 +4930.0	C_6D_6 C_6D_6	*c*	19 19	^{13}C, ^{15}N, ^{29}Si ^{13}C, ^{15}N, ^{29}Si	14, 19 19
		+4904.0	C_6D_6	*d*	144	^{13}C, ^{15}N, ^{119}Sn	144

Notes:

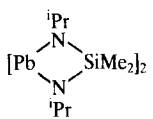
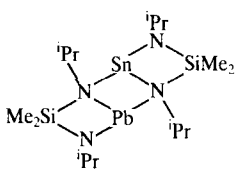
[a] $^1J(^{207}Pb\,^{15}N) = 656.7$ Hz.

[b] Slightly associated in solution.

[c] $^1J(^{207}Pb\,^{15}N) = 671.4$ Hz.

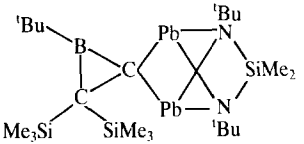
[d] $^1J(^{207}Pb\,^{15}N)$ 560.0 Hz; $^2J(^{207}Pb\,^{119}Sn) < 150.0$ Hz.

Table 12. Plumbocenes and miscellaneous lead(II) compounds.

Compound	δ^{207}Pb	Solvent	Notes	Refs.	Other nuclei	Refs.
$(\eta^5\text{-}C_5H_5)_2Pb$	−5030	C_6D_6		111		
$(\eta^5\text{-}C_5^tBu_2H_3)_2Pb$	−4756	$CDCl_3$	*h*	197	^{13}C	197
$(\eta^5\text{-}C_5Me_5)_2Pb$	−4390	C_6D_6		111		
	−4384	C_6D_6		194	^{13}C	194
$(\eta^5\text{-}C_5Ph_5)_2Pb$ (solid)	−6150	—		111	^{13}C	111
$(\eta^5\text{-}C_5Me_5)PbBF_4$	−5041.6	$CDCl_3$		194	^{11}B, ^{13}C, ^{19}F	194
$(\eta^5\text{-}C_5Me_5)PbCF_3SO_3$	−4961.6	$CDCl_3$		194	^{13}C, ^{19}F	194
$(\eta^5\text{-}C_5Me_5)Pb\text{-}bpyBF_4$	−4876	$CDCl_3$	*g*	194	^{11}B, ^{13}C	194
$(\eta^5\text{-}C_5Me_5)Pb\text{-}bpyCF_3SO_3$	−4381.7	$CDCl_3$	*g*	194	^{13}C	194
closo-1-Pb-2,3-$(SiMe_3)_2$-2,3-$C_2B_4H_4$	−1373.8	C_6D_6		186	^{11}B, ^{13}C	186
$Pb[CH(SiMe_3)_2]_2$	+9112	C_7D_8		145	^{13}C	145
	+2284	Et_2O	*a*			
	+2956	C_7D_8	*b*	156	^{13}C, ^{29}Si	156
	+2930	C_7D_8	*c*	156	^{29}Si, ^{119}Sn	156

(Continued)

Table 12. (*Continued*)

Compound	δ^{207}Pb	Solvent	Notes	Refs.	Other nuclei	Refs.
	+4935 +4818	C_6D_6 C_7D_8 (−40°C)		145	^{11}B, ^{13}C	145
PbO-yellow (solid)	+3770	—	*d*, *e*	104		
PbO-red (solid)	+38	—	*d*	104		
PbS (solid)	+1076	—	*f*	103		
PbSe (solid)	+2400	—	*f*	103		
PbTe (solid)	+357	—	*f*	103		

Notes:

[a] Presumably the ether adduct.

[b] Monomer–dimer equilibrium at room temperature or above; intramolecular rearrangement dominates below room temperature.

[c] $^2J(^{207}\text{Pb}\,^{119}\text{Sn}) = 530.0$ Hz.

[d] The δ^{207}Pb values were measured by the field-sweep method and given in gauss; the calculation of the δ^{207}Pb values (on the basis that $\delta^{207}\text{Pb} = -2961$ for an aqueous $Pb(NO_3)_2$ solution) gave significantly different values from those given in Ref. 105.

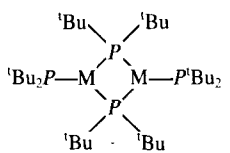
[e] According to Ref. 172, there is only a small difference in the δ^{207}Pb values for red and yellow PbO; however, no proper reference was given for the δ^{207}Pb values.

[f] The δ^{207}Pb values were measured by the field-sweep method and reported in gauss (cf. note *d*).

[g] bpy = 2,2′-Bipyridine.

[h] $(\eta^5\text{-}C_5{}^t\text{Bu}_2\text{H}_3)\text{PbBF}_4$: δ^{207}Pb −5461.8 in $CDCl_3$.

Table 13. Selected $^{1}J(^{207}PbX)$, $^{1}J(^{119}SnX)$ values (in Hz) and reduced coupling constants $^{1}K(^{207}PbX)$, $^{1}K(^{119}SnX)$ (in 10^{20} N A^{-2} m^{-3}).

Compound (M = Pb, Sn)	X	$^{1}J(^{207}PbX)$	Refs.	$^{1}K(^{207}PbX)$	$^{1}K(^{119}SnX)$	$^{1}J(^{119}SnX)$	Refs.	Notes
Me_3M-H	^{1}H	+2295	157	+92.3	+39.0	−1744.0	122	
Me_2MH_2	^{1}H	+2454.6	157	+98.7	+40.2	−1797.0	157	
Me_3M-BH_3	^{11}B	+460.0	187	+57.6	+38.6	−554.0	158	
$Me_3M-B[N(Me)CH_2]_2$	^{11}B	+1330	94	+166.6	+64.4	−930	175	
Me_3M-CH_3	^{13}C	+250.0	115	+39.6	+30.2	−340.0	146	
(*Z*)-$Me_3M-CH=CHMe$	^{13}C	+268.0	54	+56.8	+39.7	−446.6	108	
$Me_3M-C\equiv C-Me$	^{13}C	−59.0	55	−9.3	+44.4	−502.9	55	*a*
$Li^+[Me_2M-CH_3]^-$/THF	^{13}C	−775.0	187	−122.0	−13.7	+155.0	159	
$Li^+[Ph_2M-Ph]^-$/THF	^{13}C	−1030.0	4	−218.3	−23.1	+260.0	4	*b*
$M[CH(SiMe_3)_2]_2$	^{13}C	−734.0	145	−115.6	−36.6	+414.0	154, 177	
$Me_3M-SiMe_3$	^{29}Si	−764.2	187	+152.2	+73.3	+656.0	175	
$Me_3M-SnMe_3$	^{119}Sn	−3570.0	94	+381.2	+267.3	+4460.0	91	*c*
$Me_3M-SnPh_3$	^{119}Sn	−2800.0	94	+299.0	+254.1	+4240.0	94	
$[MSn_8]^{4-}$ $4Na^+$	^{119}Sn	555.0	20	59.4	16.1	268.0	20	*c, d, e*
$Me_3M-PbMe_3$	^{207}Pb	+290	98	+55.3	+381.2	−3570.0	94	
$Me_3M-N(Me)Ph$	^{15}N	+261.0	94	−102.8	+0.5	+2.2	94	
$Me_3M-N(H)Si(^tBu)Me_2$	^{15}N	+249.3	169	−98.2	+4.2	+19.1	169	*f*
$Me_3M-N(^tBu)SiMe_3$	^{15}N	+199.0	169	−78.4	1.2	5.4	178	*g*
$M[N(SiMe_3)_2]_2$	^{15}N	+564.0	14	−223.7	−80.2	−366.0	14	
Me_3M-PPh_2	^{31}P	−1335	94	−131.3	−32.9	+596.0	61	
$[M(dppe)]^{2+}(SbF_6)_2$	^{31}P	1714	59	170.0	92.2	1665	59	*e*
	^{31}P	2452	184	243.3	98.7	1782	185	*e*
	$^{31}P(\mu)$	1100	184	109.1	59.3	1071	185	*e*

(Continued)

Table 13. (*Continued*)

Compound (M = Pb, Sn)	X	$^1J(^{207}PbX)$	Refs.	$^1K(^{207}PbX)$	$^1K(^{119}SnX)$	$^1J(^{119}SnX)$	Refs.	Notes
$[M(P^tBu_2)_3Li \cdot THF]$	^{31}P	1770	7	175.6	75.3	1360	7	*e*
$Me_3M-SeMe$	^{77}Se	−1170	94	−244.2	−118.9	+1015.0	160	
MCl_4	^{35}Cl	705	99	288.9	85.0	375	99	*e*, *h*
$K_2[MCl_6]$	^{35}Cl	300	128	122.9	67.9	300	182	*e*, *i*
$Me_3M-W(CO)_3(C_5H_5)$	^{183}W	+170	171	159.5	+80.5	−150.0	175	
cis-$[Pt(MPh_3)Ph(PPh_3)_2]$	^{195}Pt	+18 380	42	+3403	+1318	−12 686	183	

Notes:

[a] In C_6D_6 solution.

[b] Similar values are obtained in other solvents (e.g. 2-Me−THF, $MeOCH_2CH_2OMe$) and with Na^+, K^+ instead of Li^+.

[c] $^1J(^{119}Sn^{119}Sn)$ values are calculated from $^1J(^{119}Sn^{117}Sn)$ by multiplication by 1.0465.

[d] Dependent on the counterion.

[e] The sign of $^1J(MX)$ has not been determined and there are no comparable compounds for which the sign of $^1J(MX)$ is known.

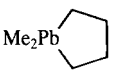
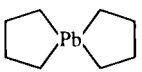
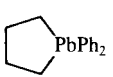
[f] $^2J(^{207}Pb^{29}Si) = 46.5$ Hz; $^2J(^{119}Sn^{29}Si) = 10.0$ Hz.

[g] $^2J(^{207}Pb^{29}Si) = 21.3$ Hz; $^2J(^{119}Sn^{29}Si) = 20.0$ Hz.

[h] Determined by the measurement of relaxation rates.

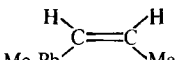
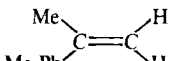
[i] Determined from solid-state ^{207}Pb NMR spectra (see Fig. 5); both values $^1J(M^{35}Cl) = \pm 30$ Hz.

Table 14. Selected $^{n}J(^{207}Pb\,^{13}C)$ and $^{2}J(^{207}Pb\,^{1}H)$ values for tetraorganylplumbanes.

Compound	$^{1}J(Pb\,^{13}C)$	$^{2}J(Pb\,^{1}H)$	$^{n}J(Pb\,^{1}H)$	$^{2}J(Pb\,^{13}C)$	$^{n}J(Pb\,^{13}C)$	Notes	Refs.
Me_4Pb	+250.0	−60.5	—	—	—		78
Me_3Pb-Et	196.0(Me)	56.4			—		78, 110
	346.0(Et)		151.4	37.0	—		
$Me_3Pb-{}^{i}Pr$	152.0(Me)	51.3					78, 110
	431.0(CH)		150.5	16.0			
Me_2PbEt_2	151.0(Me)				—		78
	292.0(Et)			34.0			
	154.0(Me)				—		107
	262.0(CH_2)			47.0			
$MePbEt_3$	244.0(Et)			32.0	—		78
Et_4Pb	200.0	−42.0	+127.0	30.0	—		96
	170.0			42.0	—		107
Bu_4Pb	190.0			28.0	74.0(^{3}J)		78
Me_3Pb-Ph	274.0(Me)	63.2			66.0(^{3}J)		90
	348.0(Ph)			63.0	16.0(^{4}J)		
Et_3Pb-Ph	256.0(Et)			34.0(Et)	51.0(^{3}J)		62
	143.0(Ph)			51.0(Ph)	13.0(^{4}J)		
Me_2PbPh_2	295.0(Me)	64.7			72.0(^{3}J)		90
	395.0(Ph)			65.0	19.0(^{4}J)		
Et_2PbPh_2	324.0(Et)			38.0(Et)	60.0(^{3}J)		62
	237.0(Ph)			56.0(Ph)	15.0(^{4}J)		
	290.0(CH_2)			55.0(CH_2)			107
	284.0(Ph)						

(Continued)

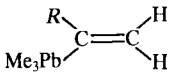
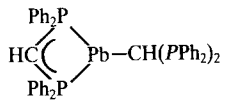
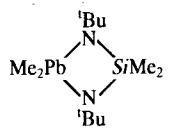
Table 14. (*Continued*)

Compound	$^1J(Pb^{13}C)$	$^2J(Pb^1H)$	$^nJ(Pb^1H)$	$^2J(Pb^{13}C)$	$^nJ(Pb^{13}C)$	Notes	Refs.
$MePbPh_3$	321.0(Me)	68.5			77.0(^3J)		90
	439.0(Ph)			67.0	19.0(^4J)		
$EtPbPh_3$	404.0(Et)			43.0(Et)	70.0(^3J)		62
	349.0(Ph)			62.0(Ph)	17.0(^4J)		
Ph_4Pb	481.0		81.0(^3J)	68.0	80.0(^3J)		76, 80
			26.2(^4J)		20.0(^4J)		
			15.2(^5J)				
	268.0(Me)	64.0					
	359.0(C=)	188.0	270.0(^3J)	⩽1	82.0(^3J)		54
	245.0(Me)	62.0					
	378.0(C=)		84.0(^3J, Me)	91.0(Me)			54
			128.0(*cis*)	62.0(C=)			
			283.0(*trans*)				
$Pb(CH{=}CH_2)_4$	454.1	213.3	331.8(*trans*)	⩽1			45, 70, 118
$Me_3Pb{-}C{\equiv}C{-}Me$	373.0(Me)	−76.2				*a*	55
	(−)59.0(C≡)		10.7(^4J)	10.0	7.0(^3J)		
$Et_3Pb{-}C{\equiv}C{-}Me$	319.0(Et)			41.0(Et)		*a*	55
	(−)277.6(C≡)			41.0(C≡)	5.0(^3J)		
$Me_2Pb(C{\equiv}C{-}Me)_2$	574.3(Me)	−100.9	13.5(^4J)			*a*	55
	(+)208.0(C≡)			70.3	9.2(^3J)		
$Et_2Pb(C{\equiv}C{-}Me)_2$	(+)531.6(Et)	−68.0	+224.5(^3J)	(−)61.0		*a*	55, 168
	(−)80.8(C≡)		9.8(^4J)	4.9	5.9(^3J)		
$Pb(C{\equiv}C{-}Me)_4$	(+)1624.5			347.4	30.5(^3J)		55

Note:

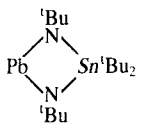
[a] In C_6D_6; the $^1J(^{207}Pb^{13}C{\equiv})$ values in $CDCl_3$ differ from those in C_6D_6: greater values indicate a negative sign and smaller values for $CDCl_3$ solutions a positive sign of $^1J(^{207}Pb^{13}C{\equiv})$.

Table 15. Selected geminal coupling constants $^2J(^{207}PbEX)$ (in Hz) ($X \neq {}^1H, {}^{13}C$).

Compound		X	E	$^2J(^{207}PbEX)$	Notes	Refs.
	n					
$(Me_3Pb)_nC(SnMe_3)_{4-n}$	1	^{119}Sn	C	508.6		21
	2	^{119}Sn	C	487.4		21
	3	^{119}Sn	C	463.3		21
	*R*					
	Me_3Si	^{29}Si	C=	111.4		5
	Me_3Sn	^{119}Sn	C=	896.5		5
	Me_3Pb	^{207}Pb	C=	1172.2	*a*	5
		^{31}P	C	165.0	*b*	8, 9
$(Me_3Pb)_2C{=}PMe_3$		^{31}P	C=	28.8		83
$Me_3Pb{-}CF_3$		^{19}F	C	240.6		116
$Me_2Pb(CF_3)_2$		^{19}F	C	379.0		116
$Pb(CF_3)_4$		^{19}F	C	808.0		195
$Me_3Pb{-}N(^tBu)SiMe_3$		^{29}Si	N	21.3		169
$Me_3Pb{-}N(SiMe_3)_2$		^{29}Si	N	9.9		169
		^{29}Si	N	5.6		169

(Continued)

Table 15. (*Continued*)

Compound	X	E	$^2J(^{207}PbEX)$	Notes	Refs.
$Me_2Pb[N(^tBu)SiMe_2]_2$	^{29}Si	N	62.3		144
$Pb[N(SiMe_3)_2]_2$	^{29}Si	N	29.0		25
$Pb[N(^tBu)SiMe_3]_2$	^{29}Si	N	$\leqslant 10.0$		154
$Pb[N(^tBu)SiMe_2]_2$	^{29}Si	N	27.1		19
$Me_3Pb-N(^tBu)SnMe_3$	^{119}Sn	N	135.0		57
$Me_3Pb-N(SnMe_3)_2$	^{119}Sn	N	417.0		57
$(Me_3Pb)_2N-SnMe_3$	^{119}Sn	N	502.0		57
	^{119}Sn	N	<150		144
$[Pb(OPchex_3)_3]^{2+}$	^{31}P	O	62.0		47
$[Pb(OPPh_3)_3]^{2+}$	^{31}P	O	45.0		59
$Ph_3Pb-S-PbPh_3$	^{207}Pb	S	381.0	*c*	124
$[Pb(SPchex_3)_3]^{2+}$	^{31}P	S	31.0		47
$[Pb((SePchex_3)_3]^{2+}$	^{31}P	Se	50.0		47
cis-$[Pt(PPh_3)_2(C\equiv C-{}^tBu)(PbMe_3)]$	^{31}P	Pt	3002.0(*trans*) 189.0(*cis*)		163
cis-$[Pt(PPh_3)_2(Ph)(PbPh_3)]$	^{31}P	Pt	3460.0(*trans*) 260.0(*cis*)		42, 106

Notes:

[a] The compound studied is $(Me_3Pb)_2C=C(Me)H$.

[b] At $-20^\circ C$; at higher temperatures all ^{31}P nuclei become equivalent owing to rapid intramolecular exchange.

[c] Measured via observation of ^{13}C satellites in the ^{207}Pb NMR spectrum; the lead atoms are crystallographically non-equivalent in the solid state, allowing for the observation of ^{207}Pb satellites in the CP MAS ^{207}Pb NMR spectrum: $^2J(^{207}Pb\,^{207}Pb) = 351$ Hz.

REFERENCES

1. P. Granger, C. Brevard and M. Devaud, *J. Magn. Reson.*, 1988, **76**, 232.
2. M. Björgvinsson, J.F. Sawyer and G. Schrobilgen, *Inorg. Chem.*, 1987, **26**, 741.
3. E. Capek and K.E. Schwarzhans, *Monatsh. Chem.*, 1987, **118**, 419.
4. U. Edlund, T. Lejon, P. Pyykkö, T.K. Venkatachalam and E. Buncel, *J. Am. Chem. Soc.*, 1987, **109**, 5982.
5. T.N. Mitchell and W. Reimann, *Magn. Reson. Chem.*, 1987, **25**, 1019.
6. W. Adcock, H. Gangodawila, G.B. Kok, V.S. Iyer, W. Kitching, G.M. Drew and D. Young, *Organometallics*, 1987, **6**, 156.
7. A.M. Arif, A.H. Cowley, R.A. Jones and J.M. Power, *J. Chem. Soc. Chem. Commun.*, 1986, 1446.
8. A.L. Balch and D.E. Oram, *Organometallics*, 1986, **5**, 2159.
9. A.L. Balch and D.E. Oram, *Inorg. Chem.*, 1987, **26**, 1906.
10. T. Tsuda, H. Yasuoka and J.P. Remeika, *J. Phys. Soc. Jpn*, 1987, **56**, 3032.
11. T.N. Mitchell, R. Wickenkamp, A. Amamria, R. Dicke and U. Schneider, *J. Org. Chem.*, 1987, **52**, 4868.
12. F.H. Köhler, W.A. Geike and N. Hertkorn, *J. Organomet. Chem.*, 1987, **334**, 359.
13. A.M.A. Da Costa, H.D. Burrows, C.F.G.C. Geraldes, J.J.C. Teixeira-Dias, C.G. Bazuin, D. Guillon, A. Skoulios, E. Blackmore, G.J.T. Tiddy and D.L. Turner, *Liquid Crystals*, 1986, **1**, 215.
14. C. Stader and B. Wrackmeyer, *J. Magn. Reson.*, 1987, **72**, 544.
15. B. Topic, U. Haeberlen, R. Blinc and H. Arend, *J. Phys. Chem.: Solid State Phys.*, 1986, **19**, 3925.
16. T.N. Mitchell and W. Reimann, *J. Organomet. Chem.*, 1987, **322**, 151.
17. P.J. Watkinson and K.M. MacKay, *J. Organomet. Chem.*, 1984, **275**, 39.
18. I. Novak and A.W. Potts, *J. Electron Spectrosc. Rel. Phenom.*, 1984, **33**, 1.
19. K. Horchler, C. Stader and B. Wrackmeyer, *Inorg. Chim. Acta*, 1986, **117**, L39.
20. W.L. Wilson, R.W. Rudolph, L.L. Lohr, R.C. Taylor and P. Pyykkö, *Inorg. Chem.*, 1986, **25**, 1535.
21. T.N. Mitchell and R. Wickenkamp, *J. Organomet. Chem.*, 1985, **291**, 179.
22. S. Kerschl, A. Sebald and B. Wrackmeyer, *Magn. Reson. Chem.*, 1985, **23**, 514.
23. C.T. Aitken and M. Onyszchuk, *J. Organomet. Chem.*, 1985, **295**, 149.
24. B. Wrackmeyer, *J. Organomet. Chem.*, 1985, **297**, 265.
25. B. Wrackmeyer, *J. Magn. Reson.*, 1985, **61**, 536.
26. N. Kleiner and M. Dräger, *J. Organomet. Chem.*, 1985, **293**, 323.
27. M. Dräger and N. Kleiner, *Z. Anorg. Allg. Chem.*, 1985, **522**, 48.
28. T.C. Wong, *J. Magn. Reson.*, 1985, **63**, 179.
29. N. Kleiner and M. Dräger, *Z. Naturforsch.*, 1985, **40b**, 477.
30. N. Kleiner and M. Dräger, *J. Organomet. Chem.*, 1984, **270**, 151.
31. F. Bucholtz and P.J. Bray, *J. Non-Cryst. Solids*, 1983, **54**, 43.
32. P.G. Harrison and M.A. Healy, *Inorg. Chim. Acta*, 1983, **80**, 279.
33. P.G. Harrison, M.A. Healy and A.T. Steel, *J. Chem. Soc. Dalton Trans.*, 1983, 1845.
34. T.N. Mitchell, *J. Organomet. Chem.*, 1983, **255**, 279.
35. F. Teixidor, M.L. Luetkens and R.W. Rudolph, *J. Am. Chem. Soc.*, 1983, **105**, 149.
36. J.J.I. Arsenault and P.A.W. Dean, *Can. J. Chem.*, 1983, **61**, 1516.
37. P.A.W. Dean, *Can. J. Chem.*, 1983, **61**, 1795.
38. N.P. Erchak, A.R. Ashmane, Yu. Yu. Popelis and E. Lukevits, *Zh. Obshch. Khim.*, 1983, **53**, 383.
39. T.T. Nakashima and D.L. Rabenstein, *J. Magn. Reson.*, 1983, **51**, 223.

40. H. Morikawa, Y. Tagaki and H. Ohno, *J. Non-Cryst. Solids*, 1982, **53**, 173.
41. C.A. Fyfe, G.C. Gobbi, J.S. Hartman, R.E. Lenkinski and J.H. O'Brien, *J. Magn. Reson.*, 1982, **47**, 168.
42. S. Carr, R. Colton and D. Dakternieks, *J. Organomet. Chem.*, 1982, **240**, 143.
43. S.B. Nagelberg, C.E. Reinhold, B.R. Willeford, M.P. Bigwood, K.C. Molloy and J.J. Zuckerman, *Organometallics*, 1982, **1**, 851.
44. P.G. Harrison, M.A. Healy and A.T. Steel, *Inorg. Chim. Acta*, 1982, **67**, L15.
45. B. Wrackmeyer, *Spectrosc. Int. J.*, 1982, **1**, 201.
46. D. Steinborn, R. Taube and R. Radeglia, *J. Organomet. Chem.*, 1982, **229**, 159.
47. P.A.W. Dean, *Can. J. Chem.*, 1982, **60**, 2921.
48. P. Pyykkö, *J. Organomet. Chem.*, 1982, **232**, 21.
49. J. Otera, A. Kusaba, T. Hinoishi and Y. Kawasaki, *J. Organomet. Chem.*, 1982, **228**, 223.
50. P.P. De Witt, H.O. Van Der Koi and J. Wolters, *J. Organomet. Chem.*, 1981, **216**, C9.
51. G.R. Hays, D.G. Gillies, L.P. Blaauw and A.D.H. Clague, *J. Magn. Reson.*, 1981, **45**, 102.
52. B.S. Pons, D.J. Santure, R.C. Taylor and R.W. Rudolph, *Electrochim. Acta*, 1981, **26**, 365.
53. R. Radeglia, D. Steinborn and R. Taube, *Z. Chem.*, 1981, **21**, 365.
54. T.N. Mitchell and H.C. Marsmann, *Org. Magn. Reson.*, 1981, **15**, 263.
55. B. Wrackmeyer, *J. Magn. Reson.*, 1981, **42**, 287.
56. A. Sebald and B. Wrackmeyer, *Spectrochim. Acta*, 1981, **37A**, 365.
57. W. Biffar, T. Gasparis-Ebeling, H. Nöth, W. Storch and B. Wrackmeyer, *J. Magn. Reson.*, 1981, **44**, 54.
58. P. Pyykkö and W. Wiesenfeld, *Mol. Phys.*, 1981, **43**, 557.
59. P.A.W. Dean, D.D. Phillips and L. Polensek, *Can. J. Chem.*, 1981, **59**, 50.
60. R.W. Kunz, *Helv. Chim. Acta*, 1980, **63**, 2054.
61. J.D. Kennedy, W. McFarlane, G.S. Pyne and B. Wrackmeyer, *J. Organomet. Chem.*, 1980, **195**, 285.
62. D.C. Van Beelen, A.E.J. Van Kampen and J. Wolters, *J. Organomet. Chem.*, 1980, **187**, 43.
63. G. Schmid, F. Schmidt and R. Boese, *Chem. Ber.*, 1985, **118**, 1949.
64. O. Lutz and A. Nolle, *Z. Phys.*, 1980, **36B**, 323.
65. D. J. Burton, R. K. Harris and L. H. Merwin, *J. Magn. Reson.*, 1980, **39**, 159.
66. E.H. Curzon, N. Herron and P. Moore, *J. Chem. Soc. Dalton Trans.*, 1980, 721.
67. M.J. Vaikus and D.G. Anderson, *Org. Magn. Reson.*, 1980, **14**, 278.
68. V. Lucchini and P. R. Wells, *J. Organomet. Chem.*, 1980, **199**, 217.
69. M. Birkhahn, R. Hohlfeld, W. Massa, R. Schmidt and J. Lorberth, *J. Organomet. Chem.*, 1980, **192**, 47.
70. R. H. Cox, *J. Magn. Reson.*, 1979, **33**, 61.
71. B. Wrackmeyer, *J. Organomet. Chem.*, 1979, **166**, 353.
72. D. De Vos, D.C. Van Beelen and J. Wolters, *J. Organomet. Chem.*, 1979, **172**, 303.
73. D.C. Van Beelen, H. O. Van Der Kooi and J. Wolters, *J. Organomet. Chem.*, 1979, **179**, 37.
74. O. Lutz and A. Nolle, *Z. Phys.*, 1979, **35B**, 245.
75. T. Majima and Y. Kanosaki, *Bull. Chem. Soc. Jpn*, 1979, **52**, 73.
76. D. De Vos, W.A.A. Barneveld, D.C. Van Beelen and J. Wolters, *Recl. Trav. Chim. Pays-Bas*, 1979, **98**, 202.
77. N.W. Alcock, N. Herron and P. Moore, *J. Chem. Soc. Dalton Trans.*, 1979, 1486.
78. T.N. Mitchell, J. Gmehling and F. Huber, *J. Chem. Soc. Dalton Trans.*, 1978, 960.

79. R.W. Rudolph, W.L. Wilson, F. Parker, R.C. Taylor and D.C. Young, *J. Am. Chem. Soc.*, 1978, **100**, 4629.
80. D. De Vos and J. Wolters, *Recl. Trav. Chim. Pays-Bas*, 1978, **97**, 181.
81. D.J. Cane, W.A.G. Graham and L. Vancea, *Can. J. Chem.*, 1978, **56**, 1538.
82. H. Fußstetter, H. Nöth, B. Wrackmeyer and W. McFarlane, *Chem. Ber.*, 1977, **110**, 3172.
83. H. Schmidbaur, J. Eberlein and W. Richter, *Chem. Ber.*, 1977, **110**, 677.
84. R. Grüning, P. Krommes and J. Lorberth, *J. Organomet. Chem.*, 1977, **127**, 167.
85. D.L. Lichtenberger and T.L. Brown, *J. Am. Chem. Soc.*, 1977, **99**, 8187.
86. J.D. Kennedy, W. McFarlane and G.S. Pyne, *J. Chem. Soc. Dalton Trans.*, 1977, 2332.
87. A. Nolle, *Z. Naturforsch.*, 1977, **32a**, 964.
88. K.S. Kim, P.J. Bray and S. Merrin, *J. Chem. Phys.*, 1976, **64**, 4459.
89. M.E. Stoll, W.-K. Rhim and R.W. Vaughan, *J. Chem. Phys.*, 1976, **64**, 4808.
90. D. De Vos, *J. Organomet. Chem.*, 1976, **104**, 193.
91. W. McFarlane, *J. Chem. Soc.* (A), 1968, 1630.
92. M. Bullpitt, W. Kitching, W. Adcock and D. Doddrell, *J. Organomet. Chem.*, 1976, **116**, 161.
93. L. Vancea, R. K. Pomeroy and W.A.G. Graham, *J. Am. Chem. Soc.*, 1976, **98**, 1407.
94. J.D. Kennedy, W. McFarlane and B. Wrackmeyer, *Inorg. Chem.*, 1976, **15**, 1299.
95. W. McFarlane, *J. Organomet. Chem.*, 1976, **116**, 315.
96. D.C. Van Beelen, D. De Vos, G.J.M. Bots, L.J. Van Doorn and J. Wolters, *Inorg. Nucl. Chem. Lett.*, 1976, **12**, 581.
97. M. J. Cooper, A.K. Holliday, P.H. Makin and R.J. Puddephatt, *J. Organomet. Chem.*, 1974, **65**, 377.
98. J.D. Kennedy and W. McFarlane, *J. Organomet. Chem.*, 1974, **80**, C47.
99. R.M. Hawk and R.R. Sharp, *J. Chem. Phys.*, 1974, **60**, 1009.
100. M. Aritomi and Y. Kawasaki, *J. Organomet. Chem.*, 1974, **81**, 363.
101. A.C. Gossard, F.J. di Salvo and H. Yasouka, *Phys. Rev.*, 1974, **B9**, 3965.
102. G.E. Maciel and J.L. Dallas, *J. Am. Chem. Soc.*, 1973, **95**, 3039.
103. I. Weinberg, *J. Chem. Phys.*, 1962, **36**, 1112.
104. L.H. Piette and H.E. Weaver, *J. Chem. Phys.*, 1958, **28**, 735.
105. J.D. Kennedy and W. McFarlane, in *NMR and The Periodic Table* (ed. R.K. Harris and B.E. Mann), p. 366. Academic Press, London, 1978.
106. S. Carr, R. Colton and D. Dakternieks, *J. Magn. Reson.*, 1982, **47**, 156.
107. D.C. Van Beelen, Thesis, University of Leiden, The Netherlands, 1980.
108. T.N. Mitchell and C. Kummetat, *J. Organomet. Chem.*, 1978, **157**, 275.
109. T.A.K. Al-Allaf, *J. Iraqi Chem. Soc.*, 1986, **11**, 25.
110. G. Singh, *J. Organomet. Chem.*, 1975, **99**, 251.
111. C. Janiak, H. Schumann, C. Stader, B. Wrackmeyer and J.J. Zuckerman, *Chem. Ber.*, 1988, **121**, 1745.
112. G. Schmid, D. Zaika, J. Lehr, N. Augart and R. Boese, *Chem. Ber.*, 1988, **121**, 1873.
113. H.D. Burrows, C.F.G.C. Geraldes, T.J.T. Pinheiro, R.K. Harris and A. Sebald, *Liquid Crystals*, 1988, **3**, 853.
114. P.T. Narasimhan and M.T. Rogers, *J. Chem. Phys.*, 1961, **34**, 1049.
115. W. McFarlane, *Mol. Phys.*, 1967, **13**, 587.
116. R. Eujen and R.J. Lagow, *J. Chem. Soc. Dalton Trans.*, 1978, 541.
117. D. Doddrell, K. G. Lewis, C.E. Mulquiney, W. Adcock, W. Kitching and M. Bullpitt, *Aust. J. Chem.*, 1974, **27**, 417.
118. P. Krebs and H. Dreeskamp, *Spectrochim. Acta*, 1969, **25A**, 1399.

119. R.J.H. Clark, A.G. Davies, R.J. Puddephatt and W. McFarlane, *J. Am. Chem. Soc.*, 1969, **91**, 1334.
120. G.D. Shier and R.S. Drago, *J. Organomet. Chem.*, 1966, **6**, 359.
121. H.P. Fritz and K.-E. Schwarzhans, *Chem. Ber.*, 1964, **97**, 1390.
122. N. Flitcroft and H.D. Kaesz, *J. Am. Chem. Soc.*, 1963, **85**, 1377.
123. H.P. Fritz and K.-E. Schwarzhans, *J. Organomet. Chem.*, 1964, **1**, 297.
124. R.K. Harris and A. Sebald, *Magn. Reson. Chem.*, 1989, **27**, 81.
125. R.M. Hawk and R.R. Sharp, *J. Chem. Phys.*, 1974, **60**, 1522.
126. A. Sebald and A.R. Grimmer, Unpublished results.
127. A. Sebald, Manuscript in preparation.
128. K. Horchler, A. Sebald and B. Wrackmeyer, Unpublished results.
129. R.K. Harris, P. Reams and K.J. Packer, *J. Mol. Struct.*, 1986, **141**, 13.
130. R.K. Harris and A. Sebald, *Magn. Reson. Chem.*, 1987, **25**, 1058.
131. J.D. Kennedy and W. McFarlane, in *Multinuclear NMR* (ed. J. Mason), p. 305. Plenum Press, London, 1987.
132. W. McFarlane, *Proc. R. Soc. Lond.*, 1968, **A306**, 185.
133. (a) W. McFarlane, in *Annual Reports on NMR Spectroscopy*, Vol. 1 (ed. E.F. Mooney), p. 135. Academic Press, London, 1968.
(b) W. McFarlane, in *Annual Reports, on NMR spectrocopy*, Vol. 5A (ed. E.F. Mooney), p. 353. Academic Press, London, 1972.
134. (a) G.A. Morris and R. Freeman, *J. Am. Chem. Soc.*, 1979, **101** 760.
(b) G.A. Morris, *J. Am. Chem. Soc.*, 1980, **102**, 428.
(c) G.A. Morris, *J. Magn. Reson.*, 1980, **41**, 185.
(d) D.P. Burum and R.R. Ernst, *J. Magn. Reson.*, 1980, **39**, 163.
135. (a) D.T. Pegg, D.M. Doddrell, W.M. Brooks and M.R. Bendall, *J. Magn. Reson.*, 1981, **44**, 32.
(b) D.T. Pegg, D.M. Doddrell and M.R. Bendall, *J. Chem. Phys.*, 1982, **77**, 2745.
136. (a) A. Allerhand and S.R. Maple, *Anal. Chem.*, 1987, **59**, 441A.
(b) E.W. Bastiaan, J. Bulthuis and C. MacLean, *Magn. Reson. Chem.*, 1986, **24**, 723.
137. (a) W.S. Brey (ed.) *Pulse Methods in 1D and 2D Liquid-Phase NMR*. Academic Press, New York, 1988.
(b) W.R. Croasman and R.M.K. Carlson (eds.) *Two-Dimensional NMR Spectroscopy*. VCH Publishers, Weinheim, 1987.
138. (a) R.R. Ernst, G. Bodenhausen and A. Wokaun, *Principles of Nuclear Magnetic Resonance in One and Two Dimensions*, pp. 468 ff. Clarendon Press, Oxford, 1987.
(b) J. Cavanagh, C.A. Hunter, D.N.M. Jones, J. Keeler and J.K.M. Sanders, *Magn. Reson. Chem.*, 1988, **26**, 667.
(c) R. Benn and A. Rufinska, *Magn. Reson. Chem.*, 1988, **26**, 895.
139. O. Howarth, in *Multinuclear NMR* (ed. J. Mason), p. 133. Plenum Press, London, 1987 (and references cited therein).
140. N.F. Ramsey, *Phys. Rev.*, 1950, **77**, 567; *Ibid.*, 1950, **78**, 699; *Ibid.*, 1951, **83**, 540; *Ibid.*, 1952, **86**, 243.
141. P. Pyykkö, *Chem. Phys.*, 1983, **74**, 1.
142. H.C.E. McFarlane and W. McFarlane, *J. Chem. Soc. Dalton Trans.*, 1973, 2416.
143. R.J. Goodfellow, in *Multinuclear NMR* (ed. J. Mason), p. 563. Plenum Press, London, 1987.
144. B. Wrackmeyer, K. Horchler and C. Stader, *J. Magn. Reson.*, 1989, **83**, 601.
145. H. Meyer, Dissertation, University of Marburg, 1988. A. Berndt, Personal Communication.

146. B. Wrackmeyer, in *Annual Reports on NMR Spectroscopy*, Vol. 16 (ed. G. A. Webb), p. 73. Academic Press, London, 1985.
147. S. Sharma, N. Weiden and Al. Weiss, *Z. Naturforsch.*, 1987, **42a**, 1313.
148. V.S. Petrosyan, *Prog. NMR Spectrosc.*, 1977, **11**, 115.
149. N.F. Ramsey, *Phys. Rev.*, 1953, **91**, 303.
150. B. Wrackmeyer and K. Wagner, *Chem. Ber.*, 1989, **122**, 857.
151. J.A. Pople and D.P. Santry, *Mol. Phys.*, 1964, **8**, 1.
152. P. Pyykkö, *Chem. Phys.*, 1977, **22**, 289.
153. G. Breit, *Phys. Rev.*, 1930, **35**, 1447.
154. C. Stader and B. Wrackmeyer, *Z. Naturforsch.*, 1987, **42b**, 1515.
155. B. Wrackmeyer, S. Kerschl, C. Stader and K. Horchler, *Spectrochim. Acta*, 1986, **42A**, 1113.
156. B. Wrackmeyer, K. Horchler, H. Zhou and M. Veith, *Z. Naturforsch.*, 1989, **44b**, 288.
157. C. Schumann and H. Dreeskamp, *J. Magn. Reson.*, 1970, **3**, 204.
158. W. Biffar, H. Nöth, H. Pommerening, R. Schwerthöffer, W. Storch and B. Wrackmeyer, *Chem. Ber.* 1981, **114**, 49.
159. J.D. Kennedy and W. McFarlane, *J. Chem. Soc. Chem. Commun.*, 1974, 983.
160. J.D. Kennedy and W. McFarlane, *J. Chem. Soc. Dalton Trans.*, 1973, 2134.
161. J.D. Kennedy, W. McFarlane and G.S. Pyne, *Bull. Soc. Chim. Belg.*, 1975, **84**, 289.
162. B.E. Mann and B.F. Taylor, *^{13}C-NMR Data for Organometallic Compounds.* Academic Press, London, 1981.
163. A. Sebald, Diploma-Thesis, University of Munich, 1980.
164. R. G. Barnes and W. V. Smith, *Phys. Rev.*, 1954, **93**, 95.
165. H.O. Kalinowski, H.-O. Berger and S. Braun, *^{13}CNMR Spektroskopie.* Thieme, Stuttgart, 1984.
166. (a) A. Pines, M.G. Gibby and I.S. Waugh, *J. Chem. Phys.*, 1973, **59**, 569.
(b) J. Schaefer and E. O. Steijskal, *J. Am. Chem. Soc.*, 1976, **98**, 1031.
(c) C. S. Yannoni, *Acc. Chem. Res.*, 1982, **15**, 201.
167. A. Sebald, Dissertation, University of Munich, 1983.
168. B. Wrackmeyer and K. Horchler, Unpublished results, 1988.
169. B. Wrackmeyer and H. Zhou, Unpublished results, 1988.
170. K.V. Schenker and W.V. Philipsborn, *J. Magn. Reson.*, 1985, **61**, 294.
171. M.M. Kubicki, J.-I. Le Gall, R. Kergoat and L.C.G. de Lima, *Can. J. Chem.*, 1987, **65**, 1292.
172. K.S. Kim and P.J. Bray, *J. Magn. Reson.*, 1974, **16**, 334.
173. R. M. Hawk and R. R. Sharp, *J. Magn. Reson.*, 1973, **10**, 385.
174. J.M. Rocard, M. Bloom and L.B. Robinson, *Can. J. Phys.*, 1959, **28**, 735.
175. J.D. Kennedy, W. McFarlane, G.S. Pyne and B. Wrackmeyer, *J. Chem. Soc. Dalton Trans.*, 1975, 386.
176. P.J. Bray, M. Leventhal and H.O. Hooper, *Phys. Chem. Glasses*, 1963, **4**, 47.
177. K.W. Zilm, G.A. Lawless, R.M. Merill, J.M. Millar and G.G. Webb, *J. Am. Chem. Soc.*, 1987, **109**, 7236.
178. B. Wrackmeyer, S. Kerschl, C. Stader and K. Horchler, *Spectrochim. Acta*, 1986, **42A**, 1113.
179. A. Sebald and M. Dräger, Unpublished results.
180. J.R. Ascenso, R.K. Harris and P. Granger, *J. Organomet. Chem.*, 1986, **301**, C23.
181. A. Sebald and R.K. Harris, Unpublished results.
182. P. Reams, PhD Thesis, University of Durham, 1987.
183. S. Carr, R. Colton and D. Dakternieks, *J. Organomet. Chem.*, 1983, **249**, 327.

184. A.H. Cowley, D.M. Giolando, R.A. Jones, C.M. Nunn and J.R. Power, *Polyhedron*, 1988, **7**, 1909.
185. W.-W. du Mont and H.-J. Kroth, *Angew. Chem.*, 1977, **89**, 832; *Angew. Chem. Int. Ed. Engl.*, 1977, **16**, 792.
186. N.S. Hosmane, U. Siriwardane, H. Zhu, G. Zhang and J.A. Maguire, *Organometallics*, 1989, **8**, 566.
187. B. Wrackmeyer and K. Horchler, *Z. Naturforsch.*, 1989, **44b**, in press.
188. B. Wrackmeyer and K. Horchler, *Magn. Reson. Chem.*, 1990, **28**, in press.
189. R. Köster, G. Seidel, B. Wrackmeyer, K. Horchler and D. Schlosser, *Angew. Chem.*, 1989, **101**, 945; *Angew. Chem. Int. Ed. Engl.*, 1989, **28**, 918.
190. P.A. Scherr and J.P. Oliver, *J. Am. Chem. Soc.*, 1972, **94**, 8026.
191. B. Wrackmeyer, K. Horchler and R. Boese, *Angew. Chem.*, 1989, **101**, in press; *Angew. Chem. Int. Ed. Engl.*, 1989, **28**, in press.
192. A.M. Bond, J.R. Bradbury, P.J. Hanna, G.N. Howell, H.A. Hudson, S. Strother and M.J. O'Connor, *Anal. Chem.*, 1984, **56**, 2392.
193. G.N. Howell, M.J. O'Connor, A.M. Bond, H.A. Hudson, P.J. Hanna and S. Strother, *Aust. J. Chem.*, 1986, **39**, 1167.
194. P. Jutzi, R. Dickbreder and H. Nöth, *Chem. Ber.*, 1989, **122**, 865.
195. T.J. Juhlke, J.I. Glanz and R.J. Lagow, *Inorg. Chem.*, 1989, **28**, 980.
196. M. Nizam, M. Allavena, Y. Bouteiller, B.H. Suits and D. White, *J. Magn. Reson.*, 1989, **82**, 441.
197. P. Jutzi and R. Dickbreder, *J. Organomet. Chem.*, 1989, **373**, 301.

Nuclear Spin Relaxation in Diamagnetic Fluids

Part 1. General Aspects and Inorganic Applications

JOZEF KOWALEWSKI

Divison of Physical Chemistry, Arrhenius Laboratory, University of Stockholm, S-106 91 Stockholm, Sweden

1. Introduction 308
2. Relaxation theory 309
   2.1. General aspects 310
   2.2. Relaxation mechanisms 313
   2.3. Reorientational dynamics—rigid molecules 322
   2.4. Reorientational dynamics—flexible molecules 329
   2.5. Distortional dynamics 335
   2.6. Translational dynamics 338
   2.7. Relaxation and exchange 341
3. Experimental methods 344
   3.1 Spin–lattice relaxation 344
   3.2 Spin–spin relaxation and spin–lattice relaxation in the rotating frame 349
   3.3 Cross-relaxation and nuclear Overhauser enhancement . . 352
   3.4 Other relaxation experiments 357
   3.5 Analysis of relaxation data 361
4. Relaxation measurements in gases 362
5. Relaxation in inorganic systems 365
   5.1 Pure inorganic liquids other than water 366
   5.2 Water and aqueous solutions of simple electrolytes . . . 367
   5.3 Main-group metal compounds and complexes in solution . . 375
   5.4 Transition-metal compounds and complexes in solution . . 385
   5.5 Other inorganic systems 393
   Acknowledgements 394
   References 395

ANNUAL REPORTS ON NMR SPECTROSCOPY
VOLUME 22 ISBN 0-12-505322-3

Copyright © 1989 Academic Press Limited
All rights of reproduction in any form reserved

1. INTRODUCTION

The concept of "relaxation time" was introduced to the vocabulary of nuclear magnetic resonance in 1946 by Bloch in his famous equations of motion for nuclear magnetization.[1] The phenomenological Bloch equations assume the magnetization component along the external magnetic field (the longitudinal magnetization) to relax exponentially to its equilibrium value. The time constant for the process is called the spin–lattice or longitudinal relaxation time, and is denoted by T_1. The magnetization components perpendicular to the magnetic field (the transverse magnetization) are also assumed to relax in an exponential manner to their equilibrium value of zero. The time constant for this process is called the spin–spin or transverse relaxation time and is denoted by T_2. The inverse of a relaxation time is referred to as the relaxation rate.

Shortly afterwards, a microscopic theory for the phenomenon of nuclear spin relaxation was presented by Bloembergen, Purcell and Pound (BPP).[2] They related the spin–lattice relaxation rate to the transition probabilities between the nuclear spin energy levels. The transition probabilities were calculated for the case of the dipole–dipole interaction (see below), modulated by random motions in a liquid. The transition probabilities for such a case can be related to the spectral densities characterizing the random process. The spectral densities in the simplest cases can be specified in terms of the "interaction strength" (for the dipole–dipole case, simply related to the cube of the inverse distance between the dipoles) and the "correlation time", the characteristic time for the decay of correlations in the course of the random process. The BPP paper is the foundation on which most of the subsequent theory has been built, but contains some errors, which were corrected by Solomon[3] in 1955. The subsequent development of the relaxation theory has been reflected in NMR textbooks, among which one should mention in particular the works of Slichter,[4] Abragam,[5] and more recently McConnell.[6]

Studies of nuclear spin relaxation phenomena are a rich source of dynamic and structural information about species ranging from simple fluids to complex macromolecular systems. There are many reviews of relaxation measurements and applications; these usually cover either relaxation studies of a particular nuclide or applications within a specialized narrow field. A notable exception to this rule is provided by the reviews by Weingärtner, published on a yearly basis by the Royal Society of Chemistry.[7] The goal of the present paper is to provide a wide (although not fully comprehensive) review of the applications of nuclear magnetic relaxation measurements. The scope is in fact similar to that adopted by Weingärtner[7] and the period covered is 1980–1988, supplemented with a selection of

important (or—for the reviewer—especially interesting) earlier work. Emphasis is placed on work of physico-chemical and chemical interest. Some additional limits are imposed on the coverage, in order to keep the already huge list of references from diverging completely. Thus attention is confined to diamagnetic systems; the theoretical aspects of paramagnetic systems have been reviewed[8] and these systems have also been considered in a monograph.[9] The phenomena of chemical exchange and self-diffusion, though related to relaxation, are in principle not covered. The chemical systems of main interest for the reviewer are small molecules in isotropic solution—this is reflected in the comprehensiveness of the coverage of this area. Some other systems are also included, as comparisons or generalizations. The guidelines for the selection of this part of the material are largely personal. Thus the survey covers relaxation in gases and in small molecules dissolved in anisotropic media and includes physically oriented work within the field of macromolecules in (dilute) solution. Complex aqueous systems, such as micelles and water-based liquid-crystalline systems, are also included. On the other hand, work judged by the reviewer as biochemistry-oriented is not covered. All *in vivo* work is excluded. Likewise, salt and polymer melts, non-aqueous liquid-crystalline phases, glasses and similar systems are not included. All work on solids and on liquid helium is excluded.

The organization of the review is as follows. In Section 2 the theory of nuclear spin relaxation is reviewed. Section 3 deals with the experimental and methodological aspects of relaxation studies. The remaining sections are devoted to applications. Section 4 deals with relaxation measurements in gases. Section 5 covers relaxation measurements in inorganic liquid systems (for the purpose of this review, every system containing metal atoms or ions is assumed to belong to this category!). In the process of writing this review, it turned out that it would be more practical to divide the review into two parts. Thus Part 1 (completed during spring 1989) closes after Section 5.

Part 2 will appear in Volume 23 of this series. it will contain two major application sections (organic liquids and solutions of small molecules; macromolecules and aggregates in solutions) and concluding remarks.

2. RELAXATION THEORY

In this section we review theoretical work on nuclear spin relaxation in fluids in general and on spin–lattice and spin–spin relaxation in liquids in particular. Theoretical work dealing with other types of NMR relaxation phenomena (nuclear Overhauser enhancement, relaxation of multiple quantum coherences etc.) and theoretical discussions related specifically to

certain experimental situations will be reviewed in Section 3. The specific theoretical problems connected with relaxation in gases will be discussed in Section 4.

2.1. General aspects

During the nineteen fifties the basic ideas of the BPP theory was developed into a complete theoretical framework by Wangness, Bloch and Redfield (WBR).[10-14] Rather than dealing with the concepts of magnetizations or energy-level populations, the WBR theory is given in terms of a density matrix (for general reviews of the density matrix formalism see the books by Blum[15] and Ernst, Bodenhausen and Wokaun[16]). Briefly, the density matrix describes the average behaviour of an ensemble of quantum-mechanical systems. Consider one of the systems at a particular instant. Solving the Schrödinger equation for this system gives a complete set of eigenstates $|n\rangle$. The state of any other system in the ensemble at any time can be expressed as a linear combination of these eigenstates with coefficients c_n. Given the coefficients, we can form products $c_n c_m^*$ and then take an ensemble average of the products. We denote these ensemble-averaged products of coefficients by ρ_{nm} and let them form a square matrix $\boldsymbol{\rho}$. This matrix is called the density matrix for our ensemble of systems in the basis of the eigenstates chosen originally.

If the density matrix $\boldsymbol{\rho}$ for the system is known, it is possible to calculate any observable $\langle Q \rangle$ by taking the trace of the product of the density matrix and the matrix representation $\mathbf{Q}$ of the corresponding operator Q in the same basis set:[4,5,15,16]

$$\langle Q \rangle = \mathrm{Tr}(\boldsymbol{\rho}\mathbf{Q}). \tag{1}$$

Thus knowledge of the time evolution of the density matrix is sufficient to describe any experiment on a macroscopic system.

The basic physical model behind the WBR theory—or the Redfield theory, as it is often called—is the division of the total system into a spin system comprising the relevant spin-dependent degrees of freedom and a lattice containing the remaining (molecular) degrees of freedom. The density matrix for the total system is written as a "direct product" of the density matrices for the spin system and the lattice. The lattice is assumed to act merely as a thermal reservoir of infinite heat capacity and remains in thermal equilibrium throughout the NMR experiment. Thus the full density matrix can be averaged over the lattice degrees of freedom and one can concentrate on the spin-system density matrix. The coupling between the two subsystems is assumed to be weak and the total Hamiltonian is

expressed using the semiclassical spin-Hamiltonian approach:

$$H = H_0 + H_1(t). \tag{2}$$

H_0 contains the spin Zeeman term and other time-independent interactions (such as the indirect spin–spin coupling in liquids), and $H_1(t)$ is the time-dependent spin–lattice coupling giving rise to relaxation. $H_1(t)$ is generally a sum of terms describing various possible interactions. Each of these terms can be conveniently written as a product of irreducible tensor operators:[5,6]

$$H_1 = \sum_m (-1)^m T^{(L)}_{-m} A^{(L)}_m. \tag{3}$$

$T^{(L)}_{-m}$ is the $-m$-component of a tensor operator of rank L, and depends only on the lattice variables, and $A^{(L)}_m$ is a tensor operator involving only spin coordinates. It can be shown[4-6,13,14] that, under certain assumptions, the spin density-matrix elements obey an equation of motion

$$\frac{\mathrm{d}\boldsymbol{\rho}}{\mathrm{d}t} = \mathrm{i}[\boldsymbol{\rho}, H] = \mathrm{i}[\boldsymbol{\rho}, H_0] - \mathbf{R}(\boldsymbol{\rho} - \boldsymbol{\rho}^{\mathrm{T}}). \tag{4}$$

$\boldsymbol{\rho}^{\mathrm{T}}$ is the thermal equilibrium density matrix. $\mathbf{R}$ is the relaxation matrix, with elements

$$\begin{aligned} R_{\alpha\alpha'\beta\beta'} = \sum_m [&\delta_{\alpha\beta}(A_{-m})_{\beta'\gamma}(A_m)_{\gamma\alpha'} J_{m,-m}(\omega_{\beta'\gamma}) \\ &+ \sum_\gamma \delta_{\alpha'\beta'}(A_m)_{\alpha\gamma}(A_{-m})_{\gamma\beta} J_{m,-m}(\omega_{\gamma\beta}) \\ &- 2(A_{-m})_{\alpha\beta}(A_m)_{\beta'\alpha'} \operatorname{Re}\{J_{m,-m}(\omega_{\alpha\beta})\}], \end{aligned} \tag{5}$$

where α, β and γ label the eigenstates of H_0, and $\omega_{\alpha\beta} = (E_\alpha - E_\beta)/\hbar$. The relaxation matrix may be complex. The imaginary components of $\mathbf{R}$ are referred to as dynamic frequency shifts.[17] The complex spectral density is defined as a Fourier–Laplace transform

$$J_{m,-m}(\omega) = \int_0^\infty G_{m,-m}(\tau) \mathrm{e}^{-\mathrm{i}\omega\tau}\, \mathrm{d}\tau \tag{6}$$

of the correlation function

$$G_{m,-m}(\tau) = (-1)^m \langle T_m(\tau) T_{-m}(0) \rangle. \tag{7}$$

Here the symbol $\langle\ \rangle$ denotes an ensemble average. Equation (4) can be combined with (1) to provide an equation for the evolution of a certain magnetization component. As we shall see below, the relaxation times T_1 and T_2 cannot always be defined. The Redfield theory is very well

established and has been used to derive the relaxation characteristics in a variety of situations. We shall return to this point in Section 2.2. Here we are going to review some recent papers dealing with the general aspects of relaxation theory.

Sanctuary and Selwyn[18] derived Redfield relaxation equations for multi-spin systems of arbitrary number of spins with arbitrary spin magnitudes. This was done for various relaxation mechanisms and the equations were formulated using the Liouville space (superoperator) formalism.[16,19,20] More recently, an even more general reformulation of the WBR theory based on the Liouville formalism was presented by Szymanski, Gryff-Keller and Binsch.[21] In this formalism, (4) is written as

$$\frac{\mathrm{d}|\rho)}{\mathrm{d}t} = -\mathrm{i}\hat{\hat{L}}_0|\rho) - \hat{\hat{R}}[|\rho) - |\rho^{\mathrm{T}})]. \tag{8}$$

$|\rho)$ stands for the density operator for the spin system, $\hat{\hat{L}}_0$ for the Liouville superoperator corresponding to H_0 (commutator with H_0), and $\hat{\hat{R}}$ is now a relaxation superoperator. In Ref. 21, which is the first of a projected series, the authors derive a compact and coherent formulation of the theory that is also suitable for computer calculations. The assumptions inherent in the theory are analysed thoroughly. The most fundamental assumption is the so-called "strong narrowing condition", which the authors state as implying the existence of two characteristic times, τ_c and t, which satisfy the strong inequalities

$$\tau_c \ll t \ll 1/|\langle H_1\rangle|, \tag{9}$$

where the correlation time τ_c is the characteristic time for the decay of G in (7), t is the typical time scale of the nuclear relaxation process and $|\langle H_1\rangle|$ is the strength of the interaction leading to the relaxation. The strong narrowing condition should not be confused with the extreme narrowing condition, which for a homonuclear spin system is

$$\tau_c \ll 1/|\omega_0|, \tag{10}$$

where ω_0 is the Larmor frequency for the nucleus under consideration.

Szymanski *et al.*[21] analyse in detail the simplifications that can be obtained by considering the symmetry properties. The symmetry properties of the relaxation superoperator are divided into intrinsic and extrinsic properties. The former are inherent in the basic structure of the theory or in the properties of the spin systems,[20,22,23] and the authors argue that these can only be handled properly in the Liouville representation. The extrinsic properties depend on a physical situation (such as, for example, properties of isotropic media[24] or the extreme narrowing condition) or the design of the experiment. The paper by Szymanski *et al.*[21] is a completely quantum-

mechanical treatment. It should be noted, however, that in the same year and in the same journal, there appeared an entirely classical theory of NMR relaxation.[25]

The range beyond the limit of (9), where the Redfield theory is not valid, is often designated the "slow-motion region". The slow-motion situation is unusual in the type of systems of interest in this review, but some work should nevertheless be mentioned here. Lynden-Bell[20] and Freed *et al.*[26] showed, following Kubo,[27] that in this range the equation of motion (8) must be replaced by a more general equation:

$$\frac{\mathrm{d}|\chi)}{\mathrm{d}t} = -\mathrm{i}\hat{\hat{L}}|\chi) - \hat{\hat{K}}[|\chi) - |\chi^{\mathrm{T}})]. \tag{11}$$

$|\chi)$ is the density operator involving spin as well as the part of the lattice to which the spin is strongly coupled, which usually means rotation. $\hat{\hat{L}}$ is the Liouville superoperator, dependent on spin and rotational degrees of freedom, averaged over other degrees of freedom. $\hat{\hat{K}}$ is a stochastic operator, which for example can be identified with a rotational diffusion operator.[20] Equation (11) is often referred to as the stochastic Liouville equation (SLE). The SLE has been most widely used in ESR.[28] It has also found applications in NMR of paramagnetic molecules[8] and in the studies of NMR relaxation and lineshapes in liquid crystals.[29] Within the field covered by this review, the SLE formalism has recently been used to calculate relaxation in systems subject to slow overall reorientation and rapid internal motion.[30,31]

Finally, it should be noted in the present context that there is a thermodynamic interpretation of spin relaxation. This interpretation and the connection between spin relaxation and other irreversible phenomena and entropy production have been discussed by Lenk.[32,33]

2.2. Relaxation mechanisms

In this section we review the basic features of various relaxation mechanisms corresponding to a different physical nature of the interaction in (3). Work dealing with the dynamic models, and giving physical significance to (7), will be presented in Sections 2.3–2.6.

Dipole–dipole (DD) interaction was pointed out as a relaxation mechanism in the BPP paper[2] and proved subsequently to be very important for many light spin-$\frac{1}{2}$ nuclei. The operators A and lattice functions T of (3) in the BPP paper were given in the form known in more recent literature as the "dipolar alphabet". The spherical tensor ($L = 2$) form of the A s and T s can be found, for example, in the books by Abragam[5] and McConnell.[6] It

is sufficient to say that the T s are suitably normalized products of the inverse cube of the distance between the interacting dipoles and $L = 2$ spherical harmonics. Correct expressions for the DD relaxation in a two-spin (I and S) system were first given by Solomon,[3] who found that the relaxation of the longitudinal magnetization components, proportional to the expectation values of I_z and S_z operators, was described by a set of two coupled equations:

$$\left.\begin{aligned}\frac{d\langle I_z\rangle}{dt} &= -(W_0 + 2W_{1I} + W_2)(\langle I_z\rangle - I_z^0) - (W_2 - W_0)(\langle S_z\rangle - S_z^0),\\ \frac{d\langle S_z\rangle}{dt} &= -(W_2 - W_0)(\langle I_z\rangle - I_z^0) - (W_0 + 2W_{1S} + W_2)(\langle S_z\rangle - S_z^0),\end{aligned}\right\} \tag{12}$$

or

$$\left.\begin{aligned}\frac{d\langle I_z\rangle}{dt} &= -\rho_I(\langle I_z\rangle - I_z^0) - \sigma(\langle S_z\rangle - S_z^0),\\ \frac{d\langle S_z\rangle}{dt} &= -\sigma(\langle I_z\rangle - I_z^0) - \rho_S(\langle S_z\rangle - S_z^0).\end{aligned}\right\} \tag{13}$$

The meaning of the transition probabilities W_0, W_{1I}, W_{1S} and W_2 in the two-spin, four-level system is made clear in Fig. 1. I_z^0 and S_z^0 are the equilibrium longitudinal magnetizations of the I and S spins respectively. The general solutions of (12) or (13) for $\langle I_z\rangle$ and $\langle S_z\rangle$ are sums of two exponentials, i.e. the longitudinal magnetizations in a two-spin system do not obey the Bloch equations. Solomon showed that the simple exponential behaviour of the longitudinal magnetization is recovered under certain conditions.

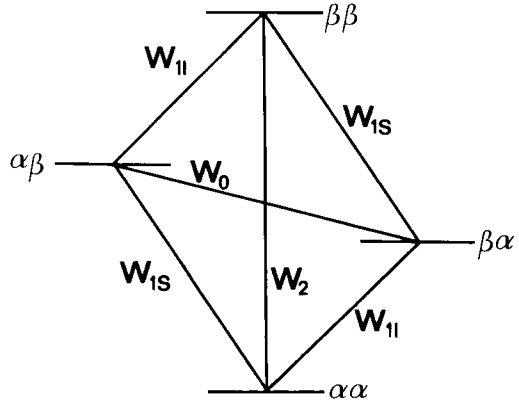


Fig. 1. Definitions of transition probabilities for an IS spin system.

(i) The two spins are identical, as for example the two protons in the water molecule. $W_{1I} = W_{1S} = W_1$, and the spin–lattice relaxation rate is given by

$$T_1^{-1} = 2(W_1 + W_2). \tag{14}$$

(ii) One of the spins, say S, is characterized by another relaxation mechanism, so efficient that on the time scale of the I-spin relaxation, the S spin remains in thermal equilibrium. This is a typical situation in paramagnetic systems where S is an electron spin. The spin–lattice relaxation rate of I, T_{1I}^{-1} or ρ_I, then becomes

$$\rho_I = T_{1I}^{-1} = W_0 + 2W_{1I} + W_2. \tag{15}$$

(iii) One of the spins, say S again, is saturated by an intense radio frequency (RF) field at its resonance frequency—conditions applying for example for ^{13}C as I spin under broadband decoupling of protons (S spins). The relaxation rate in this case is also given by (15). In addition, the steady state solution for I_z is modified to

$$\langle I_z \rangle_\infty = I_z^0 + \frac{\sigma}{\rho_I} S_z^0. \tag{16}$$

The phenomenon is referred to as the nuclear Overhauser enhancement and $\sigma = W_2 - W_0$ is called the "cross-relaxation rate".

Solomon also derived expressions for the transition probabilities W_0, W_1 and W_2. These are proportional to spectral densities characterizing the frequency distribution of the dipole–dipole interaction energy, as given in (6). The correlation functions $G_{m,-m}(\tau)$ of (7) are related to the decay of the correlation between an $L = 2$ spherical harmonic, describing the orientation of the dipole–dipole axis at a certain instant, and the same spherical harmonic at an instant τ later. Under certain conditions, discussed in more detail in the following sections, $G_{m,-m}(\tau)$ can be assumed to decay exponentially with the time constant ("correlation time") τ_c. The exponential correlation functions lead to Lorentzian spectral densities, and the relaxation rates in (14) and (15) become linear combinations of terms $\tau_c/(1 + \tau_c^2\omega^2)$, where ω corresponds to the energy differences in Fig. 1. In the "extreme narrowing" region, $\tau_c \ll \omega^{-1}$, each of the Lorentzians becomes equal to the correlation time; T_1 is thus proportional to the product τ_c/r^6 (it was pointed out by Pyper[34] that "r^{-6}" should really be interpreted as a square of the expectation value of r^{-3} over the vibrational wavefunction) and independent of the frequency. Solomon,[3] Abragam[5] and McConnell[6] also derived expressions for the rates of transverse relaxation. The transverse relaxation is shown to obey the Bloch equations. Under the extreme narrowing conditions, and when T_1 is defined, the two relaxation

times are equal. In a system of two spin-$\frac{1}{2}$ nuclei one can also define other relaxation rates. We shall return to this point in Sections 3.2 and 3.4.

Equations (12)–(16) can be formally derived within the framework of the density operator theory (see e.g. Ref. 5). The system of two spin-$\frac{1}{2}$ nuclei was also considered by Werbelow,[35] who discussed the frequency dependence of relaxation rates and nuclear Overhauser enhancements for coupled nuclei with magnetogyric ratios of opposite signs, where care has to be taken with respect to the relative signs of Larmor frequencies.

DD relaxation in spin systems of more than two spins and in systems with indirect spin–spin coupling (and possibly chemical equivalence and double resonance irradiation) has been an active field of research from the early nineteen seventies up to the present. The early development has been reviewed in excellent papers by Werbelow and Grant[36] and Vold and Vold.[37] Among numerous important findings of this period summarized in these papers, we should like in particular to stress the following.

(i) Longitudinal relaxation in a coupled spin system follows a set of coupled differential equations. One can define suitable "normal modes" of relaxation, which reduce the size of the equation system.
(ii) Double irradiation (decoupling) experiments simplify the equation system, but do not necessarily lead to single exponential relaxation processes in spin systems such as AX_2 (e.g. $^{13}CH_2$ group) or AX_3 (e.g. $^{13}CH_3$).
(iii) Different dipolar interactions (e.g. CH and CH′ in a CH_2 group) can be correlated and lead to cross-correlation or interference spectral densities in the expressions for the relaxation matrix elements.

During the nineteen eighties multispin effects have also attracted the attention of numerous investigators. Brondeau and Canet[38] examined the magnetization modes in weakly coupled spin systems without magnetic equivalence. The relaxation behaviour in such systems is Solomon-like,[3] in the sense that the relaxation matrix simplifies to a transition probability matrix. These authors also considered the symmetry simplification for the relaxation matrix. Kartochwill[39] and Brondeau *et al.*[40] also reported calculations of the transition probability matrix elements for strongly coupled systems. Relaxation in a strongly coupled ABX spin system was studied by Thevand and coworkers.[41] Longitudinal relaxation in an ABX spin system, such as in a $^{13}C-^{13}C-^{1}H$ fragment, was also studied by Canet *et al.*[42] in the presence and in the absence of proton irradiation. The longitudinal relaxation for a rare spin-$\frac{1}{2}$ nucleus X (^{13}C or ^{15}N) coupled to a strongly irradiated proton system of arbitrary complexity (ABCD...) was studied by Brondeau and Canet.[43] They generalized Solomon's[3] finding

that the longitudinal relaxation of X should be single exponential under decoupling, provided that the proton spin system did not possess any symmetry. Werbelow *et al.*[44] investigated the perturbation–response characteristics of an AMX_2 spin system, including the effect of saturation of the X_2 grouping. Blicharska[45] described proton relaxation in a methyl group. Prestegard and Grant[46] studied transverse relaxation in the relatively simple AX_2 spin system under the complicated motional regime present in fatty acid micelles. Finally, Werbelow *et al.*[47] studied magnetization modes and evolution matrices for some simple spin systems in anisotropic media.

Different aspects of the relaxation of a spin-$\frac{1}{2}$ nucleus due to dipolar interaction with quadrupolar nucleus (or nuclei) have been studied by several authors. The quadrupolar ($I > \frac{1}{2}$) nuclei are characterized by an independent efficient relaxation mechanism (see below). Longitudinal relaxation in a multipolar AX system was investigated by Werbelow and coworkers.[48] They found that the behaviour of the system under certain conditions could differ dramatically from both the system of two spin-$\frac{1}{2}$ nuclei and from the isolated quadrupolar nucleus. Werbelow also considered linewidths in the same type of system[49] and the additivity of relaxation rates for the AX_2 spin system,[50] where A is a quadrupolar nucleus. A system containing one $I = \frac{1}{2}$ spin and two quadrupolar nuclei, the $^{13}CD_2$ group, was also investigated.[51] Winter and Kimmich[52] considered the spin–lattice relaxation of an $I = \frac{1}{2}$ nucleus, dipole-coupled to a quadrupolar $I = 1$ nucleus, e.g. for a proton in a ^{14}NH group. They found that the I-spin relaxation rate varied with the resonance frequency non-monotonically, displaying so-called "quadrupolar dips" at the frequencies where the Zeeman splitting matched the quadrupolar splitting. The phenomenon of "quadrupolar dips" was also considered by Westlund and Wennerström,[53] who used a formalism originally developed for relaxation in paramagnetic systems and imposing no restrictions on the strong narrowing condition for relaxation of the quadrupolar nucleus. They found that the dip in the relaxation time versus frequency plots appeared as the reorientational motion slowed down.

The dominant relaxation mechanism for nuclei with a spin greater than $\frac{1}{2}$ is quadrupolar relaxation. The form of the interaction can be found in the books by Abragam[5] or McConnell.[6] The quadrupolar Hamiltonian was also discussed by Pettitt.[54] In analogy with the DD interaction, the quadrupolar interaction corresponds to a tensor rank of $L = 2$. If the symmetry at the side of the nucleus is lower than octahedral or tetrahedral then molecular tumbling will modulate the interaction and provide a relaxation mechanism. Quadrupolar relaxation rates of an $I > \frac{1}{2}$ nucleus are derived in Abragam's book,[5] as well as in that by McConnell.[6] Abragam[5]

showed that quadrupolar relaxation is exponential under extreme narrowing conditions, where

$$T_1^{-1} = T_2^{-1} = \frac{3}{40}\frac{2I+3}{I^2(2I-1)}(1+\tfrac{1}{3}\varepsilon^2)\frac{e^2qQ}{\hbar}^2\tau_c. \tag{17}$$

It should be noted that the quadrupolar relaxation rate depends on three factors: (a) the nuclear properties (spin quantum number I and quadrupole moment Q); (b) the electronic properties (the principal field gradient component q and the asymmetry parameter ε); (c) a dynamic property (the correlation time for the principal axis of the field gradient tensor). e^2Qq/h is often called the "quadrupolar coupling constant", QCC. The correlation time in (17) has a similar meaning to the τ_c discussed in connection with DD relaxation. The two correlation times in fact become identical under certain conditions (see below).

Outside the extreme narrowing region, the relaxation of $I = 1$ spins obeys the Bloch equations, with T_1 different from T_2. For $I > 1$ the relaxation outside the extreme narrowing region is non-exponential. The non-exponential relaxation of quadrupolar nuclei in this region was considered by Hubbard,[55] who found that the relaxation of both the longitudinal and transverse components consisted of I decaying exponential terms if I is an integer and $I + \frac{1}{2}$ exponential terms if I is half an odd integer. Hubbard also gave expressions for exponents and coefficients of the two exponentials for $I = \frac{3}{2}$. McConnell[56] analysed quadrupolar relaxation for nuclei in a molecule of arbitrary shape using the stochastic rotation operator method (see below).

Reuben and Luz[57] considered non-exponential spin–lattice relaxation for $I = \frac{7}{2}$ outside the extreme narrowing region, while Bull *et al.*[58] presented numerical solutions for the longitudinal and transverse components of multiexponential relaxation for $I = \frac{5}{2}$ and $\frac{7}{2}$. Transverse relaxation of these high half-integer spins was studied more recently by Westlund and Wennerström,[59] who also derived analytical expressions for the lineshapes under non-extreme narrowing conditions. Halle and Wennerström[60] reported a perturbation treatment of quadrupolar relaxation for $I = \frac{3}{2}$, $\frac{5}{2}$ and $\frac{7}{2}$. They found that, assuming only weakly frequency-dependent effective spectral densities, the relaxation was nearly exponential. Calculations were also carried out for a system exchanging between a "free" site, where the extreme narrowing conditions prevail, and a "bound" site, where the reorientation is slow because of interactions with a macromolecule or an aggregate. The relation between chemical exchange and nuclear relaxation will be discussed further in Section 2.7.

Werbelow and Marshall[61,62] showed that the two Lorentzian components describing the transverse relaxation (or lineshape) of $I = \frac{3}{2}$ outside the

extreme narrowing region are shifted in frequency relative to each other, because of the effects of the imaginary part of complex spectral densities in (6) or the second-order dynamic frequency shifts. The existence of these shifts was demonstrated experimentally for ^{23}Na ($I = \frac{3}{2}$) by Marshall *et al.*[63] Dynamic shifts for $I = \frac{5}{2}$ and $\frac{7}{2}$ were discussed by Westlund and Wennerström.[59]

The third relaxation mechanism corresponding to an interaction with a tensor of rank $L = 2$ in (3) is related to anisotropy in the chemical-shift tensor. This interaction can also be modulated by the rotational tumbling of molecules in solution, and chemical-shielding anisotropy (CSA) relaxation was also treated by Abragam.[5] For a cylindrically symmetric shielding tensor and an extreme narrowing region, the CSA relaxation obeys the Bloch equations with the rates

$$T_1^{-1} = \tfrac{6}{40}\,\gamma^2 B_0^2 (\Delta\sigma)^2 \tau_c, \tag{18}$$

$$T_2^{-1} = \tfrac{7}{40}\,\gamma^2 B_0^2 (\Delta\sigma)^2 \tau_c, \tag{19}$$

where $\Delta\sigma = \sigma_{zz} - \sigma_{iso}$, σ_{iso} is the isotropic chemical shift and σ_{zz} is the principal tensor component that deviates most from σ_{iso}. Again, τ_c is similar to the case of DD or quadrupolar relaxation. It should be noted that the CSA contributions to T_1 and T_2 are unequal (even under extreme narrowing conditions), and there is a characteristic B_0^2 dependence of the relaxation rates. This field dependence allows the CSA relaxation to be separated from other mechanisms. The equations of Abragam[5] were generalized to more complicated molecular shapes and motional situations by McConnell.[64,65] Lynden-Bell[66] pointed out that the nuclear shielding tensor has nine independent spherical components and can be resolved into an isotropic ($L = 0$) part, a symmetric ($L = 2$) tensor and an antisymmetric ($L = 1$) tensor. The antisymmetric tensor can also contribute to CSA relaxation and under certain conditions can make T_2 longer than T_1.

Indirect nuclear spin–spin (scalar) coupling between spins I and S can also lead to relaxation under certain circumstances. This scalar (SC) relaxation mechanism was first proposed and observed by Solomon and Bloembergen.[67] The system studied was hydrogen fluoride and these authors observed that the chemical exchange of protons between different molecules provided the modulation of the scalar coupling and thus modified the relaxation behaviour of both protons and fluorines. Solomon and Bloembergen[67] pointed out that the scalar relaxation can also lead to nuclear Overhauser enhancement, in analogy with the DD mechanism, but of the opposite sign. Abragam[5] introduced the concepts of scalar relaxation "of the first kind", where the coupling was modulated by exchange as in the work of Solomon and Bloembergen,[67] and "of the second kind", where the

relaxation of nucleus I resulted from the modulation of the coupling by the rapid relaxation of nucleus S. The equations for T_1 and T_2 for scalar relaxation of the second kind are

$$T_1^{-1} = \tfrac{2}{3} A^2 S(S+1) \frac{\tau_2}{1 + (\omega_I - \omega_S)^2 \tau_2^2}, \tag{20}$$

$$T_2^{-1} = \tfrac{1}{3} A^2 S(S+1) \left[\frac{\tau_2}{1 + (\omega_I - \omega_S)^2 \tau_2^2} + \tau_1 \right], \tag{21}$$

where A is the coupling constant, and ω_I and ω_S are Larmor frequencies. τ_1 and τ_2 are the spin–lattice and spin–spin relaxation times for the (usually quadrupolar) nucleus S. The expressions for scalar relaxation of the first kind are obtained by setting $\tau_1 = \tau_2 = \tau_e$, the exchange lifetime. The usual situation is that $(\omega_S - \omega_I)^2 \tau_2^2 \gg 1$, $\tau_1 = \tau_2$, and $T_2^{-1} \gg T_1^{-1}$. Thus a measurable scalar contribution to T_2^{-1} is much more common than that to T_1^{-1}. Johnston[68] has pointed out that this statement does not apply to a system of two spin-$\frac{1}{2}$ nuclei, unequally coupled to a quadrupolar nucleus and strongly coupled to each other. Pyper presented the theory for scalar relaxation of the second kind using the Liouville space formalism,[69] and more recently applied it to investigate the requirements for double resonance decoupling in a system undergoing scalar relaxation of the second kind.[70]

Briguet *et al.*[71] investigated scalar relaxation of the second kind for a spin-$\frac{1}{2}$ nucleus I coupled to more than one quadrupolar nucleus (S and S') and concluded that non-additivity of the relaxation rates originating from couplings to S and S' might occur because of the correlation between their relaxation mechanisms. Mlynarik[72] devised an ingenious experiment that would allow observation of such cross-correlation effects, but did not find any. Blicharski[73] derived equations for relaxation due to anisotropic indirect spin–spin coupling. Balonga[74] considered intermolecular scalar coupling and its effect on intermolecular nuclear Overhauser enhancement. Intermolecular spin–spin coupling and scalar relaxation were considered by Laaksonen *et al.*,[75] who used quantum-chemical calculations and Monte Carlo simulations to estimate the average intermolecular proton–fluorine coupling for aqueous fluoride ion.

The fifth relaxation-causing interaction is probably more obscure for NMR spectroscopists in general. It is the spin–rotation interaction (SR) by means of which the nuclear spin couples to the angular-momentum operator for the molecule's motion. The strength of the coupling between the two angular momenta is described by the spin–rotation coupling tensor. The simple physical explanation of the phenomenon is that, as the molecule rotates, so does its electronic charge distribution. The rotating charges give rise to a magnetic field, which can interact with the nuclear magnetic

moment. There is a similarity between spin–rotation coupling and magnetic shielding, where we also deal with a secondary magnetic field caused by rotating electrons, the rotation in this case being caused by the external magnetic field rather than the molecular motion. The relation between magnetic shielding and spin–rotation coupling was put into quantitative terms by Deverell.[76]

The theory of relaxation by the spin–rotation mechanism was first presented by Hubbard.[77] He found that the SR relaxation should obey the Bloch equations, with the relaxation rates for a spherical molecule under extreme narrowing conditions given by

$$T_1^{-1} = T_2^{-1} = \frac{2IkT}{3\hbar^2}(2C_\perp^2 + C_\parallel^2)\tau_{SR}, \tag{22}$$

where I is the moment of inertia and $C_\perp$ and $C_\parallel$ are the components of the spin–rotation coupling tensor, assumed to be cylindrically symmetric. τ_{SR} is the spin–rotation correlation time, very different from the τ_c occurring in the expressions for DD, CSA and quadrupolar relaxation. τ_{SR} is a measure of the decay time for the angular-velocity correlation function and, as shown by Hubbard,[77] it can be inversely proportional to the rotational correlation time τ_c under certain conditions (see below). In fact, the theory for SR relaxation contains correlation functions involving both the reorientation and angular velocity, and the dynamic aspects are therefore in a way more complicated than for other mechanisms. More sophisticated models for rotational Brownian motion were introduced in the context of SR relaxation by McClung,[78] Hubbard[79] and McConnell.[65,80–82]

One additional relaxation mechanism often mentioned in the literature is the so-called "random field" relaxation. This is really a simple model used, for example by Slichter[4] and Rorschach,[25] to illustrate how general equations for a certain relaxation theory could work. The nuclear spin is simply submitted to a Zeeman interaction with a randomly varying magnetic field. The random-field terms are often used to mimic unspecified relaxation contributions occurring along with specified ones.

Besides the five relaxation mechanisms mentioned above, relaxation phenomena can also be caused by "interference" terms corresponding to correlations between two different interactions. Such correlations can exist provided the tensor ranks of the two interactions are the same. Interference effects (between CSA and DD mechanisms) were first mentioned in connection with NMR by Shimizu[83] (they were recognized even earlier in the ESR literature) and were discussed in detail by Blicharski.[84,85] Werbelow and Grant[86] pursued this line further, treating the DD–CSA interference in a system consisting of three identical spin-$\frac{1}{2}$ nuclei, while Werbelow *et al.*[44] considered the combined effect of DD and CSA

interactions in a AMX_2 system. Bain and Lynden-Bell[87] treated relaxation matrices for AX_2 and AX_3 systems, including all possible combinations of DD, CSA, SR and random-field mechanisms. Among the more recent theoretical contributions, mention should be made of the work of Goldman[88] and Farrar and coworkers,[89,90] dealing with the DD–CSA cross-terms. The abovementioned work on the dipolar relaxation of spin-$\frac{1}{2}$ nuclei by quadrupolar nuclei[48-53] deals essentially with the dipolar–quadrupolar interference. Indeed, the "pure" DD relaxation in higher-spin systems[36-47] is affected by the interference terms between different dipolar interactions. Thus the interference terms seem to be almost ubiquitous, and one tends to agree with Szymanski *et al.*,[21] who favour denoting a pair of interaction indices, rather than a single one, as a relaxation mechanism.

2.3. Reorientational dynamics—rigid molecules

In this and the following sections we shall review the theory required to obtain the correlation functions in (7). We begin with the case of reorientational modulation of an interaction, the strength of which remains constant in some particular frame. Different parts of the material covered in this section have been reviewed by Huntress,[91] Spiess,[92] Boeré and Kidd[93] and Dölle and Bluhm.[94] The equations for the relaxation rates presented in Section 2.2 assume that the correlation functions of (7) decay exponentially with time constant τ_c. We shall now elucidate the meaning of this correlation time.

Assume that the interaction leading to relaxation has a constant magnitude in a molecule-fixed coordinate frame. This corresponds to a constant distance between the two dipoles in the case of the DD relaxation, to a constant field-gradient tensor arising from the molecular charge distribution, etc. The number of parameters required to describe the lattice part of the interaction is lowest in its principal, molecule-fixed axis system. On the other hand, we wish to handle the spin operators in the laboratory frame, because of their dominant Zeeman interaction with the magnetic field. All terms in the interaction Hamiltonian (3) must be referred to a common coordinate system, and we choose to transform the components of $T_m^{(L)}$ to the laboratory frame (we omit the rank index L for clarity):

$$T_m(\text{lab}) = \sum_{m'=-L}^{L} T_{m'}(\text{mol}) D_{mm'}(\Omega). \tag{23}$$

$D_{mm'}(\Omega)$ is the Wigner rotation matrix[92] and Ω denotes the set of Euler angles transforming the principal axis frame into the laboratory frame. $T_{m'}(\text{mol})$ are constant and the time dependence of $T_m(\text{lab})$ comes from the

molecular tumbling, which changes Ω. The correlation functions $G(\tau)$ become

$$G_{m,-m}(\tau) = \sum_{m'} \sum_{m''} T_{m'}(\text{mol}) T_{m''}(\text{mol}) \langle D_{m'm}(\Omega(0)) D^*_{m''m}(\Omega(\tau)) \rangle$$

$$= \sum_{m'} \sum_{m''} T_{m'}(\text{mol}) T_{m''}(\text{mol}) \int\int D_{m'm}(\Omega_0) D^*_{m''m}(\Omega) P(\Omega_0) P(\Omega_0 \mid \Omega, \tau) \times \mathrm{d}\Omega_0 \, \mathrm{d}\Omega. \quad (24)$$

$P(\Omega_0)$ is the probability of an orientation Ω_0 and $P(\Omega_0 \mid \Omega, \tau)$ is the conditional probability of the orientation given by Euler angles Ω at time τ, provided that it was Ω_0 at time zero. The problem is reduced to calculating the two probabilities. For isotropic fluids additional simplifications occur. $P(\Omega_0)$ is constant and needs only be suitably normalized. Moreover, as shown by Hubbard,[24] the correlation function does not depend on m. We can thus concentrate on $m = 0$ Wigner matrices, which are proportional to spherical harmonics. The calculation of the conditional probability is the remaining step.

For the small-step rotational-diffusion model $P(\Omega_0 \mid \Omega, \tau)$ can be obtained from the diffusion equation. The derivation for the case of isotropic reorientation (spherical top), which can be traced back to Einstein and Debye, is sketched by Abragam.[5] Another derivation for the same case was given by Furry.[95] The result is an exponentially decaying $G^{(L)}_{m,-m}(\tau)$:

$$G^{(L)}(\tau) = G(0) \mathrm{e}^{-\tau/\tau_L}, \quad (25)$$

where τ_L is inversely proportional to the rotational diffusion constant D_R:

$$\tau_L = \frac{1}{L(L+1)D_R}, \quad (26)$$

where L is the tensor rank of the interaction. The correlation times appearing in the relaxation-rate expressions for the DD, quadrupolar and CSA mechanisms are thus identical with τ_2.

A more general case of the small-step rotational diffusion of a molecule of arbitrary shape (asymmetric top) has been solved by Perrin,[96] Favro,[97] Woessner,[98] Shimizu[99] and Huntress,[100] and the calculations have been reviewed by Huntress[91] and Spiess.[92] The correlation function for $L = 2$ then becomes a weighted sum of five exponentials. The exponents can be expressed in terms of the three principal components of the diffusion tensor (also called "rotational diffusion constants") D_{xx}, D_{yy} and D_{zz}, while the coefficients depend on the Euler angles (polar angles for a cylindrically symmetric interaction) transforming the principal frame of the interaction into the principal frame of the diffusion tensor. The orientation of the

principal axis of the diffusion tensor relative to the principal axis of the inertial tensor (which determines the rotational properties of a molecule in the gas phase) was considered in detail by Dölle and Bluhm.[94]

Two situations with symmetry intermediate between that of a sphere and that of a general asymmetric top are of interest. The first is the symmetric top. The molecules belonging strictly to this category possess a threefold, or higher, symmetry axis. As a consequence of the symmetry, symmetric tops have two of the principal components of the inertial tensor (or the diffusion tensor) equal. Moreover, the principal axis corresponding to the unique principal component of the inertial tensor, or the diffusion tensor, coincides with the symmetry axis. The correlation function for reorientation of an arbitrary molecule-fixed axis in a symmetric top consists of three exponentials, and the corresponding spectral density (for $L = 2$) becomes

$$J(\omega) = K \sum_{m=0}^{2} \frac{C_m \tau_m}{1 + \omega^2 \tau_m^2}, \tag{27}$$

where K is a proportionality constant dependent on the relaxation mechanism (DD, CSA, quadrupolar) and its interaction strength. C_m (A, B and C in the often-used notation of Woessner[98]) are geometrical factors dependent only on the angle between the axis under consideration and the symmetry axis, and the τ_m are given by

$$\tau_m^{-1} = (6 - m^2) D_\perp + m^2 D_\parallel, \tag{28}$$

where $D_\perp$ and $D_\parallel$ are the rotational-diffusion constants perpendicular and parallel respectively to the symmetry axis. Under extreme narrowing conditions (but only then!), one can define an "effective correlation time" τ_{eff}:

$$\tau_{\text{eff}} = \sum_{m=0}^{2} C_m \tau_m \tag{29}$$

The symmetric-top model is very simple to use and has often been applied even in systems which do not fulfill the symmetry requirements for a symmetric top (see below).

The other special case is that of a planar molecule. The simplifications in this case are not as significant as for the symmetric top. The spectral densities for a planar rotor under extreme narrowing conditions were recently discussed by Diez *et al.*[101]

Rotational correlation times or the rotational diffusion constants are often interpreted in hydrodynamic terms, which corresponds to treating the solvent as a continuous viscous medium. A simple proportionality relation between τ_2 and solution viscosity (the Stokes–Einstein–Debye (SED)

equation) was suggested in the NMR context in the classical BPP paper.[2] An early modification of the SED approach was suggested by Gierer and Wirtz,[102] who introduced the concept of microviscosity corrections related to finite values of the size ratio between the solute and the solvent molecules. Reviews of the subsequent development of the hydrodynamic and related models for the rotational correlation time were given, among others, by Boeré and Kidd[93] and Dote *et al.*[103] In the notation of the latter, τ_2 is written as

$$\tau_2 = \frac{V_p \eta f_{stick} C}{kT} + \tau_2^0, \tag{30}$$

where V_p is the volume of the rotating molecule, η is the viscosity, f_{stick} is the hydrodynamic friction coefficient for the sticking boundary condition, dependent on the shape of the molecule,[96,98] and C is a dimensionless constant, dependent on the prevailing boundary condition. The SED equation is obtained by setting $f_{stick} = 1$, $C = 1$ and $\tau_2^0 = 0$. The first two conditions are valid for a sphere under the sticking boundary condition. Friction coefficients and C constants for spheroids reorienting subject to a slipping boundary were calculated by Hu and Zwanzig.[104] We note that C for a sphere reorienting under slipping boundary condition is zero, i.e. the correlation time is viscosity-independent. More general ellipsoids were studied by Youngren and Acrivos,[105] and calculations for spherocones, spherocylinders and fused spheres were reported by Dote and Kivelson.[106] The term τ_2^0 in (30) was originally suggested by Alms *et al.*[107] and explained in terms of free or inertial rotation. More recently, Evans and Kivelson[108] attributed the intercept in the correlation time versus η/T plots to cross-correlations between the torques and the kinetic or convective terms. Besides treating the solvent as a continuous viscous medium, one can also take its dielectric properties into consideration. When a polar solute molecule reorients in a dielectric medium, its motion is slowed down by slowly relaxing dipolar torques. The effect is called "dielectric friction" and was recently discussed by Madden and Kivelson.[109]

We now turn to the correlation functions occurring in the theory of relaxation by the spin–rotation interaction. These are more complicated[6,77] because the time variation of $H_1(t)$ here comes from both the reorientation of the molecular frame and the time dependence of the angular momentum. Hubbard[77] showed that, for a spherical molecule whose reorientation follows the rotational diffusion equation, the SR relaxation rates can be expressed in terms of the rotational correlation time τ_c and the correlation time describing the exponential decay of the angular momentum correlation function, τ_J. Moreover, Hubbard derived the relation between τ_c (for a tensor of rank L) and τ_J, valid for the small-step rotational diffusion

model:

$$\tau_J \tau_L = \frac{I}{L(L+1)kT}. \tag{31}$$

I is the moment of inertia (a scalar for a sphere). Equation (22) is obtained in the limit of $\tau_J \ll \tau_c$, where also $\tau_{SR} = \tau_J$. The inverse proportionality of τ_2 and τ_J implied by (31) can be given the following simple interpretation. The rotational correlation time is a measure of the time it takes for a molecule to reorient one radian. On the other hand, the angular-momentum correlation time is a measure of the average time between collisions. Now, if collisions are frequent (short τ_J), the reorientation by one radian will require many steps and thus take a long time.

An obvious equation in the discussion of the motion of small molecules in low-viscosity solvents is whether small-step rotational diffusion is a suitable model for the dynamics. One way to test the validity of the model is to control whether the Hubbard relation (31) is indeed fulfilled. This can be done experimentally only under very advantageous conditions.[110] A simpler and more approximate "χ test" was suggested by Wallach and Huntress.[111] χ is the ratio of τ_2 to the mean period for free rotation of a body with a given moment of inertia. Gillen and Noggle[112] proposed a somewhat arbitrary classification of motion as "inertial" if $\chi < 3$ and "diffusive" if $\chi > 5$, with the region in-between designated as "intermediate".

Development of more sophisticated models for the dynamic behaviour of molecules in liquids is a very active field of research. We have no intention of reviewing the field comprehensively. Rather, we shall select a few methods that have proved to have direct implications for NMR relaxation theory. An extension of the small-step diffusion model allowing for uninterrupted free rotation steps of arbitrary size was proposed by Gordon.[113] He proposed the "extended diffusion" (ED) treatment according to two models. In the J-diffusion model one assumes that the magnitude and direction of the angular momentum is randomized upon every collision ("strong collision" regime). In the M-diffusion model only the direction of the angular momentum is randomized, while the magnitude is conserved. The rotation between collisions is free and the collisions are assumed to be instantaneous. The correlation functions for either the DD, quadrupolar and CSA mechanisms, or the SR relaxation for a linear molecule, can be specified in terms of the reduced angular frequency $(kT/I)^{1/2}$ and the average time between collisions τ_J. The rotational correlation functions are not simply exponential, but rather are Gaussian-like for short times. McClung generalized the extended diffusion models to spherical tops[78] and symmetric tops.[114] He also reviewed the field.[115] More recently, extended diffusion models were also presented for asymmetric tops.[116,117] Here we

wish only to make two comments. First, extended J-diffusion (but not M-diffusion) was shown to have the classical small-step diffusion as a limiting case.[78] Secondly, extended diffusion models for symmetric (and asymmetric) tops retain the concept of a single mean time between collisions. As discussed by Spiess,[92] this hardly has attractive consequences in the limit of small-step diffusion. The ratio of the two rotational diffusion constants would then be inversely proportional to the ratio of corresponding principal component of the inertial tensor, which is not verified experimentally in systems with strong intermolecular forces. For example, Böhm *et al.*[118] compared the extended diffusion model with molecular-dynamics simulations and NMR data for acetonitrile and found the ED method to be rather unsuccessful.

Another extension of the simple rotational diffusion model in the context of NMR relaxation theory was proposed by Hubbard,[79] who based his work on solutions of the Fokker–Planck equation within the Langevin model (the FPL approach). The joint probability density of orientation and angular velocity can be obtained using this method. Again, the small-step diffusion is obtained as a special case. A somewhat different approach to the solution of the FPL equations for spherical and linear molecules[119] and later for symmetric tops[120] was proposed by McClung. Lévi and coworkers[121] compared the reorientational correlation functions and the correlation functions of importance for the SR relaxation obtained using the FPL and ED methods for linear and spherical molecules. More recently, Lee and McClung[122] developed the FPL approach to include asymmetric tops and compared the results with the ED data.[123] McConnell also considered the description of rotational Brownian motion by means of Langevin (or Langevin–Euler) equation, and most of the work is summarized in his book.[6] McConnell's work is not cited by McClung, and vice versa. However, to the reviewer the two approaches seem similar.

All the work reviewed so far in this section deals with isotropic fluids. We wish to finish the section by mentioning a few papers on the basic aspects of the reorientation of rigid molecules in an anisotropic and heterogeneous environment. Again we do not intend to give a comprehensive review. The area of spin relaxation in liquid crystals was recently reviewed by Vold[124] and Vold and Vold.[125]

In general, NMR spectra of molecules dissolved in an anisotropic solvent require a modification of the Hamiltonian (2). Following Vold and Vold,[37] we write

$$H = H_0 + \langle H_1 \rangle + H''(t), \tag{32}$$

where $\langle H_1 \rangle$ is the time-independent, motionally averaged value of H_1 of (2) and $H''(t) = H_1(t) - \langle H_1 \rangle$. The usual Redfield treatment of relaxation is

applicable, but the fact that the environment is anisotropic influences the spectral densities. Equation (24) is still valid, but the probability distribution $P(\Omega_0)$ is not isotropic. This has the consequence that the spectral densities in (6) become dependent on the index m. This implies in turn that testing of dynamic models is also possible for small, rapidly rotating solute molecules provided that ingenious relaxation experiments can be designed to disentangle individual spectral densities (see below).

If the ordering potential is known, it is easy to obtain the probability distribution $P(\Omega_0)$. The conditional probability $P(\Omega_0 \mid \Omega, \tau)$ was calculated using a diffusion equation in the presence of simple forms of restoring potential by Nordio *et al.*[126] and by Polnaszek *et al.*[127,128] These authors discussed two cases:

(i) the diffusion tensor is time-independent in the molecule-fixed frame (in complete analogy with the isotropic liquid case; see above);
(ii) the diffusion tensor is time-independent in the frame fixed with respect to the director axis of the liquid crystal.

Freed[129] developed the theory further and included the effects of the slower fluctuations of the director of the liquid crystal. References 126–129 deal with ESR relaxation. Similar work in the context of quadrupolar relaxation was presented by Jacobsen *et al.*[130] and, in an earlier but less detailed paper, by Wennerström *et al.*[131] The latter authors point out that the correlation functions and the relaxation rates in anisotropic systems are expected to be dependent on the orientation of the liquid-crystal director relative to the magnetic field. A different procedure for solving the diffusion equation in the presence of a restoring potential was presented by Bernassau *et al.*[132] The rotational correlation functions in anisotropic systems and their symmetry properties were also discussed by Halle and Wennerström.[133] More sophisticated models for rotational motion of molecules dissolved in liquid crystals were recently proposed by Vold and Vold.[134]

Wennerström and coworkers[131,133] also discussed systems, such as micelles or macromolecule solutions, which are macroscopically isotropic but display local order or local heterogeneity. They proposed the following model for the motion of water in the vicinity of such a local heterogeneity. The rapid reorientation of water molecules becomes slightly anisotropic in such an environment—in the sense that it does not completely average out the quadrupolar interaction. The remaining quadrupolar coupling, proportional to a local order parameter, is averaged out by slower motions, such as lateral diffusion or the aggregate reorientation. Both motions contribute to the correlation functions and spectral densities. Very similar ideas were also presented by Freed,[129] who discussed the isotropic phase of a nematogen above the nematic–isotropic phase transition and proposed the existence of

slowly relaxing local order contributing to the spin relaxation. The close analogy of Freed's "slowly relaxing local structures" and the "bound" water was pointed out by Poupko *et al.*[135]

2.4. Reorientational dynamics—flexible molecules

We turn now to molecules possessing internal motional degrees of freedom. A critical review of the field, with particular emphasis on the unsolved problems, was given by Hertz.[136] We begin the discussion with a single internal degree of freedom. A typical example of this class of systems is a molecule with a methyl group attached to a rigid framework.

Woessner[137] studied the rotational correlation functions and spectral densities for a spin pair reorienting randomly about an axis that in turn tumbles randomly. The two motions were treated as independent and the overall tumbling was described as isotropic small-step diffusion. For the internal motion Woessner considered two models: random jumps between three equivalent equilibrium positions and stochastic diffusion. The results were similar to the case of the rigid symmetric top. For the extreme narrowing case (but, again, only then) an effective correlation time can be defined as

$$\tau_{\text{eff}} = \frac{A}{6D_{\text{R}}} + \frac{B}{6D + D_{\text{i}}'} + \frac{C}{6D + D_{\text{i}}''}, \tag{33}$$

where A, B and C are geometrical functions of the angle between the principal axis of the interaction (the internuclear axis for the DD interaction) and the internal rotation axis, D_{R} is the rotational diffusion constant for the isotropic overall tumbling. D_{i}' and D_{i}'' are related to the internal rotation rate and depend on the motional model. For the random-jump model Woessner found $D_{\text{i}}' = D_{\text{i}}'' = \frac{3}{2}R_{\text{i}}$, where R_{i} is the specific rate of random jumps. For the diffusion model $D_{\text{i}}' = \frac{1}{4}D_{\text{i}}'' = D_{\text{i}}$. The Woessner model was applied to the case of ^{13}C relaxation under proton-decoupling conditions by Doddrell *et al.*,[138] who concentrated in particular on the region outside the extreme narrowing regime. Tsutsumi[139] extended the Woessner model to the case of internal motion occurring as random jumps between three sites, only two of which were equivalent, and Woessner[140] allowed for the modulation of the interaction strength (specifically, the internuclear distance for the DD mechanism) by the internal motion. London[141] considered a system undergoing isotropic rotational diffusion as well as internal conformational fluctuation between two stable states.

Woessner[142] also solved the case of internal rotation superimposed on the tumbling of an axially symmetric ellipsoid, while the interaction-strength

modulation within this model was considered by Bovée *et al.*,[143] Tropp[144] and John and McClung.[145] Fully anisotropic diffusion with internal rotation was treated by Buu Ban,[146] Levy *et al.*[147] and Bluhm.[148] The internal motion in these three papers was modelled as random jumps between two sites,[146] three equivalent sites[147] or two equivalent and one non-equivalent site.[148] Finally, Canet and Brondeau[149] proposed an extension of Woessner's[137] model to the anisotropic environment.

Several authors adopted a more sophisticated view of the process of internal rotation. London and Avitabile[150] studied a model assuming internal rotational diffusion to be subject to a boundary condition restricting the range of motion. Edholm and Blomberg[151] treated the internal rotation as a diffusion in the potential and described the process by means of the Smoluchowski equation. In this description the methyl group can both diffuse over the potential barrier and librate around the bottom of the potential well, and both these motions influence the spectral densities. A combination of rotation and libration was also considered by Mendonca *et al.*[152] in the context of spin–rotation relaxation of methyl ^{13}C nuclei. Moro[153] considered a more general and less mobile internal rotor. He proved that when the two parts of the molecule moving relative each other are similar in size, the assumption of uncorrelated motions is no longer valid and one has to consider the coupling between the overall motion and the conformational transition.

Bull[154] proposed an extension of the extended J-diffusion model to the case of a symmetric top with internal motion. It is assumed that the angular momentum related to the internal motion is also randomized by collisions and characterized by the same correlation time τ_J as the angular momentum of overall rotation. Versmold[155] treated the case when the overall rotation was diffusional and isotropic, but the rapid internal motion could occur in large angular steps described by the extended diffusion models. Kook Joe Shin *et al.*[156] pointed out that Versmold's[155] treatment was valid only for the case where the internal extended diffusion correlation functions are close to exponential and proposed a generalization to larger inertial effects. The same group of authors also presented an internal extended diffusion description of spin–rotation relaxation.[157]

Wallach[158] generalized Woessner's[137] derivation for the case of multiple internal rotation. In analogy with Woessner's work, Wallach assumed the overall reorientation to be isotropic and considered the case of each internal rotation behaving as either a random jump between three sites or an unrestricted diffusion. Wallach[158] gave general expressions for the correlation functions in terms of averages over the internal motion and computed the averages for certain limiting cases. Levine *et al.*[159] reported numerical calculations within the Wallach model for a hydrocarbon chain attached to

a rigid (macro)molecule for variety of conditions. They found that, for internal rotation faster than overall tumbling, the correlation functions for axes fixed in the first few methylenes adjacent to the rigid part of the molecule would deviate from single exponential form. Similar work was reported more recently by Beckmann.[160] Levine *et al.*[161] also generalized the model to the case of anisotropic overall rotational diffusion. Bull[162] simplified the multiple rotation problem by approximating the side-chain motion as the diffusion of a rod, in a conical hole embedded in the macromolecules, and attached at the apex of the cone. The correlation functions were calculated using the extended diffusion method.

By the late nineteen seventies, the models became more sophisticated and began to include, in one way or another, restrictions on the motion. Edholm and Blomberg[163] studied the decay of angular correlation functions in paraffin chains using multiple rotational diffusion in a potential model, extending their work on methyl rotation.[151] Both Wallach models were obtained as limiting cases of no potential barrier (rotational diffusion) and very high barrier (random jump). London and Avitable[150] and Wittebort and Szabo[164] presented essentially identical models including multiple internal rotations of a restricted amplitude. Wittebort and Szabo[164] argued that restriction of the internal rotations within a specific angular region is a heuristic way to take into consideration excluded-volume effects and other shortcomings of the free and independent rotation approach.[158-161] Wittebort and Szabo[164] also considered a jump-model description of the restricted internal motion and found it preferable to the diffusional approach. An even more sophisticated extension of this approach was proposed by Wittebort *et al.*,[165] who allowed for the backbone motions to be characterized by a distribution of correlation times.[166]

Another type of restricted motion was proposed by Howarth.[167,168] He assumed that the side chain moved by an internal rotation (analogous to the Woessner[137] or Doddrell *et al.*[138] cases) superimposed on a libration or a stochastic variation of the angle between the internal rotor axis and the dipole–dipole (or quadrupole) axis; this angle determines the constants A, B and C in (33). A rigorous mathematical treatment of Howarth's "three correlation times" ideas was presented by Murayama *et al.*[169]

Numerous papers presented models similar to the "restricted diffusion" and "libration" approaches, but designed more specifically for certain types of macromolecules. For the case of proteins, one should mention the "wobbling in a cone" model of Richarz *et al.*[170] and the "diffusion in a cone" model of Lipari and Szabo.[171] Related models, but designed more specifically for nucleic acids, were presented by Hogan and Jardetzky,[172,173] Lipari and Szabo[174] and Keepers and James.[175]

The increasing complexity of the physical models described in the

preceding paragraphs leads to problems regarding the uniqueness of the physical picture and the overinterpretation of the data. Therefore there has been a reaction to this development. Lipari and Szabo[176] proposed a single-exponential approximation to the complicated restricted diffusion correlation function based on the Padé approximants method. King and coworkers[177,178] proposed a "model-free" approach assuming that every motion contributing to the relaxation is a Markov process (i.e. a stochastic process in which the probability of each step is independent of the previous history of the system). In this way, they obtained an expression for the spectral density in terms of a linear combination of Lorentzians with individual amplitude and rate parameters, which can be treated as unknowns at the outset and be assigned definite values as the number of experimental observations increases. An even more radically "model-free" approach was developed by Lipari and Szabo.[179] They demonstrated that unique information on fast internal motions can be completely specified by two model-independent quantities: (i) a generalized order parameter S, which measures the degree of spatial restriction or the anisotropy of the fast motion; and (ii) an effective correlation time τ_e, which is a measure of the rate of motion. For isotropic overall motion characterized by an arbitrary correlation time τ_M and rapid motion of arbitrary nature, but in the extreme narrowing regime, the following simple expression for the spectral density (not including the interaction strength) is obtained:

$$J(\omega) = \frac{2}{5}\left[\frac{S^2\tau_M}{1 + (\tau_M\omega)^2} + \frac{(1 - S^2)\tau}{1 + (\tau\omega)^2}\right], \tag{34}$$

with

$$\tau^{-1} = \tau_M^{-1} + \tau_e^{-1}. \tag{35}$$

The King *et al.*[177,178] and Lipari and Szabo[179] approaches are operationally similar but, as discussed in the latter work, have different motivations and reach different conclusions. In particular, Lipari and Szabo[179] argued that, no matter how much experimental data are gathered, the rapid motions cannot be described by more than the two parameters. The work of Lipari and Szabo[179] is widely recognized and gets the credit it well deserves, not least for the clarity of presentation. It is less well known that very similar ideas were in fact presented much earlier in the two-step model of Wennerström *et al.*,[131] formulated originally for quadrupolar ion relaxation in micelles. In the first step the fast local motions average out most of the quadrupolar interaction, leaving a residual, which is averaged in the second step by micelle reorientation or lateral diffusion of the ion. The two-step model for the case of the CH_2 groups in hydrocarbon chains in micelles, a dynamic problem similar to that of side chains imbedded in

proteins, was presented by Wennerström *et al.*[180] a few years before the Lipari and Szabo paper.[179]

More recently, a modification of the model-free approach towards increased complexity, was proposed by Fedotov and Kivayeva,[181] who described the internal motions by a distribution of correlation times. Halle,[182] on the other hand, directed attention towards the slow part of the two-step model and treated the problem of relaxation induced by lateral diffusion on a fixed or rotating spheroidal surface.

The work on internal motions and relaxation in macromolecules discussed so far assumes the existence of a more or less rigid entity to which the more mobile parts of the system (macromolecule or aggregate) are attached. In an important review of NMR relaxation and models for backbone motions of macromolecules in solution by Heatley,[183] systems of this kind are referred to as "stiff macromolecules", which are contrasted with "flexible chain" macromolecules, such as synthetic linear polymers. In these very long chains the idea of independent or uncoupled rotations[158-161] is obviously inapplicable. The work on flexible chain systems was reviewed comprehensively by Heatley,[183] and we limit ourselves here to point out some of the highlights. Schaefer[166] introduced early the idea of the distribution of correlation times. A more detailed physical picture emerged from consideration of the kinetics of the concerted conformational transitions in polymers, such as that presented by Helfand[184] in the early nineteen seventies and developed, among others, by Valeur *et al.*[185-187] (the VJGM model) and Hall and Helfand.[188] Skolnick and Yaris[189,190] presented solutions for the VJGM model for different degrees of motional correlation. During the last few years, several authors have attempted to unify the approaches developed for "stiff" and "flexible" systems. Skolnick *et al.*[191] incorporated segment–segment interaction into the restricted rotational diffusion model. Yamakawa and Fujii[192] analysed relaxation in flexible and stiff chain polymers using the discrete helical worm-like chain model. Ferrarini *et al.*[193] studied the conformational kinetics of aliphatic chains, including the case of chains attached to a massive core. The analysis involves the reduction of the diffusion equation in the presence of a potential to a master equation for a random walk between the discrete conformational states.[194,195] In the description of the chain, no factorization of the internal variables is assumed and all the parameters are defined on a microscopic level. The effects of the overall reorientation are included in the final stage. Baldo *et al.*[196] proposed a somewhat different approach. Their dynamic description includes jumps between energetically preferred conformations and restricted diffusion ("oscillation") within the potential wells. The case of a side chain bound to a macromolecule is treated, but the authors claim (referring to "...previous procedure, ... to be published"!)

that the model can easily be extended to the case of a single long-chain molecule.

We should like to conclude this section on reorientational dynamics in non-rigid molecules by reviewing some computer simulation studies. Levy *et al.*[197] calculated the correlation functions and spectral densities of (6)–(7) from the trajectories obtained from stochastic simulations based on the Langevin equation. The correlation functions calculated from the trajectories are exact within the model used for the potential and the stochastic treatment of the solvent. Two systems were considered: butane and heptane in water. The analysis of the heptane system was performed in such a way that the results could be considered to model a side chain attached to a macromolecule. The correlation functions were evaluated using, on the one hand, the complete dynamics and, on the other, assuming uncoupled internal and overall motions. For small molecules tumbling in the extreme narrowing regime, the results indicate that it is indeed possible to assume the two motions to be uncorrelated. In the analysis of side-chain motion, the independence of the internal and overall motions is necessary within the model. The side-chain internal dynamics were shown to separate into two time scales, corresponding to the torsional fluctuations and transitions between different potential minima, with the latter being more important for NMR relaxation. The uncorrelated multiple-internal-rotation model and the random-jump model[158] give an incorrect description of the short- and long-time behaviour of the correlation function, but the resulting total description of the NMR relaxation is reasonably good.

Levy *et al.*[198] also reported more sophisticated molecular-dynamics (where the trajectory calculations are based on the successive integration of the Newton rather than the Langevin equation) simulations of the rotational correlation functions in a close-packed structure modelling a native protein pancreatic trypsin inhibitor (PTI). The picosecond time-scale atomic fluctuations were shown to cause a significant initial decay of the correlation functions (see the schematic diagram of Fig. 2). The same trajectories were also used by Levy *et al.*[199] to calculate the dipolar relaxation rates for non-protonated carbons, and by Lipari *et al.*[200] The latter authors evaluated the experimental data of Richarz *et al.*[170] using the model-free approach of Lipari and Szabo[179] and compared the fitted generalized order parameters for different sites in the molecules with the order parameter derived from the trajectories under certain assumptions. The two sets of data agreed well, which is a little surprising considering the fact that the experimental data in aqueous solution were compared with a simulation *in vacuo*. The four trajectory calculation papers were summarized and discussed by Levy and Karplus.[201]

Yasukawa *et al.*[202] proposed another type of simulation to obtain the

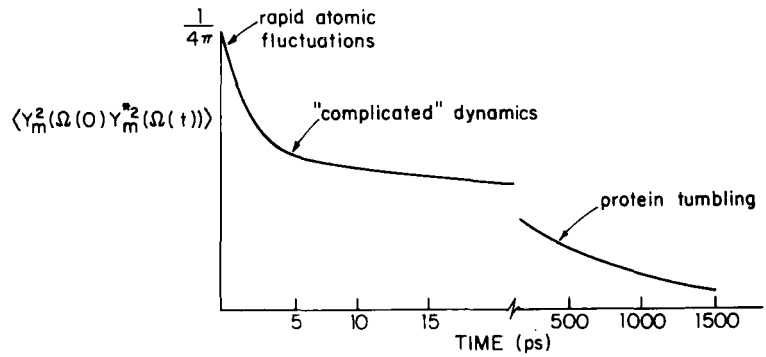


Fig. 2. Schematic behaviour of the decay of orientational correlation functions in proteins. (Reprinted with permission from R.M. Levy, M. Karplus and J.A. McCammon, *J. Am. Chem. Soc.*, **103**, 994. Copyright 1981 American Chemical Society.)

spectral densities for flexible chains. In their approach the spectral densities for the internal motion are obtained by a kind of Monte Carlo procedure, assuming the consecutive configurations to differ by a certain constant time step.

2.5. Distortional dynamics

We now turn to another dynamic situation, in which the average interaction strength is zero by symmetry. The instantaneous distortions of the symmetry lead to a non-zero average of the square of the interaction strength. The magnitude of the fluctuations and their dynamics together determine the relevant spectral densities. This dynamic situation is most common for the quadrupolar relaxation of nuclei in simple ions (such as $^{23}Na^{+}$ or $^{35}Cl^{-}$, both with $I = \frac{3}{2}$) in solution, and developments up to the mid-nineteen-seventies was reviewed well by Lindman and Forsén.[203]

The main (and still not entirely resolved) problem in the theory of quadrupolar relaxation in highly symmetric systems is the origin of the field gradient fluctuations. Early on, Valiev[204] proposed that the origin of the fluctuations should be sought in the vibrations of the complex formed by the ion and the solvent molecules, while Hertz[205] suggested that the fluctuations were of electrostatic origin and could be related to the motions of water molecules, treated as point dipoles, in the vicinity of the ion. A more recent version of the Hertz theory was presented in 1973,[206,207] and we concentrate here on this later version.

The general expression for the quadrupolar relaxation rate under extreme

narrowing conditions is given by:[203,206]

$$T_1^{-1} = T_2^{-1} = \frac{1}{4}\frac{2I+3}{I^2(2I-1)}\left(\frac{eQ}{\hbar}\right)^2 \int_0^\infty \langle V_q(0)V_{-q}(t)\rangle \, dt, \qquad (36)$$

where $V_q(t)$ denotes an $L = 2$, $q = 1$ or 2 spherical component of the field gradient tensor at the site of the nucleus at time t, expressed in the laboratory frame. The extreme narrowing conditions in the present context are to be understood as implying frequency-independent spectral densities; the integral in (36) is thus a zero-frequency value of the relevant spectral density. Hertz[206] expressed the instantaneous field gradient at the site of the ion as a sum of an "electronic" contribution, proposed earlier by Deverell[208] and due to overlap between the electronic charge distribution of the ion and other species in solution, and an "electrostatic" term. The Hertz paper[206] concentrates mainly on the latter term. He considered first random distribution of water molecules around the ion and found that the "electrostatic" field gradient correlation function for such a case could be expressed as

$$\langle V_q(0)V_{-q}(t)\rangle = \frac{24\pi}{5}\frac{[m(1+\gamma_\infty)]^2}{r_0^5} c_{H_2O} \exp\left(-\frac{t}{\tau_{H_2O}}\right), \qquad (37)$$

where m is the electric dipole moment of a water molecule, r_0 the distance between the central nucleus and the point dipole in the first hydration sphere, c_{H_2O} the water concentration, and $1+\gamma_\infty$ the Sternheimer antishielding factor, a measure of the enhancement of the field gradient from external sources caused by the polarizable electronic distribution of the ion. The time variation of the correlation function is exponential, with $\tau_{H_2O}^{-1}$ equal to the sum of the inverse correlation times for the reorientation of the water dipole relative to the ion–water vector and for the reorientation of this vector. Hertz also discussed at length the water–water correlations and many-body effects and proposed that these effects could be approximately taken into account by including in (37) a polarization factor simply related to the dielectric constant. In the second paper of the series,[207] Hertz also included the effects of other point charges (present at the finite electrolyte concentration), of the ion–water correlations and of the modification of the water–water correlations due to other ions.

The Hertz papers[205–207] were widely used (see below) but received some criticism. Hynes and Wolynes[209] pointed out that the work by Hertz involved a mixture of molecular and continuum concepts and proposed instead a theory using the continuum approach consistently. In their approach the polar solvent is treated as a dielectric continuum and the field-gradient correlation function is related to molecular torques expe-

rienced by the quadrupole as it rotates in the medium (the quadrupolar friction). In comparison with the Hertz theory, Hynes and Wolynes point out in particular that the polarization factor of the Hertz model is incorrect. The approach of Hynes and Wolynes was generalized by Stiles and Byrnes,[210] who also allowed for fluctuations due to translational motion (and suggested some corrections to the Hynes and Wolynes equations).

On the other hand, an entirely molecular picture of the quadrupolar relaxation of spherically symmetric ions has been adopted in the simulation work. Engström and coworkers[211,212] reported Monte Carlo simulations of the fluctuations of the field gradient tensor in aqueous solutions of Li^+, Na^+ and Cl^-. The simulations, based on *ab initio* calculations of the interaction energies and the field gradients, reveal that the fluctuations are dominated by the contributions from the first hydration sphere. For the cations the main part of the fluctuations comes from the translational motion of water molecules within the hydration sphere, while for the chloride anion the translations and rotations give similar contributions. Comparison with the classical electrostatic description showed qualitative and quantitative differences. The form of Hertz's polarization factor was discussed and the conclusions confimed the criticism by Hynes and Wolynes.[209] More recently, Engström *et al.*[213] reported molecular-dynamics simulations of the field-gradient correlation function for the same systems. The calculated correlation functions show a complex time dependence not describable by a single exponential decay. For each ion the correlation function starts with a rapid initial decay, which is partly attributable to correlated water motions in the first hydration sphere. The authors conclude that important aspects of the relaxation process are missing in the electrostatic theories of Hertz[206] and Hynes and Wolynes.[209]

Versmold[214] reinvestigated the electrostatic theory, using purely microscopic concepts. He treated the quadrupolar relaxation as a "collision-induced" phenomenon and expressed the field-gradient correlation function in terms of ion–solvent multipole (dipole and quadrupole) and ion–ion contributions. The final expressions for the relaxation rates explicitly contain two-particle and three-particle correlations. Versmold finds that the rapid initial decay and a weak long-time tail, obtained in molecular-dynamics simulations,[213] are to be expected from his theory.

Two papers have dealt with the quadrupolar relaxation for nuclei residing at sites of symmetry lower than spherical, but still sufficiently high (e.g. tetrahedral or octahedral) to result in zero static field gradient. Brown and Colpa[215] considered non-ionic species and related the quadrupolar relaxation to the non-zero average of the field gradient present in an excited state of a degenerate vibration. Osten and Jameson[216] investigated the same problem and found that the vibrational contributions to the relaxation

should not be of importance. Instead, they proposed the collisional deformation mechanism, related to the early suggestions by Deverell.[208]

Finally, we wish to mention the earlier paper by Schwartz,[217] who considered relaxation of spin-$\frac{1}{2}$ nuclei of heavy atoms in electrolyte solutions. He derived equations for the relaxation rates caused by transient chemical-shift anisotropy and spin–rotation mechanisms and a dynamic model in which the electronic distribution surrounding the monatomic ion fluctuated owing to ion–solvent and ion–ion interactions.

2.6. Translational dynamics

The quadrupolar relaxation due to the fluctuations of the field gradient caused at the site of a spherically symmetric ion by the surrounding molecules can, if desired, be designated as "intermolecular". In this section we shall deal with another type of intermolecular process: intermolecular dipole–dipole relaxation. The nucleus under consideration here (usually $I = \frac{1}{2}$) interacts with another nuclear dipole, residing in another molecule. The translational diffusion of the two species relative to each other modulates the interaction and can lead to relaxation.

Nuclear spin relaxation rates due to the intermolecular dipole–dipole interaction modulated by relative translational motion were first obtained by Torrey[218] and discussed by Abragam.[5] Finding the nuclear spin relaxation rates for this case involves computing the spectral densities corresponding to the correlation function, which can be written as

$$G_m(\tau) = N \int\int \frac{Y_{2m}(\Omega_0)}{r_0^3} P(r_0) \frac{Y_{2m}(\Omega)}{r^3} P(r_0 \mid rt)\, \mathrm{d}\boldsymbol{r}_0\, \mathrm{d}\boldsymbol{r}. \tag{38}$$

N is the density of spins and Y_{2m} are suitably normalized $L = 2$ spherical harmonics. r_0 is the distance between spins at time zero and r is the distance at time t. $P(r_0)$ is the probability of the relative radius vector being r_0, and $P(r_0 \mid r, t)$ is the conditional probability (propagator) similar to its rotational counterpart in (24). Abragam[5] presented a simple way to treat the problem implied by (38): he assumed $P(r_0)$ to be uniform and $P(r_0 \mid r, t)$ to be given by the solution of the diffusion equation. After a series of approximations (all molecules are spheres of radius a; extreme narrowing conditions apply; the diffusion constant is given by the macroscopic Stokes law) Abragam found that the relaxation rate should be proportional to the concentration of spins and to viscosity.

The approach of Abragam can be improved and generalized in several ways. A more general "random-flight" or "jump-diffusion" treatment of $P(r_0 \mid r, t)$ (containing the usual diffusion equation used by Abragam as a

limiting case) was reported by Torrey.[218] Torrey gave expressions for the intermolecular relaxation rate in terms of the translational diffusion constant and the distance of closest approach of the two spins. Elwenspoek[219] investigated the case of a highly viscous liquid. In such systems it takes a long time before the molecules have moved a distance of the order of a molecular dimension. Rapid oscillations around the quasi-equilibrium position can occur and can be of importance for the relaxation. Using the Torrey concepts, the distance of closest approach becomes dependent on the amplitude of this oscillation. The influence of inertial effect in translational Brownian motion on correlation functions of (38) were studied by Ivanov and Shermatov.[220]

The assumption of uniform distribution $P(r_0)$ is neither realistic nor necessary. Harmon and Muller[221] extended Torrey's theory by setting the distribution $P(r_0)$ identical with the pair correlation function (p.c.f.) $g(r)$ for the liquid. A major advance in the theory of relaxation due to translational motion was made in 1975 by Hwang and Freed.[222] First, they showed that the "independent diffusion" model of Torrey and Abragam was erroneous because it neglected the boundary-value problem implied by the existence of a distance of closest approach. The model obtained after correcting for the boundary condition (also developed independently by Ayant *et al.*[223]) is called the "force-free diffusion model". Secondly, Hwang and Freed[222] showed that the way of including the p.c.f. in the treatment suggested by Harmon and Muller[221] was only partly correct; it described properly the initial equilibrium distribution but it did not influence the conditional probability in (38), i.e. it led to a uniform distribution at long time. In order to resolve this problem, Hwang and Freed[222] proposed that $P(r_0 \mid r, t)$ should be obtained from the Smoluchowski equation, which guarantees the correct long-time limit. Besides the force-free diffusion case ($g(r) = 0$ for $r < d$, $g(r) = 1$ for $r > d$), Hwang and Freed[222] used the p.c.f. computed by solving the Percus–Yevick equation for hard spheres and by molecular-dynamics simulations. Another relation between the intermolecular relaxation rate and the pair correlation function was derived by Yulmetev.[224] Freed[225] further extended the Hwang and Freed treatment to include the cases where (i) the S spin was relaxing rapidly, (ii) the diffusion was described by finite jumps, and (iii) the diffusion coefficient was frequency-dependent. Sholl[226] analysed the general frequency dependence of the relaxation rates predicted by the models presented above. He found that the zero-frequency limit ($\omega\tau \ll 1$, where τ is a suitably defined correlation time) was model-dependent, but that the next term in the expansion of $J(\omega)$ for small ω was always of the form $A\omega^{1/2}$, with A being model-independent. Sholl also studied the high-frequency limit and again found it to be model-dependent.

The relation between the intermolecular relaxation rate on the one hand and the pair correlation functions and intermolecular interactions on the other was discussed in a review by Hertz *et al.*[227] Hwang and Chang-Yuan Ju[228,229] applied the Freed and Hwang model, together with the p.c.f.s obtained from the reference interaction site model (RISM) as the equilibrium distribution and the source of the effective pair potential, in order to interpret the proton relaxation data for some simple liquids. Similar investigations were also reported for a number of paramagnetic systems.[8]

Another approach to correcting the Torrey–Abragam model was originally suggested by Hubbard.[230] He studied the case of relaxation by intermolecular dipole–dipole interaction, allowing the spins to reside at a distance b from the centre of a spherical molecule of radius a, and found that in the extreme narrowing region the relaxation rates could be expanded in even powers of b/a. Zeidler[231] considered joint effects of the off-centre location of the spins and pair correlation functions, including orientational correlations. Ayant, Fries and coworkers considered the "spin eccentricity" within the framework of the force-free diffusion model[232] and in combination with the Smoluchowski equation,[233,234] as in the Hwang and Freed model.[222] Belorizky and Fries[235] commented on the paper by Sholl[226] and pointed out that the models including eccentricity still had the $\omega^{1/2}$ dependence at low frequencies but that the $\omega\tau \gg 1$ limit was strongly dependent on the b/a ratio. Fries[236] considered the case of spins I and S residing in different "groups of atoms", which could react, with each other and thus either be bound together or move independently. In the former case (molecular complex) the modulation of the dipole–dipole interaction would be essentially rotational, while in the latter case the modulation would be governed by translational motion.

The correlation function (38) can also be obtained by molecular dynamics simulations. Gladkii and Daragan[237] simulated a system consisting of Lennard-Jones spheres with the radii corresponding to argon and tetramethylsilane. They found that the decay of the correlation function could be described by the force-free diffusion model for times longer than about 2 ps for argon and 5 ps for tetramethylsilane. Moreover, they showed that the effective distance of closest approach for the Lennard-Jones liquid was smaller than the distance corresponding to the potential minimum. Westlund and Lynden-Bell[238] simulated a more complicated system, liquid acetonitrile. The correlation function (38), evaluated for two protons residing in different molecules, was found to decay rapidly and non-exponentially during the first picosecond to about 25% of the initial value; at longer times the motion becomes diffusive. For the hypothetical case of a spin in the molecular centre of mass the initial rapid decay was found to be much less dramatic, demonstrating the importance of the eccentricity effect.

The factorization of the correlation function into a distance term and an angular term was found to be a good approximation.

2.7. Relaxation and exchange

Chemical exchange processes have an important impact on the NMR lineshapes, as discovered by Gutowsky *et al.*[239] in the very early days of magnetic resonance and explained in length in more recent monographs.[240,241]

The relation between the phenomena of nuclear spin relaxation and chemical exchange is complicated. We follow here the presentation of the problem by Halle,[242] from where we also reproduce Fig. 3. As can be seen from the figure, the derivation of the relaxation rates can be divided into three stages. Assuming an interaction model, we can derive the distribution functions such as $P(\Omega_0)$ and $P(\Omega_0 \mid \Omega, \tau)$ in (24) or more general distributions in (38). In the second stage the fluctuating spin–lattice coupling is averaged over the distribution functions, giving the correlation functions (this implies evaluation of (24) and (38)) or, after Fourier–Laplace transformation, the spectral densities. In the final stage the spectral densities are substituted into (5) and the macroscopic relaxation rates are evaluated through (4) and (1). The chemical exchange can enter the process sketched in Fig. 3 at different stages and in different ways. The simplest effect is

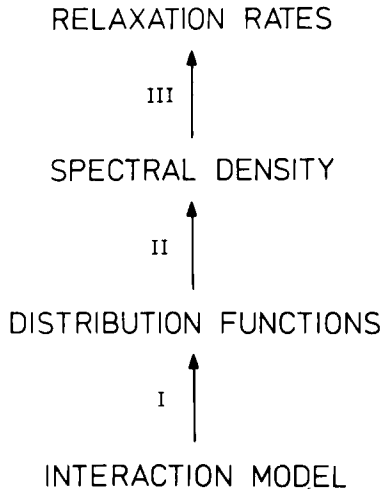


Figure 3. The three basic stages in the theory of nuclear spin relaxation. (Reproduced with permission from B. Halle, *Mol. Phys.*, 1989, **53**, 1427.) (Copyright © Taylor and Francis Ltd.)

obtained if the chemical exchange is slow compared with the molecular motions responsible for the relaxation. The exchange dynamics is then simply included in Stage III by means of the modified Bloch equations[243] or by generalizing the equation of motion for the density operator, (8):[16,240,241]

$$\frac{\mathrm{d}|\rho)}{\mathrm{d}t} = -\mathrm{i}\hat{\hat{L}}_{\mathrm{o}}|\rho) - \hat{\hat{R}}[|\rho) - |\rho^{\mathrm{T}})] + \hat{\hat{\Xi}}|\rho), \tag{39}$$

where $\hat{\hat{\Xi}}$ is the exchange superoperator, describing the effects of chemical transformations. Alternatively, but still within Stage III, the influence of the exchange on relaxation can be described using the theory of Markov processes.[244,245]

An interesting limiting condition corresponds to an exchange rate that is much larger than both the relaxation rate and the chemical-shift difference ("fast exchange conditions"). For a simple two-site exchange characterized by exponential relaxation in both sites the relaxation of the averaged signal can be described by relaxation rates T_1^{-1} and T_2^{-1}, given as weighted averages of the two sites A and B:

$$T_i^{-1} = p_{\mathrm{A}} T_{i\mathrm{A}}^{-1} + p_{\mathrm{B}} T_{i\mathrm{B}}^{-1}, \tag{40}$$

where $i = 1$ or 2, and p_{A} and p_{B} are the relative weights of the two sites, characterized by the relaxation rates $T_{i\mathrm{A}}^{-1}$ and $T_{i\mathrm{B}}^{-1}$ respectively. The situation becomes more complicated if relaxation in one of the sites is non-exponential. Several studies have dealt with specific formulation and solution of (39) for the case of quadrupolar nuclei in ions such as Na^+, Mg^{2+} and Cl^- exchanging between a bound site on the surface of a macromolecule or an aggregate and a free site in bulk solution. The bound site may be outside of the extreme narrowing region and will thus be characterized by multiexponential relaxation as discussed in Section 2.2. The problem for $I = \frac{3}{2}$ was solved by Bull.[246] The cases of $I = \frac{5}{2}$ and $\frac{7}{2}$ were solved numerically by Bull *et al.*[58] and more recently by Westlund and Wennerström,[59] who included the effect of the dynamic shifts and presented analytical expressions for the lineshapes. Eliav *et al.*[247] considered a similar, though more complicated case, where the bound site was not only outside the extreme narrowing region (10) but also outside the Redfield (strong narrowing) limit (9). Their calculations are based on solutions of stochastic Liouville equations for the two sites, coupled by exchange.

A qualitatively different physical situation occurs when the mean residence time of a nucleus in a particular site is of similar magnitude to or shorter than the relevant correlation times. In the terminology of Halle[242] (Fig. 3), the exchange must then be introduced at Stage I. This approach

was adopted by several groups in the late nineteen sixties and early nineteen seventies.[248-251] A more general approach was proposed by Wennerström.[252] He included the exchange process explicitly in the spin Hamiltonian by writing

$$H = \sum_i f_i(t) H_i, \tag{41}$$

where H_i is the Hamiltonian in site i and $f_i(t)$ is equal to unity if the nucleus is in site i at time t and zero otherwise. Burnell *et al.*[253] considered the case of a water molecule exchanging between a "free" and a "bound" site. The relaxation in the bound site is exponential and describable by the two-step model;[131,133] furthermore, the exchange rate is slow compared with the rapid motion, but fast compared with the slow component of the two-step model. More recently, Latanowicz[254] studied the case of the dipolar relaxation modulated by reorientation and rapid exchange between two sites of unequal energy.

Halle[242] concentrated his attention on intramolecular relaxation in locally ordered fluids. He argued that for this type of system the "discrete exchange" models discussed above have several weaknesses. The crudeness of the assumption that a spin just outside the perturbed region is dynamically equivalent to one far removed is clear. A less obvious but even more important shortcoming of the discrete model is the assumption that the orientational correlation induced by the surface is lost immediately and irretrievably when the spin leaves the perturbed region. Halle[242] proposed replacing the discrete model by a more realistic continuous diffusion model (CDM), in which the translational diffusion of the spin-bearing species is described by the Smoluchowski diffusion equation. This is Stage I of Fig. 3. Halle then proceeds to Stage II and derives the correlation functions. In this way, all the effects of the translational motion are included in a self-consistent manner. The relaxation behaviour predicted by the CDM approach is qualitatively different from the prediction of the discrete exchange model, mainly because of the inclusion in the former of the possibility of diffusional reencounters. In this first paper, Halle[242] treated systems with planar interfaces. The model was subsequently refined[255] and extended to cover cylindrical interfaces[256] and to perform lineshape calculations.[257]

Diffusive exchange in heterogeneous systems was also studied by Belton and Hills.[258,259] Their philosophy, however, was quite different from Halle's. They introduced the diffusive exchange at Stage III of Fig. 3 by including the diffusion terms into the generalized form of Bloch equations, originally proposed by Torrey.[260]

3. EXPERIMENTAL METHODS

In this section we review the experimental techniques for relaxation-related measurements. Papers dealing with a theoretical description of a particular experimental situation are also covered here.

Relaxation measurements are covered in most NMR books. A useful general reference work for conventional one-dimensional experiments is the book by Martin *et al.*[261] For a thorough analysis of the more sophisticated experiments, the monograph by Ernst *et al.*[16] is invaluable.

3.1. Spin–lattice relaxation

As discussed in Section 2.2, spin–lattice relaxation is not necessarily exponential. Exponential (or nearly exponential) relaxation occurs for

(i) quadrupolar nuclei ($I = 1$; for $I > 1$ only under extreme narrowing);
(ii) isolated pairs of magnetically equivalent spin-$\frac{1}{2}$ nuclei (such as protons in water);
(iii) rare spin-$\frac{1}{2}$ nuclei, relaxed either by the CSA and SR mechanisms or by dipolar interactions with another nuclear species, whose signals are saturated by double resonance irradiation; the most notable example of the latter category is ^{13}C relaxation studied under the usual conditions, i.e. with broadband irradiation of protons.

If the spin–lattice relaxation is non-exponential, many of the experiments discussed below can still be performed. The non-exponentiality of the relevant processes can be taken into consideration in the data analysis (see Section 3.5). Moreover, one can sometimes create several different initial non-equilibrium states and follow the evolution of the spin system under different conditions.

Spin–lattice relaxation measurements are usually performed using simple sequences of non-selective ("hard") pulses, with or without double resonance irradiation. The most usual experiments are "inversion–recovery" (consisting of a 180°–variable delay–90° pulse sequence), "saturation–recovery" (where the inverting 180° pulse is replaced by a saturating sequence) and "progressive saturation" (consisting of a series of 90° pulses leading to a steady state). All these techniques are discussed thoroughly in the book by Martin *et al.*[261] The factors affecting the accuracy in ^{13}C spin–lattice relaxation measurements were carefully analysed in a review by Craik and Levy,[262] who recommended using the "fast" version of the inversion–recovery sequence (FIR).[263] The optimization of the

experimental design and the statistical analysis of the data was recently discussed in a comprehensive way in a review by Weiss and Ferretti.[264] Therefore we see no need to review these aspects of the "standard" experiments and their modifications in any detail. We only wish to mention two improvements of the traditional schemes. The first one was proposed by Levitt and Freeman,[265] who designed a "composite pulse" (a sequence of phase-shifted pulses immediately after each other) providing a more broad-banded inversion than the single nominal 180° pulse. The subject of composite pulses was recently reviewed by Levitt[266] and continues to attract considerable attention.[267–269] The other improvement is also related to the imperfections of the 180° pulses. Vold and Bodenhausen[270] proposed an inversion–recovery sequence using a suitable alternation ("cycling") of the phases of both pulses and the receiver reference.

Other methods or extensions of these three basic schemes, aiming at improved speed, sensitivity or accuracy have also been proposed. The variable-nutation method (which is similar to the progressive-saturation technique but uses the pulse angle rather than pulse delay as the variable parameter), originally proposed by Christenen *et al.*,[271] was advocated by Gupta and coworkers[272,273] and Homer and Beevers.[274] Ejchart *et al.*[275] proposed a combination of the inversion–recovery and variable-nutation methods. Metz and Briggs[276] developed a two-dimensional version of the saturation–recovery experiment, in which the delay between the saturating sequence and the observed pulse functioned as the second time domain. Daxiong Ji *et al.*[277] discussed measurements of spin–lattice relaxation time by rapid-scan correlation spectroscopy.

Special techniques were developed to deal with other problems complicating the spin–lattice relaxation measurements. One such problem is related to the dynamic range. It was addressed by Brondeau *et al.*,[278] who demonstrated that using the DANTE sequence for selective inversion and monitoring made it possible to measure spin–lattice relaxation for a weak signal in the presence of a large (about 6000 times more intense) peak. Sankar *et al.*[279] described the use of the 1, 3, 3, 1 sequence for selective-excitation proton relaxation measurements for solute in millimolar concentration in water. Another complication occurs if proton measurements are to be carried out on small molecules in a macromolecular solution. The macromolecule signals give rise to a broad envelope, superimposed by the narrow signals from small molecules. Rabenstein *et al.*[280] proposed a combination of the inversion–recovery and spin-echo (see below) sequences to solve this problem. Still another difficulty in relaxation measurements—again particularly acute in proton work on large molecules—is due to overlapping signals. This problem was addressed by Arseniev *et al.*,[281] who proposed a combination of the inversion–recovery method with

two-dimensional (2D) homonuclear correlated spectroscopy (COSY). The technique essentially includes an inverting 180° pulse preceding, by a variable delay τ, the $90°-t_1-90°$ COSY sequence. The full 2D experiment is repeated with different delays τ and the intensity of the cross-peaks is followed. The same basic idea was used by Saunders and Stevens,[282] who applied the partially relaxed COSY to separate signals from protons characterized by different relaxation rates. Kay and Prestegard[283] proposed a "2D accordion" version of the same experiment, where a single 2D experiment would suffice to provide the same information.

An alternative way to deal with problems of spin–lattice relaxation measurements in systems with low sensitivity or crowded spectra involves use of heteronuclear polarization transfer.[16] Avent and Freeman[284] and Morris[285] were the first to propose using well-separated ^{13}C signals to follow the relaxation rates of proton bound to them. The scheme of Avent and Freeman involves initial saturation of the proton signal, after which the proton magnetization recovers by spin–lattice relaxation during a variable delay. This is followed by essentially a 2D heteronuclear shift-correlation experiment. The procedure of Morris[285] is one-dimensional; the initial inversion of the proton magnetization is followed, after a variable delay, by an INEPT polarization transfer to the carbons. A very similar experiment, also allowing selective pulses, was proposed by Bigler.[286] The INEPT polarization transfer was also applied by Kowalewski and Morris,[287] with the purpose of increasing sensitivity of low magnetogyric ratio nuclei. They used INEPT to prepare a highly polarized initial state for nuclei such as ^{13}C, ^{15}N and ^{29}Si as the first step of an experiment; the rest was essentially recovery under broadband decoupling conditions, followed by the monitoring 90° pulse. An even more efficient method to increase ^{13}C (or similar nucleus) sensitivity involves indirect detection, i.e. monitoring changes in ^{13}C magnetization by using the more sensitive proton resonance. This approach was proposed for ^{13}C spin–lattice relaxation experiments by Sklenar *et al.*[288] and Kay *et al.*[289] Even more recently, a two-dimensional version of the experiment involving double polarization transfers was proposed by Nirmala and Wagner.[290] Less complicated combinations of experiments on one nucleus aiming at obtaining the relaxation information on another were proposed early by London *et al.*[291] They noted that the comparison of the proton relaxation rates of the species with the proton bonded to ^{12}C and the ^{13}C satellites made it possible to evaluate the $^{13}C-^{1}H$ dipolar contribution to the carbon relaxation. Similar work, but including selective and biselective excitation (see below) was presented by Rossi and Niccolai.[292] Marchal, Canet and Werbelow[293,294] described partial ^{13}C Overhauser experiments (see Section 3.3) as a method to determine proton relaxation rates. A quite different heteronuclear relaxa-

tion experiment involves studies of the resonance of a spin-$\frac{1}{2}$ nucleus coupled to a quadrupolar nucleus, the relaxation of which influences the lineshape. This type of measurement was the subject of a recent review.[295]

Some papers have dealt with experiments where the inversion of one nuclear species was succeeded by observation of its heteronuclear coupling partner. Fuson and Prestegard[296] and Brondeau *et al.*[297] demonstrated that this type of experiment on a $^{13}CH_2$ group (or another AX_2 system) could provide dipolar cross-correlation spectral densities. Farrar and Locker[90] used this type of "semiselective" spin–lattice relaxation experiment to derive interference DD–CSA spectral densities.

The nomenclature of "selective" and "semiselective" pulses is usually used in connection with experiments on coupled proton systems.[37] Most of the recent relaxation-related work on complicated proton spin systems has been concerned with cross-relaxation networks and will be reviewed in Section 3.3. Here we only wish to mention the paper by Huang *et al.*[298] on the use of a "spy" nucleus (such as ^{13}C) to study the relaxation matrix for a proton system coupled to it.

Some interesting papers have been concerned with the complications in the relaxation behaviour (in systems that are either anisotropic or outside the extreme narrowing region) and the effect of the flip angle of the observed pulse in these systems. Bernassau and Grant[299] and Courtieu *et al.*[300] considered the case of "soft" (selective) and "hard" (non-selective) perturbing pulses applied to the A_3 spin system in an anisotropic medium. They found that varying the flip angle of the observed pulse may allow the separation of the quartet and doublet contributions to the cental line. Werbelow[301] and Einarsson and Westlund[302] considered the perturbation response in high-spin systems. The density operator for such systems can acquire non-zero contributions from multipole operators or the $L \geqslant 2$ irreducible tensor operators.[22,23] Both papers consider a sequence of events involving: (i) creation of a non-equilibrium state (e.g. an inverting 180° pulse); (ii) evolution (relaxation); (iii) observing pulse of angle Θ; (iv) detection of the FID and the Fourier transformation. Werbelow[301] discusses how the observed intensity of different multipoles is influenced by the choice of the angle Θ. Einarsson and Westlund[302] concentrate on the effect of the multipoles on the lineshapes in an inversion–recovery experiment for $I = \frac{3}{2}, \frac{5}{2}$ and $\frac{7}{2}$ in isotropic systems outside the extreme narrowing range.

In addition to the measurement methods mentioned above, there exists a group of "hybrid" experiments, where the spin–lattice relaxation rate is measured together with another relaxation parameter (spin–spin relaxation rate or nuclear Overhauser enhancement). We shall return to this type of experiment in the following sections.

All the experimental techniques for relaxation measurements mentioned

above are designed to work at high—and constant—magnetic field. A review of experimental aspects of spin–lattice relaxation cannot, however, be complete without mentioning another branch of techniques: field-cycling. This type of measurement is designed to provide relaxation information at low magnetic field, and the experimental set-up is such that, given sufficient signal intensity, performing a variable-field spin–lattice relaxation (nuclear magnetic relaxation dispersion, NMRD) experiment is easier than performing a variable-temperature experiment on a conventional spectrometer. The course of the experiment is displayed schematically in Fig. 4, which is taken from the work of Koenig and Brown.[303] During the "soak" period the spins are allowed to equilibrate at a particular field. After that, the field is switched rapidly to the B_0 value at which the relaxation rate is to be measured. The magnetization relaxes towards the equilibrium at B_0. After a variable time τ at this field, the magnetic field is switched again, now

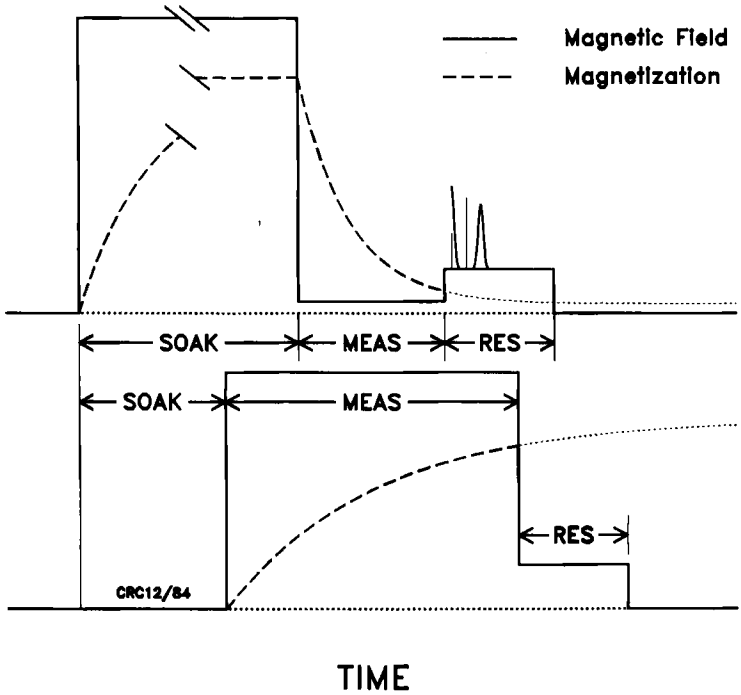


Figure 4. Representation of the time variation of the magnetic field and magnetization in a field-cycling relaxometer. (Reprinted with permission from *NMR Spectroscopy of Cells and Organisms*, Vol. 2 (ed. R.K. Gupta), p. 75 (chapter by S.H. Koenig and R.D. Brown), 1987. Copyright The Chemical Rubber Co., CRC Press, Inc.)

to the "resonance" field at which the signal is detected. Depending on whether B_0 is lower or higher than the detection field, the "soaking" field is either high or essentially zero, as indicated. After such a "field cycle", one returns to the "soaking" stage and can start the next cycle, with a different τ and/or at another B_0. NMR field cycling spectroscopy was recently reviewed comprehensively by Noack.[304]

The magnetic field strength or the Larmor frequency is clearly an intrinsic parameter for the NMR experiment. Thus the way in which relaxation properties of a given system vary with magnetic field is important from the point of view of both the theory and practice of magnetic resonance. Other variables at the spectroscopist's disposal, such as temperature or pressure, are extrinsic to the NMR experiment but of central importance for the physico-chemical properties of the systems. The variability of temperature has for a long time been taken for granted in commercially available spectrometers (even though the precision and constancy of temperature is sometimes a problem[305]), but high-pressure NMR remains the domain of a limited number of laboratories. Nevertheless, variable-pressure relaxation studies are numerous and have been summarized in several reviews.[306-308]

3.2. Spin–spin relaxation and spin–lattice relaxation in the rotating frame

The spin–spin relaxation time T_2, under ideal conditions, is simply related to the linewidth of the NMR line at half-height, $T_2^{-1} = \pi \Delta\nu_{1/2}$. Thus the simplest method of determining T_2 is to measure the linewidth. Ideal conditions imply, in the first place, that the line broadening due to an inhomogeneous B_0 field should be negligible compared with the natural linewidth. In the case of high-resolution instrumentation this requirement is not a problem for rapidly relaxing quadrupolar nuclei, but can be difficult to fulfill for spin-$\frac{1}{2}$ nuclei (it was, however, demonstrated by Allerhand and Dohrenwend[309] that accurate determination of T_2 from linewidths as low as 0.5 Hz is possible for ^{13}C using commercial instruments, provided that appropriate precautions are taken). If the lines are too broad, on the other hand, one often encounters problems with the rolling baseline, caused by the acoustic ringing of the NMR probes. Methods for avoiding this phenomenon were recently reviewed by Gerothanassis.[310] If one wishes to determine the linewidth and/or the chemical shift for a quadrupolar nucleus that displays overly broad lines under normal conditions, one can try to use a supercritical fluid solvent and thus reduce the linewidth by reducing viscosity.[311,312]

If the field-inhomogeneity broadening is disturbing, it can be suppressed by employing the spin-echo technique. The most common version of the spin-echo experiment is the so-called Carr–Purcell–Meiboom–Gill (CPMG) experiment, discussed thoroughly by Martin *et al.*[261] Briefly, the experiment consists of a 90° pulse, followed by a series of 180° pulses (with the radio-frequency field phase-shifted by 90°) at times τ, 3τ, 5τ etc. after the initial pulse. At times 2τ, 4τ etc. the spin isochromates, dephased by the field inhomogeneity, refocus and produce an echo. The echo intensity envelope decay corresponds to the transverse relaxation. CPMG experiments are in general more difficult to perform accurately than T_1 measurements by inversion–recovery experiments. Experimental conditions for accurate measurements of long spin–spin relaxation times were discussed by Tiffon *et al.*[313] Levitt and Freeman[314] proposed composite refocusing pulses, designed to be less sensitive to pulse-length errors and to spatial inhomogeneity of the radio-frequency field. A two-dimensional version of the spin-echo experiment was proposed by Metz and Briggs[276] as a method for determining T_2.

Theoretical discussions of the Carr–Purcell spin-echo experiment in the presence of chemical exchange were presented by Lankhorst *et al.*[315] The time evolution of the transverse magnetization for a spin I coupled to a rapidly relaxing spin S was calculated in the presence of scalar relaxation of both the first and the second kind. The exchange process was treated in a way similar to that introduced by Wennerström.[252] Vega[316] presented a classification of various forms of relaxation-rate expressions for a wide range of spin-echo and related experiments. He showed that there are four basic kinds of parametric expression for T_2, the validity conditions of which are determined by relative magnitudes of the correlation time for the random motion, the characteristic period of the spin-echo experiment and the magnitude of the fluctuating spin interaction. We shall return to other types of echo experiments in Section 3.4.

As discussed in the book by Martin *et al.*,[261] a technically easier alternative to the CPMG experiment may be the spin-locking experiment. This experiment consists of a 90° pulse, turning the magnetization to the transverse plane in the direction perpendicular to the radio-frequency field. The pulse is followed immediately by a weaker RF field in the direction perpendicular to the first pulse, i.e. in the same direction as the magnetization. The magnetization becomes locked in the direction of the RF field and does not defocus. The magnetization decay follows a relaxation time denoted by $T_{1\rho}$ (for T_1 in the rotating frame). The theory of $T_{1\rho}$ (and $T_{2\rho}$) was discussed for all the common relaxation mechanisms by Blicharski.[317] He found that $T_{1\rho}$ should be identical with T_2 if the molecular motions are

not too slow, $\omega_e \tau_c \ll 1$, where ω_e is the angular velocity corresponding to the spin-locking RF field ($\omega_e = B_1/\gamma$) and τ_c is the appropriate correlation time. Note that the inequality may not be satisfied if the "correlation time" is to be identified with the exchange lifetime for slow processes. The relation between spin-echo and spin-locking was also discussed by Vega,[316] who considered them as essentially identical phenomena. James *et al.*[318] found that a modification of the $T_{1\rho}$ experiment where the locking field was set off-resonance (thus modifying its effective magnitude) could directly provide the spectral density components at low frequencies. The findings of James *et al.*[318] were to a certain extent reinterpreted by Bendel.[319]

Still another way to measure T_2 was proposed by Bain *et al.*[320] The experiment involves measuring the signal intensity, after saturation of the signal with CW irradiation, as a function of the irradiation offset. The form of the resulting curve can be predicted from the solution of Bloch equations under saturating conditions. Provided that the T_1 and the magnitude of the saturating field are known, T_2 can be determined by fitting the experimental curve to its theoretical form. A modification of the experiment, involving repetitive small-angle pulses instead of the CW saturation, was presented by Leon *et al.*[321] Since T_1 must be known to evaluate T_2, we can consider this method of T_2 determination as belonging to a category of "hybrid" experiments. Eisenstadt[322-324] proposed an experiment in which the magnetization is moved back and forth between the longitudinal direction and the transverse plane. For a one-component system the measurement provides a hybrid relaxation rate T_{12}^{-1}, which is a weighted average of T_1^{-1} and T_2^{-1}. The papers aim actually at studies of two-phase systems with chemical exchange, and for such a case the formulation becomes more complex. Kronenbitter and Schwenk[325] proposed two hybrid experiments, designed for slowly relaxing systems. The first experiment consisted of a series of periodic RF pulses. The measurement of amplitude of the steady-state signal as a function of the pulse angle provides the T_1/T_2 ratio. The other experiment follows the build-up of the steady state and yields $T_1 + T_2$. The combination of the two experiments gives both relaxation times. The steady-state method and its applications were reviewed by Schwenk.[326] An improved preparation method for the experiments of this kind was recently proposed by Kreibich and Schwenk.[327] Finally, we should mention the hybrid method of Metz and Briggs[276] for a single-line spectrum. The method combines the spin-echo experiment in one time domain with the saturation–recovery experiment in the other. After two-dimensional Fourier transform, one obtains a line with the linewidth equal to $1/\pi T_2$ in one frequency domain and $1/\pi T_1$ in the other frequency domain.

3.3. Cross-relaxation and nuclear Overhauser enhancement

As mentioned at the beginning of Section 2.2, the saturation of a nucleus S interacting through dipole–dipole (or scalar) interaction with another nucleus I influences the steady-state intensity of the I signal, leading to the phenomenon of nuclear Overhauser enhancement (NOE). We are going to classify the NOE experiments with respect to the way the double-resonance irradiation is carried out, beginning with broadband heteronuclear irradiation and going on to selective irradiation and the rich variety of modifications of the basic frequency-resolved experiment.

The theory and methodology of heteronuclear broadband irradiation are fairly straightforward. Under extreme narrowing conditions, the heteronuclear NOE factor for I determined under broadband decoupling of S can be used to determine the dipole–dipole (IS) contribution (T_{1DD}^{-1}) to the observed spin–lattice relaxation rate of I (T_{1obs}^{-1}) through the simple relation[261]

$$T_{1DD}^{-1} = \frac{\eta_{obs}}{\eta_{max}} T_{1obs}^{-1}. \tag{42}$$

η_{obs} is the observed NOE factor and η_{max} is the maximum value corresponding to the pure DD relaxation, equal to $\gamma_S/2\gamma_I$. Equation (42) assumes that only the DD relaxation contributes to W_0 and W_2 in (12). This neglects the possible contribution of scalar relaxation, a fully acceptable assumption for the carbon–proton case. The CSA and SR mechanisms only contribute to W_1 and thus, according to (13)–(16), reduce the NOE.

Under non-extreme narrowing conditions, the broadband heteronuclear NOE is also reduced from its maximal value. The relaxation of proton-bearing carbons in larger molecules, characterized by long rotational correlation time, is usually assumed to be dominated by the dipole–dipole mechanism. With this assumption, the measured NOE is an independent dynamic parameter that can be used for characterizing molecular motions and testing dynamic models. Calculations of ^{13}C NOE caused by broadband proton irradiation have been reported by many authors for a variety of dynamic models discussed above (see Refs. 138, 139, 149, 150, 165–171, 173–175, 178, 179, 181, 183, 191, 192, 196, 197).

Broadband irradiation NOE experiments were introduced in the early nineteen seventies. Still important with today's technology is the gated decoupling technique introduced by Freeman *et al.*[328] for obtaining proton-decoupled ^{13}C spectra without NOE. The experiment is based on the fact that NOE build-up is a relatively slow process, governed by spin–lattice relaxation processes, while the decoupling is instantaneous. Thus gating the proton decoupler off (during at least $10T_1$ before the carbon pulse[329,330])

results in an NOE-free intensity, and switching it on simultaneously with the pulse removes spin–spin couplings. The experiment can also be performed by switching on the decoupler a time τ before the pulse. By varying τ, one obtains the "dynamic NOE" experiment, proposed by Freeman *et al.*[328] and "rediscovered" in the late nineteen seventies by several groups[331–333] as a method for simultaneous determination of T_1 and NOE. Among more recent work on the theoretical and methodological aspects of heteronuclear broadband NOE experiments, one should mention the work of Borzo and Maciel[334] on NOE in exchanging systems and two papers on estimating peak areas by Weiss, Ferretti and coworkers.[335,336]

On the other hand, the last decade has seen a period of intense activity in the field of frequency-resolved NOE (and related) experiments, in which the NOE has been determined as a function of the double resonance irradiation frequency. This frequency resolution can be obtained in a series of one-dimensional experiments with varying irradiation frequency or in a two-dimensional experiment. The experiment may be homo- or heteronuclear, and the irradiation can be applied continuously (steady-state NOE experiment) or in the form of pulses (transient NOE experiment).

We begin the discussion with homonuclear one-dimensional experiments. The theory and experimental practice of steady-state NOE experiments were described in a book by Noggle and Schirmer[337] and in a review by Sanders and Mersh.[338] The situation for a two-spin system is summarized in the Solomon equations (12)–(16). The measurement of T_1 and NOE directly yields the cross-relaxation rate σ. The two-spin system was also analysed in detail by Bain *et al.*[339] In the case of a multispin system the situation is more complicated. The general cases of multispin systems with spin–spin splittings were treated by Werbelow and Grant[36] and Vold and Vold.[37] In the remainder of this section we concentrate the presentation on systems without spin–spin splittings. The equation system for the time evolution of longitudinal magnetization components may then be written in the following matrix form,[16,337] generalizing the Solomon equations:

$$\frac{\mathrm{d}\ \Delta \boldsymbol{M}_z}{\mathrm{d}t} = -\mathbf{R}\ \Delta \boldsymbol{M}_z, \tag{43}$$

where $\Delta \boldsymbol{M}_z$ is a vector with components ΔM_{zi}, $i = 1, \ldots, N$. N is the number of spins in the system. ΔM_{zi} is the deviation of the longitudinal magnetization of the ith spin from its equilibrium value. $\mathbf{R}$ is the relaxation matrix. Its diagonal elements R_{ii} are

$$R_{ii} = \sum_{j \neq i} \rho_{ij} + \rho_i^*, \tag{44}$$

where ρ_{ij} are the analogues of ρ_I and ρ_S in (13) and ρ_i^* is the relaxation rate

of spin i due to other relaxation paths. The off-diagonal elements of **R** are the cross-relaxation rates σ_{ij}.

Assume that all transitions of some spins S are saturated, that some other spins N are unaffected by the irradiation, and that spins I are observed. The steady-state solution of generalized Solomon equations for this case was given by Schirmer and Noggle:[337]

$$\eta_I^{(S)} = \sum_S \frac{\sigma_{IS}}{R_{II}} - \frac{1}{R_{II}} \sum_N \sigma_{IN}\eta_N(S). \tag{45}$$

The last term in (45) describes the so-called "three-spin effect". It arises because saturation of S leads to an enhancement of the population difference across the N transitions, which in turn decreases the intensity of the I transitions by dipolar IN coupling.[340] Clearly, the presence of the three-spin effect makes the analysis of cross-relaxation networks from steady-state NOEs quite complicated, even for small molecules.

Other possible experiments providing the cross-relaxation rates are of the transient (time-dependent) rather than steady-state type. Some such experiments were discussed in the book by Noggle and Schirmer.[337] The experiments in this category follow the time evolution of various longitudinal magnetization components after an initial perturbation. An important concept in this context, introduced by Freeman *et al.*,[341] is the initial rate of recovery. Freeman *et al.*[341] showed that immediately after the perturbing pulse the recovery can, within reasonable accuracy, be described as single exponential, characterized by an "initial relaxation rate". As demonstrated by Freeman *et al.*[340] and Hall and Hill,[342] the combination of non-selective inversion–recovery experiments with selective inversion experiments, where magnetizations corresponding to one or two protons are inverted, can be an alternative source of the cross-relaxation data—sometimes more efficient than the steady-state NOE experiments. This type of experiment was recently reviewed by Dais and Perlin.[343]

The work described in the previous paragraph is concerned with small molecules, characterized by short correlation times. The dependence of the homonuclear NOE on the molecular mobility was discussed by several authors in the mid-nineteen-seventies. Werbelow[344] studied a pair of spins undergoing an isotropic overall tumbling and internal motion (one degree of freedom) under different motional conditions. He found that the NOE was mainly sensitive to the overall motion. Similar work was also reported by Tropp.[144] Kalk and Berendsen[345] discussed proton relaxation in proteins and stressed the importance of spin exchange (cross-relaxation) in extended spin systems, the effect denoted in solids as "spin diffusion". The role of spin diffusion for proton relaxation under double-irradiation conditions was also discussed by Akasaka.[346] The differences between the NOE

experiments in small and large molecules were summarized by Bothner-By.[347]

Spin diffusion makes the steady-state NOE experiments on large molecules less specific and therefore less useful. By the late nineteen seventies, several groups of authors discussed the possibilities of overcoming this lack of specificity by means of transient experiments in the context of studies of large molecules. Wüthrich and coworkers proposed using selective inversion pulse[348] (a similar experiment was also proposed by Tropp[144]) and the so-called truncated driven Overhauser experiment.[349] The theoretical aspects of experiments of this kind were discussed by Bothner-By and Noggle,[350,351] while the practical aspects of time-dependent NOE experiments were analysed by Dobson *et al.*[352] Recently, Andersen, Eaton and coworkers[353,354] discussed the rapid-acquisition versions of the transient and driven experiments and compared the merits of the two approaches. In another recent paper, Kerwood and Bolton[355] proposed a field-cycling or low-field NOE-type experiment, in which the equilibration and selective inversion at high field is followed by relaxation at low field; the detection occurs again at the high field. By means of this experiment, it is possible to combine the sensitivity of the high field with the simplicity of the relaxation phenomena in extreme narrowing for slowly tumbling molecules. Heteronuclear frequency-selective NOE-type experiments were first proposed by Campbell and Freeman,[356] who used selective and biselective pulses. Similar experiments were discussed more recently by Rossi and Niccolai[292,357] and by Kövér and Batta,[358] who also published an extensive review of the field of one- and two-dimensional heteronuclear NOE measurements.[359] It should be pointed out that experiments of this type are most useful for smaller molecules.

The experience of the last ten years shows that the best method for studies of homonuclear cross-relaxation processes in large molecules is two-dimensional exchange spectroscopy (2D NOE, NOESY). It was first described by Jeener *et al.*[360] as a method for studying general exchange processes (chemical exchange and/or spin exchange by cross-relaxation) and by Macura and Ernst[361] as a tool for studies of cross-relaxation. The method is presented in detail in the book by Ernst *et al.*[16] and we therefore describe it here rather briefly. The basic pulse sequence of the method consists of three non-selective 90° pulses. The first pulse creates transverse magnetization. The interval between the first two pulses is the t_1 period, incremented in the course of the 2D experiment. The transverse magnetization components precess freely during this period and acquire frequency labels. The second pulse converts the transverse magnetization back into longitudinal magnetization. The interval between the second and the third pulse is called the mixing period τ_M; during this period the longitudinal

magnetization components undergo cross-relaxation. The final pulse again generates transverse magnetization, which can be detected as an FID during the detection period t_2. The experiment leads to cross-peaks in the 2D spectrum joining the resonances, which cross-relax each other. Kumar *et al.*[362] reported 2D NOE studies with variable mixing time and were able to measure the build-up rates of the first-order NOE between closely spaced protons as well as the second-order Overhauser effects due to spin diffusion.

The procedures for obtaining 2D absorption-mode lineshapes in the 2D NOE spectra were proposed by States *et al.*,[363] Keeler and Neuhaus[364] and Johnston *et al.*[365] The advantages of phase-sensitive experiments for the purpose of quantitative determination of cross-peak volumes were discussed by Olejniczak *et al.*[366] Cutnell[367] proposed a scheme for obtaining 2D NOE spectra with solvent signal suppression. Bremer *et al.*[368] presented a modification of the NOESY scheme, called "skewed exchange spectroscopy" (SKEWSY). Bull[369] investigated the possible role of cross-correlation effects on NOESY spectra and found the method rather insensitive to these effects. Modifications of the standard experiment, which use multiple-quantum filtering (see Section 3.4) and enable relatively direct measurements of cross-correlations, were also discussed. Clore and Gronenborn[370] and van de Ven *et al.*[371] studied the "transferred" or "chemically relayed" Overhauser effect, i.e. the NOE transferred by chemical exchange between nuclei without direct dipolar interaction.

2D NOE spectroscopy for systems with spin–spin couplings is somewhat more complicated. As discussed by Macura *et al.*,[372,373] scalar spin–spin interactions can lead to additional cross-peaks, called "*J*-peaks". Methods for suppressing the *J*-peaks were described by Macura *et al.*[374] and Rance *et al.*[375] Moreover, if the pulse angles in the NOESY experiment deviate from 90°, the coupled spin system may reach a state of so-called "longitudinal two-spin order",[376] leading to "*zz* signals". As shown by Wagner *et al.*,[377] the occurrence of the longitudinal two-spin order can be turned into an advantage, since it allows for the separation of chemical-exchange and cross-relaxation effects and of cross-relaxation phenomena within coupled spin systems and between different spin systems. Oschkinat *et al.*[378] proposed a "small-angle NOESY" experiment for coupled systems, allowing separate determination of the transition probabilities between pairs of energy levels in a coupled spin system. The heteronuclear 2D NOE experiment (HOESY) was proposed by Rinaldi[379] and Chin Yu and Levy.[380] The pure-absorption version was introduced by Kövér and Batta,[381] who also reviewed the field.[359] Modifications of the basic scheme was recently presented by Bigler and Müller,[382] Kövér and Batta[383] and Muhandiram and McClung.[384] Griffey and Redfield[385] reviewed applications of proton-

detected heteronuclear edited techniques for studies of nuclear Overhauser effect.

As discussed by Macura and Ernst,[361] a proton pair tumbling isotropically in solution has zero NOE if the motional conditions are such that $\omega_0\tau_c = \frac{1}{2}\sqrt{5}$. Thus the conventional NOESY experiment will not lead to any cross-peaks, independently of the strength of the dipole–dipole coupling. Bothner-By *et al.*[386] devised an experiment that can replace NOESY under these conditions: the transient NOE experiment in the rotating frame or the CAMELSPIN experiment. The experiment can be performed either as a one-dimensional difference measurement or in a two-dimensional version. In the one-dimensional case the reference spectrum is generated by a spin-locking experiment. The cross-relaxation spectrum is generated in a similar way, but including a selective inversion pulse immediately prior to the 90° pulse. The cross-relaxation rate available from the CAMELSPIN experiment is known as the "transverse cross-relaxation rate". Bax and Davis[387] discussed the practical aspects of the experiment, which they called "rotating-frame Overhauser enhancement spectroscopy" (ROESY). Davis[388] found that comparing the longitudinal and transverse cross-relaxation rates could determine the correlation time uniquely. Suppression of artifacts in the ROESY experiment was discussed by Cavanagh and Keeler[389] and Farmer and Brown.[390] Finally, Farmer *et al.*[391] performed a theoretical investigation of the effects of the molecular motion on the NOESY and ROESY cross-relaxation rates for AX and AX_3 spin systems, while Bull[392] presented the ROESY relaxation matrices for a variety of spin systems and proposed a multiple-quantum (see below) ROESY experiment.

3.4. Other relaxation experiments

In this section we cover three topics: multiple quantum phenomena, relaxation-allowed coherence transfer, and some relaxation experiments specifically designed for oriented systems. As shown below, the three topics are in fact related to each other.

The elements ρ_{mn} of the density matrix, formulated in the basis of the eigenstates of a high-field Hamiltonian (i.e. a Hamiltonian dominated by the Zeeman interaction), can be characterized by the difference ΔM_{mn} between the total magnetic quantum numbers of the eigenstates n and m. This difference is called the "coherence order". The coherence order can be zero (for example, $\Delta M_{mm} = 0$ for diagonal elements of the density matrix) or any integer up to$N$, where N is the total number of Zeeman levels for a

spin system (for a system of K spin-$\frac{1}{2}$ nuclei $N = K + 1$, for an isolated quadrupolar nucleus $K = 2I + 1$, etc.). The observable NMR signals originate from the density-matrix elements corresponding to $\Delta M_{mn} = 1$, called "single-quantum coherences". The density matrix elements corresponding to other ΔM_{mn} are called "multiple-quantum (MQ) coherences". Alternatively, one can say that the MQ coherences correspond to the $M > 1$ components in the expansion of the density operator in irreducible tensor operators $T_M^{(L)}$. Multiple-quantum coherences can be detected indirectly in 2D experiments, and the field of MQ NMR spectroscopy has been the subject of several reviews.[16,393-396]

The Redfield relaxation theory is valid for the time evolution of density matrix elements of any coherence order. The expressions for the decay rates of the MQ coherences in coupled systems of spin-$\frac{1}{2}$ nuclei, caused by the DD and the random-field mechanisms, were derived by Wokaun and Ernst.[397] They found that the relaxation of the non-degenerate coherences should be exponential. The time constant for MQ decay, which can be called T_2 for a forbidden MQ transition, is sensitive to cross-correlations between different interactions. The case of quadrupolar nuclei was treated by the Volds and coworkers[398-400] and by Werbelow and Pouzard.[401] For high-spin systems the quadrupolar relaxation rates for MQ coherences can provide combinations of spectral densities, different from those available from other experiments. Kowalewski and Larsson[402,403] studied the scalar relaxation of multiple quantum coherences in an AMS system, where A and M denote spin-$\frac{1}{2}$ nuclei and S represents one, or several, quadrupolar nuclei. Comparisons of zero-quantum and double-quantum relaxation rates were shown to yield relative signs of the AS and MS coupling constants.

Experimentally, the MQ relaxation rates can be determined as follows. Assume that the spin system under consideration is described by a spin Hamiltonian containing terms bilinear in nuclear spins (scalar, dipolar or quadrupolar interaction). A suitable sequence of pulses and free precession intervals can then create a state of MQ coherence. The MQ coherence is allowed to evolve during time t_1 and is then transferred into an observable single-quantum coherence, detected during t_2. After Fourier transformation with respect to t_2 and t_1, the MQ relaxation rate is determined from the linewidths in the ω_1 frequency domain, in analogy with the spin–spin relaxation for the allowed single-quantum transitions. In analogy with the studies of the usual T_2, one has to get rid of the inhomogeneous broadening. The multiple-quantum spin-echo experiment was proposed by Bodenhausen *et al.*[399]

Multiple-quantum phenomena can have other implications for studies of relaxation processes. Benn[404] reported spin–lattice relaxation-time measurements of ^{13}C satellites of the ^{13}C resonances without isotope enrichment.

This could be achieved by a combination of the ideas of progressive saturation and the INADEQUATE experiment, where the resonances corresponding to isolated ^{13}C are suppressed by forcing the systems to pass through a state of double-quantum coherence (double-quantum filtering).

Several other papers have dealt with multiple-quantum filtered relaxation experiments, in which the multiple-quantum phenomena enter in a more subtle way. We begin the discussion with the case of quadrupolar nuclei. Jaccard *et al.*[405] showed that MQ coherence can be created for quadrupolar nuclei with $I \geqslant \frac{3}{2}$, even in the absence of bilinear splittings, if the system is outside the extreme narrowing region and is thus characterized by multi-exponential relaxation. Jaccard *et al.*[405] proposed experiments designed to monitor the non-exponentiality of the longitudinal as well as the transverse relaxation. A similar procedure was proposed by Pekar and Leigh,[406] who found that double-quantum filtering of the ^{23}Na signal ($I = \frac{3}{2}$) outside the extreme narrowing region facilitated the detection of biexponential transverse relaxation. The double-quantum ^{23}Na spectrum of an isotropic system outside the extreme narrowing region was reported by Rooney *et al.*[407]

The creation of double-quantum coherence in a spin system without bilinear splitting, such as a quadrupolar nucleus in the isotropic environment discussed in the last paragraph, is in conflict with the usual coherence transfer rules.[16] Similar observations were also made in other systems with non-exponential relaxation. Müller *et al.*[408] and Rance and Wright[409] observed violations of the coherence transfer selection rules in 2D spectra of systems of spin-$\frac{1}{2}$ nuclei with degenerate transitions. As explained at length by Müller *et al.*,[410] these phenomena are closely related to the relaxation-promoted occurrence of higher-magnetic multipoles (irreducible tensor operators with $L > 1$) in the density operator for the system. The work of Jaccard *et al.*,[405] Leigh and Pekar[406] and Rooney *et al.*[407] is thus related to the discussion of the simple inversion–recovery experiment for quadrupolar nuclei outside the extreme narrowing region presented by Einarsson and Westlund.[302] Kay and Prestegard[411] used the intensity of the double-quantum filtered signals from methyl-group protons to extract cross-correlation spectral densities—information identical with that obtained by Bendall and Pegg[412] from a polarization-transfer experiment. Müller[413] reported an experiment known by the acronym MERCY (multiple-exponential relaxation spectroscopy), very similar to that of Jaccard *et al.*,[405] for the protons in a methyl group outside the extreme narrowing region. Non-exponential relaxation can also occur in systems of spin-$\frac{1}{2}$ nuclei without magnetic equivalence if cross-correlation effects are present. Jaccard *et al.*[414] used this fact to study CSA–DD interference relaxation, and Wimeris and Bodenhausen[415] observed relaxation-allowed coherence

transfer in systems of three and four spin-$\frac{1}{2}$ nuclei with cross-correlated dipolar interactions.

We now turn to two types of special experiment designed for oriented systems in general and the quadrupolar nuclei in such systems in particular. Both types of experiment have been discussed in reviews of relaxation measurements in liquid-crystalline solutions.[124,125] The first of these experiments was originally proposed by Jeener and Broekaert (JB).[416] They showed that a sequence of two pulses, phase-shifted relative to each other by 90° and separated by an interval of order T_2, could create dipolar order in solids. The efficiency is highest if the first pulse is a 90° pulse, while the second is a 45° pulse. The (macroscopic) state of dipolar order is characterized by excess population of the $\alpha\alpha$ and $\beta\beta$ states ($M = \pm 1$ in the coupled representation) and reduced populations of the $\alpha\beta$ and $\beta\alpha$ ($M = 0$) states. The dipolar order has an analogue in scalar-coupled (scalar order) and quadrupolar (quadrupolar order) systems. The decay of scalar order was studied by Jaccard *et al.*[414] Ahmad and Packer[417] analysed the evolution of a $I = 1$ system in an anisotropic environment after the creation of quadrupolar order by the JB sequence, as monitored by a third pulse with pulse angle 45°. Vold *et al.*[418] demonstrated that it was possible in this way to measure the recovery of Zeeman order and the decay of quadrupolar order from a single set of recovery curves, thus providing the spectral densities $J_1(\omega_0)$ and $J_2(2\omega_0)$. Modifications of the JB experiment were subsequently proposed by Barbara *et al.*,[419] who combined the JB excitation with a MQ sequence, and by Wimperis and Bodenhausen,[420] who proposed a broadband (i.e. efficient over a range of quadrupolar couplings) version of the experiment.

The other type of experiment is designed to provide information on transverse relaxation, and thus zero-frequency spectral density. As discussed in the classical paper by Solomon,[421] the quadrupolar-split lines in single crystals are usually broadened because of the distribution of the quadrupole constants, which are in turn due to crystal imperfections. In order to circumvent this problem, Solomon proposed the quadrupolar echo (QE) experiment. In analogy with the JB experiment, the QE experiment also consists of a pair of pulses phase shifted by 90° and separated by an interval τ. Here the pulse angle of both pulses is set at 90°. At time 2τ after the first pulse the static quadrupolar interaction is refocused and an echo occurs. The QE experiment found a large number of applications as a tool for obtaining deuteron spectra in oriented systems.[422,423] Ahmad *et al.*[424] applied the QE experiment to study the transverse relaxation of the deuteron in D_2O in heterogeneous systems. Vold and Vold[425] and later Müller and Chan[426] proposed a two-dimensional version of the QE experiment. Recently, Furo *et al.*[427] described the 2D QE experiment, as

well as a two-dimensional combination of QE and the usual (Carr–Purcell) echo, for quadrupolar nuclei with $I > 1$.

3.5. Analysis of relaxation data

Analysis of relaxation data can be carried out in different ways and on different levels. First, there is the evaluation of the time constants for exponential relaxation (relaxation rates or initial rates) from the sets of inversion–recovery or spin-echo spectra. This subject has been discussed at length in reviews mentioned above,[37,262,264] and we have nothing to add here. Then there is the interpretation of non-exponential relaxation data, such as full recovery curves from coupled spin systems and cross-peak intensities in NOESY experiments. Finally, one can analyse a set of relaxation rates and related data, obtained for various positions in a molecule and, possibly, as a function of magnetic field in terms of the parameters of the dynamic models discussed in Sections 2.3–2.6.

Canet[428] described a procedure, and its implementation in the form of a computer program, for the analysis of the inversion–recovery data in coupled spin systems. The procedure allows calculations of theoretical recovery curves from a given set of autocorrelation and cross-correlation spectral densities and fitting of the spectral densities to the observed recovery data. Fuson *et al.*[429] expressed the spectral densities derived from the analysis of an AX_2 spin system in terms of cartesian correlation times. They pointed out that this representation has the advantage of not being biased towards any particular model. Piveteau *et al.*[430] developed a simulation program, BOWMAN, for multipulse experiments on weakly coupled spin systems, including the effects of relaxation.

A large number of papers have been devoted to the analysis of cross-relaxation data in the NOESY experiment. The papers mentioned in this section deal specifically with problems of data analysis, and their selection is to a certain extent arbitrary. Expressions for the cross-peak intensities as functions of the relaxation matrix of (43) were given by Macura and Ernst.[361] They also demonstrated that the cross-peak intensities at short mixing times were simply related to the corresponding cross-relaxation rates, which in turn are proportional to the sixth power of the ratio of the internuclear distances. Clore and Gronenborn[431] assessed the errors involved in the determination of interproton distances in one- and two-dimensional NOE experiments; in particular, they addressed the problem of errors introduced by the use of simple relations between the relative distances and the cross-peak intensities. Macura *et al.*[432] proposed an improved method for the evaluation of cross-relaxation rates within the

initial rate approximation for the NOE build-up, where the cross-peak intensities are scaled relative to the diagonal ones. Keepers and James[433] described a procedure for distance determination from NOESY data, avoiding the initial rate approximation by working with the complete relaxation matrix in (43). They found that recording cross-peak intensities at several mixing times was important for obtaining accurate distances and that an approximate description of the motional dynamics might be adequate. A similar procedure was also proposed by Olejniczak *et al.*[434] Boelens *et al.*[435] modified the relaxation-matrix method, in which the experimental NOEs are supplemented with calculated ones based on a molecular model. Madrid and Jardetzky[436] evaluated the sensitivity of the relaxation-matrix approach to structural studies and estimated the magnitude of errors that can be expected when NOESY spectra are interpreted without prior knowledge of structure. Kay *et al.*[437] described a two-dimensional simulation program for NOESY (and other 2D experiments) including the strong-coupling effects and describing the spin–lattice relaxation with the full form of (43). Mirau[438] proposed a procedure for quantitative interpretation of a single NOESY spectrum, employing one-dimensional selective relaxation-rate data for normalizing peak volumes.

We now turn to papers concerned with the analysis of sets of relaxation times, and possibly heteronuclear NOEs, in terms of motional models and parameters. Fujiwara *et al.*[439] described a least-squares program for the analysis of ^{13}C relaxation data for a symmetric rotor. Allouche and Pouzard[440] reported a program, called ISHTAR, for quantitative investigation of dipolar and quadrupolar spin–lattice relaxation within the model of anisotropic rotational diffusion. The implementations and practical function of "model-free" approaches to relaxation in molecules with internal motion degrees of freedom were described by Lipari and Szabo[441] and Fedotov and Kivayeva.[442] Error sources in the model-free treatment and the statistical analysis of the data were discussed by McCain *et al.*[443] Finally, Craik *et al.*[444] presented a comprehensive and general program (MOLDYN) for the interpretation of relaxation data in terms of a large number of dynamics models. The program is also designed to assist in the testing and evaluation of new motional models.

4. RELAXATION MEASUREMENTS IN GASES

Nuclear spin relaxation in gases has been reviewed recently.[445,446] Therefore we see no need to make this section comprehensive. Instead, we present here a personal selection of papers, concentrating on the aspects of the nuclear

spin relaxation phenomena in gases that we judge to be of interest for work on liquids.

Following Armstrong,[445] we can divide gas-phase relaxation studies into three regimes. In the high-density or dense-fluid region a gas is not vastly different from a liquid. In fact, Bull[447] reported variable-temperature measurements of quadrupolar deuteron and nitrogen relaxation in neat deuterated acetonitrile, covering the liquid and gaseous regions. The relaxation rates varied continuously with temperature and could be interpreted using the extended diffusion model. Topol *et al.*[448] studied proton T_1 in HCl and H_2S in fluids on both sides of the critical point. Except for a dip in the very vicinity of the critical point, the temperature dependence of the relaxation rates was also smooth here. Topol[449] reported calculations of spin–lattice relaxation times in fluids slightly above the critical point. Jonas and coworkers[450–452] reported ^{19}F spin–lattice relaxation in gaseous SF_6 and CF_4 at variable temperature and high (and variable) pressure. The relaxation was dominated by the spin–rotation interaction and displayed a strongly non-linear pressure dependence. Zerda *et al.*[453] compared the τ_J values obtained from these measurements for SF_6 with the τ_2 data from Raman spectroscopy and analysed the data using the ED and FPL models (see Section 2.3). Lamb and Jonas[454] studied proton relaxation in compressed supercritical water ($t_c = 374°C$) and in water vapour under high pressure in the temperature range 150–350°C. The relaxation rate in the supercritical region was found to be dominated by the SR mechanism with T_1 linear with density up to rather high densities. At lower temperatures the contribution of the DD mechanism was found to become more important.

Relaxation in the low- and intermediate-density regimes is dominated by binary collisions and differs more from the liquid state. An early and important study of relaxation in gases of polyatomic molecules was made by Bloom *et al.*,[455] who studied proton and deuteron spin–lattice relaxation in deuterated methanes. They expressed the relaxation rate as the sum of three terms: (i) an intramolecular contribution depending on the reorientational spectral densities of the $L = 2$ spherical harmonics (DD or quadrupolar relaxation); (ii) an intermolecular DD contribution; and (iii) a spin–rotation contribution. In the low- or intermediate-density range the intermolecular term can safely be neglected. Bloom *et al.*[455] estimated the SR contribution to proton T_1^{-1} as about 80–95%, while the quadrupolar relaxation dominated the deuteron relaxation in the deuterated species. Using a simple collision-theory argument, they found that the SR relaxation time, at constant temperature and not too low pressure, should be proportional to density ρ and that the temperature dependence should follow the power law $T_1/\rho \propto T^{-3/2}$. Both of these expectations were confirmed

experimentally. T_1/ρ for CD_4 was found experimentally to vary only slightly with temperature, which Bloom *et al.* were able to rationalize.

The conclusion that the SR mechanism is dominant in gases seems to be valid for most spin-$\frac{1}{2}$ nuclei. Weiss-Lopez, Folkendt and coworkers recently reported studies of proton relaxation in gaseous furan[456] and of proton and carbon relaxation in gaseous benzene.[457] In both papers it was found that spin–lattice relaxation was dominated by the SR mechanism and its density dependence for protons could be described reasonably well by the simple relation

$$T_1 = A\rho + B/\rho. \tag{46}$$

The first term describes the linear part of the T_1 versus density curve, characteristic of the intermediate-density range, while the second term describes the variation of T_1 in the vicinity of a minimum, characteristic of the low-density regime. The density dependence of the proton T_1 in gaseous benzene at 381 K is shown in Fig. 5. For ^{13}C it was only possible to study the intermediate-density region. Using density-dependent data, the authors were able to determine the spin–rotation coupling constants and the angular-momentum reorientation cross-section, a measure of the efficiency of the transfer of angular momentum. The use of (46) in the case of benzene was found to give a small systematic error, similar to the deviation from the linear density dependence observed earlier by Lemaire and Armstrong[458] for protons in HCl and NH_3. Lemaire and Armstrong[458] explained their

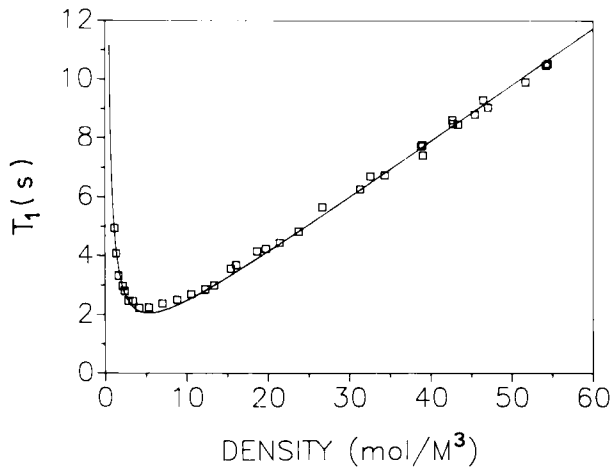


Fig. 5. Density dependence of proton T_1 for benzene gas at 381 K. (Reprinted with permission from M.M. Folkendt, B.E. Weiss-Lopez and N.S. True, *J. Phys. Chem.*, **92**, 4859. Copyright 1988 American Chemical Society.)

observations using the so-called "multilevel relaxation-time approximation".

A nuclear species that has received some attention in work on dilute gases is ^{19}F. Spring and True[459] studied axial and equatorial ^{19}F spin relaxation in sulphur tetrafluoride, while Jameson and Jameson studied SF_6 [460] and the analogous selenium and tellurium hexafluorides.[461] Ursu *et al.*[462] investigated hexafluorides of tungsten, molybdenum and uranium. In all cases ^{19}F spin–lattice relaxation was dominated by the SR mechanism. The SR mechanism also dominated ^{77}Se and ^{125}Te (both $I = \frac{1}{2}$) relaxation in SeF_6 and TeF_6,[461] which made it possible to determine absolute nuclear shieldings for these nuclei. Ursu *et al.*[463] also studied the linewidth of ^{19}F in gaseous UF_6 as a function of ^{235}U enrichment. The presence of this isotope was found to broaden the fluorine line, owing to the scalar relaxation of the second kind originating in the rapid quadrupolar relaxation of ^{235}U.

A diatomic molecule that we wish to mention here is nitrogen. Golubev *et al.*[464] studied linewidths of ^{15}N ($I = \frac{1}{2}$) in the isotopic species $^{15}N_2$ and of ^{14}N ($I = 1$) in $^{14}N_2$. Relaxation of the former is dominated by the SR mechanism (correlation time τ_J), while the latter is relaxed by quadrupolar interaction (correlation time τ_2). The authors were able to establish that in the density range under investigation the two correlation times were proportional to each other, in agreement with the extended J-diffusion model. Jameson *et al.*[465] studied spin–lattice relaxation of ^{15}N in nitrogen gas and mixtures of N_2 with buffer gases. They were able to determine the cross-sections for angular-momentum transfer. The cross-sections were found to be temperature-dependent (which leads to deviations from the $T^{-3/2}$ power law); such a deviation is indicative of the anisotropic intermolecular potential.[466,467] Work of this type seems to have gained popularity during the last few years. Jameson *et al.* reported studies of ^{13}C relaxation in CO [468] and CO_2 [469] in mixtures with other gases, while Reddy and coworkers investigated ethyne[470] and ethene[471] in mixtures with helium, argon and nitrogen.

In concluding this section, we mention briefly the work of Brinkmann and Kuhn,[472] who studied relaxation of quadrupolar ^{83}Kr in krypton gas. The relevant relaxation mechanism was found to be the collision-induced quadrupolar interaction.

5. RELAXATION IN INORGANIC SYSTEMS

Chemical and physico-chemical applications of nuclear spin relaxation measurements in liquids will be presented in this section and in Part 2 of this

review. The division of the material is based on chemical classification into inorganic, organic and macromolecular systems.

In this section we review nuclear spin relaxation measurements in inorganic liquid systems. The "inorganic system" is defined here as either any system not containing carbon atoms or any low-molecular-weight system containing metal atoms. Within the general subject of inorganic systems, according to the definition above, we are going to begin in Section 5.1 with pure liquids other than water. We continue in Section 5.2 with water and aqueous solutions of simple electrolytes. By "simple electrolyte solutions", we mean solutions of small inorganic ions. Other solutions of main-group metal compounds and complexes will be reviewed in Section 5.3, followed by transition-metal compounds in Section 5.4. Finally, Section 5.5 contains the remaining types of inorganic systems.

5.1. Pure inorganic liquids other than water

This short section covers papers on liquids of small molecules. The problems addressed are not substantially different from those studied in dense gases: determination of rotational and angular-momentum correlation times is an important topic, evaluation of models for the reorientational dynamics is another. The variable parameter of the experimental series is usually temperature. The temperature dependence of the rotational correlation time is often approximated by an "Arrhenius equation":

$$\tau_2 = \tau_2^0 \, e^{E_a/RT}, \tag{47}$$

where E_a is an "activation energy", a useful quantity for reduction of experimental data but with a somewhat obscure physical interpretation.

Topol *et al.*[448] studied proton relaxation in liquid HCl and H_2S along the liquid–vapour coexistence curve up to (and above) the critical point. Hauer *et al.*[473] studied the temperature and pressure dependences of T_1 for protons in H_2S and for deuterons in D_2S. The contributions of different relaxation mechanisms were separated and the dynamics were interpreted using the extended J-diffusion model. Facey *et al.*[474] reported deuteron and ^{77}Se relaxation for different condensed phases of hydrogen selenide. The motion in the liquid phase was very rapid and the ^{77}Se ($I = \frac{1}{2}$) relaxation was dominated by the SR mechanism. Wasylishen *et al.*[475] studied the quadrupolar relaxation of ^{33}S and ^{17}O in liquid sulphur dioxide. Using the sulphur QCC from other sources, they were able to derive the rotational correlation time. Assuming the same effective correlation time to govern the ^{17}O relaxation rate, they were also able to estimate the ^{17}O QCC.

Quadrupolar relaxation of ^{14}N in liquid ammonia (NH_3 and ND_3) and of

the deuteron in the deuterated species was studied early on by Atkins *et al.*[476] More recently, Hauer *et al.*[477] studied longitudinal proton and deuteron relaxation in liquid ammonia as a function of temperature and pressure. At temperatures below about 350 K the molecular reorientation could be described as isotropic small-step rotational diffusion. Sawyer and Powles[478] studied ^{31}P, ^{1}H and ^{2}H relaxation rates in liquid (and solid) mixtures of PH_3 and PD_3 as functions of temperature. The relaxation mechanisms were analysed and the molecular reorientation dynamics were discussed. In another early paper, Allerhand[479] studied the anisotropy of the rotational motion of liquid boron trichloride by means of measurements of the relaxation rates for quadrupolar ^{11}B and ^{35}Cl nuclei.

Briguet *et al.*[480] studied molecular reorientation of silicon tetrachloride, $SiCl_4$, in the pure liquid. The ^{35}Cl relaxation data were the source of rotational correlation times, while the SR-dominated relaxation of ^{29}Si provided the angular-momentum correlation time τ_J. The data were found to be consistent with the Hubbard relation (31) and with the small-step diffusion model. The same authors also analysed the behaviour of τ_J in $SiCl_4$ along the liquid–vapour coexistence curve.[481] Larsson *et al.*[110] studied ^{29}Si and ^{35}Cl relaxation in a similar compound, trichlorosilane ($SiHCl_3$). The presence of the directly bonded proton made the ^{29}Si spin–lattice relaxation a mixture of the DD and SR mechanisms, and the authors used the relaxation data from this nucleus alone to evaluate the validity of the Hubbard relation. Garg *et al.*[482] studied ^{19}F relaxation in liquid ClO_3F and found its reorientation to follow the extended J-diffusion model. Virlet and Tantot[483] reported an ^{17}O relaxation study for the same compound and for related chlorine oxyfluorides. Some transition-metal compounds have been studied in the form of pure liquids. We defer the review of this work to Section 5.4.

5.2. Water and aqueous solutions of simple electrolytes

The pure inorganic liquid that has received by far the most attention is of course water. Early NMR work on water was reviewed by Glasel[484] in the first volume of the comprehensive treatise on aqueous systems, edited by Franks. Relaxation work on liquid water can provide information on molecular reorientation processes and proton exchange. We begin with work concerned with reorientation dynamics. This type of information can be obtained from measurements on three nuclear species: ^{1}H, ^{2}H or ^{17}O, the last two either at natural abundance or after enrichment. The proton work has the advantage of high sensitivity; however, the separation of different contributions (inter- and intra-molecular DD, spin rotation) is

rather troublesome, and it can be more informative to study the quadrupolar ^2H or ^{17}O nuclei characterized by a relaxation mechanism that is both simple and directly related to molecular rotation. Hindman *et al.* reported spin–lattice relaxation rates for ^1H in H_2O,[485] for ^2H in D_2O[486] and for ^{17}O in enriched water.[487] The measurements extended over the temperature range from supercooled liquid to above boiling point. The logarithm of the relaxation rate was found to vary with inverse temperature in a non-linear fashion, i.e. the data did not follow the Arrhenius-type relation (47). The temperature dependence of the nuclear spin–lattice relaxation rates in water was also discussed by Melnichenko and Chizhik.[488] Yashkichev[489] proposed a mechanism for proton relaxation in water, based on a model of collective motions. Jonas and coworkers[490–492] studied proton and deuteron relaxation in water as a function of both temperature and pressure, up to several megapascals. The initial compression was found to result in higher motional freedom, leading to a maximum in the T_1 versus pressure curves. For D_2O Jonas and coworkers[490,491] combined ^2H T_1 data with measurements of viscosity in order to estimate the temperature and pressure dependence of the deuteron QCC.

Hindman[493] reported measurements of ^{17}O T_1 in water in n-heptane emulsions; in this way, it is possible to reach further down in temperature in the supercooled region. He also discussed the temperature dependence of the relaxation rate in terms of two kinetic processes. Lang and Lüdemann extended this approach to low-temperature measurements and reported data for protons,[494] deuterons[495] and ^{17}O.[496,497] The lower end of the variable temperature was extended to $-87^\circ C$ and the measurements were performed under variable pressure (up to 250 MPa) conditions. At sufficiently low temperature the motion of water molecules becomes so slow that the system is no longer in the extreme narrowing region. Assuming isotropic motion, they were able to estimate the correlation time at the minimum of the T_1 versus temperature curve, and consequently to derive the deuteron QCC of 214 kHz.[495] The assumption of isotropic reorientation was consistent with observed relaxation data for different nuclei. The temperature dependence of the rotational correlation times was fitted to equations of different forms. Outside the extreme narrowing region the spin–lattice relaxation times become frequency-dependent, which was recently demonstrated for ^1H, ^2H and ^{17}O relaxation in water by Lang and Lüdemann.[498] Lang *et al.*[499] also reported variable-temperature, -pressure and -frequency measurements of both T_1 and T_2 for deuterons in D_2O (see Fig. 6) and analysed the data using a model describing the orientational fluctuations of water molecules in terms of fast librational oscillations and a slower diffusional motion. The magnitude of the deuteron QCC was discussed and it was concluded that it could be considered approximately as

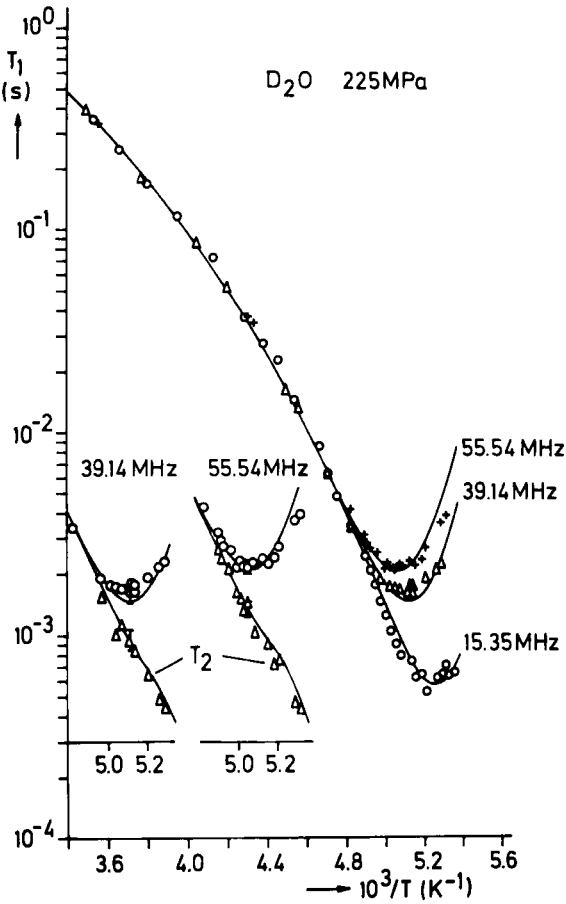


Fig. 6. Deuteron relaxation times in supercooled D_2O under 225 MPa pressure as a function of the inverse temperature at several resonance frequencies. (Reproduced with permission from E.W. Lang, H.-D. Lüdemann and L. Piculell, *J. Chem. Phys.*, 1989, **81**, 3820.) (Copyright © 1989 American Chemical Society.)

a temperature- and pressure-independent parameter. The deuteron QCC in liquid water was also discussed by Halle and Wennerström[133] and Cummins *et al.*,[500] who reported *ab initio* calculations for water clusters.

A different method for determining the rotational correlation time for water molecules, applicable in the extreme narrowing range, was mentioned by Lang and Lüdemann[497] and described fully by Lankhorst *et al.*[501] They proposed comparing the proton relaxation rates in enriched and natural-abundance samples. This provides the dipolar contribution to the proton

relaxation from ^{17}O. The OH distance is short, which makes this contribution predominantly intramolecular. It is also a well-known quantity, which provides the interaction strength and, as a consequence, the rotational correlation time. Van der Maarel *et al.* found the dynamic information from this method consistent with the isotropic reorientation of water molecules[502] and discussed the magnitudes of the QCCs. Mulder *et al.*[503] presented a general discussion of the strategies for possible experimental detection of picosecond time-scale motional anisotropy for water molecules and stressed the importance of the $^{1}H-^{17}O$ dipolar contribution. In an application of the strategy, however, no such anisotropy was found in pure water.[504] Another type of isotope effect was studied by Kakihana *et al.*,[505] who examined the dependence of deuteron relaxation time on the composition of the H_2O/D_2O mixture.

We now turn to work on proton exchange. While work on reorientation dynamics usually employs T_1 measurements, proton-exchange work is based on studies of T_2 or related data (an exception to this rule is the work of Latanowicz,[254] who measured the proton T_1 as a function of composition in an H_2O/D_2O mixture and related it to proton exchange). As first explained by Meiboom,[506] the relaxation mechanism involved is the scalar relaxation of the first kind (exchange-modulated coupling) and it influences proton and ^{17}O linewidth. Deuteron linewidth is affected to a lesser extent, as its coupling constant to ^{17}O is 6.5 times smaller. The ^{1}H linewidth work of Meiboom was recently extended to higher ^{17}O enrichments by Yeung and Lent.[507] Lamb *et al.*[508] measured the average residence time τ_e of a proton on a water molecule by ^{1}H $T_{1\rho}$ measurements at varying temperature and pressure, while Graf *et al.*[509] determined τ_e by measuring the proton T_1 at very low frequencies by means of the field-cycling technique. Turner[510] and Halle and Karlström[511] measured the ^{17}O linewidth and worked with both H_2O and D_2O.

Nuclear spin relaxation in simple electrolyte solutions has been reviewed by Hertz[512] and Holz.[513] Moreover, several articles of interest can be found in the two-volume treatise edited by Laszlo.[514] Therefore we cover the field rather briefly and limit this review strictly to work published during the nineteen eighties.

We begin with investigations involving measurements on the water nuclei and involving the problems discussed above for pure water. Lang and coworkers[515-519] studied deuteron relaxation in supercooled aqueous solutions of alkali-metal and magnesium halides. The measurements were carried out as functions of composition, temperature and pressure. Lang and Prielmeier[520] supplemented this work with similar measurements of proton relaxation. The anomalous increase of molecular mobility upon compression, observed in pure water, becomes less pronounced or reverts to

normal with increasing salt concentration. Van der Maarel *et al.*[521] studied water dynamics in solutions of alkali-cation and magnesium salts, using proton, deuteron and ^{17}O relaxation. The ions were found to introduce moderate changes in the deuteron QCC and in the OH distance. On the other hand, the correlation times changed significantly, and the rotational motion acquired a moderate anisotropy. The same group also studied the structure and dynamics of water in $AlCl_3$ solutions.[522] Nakamura *et al.*[523] studied water-proton relaxation (as well as translational diffusion) in concentrated $ZnCl_2$ solutions and found the translational motion to be more retarded than the rotational motion. Purcell and Pessen[524] studied water-proton spin–lattice relaxation in aqueous solutions of orthophosphoric acid as a function of the acid concentration. Hertz *et al.*[525] studied the effect of added salt on the proton exchange rates, determined from ^{17}O linewidths. Hertz and Maurer[526,527] reported proton, deuteron, ^{17}O and ^{35}Cl measurements for an aqueous solution of hydrochloric acid and determined, among other properties, the rate of intermolecular proton exchange.

Several papers concentrated on the structural and dynamic properties of the hydration shell. Madden and Impey[528] discussed experimental data on the dynamics of coordinated water and compared them with simulation results. Chizhik *et al.*[529,530] studied deuteron and quadrupolar ion relaxation in alkali-metal salts in neutral and alkaline water solutions and deduced water mobilities and hydration numbers. Struis *et al.*[531] studied relaxation rates of ^{2}H and ^{17}O in concentrated aqueous solutions of $MgCl_2$ and interpreted the results in terms of a two-phase model corresponding to water molecules in fast exchange between the $Mg(H_2O)_6^{2+}$ moieties and the bulk water. Helm *et al.*[532] reported a high-pressure ^{17}O lineshape NMR study of water exchange in tetraaquoplatinum(II). They were able to estimate from these measurements the ^{17}O quadrupolar relaxation rate in the complex as a function of temperature and pressure (this is the reason for including the paper in this review; chemical exchange studies based on line-broadening or lineshape measurements are as a rule not included here). Miura *et al.*[533] studied aqueous solutions of $Al(ClO_4)_3$ at low temperatures, a case where the water exchange between the hydration sphere of the cation and the bulk was so slow that two separate proton signals were obtained. They measured the proton spin–lattice relaxation rates for both signals and concluded that the coordinated water reoriented anisotropically, while the bulk-water molecules underwent isotropic reorientation.

Next we turn to the relaxation of nuclei residing in the ions and begin with cations. Monovalent cations of alkali metals have been studied in detail. Mazitov[534] studied quadrupolar relaxation of several alkali (and some alkaline earth) cations and halide anions. He related the relaxation rate to

ligand oscillations and the lifetimes of molecules in the hydration sphere. Several groups studied the lithium cation, which is interesting because the quadrupole moment of ^{7}Li is low and the DD mechanism can compete with the quadrupolar interaction. Weingärtner[535] studied aqueous solutions of LiI under variable-temperature conditions and separated the two mechanisms by varying the H_2O/D_2O ratio. Proton and deuteron relaxation was also studied. The three nuclei displayed maximal relaxation rates at the same temperature. Mazitov *et al.*[536] studied ^{7}Li relaxation for LiCl dissolved in water of different isotopic composition (H_2O, D_2O, $^{17}OD_2$) and were able to determine the orientation of the water-molecule dipole in the first hydration sphere. Tokuhiro[537] studied the non-exponentiality of ^{7}Li relaxation in highly concentrated LiCl solutions outside the extreme narrowing region. On the other hand, Holz and Sacco[538] studied the quadrupolar contribution to ^{7}Li spin–lattice relaxation in very dilute LiCl solution and found it to follow the $c^{1/2}$ law at low concentrations, which was interpreted in terms of the Debye–Hückel ion–ion distribution. Similar work on sodium salts using ^{23}Na relaxation was reported by Sacco *et al.*[539] ^{23}Na relaxation in NaOH solutions was studied by Kunze *et al.*[540] as a function of temperature and concentration. Hertz and Mazitov[541] studied quadrupolar relaxation of ^{87}Rb and ^{133}Cs (as well as ^{81}Br) in aqueous solutions of these heavier alkali-metal ions and were able to find the evidence for higher ion–ion correlations. Two papers have dealt with monovalent cations other than the alkali metals. Pfister *et al.*[542] studied the longitudinal and transverse relaxation of ^{109}Ag in aqueous solutions of silver nitrate. Longitudinal relaxation was found to be extremely slow, with the T_1 of the order of 600–1200 s and T_2 about 3–9 times shorter. It was concluded that longitudinal relaxation was probably dominated by the CSA mechanism modulated by exchange and reorientation. Perrin and Gipe[543] studied ^{15}N relaxation and NOE in the ammonium ion as functions of temperature and determined the rotational correlation times.

Divalent cations have not attracted as much attention. Helm and Hertz[544] measured the quadrupolar relaxation rates of ^{25}Mg, ^{43}Ca, ^{87}Sr and ^{137}Ba in aqueous solutions of bromides and perchlorates of the alkaline-earth cations as functions of concentration. The results were interpreted using electrostatic theories. Köhnlein *et al.*[545] reported ^{67}Zn ($I = \frac{5}{2}$) relaxation-time measurements in aqueous solutions of zinc nitrate and sulphate. Hays *et al.*[546] studied the field dependence of ^{207}Pb ($I = \frac{1}{2}$) relaxation in aqueous solution and found no evidence of the CSA mechanism. In contrast, the CSA mechanism was found to be dominant for ^{195}Pt relaxation in the square planar $Pt(H_2O)_4^{2+}$ complex, studied by Gröning *et al.*[547] Interest has been greater in trivalent ions. Kodweiss *et al.*[548] studied linewidths and spin–lattice relaxation of quadrupolar nuclei ^{27}Al, ^{69}Ga, ^{71}Ga and ^{115}In in

aqueous salt solutions. The relaxation of the four nuclides was found to vary in a similar way upon changing concentration and temperature. ^{69}Ga and ^{71}Ga relaxation in aqueous salt solution was also studied by Tarasov *et al.*[549] Takahashi[550] studied ^{27}Al spin–lattice relaxation as a function of HCl concentration in aqueous solutions of aluminium chloride. Akitt and coworkers[551,552] studied the linewidth of ^{27}Al in solutions containing highly symmetric slowly relaxing $Al(H_2O)_6^{3+}$ species and species of lower symmetry. The measurements were carried out as functions of pH, concentration or temperature, which justifies the inclusion of this work here—papers referring to isolated linewidth measurements on common quadrupolar nuclei will in general not be covered in this review. In another paper by Akitt *et al.*[553] ^{27}Al linewidths in sodium aluminate solutions were correlated with solution viscosity. Relaxation of the magnetic nuclei of Group IIIb cations (^{45}Sc, $I=\frac{7}{2}$, ^{89}Y, $I=\frac{1}{2}$, ^{138}La, $I=5$, ^{139}La, $I=\frac{7}{2}$) in aqueous salt solutions was studied by Lutz and Oehler,[554] Schwenk[555] and Haid *et al.*[556] Finally, Navon[557] studied spin–lattice relaxation of ^{59}Co in the $Co(H_2O)_6^{3+}$ complex. No evidence of a paramagnetic high-spin species was found. The relaxation rate was found to increase at higher temperatures, which was associated with increased formation of lower-symmetry species.

We now turn to work on relaxation of nuclei residing in anions. As the chemistry of anions is different from that of cations, we shall discuss anions according to the number of atoms in them, rather than the total charge. Thus we begin with the halide anions. Among those, F^- has a special position, since the only naturally occurring fluorine isotope (^{19}F) is a spin-$\frac{1}{2}$ nucleus. ^{19}F dipolar relaxation due to the solvent nuclei in water of different isotopic composition was studied by Müller and Hertz.[558] They concluded that the water arrangement in the hydration sphere of F^- was symmetric with respect to the FO radial direction, which is contrary to the prevalent notion of the hydrogen-bonded structure.[559] From the point of view of nuclear spin relaxation, heavier halide anions are similar to the alkali-metal cations, i.e. they are relaxed by transient quadrupolar interaction (see Section 2.5). Earlier work on chlorine, bromine and iodine relaxation was reviewed by Lindman and Forsén.[203,514] Among more recent work on simple electrolytes, we mention the paper by Yudasaka *et al.*[560] on potassium chloride (as well as tetraethylammonium chloride) and the work of Soffer and Marcus[561] on ^{81}Br relaxation in concentrated hydrobromic acid solutions.

Some papers have dealt with diatomic and triatomic anions in aqueous solution. Wasylishen *et al.*[562] studied ^{14}N and ^{13}C relaxation in the cyanide ion. The ^{14}N data provided an estimate of the rotational correlation time. The ^{13}C T_1 were found to be field-independent and to decrease upon increasing temperature, which is consistent with the SR mechanism. De

Nicholas and Wasylishen[563] studied ^{14}N relaxation in triatomic anions, $SeCN^-$, SCN^-, OCN^-, and N_3^-. The latter species was also studied by Loewenstein.[564]

Oxo-anions have attracted the attention of many investigators. De Nicholas and Wasylishen[565] studied the rotational correlation times of nitrate and carbonate ions in dilute solutions. The ^{14}N data were used to derive the reorientation of the C_3 axis, while ^{17}O relaxations provided information on the in-plane motion. Using the same methodology, the same authors also studied the effects of a variety of cations on the rotational motion of nitrate anions.[566] Adachi *et al.*[567] combined ^{14}N and ^{17}O NMR relaxation data for the nitrate anion with Raman lineshape analysis. McCain[568] studied ^{13}C relaxation in carbonate and squarate ($C_4O_4^{2-}$) ions as a function of temperature and magnetic field. The rotational correlation times were estimated from the CSA relaxation rate.

Masuda and coworkers[569-571] studied rotational motion of tetrahedral oxo-anions (perchlorate, sulphate, phosphate) by means of ^{17}O spin–lattice relaxation measurements at variable concentration.The field gradients at the site of the oxygen nucleus were calculated by *ab initio* quantum-chemical methods. Nakahara and Ibuki[572,573] interpreted NMR data on the rotational motion of the tetrahedral oxo and nitrate anions within the framework of dielectric friction theory. Several groups studied the relaxation of the central atom nucleus in the same anions. Miller *et al.*[574] reported the ^{35}Cl relaxation rate in the perchlorate anion as a function of temperature and NaOH concentration. James and Cutler[575] studied ^{17}O and ^{35}Cl (and in some cases ^{25}Mg) linewidths in solutions of alkaline-earth perchlorates and interpreted the results in terms of ion–ion solvent interactions. Quadrupolar relaxation for ^{33}S in inorganic sulphates was studied by Hinton and Shungu,[576] who reported spin–lattice relaxation measurements as a function of temperature and concentration and by Belton *et al.*,[577] who investigated the effects of counterion binding, pH and viscosity on T_1 and T_2. McCain and Markley[578] studied the mechanism of the spin–lattice relaxation of ^{31}P ($I=\frac{1}{2}$) in orthophosphate solution. In rigorously purified samples, the spin–lattice relaxation rate was nearly independent of concentration or pH. The dipole–dipole and CSA contributions were identified; moreover, an additional contribution with the efficiency increasing with increasing temperature was observed. Hinton and Buster[579] studied the ^{33}S spin–lattice relaxation of the only observable sulphur resonance in the thiosulphate anion $S_2O_3^{2-}$.

Silicate solutions contain mixtures of various anionic species, which have been subject to several studies using ^{29}Si relaxation. Wang *et al.*[580] studied the concentration dependence of ^{29}Si spin–lattice relaxation in sodium silicate solution. Kinrade and Swaddle[581,582] studied exchange dynamics

and mechanisms for spin–lattice relaxation in alkali-metal silicates. They identified the DD interaction between ^{29}Si and alkali-metal nuclei as an important relaxation mechanism. For larger cage-like silicate anions Knight and Harris[583] found that DD relaxation with protons was of primary importance. Finally, Balz *et al.*[584] studied the relaxation of two quadrupolar boron nuclei, ^{10}B and ^{11}B, in dilute solutions of boric acid and borates.

5.3. Main-group metal compounds and complexes in solution

This section is organized according to the main group of the periodic table to which the metals belong. As an introduction and general reference to the area, we mention Laszlo's book[514] and some recent reviews. The NMR of the main group metal nuclides was reviewed by Dechter.[585] The topic of ion–molecule interactions was reviewed by Detellier and Laszlo.[586] The field of NMR of less common quadrupolar nuclei was reviewed by Drakenberg.[587]

We begin this section by discussing papers dealing with the measurement of relaxation rates of alkali-metal cations in simple electrolytes dissolved in non-aqueous solvents or solvent mixtures. Weingärtner and Hertz[588] studied the relaxation of quadrupolar nuclei of alkali-metal and halide ions in solutions of simple 1 : 1 salts in several polar organic solvents. The concentration-dependent data were interpreted using Hertz' electrostatic theory (see Section 2.5). Uchibayashi *et al.*[589] studied spin–lattice relaxation of ^{7}Li in concentrated $LiNO_3$ solutions in liquid ammonia. The data were correlated with solution viscosities. Birkel and Hertz[590] studied the relaxation of ^{19}F in solutions of RbF in methanol and formamide with a varying extent of deuteration. The results allowed the determination of the orientation of the solvent molecules around the fluoride ion. Hofmann and Holz[591] studied the relaxation of ^{23}Na, ^{87}Rb and ^{35}Cl in simple electrolyte solutions in various solvents, in the presence of a direct electric field and thus electric current. In some non-aqueous systems the relaxation rate changed in the presence of the electric field. Weingärtner[592,593] used quadrupolar ion relaxation measurements in order to study ion-pair formation and related ion–ion interactions in simple 1 : 1 salt solutions in non-aqueous solvents. Similar studies were reported by Detellier and Gerstmans[594] and by Mishustin and coworkers.[595,596] Mishustin and Podkovyrin[597,598] also studied the solvation dynamics, using temperature-dependent ^{7}Li relaxation experiments in organic solutions of $LiClO_4$ and Monte Carlo simulations.

Some authors investigated the effect of added salt on the nuclear spin

relaxation and molecular dynamics in simple organic liquids. Ansari and Hertz[599] investigated the modification of reorientational correlation times in various isotopic species of ethanol caused by adding alkali halides. The results were discussed in relation to current theories for internal motion (see Section 2.4). A later paper by the same authors[600] also discussed the effect of adding water to the ethanolic LiCl solutions. Lambert and Vlasak Simpson[601] studied the effect of added lithium chloride on the proton and carbon relaxation in acetic acid, ethanol and their fluorinated analogues. Finally, Saint Germain and Vincendon[602] studied proton, ^{13}C and ^{7}Li relaxation in a *N,N*-dimethylacetamide solution of LiCl, with the purpose of elucidating the unusual solvent properties of the system.

We now turn to papers dealing with relaxation studies of simple electrolytes in solvent mixtures (work on solvent mixtures without electrolyte will be deferred to Part 2 of this review). The chemical phenomena occurring in mixed solvents, as opposed to pure ones, are preferential solvation and reduction of the symmetry of the solvation shell. We begin with mixtures containing water as one of the components. Braun and Holz[603,604] studied ^{23}Na and ^{87}Rb relaxation in mixtures of water and acetonitrile. Starting from pure acetonitrile, quadrupolar relaxation rates were demonstrated to increase rapidly upon adding a small amount of water, indicating a disturbance of the symmetry of the solvation shell. The symmetry quenching could also be confirmed by comparing variable temperature relaxation measurements for the ion nuclei with the relaxation rates for the ^{14}N in acetonitrile. Huang *et al.*[605] studied ^{23}Na relaxation in solutions of $NaClO_4$ in water–acetone, water–acetonitrile and water–ethanol mixtures (and organic-soluble sodium salts in organic mixed solvents). Some time ago Holz[606] proposed a method for studying the preferential solvation by measuring the H_2O/D_2O isotope effect on the quadrupolar relaxation rates of alkali-halide nuclei. In binary solvent mixtures the isotope effect was found to be composition-dependent. Holz and coworkers applied the method to studies of preferential solvation of Na^+ in mixtures of water with small amides[607] and with strongly solvating hexamethylphosphoric triamide (HMPA).[608] The latter paper also reported relaxation rates for the quadrupolar nuclei in the solvent molecules. Finter and Hertz[609,610] measured proton relaxation rates in selectively deuterated species of formamide in the presence of Na^+ and I^- ions and derived from the measurements the structural information on the solvation shell. Corresponding measurements were also performed in water–formamide solvent mixtures, in order to study preferential solvation. Merbolt and Frahm[611] studied water-proton relaxation in aqueous solutions of deuterated organic solvents in the presence of added nitrates of Na^+, Be^{2+} and Al^{3+}. Yudasaka *et al.*[612] investigated the line broadening of the ^{35}Cl resonance of

KCl in aqueous solutions of non-electrolytes. Farrar and coworkers[90,613,614] studied PHO_3^{2-} and PFO_3^{2-} anions in mixtures of water and ethylene glycol. They investigated longitudinal relaxation, differential line broadening and $T_{1\rho}$ in the coupled heteronuclear systems of two spin-$\frac{1}{2}$ nuclei (PH, PF). Interference effects between the DD and CSA interactions were clearly demonstrated in viscous solutions outside the extreme narrowing range.

Delville, Chalais and coworkers[615,616] studied solutions of sodium salts in binary solvent mixtures of tetrahydrofuran with amines. The variation of the ^{23}Na linewidth with the composition of the solvent mixture was analysed in terms of successive ligand replacements in discrete solvates. Mishustin and coworkers[617-625] studied ^{7}Li (and in some cases ^{23}Na) relaxation in salt solutions in a large number of non-aqueous binary solvent mixtures. The data were interpreted in terms of the thermodynamics of solvation.

We now turn to other alkali-metal-containing systems and begin with lithium compounds. Mazitov *et al.*[626] studied ^{7}Li relaxation in systems containing lithium formate, another (zinc, cadmium, caesium, ammonium) formate and water. Grace and Krane[627] studied ^{7}Li and ^{13}C relaxation in aqueous solutions of noradrenaline and lithium chloride, attempting (unsuccessfully) to detect complex formation.

Complexation of lithium was detected by Olsher *et al.*[628] in solutions containing polydentate amido ethers, using, among others, ^{7}Li T_1 data. van Lier *et al.*[629] investigated interactions between lithium salts and organic phosphates by means of multinuclear NMR measurements, including ^{7}Li, ^{35}Cl and ^{81}Br linewidth studies. Nöth *et al.*[630] investigated the dependence of ^{7}Li (and ^{27}Al) linewidth in $LiAlH_4$ in ethers on solvent, concentration and temperature. Organic lithium compounds have been subject to numerous NMR studies, some of which also employed relaxation studies. Some time ago, Jackman and Trewella[631] proposed an isotope-substitution technique, employing the difference between the magnetic moments of ^{1}H and ^{2}H. A comparison of ^{13}C relaxation times in the species containing both isotopes allows the determination of CH distances. Jackman and Scarmoutzos[632] used a similar technique to study the structure of phenyllithium in solution, but employed the $^{7}Li/^{6}Li$ substitution. The structure in a mixed (hydrocarbon–ether) solvent was found to be tetrameric, with the same geometry as in the solid state. Jackman and coworkers also studied aggregation phenomena in lithium phenolates[633,634] and other organolithium systems.[635,636] In all these papers the authors estimated the lithium QCC by the technique often known as the "dual spin-probe method". The method makes use of ^{13}C spin–lattice relaxation measurements for proton-bearing carbons in order to derive an effective rotational correlation time

for the molecule under consideration. This rotational correlation time and the measured relaxation rate for a quadrupolar nucleus (here ^{7}Li) are then used to evaluate the QCC by means of (17). Similar work on the lithium enolate of acetaldehyde was also reported by Jing Quan Wen and Grutzner.[637] Work dealing with lithium (and other alkali cations) in systems containing crown ethers and related macrocylic compounds will be discussed below.

Sodium salts of simple organic sulphonic acids in aqueous solution have been studied by two groups. Koda and Nomura[638] found that ^{23}Na spin–lattice relaxation data showed no indication of specific ion–ion interactions. On the other hand, proton relaxation times for methylsulphate protons indicated anion–water interactions. Uedaira and Uedaira[639] studied ^{23}Na and water-deuteron relaxation and the effect of various anions on the water rotational correlation times. Two other papers also concentrated on organic anions. Baltzer and Becker[640] studied the solvation of organic oxyanions (*p*-nitrophenolate, benzoate) and corresponding methyl esters in several solvents by means of ^{17}O linewidth measurements. The relaxation rate in the neutral species varied linearly with viscosity, whereas anions showed a more complicated behaviour. Pascal *et al.*[641] studied ^{13}C spin–lattice relaxation, with and without proton decoupling, in concentrated methanolic solutions of lithium and sodium methanolates. The relaxation was non-exponential, which was ascribed to the interference between cross-correlation effects and chemical exchange.

The sodium salt of tetraethylaluminate (TEA) has been studied by multinuclear NMR methods by two groups. Gray and Maciel[642] studied NaTEA in mixtures of a polar solvent (tetrahydrofuran or pyridine) and *m*-xylene. The dependence of the ^{23}Na linewidth (in combination with other parameters) on the solution composition provided information on the ion-pairing and aggregation. Medley *et al.*[643] studied NaTEA in mixtures of benzene and HMPA.

Lerner and Torchia[644] analysed non-Lorentzian ^{23}Na lineshapes in two model systems. Analysis of the field and temperature dependences of T_1 and T_2 in aqueous solution of sodium laurate indicated that relaxation of the main species was in the extreme narrowing region (contrary to the findings of Marshall *et al.*[63]), and the non-Lorentzian lineshape resulted from exchange. The other model system, sodium chloride in glycerol, however, was found to consist of a single population of ions outside of the extreme narrowing region. A different application of ^{23}Na spin–lattice relaxation in the context of medium-sized molecules was reported by Amat *et al.*,[645] who used the relaxation rates to derive the rate of chemical exchange between a monensin (polyether) complexed site and a methanol-solvated site. The effects of the pH and water content were also investigated. Complexes

between the sodium cation and acyclic polyethers were studied by Grandjean *et al.*,[646] who reported ^{23}Na linewidths and proton spin–lattice relaxation times.

We now turn to work on alkali-ion complexes with crown ethers and related macrocyclic ligands. Several authors studied complexation kinetics in systems of this type using ^{23}Na NMR. The temperature dependence of ^{23}Na linewidth was applied for this purpose by Strasser and Popov[647] and Phillips *et al.*[648] Stöver, Delville and coworkers[649–651] studied spin–lattice and spin–spin relaxation rates for ^{23}Na in the sodium cation complexed by large crown ethers. For dibenzo-24-crown-8 complexes[649,650] the T_1 results were found to be field-independent, while T_2 changed with magnetic field. The exchange contribution to the spin–spin relaxation rates could be separated. For the even larger dibenzo-30-crown-10 complex the linewidth (T_2) at low field was found to agree with the T_1 measurement at a higher field, which excluded exchange broadening. The variation of the ^{23}Na linewidth with solution composition could be interpreted in terms of equilibria between different complexes.[651] The same group[652] also reported similar work, using ^{39}K relaxation, for the complexes of the same crown ether with potassium thiocyanate. Amat *et al.*[653] used changes in ^{23}Na T_1 upon complexation for evaluating the kinetics of the complexation reactions. They employed the approach developed by Strehlow and Frahm[654] and Lambert and Keepers,[655] based on the fact that the apparent spin–lattice relaxation rates for two exchanging sites are dependent on both the "real" relaxation rates and the exchange lifetimes. Rubidium complexes with 18-crown-6 and cryptand-222 were studied by Khazaeli *et al.*,[656] who reported some solvent- and concentration-dependent ^{87}Rb linewidths.

Holton, Ellaboudy and coworkers[657–659] recently reported a study of ^{23}Na relaxation in the sodide anion (Na^-), occurring along with Na^+–crown ether complexes upon dissolving sodium metal (or sodium alloys with other alkali metals) in a neat crown ether. The quadrupolar-dominated ^{23}Na spin–lattice relaxation was found to be inefficient, essentially independent of the counterion and dependent only weakly on the sodide concentration. A very low r.m.s. value of the QCC was estimated, in agreement with only minor perturbation of the gas-like electronic structure. Edwards *et al.*[660] compared the ^{23}Na linewidth in the sodide solution with the linewidths of ^{39}K and ^{87}Rb in the corresponding potasside and rubidide solutions. The increase of linewidth with atomic number is interpreted in terms of increasing solution perturbation of the electronic structure. NMR studies of alkali anions were recently reviewed by Edwards *et al.*[660]

Several authors have studied the effects of cation–macrocycle complexation on the relaxation rates of nuclei residing in the macrocyclic ligand,

with the purpose of obtaining information on the reorientation dynamics and intermolecular interactions. Popov *et al.*[661] used ^{17}O linewidths for this purpose and, in some cases, ^{13}C spin–lattice relaxation rates. They found that complexation rigidifies the structure of the flexible ligand, if the size of a cation fits the cavity size. This increases the effective correlation times and the relaxation rates. On the other hand, complexation of a cation by a crown ether with too large a cavity was found to shorten the effective correlation times by creating additional possible conformational processes. Schmidt *et al.*[662] studied ^{13}C relaxation in Na^+ and K^+ complexes of cryptand-221 in interacting and non-interacting solvents. The two types of solvent were found to have different effects on the relative behaviour of the relaxation rates in the series free-ligand–Na^+ complex–K^+ complex. Alkali and alkaline-earth cryptand complexes were also studied by ^{13}C T_1 measurements by Durst, Echegoyen and coworkers.[663,664] The relaxation rates were found to decrease upon binding an alkali cation (especially for Li^+), and to increase upon binding calcium or barium cations. Echegoyen, Kaifer and coworkers[665,666] also investigated ^{13}C relaxation in macrocycles with one oxygen atom replaced by an alkylated nitrogen or with a side chain containing ether oxygens. Buchanan *et al.*[667] reported ^{13}C spin–lattice relaxation measurements for sodium and potassium cation complexes with *cis*-cyclohexyl-15-crown-5. Erk[668] studied the temperature dependence of ^{13}C spin–lattice relaxation in 12-crown-4 and its complexes with Li^+, Ca^{2+} and Mg^{2+}. The present reviewer finds the interpretation of the data inconclusive.

Several groups combined measurements of the quadrupolar relaxation rate for the cation nucleus with ^{13}C T_1 studies and used the data to derive the QCC for the cations (the dual spin-probe technique mentioned above in connection with ^7Li compounds). Bisnaire *et al.*[669] reported such work for the Na^+–dibenzo-24-crown-8 complex, while Saito and Tabeta[670] studied sodium complexes with several ionophores. Neurohr *et al.*[671] studied complexes of potassium with various ionophores; combined ^{13}C and ^{39}K measurements were also reported by Detellier and Robillard[672] for the complex between K^+ and dibenzo-30-crown-10. Eliasson *et al.*[673] studied ^{13}C, ^{17}O and metal relaxation in complexes of Li^+, Na^+ and K^+ with 12-crown-4, 15-crown-5 and 18-crown-6. Comparison of ^{13}C and ^{17}O data indicates that complex formation reduces the internal mobility of the crown ethers. QCCs for the alkali cations derived by means of the dual spin-probe method were also compared with *ab initio* calculations for model compounds.

A different type of application of relaxation measurements to crown-ether–alkali-cation systems was presented by Sugawara *et al.*[674] They studied the ^{35}Cl linewidth for the chloride counterion to the K^+–18-crown-

6 complex as a function of KCl concentration in water and some organic solvents. The data in aqueous solution were interpreted in terms of ion-pair formation, while the results in acetonitrile solution were found to be consistent with the presence of a "naked" anion.

Among alkaline earths, ^{25}Mg and ^{43}Ca NMR have attracted the most attention, not least because of the biological importance of Mg^{2+} and Ca^{2+} ions. NMR of these two nuclides was reviewed by Neurohr *et al.* in Vol. 2 of Laszlo's book.[514] The number of papers to be reviewed here is rather limited.

We begin here with simple salt solutions in non-aqueous and mixed solvents. James and Cutler[675] studied ^{17}O, ^{25}Mg and ^{35}Cl linewidths in acetone solutions of $Mg(ClO_4)_2$ and $Sr(ClO_4)_2$ as functions of concentration and estimated solvation numbers. Echegoyen *et al.*[676] investigated perchlorates of magnesium, calcium and barium in HMPA solution by measuring ^{35}Cl linewidth. The calcium-salt solution deviated from the other ones by the exceptionally large linewidth, indicating strong ionic association.

Frahm and Merboldt[611,677,678] studied water-proton relaxation in solutions of beryllium nitrate in binary mixtures of water with organic solvents. The kinetics of proton exchange was studied as a function of temperature, solvent composition and beryllium concentration by means of proton T_2 (spin-echo) experiments.[677] The two other papers[611,678] described T_1 and T_2 measurements as functions of mixture composition, temperature and magnetic field. The dependence of the measured spin–lattice relaxation rate on the mole fraction of water in the solvent mixture was enhanced by adding the electrolyte. At low temperatures the T_1 became field-dependent and featured a characteristic minimum as a function of temperature (cf. Fig. 6 above). The molecular dynamics was described using distributions of correlation times, the mean value of which was sensitive to the mole fraction of electrolyte.

Kowalewski and Maliniak[679] studied metal-nucleus and ^{13}C relaxation in magnesium and calcium acetylacetonates and estimated the QCC values and the field gradients at the metal site. Comparisons were made with earlier work by Wehrli[680] on beryllium acetylacetonate and conclusions were drawn on the symmetry distortions in the series of compounds. Koehler *et al.*[681] studied ^{25}Mg relaxation in complexes with mono- and dicarboxylic acid ligands. They analysed the concentration dependence of the relaxation rates and estimated apparent QCCs for various complexes present in aqueous solution. Drakenberg[682] studied ^{43}Ca spin–lattice relaxation in some small calcium complexes with polydentate ligands in aqueous solution. By deriving the correlation times from ^{13}C relaxation rates, he also estimated the QCC values for calcium. Huet and Gaudemer[683] studied ^{13}C

relaxation in magnesium–porphyrin complexes. Some of the ^{13}C relaxation work on alkali-cation–crown-ether (or cryptand) complexes also included data for alkaline-earth compounds.[664,666,668]

Group IIIa of the periodic table contains several nuclear species of interest for NMR spectroscopists. For recent reviews we refer to the book edited by Laszlo,[514] and to the papers by Siedle[684] on ^{11}B (for the purpose of this review, we consider boron to be a metal and include it here), by Akitt[685] on multinuclear studies of aluminium compounds and by Hinton *et al.*[686] on thallium NMR.

Several papers have dealt with aluminium halide solutions in non-aqueous solvents and solvent mixtures. Koch *et al.*[687] studied solvation of Al^{3+} in methanol. At low temperature the ligand exchange between the solvation sphere and the bulk was found to be slow and two separate methyl signals were obtained. The measured spin–lattice relaxation rates for the two signals were influenced by the exchange (the coalescence of relaxation rates[655]). Merboldt and Frahm[611] studied water-proton T_1 and T_2 in the solvent system water–HMPA in the presence of aluminium nitrate. ^{27}Al linewidths were measured by Akitt and Lelievre[688] in $AlCl_3$ and $Al(ClO_4)_3$ solutions in alcohols and alcohol/chloroform mixtures, by Wehrli and Wehrli[689] for aluminium halide solutions in acetonitrile and in acetonitrile–water, and by Sloan *et al.*[690] for aluminium perchlorate in dimethylformamide–dimethylsulphoxide mixtures. The linewidth was related to the symmetry of the solvates. Garrison and Crumbliss[691] studied the linewidth of the ^{27}Al signal in mixed acetone–water–perchloric acid solutions. The linewidth was found to vary linearly with the correlation time (estimated from viscosity by the Gierer–Wirtz[102] relation), indicating that acetone does not enter the first solvation sphere of the ion. The aluminium QCC for the hexaaquo complex was determined.

Several groups studied anionic halide complexes of the Group IIIa metals. Tarasov *et al.*[692] reported measurements of T_1 and T_2 for ^{27}Al, ^{69}Ga, ^{71}Ga and ^{14}N in the anions $MCl_nBr_{4-n}^-$ and the solvate complexes with acetonitrile. Evidence was found for scalar relaxation of the second kind being operative. McGarvey *et al.*[693,694] and Colton *et al.*[695] studied the metal-nucleus linewidth in gallium and indium tetrahalometallates.

Dechter *et al.*[696] studied metal-nucleus QCC in aluminium, gallium and indium acetylacetonates, using the dual spin-probe technique. Trends in the QCC as a function of the central atom in the series were discussed. The unusually low linewidth of the ^{27}Al signal in tris bidentate complexes was also discussed by Akitt.[697] Thompson *et al.*[698] investigated aluminium(III) hydrolysis products by combining the solution relaxation-rate measurements for ^{27}Al and ^{17}O with solid-state determinations of the QCCs.

Group IIIa metals form numerous hydrides and organometallic com-

pounds. Gibb and Kennedy[699] studied ^{1}H and ^{11}B longitudinal relaxation rates in decaborane $B_{10}H_{14}$ as a function of temperature. Privalov *et al.*[700] reported ^{1}H and ^{11}B relaxation times measurements for the anionic species $B_6H_7^-$. Solutions of tetrahydridoaluminates were studied by ^{27}Al (as well as ^{1}H and ^{2}H measurements) by Nöth *et al.*[630] and Tarasov *et al.*[701] Vestin *et al.*[702] studied ^{27}Al linewidths and ^{13}C spin–lattice relaxation in triethylaluminium in toluene solution over an extended temperature interval. The effective correlation times at different positions were determined and used for qualitative discussion of internal motions. Two groups studied the tetraethylaluminate systems. The multinuclear studies of Gray and Maciel[642] have already been mentioned in connection with ^{23}Na work. Day *et al.*[703] proposed using ^{27}Al relaxation in the $NaAlEt_4$–benzene–donor system to determine solvent donicity towards sodium. The approach was also applied to the case of HMPA as donor.[704]

Some papers have dealt with ^{205}Tl ($I = \frac{1}{2}$) relaxation in dialkylthallium compounds. Brady *et al.*[705] demonstrated that ^{205}Tl spin–lattice relaxation in high magnetic fields was dominated by the CSA mechanism. They also showed that measurement of the lineshape of protons coupled to ^{205}Tl offered an easy method to monitor changes in ^{205}Tl relaxation. Forster and coworkers[706,707] studied ^{205}Tl spin–lattice relaxation in the dimethylthallium(III) cation as a function of temperature and magnetic field. The CSA mechanism dominated in aqueous solution,[706] but the contribution from the SR interaction could also be quantified. The interaction strength constants and the activation energies for $\tau_\perp$ and τ_J were determined. In a viscous solvent[707] (water–glycerol mixture) CSA relaxation was the only efficient mechanism. At sufficiently high field and low temperature the region outside the extreme narrowing region was reached, which could be seen in the temperature dependence of the spin–lattice and spin–spin relaxation rates and their ratio. Finally, ^{205}Tl linewidths (and some T_1 values) were reported for complexes of thallium salts with an ionophoric antibiotic.[708]

We turn next to the systems containing heavier elements of Group IV—work on silicon compounds not containing carbon has already been reviewed in Sections 5.1 and 5.2. The review of relaxation studies for silicon–organic systems is deferred to Part 2 of this review.

General aspects of ^{73}Ge NMR were discussed by Wilkins *et al.*[709] ^{73}Ge is a quadrupolar nucleus ($I = \frac{9}{2}$) with a low magnetogyric ratio and moderate natural abundance, making NMR work rather difficult. Wilkins *et al.*[709] list the T_1 and T_2 values for a variety of germanium compounds, and discuss the dominant quadrupolar mechanism, the QCCs and the correlation times. A group of germanium compounds that have attracted some attention (and some controversy) are tetrahalogermanes. Tarasov *et al.*[710] studied ^{73}Ge

relaxation in neat $GeCl_4$ and $GeBr_4$ and their mixture, in which resonances of lower-symmetry compounds can be seen. The germanium spin–lattice relaxation in $GeCl_4$ was found to display a temperature dependence characteristic of two competing mechanisms, quadrupolar and spin–rotation. Harazono *et al.*[711,712] studied ^{73}Ge T_1 and T_2 in GeH_4 and symmetric tetrahalogermanes GeX_4 in benzene and CS_2 solutions. For X = Cl and Br spin–lattice relaxation was found to be dominated by the quadrupolar interaction, while scalar relaxation of the second kind contributed significantly to T_2. For X = I, $T_1 = T_2$ was obtained, in agreement with quadrupolar dominance in both rates. Sekacis *et al.*[713] and Takeuchi *et al.*[714] studied ^{73}Ge spin–lattice relaxation times in organogermanium compounds.

NMR spectroscopy of ^{119}Sn was reviewed by Wrackmayer.[715] Blunden *et al.*[716] measured ^{119}Sn ($I = \frac{1}{2}$) spin–lattice relaxation times and tin–proton NOEs in some organotin compounds. The SR and DD mechanisms compete, with the latter dominating for larger molecules. Birchall and Manivannan[717] studied tin spin–lattice relaxation in dialkyltin cations in highly acidic solutions. The spin–lattice relaxation rate at high magnetic field was found to be dominated by the CSA mechanism. A comparison of T_1 and T_2 indicated the presence of a rapid exchange process. Axelson *et al.*[718] reported measurements of ^{13}C spin–lattice relaxation times in sterically crowded organotin derivatives and discussed internal mobilities of various groups bonded to tin. Daragan *et al.*[719] studied ^{13}C and ^{1}H relaxation in neat tetramethyllead in an extended temperature interval. The carbon measurements were performed with and without proton decoupling and the molecular dynamics was discussed.

Work on relaxation in inorganic compounds of nitrogen and phosphorus (other than aqueous solutions of simple electrolytes) will be discussed in Section 5.5. Concerning compounds of heavier Group Va elements, we have been able to trace just one paper on nuclear relaxation published during the nineteen eighties: Morgan *et al.*[720] reported ^{209}Bi ($I = \frac{9}{2}$) and ^{19}F relaxation data for hexafluorobismuthate(V) ion BiF_6^-. The relaxation was presumably dominated by the quadrupolar interaction, but the linewidth was only moderate because of the high symmetry of the bismuth site.

We turn now to compounds containing heavier Group VI elements, selenium and tellurium. Pappalardo[721] reported ^{13}C T_1 data for dipirydyl dichalcogenides Py_2X_2, X = S, Se, Te. Three papers have dealt with ^{77}Se ($I = \frac{1}{2}$) relaxation. Jakobsen *et al.*[722] studied ^{77}Se spin–lattice relaxation in H_2Se in deuterochloroform solution and found it to be dominated by the spin–rotation mechanism. Abel *et al.*[723] studied ^{1}H and ^{77}Se spin–lattice relaxation times in a series of organochalcogen compounds. The proton relaxation rates were found to be due primarily to the DD interaction, while

the selenium nucleus relaxed by a mixture of the CSA and SR mechanisms. Wong *et al.*[724] reported ^{77}Se T_1 results in selenoketones and diphenyldiselenide as a function of temperature at three magnetic fields. The CSA mechanism was found very significant at high field. Tellurium compounds also attracted some attention. Granger and Chapelle[725,726] studied ^{125}Te and ^{123}Te (both $I=\frac{1}{2}$) relaxation times T_1 and T_2 in dimethyltelluride as functions of temperature and magnetic field. Proton and ^{13}C relaxation rates were also reported. Tellurium relaxation was found to be governed by the SR mechanism, while both SR and DD contributed to the relaxation of the light nuclei. Granger *et al.*[727] also reported ^{125}Te T_1 values for diaryltellurides.

5.4. Transition-metal compounds and complexes in solution

In analogy with Section 5.3, this section is also organized according to the periodic system. As general references to the NMR of transition-metal nuclei, we mention the book edited by Laszlo[514] and the reviews by Dechter[728] and Drakenberg.[587]

Many of the magnetic nuclei of transition metals belong to the category "less common" and literature on their NMR data is scarce. Therefore we choose here to be somewhat more liberal in reviewing papers reporting only isolated linewidth data. We begin with systems containing elements of Group Ib (Cu, Ag, Au). NMR work on paramagnetic copper(II) complexes is fairly common; in contrast, only few papers concerned with nuclear spin relaxation in diamagnetic Group Ib element compounds have appeared during the nineteen eighties. Tetrahedrally coordinated copper(I) complexes have been studied by means of ^{63}Cu ($I=\frac{3}{2}$) NMR by three groups. Ochsenbein and Schläpfer[729] studied the ^{63}Cu linewidth in tetrapyridine and tetraacetonitrile solvates as a function of temperature, counterion and the solvent mixture composition. Kroneck *et al.*[730] reported copper linewidths in phosphine and phosphite complexes and related them to the metal π-acceptor properties of the ligands. Phosphite complexes were also studied by Marker and Gunter,[731] who combined ^{63}Cu and ^{31}P linewidth studies. The signals of both nuclei were split owing to scalar coupling, with the components broadened owing to copper relaxation and exchange. Kronenbitter *et al.*[732] studied the extremely long relaxation times T_1 and T_2 for ^{109}Ag in the silver ion solvated in water–ethylamine mixtures. Jans-Bürli and Pregosin[733] studied ^{31}P spin–lattice relaxation in gold(I) (and iridium(I)) complexes of arylphosphines. Phosphorus relaxation mechanisms were discussed.

Group IIb compounds have attracted more attention. Zhi-fen Li and

Popov[734] studied the ^{67}Zn ($I = \frac{5}{2}$) linewidths in solutions of zinc salts in water, methanol, dimethylformamide and binary solvent mixtures. Effects of adding additional complexing ligands were also reported. Köhnlein *et al.*[545] measured ^{67}Zn relaxation times in aqueous solutions of zinc sulphate and nitrate as functions of added citrate concentration. Shimizu, Kodaka and Hatano[735-737] studied zinc relaxation in several complexes of Zn^{2+} with ligands of biochemical interest in aqueous solution. Carson and Dean[738] reported linewidths of metal NMR signals for ^{67}Zn and ^{199}Hg ($I = \frac{1}{2}$) in thiolate and phenylselenolate complexes, while Huet and Gaudemer[683] studied ^{13}C relaxation in Zn^{2+}–porphyrin complexes. Bammel and Evilia[739] investigated ^{67}Zn relaxation by studying the scalar relaxation of ^{15}N in ligands complexed by ^{67}Zn-enriched zinc ions.

The other two Group IIb elements, cadmium and mercury, have magnetic isotopes with $I = \frac{1}{2}$ and their relaxation mechanisms are fairly complicated, especially for ^{113}Cd. Some of the ^{113}Cd relaxation work is also quite sophisticated, from the point of view of NMR relaxation as well as chemistry. Jensen *et al.*[740] studied cadmium–EDTA and perdeutero-EDTA complexes. They reported ^{113}Cd T_1 and NOE data at three magnetic fields and several pH values, as well as ^{13}C T_1 for the ligand nuclei. The acid–base equilibria in the system were studied. ^{113}Cd spin–lattice relaxation in the low-pH form was dominated by the DD interaction with protons at low field and by the CSA mechanism at high field. At high pH the apparent relaxation rates were influenced by the exchange. In another paper from the same group, Ellis *et al.*[741] studied solid-state ^{113}Cd spectra (which yielded the shift anisotropy), as well as ^{113}Cd and ^{13}C relaxation in solution for a cadmium(II)–porphyrin complex. ^{13}C relaxation provided a correlation time for the reorientation of an axis in the plane of the porphyrin. Given the shift anisotropy, the T_1 CSA for ^{113}Cd provided the correlation time for the reorientation of an axis perpendicular to the porphyrin plane and allowed the characterization of motional anisotropy. Bryden and Reilley[742] studied cadmium cyclohexanediamine-tetraacetate in H_2O and D_2O solution. They reported ^{113}Cd T_1 results and non-selective and selective $^{113}Cd-^{1}H$ NOEs. The results demonstrated that water did not penetrate the coordination sphere of the ion. Dechter *et al.*[743] studied ^{113}Cd spin–lattice relaxation in DMSO and pyridine solutions as a function of temperature at three magnetic fields. The relaxation rates were generally low. The data for the DMSO solution could be analysed in terms of DD, CSA and SR contributions. By comparing the CSA contribution to the ^{113}Cd relaxation rate with the ^{13}C spin–lattice relaxation rate, an estimate of the shift anisotropy was obtained. Similar variable-temperature multinuclear multifield relaxation work was also reported by Keller *et al.*[744] for ^{113}Cd in several small dynamically stable cadmium complexes in aqueous

solution. Casu *et al.*[745] reported single-temperature single-field ^{113}Cd T_1 for aqueous systems at two pH values, containing cadmium salts and ATP. Radics and Kajtar-Peredy[746] studied a complex between Cd^{2+} and the carboxylic acid ionophore antibiotic griseochelin. The ^{13}C T_1 data provided the dynamic information, which was combined with proton–proton NOEs (and spin–spin couplings) to give the solution conformation. Finally, Vlasov and Antonov[747] studied proton relaxation in methanol solution of sodium iodide and cadmium iodide.

Mercury compounds have been the subjects of four papers. Gillies *et al.*[748] studied ^{199}Hg spin–lattice relaxation in diphenylmercury and found it to be dominated by the CSA interaction, even at fairly low field. Combining the ^{199}Hg and ^{13}C relaxation data, they were able to determine the shielding anisotropy for ^{199}Hg. Bain[749] reported ^{199}Hg, ^{13}C and ^{15}N spin–lattice relaxation times for various species present in the Hg(II)–$Hg(CN)_2$–D_2O system. Wasylishen *et al.*[750] studied several Hg(II) compounds at two magnetic fields. The CSA mechanism was found to be dominant for ^{199}Hg in compounds with a mercury coordination number of two. In most cases, the authors also measured ^{13}C or ^{14}N relaxation rates and estimated the shielding anisotropy for mercury. In the four-coordinated tetrahedral complexes, the symmetry precludes efficient CSA relaxation and the ^{199}Hg relaxation becomes two orders of magnitude slower. Thomas and Rowland[751] reported a ^{13}C T_1 investigation of internal motions in arylmercury compounds.

We turn next to Group IIIb (Sc, Y, La, Ac) and also include lanthanides and actinides. The linewidth of ^{45}Sc ($I = \frac{7}{2}$) in aqueous scandium salts solutions was studied by Rehder and Speh.[752] Levy *et al.*[753] studied spin–lattice relaxation of ^{89}Y ($I = \frac{1}{2}$) in aqueous and DMSO salt solutions in the absence and in the presence of crown ethers. Relaxation times of several hundreds of seconds were reported, the main relaxation mechanisms being SR and DD with the solvent protons. Evans and Missen[754] reported ^{139}La ($I = \frac{7}{2}$) linewidths for a variety of lanthanum complexes in acetonitrile solution, while Geraldes and Sherry[755] studied another series of lanthanum complexes in water. The last member of the lanthanide series, lutetium, was studied by Brücher *et al.*[756] They investigated $Lu(ClO_4)_3$ in acetone–water solution by means of ^{35}Cl relaxation, which indicated the formation of an inner-sphere perchlorate complex. Two uranium compounds have been studied by NMR relaxation measurements. Ursu *et al.*[757–759] studied neat liquid UF_6. They measured ^{19}F T_2[757] and $T_{1\rho}$[758,759] as functions of enrichment in ^{235}U. The transverse relaxation of ^{19}F bonded to this particular isotope is dominated by scalar relaxation of the second kind, caused by the rapid quadrupolar relaxation. Jung *et al.*[760] reported ^{17}O relaxation measurements in aqueous solutions of uranyl salts. The water

^{17}O linewidth variation with concentration, temperature and anion was investigated. Both T_1 and T_2 were reported for the uranyl oxygen, which relaxed exceptionally slowly.

We now turn to Group IVb (Ti, Zr, Hf) compounds. Titanium has two magnetic isotopes, ^{47}Ti ($I = \frac{5}{2}$) and ^{49}Ti ($I = \frac{7}{2}$), whose linewidths in different complexes were explored by Hao *et al.*[761] Zirconium has a magnetic isotope, ^{91}Zr ($I = \frac{5}{2}$), whose linewidth in different compounds was studied by Sayer *et al.*[762]

Group Vb (V, Nb, Ta) compounds have been studied more diligently. Among systems reviewed in this section, vanadium compounds have received a relatively large amount of attention. Three groups reported independently very similar studies on neat liquid vanadyl trichloride $VOCl_3$.[763-765] The relaxation rates were measured for the two magnetic isotopes, the common ^{51}V ($I = \frac{7}{2}$) and the rare ^{50}V ($I = 6$). By comparing the relaxation rates of the two nuclides, it was possible to determine the nuclear quadrupole moment of the rare isotope. Brownlee and Shehan[766] reported spin–lattice relaxation for ^{17}O and ^{51}V in $V(CO)_6^-$ and derived the corresponding QCCs by comparison with hexacarbonyl compounds of other metals. Spin–lattice relaxation of ^{51}V in the vanadate ion VO_4^{3-} was studied by Tarasov *et al.*[767,768] (over a wide temperature interval, also ^{50}V) and by Haid *et al.*[769] (as a function of the vanadate and NaOH concentration). Tarasov *et al.*[767,768] also studied a large number of other T_d-symmetry oxo-complexes and discussed a model for quadrupolar relaxation in these compounds. ^{51}V relaxation was also studied in polyoxovanadates by Habayeb and Hileman.[770] Besecker *et al.*[771] studied similar compounds of vanadium, niobium and tantalum by means of ^{17}O NMR and discussed the effects of the metal-nucleus relaxation of the oxygen linewidth. Domaille[772] reported ^{51}V spin–lattice relaxation times in heteropolymetalates containing vanadium and tungsten. Rehder and Basler[773] reported some measurements of ^{181}Ta linewidths.

Several authors have reported work on compounds of Group VIb metals (Cr, Mo, W). Among the magnetic isotopes of these metals, mention should be made of ^{53}Cr ($I = \frac{3}{2}$), ^{95}Mo and ^{97}Mo (both $I = \frac{5}{2}$) and ^{183}W ($I = \frac{1}{2}$). The papers on oxo-anions referred to above also included relaxation measurements for the metal nucleus in chromates,[767-769] molybdates,[767,768,771] tungstates[771] and vanadotungstates.[772] Oxomolybdenum compounds were also studied by means of combined ^{95}Mo and ^{17}O linewidth studies by Freeman *et al.*[774] and, by means of ^{95}Mo linewidths, by Young and Enemark[775] and Gheller *et al.*[776] Kroneck *et al.*[777] reported linewidth data for ^{95}Mo, ^{97}Mo, ^{17}O and ^{33}S in thiomolybdates. The linewidths of the latter two nuclei in thiomolybdates and thiotungstates were also studied by Belton *et al.*[778]

Other types of compound of Group VIb metals have also attracted attention. ^{53}Cr linewidths were reported by Hafner *et al.*[779] for a large number of pentacarbonylchromium–carbene complexes. Haslinger and Robien[780] studied non-exponential ^{1}H spin–lattice relaxation in biphenyltricarbonylchromium compounds. Brownlee and coworkers[776,781] studied hexacarbonyl complexes of chromium, molybdenum and tungsten by combined metal-nucleus and oxygen spin–lattice relaxation measurements and estimated the QCCs. The same group also studied ^{95}Mo relaxation in other molybdenum–organic compounds.[782–784] Moreover, Donovan-Mtuzi *et al.*[785] studied ^{15}N relaxation in dinitrogen complexes of molybdenum and tungsten. Crabtree, Hamilton and coworkers[786–788] studied the proton T_1 of the hydride resonance in tungsten (and other transition-metal) hydride complexes, in order to determine whether the structure was classical or non-classical. The non-classical structure implies that a hydrogen molecule is bonded to a metal atom relatively intact; consequently the proton–proton distance is short and so is T_1.

Compounds of group VIIb metals (Mn, Tc, Re) have also received some attention. The metal nuclei of interest here are ^{55}Mn ($I = \frac{5}{2}$), ^{99}Tc ($I = \frac{9}{2}$) and ^{187}Re ($I = \frac{5}{2}$). Quadrupolar relaxation of the central metal nucleus in the tetrahedral oxo-complexes of all three metals was studied by Tarasov *et al.*[767,768] ^{55}Mn relaxation in MnO_4^- was also studied by Haid *et al.*,[769] while ^{99}Tc relaxation in the analogous TcO_4^- anion was reported by Buckingham *et al.*,[789] Tarasov *et al.*[790] and Kidd.[791] The latter author also discussed the quadrupolar nucleus QCCs in a series of seven MO_4^{n-} compounds. Work on other systems containing Group VIIb metals has been scarce. Farrar and Quinting[792] reported proton and ^{55}Mn relaxation times in $HMn(CO)_5$. Proton spin–lattice relaxation was dominated by the DD interaction with ^{55}Mn. By measuring ^{1}H T_1 as a function of temperature at the minimum in the T_1 versus temperature curve, the authors were able to determine the proton–manganese distance. ^{1}H T_2 contained an important contribution from the scalar relaxation of the second kind. By combining the proton T_2 with manganese T_1, it was also possible to evaluate the scalar coupling constant J_{HMn}. Another manganese carbonyl complex was studied by Aime *et al.*,[793] by means of ^{17}O relaxation measurements. Franklin *et al.*[794] reported ^{99}Tc and ^{17}O spin–lattice relaxation times for several technetium-(VII) compounds in solution. Donovan-Mtuzi *et al.*[785] studied ^{15}N relaxation in dinitrogen complexes of rhenium, while Hamilton and Crabtree[788] used ^{1}H T_1 measurements to distinguish between classical and non-classical (see above) rhenium hydride structures.

We proceed with Group VIII compounds. All the iron-group metals (Fe, Ru, Os) have magnetic isotopes. In the case of iron it is ^{57}Fe ($I = \frac{1}{2}$), one of the most difficult nuclei to observe. Nozawa *et al.*[795] were first to report

the spin–lattice relaxation rates for iron in $Fe(CO)_5$ and ferrocene. The experiments were performed at a single temperature and a single magnetic field, but the authors nevertheless tried to analyse the relaxation mechanism. Baltzer *et al.*[796] reported variable-field ^{57}Fe T_1 experiments for a ferrocene derivative and found the relaxation process to be dominated by the CSA mechanism. A more comprehensive study of ^{57}Fe spin–lattice and spin–spin relaxation was presented by Hafner *et al.*,[797] who performed measurements on several compounds at several temperatures and at two magnetic fields. Two competing mechanisms, SR and CSA, were identified, with the latter generally dominating at high field.

Several papers have dealt with relaxation of ligand nuclei in metallo-organic iron-group compounds. Aime and coworkers[793,798–800] presented a series of papers in which they estimated the QCC for oxygen in carbonyl ligands from ^{17}O relaxation rates. In the earliest paper[793] a series of carbonyl complexes of the iron-group metals, manganese and rhodium were studied and the correlation times necessary for deriving the QCC were estimated using the Stokes–Einstein relation. Later, the authors[798] studied organometallic carbonyl complexes of iron, osmium and cobalt and obtained the τ_c from ^{13}C relaxation of the proton-bearing carbons in the organic ligands. More recently, the correlation time has been estimated from the CSA contribution to the ^{13}C relaxation in the carbonyl ligands in $M_3(CO)_{12}$ clusters with M = Fe, Ru, Os[799] and in other iron and rhodium carbonyl complexes.[800] Aime and Occhiello[801] studied ^{13}C and ^1H relaxation in binuclear complexes of iron-group metals containing the cyclopentadienyl moiety. The carbon data allowed estimation of the correlation times, while ^1H T_1 and NOE yielded geometrical information. Iron cyclopentadienyl complexes were also studied by means of ^{13}C spin–lattice relaxation-time and NOE measurements by Mann *et al.*[802] Appel *et al.*[803] measured ^{31}P spin–lattice relaxation times in ruthenium (and platinum) complexes with phosphorus-containing ligands. Hamilton and Crabtree[787,804] studied iron-group metal hydride complexes, using ^1H T_1 measurements for structural studies. Similar work was also reported by Bautista *et al.*,[805] Aime *et al.*[806] (for ruthenium and osmium clusters) and Drake[807] for osmium carbonyl hydrido clusters. Amman *et al.*[808] studied proton T_1 in a series of ruthenium (as well as other Group VIII metal) hydrides and showed that the relaxation rate could vary by at least an order of magnitude also within the group of hydrides with classical structures. VanderVelde *et al.*[809] reported selective and non-selective proton spin–lattice relaxation experiments in ruthenium and osmium clusters with two types of proton.

Ruthenium has two magnetic isotopes, ^{99}Ru and ^{101}Ru, both with $I = \frac{5}{2}$. The relaxation properties of these nuclei in RuO_4 were studied by Tarasov

et al.,[767,768] Brevard and Granger[810] and Dykstra and Harrison.[811] The latter authors also studied ruthenium signal linewidths in a series of other compounds. Masuda and Yamatera[812] studied the trisphenanthroline complex of Ru^{2+} in water and methanol using ^{13}C T_1 measurements. The rotational correlation times were determined and discussed in terms of hydrodynamics and aggregation. The paper by Donovan-Mtunzi *et al.*[785] on ^{15}N relaxation in, among others, osmium dinitrogen complexes has been mentioned already.

We now turn to the cobalt group (Co, Rh, Ir). Cobalt compounds have been studied extensively, at least partly because of the advantageous NMR properties of ^{59}Co ($I=\frac{7}{2}$). We begin the discussion with ^{59}Co relaxation in highly symmetric complexes with small inorganic ligands and proceed towards decreasing symmetry and increasing metalloorganic character of the compounds. The discussion of cobalt compounds will be concluded by reviewing studies dealing with the relaxation of other nuclei.

In the work on highly symmetric species the authors discuss the interactions involved in the relaxation and their modulation. Chacko and Bryant[813] studied ^{59}Co, ^{13}C and ^{15}N relaxation rates in aqueous solutions of potassium hexacyanocobaltate as functions of temperature, in the presence and in the absence of Mg^{2+} ions. They found the cobalt relaxation rate to be dominated by quadrupolar interaction, with the modulation of the field gradient not coupled to rotation. The presence of Mg^{2+} outside the first coordination sphere changed the field gradient by at most 30%. Eaton *et al.*[814,815] studied the same anion in mixed solvents and in DMSO solutions containing strongly hydrogen-bonding species. Drastic increase in the linewidth was observed. Relaxation rates were not proportional to viscosity, indicating a change in the relaxation mechanism rather than simple correlation-time variation. Jordan[816] studied another highly symmetric system, $Co(NH_3)_6^{3+}$ in D_2O. The ^{59}Co relaxation rate was found to display a much weaker temperature dependence than the solvent-deuteron relaxation or the ammino-proton T_1. Jordan interpreted this observation as an indication of the quadrupolar relaxation of ^{59}Co competing with the SR mechanism. Yamasaki *et al.*[817] and Russell and Bryant[818] studied ^{59}Co relaxation in hexaamminocobalt(III) and tris(ethylenediamine)cobalt(III) ($Co(en)_3^{3+}$) in aqueous solution. The latter work aimed at studying ion-pairing effects and included ^{13}C T_1 measurements, thus making it possible to separate the effects of the rotational correlation time and of the field gradient. Buist and Eaton[819] studied $T_{1\rho}$ for ^{59}Co in $Co(en)_3^{3+}$ and hexanitrocobaltate solutions. They found a substantial contribution from the scalar relaxation (due to ^{14}N) and determined the cobalt–nitrogen coupling constants. Doddrell *et al.*[820] studied ^{59}Co relaxation in symmetric, bidentate cobalt complexes, e.g. trisacetylacetonatocobalt(III) ($Co(acac)_3$).

They interpreted the data in terms of Valiev's theory (see Section 2.5), involving excitation of vibrational modes of an octahedron. A more recent study of $Co(acac)_3$, presented by Grahn *et al.*,[821] did not confirm the conclusions of Doddrell *et al.*

Au-Yeung, Eaton and Buist[822-824] studied cobalt linewidths in a large number of cobalt complexes of varying symmetry at several magnetic fields and in several solvents. In aqueous solution the highly symmetric ions $Co(CN)_6^{3-}$ and $Co(NH_3)_6^{3+}$ featured field-independent linewidths. The linewidths of complexes of lower symmetry were field-dependent, indicating CSA contributions. Au-Yeung and Eaton[825] also proposed a point-charge model for estimating ^{59}Co linewidths in low-symmetry complexes. ^{59}Co linewidths were also reported by Tarasov *et al.*[826] in several low-symmetry complexes, by Au-Yeung and Eaton[827] in cobalt–dioxygen complexes and by Hagen *et al.*[828,829] in cobalt(III) porphyrins. Saito and Sawada[830] studied cobalt and proton relaxation in cobalt hydride carbonyl clusters.

Masuda and Yamatera[812,831] studied ^{13}C relaxation in symmetric complexes of Co^{3+} with bidentate ligands and related the rotational correlation times to solution viscosities and ion–ion interactions. For $Co(en)_3^{3+}$ the proton spin–lattice relaxation times were also measured and the motional anisotropy was investigated.[831] At infinite dilution the reorientation of the complexes was close to isotropic. Huet and Gaudemer[683] employed ^{13}C T_1 measurements to study rotational barriers around the pyridine–metal bond in porphyrin complexes of cobalt(III) and rhodium(III). Aime and coworkers[798] and Bernassau *et al.*[832] studied ^{13}C relaxation in cobalt carbonyl complexes of linear alkynes. Schwartz *et al.*[833] reported a ^{13}C relaxation study of reorientational dynamics in tetracobalt clusters with carbonyl and phosphine ligands. Storm *et al.*[834] demonstrated specific deuterium substitution effects on ligand-proton relaxation and interligand NOEs in cobalt(III) complexes.

We turn next to rhodium and iridium compounds. We have found four papers on the relaxation of ^{103}Rh, a low-magnetogyric-ratio $I = \frac{1}{2}$ nuclide. Grüninger *et al.*[835] reported a long T_1 of about 60 s for ^{103}Rh in $Rh(acac)_3$ in chloroform solution at 2.1 T. Cocivera *et al.*[836] and Benn *et al.*[837] studied several rhodium compounds at high field and found very short rhodium spin–lattice relaxation times in low-symmetry complexes. Socol and Meek[838] reported a multifield relaxation study of ^{103}Rh relaxation in a five-coordinated rhodium complex and proved the dominance of the CSA mechanism at high fields. Among studies of other nuclei in rhodium compounds, one should mention the ^{17}O relaxation work on carbonyl complexes by Aime *et al.*[793,800] and the ^{31}P studies of Jans-Bürli and Pregosin.[733] Crabtree and coworkers[786,839,840] studied hydride complexes of iridium by proton T_1 measurements.

We turn finally to the nickel-group (Ni, Pd, Pt) compounds. Nickel has a magnetic isotope (^{61}Ni, $I=\frac{3}{2}$), but has not attracted much attention from NMR spectroscopists. We mention here only a paper by Hao *et al.*[841] giving the ^{61}Ni linewidths in some tetrahedrally coordinated compounds. Wasylishen *et al.*[842] studied ^{13}C relaxation in $K_2Ni(CN)_4$ in aqueous solution at two magnetic fields and found the CSA mechanism dominant at high field. The rotational correlation time for the complex was estimated from the ^{14}N linewidth, and the role of the dipolar $^{13}C^{14}N$ interaction was discussed.

NMR relaxation work on palladium compounds has been scarce: we are aware of only a short mention of ^{1}H relaxation in a palladium hydride complex in the paper by Amman *et al.*[808] On the other hand, the heaviest element of the nickel group, platinum, has attracted considerable attention. ^{195}Pt ($I=\frac{1}{2}$) NMR was recently reviewed by Pregosin.[843] Lallemand *et al.*[844] were the first to discuss the important role of ^{195}Pt CSA relaxation based on measurements at two fields. Doddrell *et al.*[845] studied ^{195}Pt shielding anisotropy in two platinum complexes in the solid state and the platinum relaxation in solution. Ismail *et al.*[846] observed the field-dependent broadening of the ^{195}Pt satellites in the proton spectra of platinum complexes, which was related to the ^{195}Pt CSA relaxation. Dechter and Kowalewski[847] reported a dual spin-probe study of ^{13}C and ^{195}Pt relaxation in $Pt(acac)_2$ and determined the Pt shielding anisotropy. Wasylishen and Britten[848] studied ^{195}Pt relaxation mechanisms in $Pt(CN)_4^{2-}$ and in $Pt(CN)_6^{2-}$ in aqueous solution. By variable-temperature studies at two magnetic fields, they proved that both the CSA and the SR mechanisms were important in the tetracoordinated (square-planar) compound, while the SR mechanism dominated in the case of the octahedral, hexacoordinated complex. Lystbaek and Bildsoe[849] determined ^{13}C and ^{195}Pt spin–lattice relaxation times in an anionic complex of platinum(II) with tetra-n-butylammonium counterion in different solvents and discussed the internal rotation dynamics. Benn *et al.*[850] studied ^{195}Pt relaxation in phosphorus–platinum compounds as a function of the magnetic field and temperature. Finally, platinum hydrides were studied by proton T_1 measurements.[786,803,808]

5.5. Other inorganic systems

In this section we collect work on systems that are perceived as inorganic but do not conveniently fall into the categories covered in the preceding sections.

We begin with noble gases in solution. Xenon has two magnetic isotopes, ^{129}Xe ($I=\frac{1}{2}$) and ^{131}Xe ($I=\frac{3}{2}$). NMR spectroscopy of atomic xenon in the

condensed phase has been investigated by a number of workers, and was recently reviewed by Reisse.[851] Mazitov and coworkers[852] and Stengle *et al.*[853] studied ^{131}Xe spin–lattice relaxation in solutions of atomic xenon in a series of solvents. Quadrupolar relaxation was found to be rather rapid in polar solvents, and the results could be interpreted using Hertz's electrostatic theory (see Section 2.5). Quadrupolar relaxation of ^{131}Xe in water was also studied by means of a molecular-dynamics simulation by Schnitker and Geiger.[854] Krypton also has a magnetic isotope, ^{83}Kr ($I = \frac{9}{2}$). Nuclear relaxation of this nucleus in a liquid solution of atomic krypton in different solvents was studied by Mazitov *et al.*[855] The relaxation of krypton nuclei behaves as a function of solvent in a similar way to that of ^{131}Xe.

A second group of papers to be discussed here deals with relaxation studies of inorganic non-metal compounds in non-aqueous solutions. Perrin and Gipe[856] studied the rotational motion of the ammonium ion in a variety of solvents using ^{15}N T_1 and NOE measurements. Dietrich *et al.*[857] investigated a stable complex of the ammonium ion with macrobicyclic ligands (cryptands), employing proton, ^{13}C, ^{14}N and ^{15}N relaxation data. The correlation times as well as the extent of dynamic coupling between the cation and the ligand were determined. Kintzinger *et al.*[858] also studied ^{35}Cl and ^{13}C relaxation in a cryptate complex of the chloride anion and determined the chlorine QCC. Wasylishen and Nicholas[859] reported ^{14}N and ^{17}O spin–lattice relaxation rates for nitrous oxide in hexane solution. The QCC values for the two non-equivalent ^{14}N nuclei are available from microwave spectroscopy. Thus the unique correlation time for the linear molecule and consequently the oxygen QCC could be estimated. Schilling *et al.*[860] studied ^{31}P linewidths in $POCl_3$ and linear phosphorylphosphazenes in various solvents under variable-temperature conditions. Spin–rotation relaxation was found to be an important mechanism. Finally, Sammons *et al.*[861] studied the effect of ^{17}O on the ^{31}P linewidth in ^{17}O-enriched phosphoric acid in D_2O, glycerol and a mixture of the two solvents. The linewidths of the ^{31}P and ^{17}O signals were inversely proportional to each other, in agreement with the postulated scalar relaxation of the second kind.

ACKNOWLEDGEMENTS

I wish to thank Helena Kovacs for critical comments on the early version of the manuscript and Barbara Hessel for preparing the final version of the paper. I am grateful to the Swedish Natural Science Research Council for its continuing support of my own research in the field of nuclear spin relaxation.

REFERENCES

1. F. Bloch, *Phys. Rev.*, 1946, **70**, 460.
2. N. Bloembergen, E.M. Purcell and R.V. Pound, *Phys. Rev.*, 1948, **73**, 679.
3. I Solomon, *Phys. Rev.*, 1955, **99**, 559.
4. C.P. Slichter, *Principles of Magnetic Resonance*, 2nd edn. Springer-Verlag. Berlin, 1980.
5. A. Abragam, *The Principles of Nuclear Magnetism*. Clarendon Press, Oxford, 1961.
6. J. McConnell, *The Theory of Nuclear Magnetic Relaxation in Liquids*. Cambridge University Press, 1987.
7. H. Weingärtner, in *Specialist Periodical Reports on NMR*, Vol. 17 (ed. G.A. Webb) p. 84. Royal Society of Chemistry, London, 1988. See also previous volumes in the series.
8. J. Kowalewski, L. Nordenskiöld, N. Benetis and P.-O. Westlund, *Prog. NMR Spectrosc.*, 1985, **17**, 141.
9. I. Bertini and C. Luchinat, *NMR of Paramagnetic Molecules in Biological Systems*. Benjamin/Cummings, Menlo Park, California, 1986.
10. R.K. Wangness and F. Bloch, *Phys. Rev.*, 1953, **89**, 728.
11. F. Bloch, *Phys. Rev.*, 1956, **102**, 104.
12. F. Bloch, *Phys. Rev.*, 1957, **105**, 1206.
13. A.G. Redfield, *IBM J. Res. Dev.*, 1957, **1**, 19.
14. A.G. Redfield, *Adv. Magn. Reson.*, 1965, **1**, 1.
15. K. Blum, *Density Matrix Theory and Applications*. Plenum Press, New York, 1981.
16. R.R. Ernst, G. Bodenhausen and A. Wokaun, *Principles of Nuclear Magnetic Resonance in One and Two Dimensions*. Clarendon Press, Oxford, 1987.
17. C.E.M. Fouques and L.G. Werbelow, *Can. J. Chem.*, 1979, **57**, 2329.
18. B.C. Sanctuary and L. Selwyn, *J. Chem. Phys.*, 1981, **74**, 906.
19. J. Jeener, *Adv. Magn. Reson.*, 1982, **10**, 1.
20. R.M. Lynden-Bell, *Mol. Phys.*, 1971, **22**, 837.
21. S. Szymanski, A.M. Gryff-Keller and G. Binsch, *J. Magn. Reson.*, 1986, **68**, 399.
22. N.C. Pyper, *Mol. Phys.*, 1971, **21**, 1.
23. N.C. Pyper, *Mol. Phys.*, 1971, **22**, 433.
24. P.S. Hubbard, *Phys. Rev.*, 1969, **180**, 319.
25. H.E. Rorschach, *J. Magn. Reson.*, 1986, **67**, 519.
26. J.H. Freed, G.V. Bruno and C.F. Polnaszek, *J. Phys. Chem.*, 1971, **75**, 3385.
27. R. Kubo, *J. Math. Phys.*, 1963, **4**, 174.
28. D.J. Schneider and J.H. Freed, in *Lasers, Molecules, and Methods* (ed. J.O. Hirschfelder, R.E. Wyatt and R.D. Coalson), p. 387. Wiley, New York, 1989.
29. K. Müller, P. Meier, and G. Kothe, *Prog. NMR Spectrosc.*, 1985, **17**, 211.
30. Lian-Pin Hwang, *Mol. Phys.*, 1983, **49**, 1341.
31. N.T. Khazanovich and V.D. Mironov, *Mol. Phys.*, 1985, **55**, 145.
32. R. Lenk, *Prog. NMR Spectrosc.*, 1979, **13**, 271.
33. R. Lenk, *Arch. Sci. Genève*, 1985, **38**, 203.
34. N.C. Pyper, *Mol. Phys.*, 1982, **45**, 441.
35. L.G. Werbelow, *J. Magn. Reson.*, 1984, **57**, 136.
36. L.G. Werbelow and D.M. Grant, *Adv. Magn. Reson.*, 1977, **9**, 189.
37. R.L. Vold and R.R. Vold, *Prog. NMR Spectrosc.*, 1978, **12**, 79.
38. J. Brondeau and D. Canet, *J. Chem. Phys.*, 1982, **76**, 4751.
39. A. Kratochwill, *J. Magn. Reson.*, 1979, **35**, 289.
40. J. Brondeau, D. Canet, J. Brocas and A.M. Decoster, *J. Magn. Reson.*, 1982, **46**, 129.
41. A. Thevand, G. Pouzard and L. Werbelow, *J. Phys. Chem.*, 1981, **85**, 29.
42. D. Canet, H. Nery and J. Brondeau, *J. Chem. Phys.*, 1979, **70**, 2098.

43. J. Brondeau and D. Canet, *J. Chem. Phys.*, 1977, **67**, 3650.
44. L. Werbelow, D. Canet and H. Nery, *J. Magn. Reson.*, 1984, **60**, 405.
45. B. Blicharska, *Physica*, 1988, **147A**, 601.
46. J.H. Prestegard and D.M. Grant, *J. Am. Chem. Soc.*, 1978, **100**, 4664.
47. L.G. Werbelow, D.M. Grant, E.P. Black and J.M. Courtieu, *J. Chem. Phys.*, 1978, **69**, 2407.
48. L.G. Werbelow, D.A. Ikenberry and G. Pouzard, *J. Magn. Reson.*, 1983, **51**, 409.
49. L.G. Werbelow, *J. Magn. Reson.*, 1986, **67**, 66.
50. L.G. Werbelow, *J. Chem. Phys.*, 1982, **77**, 5849.
51. L.G. Werbelow, A. Allouche and G. Pouzard, *J. Phys. Chem.*, 1984, **88**, 4692.
52. F. Winter and R. Kimmich, *Mol. Phys.*, 1982, **45**, 33.
53. P.-O. Westlund and H. Wennerström, *J. Magn. Reson.*, 1985, **63**, 280.
54. B.A. Pettitt, *J. Magn. Reson.*, 1982, **48**, 309.
55. P.S. Hubbard, *J. Phys. Chem.*, 1970, **53**, 985.
56. J. McConnell, *Physica*, 1983, **117A**, 251.
57. J. Rueben and Z. Luz, *J. Phys. Chem.*, 1976, **80**, 1357.
58. T.E. Bull, S. Forsén and D.L. Turner, *J. Chem. Phys.*, 1979, **70**, 3106.
59. P.-O. Westlund and H. Wennerström, *J. Magn. Reson.*, 1982, **50**, 451.
60. B. Halle, and H. Wennerström, *J. Magn. Reson.*, 1981, **44**, 89.
61. L.G. Werbelow, *J. Chem. Phys.*, 1979, **70**, 5381.
62. L.G. Werbelow and A.G. Marshal, *J. Magn. Reson.*, 1981, **43**, 443.
63. A.G. Marshall, Tao-Chin Lin Wang, C.E. Cottrell and L.G. Werbelow, *J. Am. Chem. Soc.*, 1982, **104**, 7665.
64. J. McConnell, *Physica*, 1984, **127A**, 152.
65. J. McConnell, *Polymer*, 1985, **26**, 193.
66. R.M. Lynden-Bell, *Mol. Phys.*, 1975, **29**, 301.
67. I. Solomon and N. Bloembergen, *J. Chem. Phys.*, 1956, **25**, 261.
68. E.R. Johnston, *J. Magn. Reson.*, 1984, **60**, 366.
69. N.C. Pyper, *Mol. Phys.*, 1971, **20**, 449.
70. N.C. Pyper, *Mol. Phys.*, 1981, **42**, 1367.
71. A. Briguet, J.C. Duplan and J. Delmau, *J. Magn. Reson.*, 1981, **42**, 141.
72. V. Mlynarik, *J. Magn. Reson.*, 1988, **79**, 322.
73. J.S. Blicharski, *Z. Naturforsch.*, 1972, **27a**, 1355.
74. P.E. Balonga, *J. Magn. Reson.*, 1984, **59**, 50.
75. A. Laaksonen, J. Kowalewski and B. Jönsson, *Chem. Phys. Lett.*, 1982, **89**, 412.
76. C. Deverell, *Mol. Phys.*, 1970, **18**, 319.
77. P.S. Hubbard, *Phys. Rev.*, 1963, **131**, 1155.
78. R.E.D. McClung, *J. Chem. Phys.*, 1969, **51**, 3842.
79. P.S. Hubbard, *Phys. Rev.*, 1974, **A9**, 481 (Erratum: 1981, **A24**, 645).
80. J. McConnell, *Physica*, 1982, **112A**, 479.
81. J. McConnell, *Physica*, 1982, **112A**, 488.
82. J. McConnell, *Physica*, 1982, **111A**, 85.
83. H. Shimizu, *J. Chem. Phys.*, 1964, **40**, 3357.
84. J. S. Blicharski, *Phys. Lett.*, 1967, **24A**, 608.
85. J.S. Blicharski, *Acta Phys. Pol.*, 1970, **A38**, 19.
86. L.G. Werbelow and D.M. Grant, *J. Magn. Reson.*, 1975, **20**, 554.
87. A.D. Bain and R.M. Lynden-Bell, *Mol. Phys.*, 1975, **30**, 325.
88. M. Goldman, *J. Magn. Reson.*, 1984, **60**, 437.
89. T.C. Farrar and R.A. Quintero-Arcaya, *Chem. Phys. Lett.*, 1985, **122**, 41.
90. T.C. Farrar and I.C. Locker, *J. Chem. Phys.*, 1987, **87**, 3281.

91. W.T. Huntress, *Adv. Magn. Reson.*, 1970, **4**, 1.
92. H.W. Spiess, in *NMR Basic Principles and Progress*, Vol. 15 (ed. P. Diehl, E. Fluck and R. Kosfeld), p. 55. Springer-Verlag, Berlin, 1978.
93. R.T. Boeré and R.G. Kidd, in *Annual Reports on NMR Spectroscopy*, Vol. 13 (ed. G.A. Webb), p. 319. Academic Press, London, 1983.
94. A. Dölle and Th. Bluhm, *Prog. NMR Spectrosc.* 1989, **21**, 175.
95. W.H. Furry, *Phys. Rev.*, 1957, **107**, 7.
96. F. Perrin, *J. Phys. Radium*, 1934, **5**, 33.
97. L.D. Favro, *Phys. Rev.*, 1960, **119**, 53.
98. D.E. Woessner, *J. Chem. Phys.*, 1962, **37**, 647.
99. H. Shimizu, *J. Chem. Phys.*, 1964, **40**, 754.
100. W.T. Huntress, *J. Chem. Phys.*, 1969, **48**, 3524.
101. E. Diez, F.J. Bermejo and J. Guilleme, *J. Chem. Phys.*, 1985, **83**, 58.
102. A. Gierer and K. Wirtz, *Z. Naturforsch.*, 1953, **8a**, 532.
103. J.L. Dote, D. Kivelson and R.N. Schwartz, *J. Phys. Chem.*, 1981, **85**, 2169.
104. C.-M. Hu and R. Zwanzig, *J. Chem. Phys.*, 1974, **60**, 4354.
105. G.K. Youngren and A. Acrivos, *J. Chem. Phys.*, 1975, **63**, 3846.
106. J.L. Dote and D. Kivelson, *J. Phys. Chem.*, 1983, **87**, 3889.
107. G.R. Alms, D.R. Bauer, J.I. Brauman and R. Pecora, *J. Chem. Phys.*, 1973, **58**, 5570.
108. G.T. Evans and D. Kivelson, *J. Chem. Phys.*, 1986, **84**, 385.
109. P. Madden and D. Kivelson, *J. Phys. Chem.*, 1982, **86**, 4244.
110. K.M. Larsson, J. Kowalewski and U. Henriksson, *J. Magn. Reson.*, 1985, **62**, 260.
111. D. Wallach and W.T. Huntress, *J. Chem. Phys.*, 1969, **50**, 1219.
112. K.T. Gillen and J.H. Noggle, *J. Chem. Phys.*, 1970, **53**, 801.
113. R.G. Gordon, *J. Chem. Phys.*, 1966, **44**, 1930.
114. R.E.D. McClung, *J. Chem. Phys.*, 1972, **57**, 5478.
115. R.E.D. McClung, *Adv. Mol. Relax. Inter. Proc.*, 1977, **10**, 83.
116. J.-C. Leicknam and Y. Guissani, *Mol. Phys.*, 1981, **42**, 1105.
117. T.E. Bull and W. Egan, *J. Chem. Phys.*, 1984, **81**, 3181.
118. H.J. Böhm, R.M. Lynden-Bell, P.A. Madden and I.R. McDonald, *Mol. Phys.*, 1984, **51**, 761.
119. R.E.D. McClung, *J. Chem. Phys.*, 1980, **73**, 2435.
120. R.E.D. McClung, *J. Chem. Phys.*, 1981, **75**, 5503.
121. G. Lévi, J.P. Marsault, F. Marsault-Hérail and R.E.D. McClung, *J. Chem. Phys.*, 1980, **73**, 2443.
122. D.H. Lee and R.E.D. McClung, *Chem. Phys.*, 1987, **112**, 23.
123. D.H. Lee and R.E.D. McClung, *J. Magn. Reson.*, 1987, **73**, 34.
124. R.R. Vold, in *Nuclear Magnetic Resonance of Liquid Crystals* (ed. J.W. Emsley), p. 253. Reidel, Dordrecht, 1985.
125. R.L. Vold and R.R. Vold, *Israel J. Chem.*, 1983, **23**, 315.
126. P.L. Nordio, G. Rigatti and U. Segre, *J. Chem. Phys.*, 1972, **56**, 2117.
127. C.F. Polnaszek, G.V. Bruno and J.H. Freed, *J. Chem. Phys.*, 1973, **58**, 3185.
128. C.F. Polnaszek and J.H. Freed, *J. Phys. Chem.*, 1975, **79**, 2283.
129. J.H. Freed, *J. Chem. Phys.*, 1977, **66**, 4183.
130. J.P. Jacobsen, H.K. Bildsoe and K. Schaumburg, *J. Magn. Reson.*, 1976, **23**, 153.
131. H. Wennerström, G. Lindblom and B. Lindman, *Chem. Scr.*, 1974, **6**, 97.
132. J.M. Bernassau, E.P. Black and D.M. Grant, *J. Chem. Phys.*, 1982, **76**, 253.
133. B. Halle and H. Wennerström, *J. Chem. Phys.*, 1981, **75**, 1928.
134. R.R. Vold and R.L. Vold, *J. Chem. Phys.*, 1988, **88**, 1443.
135. R. Poupko, R.L. Vold and R.R. Vold, *J. Phys. Chem.*, 1980, **84**, 3444.

136. H.G. Hertz, *Prog. NMR Spectrosc.*, 1983, **16**, 115.
137. D.E. Woessner, *J. Chem. Phys.*, 1962, **36**, 1.
138. D. Doddrell, V. Glushko and A. Allerhand, *J. Chem. Phys.*, 1972, **56**, 3683.
139. A. Tsutsumi, *Mol. Phys.*, 1979, **37**, 111.
140. D.E. Woessner, *J. Chem. Phys.*, 1965, **42**, 1855.
141. R.E. London, *J. Am. Chem. Soc.*, 1978, **100**, 2678.
142. D.E. Woessner, B.S. Snowden and G.H. Meyer, *J. Chem. Phys.*, 1969, **50**, 719.
143. W.M.M.J. Bovée, J. Vriend, J.A. Peters, J.M.A. Baas and B. Van de Graaf, *Mol. Phys.*, 1980, **41**, 933.
144. J. Tropp, *J. Chem. Phys.*, 1980, **72**, 6035.
145. B.K. John and R.E.D. McClung, *J. Magn. Reson.*, 1982, **50**, 267.
146. B. Ban, *J. Magn. Reson.*, 1981, **45**, 118.
147. G.C. Levy, A. Kumar and D. Wang, *J. Am. Chem. Soc.*, 1983, **105**, 7536.
148. Th. Bluhm, *Mol. Phys.*, 1982, **47**, 475.
149. D. Canet and J. Brondeau, *Chem. Phys. Lett.*, 1983, **100**, 70.
150. R.E. London and J. Avitabile, *J. Am. Chem. Soc.*, 1978, **100**, 7159.
151. O. Edholm and C. Blomberg, *Chem. Phys.*, 1981, **56**, 9.
152. C. Mendonca, H.A. Farrach, C.P. Poole and P.D. Ellis, *J. Magn. Reson.*, 1981, **45**, 290.
153. G. Moro, *Chem. Phys.*, 1987, **118**, 167; *Ibid.* 1987, **118**, 181.
154. T.E. Bull, *J. Chem. Phys.*, 1976, **65**, 4802.
155. H. Versmold, *J. Chem. Phys.*, 1980, **73**, 5310.
156. Kook Joe Shin, Doo Soo Chung and Bong Soo Kim, *J. Chem. Phys.*, 1982, **77**, 5852.
157. Doo Soo Chung, Eun Mi Kim and Kook Joe Shin, *Chem. Phys. Lett.*, 1984, **108**, 283.
158. D. Wallach, *J. Chem. Phys.*, 1967, **47**, 5258.
159. Y.K. Levine, P. Partington and G.C.K. Roberts, *Mol. Phys.*, 1973, **25**, 497.
160. P. Beckmann, *Mol. Phys.*, 1980, **41**, 1227.
161. Y.K. Levine, N.J.M. Birdsall, A.G. Lee, J.C. Metcalfe, P. Partington and G.C.K. Roberts, *J. Chem. Phys.*, 1974, **60**, 2890.
162. T.E. Bull, *J. Magn. Reson.*, 1978, **31**, 453.
163. O. Edholm and C. Blomberg, *Chem. Phys.*, 1979, **42**, 449.
164. R.J. Wittebort and A. Szabo, *J. Chem. Phys.*, 1978, **69**, 1722.
165. R.J. Wittebort, A. Szabo and F.R.N. Gurd, *J. Am. Chem. Soc.*, 1980, **102**, 5723.
166. J. Schaefer, *Macromolecules*, 1973, **6**, 882.
167. O.W. Howarth, *J. Chem. Soc. Faraday Trans. 2*, 1978, **74**, 1031.
168. O.W. Howarth, *J. Chem. Soc. Faraday Trans. 2*, 1979, **75**, 863.
169. K. Murayama, F. Horii and R. Kitamaru, *Bull. Inst. Chem. Res. Kyoto Univ.*, 1983, **61**, 229.
170. R. Richarz, K. Nagayama and K. Wüthrich, *Biochemistry*, 1980, **19**, 5189.
171. G. Lipari and A. Szabo, *Biophys. J.*, 1980, **30**, 489.
172. M.E. Hogan and O. Jardetzky, *Proc. Natl Acad. Sci. USA*, 1979, **76**, 6341.
173. M.E. Hogan and O. Jardetzky, *Biochemistry*, 1980, **19**, 3460.
174. G. Lipari and A. Szabo, *Biochemistry*, 1981, **20**, 6250.
175. J.W. Keepers and T.L. James, *J. Am. Chem. Soc.*, 1982, **104**, 929.
176. G. Lipari and A. Szabo, *J. Chem. Phys.*, 1981, **75**, 2971.
177. R. King and O. Jardetzky, *Chem. Phys. Lett.*, 1978, **55**, 15.
178. R. King, R. Maas, M. Gassner, R.K. Nanda, W.W. Conover and O. Jardetzky, *Biophys. J.*, 1978, **6**, 103.
179. G. Lipari and A. Szabo, *J. Am. Chem. Soc.*, 1982, **104**, 4546.
180. H. Wennerström, B. Lindman, O. Söderman, T. Drakenberg and J.B. Rosenholm, *J. Am. Chem. Soc.*, 1979, **101**, 6860.
181. V.D. Fedotov and L.S. Kivayeva, *Biopolim. Kletka*, 1987, **3**, 171; *J. Biomol. Struct. Dyn.*, 1987, **4**, 599.

182. B. Halle, *Mol. Phys.*, 1987, **61**, 963.
183. F. Heatley, in *Annual Reports on NMR Spectroscopy*, Vol. 17 (ed. G.A. Webb), p. 179. Academic Press, London, 1986.
184. E. Helfand, *J. Chem. Phys.*, 1971, **54**, 4651.
185. B. Valeur, J.P. Jarry, F. Geny and L. Monnerie, *J. Polym. Sci. Polym. Phys.*, 1975, **13**, 667.
186. B. Valeur, L. Monnerie and J.P. Jarry, *J. Polym. Sci. Polym. Phys.*, 1975, **13**, 675.
187. B. Valeur, J.P. Jarry, F. Geny and L Monnerie, *J. Polym. Sci. Polym. Phys.*, 1975, **13**, 2251.
188. C.K. Hall and E. Helfand, *J. Chem. Phys.*, 1982, **77**, 3275.
189. J. Skolnick and R. Yaris, *Macromolecules*, 1982, **15**, 1041 (Erratum: 1983, **16**, 491).
190. J. Skolnick and R. Yaris, *Macromolecules*, 1983, **16**, 266.
191. J. Skolnick, D. Perchak and R. Yaris, *J. Magn. Reson.*, 1984, **57**, 204.
192. H. Yamakawa and M. Fujii, *J. Chem. Phys.*, 1984, **81**, 997.
193. A. Ferrarini, G. Moro and P.L. Nordio, *Mol. Phys.*, 1988, **63**, 225.
194. G. Moro and P.L. Nordio, *Mol. Phys.*, 1985, **56**, 255.
195. G. Moro and P.L. Nordio, *Mol. Phys.*, 1986, **57**, 947.
196. M. Baldo, A. Grassi, B. Perly, *Mol. Phys.*, 1988, **64**, 51.
197. R.M. Levy, M. Karplus, and P.G. Wolynes, *J. Am. Chem. Soc.*, 1981, **103**, 5998.
198. R.M. Levy, M. Karplus and J.A. McCammon, *J. Am. Chem. Soc.*, 1981, **103**, 994.
199. R.M. Levy, C.M. Dobson and M. Karplus, *Biophys. J.*, 1982, **39**, 107.
200. G. Lipari, A. Szabo and R.M. Levy, *Nature*, 1982, **300**, 197.
201. R.M. Levy and M. Karplus, *Adv. Chem. Ser.*, 1983, **204**, 445.
202. T. Yasukawa, K. Murakami and C. Chachaty, *Chem. Phys. Lett.*, 1982, **88**, 74.
203. B. Lindman and S. Forsén, *Chlorine, Bromine and Iodine NMR*. Springer-Verlag, Berlin, 1976.
204. K.A. Valiev, *Sov. Phys. JETP*, 1960, **37**, 77.
205. H.G. Hertz, *Z. Elektrochem. Ber. Bunsenges. Phys. Chem.*, 1961, **65**, 20.
206. H.G. Hertz, *Ber. Bunsenges. Phys. Chem.*, 1973, **77**, 531.
207. H.G. Hertz, *Ber. Bunsenges. Phys. Chem.*, 1973, **77**, 688.
208. C. Deverell, *Mol. Phys.*, 1969, **16**, 491.
209. J.T. Hynes and P.G. Wolynes, *J. Chem. Phys.*, 1981, **75**, 395.
210. P.J. Stiles and G.B. Byrnes, *Chem. Phys.*, 1985, **100**, 217.
211. S. Engström and B. Jönsson, *Mol. Phys.*, 1981, **43**, 1235.
212. S. Engström, B. Jönsson and B. Jönsson, *J. Magn. Reson.*, 1982, **50**, 1.
213. S. Engström, B. Jönsson and R.W. Impey, *J. Chem. Phys.*, 1984, **80**, 5481.
214. H. Versmold, *Mol. Phys.*, 1986, **57**, 201.
215. R.J.C. Brown and J.P. Colpa, *J. Chem. Phys.*, 1982, **77**, 1501.
216. H.J. Osten and C.J. Jameson, *Mol. Phys.*, 1986, **57**, 553.
217. R.N. Schwartz, *J. Magn. Reson.*, 1976, **24**, 205.
218. H.C. Torrey, *Phys. Rev.*, 1953, **92**, 962.
219. M. Elwenspoek, *Mol. Phys.*, 1979, **37**, 689.
220. E.N. Ivanov and E.N. Shermakov, *Fiz. Zhidk. Sostoyaniya*, 1982, **10**, 112 (*Chem. Abstr.*, 1984, 100:215655m).
221. J.F. Harmon and B.H. Muller, *Phys. Rev.*, 1969, **182**, 400.
222. Lian-Pin Hwang and J.H. Freed, *J. Chem. Phys*, 1975, **63**, 4017.
223. Y. Ayant, E. Belorizky, J. Alizon and J. Gallice, *J. Physique*, 1975, **36**, 991.
224. R.M. Yulmetev, *Acta Phys. Polon.*, 1980, **A58**, 801.
225. J.H. Freed, *J. Chem. Phys.*, 1978, **68**, 4034.
226. C.A. Sholl, *J. Phys.*, 1981, **C14**, 447.
227. H.G. Hertz, A. Kratochwill and H. Weingärtner, *Proc. Ind. Acad. Sci. Chem. Sci.*, 1985, **94**, 337.
228. Lian-Pin Hwang, *Mol. Phys.*, 1984, **51**, 1235.

229. Chang-Yuan Ju and Lian-Pin Hwang, *J. Chin. Chem. Soc. (Taipei)*, 1985, **32**, 231.
230. P.S. Hubbard, *Phys. Rev.*, 1963, **131**, 275.
231. M.D. Zeidler, *Mol. Phys.*, 1975, **30**, 1441.
232. Y. Ayant, E. Belorizky, P. Fries and J. Rosset, *J. Physique*, 1977, **38**, 325.
233. P. Fries and E. Belorizky, *J. Physique*, 1978, **39**, 1263.
234. P.H. Fries and B.M. Rigobello, *J. Physique*, 1982, **43**, 1397.
235. E. Belorizky and P.H. Fries, *J. Phys.*, 1981, **C14**, L521.
236. P.H. Fries, *Mol. Phys.*, 1983, **48**, 503.
237. A.M. Gladkii and V.A. Daragan, *Zh. Fiz. Khim.*, 1984, **58**, 1083.
238. P.-O. Westlund and R.M. Lynden-Bell, *J. Magn. Reson.*, 1987, **72**, 522.
239. H.S. Gutowsky, D.W. McCall and C.P. Slichter, *J. Chem. Phys.*, 1953, **21**, 279; H. S. Gutowsky and A. Saika, *J. Chem. Phys.*, 1953, **21**, 1688.
240. J.I. Kaplan and G. Fraenkel, *NMR of Chemical Exchanging Systems*. Academic Press, New York, 1980.
241. J. Sandström, *Dynamic NMR Spectroscopy*. Academic Press, London, 1982,
242. B. Halle, *Mol. Phys.*, 1984, **53**, 1427.
243. H.M. McConnell, *J. Chem. Phys.*, 1958, **28**, 430.
244. J.R. Zimmerman and W.E. Brittin, *J. Phys. Chem.*, 1957, **61**, 1328.
245. H. Winkler and A. Gutsze, *Adv. Molec. Relax. Inter. Proc.*, 1981, **21**, 159.
246. T.E. Bull, *J. Magn. Reson.*, 1972, **8**, 344.
247. U. Eliav, A. Baram and G. Navon, *J. Chem. Phys.*, 1988, **89**, 5584.
248. D. Beckert and H. Pfeifer, *Ann. Phys.*, 1965, **16**, 262.
249. H.G. Hertz, *Ber. Bunsenges. Phys. Chem.*, 1967, **71**, 979.
250. J.E. Anderson and P.A. Fryer, *J. Chem. Phys.*, 1969, **50**, 3784.
251. A.G. Marshal, *J. Chem. Phys.*, 1970, **52**, 2527.
252. H. Wennerström, *Mol. Phys.*, 1972, **24**, 69.
253. E.E. Burnell, M.E. Clark, J.A.M. Hinke and N.R. Chapman, *Biophys. J.*, 1981, **33**, 1.
254. L. Latanowicz, *Ber. Bunsenges. Phys. Chem.*, 1987, **91**, 237.
255. B. Halle, *Mol. Phys.*, 1985, **56**, 209.
256. B. Halle, *Mol. Phys.*, 1987, **60**, 319.
257. B. Halle and P.-O. Westlund, *Mol. Phys.*, 1988, **63**, 97.
258. P.S. Belton and B.P. Hills, *Mol. Phys.*, 1987, **61**, 999.
259. P.S. Belton and B.P. Hills, *Mol. Phys.*, 1988, **65**, 313.
260. H.C. Torrey, *Phys. Rev.*, 1956, **104**, 563.
261. M.L. Martin, G.J. Martin and J.-J. Delpuech, *Practical NMR Spectroscopy*. Heyden, London, 1980.
262. D.J. Craik and G.C. Levy, in *Topics in Carbon-13 NMR Spectroscopy*, Vol. 4 (ed. G.C. Levy), Chap. 9. Wiley, New York, 1984.
263. D. Canet, G.C. Levy and I.R. Peat, *J. Magn. Reson.*, 1975, **18**, 199.
264. G.H. Weiss and J.A. Ferretti, *Prog. NMR Spectrosc.*, 1988, **20**, 317.
265. M.H. Levitt and R. Freeman, *J. Magn. Reson.*, 1979, **33**, 473.
266. M.H. Levitt, *Prog. NMR Spectrosc.*, 1986, **18**, 61.
267. D.B. Zax, G. Goelman and S. Vega, *J. Magn. Reson.*, 1988, **80**, 375.
268. Jintong Mao, T.H. Mereci and E.R. Andrew, *J. Magn. Reson.*, 1988, **79**, 1.
269. Z. Starcuk, L. Pucek and Z. Starcuk, *J. Magn. Reson.*, 1988, **80**, 352.
270. R.R. Vold and G. Bodenhausen, *J. Magn. Reson.*, 1980, **39**, 363.
271. K.A. Christensen, D.M. Grant, E.M. Schulman and C. Walling, *J. Phys. Chem.*, 1974, **78**, 1971.
272. R.K. Gupta, *J. Magn. Reson.*, 1977, **25**, 231.
273. R.K. Gupta, G.H. Weiss, J.A. Ferretti and E.D. Becker, *J. Magn. Reson.*, 1979, **35**, 301.
274. J. Homer and M.S. Beevers, *J. Magn. Reson.*, 1985, **63**, 287.

275. A. Ejchart, P. Oleski and K. Wroblewski, *J. Magn. Reson.*, 1986, **68**, 207.
276. K.R. Metz and R.W. Briggs, *J. Magn. Reson.*, 1985, **61**, 526.
277. Daxiong Ji, Dongsheng Wang and Xuewen Wu, *Kexue Tongbao (Foreign Language Edn)*, 1986, **31**, 1598 (*Chem. Abstr.*, 1987, 107: 50591s).
278. J. Brondeau, B. Diter and D. Canet, *J. Magn. Reson.*, 1981, **42**, 110.
279. S.S. Sankar, P.A. Molé and R.L. Coulson, *Magn. Reson. Med.*, 1986, **3**, 958.
280. D.L. Rabenstein, T. Nakashima and G. Bigam, *J. Magn. Reson.*, 1979, **34**, 675.
281. A.S. Arseniev, A.G. Sobol and V.F. Bystrov, *J. Magn. Reson.*, 1986, **70**, 427.
282. J.K. Saunders and J.D. Stevens, *Magn. Reson. Chem.*, 1986, **24**, 1023.
283. L.E. Kay and J.H. Prestegard, *J. Magn. Reson.*, 1988, **77**, 599.
284. A.G. Avent and R. Freeman, *J. Magn. Reson.*, 1980, **39**, 169.
285. G.A. Morris, *J. Magn. Reson.*, 1980, **41**, 185.
286. P. Bigler, *J. Magn. Reson.*, 1987, **75**, 162.
287. J. Kowalewski and G.A. Morris, *J. Magn. Reson.*, 1982, **47**, 331.
288. V. Sklenar, D. Torchia and A. Bax, *J. Magn. Reson.*, 1987, **73**, 375.
289. L.E. Kay, T.L. Jue, B. Bangerter and P.C. Demou, *J. Magn. Reson.*, 1987, **73**, 558.
290. N.R. Nirmala and G. Wagner, *J. Am. Chem. Soc.*, 1988, **110**, 7557.
291. R.E. London, T.E. Walker, V.H. Kollman and N.A. Matwiyoff, *J. Magn. Reson.*, 1977, **26**, 213.
292. C. Rossi and N. Niccolai, *Chem. Phys. Lett.*, 1987, **142**, 418.
293. J.P. Marchal and D. Canet, *J. Magn. Reson.*, 1984, **57**, 269.
294. L. Werbelow, J.P. Marchal and D. Canet, *J. Magn. Reson.*, 1985, **61**, 457.
295. V. Mlynarik, *Prog. NMR Spectrosc.*, 1986, **18**, 277.
296. M.M. Fuson and J.H. Prestegard, *J. Magn. Reson.*, 1980, **41**, 179.
297. J. Brondeau, D. Canet, C. Millot, H. Nery and L. Werbelow, *J. Chem. Phys.*, 1985, **82**, 2212.
298. Y. Huang, G. Bodenhausen and R.R. Ernst, *J. Am. Chem. Soc.*, 1981, **103**, 6988.
299. J.M. Bernassau and D.M. Grant, *J. Magn. Reson.*, 1981, **44**, 262.
300. J. Courtieu, C.L. Mayne, D.M. Grant and J.M. Bernassau, *J. Magn. Reson.*, 1982, **48**, 346.
301. L.G. Werbelow, *J. Magn. Reson.*, 1983, **52**, 282.
302. L. Einarsson and P.-O. Westlund, *J. Magn. Reson.*, 1988, **79**, 54.
303. S.H. Koenig and R.D. Brown, in *NMR Spectroscopy of Cells and Organisms*, Vol. 2 (ed. R.K. Gupta), p. 75. CRC Press, Boca Raton, 1987. A review of the NMRD work from this group is to appear in *Prog. NMR Spectrosc.*
304. F. Noack, *Prog. NMR Spectrosc.*, 1986, **18**, 171.
305. R.L. Vold and R.R. Vold, *J. Magn. Reson.*, 1983, **55**, 78.
306. J. Jonas, *Acc. Chem. Res.*, 1984, **17**, 74.
307. J. Jonas, in *High Pressure Chemistry and Biochemistry* (ed. R. van Eldik and J. Jones), p. 193. Reidel, Dordrecht, 1987.
308. A.E. Merbach, in *High Pressure Chemistry and Biochemistry* (ed. R. van Eldik and J. Jones), p. 311. Reidel, Dordrecht, 1987.
309. A. Allerhand and M. Dohrenwend, *J. Am. Chem. Soc.*, 1985, **107**, 6684.
310. I.P. Gerothanassis, *Prog. NMR Spectrosc.*, 1987, **19**, 267.
311. J.M. Robert and R.F. Evilia, *J. Am. Chem. Soc.*, 1985, **107**, 3733.
312. D.M. Lamb, D.G. Vander Velde and J. Jonas, *J. Magn. Reson.*, 1987, **73**, 345.
313. B. Tiffon, B. Ancian and J.-E. Dubois, *Anal. Chim. Acta*, 1981, **124**, 415.
314. M.H. Levitt and R. Freeman, *J. Magn. Reson.*, 1981, **43**, 65.
315. D. Lankhorst, J. Schriever and J.C. Leyte, *J. Magn. Reson.*, 1983, **51**, 430.
316. A.J. Vega, *J. Magn. Reson.*, 1985, **65**, 252.
317. J.S. Blicharski, *Acta Phys. Polon.*, 1972, **A41**, 223.
318. T.L. James, G.B. Matson, I.D. Kuntz and R.W. Fisher, *J. Magn. Reson.*, 1977, **28**, 417.

319. P. Bendel, *J. Magn. Reson.*, 1981, **42**, 364.
320. A.D. Bain, W.P.Y. Ho and J.S. Martin, *J. Magn. Reson.*, 1981, **43**, 328.
321. V. Leon, E. Valdivieso and J. Espidel, *Appl. Spectrosc.*, 1987, **41**, 159.
322. M. Eisenstadt, *J. Magn. Reson.*, 1980, **38**, 507.
323. M. Eisenstadt, *J. Magn. Reson.*, 1980, **39**, 263.
324. M. Eisenstadt, *J. Magn. Reson.*, 1980, **39**, 275.
325. J. Kronenbitter and A. Schwenk, *J. Magn. Reson.*, 1977, **25**, 147.
326. A. Schwenk, *Prog. NMR Spectrosc.*, 1985, **17**, 69.
327. W. Kreibich and A. Schwenk, *J. Magn. Reson.*, 1988, **77**, 308.
328. R. Freeman, H.D.W. Hill and R. Kaptein, *J. Magn. Reson.*, 1972, **7**, 327.
329. D. Canet, *J. Magn. Reson.*, 1976, **23**, 361.
330. S.J. Opella, D.J. Nelson and O. Jardetzky, *J. Chem. Phys.*, 1976, **64**, 2533.
331. J. Kowalewski, A. Ericsson and R. Vestin, *J. Magn. Reson.*, 1978, **31**, 165.
332. J.C. Duplan, A. Briguet, G. Tetu and J. Delmau, *J. Magn. Reson.*, 1978, **31**, 509.
333. S.J. Opella, R.A. Friedman, M.C. Jarema and P. Lu, *J. Magn. Reson.*, 1979, **36**, 81.
334. M. Borzo and G.E. Maciel, *J. Magn. Reson.*, 1981, **43**, 175.
335. G.H. Weiss, J.A. Ferretti, J.E. Kiefer and L. Jacobson, *J. Magn. Reson.*, 1983, **53**, 7.
336. G.H. Weiss and J.A. Ferretti, *J. Magn. Reson.*, 1983, **55**, 397.
337. J.H. Noggle and R.E. Schirmer, *The Nuclear Overhauser Effect*. Academic Press, New York, 1971.
338. J.K.M. Sanders and J.D. Mersh, *Prog. NMR Spectrosc.*, 1982, **15**, 353.
339. A.D. Bain, J.C. MacDonald and M. Mazurek, *J. Magn. Reson.*, 1981, **44**, 531.
340. R. Freeman, H.D.W. Hill, B.L. Tomlinson and L.D. Hall, *J. Chem. Phys.*, 1974, **61**, 4466.
341. R. Freeman, S. Wittekoek and R.R. Ernst, *J. Chem. Phys.*, 1970, **52**, 1529.
342. L.D. Hall and H.D.W. Hill, *J. Am. Chem. Soc.*, 1976, **98**, 1269.
343. P. Dais and A.S. Perlin, *Adv. Carbohydr. Chem. Biochem.*, 1987, **45**, 125.
344. L.G. Werbelow, *J. Am. Chem. Soc.*, 1974, **96**, 4747.
345. A. Kalk and H.J.C. Berendsen, *J. Magn. Reson.*, 1976, **24**, 343.
346. K. Akasaka, *J. Magn. Reson.*, 1981, **45**, 337.
347. A.A. Bothner-By, in *Biological Applications of Magnetic Resonance* (ed. R.G. Shulman), p. 177. Academic Press, New York, 1979.
348. S.L. Gordon and K. Wüthrich, *J. Am. Chem. Soc.*, 1978, **100**, 7094.
349. G. Wagner and K. Wüthrich, *J. Magn. Reson.*, 1979, **33**, 675.
350. A.A. Bothner-By and J.H. Noggle, *J. Am. Chem. Soc.*, 1979, **101**, 5152.
351. J.H. Noggle, *J. Am. Chem. Soc.*, 1980, **102**, 2230.
352. C.M. Dobson, E.T. Olejniczak, F.M. Poulsen and R.G. Ratcliffe, *J. Magn. Reson.*, 1982, **48**, 97.
353. N.H. Andersen, K.T. Nguyen, C.J. Hartzell and H.L. Eaton, *J. Magn. Reson.*, 1987, **74**, 195.
354. H.L. Eaton and N.H. Andersen, *J. Magn. Reson.*, 1987, **74**, 212.
355. D.J. Kerwood and P.H. Bolton, *J. Magn. Reson.*, 1986, **68**, 588.
356. I.D. Campbell and R. Freeman, *J. Chem. Phys.*, 1973, **58**, 2666.
357. C. Rossi, *J. Chem. Phys.*, 1986, **84**, 6581.
358. K.E. Kövér and G. Batta, *J. Magn. Reson.*, 1987, **73**, 512.
359. K.E. Kövér and G. Batta, *Prog. NMR Spectrosc.*, 1987, **19**, 223.
360. J. Jeener, B. H. Meier, P. Bachmann and R.R. Ernst, *J. Chem. Phys.*, 1979, **71**, 4546.
361. S. Macura and R.R. Ernst, *Mol. Phys.*, 1980, **41**, 95.
362. A. Kumar, G. Wagner, R.R. Ernst and K. Wüthrich, *J. Am. Chem. Soc.*, 1981, **103**, 3654.
363. D.J. States, R.A. Haberkorn and D.J. Ruben, *J. Magn. Reson.*, 1982, **48**, 286.
364. J. Keeler and D. Neuhaus, *J. Magn. Reson.*, 1985, **63**, 454.

365. E.R. Johnston, M.J. Dellwo and J. Hendrix, *J. Magn. Reson.*, 1986, **66**, 399.
366. E.T. Olejniczak, J.C. Hoch, C.M. Dobson and F.M. Poulsen, *J. Magn. Reson.*, 1985, **64**, 199.
367. J.D. Cutnell, *J. Am. Chem. Soc.*, 1982, **104**, 362.
368. J. Bremer, G.L. Mendz and W.J. Moore, *J. Am. Chem. Soc.*, 1984, **106**, 4691.
369. T.E. Bull, *J. Magn. Reson.*, 1987, **72**, 397.
370. G.M. Clore and A.M. Gronenborn, *J. Magn. Reson.*, 1982, **48**, 402.
371. F.J.M. van de Ven, H.G.J.M. Janssen, A. Gräslund and C.W. Hilbers, *J. Magn. Reson.*, 1988, **79**, 221.
372. S. Macura, Y. Huang, D. Suter and R.R. Ernst, *J. Magn. Reson.*, 1981, **43**, 259.
373. S. Macura, K. Wüthrich and R.R. Ernst, *J. Magn. Reson.*, 1982, **47**, 351.
374. S. Macura, K. Wüthrich and R.R. Ernst, *J. Magn. Reson.*, 1982, **46**, 269.
375. M. Rance, G. Bodenhausen, G. Wagner, K. Wüthrich and R.R. Ernst, *J. Magn. Reson.*, 1985, **62**, 497.
376. G. Bodenhausen, G. Wagner, M. Rance, O.W. Soerensen, K. Wüthrich and R.R. Ernst, *J. Magn. Reson.*, 1984, **59**, 542.
377. G. Wagner, G. Bodenhausen, N. Müller, M. Rance, O.W. Soerensen, R.R. Ernst and K. Wüthrich, *J. Am. Chem. Soc.*, 1985, **107**, 6440.
378. H. Oschkinat, A. Pastore and G. Bodenhausen, *J. Am. Chem. Soc.*, 1987, **109**, 4110.
379. P.L. Rinaldi, *J. Am. Chem. Soc.*, 1983, **105**, 5167.
380. Chin Yu and G.C. Levy, *J. Am. Chem. Soc.*, 1983, **105**, 6994; *Ibid.*, 1984, **106**, 6533.
381. K.E. Kövér and G. Batta, *J. Magn. Reson.*, 1986, **69**, 519.
382. P. Bigler and C. Müller, *J. Magn. Reson.*, 1988, **79**, 45.
383. K.E. Kövér and G. Batta, *J. Magn. Reson.*, 1988, **79**, 206.
384. D.R. Muhandiram and R.E.D. McClung, *J. Magn. Reson.*, 1988, **80**, 539.
385. R.H. Griffey and A.G. Redfield, *Q. Rev. Biophys.*, 1987, **19**, 51.
386. A.A. Bothner-By, R.L. Stephens, Ju-mee Lee, C.D. Warren and R.W. Jeanloz, *J. Am. Chem. Soc.*, 1984, **106**, 811.
387. A. Bax and D.G. Davis, *J. Magn. Reson.*, 1985, **63**, 207.
388. D.G. Davis, *J. Am. Chem. Soc.*, 1987, **109**, 3471.
389. J. Cavanagh and J. Keeler, *J. Magn. Reson.*, 1988, **80**, 186.
390. B.T. Farmer and L.R. Brown, *J. Magn. Reson.*, 1987, **72**, 197.
391. B.T. Farmer, S. Macura and L.R. Brown, *J. Magn. Reson.*, 1988, **80**, 1.
392. T.E. Bull, *J. Magn. Reson.*, 1988, **80**, 470.
393. G. Bodenhausen, *Prog. NMR Spectrosc.*, 1981, **14**, 137.
394. D.P. Weitekamp, *Adv. Magn. Reson.*, 1983, **11**, 111.
395. M. Munowitz and A. Pines, *Science*, 1986, **233**, 501.
396. M. Munowitz and A. Pines, *Adv. Chem. Phys.*, 1987, **64**, 1.
397. A. Wokaun and R.R. Ernst, *Mol. Phys.*, 1978, **36**, 317.
398. R. Poupko, R.L. Vold and R.R. Vold, *J. Magn. Reson.*, 1979, **34**, 67.
399. G. Bodenhausen, R.L. Vold and R.R. Vold, *J. Magn. Reson.*, 1980, **37**, 93.
400. D. Jaffe, R.L. Vold, and R.R. Vold, *J. Magn. Reson.*, 1982, **46**, 496.
401. L. Werbelow and G. Pouzard, *J. Phys. Chem.*, 1981, **85**, 3887.
402. J. Kowalewski and K.M. Larsson, *Chem. Phys. Lett.*, 1985, **119**, 157.
403. K.M. Larsson and J. Kowalewski, *Spectrochim. Acta*, 1987, **43A**, 545.
404. R. Benn, *J. Magn. Reson.*, 1984, **59**, 164.
405. G. Jaccard, S. Wimperis and G. Bodenhausen, *J. Chem. Phys.*, 1986, **85**, 6282.
406. J. Pekar and J.S. Leigh, *J. Magn. Reson.*, 1986, **69**, 582.
407. W.D. Rooney, T.M. Barbara and C.S. Springer, *J. Am. Chem. Soc.*, 1988, **110**, 674.
408. N. Müller, G. Bodenhausen, K. Wüthrich and R.R. Ernst, *J. Magn. Reson.*, 1985, **65**, 531.

409. M. Rance and P.E. Wright, *Chem. Phys. Lett.*, 1986, **124**, 572.
410. N. Müller, G. Bodenhausen and R.R. Ernst, *J. Magn. Reson.*, 1987, **75**, 297.
411. L.E. Kay and J.H. Prestegard, *J. Am. Chem. Soc.*, 1987, **109**, 3829.
412. M.R. Bendall and D.T. Pegg, *J. Magn. Reson.*, 1983, **53**, 40.
413. N. Müller, *Chem. Phys. Lett.*, 1986, **131**, 218.
414. G. Jaccard, S. Wimperis and G. Bodenhausen, *Chem. Phys. Lett.*, 1987, **138**, 601.
415. S. Wimperis and G. Bodenhausen, *Chem. Phys. Lett.*, 1987, **140**, 41.
416. J. Jeener and P. Broekaert, *Phys. Rev.*, 1967, **157**, 232.
417. S.B. Ahmad and K.J. Packer, *Mol. Phys.*, 1979, **37**, 47.
418. R.L. Vold, W. H. Dickerson and R.R. Vold, *J. Magn. Reson.*, 1981, **43**, 213.
419. T.M. Barbara, R.L. Vold, and R.R. Vold, *J. Magn. Reson.*, 1984, **59**, 478.
420. S. Wimperis and G. Bodenhausen, *Chem. Phys. Lett.*, 1986, **132**, 194.
421. I. Solomon, *Phys. Rev.*, 1958, **110**, 61.
422. J.H. Davis, K.R. Jeffrey, M. Bloom, M.I. Valic and T.P. Higgs, *Chem. Phys. Lett.*, 1976, **42**, 390.
423. J.H. Davis, *Biochem. Biophys. Acta*, 1983, **737**, 117.
424. S.B. Ahmad, K.J. Packer and J.M. Ramsden, *Mol. Phys.*, 1977, **33**, 857.
425. R.L. Vold and R.R. Vold, *J. Magn. Reson.*, 1981, **42**, 173.
426. L. Müller and S.I. Chan, *J. Chem. Phys.*, 1983, **78**, 4341.
427. I. Furo, B. Halle and T.C. Wong, *J. Chem. Phys.*, 1988, **89**, 5382.
428. D. Canet, *Mol. Phys.*, 1978, **36**, 1731.
429. M.M. Fuson, M.S. Brown, D.M. Grant and G.T. Evans, *J. Am. Chem. Soc.*, 1985, **107**, 6695.
430. D. Piveteau, M.A. Delsuc and J.-Y. Lallemand, *J.Magn. Reson.*, 1986, **70**, 290.
431. G.M. Clore and A.M. Gronenborn, *J. Magn. Reson.*, 1985, **61**, 158.
432. S. Macura, B.T. Farmer and L.R. Brown, *J. Magn. Reson.*, 1986, **70**, 493.
433. J.W. Keepers and T.L. James, *J. Magn. Reson.*, 1984, **57**, 404.
434. E.T. Olejniczak, R.T. Gampe and S.W. Fesik, *J. Magn. Reson.*, 1986, **67**, 28.
435. R. Boelens, T.M.G. Koning and R. Kaptein, *J. Mol. Struct.*, 1988, **173**, 299.
436. M. Madrid and O. Jardetzky, *Biochim. Biophys. Acta*, 1988, **953**, 61.
437. L.E. Kay, J.N. Scarsdale, D.R. Hare and J.H. Prestegard, *J. Magn. Reson.*, 1986, **68**, 515.
438. P.A. Mirau, *J. Magn. Reson.*, 1988, **80**, 439.
439. H. Fujiwara, T. Takagi, M. Sugiura and Y. Sasaki, *J. Chem. Soc. Perkin Trans. 2*, 1983, 903.
440. A. Allouche and G. Pouzard, *J. Comput. Chem.*, 1985, **6**, 610.
441. G.Lipari and A. Szabo, *J. Am. Chem. Soc.*, 1982, **104**, 4559.
442. V.D. Fedotov and L.S. Kivayeva, *Biopolim. Kletka*, 1987, **3**, 178.
443. D.C. McCain, E.L. Ulrich and J.L. Markley, *J. Magn. Reson.*, 1988, **80**, 296.
444. D.J. Craik, A. Kumar and G.C. Levy, *J. Chem. Inf. Comput. Sci.*, 1983, **23**, 30.
445. R.L. Armstrong, *Magn. Reson. Rev.*, 1987, **12**, 91.
446. R.L. Armstrong and C. Lemaire, *Bull. Magn. Reson.*, 1987, **9**, 20.
447. T.E. Bull, *J. Chem. Phys.*, 1975, **62**, 222.
448. R. Topol, K. Krynicki and J.G. Powles, *Mol. Phys.*, 1979, **37**, 1655.
449. R. Topol, *Mol. Phys.*, 1980, **40**, 161.
450. J. DeZwaan and J. Jonas, *J. Chem. Phys.*, 1975, **63**, 4606.
451. R.J. Finney, M. Wolfe and J. Jonas, *J. Chem. Phys.*, 1977, **67**, 4004.
452. M. Wolfe, E. Arndt, and J. Jonas, *J. Chem. Phys.*, 1977, **67**, 4012.
453. T.W. Zerda, J. Schroeder and J. Jonas, *J. Chem. Phys.*, 1981, **75**, 1612.
454. W.J. Lamb and J. Jonas, *J. Chem. Phys.*, 1981, **74**, 913.
455. M. Bloom, F. Bridges and W.N. Hardy, *Can. J. Phys.*, 1967, **45**, 3533.
456. B.E. Weiss-Lopez, E.D. Winegar and N.S. True, *J. Phys. Chem.*, 1988, **92**, 4052.

457. M.M. Folkendt, B.E. Weiss-Lopez and N.S. True, *J. Phys. Chem.*, 1988, **92**, 4859.
458. C. Lemaire and R.L. Armstrong, *J. Chem. Phys.*, 1984, **81**, 1626.
459. C.A. Spring and N.S. True, *J. Magn. Reson.*, 1984, **58**, 338.
460. C.J. Jameson and A.K. Jameson, *J. Chem. Phys.*, 1988, **88**, 7448.
461. C.J. Jameson and A.K. Jameson, *Chem. Phys. Lett.*, 1987, **135**, 254.
462. I. Ursu, M. Bogdan, P. Fitori, A. Darabont and D.E. Demco, *Mol. Phys.*, 1985, **56**, 297.
463. I. Ursu, D.E. Demco, M. Bogdan, P. Fitori and A. Darabont, *J. Physique. Lett.*, 1985, **46**, L493; D.E. Demco, M. Bogdan, P. Fitori, F. Balibanu and A. Darabont, *Rev. Roum. Phys.*, 1988, **33**, 509.
464. N.S. Golubev, A.I. Burshtein and S.I. Temkin, *Chem. Phys. Lett.*, 1982, **91**, 139.
465. C.J. Jameson, A.K. Jameson and N.C. Smith, *J. Chem. Phys.*, 1987, **86**, 6833.
466. M. Bloom and I. Oppenheim, *Adv. Chem. Phys.*, 1967, **12**, 549.
467. H. Van Houten, L.J.F. Hermans and J.J.M. Beenakker, *Physica*, 1985, **131A**, 64.
468. C.J. Jameson, A.K. Jameson and K. Buchi, *J. Chem. Phys.*, 1986, **85**, 697.
469. C.J. Jameson, A.K. Jameson, N.C. Smith and K. Jackowski, *J. Chem. Phys.*, 1987, **86**, 2717.
470. C.P.K. Reddy, K.L. Sarkar and L. Pandey, *J. Magn. Reson.*, 1983, **55**, 177.
471. C.P.K. Reddy and K.L. Sarkar, *J. Chem. Phys.*, 1984, **80**, 3038.
472. D. Brinkmann and D. Kuhn, *Phys. Rev.*, 1980, **A21**, 163.
473. J. Hauer, E.W. Lang and H.-D. Lüdemann, *Chem. Phys.*, 1981, **62**, 195.
474. G. Facey, R.E. Wasylishen, M.J. Collins, C.I. Ratcliffe and J.A. Ripmeester, *J. Phys. Chem.*, 1986, **90**, 2047.
475. R.E. Wasylishen, J.B. Macdonald and J.O. Friedrich, *Can. J. Chem.*, 1984, **62**, 1181.
476. P.W. Atkins, A. Loewenstein and Y. Margalit, *Mol. Phys.*, 1969, **17**, 329.
477. H. Hauer, E.W. Lang and H.-D. Lüdemann, *Ber. Bunsenges. Phys. Chem.*, 1979, **83**, 1262.
478. D.W. Sawyer and J.G. Powles, *Mol. Phys.*, 1971, **21**, 83.
479. A. Allerhand, *J. Chem. Phys.*, 1970, **52**, 3596.
480. A. Briguet, J.C. Duplan and J. Delmau, *Mol. Phys.*, 1980, **39**, 1541.
481. A. Briguet, J.C. Duplan and J. Delmau, *J. Phys.*, 1980, **C13**, L289.
482. S.K. Garg, J.A. Ripmeester and D.W. Davidson, *J. Chem. Phys.*, 1980, **72**, 567.
483. J. Virlet and G. Tantot, *Chem. Phys. Lett.*, 1976, **44**, 296.
484. J.A. Glasel, in *Water. A Comprehensive Treatise*, Vol. 1 (ed. F. Franks), Chap. 6. Plenum Press, New York, 1972.
485. J.C. Hindman, A. Svirmickas and M. Wood, *J. Chem. Phys.*, 1973, **59**, 1517.
486. J.C. Hindman, A.J. Zielen, A. Svirmickas and M. Wood, *J. Phys. Chem.*, 1971, **54**, 621.
487. J.C. Hindman, A. Svirmickas and M. Wood, *J. Phys. Chem.*, 1970, **74**, 1266.
488. N.A. Melnichenko and V.I. Chizhik, *Zh. Strukt. Khim.*, 1981, **22**, 76.
489. V. I. Yashkichev, *Zh. Fiz. Khim.*, 1981, **55**, 709.
490. Y. Lee and J. Jonas, *J. Chem. Phys.*, 1972, **57**, 4233.
491. J. Jonas, T. DeFries and D.J. Wilbur, *J. Chem. Phys.*, 1976, **65**, 582.
492. T. DeFries and J. Jonas, *J. Chem. Phys.*, 1977, **66**, 896.
493. J.C. Hindman, *J. Chem. Phys.*, 1974, **60**, 4488.
494. E. Lang and H.-D. Lüdemann, *J. Chem. Phys.*, 1977, **67**, 718.
495. E. Lang and H.-D. Lüdemann, *Ber. Bunsenges. Phys. Chem.*, 1980, **84**, 462.
496. E.W. Lang and H.-D. Lüdemann, *Ber. Bunsenges. Phys. Chem.*, 1981, **85**, 603.
497. E.W. Lang and H.-D. Lüdemann, *Ber Bunsenges. Phys. Chem.*, 1981, **85**, 1016.
498. H.-D. Lüdemann and E.W. Lang, *J. Physique Colloq.*, 1984, **45**, C7, 41.
499. E.W. Lang, H.-D. Lüdemann and L. Piculell, *J. Chem. Phys.*, 1984, **81**, 3820.
500. P.L. Cummins, G. B. Bacskay, N.S. Hush, B. Halle and S. Engström, *J. Chem. Phys.*, 1985, **82**, 2002.
501. D. Lankhorst, J. Schriever and J.C. Leyte, *Ber. Bunsenges. Phys. Chem.*, 1982, **86**, 215.

502. J.R.C. Van der Maarel, D. Lankhorst, J. de Bleijser and J.C. Leyte, *Chem. Phys. Lett.*, 1985, **122**, 541.
503. C.W.R. Mulder, J. Schriever and J.C. Leyte, *J. Phys. Chem.*, 1983, **87**, 2336.
504. R.P.W.J. Struis, J. de Bleijser and J.C. Leyte, *J. Phys. Chem.*, 1987, **91**, 1639.
505. M. Kakihana, M. Okamoto and T. Nagumo, *Z. Naturforsch.*, 1985, **40a**, 1085.
506. S. Meiboom, *J. Chem. Phys.*, 1961, **34**, 375.
507. H.N. Yeung and A.H. Lent, *Magn. Reson. Med.*, 1987, **5**, 87.
508. W.J. Lamb, D.R. Brown and J. Jonas, *J. Phys. Chem.*, 1981, **85**, 3883.
509. V. Graf, F. Noack and G.J. Béné, *J. Chem. Phys.*, 1980, **72**, 861.
510. D.L. Turner, *Mol. Phys.*, 1980, **40**, 949.
511. B. Halle and G. Karlström, *J. Chem. Soc. Faraday. Trans. 2*, 1983, **79**, 1031.
512. H.G. Hertz, in *Water. A Comprehensive Treatise*, Vol. 3 (ed. F. Franks), Chap. 7. Plenum Press, New York, 1973.
513. M. Holz, *Prog. NMR Spectrosc.*, 1986, **18**, 327.
514. P. Laszlo (ed.), *NMR of Newly Accessible Nuclei*. Academic Press, New York, 1983.
515. E.W. Lang, W. Fink and H.-D. Lüdemann, *J. Physique Colloq.*, 1984, **45**, C7, 173.
516. E.W. Lang and H.-D. Lüdemann, *Ber. Bunsenges. Phys. Chem.*, 1985, **89**, 508.
517. W. Fink and E.W. Lang, *J. Phys. Chem.*, 1988, **92**, 6440.
518. W. Fink, H. Radkowitsch and E.W. Lang, *Chem. Phys.*, 1988, **124**, 239.
519. W. Fink, H. Radkowitsch and E.W. Lang, *Z. Naturforsch.*, 1988, **43a**, 538.
520. E.W. Lang and F.X. Prielmeier, *Ber. Bunsenges. Phys. Chem.*, 1988, **92**, 717.
521. J.R.C. Van der Maarel, D. Lankhorst, J. de Bleijser and J.C. Leyte, *J. Phys. Chem.*, 1986, **90**, 1470.
522. J.R.C. Van der Maarel, H.R.W.M. de Boer, J. de Bleijser, D. Bedeaux and J.C. Leyte, *J. Chem. Phys.*, 1987, **86**, 3373.
523. Y. Nakamura, S. Shimokawa, K. Futamata and M. Shimoji, *J. Chem. Phys.*, 1982, **77**, 3258.
524. J.M. Purcell and H. Pessen, *Anal. Lett.*, 1986, **19**, 1917.
525. H.G. Hertz, H. Versmold and C. Yoon, *Ber. Bunsenges. Phys. Chem.*, 1983, **87**, 577.
526. H.G. Hertz, *Z. Phys. Chem. (Munich)*, 1983, **135**, 89.
527. H.G. Hertz and R. Maurer, *Z. Phys. Chem. (Munich)*, 1983, **135**, 107.
528. P.A. Madden and R.W. Impey, *Ann. NY Acad. Sci.*, 1986, **482**, 91.
529. V.I. Chizhik, V.I. Mikhailov, T.T. Ermolaeva, G.V. Karpenko and T.N. Mayorova, *Zh. Strukt. Khim.*, 1981, **22**, 178.
530. V.I. Chizhik, V.I. Mikhailov and Su Chan Pak, *Vestn. Leningr. Univ. Fiz. Khim.*, 1985, 78; *Teor. Eksp. Khim.*, 1986, **22**, 503.
531. R.P.W.J. Struis, J. de Bleijser and J.C. Leyte, *J. Phys. Chem.*, 1987, **91**, 6309.
532. L. Helm, L. I. Elding and A.E. Merbach, *Inorg. Chem.*, 1985, **24**, 1719.
533. K. Miura, K. Hashimoto, H. Fukui, E. Yamada and S. Shimokawa, *J. Phys. Chem.*, 1985, **89**, 5098.
534. R.K. Mazitov, *Dokl. Akad. Nauk SSSR*, 1981, **260**, 1402; *Radiospektroskopiya*, 1983, **15**, 44 (*Chem. Abstr.*, 1984, 101:82846w).
535. H. Weingärtner, *J. Magn. Reson.*, 1980, **41**, 74.
536. R. Mazitov, K.J. Müller and H.G. Hertz, *Z. Phys. Chem. (Munich)*, 1984, **140**, 55.
537. T. Tokuhiro, *J. Magn. Reson.*, 1988, **76**, 22.
538. M. Holz and A. Sacco, *Z. Phys. Chem. (Munich)*, 1987, **155**, 133.
539. A. Sacco, M. Holz and H.G. Hertz, *J. Magn. Reson.*, 1985, **65**, 82.
540. J. Kunze, A. Ebert, H. Lang and B. Philipp, *Z. Phys. Chem. (Leipzig)*, 1985, **266**, 49.
541. H.G. Hertz and R. Mazitov, *Ber. Bunsenges. Phys. Chem.*, 1981, **85**, 1103.
542. H. Pfister, A. Schwenk and D. Zeller, *J. Magn. Reson.*, 1986, **68**, 138.

543. C.L. Perrin and R.K. Gipe, *J. Am. Chem. Soc.*, 1986, **108**, 1088.
544. L. Helm and H.G. Hertz, *Z. Phys. Chem. (Wiesbaden)*, 1981, **127**, 23.
545. D. Köhnlein, O. Lutz and P. Ruppert, *J. Magn. Reson.*, 1984, **57**, 486.
546. G.R. Hays, D.G. Gillies, L.P. Blaauw and A.D.H. Clague, *J. Magn. Reson.*, 1981, **45**, 102.
547. Ö. Gröning, T. Drakenberg and L.I. Elding, *Inorg. Chem.*, 1982, **21**, 1820.
548. J. Kodweiss, D. Köhnlein, G. Kössler, O. Lutz, W. Messner, K.R. Mohn, A. Nolle, G. Nothaft, P. Ruppert, N. Steinhauser, D. Zepf, E. Haid and W. Schich, *Z. Naturforsch.* 1986, **41a**, 471.
549. V.P. Tarasov, V.I. Privalov and Yu A. Buslaev, *Zh. Strukt. Khim.*, 1981, **22**, 64.
550. A. Takahashi, *J. Phys. Soc. Jpn*, 1980, **48**, 1049.
551. J.W. Akitt, J.A. Farnsworth and P. Letellier, *J. Chem. Soc. Faraday Trans. 1*, 1985, **81**, 193.
552. J.W. Akitt and J.M. Elders, *J. Chem. Soc. Faraday Trans. 1*, 1985, **81**, 1923.
553. J.W. Akitt, W. Gessner and M. Weinberger, *Magn. Reson. Chem.*, 1988, **26**, 1047.
554. O. Lutz and H. Oehler, *J. Magn. Reson.*, 1980, **37**, 261.
555. A. Schwenk, *J. Magn. Reson.*, 1980, **37**, 551.
556. E. Haid, D. Köhnlein, G. Kössler, O. Lutz, W. Messner, K.R. Mohn, G. Nothaft, B. van Rickelen, W. Schich and N. Steinhauser, *Z. Naturforsch.*, 1983, **38a**, 317.
557. G. Navon, *J. Phys. Chem.*, 1981, **85**, 3547.
558. K.J. Müller and H.G. Hertz, *Z. Phys. Chem. (Munich)*, 1984, **140**, 31.
559. R. Ahlrichs, H.-J. Böhm, H.G. Hertz and K.J. Müller, *Z. Phys. Chem. (Munich)*, 1984, **142**, 67.
560. M. Yudasaka, T. Sugawara, H. Iwamura and T. Fujiyama, *Bull. Chem. Soc. Jpn*, 1981, **54**, 1933.
561. N. Soffer and Y. Marcus, *Ber. Bunsenges. Phys. Chem.*, 1982, **86**, 72.
562. R.E. Wasylishen, W. Danchura and K. Marat, *J. Magn. Reson.*, 1980, **40**, 221.
563. A.M. de P. Nicholas and R.E. Wasylishen, *Can. J. Chem.*, 1986, **64**, 1839.
564. A. Loewenstein, *J. Magn. Reson.*, 1982, **49**, 332.
565. A.M. de P. Nicholas and R.E. Wasylishen, *J. Phys. Chem.*, 1985, **89**, 5446.
566. A.M. de P. Nicholas and R.E. Wasylishen, *Can. J. Chem.*, 1987, **65**, 951.
567. A. Adachi, H. Kiyoyama, M. Nakahara, Y. Masuda, H. Yamatera, A. Shimizu, and Y. Taniguchi, *J. Chem. Phys.*, 1989, **90**, 392.
568. D.C. McCain, *J. Magn. Reson.*, 1986, **69**, 128.
569. Y. Masuda, M. Sano and H. Yamatera, *J. Phys. Chem.*, 1985, **89**, 3086.
570. Y. Masuda, M. Sano, and H. Yamatera, *J. Chem. Soc. Faraday Trans. 1*, 1985, **81**, 127.
571. Y. Masuda and H. Yamatera, *Chem. Lett.*, 1988, 171.
572. M. Nakahara and K. Ibuki, *J. Chem. Phys.*, 1986, **85**, 4654.
573. K. Ibuki and M. Nakahara, *J. Chem. Phys.*, 1989, **90**, 386.
574. A.G. Miller, J.A. Franz and J.W. Macklin, *J. Phys. Chem.*, 1985, **89**, 1190.
575. D.W. James and P.G. Cutler, *Aust. J. Chem.*, 1986, **39**, 137.
576. J.F. Hinton and D. Shungu, *J. Magn. Reson.*, 1983, **54**, 309.
577. P.S. Belton, I.J. Cox and R.K. Harris, *Magn. Reson. Chem.*, 1986, **24**, 171.
578. D.C. McCain and J.L. Markley, *J. Am. Chem. Soc.*, 1980, **102**, 5559.
579. J.F. Hinton and D. Buster, *J. Magn. Reson.*, 1984, **58**, 324.
580. Jinxi Wang, Rongsan Chen, Yan Mao, Chongde Li, Jinhua Wei, Haicheng Liu and Anpang Tai, *Huaxue Xuebao*, 1984, **42**, 308 (*Chem. Abstr.*, 1984, 100:220422n).
581. S.D. Kinrade and T.W. Swaddle, *J. Chem. Soc. Chem. Commun.*, 1986, 120; *Inorg. Chem.*, 1988, **27**, 4259.
582. S.D. Kinrade and T.W. Swaddle, *J. Am. Chem. Soc.*, 1986, **108**, 7159.
583. C.T.G. Knight and R.K. Harris, *Magn. Reson. Chem.*, 1986, **24**, 872.

584. R. Balz, U. Brändle, E. Kammerer, D. Köhnlein, O. Lutz, A. Nolle, R. Schafitel and E. Veil, *Z. Naturforsch.*, 1986, **41a**, 737.
585. J.J. Dechter, *Prog. Inorg. Chem.*, 1982, **29**, 285.
586. C. Detellier and P. Laszlo, *Proc. Ind. Acad. Sci. Chem. Sci.*, 1985, **94**, 291.
587. T. Drakenberg, in *Annual Reports on NMR Spectroscopy*, Vol. 17 (ed. G.A. Webb), p. 231. Academic Press, London, 1986.
588. H. Weingärtner and H.G. Hertz, *Ber. Bunsenges. Phys. Chem.*, 1977, **81**, 1204.
589. K. Uchibayashi, M. Niibe, and Y. Nakamura, *J. Chem. Engng Data*, 1985, **30**, 214.
590. I. Birkel and H.G. Hertz, *J. Chem. Soc. Faraday Trans. 1*, 1981, **77**, 2315.
591. R.E.S. Hofmann and M. Holz, *Chem. Phys. Lett.*, 1987, **142**, 492.
592. H. Weingärtner, *J. Chem. Soc. Faraday Trans. 1*, 1982, **78**, 3063.
593. H. Weingärtner, *Z. Phys. Chem. (Wiesbaden)*, 1982, **130**, 23.
594. C. Detellier and A. Gerstmans, *Inorg. Chim. Acta*, 1982, **65**, L157.
595. A.I. Mishustin, *Zh. Fiz. Khim.*, 1986, **60**, 336; *Ibid.*, 1986, **60**, 341.
596. V.N. Plakhotnik, N.F. Tovmash, A.I. Mishustin, V.B. Tulchinskii and E. Ya. Ivankova, *Koord. Khim.*, 1987, **13**, 447.
597. A.I. Mishustin and A.I. Podkovyrin, *Zh. Fiz. Khim.*, 1983, **57**, 101.
598. A.I. Mishustin and A.I. Podkovyrin, *Khim. Fiz.*, 1987, **6**, 60.
599. M.S. Ansari and H.G. Hertz, *J. Solution Chem.*, 1984, **13**, 877.
600. M.S. Ansari and H.G. Hertz, *Z. Phys. Chem. (Munich)*, 1985, **146**, 15.
601. J.B. Lambert and S. Vlasak Simpson, *Magn. Reson. Chem.*, 1985, **23**, 61.
602. J. Saint Germain and M. Vincendon, *Org. Magn. Reson.*, 1983, **21**, 371.
603. B.M. Braun and M. Holz, *Z. Phys. Chem. (Munich)*, 1983, **135**, 77.
604. B.M. Braun and M. Holz, *J. Solution Chem.*, 1983, **12**, 685.
605. Yining Huang, Zhifen Li and Ruilin Liu, *Wuli Huaxue Xuebao*, 1986, **2**, 133 (*Chem. Abstr.*, 1986, 105:85997q).
606. M. Holz, *J. Chem. Soc. Faraday Trans. 1*, 1978, **74**, 644.
607. M. Holz and C. Rau, *J. Chem. Soc. Faraday Trans. 1*, 1982, **78**, 1899.
608. M. Holz and A. Sacco, *Mol. Phys.*, 1985, **54**, 149.
609. C.K. Finter and H.G. Hertz, *Z. Phys. Chem. (Munich)*, 1986, **148**, 75.
610. C.K. Finter and H.G. Hertz, *J. Chem. Soc. Faraday Trans. 1*, 1988, **84**, 2735.
611. K.-D. Merboldt and J. Frahm, *Ber. Bunsenges. Phys. Chem.*, 1986, **90**, 614.
612. M. Yudasaka, T. Sugawara, H. Iwamura and T. Fujiyama, *Bull. Chem. Soc. Jpn*, 1982, **55**, 311.
613. T.C. Farrar and R.A. Quintero-Arcaya, *J. Phys. Chem.*, 1987, **91**, 3224.
614. T.C. Farrar, R.A. Quintero-Arcaya and I.C. Locker, *Z. Phys. Chem. (Munich)*, 1987, **151**, 25.
615. A. Delville, C. Detellier, A. Gerstmans and P. Laszlo, *J. Magn. Reson.*, 1981, **42**, 14.
616. S. Chalais, A. Delville, C. Detellier, A. Gerstmans and P. Laszlo, *J. Solution Chem.*, 1983, **12**, 33.
617. A.I. Mishustin, A.I. Podkovyrin and Yu.M. Kessler, *Koord. Khim.*, 1980, **6**, 236.
618. A.I. Mishustin, *Zh. Fiz. Khim.*, 1982, **56**, 1887; *Ibid.*, 1983, **57**, 2757; *Dokl. Adak. Nauk SSSR*, 1983, **268**, 641.
619. A.I. Podkovyrin, A.I. Mishustin and Yu.M. Kessler, *Zh. Strukt. Khim.*, 1983, **24**, 59.
620. A.I. Mishustin, *Zh. Fiz. Khim.*, 1983, **57**, 1486; *Ibid.*, 1985, **59**, 1021.
621. A.I. Mishustin and V.I. Egert, *Zh. Fiz. Khim.*, 1986, **60**, 2343.
622. A.I. Mishustin, V.I. Plakhotnik and N.F. Tovmash, *Zh Fiz. Khim.*, 1986, **60**, 875.
623. A.I. Podkovyrin and A.I. Mishustin, *Zh. Fiz. Khim.*, 1986, **60**, 1166.
624. A.I. Mishustin, V.A. Mozalevskaya and V.P. Ponkratov, *Zh. Fiz. Khim.*, 1986, **60**, 2948; *Ibid.*, 1987, **61**, 2810.

625. A.I. Mishustin and A.I. Kryglyak, *Zh. Obshch. Khim.*, 1987, **57**, 1806.
626. R.K. Mazitov, L.S. Itkina, E.V. Petrova and K.A. Nadzharyan, *Zh. Neorg. Khim.*, 1980, **25**, 1200.
627. D.S.B. Grace and J. Krane, *Acta Chem. Scand.*, 1982, **A36**, 235.
628. U. Olsher, G.A. Elgavish and J. Jagur-Grodzinski, *J. Am. Chem. Soc.*, 1980, **102**, 3338.
629. J.J.C. van Lier, L.J.M. van de Ven, J.W. de Haan and H.M. Buck, *J. Phys. Chem.*, 1983, **87**, 3501.
630. H. Nöth, R. Rurländer and P. Wolfgardt, *Z. Naturforsch.*, 1980, **35b**, 31.
631. L.M. Jackman and J.C. Trewella, *J. Am. Chem. Soc.*, 1976, **98**, 5712.
632. L.M. Jackman and L.M. Scarmoutzos, *J. Am. Chem. Soc.*, 1984, **106**, 4627.
633. L.M. Jackman and C.W. DeBrosse, *J. Am. Chem. Soc.*, 1983, **105**, 4177.
634. L.M. Jackman and B.D. Smith, *J. Am. Chem. Soc.*, 1988, **110**, 3829.
635. L.M. Jackman, L.M. Scarmoutzos, and C.W. DeBrosse, *J. Am. Chem. Soc.*, 1987, **109**, 5355.
636. L.M. Jackman, L.M. Scarmoutzos, B.D. Smith and P.G. Williard, *J. Am. Chem. Soc.*, 1988, **110**, 6058.
637. Jing Quan Wen and J.B. Grutzner, *J. Org. Chem.*, 1986, **51**, 4220.
638. S. Koda and H. Nomura, *J. Solution Chem.*, 1985, **14**, 355.
639. H. Uedaira and H. Uedaira, *Nippon Kagaku Kaishi*, 1986, 1265 (*Chem. Abstr.*, 1987, 106:56654r).
640. L. Baltzer and E.D. Becker, *J. Am. Chem. Soc.*, 1983, **105**, 5730.
641. Y.-L. Pascal, O. Convert and Y. Ahomadegbe, *J. Chim. Phys.*, 1981, **78**, 771.
642. J.L. Gray and G.E. Maciel, *J. Phys. Chem.*, 1983, **87**, 5290; *Ibid.*, 1983, **87**, 5418.
643. J.H. Medley, E.S. Mooberry and M.C. Day, *Can J. Chem.*, 1983, **61**, 558.
644. L. Lerner and D.A. Torchia, *J. Am. Chem. Soc.*, 1986, **108**, 4264.
645. E. Amat, B.G. Cox, J. Rzeszotarska and H. Schneider, *J. Am. Chem. Soc.*, 1988, **110**, 3368.
646. J. Grandjean, P. Laszlo, W. Offermann and P.L. Rinaldi, *J. Am. Chem. Soc.*, 1981, **103**, 1380.
647. B.O. Strasser and A.I. Popov, *J. Am. Chem. Soc.*, 1985, **107**, 7921.
648. R.C. Phillips, S. Khazaeli and J.L. Dye, *J. Phys. Chem.*, 1985, **89**, 600.
649. H.D.H. Stöver, A. Delville and C. Detellier, *J. Am. Chem. Soc.*, 1985, **107**, 4167.
650. A. Delville, H.D.H. Stöver and C. Detellier, *J. Am. Chem. Soc.*, 1985, **107**, 4172.
651. H.D.H. Stöver, L.J. Maurice, A. Delville and C. Detellier, *Polyhedron*, 1985, **4**, 1091.
652. H.D.H. Stöver, M. Robillard, and C. Detellier, *Polyhedron*, 1987, **6**, 577.
653. E. Amat, B.G. Cox, and H. Schneider, *J. Magn. Reson.*, 1987, **71**, 259
654. H. Strehlow and J. Frahm, *Ber. Bunsenges. Phys. Chem.*, 1975, **79**, 57.
655. J.B. Lambert and J.W. Keepers, *J. Magn. Reson.*, 1980, **38**, 233.
656. S. Khazaeli, J.L. Dye and A.I. Popov, *Spectrochim. Acta*, 1983, **39A**, 19.
657. D.M. Holton, A. Ellaboudy, N.C. Pyper and P.P. Edwards, *J. Chem. Phys.*, 1986, **84**, 1089.
658. A.S. Ellaboudy, D.M. Holton, N.C. Pyper, P.P. Edwards, B. Wood and W. McFarlane, *Nature*, 1986, **321**, 684.
659. P.P. Edwards, A.S. Ellaboudy and D.M. Holton, *Nature*, 1985, **317**, 242.
660. P.P. Edwards, A.S. Ellaboudy, D.M. Holton and N.C. Pyper, in *Annual Reports on NMR Spectroscopy*, Vol. 20 (ed. G.A. Webb), p. 315. Academic Press, London, 1988.
661. A.I. Popov, A.J. Smetana, J.-P. Kintzinger and Thi Thanh-Tam Nguyen, *Helv. Chim. Acta*, 1980, **63**, 668.
662. E. Schmidt, J.-M. Tremillon, J.-P. Kintzinger and A.I. Popov, *J. Am. Chem. Soc.*, 1983, **105**, 7563.
663. H.D. Durst, L. Echegoyen, G.W. Gokel and A. Kaifer, *Tetrahedron Lett.*, 1982, **23**, 4449.

664. L. Echegoyen, A. Kaifer, H.D. Durst and G.W. Gokel, *J. Org. Chem.*, 1984, **49**, 688.
665. A. Kaifer, H.D. Durst, L. Echegoyen, D.M. Dishong, R.A. Schultz and G.W. Gokel, *J. Org. Chem.*, 1982, **47**, 3195.
666. L. Echegoyen, A. Kaifer, H. Durst, R.A. Schultz, D.M. Dishong, D.M. Goli and G.W. Gokel, *J. Am. Chem. Soc.*, 1984, **106**, 5100.
667. G.W. Buchanan, K. Bourque, G.K. Diedrich and M.Z. Khan, *Magn. Reson. Chem.*, 1987, **25**, 65.
668. C. Erk, *Spectrosc. Lett.*, 1986, **19**, 1175.
669. M. Bisnaire, C. Detellier and D. Nadon, *Can. J. Chem.*, 1982, **60**, 3071.
670. H. Saito and R. Tabeka, *Bull. Chem. Soc. Jpn*, 1987, **60**, 61.
671. K.J. Neurohr, T. Drakenberg, S. Forsén and H. Lilja, *J. Magn. Reson.*, 1983, **51**, 460.
672. C. Detellier and M. Robillard, *Can. J. Chem.*, 1987, **65**, 1684.
673. B. Eliasson, K.M. Larsson and J. Kowalewski, *J. Phys. Chem.*, 1985, **89**, 258.
674. T. Sugawara, M. Yudasaka, Y. Yokoyama, T. Fujiyama and H. Iwamura, *J. Phys. Chem.*, 1982, **86**, 2705.
675. D.W. James and P.G. Cutler, *Aust. J. Chem.*, 1986, **39**, 149.
676. L. Echegoyen, I. Nieves, J. Thompson, F. Rosa and R. Concepcion, *J. Phys. Chem.*, 1981, **85**, 3697.
677. J. Frahm, *Ber. Bunsenges. Phys. Chem.*, 1980, **84**, 754.
678. J. Frahm, *J. Phys. Chem.*, 1980, **84**, 1393.
679. J. Kowalewski and A. Maliniak, *J. Magn. Reson.*, 1985, **62**, 316.
680. F. Wehrli, *J. Magn. Reson.*, 1978, **30**, 193.
681. L.S. Koehler, F. Jarnagin, R.G. Hiskey, L.G. Pedersen and K.A. Koehler, *J. Inorg. Biochem.*, 1987, **29**, 153.
682. T. Drakenberg, *Acta Chem. Scand.*, 1982, **A36**, 79.
683. J. Huet and A. Gaudemer, *Org. Magn. Reson.*, 1981, **15**, 347.
684. A.R. Siedle, in *Annual Reports on NMR Spectroscopy*, Vol. 12 (ed. G.A. Webb), p. 177. Academic Press, London, 1982; *Ibid.*, Vol. 20, p. 205, 1988.
685. J.W. Akitt, *Prog. NMR Spectrosc.*, 1989, **21**, 1.
686. J.F. Hinton, K.R. Metz and R.W. Briggs, *Prog. NMR Spectrosc.*, 1988, **20**, 423.
687. W. Koch, I. Wawer, and H.G. Hertz, *Z. Phys. Chem. (Wiesbaden)*, 1982, **132**, 161.
688. J.W. Akitt and L. Lelievre, *J. Chem. Soc. Dalton Trans.*, 1985, 591.
689. F.W. Wehrli and S. Wehrli, *J. Magn. Reson.*, 1981, **44**, 197.
690. J.B. Sloan, S.A. Cannon, E.C. Delionback and J.J. Dechter, *Inorg. Chem.*, 1985, **24**, 883.
691. J.M. Garrison and A.L. Crumbliss, *Inorg. Chem.*, 1988, **27**, 3058.
692. V.P. Tarasov, V.I. Privalov, G.A. Kirakosyan and Yu. A. Buslaev, *Z. Naturforsch.*, 1983, **38b**, 1173.
693. B.R. McGarvey, M.J. Taylor and D.G. Tuck, *Inorg. Chem.*, 1981, **20**, 2010.
694. B.R. McGarvey, C. Owens Trudell, D.G. Tuck and L. Victoriano, *Inorg. Chem.*, 1980, **19**, 3432.
695. R. Colton, D. Dakternieks and J. Hauenstein, *Aust. J. Chem.*, 1981, **34**, 949.
696. J.J. Dechter, U. Henriksson, J. Kowalewski and A.-C. Nilsson, *J. Magn. Reson.*, 1982, **48**, 503.
697. J.W. Akitt, *J. Chem. Soc. Faraday Trans. 2*, 1986, **82**, 377.
698. A.R. Thompson, A.C. Kunwar, H.S. Gutowsky and E. Oldfield, *J. Chem. Soc. Dalton Trans.*, 1987, 2317.
699. T.C. Gibb and J.D. Kennedy, *J. Chem. Soc. Faraday Trans. 2*, 1982, **78**, 525.
700. V.I. Privalov, V.P. Tarasov, M.A. Meladze, D.M. Vinitskii, K.A. Solntsev, Yu.A. Buslaev and N.T. Kuznetsov, *Zh. Neorg. Khim.*, 1986, **31**, 1113.
701. V.P. Tarasov, V. I. Privalov, A.A. Gorbik and S.I. Bakum, *Koord. Khim.*, 1985, **11**, 1626.
702. U. Vestin, J. Kowalewski and U. Henriksson, *Org. Magn. Reson.*, 1981, **16**, 119.

703. M.C. Day, J.H. Medley and N. Ahmad, *Can. J. Chem.*, 1983, **61**, 1719.
704. J.H. Medley, N. Ahmad and M.C. Day, *Can. J. Chem.*, 1985, **63**, 2906.
705. F. Brady, R.W. Matthews, M.J. Forster and D.G. Gillies, *Inorg. Nucl. Chem. Lett.*, 1981, **17**, 155; *J. Chem. Soc. Chem. Commun.*, 1981, 911.
706. M.J. Forster, D.G. Gillies and R.W. Matthews, *Mol. Phys.*, 1987, **60**, 129.
707. M.J. Forster and D.G. Gillies, *Mol. Phys.*, 1987, **62**, 439.
708. R.W. Briggs, F.A. Etzkorn and J.F. Hinton, *J. Magn. Reson.*, 1980, **37**, 523.
709. A.L. Wilkins, P.J. Watkinson and K.M. Mackay, *J. Chem. Soc. Dalton Trans.*, 1987, 2365.
710. V.P. Tarasov, V.I. Privalov, S.G. Drobyshev and Yu. A. Buslaev, *Dokl. Akad. Nauk SSSR*, 1983, **272**, 1176.
711. T. Harazono, K. Tanaka, Y. Takeuchi and N. Kakimoto, *Chem. Lett.*, 1986, 1841.
712. T. Harazono, K. Tanaka, Y. Takeuchi and H. Fukutomi, *Inorg. Chem.*, 1987, **26**, 3851.
713. I.P. Sekacis, E.E. Liepinsh, I.A. Zicmane and E. Lukevic, *Zh. Obshch. Khim.*, 1983, **53**, 2064.
714. Y. Takeuchi, T. Harazono and N. Kakimoto, *Inorg. Chem.*, 1984, **23**, 3835.
715. B. Wrackmayer, in *Annual Reports on NMR Spectroscopy*, Vol. 16 (ed. G.A. Webb), p. 73, Academic Press, London, 1985.
716. S.J. Blunden, A. Frangou and D.G. Gillies, *Org. Magn. Reson.*, 1982, **20**, 170.
717. T. Birchall and V. Manivannan, *Can. J. Chem.*, 1985, **63**, 2211.
718. D.E. Axelson, C.E. Holloway and C.P.J. Vuik, *Org. Magn. Reson.*, 1980, **14**, 220.
719. V.A. Daragan, I.V. Edneral and E.E. Ilina, *Zh. Fiz. Khim.*, 1983, **57**, 1707.
720. K. Morgan, B.G. Sayer and G. Schrobilgen, *J. Magn. Reson.*, 1983, **52**, 139.
721. G.C. Pappalardo, A. Grassi, M. Baldo, L. Radics, A. Forchioni and K.J. Irgolic, *Chem. Phys.*, 1986, **109**, 125.
722. H.J. Jakobsen, A.J. Zozulin, P.D. Ellis and J.D. Odom, *J. Magn. Reson.*, 1980, **38**, 219.
723. E.W. Abel, K.G. Orrell and A.W.G. Platt, *Org. Magn. Reson.*, 1983, **21**, 196.
724. T.C. Wong, T.T. Ang, F.S. Guziec and C.A. Moustakis, *J. Magn. Reson.*, 1984, **57**, 463.
725. P. Granger and S. Chapelle, *J. Magn. Reson.*, 1980, **39**, 329.
726. S. Chapelle and P. Granger, *Mol. Phys.*, 1981, **44**, 459.
727. P. Granger, S. Chapelle, W.R. McWhinnie and A. Al-Rubaie, *J. Organomet. Chem.*, 1981, **220**, 149.
728. J.J. Dechter, *Prog. Inorg. Chem.*, 1985, **33**, 393.
729. U. Ochsenbein and C.W. Schläpfer, *Helv. Chim. Acta*, 1980, **63**, 1926.
730. P. Kroneck, O. Lutz, A. Nolle and H. Oehler, *Z. Naturforsch.*, 1980, **35a**, 221.
731. A. Marker and M.J. Gunter, *J. Magn. Reson.*, 1982, **47**, 118.
732. J. Kronenbitter, U. Schweizer and A. Schwenk, *Z. Naturforsch.*, 1980, **35a**, 319.
733. S. Jans-Bürli and P.S. Pregosin, *Magn. Reson. Chem.*, 1985, **23**, 198.
734. Zhi-fen Li and A.I. Popov, *J. Solution Chem.*, 1982, **11**, 17.
735. T. Shimizu, M. Kodaka and M. Hatano, *Biochem. Biophys. Res. Commun.*, 1982, **106**, 988.
736. M. Kodata, T. Shimizu and M. Hatano, *Inorg. Chim. Acta*, 1983, **78**, L55.
737. T. Shimizu and M. Hatano, *Inorg. Chim. Acta*, 1983, **76**, L177.
738. G.K. Carson and P.A.W. Dean, *Inorg. Chim. Acta*, 1982, **66**, 157.
739. B.P. Bammel and R.F. Evilia, *Inorg. Chem.*, 1984, **23**, 1574.
740. C.F. Jensen, S. Deshmukh, H.J. Jakobsen, R.R. Inners and P.D. Ellis, *J. Am. Chem. Soc.*, 1981, **103**, 3659.
741. P.D. Ellis, R.I. Inners and H.J. Jakobsen, *J. Phys. Chem.*, 1982, **86**, 1506.
742. C.C. Bryden and C.N. Reilley, *J. Am. Chem. Soc.*, 1982, **104**, 2697.
743. J.J. Dechter, O.R. Polanco and J. Kowalewski, *J. Magn. Reson.*, 1985, **65**, 395.
744. A.D. Keller, T. Drakenberg, R.W. Briggs and I.M. Armitage, *Inorg. Chem.*, 1985, **24**, 1170.
745. M. Casu, A. Lai and G. Saba, *Chem. Phys.*, 1986, **109**, 301.

746. L. Radics and M. Kajtar-Peredy, *J. Chem. Soc. Perkin Trans. 2*, 1986, 1471.
747. Yu. G. Vlasov and P.P. Antonov, *Izv. Vyssh. Uchebn. Zaved. Khim. Khim. Tekhnol.*, 1984, **27**, 755 (*Chem. Abstr.*, 1984, 101:117633d).
748. D.G. Gillies, L.P. Blaauw, G.R. Hays, R. Huis and A.D.H. Clague, *J. Magn. Reson.*, 1981, **42**, 420.
749. R.L. Bain, *J. Inorg. Nucl. Chem.*, 1981, **43**, 2481.
750. R.E. Wasylishen, R.E. Lenkinski and C. Rodger, *Can. J. Chem.*, 1982, **60**, 2113.
751. R.D. Thomas and K.E. Rowland, *Magn. Reson. Chem.*, 1988, **26**, 111.
752. D. Rehder and M. Speh, *Inorg. Chim. Acta*, 1987, **135**, 73.
753. G.C. Levy, P.L. Rinaldi and J.T. Bailey, *J. Magn. Reson.*, 1980, **40**, 167.
754. D.F. Evans and P.H. Missen, *J. Chem. Soc. Dalton Trans.*, 1982, 1929.
755. C.F.G.C. Geraldes and A.D. Sherry, *J. Magn. Reson.*, 1986, **66**, 274.
756. E. Brücher, J. Glaser, I. Grenthe and I. Puigdomenech, *Inorg. Chim. Acta*, 1985, **109**, 111.
757. I. Ursu, D.E. Demco, M. Bogdan, A. Darabont, P. Fitori, R. Grosescu and N. Valcu, *Rev. Roum. Phys.*, 1982, **27**, 451.
758. I. Ursu, M. Bogdan, P. Fitori, F. Balibanu and D.E. Demco, *Rev. Roum. Phys.*, 1987, **32**, 383.
759. I. Ursu, M. Bogdan, P. Fitori, F. Balibanu and D.E. Demco, *Mol. Phys.*, 1987, **62**, 793.
760. Woo-Sik Jung, H. Tomayasu and H. Fukutomi, *Bull. Chem. Soc. Jpn*, 1987, **60**, 489.
761. N. Hao, B.G. Sayer, G. Denes, D.G. Bickley, C. Detellier and M.J. McGlinchey, *J. Magn. Reson.*, 1982, **50**, 50.
762. B.G. Sayer, N. Hao, G. Denes, D.G. Bickley and M.J. McGlinchey, *Inorg. Chim. Acta*, 1981, **48**, 53.
763. M.A. Habayeb and O.E. Hileman, *Can. J. Chem.*, 1980, **58**, 2115.
764. V.P. Tarasov, V.I. Privalov, A.A. Gorbik and Yu. A. Buslaev, *Dokl. Akad. Nauk SSSR*, 1981, **257**, 678.
765. O. Lutz, W. Messner, K.R. Mohn and P. Kroneck, *Z. Phys.* 1981, **A300**, 111.
766. R.T.C. Brownlee and B.P. Shehan, *J. Magn. Reson.*, 1986, **66**, 503.
767. V.P. Tarasov, V.I. Privalov and Yu. A. Buslaev, *Mol. Phys.*, 1983, **50**, 1141.
768. V.P. Tarasov, V.I. Privalov and Yu A. Buslaev, *Dokl. Akad. Nauk SSSR*, 1983, **269**, 640.
769. E. Haid, D. Köhnlein, G. Kössler, O. Lutz and W. Schich, *J. Magn. Reson.*, 1983, **55**, 145.
770. M.A. Habayeb and O.E. Hileman, *Can. J. Chem.*, 1980, **58**, 2255.
771. C.J. Besecker, W.G. Klemperer, D.J. Maltbie and D.A. Wright, *Inorg. Chem.*, 1985, **24**, 1027.
772. P.J. Domaille, *J. Am. Chem. Soc.*, 1984, **106**, 7677.
773. D. Rehder and W. Basler, *J. Magn. Reson.*, 1986, **68**, 157.
774. M.A. Freeman, F.A. Schultz and C.N. Reilley, *Inorg. Chem.*, 1982, **21**, 567.
775. C.G. Young and J.H. Enemark, *Inorg. Chem.*, 1985, **24**, 4416.
776. S.F. Gheller, M. Sidney, A.F. Masters, R.T.C. Brownlee, M.J. O'Connor and A.G. Wedd, *Aust. J. Chem.*, 1984, **37**, 1825.
777. P. Kroneck, O. Lutz and A. Nolle, *Z. Naturforsch.*, 1980, **35a**, 226.
778. P.S. Belton, I.J. Cox and R.K. Harris, *J. Chem. Soc. Faraday Trans. 2*, 1985, **81**, 63.
779. A. Hafner, L.S. Hegedus, G. de Weck, B. Hawkins and K.H. Dötz, *J. Am. Chem. Soc.*, 1988, **110**, 8413.
780. E. Haslinger and W. Robien, *J. Am. Chem. Soc.*, 1980, **102**, 1237.
781. R.T.C. Brownlee, M.J. O'Connor, B.P. Shehan and A.G. Wedd, *J. Magn. Reson.*, 1985, **61**, 22.
782. R.T.C. Brownlee, M.J. O'Connor, B.P. Shehan and A.G. Wedd, *J. Magn. Reson.*, 1985, **61**, 516.
783. B.P. Shehan, M. Kony, R.T.C. Brownlee, M.J. O'Connor and A.G. Wedd, *J. Magn. Reson.*, 1985, **63**, 343.

784. R.T.C. Brownlee, M.J. O'Connor, B.P. Shehan and A.G. Wedd, *J. Magn. Reson.*, 1985, **64**, 142.
785. S. Donovan-Mtunzi, C.J. MacDonald, R.L. Richards, G.E. Hawkes and J. Mason, *J. Chem. Soc. Dalton Trans.*, 1985, 2473.
786. R.H. Crabtree, B.E. Segmuller and R.J. Uriarte, *Inorg. Chem.*, 1985, **24**, 1949.
787. R.H. Crabtree, D. Hamilton and M. Lavin, *ACS Symp. Ser.*, 1987, **357**, 223.
788. D.G. Hamilton and R.H. Crabtree, *J. Am. Chem. Soc.*, 1988, **110**, 4126.
789. M.J. Buckingham, G.E. Hawkes and J.R. Thornback, *Inorg. Chim. Acta*, 1981, **56**, L41.
790. V.P. Tarasov, V.I. Privalov and Yu. A. Buslaev, *Dokl. Akad. Nauk SSSR*, 1982, **262**, 1433.
791. R.G. Kidd, *J. Magn. Reson.*, 1981, **45**, 88.
792. T.C. Farrar and G.R. Quinting, *J. Phys. Chem.*, 1986, **90**, 2834.
793. S. Aime, R. Gobetto, D. Osella, L. Milone, G.E. Hawkes and E.W. Randall, *J. Chem. Soc. Chem. Commun.*, 1983, 794.
794. K.J. Franklin, C.J.L. Lock, B.G. Sayer and G.J. Schrobilgen, *J. Am. Chem. Soc.*, 1982, **104**, 5303.
795. T. Nozawa, M. Hatano, M. Sato, Y. Toida and E. Batholdi, *Bull Chem. Soc. Jpn*, 1983, **56**, 3837.
796. L. Baltzer, E.D. Becker, B.A. Averill, J.M. Hutchinson and O.A. Gansow, *J. Am. Chem. Soc.*, 1984, **106**, 2444.
797. A. Hafner, W. von Philipsborn and A. Schwenk, *J. Magn. Reson.*, 1987, **74**, 433.
798. S. Aime, R. Gobetto, D. Osella, G.E. Hawkes and E.W. Randall, *J. Chem. Soc. Dalton Trans.*, 1984, 1863.
799. S. Aime, M. Botta, R. Gobetto, D. Osella, *J. Chem. Soc. Dalton Trans.*, 1988, 791.
800. G.E. Hawkes, E.W. Randall, S. Aime and R. Gobetto, *J. Magn. Reson.*, 1986, **68**, 597.
801. S. Aime and E. Occhiello, *J. Chem. Soc. Dalton Trans.*, 1986, 1863.
802. B.E.Mann, C.M. Spencer, B.F. Taylor and P. Yavari, *J. Chem. Soc. Dalton Trans.*, 1984, 2027.
803. D.M. Appel. A.S.F. Boyd, I.W. Robertson, D.M. Roundhill and T.A. Stephenson, *Inorg. Chem.*, 1982, **21**, 449.
804. R.H. Crabtree and D.G. Hamilton, *J. Am. Chem. Soc.*, 1986, **108**, 3124.
805. M.T. Bautista, K.A. Earl, P.A. Maltby, R.H. Morris, C.T. Schweitzer and A. Sella, *J. Am. Chem. Soc.*, 1988, **110**, 7031.
806. S. Aime, M. Botta, R. Gobetto and D. Osella, *Inorg. Chem.*, 1987, **26**, 2551.
807. S.R. Drake, B.F.G. Johnson and J Lewis, *J. Organomet. Chem.*, 1988, **346**, 105.
808. C. Ammann, F. Isaia and P.S. Pregosin, *Magn. Reson. Chem.*, 1988, **26**, 236.
809. D.G. VanderVelde, J.S. Holmgren and J.R. Shapley, *Inorg. Chem.*, 1987, **26**, 3077.
810. C. Brevard and P. Granger, *J. Chem. Phys.*, 1981, **75**, 4175.
811. R.W. Dykstra and A.M. Harrison, *J. Magn. Reson.*, 1982, **46**, 338.
812. Y. Masuda and H. Yamatera, *J. Phys. Chem.*, 1984, **88**, 3425.
813. V.P. Chacko and R.G. Bryant, *J. Magn. Reson.*, 1984, **57**, 79.
814. D.R. Eaton, R.J. Buist and C.V. Rogerson, *Can. J. Chem.*, 1983, **61**, 1524.
815. D.R. Eaton, C.V. Rogerson and A.C. Sandercock, *J. Phys. Chem.*, 1982, **86**, 1365.
816. R.B. Jordan, *J. Magn. Reson.*, 1980, **38**, 267.
817. A. Yamasaki, Y. Miyakoshi, M. Fujita, Y. Yoshikawa and H. Yamatera, *J. Inorg. Nucl. Chem.*, 1979, **41**, 473.
818. J.G. Russell and R.G. Bryant, *J. Phys. Chem.*, 1984, **88**, 4298.
819. R.J. Buist and D.R. Eaton, *Can. J. Chem.*, 1987, **65**, 1653.
820. D.M. Doddrell, M.R. Bendall, P.C. Healy, G. Smith, C.H.L. Kennard, C.L. Raston and A.H. White, *Aust. J. Chem.*, 1979, **32**, 1219.
821. H. Grahn, U. Edlund and T.A. Holak, *Magn. Reson. Chem.*, 1987, **25**, 497.
822. S.C.F. Au-Yeung and D.R. Eaton, *J. Magn. Reson.*, 1983, **52**, 351.

823. S.C.F. Au-Yeung and D.R. Eaton, *J. Magn. Reson.*, 1983, **52**, 366.
824. S.C.F. Au-Yeung, R.J. Buist and D.R. Eaton, *J. Magn. Reson.*, 1983, **55**, 24.
825. S.C.F. Au-Yeung and D.R. Eaton, *Can. J. Chem.*, 1983, **61**, 2431.
826. V.P. Tarasov, T.Sh. Kapanadze, I.B. Baranovskii, G.V. Tsintsadze, S.G. Drobyshev and Yu. A. Buslaev, *Koord. Khim.*, 1984, **10**, 368.
827. S.C.F. Au-Yeung and D.R. Eaton, *Inorg. Chim. Acta*, 1983, **76**, L141.
828. K.I. Hagen, C.M. Schwab, J.O. Edwards and D.A. Sweigart, *Inorg. Chem.*, 1986, **25**, 978.
829. K.I. Hagen, C.M. Schwab, J.O. Edwards, J.G. Jones, R.G. Lawler and D.A. Sweigart, *J. Am. Chem. Soc.*, 1988, **110**, 7024.
830. T. Saito and S. Sawada, *Bull.Chem. Soc. Jpn*, 1985, **58**, 459.
831. Y. Masuda and H. Yamatera, *J. Phys. Chem.*, 1983, **87**, 5339.
832. J.M. Bernassau, M. Bertranne, C. Collongues and M. Fetizon, *Tetrahedron*, 1985, **41**, 3063.
833. M. Schwartz, M.G. Richmond, A.F.T. Chen, G.E. Martin and J.K. Kochi, *Inorg. Chem.*, 1988, **27**, 4698.
834. C.B. Storm, A.H. Turner and N.S. Rowan, *Inorg. Chem.*, 1985, **24**, 1269.
835. K.-D. Grüninger, A. Schwenk and B.E. Mann, *J. Magn. Reson.*, 1980, **41**, 354.
836. M. Cocivera, G. Ferguson, R.E. Lenkinski, P. Szczecinski, F.J. Lalor and D.J. O'Sullivan, *J. Magn. Reson.*, 1982, **46**, 168.
837. R. Benn, H. Brenneke and R.-D. Reinhardt, *Z. Naturforsch.*, 1985, **40b**, 1763.
838. S.M. Socol and D.W. Meek, *Inorg. Chim. Acta*, 1985, **101**, L45.
839. R.H. Crabtree and M. Lavin, *J. Chem. Soc. Chem. Commun.*, 1985, 1661.
840. R.H. Crabtree, M. Lavin and L. Bonneviot, *J. Am. Chem. Soc.*, 1986, **108**, 4032.
841. N. Hao, M.J. McGlinchey, B.G. Sayer and G.J. Schrobilgen, *J. Magn. Reson.*, 1982, **46**, 158
842. R.E. Wasylishen, G.L. Neufeld and K.J. Friesen, *Inorg. Chem.*, 1981, **20**, 638.
843. P.S. Pregosin, in *Annual Reports on NMR Spectroscopy*, Vol. 17 (ed. G.A. Webb), p. 285. Academic Press, London, 1986.
844. J.-Y. Lallemand, J. Soulié and J.-C. Chottard, *J. Chem. Soc. Chem. Commun.*, 1980, 436.
845. D.M. Doddrell, P.F. Barron, D.E. Clegg and C. Bowie, *J. Chem. Soc. Chem. Commun.*, 1982, 575.
846. I.M. Ismail, S.J.S. Kerrison and P.J. Sadler, *Polyhedron*, 1982, **1**, 57.
847. J.J. Dechter and J. Kowalewski, *J. Magn. Reson.*, 1984, **59**, 146.
848. R.E. Wasylishen and J.F. Britten, *Magn. Reson. Chem.*, 1988, **26**, 1075.
849. K. Lystbaek and H. Bildsoe, *Magn. Reson. Chem.*, 1985, **23**, 263.
850. R. Benn, H.M. Büch and R.-D. Reinhardt, *Magn. Reson. Chem.*, 1985, **23**, 559.
851. J. Reisse, *Nouv. J. Chim.*, 1986, **10**, 665.
852. R.K. Mazitov, H.G. Hertz, V.F. Garanin, K.M. Enikeev, A.V. Ilyasov and V.F. Sukhoverkhov, *Dokl. Akad. Nauk SSSR*, 1983, **273**, 131.
853. T.R. Stengle, N.V. Reo and K.L. Williamson, *J. Phys. Chem.*, 1984, **88**, 3225.
854. J. Schnitker and A. Geiger, *Z. Phys. Chem. (Munich)*, 1987, **155**, 29.
855. R.K. Mazitov, K.M. Enikeev and A.V. Ilyasov, *Z. Phys. Chem. (Munich)*, 1987, **155**, 55.
856. C.L. Perrin and R.K. Gipe, *Science*, 1987, **238**, 1393.
857. B. Dietrich, J.-P. Kintzinger, J.-M. Lehn, B. Metz and A. Zahidi, *J. Phys. Chem.*, 1987, **91**, 6600.
858. J.-P. Kintzinger, J.-M. Lehn, E. Kauffmann, J.L. Dye and A.I. Popov, *J. Am. Chem. Soc.*, 1983, **105**, 7549.
859. R.E. Wasylishen and A.M. de P. Nicholas, *Magn. Reson. Chem.*, 1986, **24**, 1031.
860. G. Schilling, C.W. Rabener and W. Lehr, *Z. Naturforsch.*, 1982, **37b**, 38.
861. R.D. Sammons, P.A. Frey, K. Bruzik and Ming-Daw Tsai, *J. Am. Chem. Soc.*, 1983, **105**, 5455.

Index

Acarides *see* Agrochemicals *and individual compounds*
13-Acetoxycycloheximide, 156
3-Acetyl-2-(2′,6′-dimethyl-5′-heptenyl) oxazolidine (insect repellant), 161
Acifluorfen, 147–148
Acifluorfen methyl, 149
Actin, ligand binding to, 108
Actinide compounds, nuclear relaxation in, 365, 387–388
Actinomycin C, interactions, 111
Actinomycin D, interactions, 111
Adenosine deaminase, ligand binding to, 105, 131–132
Adenylate kinase
  AMP bound to, 126–127, 128
  binding of AMP to, 86
  ligand binding to, 105, 106
ADH, AMP binding to, 84–86
Aggregates, ion binding to, 47–50
Agrochemicals
  assay of, 192–195
  decomposition of, stability in model systems, 174–177
  metabolic effects of, 188–191
  metabolism of, 177–188
  modes of action of, 188–191
  natural origin, 167–174
  structural analysis of, 142–167
^{27}Al, relaxation, 372–373, 382, 383
Alanine, scandium complex, 9, 10
β-Alanine. platinum complexes, 11
Alkali metal ion binding
  macromolecules, 26–30
  small ligands, 2–7
Alkali-metal compounds, relaxation in, 371–372, 375–381
Alkaline phosphatase, ^{113}Cd NMR studies of, 39, 43
Alkaline-earth metal ion binding
  macromolecules, 30–35
  small ligands, 7–8
Alkaline-earth-metal compounds, relaxation in, 372–373, 374, 381–382
Alkenyllead compounds, 276–277, 278
Alkylplumbanes, 267–271
  276–277
Alkyplumbanes, 267–271
Alkynylplumbanes, 259, 269, 278
Allethrin (insecticide), photochemical degradation of, 179
Aluminium compounds, solutions of, 373, 382, 383
4-(Aminomethyl)bicyclo[2.2.2]octane-1-carboxylic acid, (AMBOC), 70, 71
Ammonia, liquid, relaxation in, 366–367
Ammonium ion, relaxation in, 394
Ammonium lead(IV) chloride, 265, 288
AMP, binding of, 84–87, 126–127, 128
Anions, relaxation in, 373–375
Anisotropic solvents, relaxation in, 327–328
Antisickling ligands, 108
Antithrombin III interaction, 109
Apohaemoglobin, reactions with heme, 107
Aqueous solutions
  main-group-metal compounds, 376–385
  simple electrolytes, 370–375
  transition-metal compounds, 385–393
8-Arginine vasopressin (AVP), binding of, 114–116
Aryllead compounds, 274–275
Ascophyllum nodosum peroxidase, 35, 36
Assignment (of spectra), of agrochemicals, 142–152
Atrazine, detection of, 192–193

Automated instrumentation, 140
Azadirachtin (insect antifeedant), 167–168, 173
Azurines, ^{113}Cd NMR studies of, 42

^{11}B NMR, relaxation studied by, 367, 383
Band gaps
  polyacetylenes, 237, 239, 240, 242
  polyoxymethylene, 229, 230, 232, 233
Barban, detection of, 192–193
^{9}Be NMR, ion binding studies, 7
Bee venom melittin, interaction of, 112
Benzene gas, relaxation in, 364
4-Benzylaminesulphonic acid, 80
^{209}Bi NMR, relaxation studied by, 384
Bifenox, 147
Bile acid movement, 113
Bis(trimethylplumbyl)ethylene, 265
Bloch equations, 308
Bloembergen equations *see* Solomon–Bloembergen ...
Bloembergen–Purcell–Pound (BPP) theory, 308
Blue copper protein, ^{113}Cd NMR studies of, 42
Body fluids, analysis for agrochemicals, 180–182
Boron compounds, relaxation in, 383
Bovine insulin, ^{113}Cd NMR studies of, 37, 42
Bovine serine proteases, ^{113}Cd NMR studies of, 43
Bovine serum albumin (BSA)
  ^{113}Cd NMR studies of, 43
  ^{59}Co NMR studies of, 36
Bovine superoxide dismutase, ^{113}Cd NMR studies of, 42
Brush-border membrane, sodium-ion transport across, 49
Buthiobate (fungicide), 163

^{13}C–^{1}H chemical-shift correlation spectroscopy, ^{207}Pb NMR used with, 253
^{13}C–^{1}H shift-correlated spectra, agrochemicals studied by, 141, 144, 146, 156
^{13}C NMR
  agrochemicals studied by, 141, 143, 146, 147, 153, 160–161, 177. 179, 190
  configuration determined by using, 212–226
  databases, 142
  interchain interactions studied by, 226–246
  intrachain interactions studied by, 211–212
  ligand–macromolecule interactions studied by, 96, 99–100, 104–109, 120, 124, 129, 130, 132
  relaxation studied by, 373, 376, 377, 380, 381–382, 384, 386, 387, 390, 391, 392, 393
^{13}C shielding tensors
  polyacetylenes, 217–218, 219, 241
  poly(L-alanine), 224
  poly(β-benzyl L-aspartate), 225
  polyglycine, 223
  polyoxymethylene, 214, 229, 232–233, 235
^{43}Ca NMR
  ion binding studies, 8, 30–35
  relaxation studied by, 381
Cadmium compounds, relaxation in, 386–387
Calbindin D_{9k}, ion binding of, 44, 46
Calcium compounds, relaxation in, 372, 381–382
Calmodulin, ion-binding of, 31–32, 41, 44, 45
CAMELSPIN experiment, 357
Capsidiol (fungicide), 173
Carbanolate, detection of, 192–193
Carbonic anhydrase
  ligand binding to, 63–64, 67, 107
  ligand–macromolecule interactions studied by, 105, 122–124
Carbonic anhydrase isozymes, ^{113}Cd NMR studies of, 40, 43
Carboxy peptidase, ligand binding to, 107
Carboxypeptidase A, ^{113}Cd NMR studies of, 42

Carr–Purcell–Meiboom–Gill (CPMG) experiment, 350
Cations, relaxation in, 371–373
^{113}Cd NMR
  ion binding studies, 16–20, 37–46
  relaxation studied by, 386
Cells, ion binding to, 49–50
Chemical exchange, and nuclear spin relaxation, 341–343
Chemical-shielding anisotropy (CSA) relaxation, 319
  interference with dipole–dipole interaction, 321–322, 359, 377
Chemical-shift measurements. ligand–macromolecule interactions studied by, 62–67, 91–92, 104–113, 114–116, 120
Chlorine oxyfluorides, relaxation in, 367
Chlorpropham, detection of, 192–193
Chlozolinate (fungicide), hydrolysis of, 179
Cholinesterase inhibitors, insecticides as, 194–195
Chromium compounds, relaxation in, 388–389
Chromamycin A_3 interactions, 110
Chymotrypsin
  ^{113}Cd NMR studies, 43
  ligand binding to, 82, 104, 106, 120–122
Chymotrypsinogen, ^{113}Cd NMR studies, 43
CIPC, detection of, 192–193
^{35}Cl NMR
  ligand–macromolecule interactions studied by, 113
  relaxation studied by, 367, 374, 375, 380, 381
Clofentezine (acaricide), 144
  ^{13}C NMR spectra of, 146, 147
  ^{1}H NMR spectra of, 144, 145
  hydrolysis of, 176, 177, 179
  metabolism of, 182, 183
Clostridium MP apoflavodoxin, binding with, 101
CNDO/2 method, 210, 211, 212
  interaction distances underestimated by, 237
  polyacetylenes studied by, 219–222
^{59}Co NMR
  ion binding studies, 36
  ligand–macromolecule interactions studied by, 111
  relaxation studied by, 391–392
Cobalt compounds, relaxation in, 391–392
Coherence order, meaning of term, 357–358
COLOC pulse sequence, 141, 152
Computer programs, relaxation data analysis, 361–362
Computer-searchable databases, 142
Concavalin A, ^{113}Cd NMR studies of, 40–41, 44
Configuration
  at double bonds, agrochemicals, 152–153
  and nuclear shielding, 212–226
  in ring systems, agrochemicals, 153–156
Conformational properties, agrochemicals, 158–167
Continuous diffusion model (CDM) approach, 343
Continuous-wave (CW) off-resonance, 141, 351
Coordination number, ^{207}Pb NMR, 256–258
Copper compounds, relaxation in, 385
COSY spectra, 346
  agrochemicals, 141, 148, 156, 182
  kringle proteins, 65, 66, 117
  see also Relayed COSY...
^{53}Cr NMR, relaxation studied by, 388, 389
Creatine kinase, ligand binding to, 108
Cross-polarization–magic-angle-spinning (CPMAS) technique, ^{207}Pb NMR, 265, 266
Cross-relaxation, and NOE, 352–357
Cross-relaxation rate, 315
Crown ethers
  alkali-ion complexes of, 2–7
    relaxation studies of, 379, 380
  lithium ion binding to, 2
  potassium ion binding to, 6–7
  sodium ion binding to, 2–6
^{133}Cs NMR
  ion binding studies, 7

^{133}Cs NMR (*continued*)
relaxation studied by, 372
^{63}Cu NMR, relaxation studied by, 385
Cyanide ion, relaxation in, 373–374
Cyanobacterin (herbicide), 191
1,2-Cyclohexanedione, interaction of, 113
Cycloheximide (fungicide), 155, 173
Cypermethrin, metabolism of, 184–185
Cyphenothrin (insecticide), oxidation of, 176–177, 178, 179
Cytochalasin H and derivatives (plant growth regulators), 173
Cytochrome b_5, ligand binding to, 94, 95, 109
Cytochrome c
interaction of, 113
ligand binding to, 109
Cytochrome cd_1, 109

DANTE pulse sequence, 124, 345
Data analysis, relaxation data, 361–362
DBCP (nematicide), metabolites of, 181
3-Deacetyl-11-desoxyazadirachtin analogues, 169, 173
Debneyol (fungicide), 173
DEPT pulse sequence, 141, 250
Destruxins (insecticides), 173
Detigloyldihydroazadirachtin, 168–169
Deuteriated methanes, relaxation in, 363
Deuterium NMR *see* ^{2}H NMR
Deuterium oxide, relaxation in, 368–369
Diamagnetic fluids, relaxation in, 362–394
experimental methods used, 344–362
theory of, 309–343
Diaminolead(II) compounds, 260, 292
Dichlorprop (herbicide), 158
Dichlorobutrazol, 159
Dieldrin (insecticide), metabolism of, 181
Dielectric friction theory, 325, 374
3′,5′-Difluoromethotrexate, 88–89
Dihydrofolate reductase, ligand binding to, 65, 67, 75, 81, 83, 88–89, 106, 107, 118–120
Diorganolead(IV) compounds, 286–288
Diphenyl ether herbicides, 145–146
Dipolar interactions, 91, 92
Dipole–dipole (DD) interaction, 313–314, 316
interference with chemical-shielding anisotropy, 321–322, 359, 377
Dipyridamole, interaction of, 113
Displatin, 13
Distamycin A interactions, 110, 111
Distortional dynamics, 335–338
continuum approach, 336–337
electrostatic approach, 337
DNA, ionic interactions, 26–28, 33–34
DNA–ligand interactions, 110–111
DNA polymerase-I, ligand binding to, 104
Dopamine β-mono-oxygenase, ligand binding to, 95, 105
Double-quantum coherence, 359
Dual spin-probe method, 377–378, 382
Dynamic lineshape analysis, ligand–macromolecule interactions studied by, 88–90

Ecdysone, 170–171, 172, 174
Ecdysteroids, 172
Echinomycin interactions, 111
EDTA, cadmium complexes, 17–19
Electrolyte solutions, relaxation in, 370–375
Enantiomeric purity, agrochemicals, 156–158
Endrin (insecticide), metabolism of, 181–182
Enzyme–coenzyme interactions, 107–108
Enzyme–inhibitor interactions, 106–107
Enzyme–substrate interactions, 104–106
Enzymes, nucleotide binding to, 84, 125–127
Ethephon (ripening agent), decomposition of, 187–188

Extended diffusion (ED) treatment, 326, 330
Extended Hückel MO (EHMO) calculations, 210, 226, 246

^{19}F NMR
  agrochemicals analysed by, 192
  agrochemicals studied by, 180, 184, 189
  ligand–macromolecule interactions studied by, 63–64, 96, 102, 104–109, 112–113, 122, 123, 133
  relaxation studied by, 373, 384, 387
Fast inversion–recovery (FIR) sequence, 344–345
^{57}Fe NMR
  ion binding studies, 35–36
  relaxation studied by, 389–390
Fenoprop (herbicide), 158
Fenpropimorph (fungicide), mode of action of, 188–189
Fenvalerate (insecticide), metabolism of, 184
Fermi contact interactions, 91, 92
  ^{207}Pb NMR, 261, 263
Ferrocene derivatives, relaxation in, 390
Ff gene 5 protein, interactions of, 111
Field cycling spectroscopy, 348–349
Field gradient fluctuations, origin of, 335
Flavodoxins, binding with, 101–102, 109
Fluazifop-butyl (herbicide), photochemical degradation of, 179
Fluorides, solutions, 373
4-Fluorobenzenesulphonamide, 63–64, 67
4-Fluorocinnamate, 82, 122
FMN, flavodoxin binding of, 101, 109
Fokker–Planck equation within Langevin model (FPL) approach, 327
Force-free diffusion model, 339, 340
Fosmethilan, 162–163
Freeze-dried tissues, solid-state spectra from, 185
Fully coupled ^{13}C–^{1}H 2D correlation, agrochemicals studied by, 141, 150–151, 156

Gallium compounds, solutions, 372–373, 382
Gases, relaxation measurements in, 362–365
Gated decoupling technique
  pesticides studied by, 141
  relaxation studied by, 352
^{73}Ge NMR, relaxation studied by, 383–384
Geminal couplings, ^{207}Pb NMR, 263–264, 299–300
Germanium compounds, relaxation in, 383–384
Glutamate dehydrogenase, ligand binding to, 108
Glycine
  cadmium complexes, 17, 18
  platinum complexes, 11–12
Glycogen phosphorylase, ligand binding to, 102, 105, 107
Glyphosate (herbicide), degradation of, 185–186
Gramicidins
  interaction of, 112, 113
  thallium ion binding to, 22–23, 24, 47–49
Group Ib compounds, relaxation in, 385
Group IIb compounds, relaxation in, 385–387
Group IIIa compounds, relaxation in, 372–373, 382–383
Group IIIb compounds, relaxation in, 373, 387–388
Group IVa compounds, relaxation in, 383–384
Group IVb compounds, relaxation in, 388
Group Va compounds, relaxation in, 384, 394
Group Vb compounds, relaxation in, 388
Group VIa compounds, relaxation in, 384–385

Group VIb compounds, relaxation in, 388–389
Group VIIb compounds, relaxation in, 389
Group VIII compounds, relaxation in, 389–393
GTP, ligand binding to, 109
5′-Guanosine monophosphate, ^{23}Na NMR, 7

^{1}H–^{1}H 2D correlation, agrochemicals studied by, 141, 172
^{1}H NMR
  agrochemicals studied by, 141, 144–145, 153–155, 157–158, 161–166, 175, 179, 182–184, 193–195
  databases, 142
  ligand–macromolecule interactions studied by, 96, 97–98, 104–113, 117, 119, 120, 123, 130, 132
  relaxation studied by, 367, 368, 376, 384
^{2} NMR
  ligand–macromolecule interactions studied by, 96, 98–99, 105, 112–113, 122, 132
  relaxation studied by, 366, 367, 368, 369, 371, 383
^{3}H NMR, ligand–macromolecule interactions studied by, 99, 130
Haemoglobin, ligand binding to, 108
HAHA-effect, 256
n-Heptane emulsions, relaxation in, 368
Herbicides *see* Agrochemicals *and individual compounds*
Heteronuclear 2D NDE experiment (HOESY), 356
Heteronuclear broadband NOE, 352
Heteronuclear ^{13}C–^{1}H 2D correlation, agrochemicals studied by, 141, 156, 177
Heteronuclear multiple-quantum coherence (HMQC), 38, 131
Heteronuclear polarization transfer, 346
Hexamethonium 2H interactions, 111
^{199}Hg NMR
  ion binding studies, 20–21
  relaxation studied by, 386, 387
Histidine residues, study of, 65
Homonuclear one-dimensional NOE experiments, 353–354
Horse liver alcohol dehydrogenase, ^{113}Cd NMR studies of, 42
Horseradish peroxidase
  ^{113}Cd NMR studies of, 42
  ligand binding to, 76, 77
Hwang–Freed model, 339, 340
Hydration shell, properties of, 371
Hydrogen bonding, interchain interaction affected by, 242, 244
Hydrogen selenide liquid, relaxation in, 366
20-Hydroxyecdysone, 174

In vivo monitoring
  metabolic effects of agrochemicals studied by, 190–191
  metabolism of agrochemicals studied by, 187–188
Indirect spin–spin coupling, ^{207}Pb NMR, 261–264, 295–300
Indium compounds, relaxation in, 372, 382
INDO/S method, polyacetylenes studied by, 219–222
INDO/S parametrization scheme, 210
INDOR technique, 251
INEPT pulse sequence, 141, 251, 252, 346
Inorganic liquids, nuclear spin relaxation in, 366–367
Inorganic systems, relaxation in, 365–394
Insect attractants, 153
Insecticides *see* Agrochemicals *and individual compounds*
Instrumental developments, 150
Insulin
  ^{113}Cd NMR studies of, 37, 42
  ^{67}Zn NMR spectra of, 37
Interbond angles, ^{207}Pb NMR, 259–260
Interference effects, relaxation mechanisms, 321–322

Internal rotation, effects of, 329–335
Intrachain interaction, and nuclear shielding, 210–212, 226–246
Inversion–recovery sequences, 345–347
Inversion-transfer technique, ligand–macromolecule interactions studied by, 73
Ion binding
  aggregates and cells, 47–50
  macromolecules, 26–47
  small ligands, 2–26
  studies of, 1–50
Ions, relaxation in, 371–375
Iridium compounds, relaxation in, 392
Iron compounds, relaxation in, 389–390
Iron NMR *see* ^{57}Fe NMR
Isobutyl 3-(benzylmethylamino)-2-cyanocrylate (fungicide), 163–167
Isocitrate dehydrogenase, ligand binding to, 70, 71, 105
Isoleucyl tRNA synthase, ligand binding to, 105
Isoproturon (herbicide), photochemical degradation of, 179
Isotope effects, ^{207}Pb NMR, 260
Isotope labelling, 97, 133
Isotope-edited NOE spectra, ligand–macromolecule interactions studied by, 87–88, 124–125

J-diffusion model, 326, 327, 330
J-peaks, 356
J-resolved 2D NMR, agrochemicals studied by, 149
Jeener–Broekaert (JB) experiment, 360

^{39}K NMR
  ion binding studies by, 6–7, 28, 29–30
  relaxation studied by, 379
Ketosteroid isomerase, ligand binding to, 106
^{83}Kr NMR, relaxation studied by, 394
Kringle proteins, ligand binding to, 65, 66, 70, 71, 80–81, 109, 110, 116–118
Krypton, relaxation for gas in solution, 394

^{138}La NMR, relaxation studied by, 373
^{139}La NMR
  ion binding studies, 9
  relaxation studied by, 373
a-Lactalbumin, ^{113}Cd NMR studies of, 42
D-Lactate dehydrogenase, binding to, 112
Lactoperoxidase, ligand binding to, 107
Lanthanide compounds, relaxation in, 373, 387
Lanthanide shift reagents, optically active, 156–158
Lanthanum compounds, relaxation in, 373, 387
Lead compounds
  alkenyl, 259, 276–277
  alkyl, 271
  alkynyl, 278
  anions, 289, 291
  aryl, 274–275
  diaminolead(II), 260, 292
  diorganolead(IV), 286–288
  five-membered cyclic, 260, 275, 277, 293
  four-membered cyclic, 260, 292, 293
  monoorganolead(IV), 286–288
  organotrimethyl, 267–270
  organotriphenyl, 272–273
  six-membered cyclic, 260, 275, 276
  tetraalkenyl, 276–277
  tetraalkyl, 271
  tetraalkynyl, 278
  tetraaryl, 274–275
  triorganolead–element, 279–285
Lead (II) acetate, 258, 290
Lead(II) arsenofluoride, 290
Lead(II) carbonate, 290
Lead(II) chlorate, 290
Lead(II) chloride, 290
Lead(II) compounds, chemical shifts for, 260, 290–294
Lead(II) nitrate, 258, 290
Lead(II) oxide, 294
Lead(II) selenide, 294

Lead(II) sulphate, 290
Lead(II) sulphide, 294
Lead(II) telluride, 294
Lead(IV) acetate, 288
Lead(IV) chloride, 287
Lead(IV) compounds, chemical shifts for, 258–260, 267–288
Lead(IV)–element compounds, 287, 288
Lead(IV) oxide, 288
Lead NMR *see* ^{207}Pb NMR
Lectins, ^{113}Cd NMR studies, 41, 44
Leptophos (insecticide), 156–157
^{7}Li NMR
  ion binding studies, 2
  relaxation studied by, 372, 375, 376, 377
Ligand–macromolecule interactions, NMR studies of, 61–133
  applications, 103–133
  methods used, 62–95, 97
  nuclear probes used, 96, 97–103
Limonoid natural products, 167
Line broadening, 349
  suppression of, 350
Linewidth analysis
  agrochemicals studied by, 161–162
  ligand–macromolecule interactions studied by, 69–71, 123
Liouville space (superoperator) formalism, 312, 313
Lipid–protein interactions, 112
Liquid ammonia, relaxation in, 366–367
Lithium compounds, solutions, relaxation in, 372, 375–378
Long-range couplings, ^{207}Pb NMR, 264
Luciferase, ligand binding to, 108
Lutetium compounds, relaxation in, 387

M-diffusion model, 326, 327
Macromolecule–ligand interactions, NMR studies of, 61–133
  applications, 103–133
  methods used, 62–95, 97
  nuclear probes used, 96, 97–103
Macromolecules
  metal-ion binding to, 26–47
  nuclear shielding in, 205–246
Magic-angle-spinning (MAS) technique, ^{207}Pb NMR, 265, 266
Magnesium compounds, relaxation in, 372, 381
Magnetization-transfer experiments
  inversion-transfer technique used, 73
  ligand binding studied by, 74–76
  ligand–macromolecule interactions studied by, 72–76, 104–107, 109, 110
  saturation-transfer technique used, 65, 72–73, 75–76, 123
Main-group-metal compounds, solutions, relaxation in, 375–385
Manganese compounds, relaxation in, 389
Mecoprop (herbicide), 158
Membranes, ligand binding to, 132
Mercury compounds, nuclear relaxation in, 387
Mercury NMR *see* ^{199}Hg NMR
Metabolic effects, agrochemicals, 188–191
Metabolism, agrochemicals, 177–188
Metallothionein, ^{113}Cd NMR studies of, 37–39, 43
Methanethiosulphonate (MMTS) modified enzyme, 129
Methfuroxam (fungicide), oxidation of, 179
Methoxybenzoxazolinones (pesticides), 143
Methylthio-s-triazine herbicides, 177
^{25}Mg NMR
  ion binding studies by, 8, 30–35
  relaxation studied by, 381
^{55}Mn NMR, relaxation studied by, 389
^{95}Mo NMR
  ion binding studies by, 36
  relaxation studied by, 388
^{97}Mo NMR, relaxation studied by, 388
Model-free approach, 332–333
Molybdenum compounds, relaxation in, 388–389
Monoorganolead(IV) compounds, 286–288

Multiple-exponential relaxation spectroscopy (MERCY), 359
Multiple-internal-rotation model, 330–331, 334
Multiple-quantum (MQ) coherences, 358–359
Myricoside (insect antifeedant), 173
Mytomycin C interactions, 110

^{14}N NMR, relaxation studied by, 373, 374, 387, 394
^{15}N NMR
  ligand–macromolecule interactions studied by, 96, 100–102, 104, 107–109, 111–112, 114, 120, 125, 133
  relaxation studied by, 387, 391, 394
^{23}Na NMR
  ion binding studies, 3–6, 7, 26–30
  ligand–macromolecule interactions studied by, 111
  relaxation studied by, 372, 375, 376, 377, 378–379
  shift reagents used, 7
Natural products, agrochemical use of, 167–174
Nematicides *see* Agrochemicals *and individual compounds*
Neurophysins, ligand binding to, 109, 114–116
Nickel compounds, relaxation in, 393
Nitrate anion, relaxation in, 374
Nitrogen gas, relaxation in, 365, 387
4-Nitrophenyl(phenylselenyl) acetate, 122
Noble gases, relaxation for gas in solution, 393–394
NOESY, 355–356
  data analysis for, 361–362
NOESY spectra, agrochemicals studied by, 141, 164–167, 177, 178
Nogalomycin interactions, 111
Non-aqueous solutions, relaxation in, 394
Nuclear double resonance (NDR) spectroscopy, agrochemicals detected by, 192–193
Nuclear magnetic relaxation dispersion (NMRD) experiment, 348
Nuclear Overhauser enhancement (NOE), 315
  cross-relaxation and, 352–357
  isotope-edited, 87–88, 124–125
  ligand–macromolecule interactions studied by, 76, 78–88, 104–112, 122, 123–124
  measurement of, 78–79
  spectroscopy *see* NOESY
  transferred, 82–87, 125–126
Nuclear shielding
  calculation for macromolecules, 208–209
  and configuration, 212–226
  and interchain interactions, 226–246
  interpretations in terms of electronic structures, 210–246
  and intrachain interaction, 210–212
  theoretical aspects of, 206–210
Nuclear spin relaxation
  experimental methods used, 344–362
  measurement in gases, 362–365
  measurement in inorganic systems, 365–394
  ^{207}Pb NMR, 253–255
  theory of, 309–343
  see also Relaxation
Nucleic acids, ligand binding to, 132–133
Nucleotides, binding to enzymes, 84, 125–127

^{17}O NMR, relaxation studied by, 366, 368, 370, 371, 374, 381, 387, 388, 394
3-Octylthio-1,1,1-trifluoropropane-2-one (insecticide), mode of action of, 189–190
One-bond couplings, ^{207}Pb NMR, 262–263, 295–296
One-dimensional pulse NMR experiments, methods summarized, 141
Organochlorine pesticides, detection of, 192
Organophosphorus pesticides
  analysis of, 194
  enantiomeric purity of, 156–157

Organotrimethyllead compounds, 267–270
Organotriphenyllead compounds, 272–273
Oriented systems, relaxation measurement in, 360
Osteocalcin, ^{113}Cd NMR studies of, 42
Ovalifoliene analogues (plant growth regulators), 173
Oxo-anions, relaxation in, 374–375
Oxytocin, binding of, 114, 115

^{31}P NMR
  agrochemicals analysed by, 194
  agrochemicals studied by, 190, 191
  ligand–macromolecule interactions studied by, 69, 96, 102, 105–113, 120, 132
  relaxation studied by, 367, 374, 385, 394
Paclobutrazol (fungicide), 157, 159
Palladium compounds, relaxation in, 393
Paramagnetic probes
  chemical-shift measurements using, 91–92
  ligand–macromolecule interactions studied by, 90–95, 105–108, 124
  relaxation rate measurement using, 92–95
Paraquat (herbicide), 142–143
Parvalbumins, ion binding of, 44, 46
^{207}Pb isotope, NMR properties of, 210
^{207}Pb NMR
  chemical shifts, 255–260
    effect of coordination number on, 256–258
    isotope effects, 260
    lead(II) compounds, 260, 290–294
    lead(IV) compounds, 258–260, 267–288
  experimental details, 250–253
  geminal couplings, 263–264, 299–300
  indirect spin–spin couplings, 261–264, 295–300
  interbond angles in, 259–260
  ion binding studies, 23
  long-rang coupling constants for, 264
  nuclear spin relaxation in, 253–255
  one-bond couplings, 262–263, 295–296
  referencing for, 250–251
  relaxation studied by, 253–255, 372
  solid-state, 264–266
  techniques for observing resonances, 251–253
  vicinal coupling constants for, 264, 297–298
Penicillamine, zinc ion binding to, 16
Pepsin, ligand binding to, 88, 107, 124–125
Perchlorate anion, relaxation in, 374
Pesticide metabolites, 180–188
Pesticides
  NMR studies of, 139–199
  see also Agrochemicals
Pf1 coat protein, binding of, 112
Phenanthrenes (fungicide), 173
Phenothrin (insecticide), 151
Phenoxyacetic acid herbicides, metabolism of, 188
Phenylamide herbicides
  metabolic effects of, 190
  see also CIPC; Propanil
Pheromone components, 153
Phloretin 4′-*O*-β-D-glucopyranoside (insect antifeedant), 173
Phosmoglucomutase, ^{113}Cd NMR studies of, 43
Phosphocholine bilayers, tripeptide perturbation of, 113
Phosphoglucomutase, ligand binding to, 106
Phospholipase A_2, ion binding of, 33
Phospholipase C, ^{113}Cd NMR studies of, 42
Phosphoribosyl transferase, ligand binding to, 105
Phosphorus ion, relaxation in, 394
Phytoecdysteroids, 172, 173, 174
Plasminogen, kringle proteins in, 116
Plastocyanin, ^{113}Cd NMR studies, 42
Platinum compounds, relaxation in, 393
Plumbocenes, 256, 257, 258, 277, 293
Plumbylenes, 258, 292

Poisson–Boltzmann (PB) theory, 27
Polarization-transfer technique
  ligand–macromolecule interactions studied by, 95, 114
  ^{207}Pb NMR, 251, 252
Polyacetylenes
  band gaps of, 237, 239, 240, 242
  bond angles of, 216–217
  ^{13}C shielding tensors of, 217–218, 219
  configuration of, 215–223
  geometrical parameters of, 238
  interchain interaction in, 237–240
  molecular orbital calculations for, 219–222
  valence band structures of, 221
Poly(L-alanine)
  configuration of, 224
  interchain interactions in, 244–246
Poly(β-benzyl L-aspartate), configuration of, 224–226
Polyethylene
  configuration of, 212–213
  crystallographic models used in nuclear shielding calculations, 227
  interchain interaction in, 226–229
  intrachain interaction in, 211–212
Poly(ethylene oxide), relaxation rates affected by, 28
Polyglycine
  configuration of, 223–224
  interchain interactions in, 240, 242–244
Polyoxymethylene
  band gaps for, 229, 230, 232, 233
  configuration of, 213–215
  crystallographic models used in nuclear shielding calculations, 236
  interchain interaction in, 229–237
  seven-chains model, 230–236
  single-chain model, 229–230
Polypeptides
  configurations of, 223–226
  interchain interaction in, 240, 242–246
Porphobilinogen deaminase, ligand binding to, 99, 104, 107, 130–131
Porphobilinogen synthase, ligand binding to, 98–99, 105, 128–129
Potassium NMR *see* ^{39}K NMR
Pressure variability, 349
Profenofos (insecticide), 156–157
Profluralin metabolites, 180–181
Prolidase-catalysed hydrolysis, 104
Propanil (herbicide), 145, 161–162
  oxidation of, 179
Propoxur (insecticide), assay of, 194
Proteases, ligand binding to, 104
Protein C, ion binding of, 47
Protein–ligand interactions, 108–110, 114–118
Proteins, ion-binding of, 30–33, 35–47
Proteoglycans, ion binding of, 33
Proton-exchange studies, 370
^{195}Pt NMR
  ion binding studies, 11–13, 14, 15
  relaxation studied by, 372, 393
Purine riboside, binding by, 131–132
Pyrethroids, 152–153, 160
Pyrophosphatase (PPase), ^{113}Cd NMR studies of, 40, 43
Pyruvate kinase, ion binding studies, 28–29

Quadrupolar coupling constant (QCC), 318
Quadrupolar dips, 317
Quadrupolar echo (QE) experiment, 360–361
Quadrupolar relaxation, 317–318
Quantitive structure–activity relationship (QSAR) technique, agrochemicals analysed by, 195
Quinalphos (insecticide)
  hydrolysis of, 179
  photodegradation of, 175, 179
QWIKCORR pulse sequence, 152

Ramsey's theory, ^{207}Pb NMR, 255, 261
Random field relaxation, 321
Random-jump model, 329, 330, 331, 334

^{87}Rb NMR
ion binding studies, 48–49
relaxation studied by, 372, 375, 376
^{187}Re NMR, relaxation studied by, 389
Redfield theory, 310–312
see also Wangness–Bloch–Redfield (WBR) theory
Relative rotation angle, definition of, 231
Relative sliding length, definition of, 230
Relaxation
data analysis for, 361–362
exchange effects on, 341–343
experimental methods used, 344–362
interference effects between mechanisms, 321–322
measurements in gases, 362–365
measurements in inorganic systems, 365–394
^{207}Pb NMR, 253–255
theory of, 309–343
Relaxation mechanisms, 313–322
Relaxation superoperator, symmetry properties of, 312
Relaxation-time measurements, ligand–macromolecule interactions studied by, 68–69, 92–95, 105–113, 122, 123
Relayed COSY spectra, agrochemicals studied by, 141, 170–171, 172
Reorientational dynamics
flexible molecules, 329–335
computer simulation studies, 334
rigid molecules, 322–329
^{103}Rh NMR
ion binding studies, 11
relaxation studied by, 392
Rhenium compounds, relaxation in, 389
Rhodium compounds, relaxation in, 390, 392
Rhodopsin, ligand binding to, 112
Riboflavin 5′-phosphate, ligand binding to, 101, 109
Rotating frame, spin–spin relaxation in, 349–351
Rotating-frame Overhauser enhancement spectroscopy (ROESY), 357
Rotenone (insecticide), epimerization of, 179
Rubidium compounds, solutions, 372, 375
Ruthenium compounds, relaxation in, 390–391
Ryanodine (insecticide), 150–151, 156

^{33}S NMR, relaxation studied by, 366, 374
Saturation-transfer technique
agrochemicals studied by, 163–164
ligand–macromolecule interactions studied by, 65, 72–73, 75–76, 123
^{45}Sc NMR
ion binding studies, 9, 10
relaxation studied by, 373, 387
Scalar (SC) relaxation, 319–320
Scandium compounds, relaxation in, 373, 387
^{77}Se NMR
ligand–macromolecule interactions studied by, 104, 122
relaxation studied by, 366, 384–385
Selenium compounds, relaxation in, 384–385
Semiselective spin–lattice relaxation experiments, 347
Serine proteases, ligand binding to, 120–121
Sheep-kidney Na,K ATP-ase, ligand binding to, 107
^{29}Si NMR, relaxation studied by, 367, 374–375
Silicate solutions, relaxation in, 374–375
Silcon tetrachloride liquid, relaxation in, 367
Simazine, detection of, 192–193
Skewed exchange spectroscopy (SKEWSY), 356
Sliding length, definition of, 230
Small ligands
alkali-metal-ion binding to, 2–7
alkaline-earth-metal-ion binding to, 7–8

group IIA and IIIA metal ion binding to, 21–26
ion binding to, 2–26
transition-metal-ion binding to, 8–21
Small-step rotational-diffusion model, 323–324
validity of, 326
Smoluchowski diffusion equation, 339, 340, 343
^{119}Sn NMR
ion binding studies, 23–26
one-bond couplings, 262, 295–296
relaxation studied by, 384
Sodium NMR *see* ^{23}Na NMR
Sodium salts, relaxation studies of, 372, 376, 377
Solid-state analysis, freeze-dried tissues, 185–187
Solid-state NMR
interchain interactions in, 226
^{207}Pb NMR, 264–266
Solomon–Bloembergen equations, 28, 29, 47, 92
Solomon equations, 314, 353
Spectral-editing technique
ligand–macromolecule interactions studied by, 95
pesticides studied by, 141
Spin diffusion, 354
Spin–lattice relaxation, 308
measurement of, 344–349
Spin–lattice relaxation rates, 315
Spin–rotation interaction (SR), 320–321
Spin–spin relaxation time, measurement of, 349–351
Spin-echo technique, 350
Spin-locking experiment, 350–351
Stellacyanin, ^{113}Cd NMR studies of, 42
Stereochemistry, agrochemicals, 152–158
Stochastic Liouville equation (SLE), 313
Stokes–Einstein–Debye (SED) equation, 324–325
Strong narrowing condition, meaning of term, 312
Structural analysis, agrochemicals, 142–167
Sulphate anion, relaxation in, 374
Sulphur dioxide liquid, relaxation in, 366
Sulphur hexafluoride gas, relaxation in, 363, 365
Sulprofos (insecticide), 156–157
Supercritical water, proton relaxation in, 363

^{99}Tc NMR, relaxation studied by, 389
Technetium compounds, relaxation in, 389
Tellurium compounds, relaxation in, 385
Temperature variability, 349
Teramae's geometrical parameters, 237
Tetraalkenyllead compounds, 276–277, 278
Tetraalkyllead compounds, 271
Tetraaryllead compounds, 274–275
Tetraethylaluminate (TEA), sodium salt of, 378
Tetraphenylporphyrin, cadmium complex of, 19
Tetra-1-propynyllead, 251, 278
Thallium compounds, relaxation in, 383
Thallium ion binding
gramicidin channels, 22–23, 24, 47–49
macromolecules, 47
small ligands, 21–23, 24
Three-spin effect, 354
^{47}Ti NMR, relaxation studied by, 388
^{49}Ti NMR, relaxation studied by, 388
Tight-binding (TB) MO calculations, 207, 240
Tin compounds, relaxation in, 384
Tissue extracts, analysis for agrochemicals, 182, 184–185
Titanium compounds, relaxation in, 388
^{205}Tl NMR
ion binding studies, 21–23, 47
relaxation studied by, 383
Tocopherol, interaction of, 112, 113
Tomamycin interactions, 110

Torrey–Abragam model, 338–339, 340
Transferred NOE measurements, ligand–macromolecule interactions studied by, 82–87, 125–126
Transferrin, ion binding of, 47
Transition probabilities, definitions for *IS* spin system, 314
Transition-metal compounds, solutions, relaxation in, 385–393
Transition-metal ion binding
  macromolecules, 35–46
  small ligands, 8–21
Translational dynamics, 338–341
Triadimenol, 159
Trichilins (insect antifeedant), 173
Trifluralin (herbicide), 192
Triglycine, platinum complexes, 12
Trimedlure (insect attractant), 153–154
Trimethoprim derivatives, 83, 90, 106
Trimethyllead chloride, 255, 279
Trimethylorganolead compounds, 267–270
Triorganolead–element compounds, 279–285
Triphenyllead chloride, 252, 279
Triphenylorganolead compounds, 272–273
Tritium NMR *see* ^{3}H NMR
Tropomysin, ligand binding to, 109
Troponin C, ion binding of, 44, 46
Truncated driven Overhauser experiment, 355
b-Trypsin, ^{113}Cd NMR studies of, 43
Trypsinogen, ^{113}Cd NMR studies of, 43
Tryptophan-synthase-catalysed isomerization, 104
Tubulin, binding by, 109
Tungsten compounds, relaxation in, 388–389
Two-dimensional chemical exchange, ligand–macromolecule interactions studied by, 74
Two-dimensional difference spectroscopy, 95
Two-dimensional exchange spectroscopy, 355–356
  data analysis for, 361–362
Two-dimensional NMR
  lead compounds, 253
  ligand–macromolecule interactions studied by, 95, 97, 117, 119
Two-dimensional pulse NMR experiments, methods summarized, 141

Ubiquinone-10 interaction, 113
UDP-galactose-4-epimerase, ligand binding to, 108
Uranium hexafluoride, relaxation in, 365, 387
Urea-type herbicides, 154–155

^{51}V NMR
  ion binding studies by, 9–11, 35
  relaxation studied by, 388
Valence band structure, polyacetylenes, 221
Valeur–Jarry–Geny–Monnerie (VJGM) model, 333
Vanadium compounds, relaxation in, 388
Vicinal couplings, ^{207}Pb NMR, 264, 297–298
Vinclozolin (fungicide), 157
  hydrolysis of, 179
Vitamin C, platinum complexes, 12–13

^{183}W NMR, relaxation studied by, 388
Wallach models, 330–331
Wangness–Bloch–Redfield (WBR) theory, 310
  general reformulation of, 312
Water, relaxation in, 95, 367–370
Whole-cell studies, ion binding in, 49–50

^{129}Xe NMR, relaxation studied by, 393
^{131}Xe NMR, relaxation studied by, 393–394
Xenon, relaxation for gas in solution, 393–394

^{89}Y NMR, relaxation studied by, 373, 387

Zinc compounds, relaxation in, 386
Zirconium compounds, relaxation in, 388

^{67}Zn NMR
  ion binding studies, 14, 16
  relaxation studied by, 372, 386
^{91}Zr NMR, relaxation studied by, 388